INVESTIGATION OF HOST-GUEST INCLUSION COMPLEXATION OF SOME BIOLOGICALLY POTENT MOLECULES AND SOLVENT CONSEQUENCES OF SOME FOOD PRESERVATIVES WITH THE MANIFESTATION OF SYNTHESIS, CHARACTERIZATON AND INNOVATIVE APPLICATIONS

A thesis submitted to the

UNIVERSITY OF NORTH BENGAL

For the award of

DOCTOR OF PHILOSOPHY (Ph.D.)

In

CHEMISTRY

By

BIPLAB RAJBANSHI, *M.Sc. in Chemistry*

Under the supervision and guidance of

DR. MAHENDRA NATH ROY

Professor of Chemistry

Department of Chemistry

University of North Bengal

Darjeeling, PIN– 734013, WB, INDIA

February
2020

This thesis is dedicated

To

My beloved

Parents and Brother

DECLARATION

I declare that the thesis entitled "**INVESTIGATION OF HOST-GUEST INCLUSION COMPLEXATION OF SOME BIOLOGICALLY POTENT MOLECULES AND SOLVENT CONSEQUENCES OF SOME FOOD PRESERVATIVES WITH THE MANIFESTATION OF SYNTHESIS, CHARACTERIZATON AND INNOVATIVE APPLICATIONS**" has been prepared by me under the guidance of Dr. Mahendra Nath Roy, Professor of Chemistry, University of North Bengal. No part of this thesis has formed the basis for the award of any degree or fellowship previously.

Biplab Rajbanshi

Biplab Rajbanshi
Department of Chemistry
University of North Bengal
Darjeeling – 734013
West Bengal, India

Date: 17.02.2020

UNIVERSITY OF NORTH BENGAL

Prof (Dr.) M. N. Roy,

Awardee of One Time Grant from UGC,
Prof. Suresh C. Ameta awarde from ICS,
Shiksha Ratna by Govt. of West Bengal
and
Bronze Medal from CRSI

Department of Chemistry

E-mail: mahendraroy2002@yahoo.co.in

Phone : 0353 2776381
Mobile: 09434496154
Fax: 91 353 2699001
Darjeeling 734 013, INDIA
February, 2020

CERTIFICATE

I certify that Mr. Biplab Rajbanshi has prepared the thesis entitled "**INVESTIGATION OF HOST-GUEST INCLUSION COMPLEXATION OF SOME BIOLOGICALLY POTENT MOLECULES AND SOLVENT CONSEQUENCES OF SOME FOOD PRESERVATIVES WITH THE MANIFESTATION OF SYNTHESIS, CHARACTERIZATON AND INNOVATIVE APPLICATIONS**" for the award of Ph.D. degree of the University of North Bengal, under my guidance. He has carried out the research work at the Department of Chemistry, University of North Bengal.

Mahendra Nath Roy

DR. MAHENDRA NATH ROY

Professor of Chemistry

Department of Chemistry

University of North Bengal

Darjeeling – 734013

West Bengal, India

Prof. (Dr.) M. N. Roy
Department of Chemistry
&
Chairman, Sports Board
University of North Bengal
Darjeeling-734013, India

Date: 17-02-2020

URKUND

Urkund Analysis Result

Analysed Document:	Biplab Rajbanshi _Chemistry.pdf (D63579334)
Submitted:	2/7/2020 12:29:00 PM
Submitted By:	nbuplg@nbu.ac.in
Significance:	2 %

Sources included in the report:

https://www.beilstein-journals.org/bjoc/articles/15/163
https://www.ncbi.nlm.nih.gov/pmc/articles/PMC5865576/
https://pubs.rsc.org/en/content/articlelanding/2014/ra/c4ra07877b
https://www.researchgate.net/publication/304030820_Docking_and_physico-chemical_properties_of_a-_and_b-cyclodextrin_complex_containing_isopulegol_a_comparative_study
https://www.nature.com/articles/srep35764
https://cyberleninka.org/article/n/1411489
https://www.researchgate.net/publication/308987796_Study_to_explore_the_mechanism_to_form_inclusion_complexes_of_b-cyclodextrin_with_vitamin_molecules
https://www.researchgate.net/publication/265469096_Host-guest_inclusion_complexes_of_a_and_b-cyclodextrins_with_a-amino_acids
https://www.jacsdirectory.com/journal-of-advanced-chemical-sciences/admin/issues/20171031183422_3-4-02%20JACS17167%20Published.pdf

Instances where selected sources appear:

33

Biplab Rajbanshi 17.02.2020

Signature of the Candidate

Mahendra Nath Roy

Signature of the Supervisor

(17-02-2020)

Prof. (Dr.) M. N. Roy
Department of Chemistry
&
Chairman, Sports Board
University of North Bengal
Darjeeling-734013, India

ACKNOWLEDGEMENT

First of all, I would like to express my deepest sense of gratitude and inner sentiment to my respected teacher and supervisor, Dr. Mahendra Nath Roy, Professor Department of Chemistry, University of North Bengal, Darjeeling, India. Throughout my research period, I have received constant guidance, valuable suggestions, inspiration constructive criticism from him. I am deeply indebted to him for his keen interest, strong motivation, and constant encouragement and sympathetic consideration. The trust, support and freedom to create that he has provided throughout the work is very much appreciated. Without his loving care, dependable guidance and precious supervision, it would have been impossible for me to bring the present contour to this thesis.

I also express my profound sense of gratitude to the honourable faculty members, Department of Chemistry, University of North Bengal for their priceless assistance and continued inspiration the course of my research. I am grateful to the University authority for providing laboratory facilities, especially University Scientific Instrumentation Centre, University of North Bengal for helping me in my research.

The inspiration, encouragement and whole-hearted cooperation that I received from my parents is most elegantly acknowledged. No word is enough to pay my sincere gratitude to my father Sri Jatish Rajbanshi, mother Smt. Aloka Rajbanshi and brother Mr. Satrughna Rajbanshi for their contribution to my carrier building and whose inspiration went a long way to the completion of this thesis.

My special thanks goes to all of my lab mates for their valuable assistance and cooperation during my research work.

I am constantly aware of what a huge debt I owe to the sources of the information required for my research work: the numerous books, monographs, articles, computer websites etc. I put on record some measure of my gratitude to those references I have cited in this thesis.

I am thankful to State fellowship bearing Reference No. **1743/R-2017 dated 18.04.2017** for providing financial aid and instrumental assistance in order to

continue my research work. I would also like to record my thankfulness to **'ONE TIME GRANT' Ref No. F4-10/2010(BSR), UGC, New Delhi** for financial and instrumental assistance in connection with the research work.

Biplab Rajbanshi

Biplab Rajbanshi

Department of Chemistry

University of North Bengal

Darjeeling – 734013, WB, India

Date: 17.02.2020

PREFACE

The work in the thesis entitled "**INVESTIGATION OF HOST-GUEST INCLUSION COMPLEXATION OF SOME BIOLOGICALLY POTENT MOLECULES AND SOLVENT CONSEQUENCES OF SOME FOOD PRESERVATIVES WITH THE MANIFESTATION OF SYNTHESIS, CHARACTERIZATON AND INNOVATIVE APPLICATIONS"** was initiated under the supervision of Dr. Mahendra Nath Roy, Prof. of Chemistry in the Department of Chemistry, University of North Bengal. This research was become conscious within the framework of the Programme in the field of "**Host-Guest Inclusion Complexation of Some Biologically Potent Molecules & Food Preservative - Ionic Liquid interaction"** and the research group of Professor Roy.

The whole is an attempt to explore the supramolecular host – guest inclusion complexation of some biologically active molecules such as small drug molecules as well as vitamins in order to make them more bioavailable by increasing their solubility and to develop the drug delivery system for the mere water soluble newly emerging highly potential drug as inclusion complexes leads the controlled release of the drug molecules to the affected site without any chemical modification of the drug molecules. Beside this we investigated food preservative – ionic liquid interaction to minimize the doze of food preservative in foods.

During the course of my research, I was privileged to participate in several meets and seminars across the country. I was highly inspired by listening and interacting with distinguished experts and scientists. I was even fortunate enough to publish the works relating the thesis in the International Journal of repute.

In keeping with general practice of reporting scientific observation, due acknowledgement has been made whenever the work described was based on the findings of the other investigators. I must take the responsibility of any unintentional oversights and errors, which might have crept in spite of precautions.

I hope I will be given more challenges in my life so that the knowledge that I have earned during my work can be put into action in the future.

ABSTRACT

As the title of the thesis, I would like to show my deep insight into the field of Supramolecular Host-Guest Inclusion Complexation and the Food Preservative-Ionic Liquid interaction in solution phase resulting molecular synergism to show better microbial activity. In the supramolecular chemistry, various biologically potent molecules like, drugs, proteins and vitamins that are merely water-soluble and the delivery system of whose are still not so developed, were chosen for the formation of inclusion complexes with cyclodextrins in order to enhance its solubility as well as bioavailability. Different physicochemical as well as spectroscopic methodologies usually used to study the inclusion complexation exploring mechanism of their formation, stability, thermodynamic feasibility, binding ability to albumin protein and sustained oozing of the drug molecules from inclusion complexes to the dispersive media. In the field of solution chemistry, Food Preservative-Ionic liquid interaction showing molecular synergism to antimicrobial activity would become a great aspect in the area of food chemistry, as we know, there is so much of food productions all over the world but because of the process of spoilage a large proportion of these is lost. So, it requires a great attention to preserve foods, produced industrially and even at home. There are so many preservatives known, that utterly prevents spoilage of foods, but having some sort of side effects, usedness of these is an inherent threat to the world health. Now, use of these in minimal amount i.e. below the MIC (Minimal Inhibitory Concentration) in food would overcome the threat. The genesis of diverse interactions is usually exposed by measurement of the apparent molar volume (ϕ_v), limiting apparent molar volume (ϕ_v^0), molar refraction (R_M), limiting molar refraction (R_M^0) viscosity B coefficients obtained from different physicochemical methodologies. Food Preservative-Ionic liquid combinations were found to show better antimicrobial activity as obtained from the antimicrobial study on some gram positive and gram negative bacteria.

Importance of host-guest chemistry of cyclodextrins:

My research work on the supramolecular chemistry associated with and justified satisfactorily by the improvement of the following novel aspects - (a) solubility of the

drug into water for bioavailability, (b) drug delivery through HSA assisted controlled release from inclusion complexes, (c) Enhancement of fire resistivity of fire retardant, (d) Promotion of biodegradability of a water pollutant.

A drug to show greater therapeutic effectiveness needs its bioavailability and solubility to a large scale. Pharmacological response to be shown by a drug a minimum concentration of it must be achieved, in this connection aqueous solubility of the drug to a desired level is significant. Solubility of a molecule may be defined qualitatively as the spontaneous interaction of two or more substances to form a homogeneous molecular dispersion. It was found, that drug-CDs inclusion complexes enhances the aqueous solubility of drug making it more bioavailable. Encapsulation of the hydrophobic part of the guest molecule into the hydrophobic cavity of suitable dimension of CDs makes it to increase aqueous solubility. The cavity dimension of the CDs should be moderate to reduce the contact between water and the nonpolar regions of host and guest molecule. Among the CDs, α and β-cyclodextrins were used for the dimensional suitability of their cavity size.

As the organism – environment interaction is essential for its survival, on the molecular level small molecule like drug – protein/drug – gene product interaction is also essential that underlie the organism's ability to adapt to environmental changes and include those that bind, transport, and metabolize small molecules. Human serum albumin, the most abundant protein in blood plasma found to act as a carrier protein for vitamin, nutrients, hormone, steroid, drug like small molecule of low water solubility and binding ability of these molecules to HSA constitute a vibrant matter in pharmacokinetics. Here, binding property of drug to the HSA had been studied spectrofluorimetrically. Thus, HSA assists the drug to release from the inclusion complexes and makes its transportation to the affective area where adsorption of the drug molecule to be needed. Our study to form inclusion complexes of drug thus become moralised by the solubility enhancement and HSA assisted transformation and controlled release of the drug in human body.

The higher melting point of the inclusion complexes compare to its parent compound, namely, HBCDD are because of the fact that extra amount of heat is required for that compound to come out from the corresponding cyclodextrins (β-CD and HP-β-

CD respectively) cavity and also these higher values of melting point i.e. 209.5^{0}C and 210.5^{0}C clearly indicate the formation of two new inclusion complexes i.e. IC-1 and IC-2 respectively.

The aqueous solubility of HBCDD is very low in a wide range of temperature. But, the inclusion complexes were found to be fairly soluble in water at room temperature. This is the indication of a molecule to be bio-available and also bio-degradable by the microorganisms. Thus, the pollutant HBCDD which, was a non-bio-degradable in nature, now has been converted into a bio-degradable material through the newly formed inclusion complexes with β and HP-β-CD respectively.

Importance of drugs and vitamins as guest molecule: Phenylephrine hydrochloride (PEH) is a selective α1-adrenergic receptor agonist of the phenethylamine class used primarily in cold and flu conditions as an antipyretic, analgesic drug to relief pain. In the United States PEH is used as nasal decongestant. Phenylpropanolamine, pseudoephedrine and ephedrine are also used as nasal decongestant as the substitute of PEH. However, due to serious side effect (haemorrhagic stroke) phenylpropanolamine was withdrawn from market. Now, it is imperative to find out the suitability of PEH as the same done by the Phenylpropanolamine, pseudoephedrine and ephedrine for the treatment of nasal or sinus congestion and to find out the way of delivery with biocompatibility.

Alkaloid synephrine (SNP) was first extracted as a natural product from the leaves of various citrus trees are used as bronchial muscle reluctant, increases blood pressure in the patients suffering from low blood pressure. Its presence and positive retort as a bio-marker makes the orange juice like soft drinks authentic. Lipolytic stimulation by synephrine increases thermogenesis which leads to the increase in metabolic rate and fat oxidation. In weight loss products as well as in the dietary supplement “ephedra free” synephrine is frequently used and starts to earn enormous attention after the banned product ephedrine. Most of the cases patients suffering from obesity are often found to suffer from type-2 diabetes and hence synephrine in weight loss products frequently becomes beneficial to the diabetic patients.

Alverine citrate (ALVC) belonging from a class of antispasmodic drugs used to treat irritable bowel syndrome and diverticular disease. Alverine citrate acts as a

muscle relaxant and relieves abdominal pain, constipation or diarrhoea caused by the abnormal activity of the gut muscle. It also relaxes the muscle in the womb which is caused by the muscle spasms in uterus. Voltage-gated calcium channels are the main transducers of membrane potential changes into intracellular Ca^{2+} transients such a way they intervene smooth muscle contraction and activate endocrine to release hormone. The visceral pronociceptive effect of 5-HTcan be reduced as ALVC binds with 5-HT1A acting as an antagonist. ALVC when combined with simethicone, found to act more effectively in the treatment of abdominal pain in IBS. It is marketed commercially by the name Spasmonal® Forte in the form of hard capsule (Alverine citrate 60/120 mg) and soft capsule (60 mg Alverine citrate/300 mg simethicone). ALVC ultimately metabolised to two secondary metabolites through the conversion of its primary active metabolite, para hydroxy alverine (PHA).

The B vitamins and their derivatives are a class of water-soluble vitamins and naturally found in food substances. These have significant role in cell metabolism. They have major importance for food processing and biological activities such as transferring the alkyl group, fitting carbon dioxide, decarboxylation and transamination of amino acids, lipids and sugars. Fruit juices are one of the main sources of vitamins and the quality of fruit juices in industry is maintained by different techniques including pasteurization, which led to the degradation of vitamins along with other valuable food nutrients.

Importance of water pollutant: 1,2,5,6,9,10-hexabromocyclododecane(HBCDD) is mainly globally used as fire retardant additives for producing extruded or expanded polystyrene foam materials in bulk amount and has been widely manufactured from 1960. Moreover, it is used as an additive to manufacture various things such as upholstered furniture, automobile interior textiles, car cushions, electric and electronic equipment etc. In recent past decades it is one of the major environmental concern pollutant due to its persistent, toxic, bio-accumulative and biomagnifying or bio-transformative nature in environment. For these reasons this cyclic aliphatic brominated compound is very harmful to aquatic life.

Importance of food preservatives: Sodium benzoate (SBz) having inhibitory effect on the microbial growth is strongly recommended as a food preservative and

commonly used in foods like soda, fruit juice and a variety of products, such as cosmetics and pharmaceuticals. In acidic medium SBz works better on yeasts, molds, bacterial growth and prevent spoilage. In patients with acute hyper-ammonaemia, who were born with urea cycle disorders SBz acts as a therapeutic agent and also treats dental carries, blocks D-dopa in the hemi-parkinsonian rat.

Sodium salicylate (Scyt) is a significant antibacterial agent, also enhances the activities of certain antibiotics. The bacterial strains, Salmonella, Shigella including Escherichia coli that causes diarrhoea used to inhibited by bismuth subsalicylate efficiently. Being an active anti-inflammatory compound Scyt have been used as anti-inflammatory, analgesic and anti-pyretic agent still it has gastric bleeding like serious disadvantage. Scyt acts synergistically with vancomycin and enhances anti-staphylococcal activity significantly. The presence of salicylate in 5 mM concentration, vancomycin prevents biofilm formation and kill bacteria effectively below its MIC.

Importance of ionic liquids: Quaternary ammonium based ionic liquids also execute some sort of anti-microbial effects for instance positive charge on the Nitrogen atom of these ionic liquids attracts naturally the negatively charged species, such as bacterial proteins and consequently disorganization in the protein chain makes it denature. Ionic liquids, benztltriethylammonim chloride, benztltrimethylammonim chloride were used herewith in all four possible combinations to the illustrious food preservative SBz and Scyt. Anti-microbial activities of the set of four combinations were studied warily at concentrations below their MIC and found synergistic to each other.

Summary of work done:

Chapter I: This chapter contains in details about the object of the research work, their scope and applications in the contemporary science. It also includes the reason of choosing the biomolecules, drugs, vitamins, water pollutant, food preservatives, ionic liquids, cyclodextrins and the solvent systems.

Chapter II: This chapter includes the review of the earlier works in this field of research done by various scientist and researchers across the world. This chapter also provide a detail theory of investigation, where the interacting forces between the molecules have been described. Here, the theory of ^{1}H NMR, 2D ROESY, FTIR spectroscopy, UV-Visible spectroscopy, Fluorescence spectroscopy, Differential Scanning Calorimetry, Scanning Electron microscopy, Powder X-Ray Diffraction, High Resolution Mass Spectroscopy, Surface tension, Conductivity, Density, Viscosity, Refractive index have been discussed thoroughly and the significance of their use in the research work described in this thesis have been shown.

Chapter III: This chapter contains the experimental section. It covers the name, structure, physical properties, method of purification and applications of biologically active molecules, drugs, vitamins, water pollutant, cyclodextrins, food preservatives, ionic liquids and solvents used in the research work. It also includes the details about the experimental methods, the descriptions and use of the instruments involved in the research work.

Chapter IV: Host-guest interaction of two significant drugs, phenylephrine hydrochloride and synephrine with α and β-cyclodextrins were studied systematically. Initially two simple but reliable physicochemical techniques namely conductance and surface tension were employed to find out saturation concentration for the inclusion and its stoichiometry. The obtained 1:1 stoichiometry was further confirmed by two spectrometric methods, UV-Vis study and spectrofluorimetry. Significant shifts in IR stretching frequency also support the inclusion process. Relative stabilities of the inclusion complexes were established by the association constants obtained from UV-Vis spectroscopic measurements, program based mathematical calculation of conductivity data. Calculations of the thermodynamic parameters dictates thermodynamic feasibility of the inclusion process. Spectrofluorometric measurement scaffolds the UV-Vis spectroscopic measurement validating stability of the ICs once again. Mass spectroscopic measurement gives the molecular ion peaks corresponding to the inclusion complex of 1:1 molar ratio of host and guest molecules. The mechanism of inclusion was drawn by 1H-NMR and 2D ROESY spectroscopic analysis. Surface texture of the inclusion complexes was studied by SEM. Finally, the cytotoxic activities of the inclusion complexes were analyzed and found, Cell viability also balances for

non-toxic behavior of the ICs. Moreover, all the studies reveal the formation of inclusion complexes of two ephedra free, alternatively emerging drugs (after their banned product having ephedra) SNP, PEH with α and β-CD, which enriches the drug delivery system with their regulatory release without any chemical modification.

Chapter V: The host-guest inclusion of thiamine hydrochloride(guest) within the hydrophobic cavity of α and β-cyclodextrin molecules (hosts) have been studied scientifically in the solid and solution phases respectively. Various modern spectroscopic techniques had been used to establish the outcome of this work. The UV-Vis study supported the 1:1 stoichiometry of the inclusion complexes and also used to evaluate the association constants along with thermodynamic parameters with high accuracy for the determination of the feasibility of this inclusion process. From the mass spectrometric study,1:1 stoichiometry of the inclusion complexes had been confirmed in their solid state. Differential scanning calorimetric and infrared studies also supported this fact.1H-NMR and 2D ROESY spectroscopic analysis had given the mechanism of inclusion process, and the SEM study exposed their surface structures. Finally, the sustained oozing of the guest molecule from the hydrophobic cavity of the respective cyclodextrin molecules separately had been studied in the presence of human serum albumin in their aqueous buffer solutions with the help of fluorescence spectroscopic technique. This study has a truly intense effect to the stabilization of the respective guest molecule from the external hazardous, such as photolytic degradation, oxidation-reduction, thermal cleavage etc., and also predicts the releasing behavior of thiamine hydrochloride in the presence of human serum albumin without any chemical modification.

Chapter VI: Inclusion complexation of a non-biodegradable pollutant in hydrophobic cavity of β-cyclodextrin and 2-hydroxypropyl-β-cyclodextrin were synthesized and characterized to retain its fire resistance property and converted it into bio-degradable molecule. 1H NMR, 2D ROESY, HRMS, SEM, etc. studies have been executed to establish this fact. The stoichiometry of the two complexes has been obtained as 1:1. The inclusion has been established by 1H-NMR and 2D ROESY spectroscopic analysis. Substantial shifts in IR stretching frequency support the inclusion process. HRMS measurement gives the molecular ion peaks corresponding to the inclusion complex of 1:1 molar ratio of host and guest molecules. Surface texture properties of the inclusion

complexes were studied by SEM and the presence of bromine were proved by EDXS. Thermal stabilities of the inclusion complexes were illustrated by melting point analysis. The aqueous solubility of the inclusion complexes demonstrate that these are more bio-available to the microorganism making them biodegradable in nature. The biodegradability study confirms the conversion of non-biodegradable HBCDD into biodegradable material by encapsulating in the two cyclodextrins.

Chapter VII: Solubility development of supramolecular host-guest interaction between Alverine citrate with αand β-cyclodextrins were studied throughout the article. 2:1 host to guest stoichiometry of the inclusion complexation in the solution phase were confirmed by the Job's plot and further confirmation about the stoichiometry was also obtained from the mass spectra of the inclusion complexes. IR, DSC, SEM and PXRD data turn out to be supportive about the phenomenon, inclusion complexation. Association constants and thermodynamic parameters of the inclusion complexes were obtained using UV-vis and spectrofluorometric measurement. The mechanism of inclusion complexation was explored by 1H and 2D ROESY NMR spectroscopy. Binding ability of the drug molecule, Alverine citrate with the HSA and the controlled release of the drug molecule from inclusion complexes were studied at PH-7.4 by spectrofluorimetricaly. Studied phenomenon thus develops the solubility of merely soluble drug into water, consequently makes bioavailable and enriches the drug delivery system.

Chapter VIII: An analysis on the diverse molecular interactions of implausible food preservatives, Sodium benzoate (SBz), Sodium salicylate (Scyt) in the aqueous solutions of Benzyltriethylammoniun chloride (BTEACl), Benzyltrimethylammoniun chloride (BTMACl) having durable anti-bacterial effect have been explored thoroughly by various physicochemical methodologies such as Density, Refractive index, Viscosity, Electrical conductivity, at five different temperatures ranging from 298.15 K to 318.15 K. Anti-bacterial as well as the anti-fungal effects of the ternary mixtures, (BTEACl+SBz+H2O), (BTEACl+Scyt+H2O), (BTMACl+SBz+H2O) and (BTMACl+Scyt+H2O) were further analysed for better results and found to act synergistically below the MIC of both the food preservative, thus minimises the hazardous threat, caused by unnecessarily excessive consumption of food preservatives. Association constants governed by diverse intermolecular interactions

in the solution phase were studied by UV-vis spectroscopy. Construction of thermodynamic background caused by innumerable interactions taking place in the ternary mixtures were explored by calculating the free energies of various molecular associations. The genesis of diverse interactions was exposed by measurement of the apparent molar volume, limiting apparent molar volume, molar refraction, limiting molar refraction, viscosity B coefficients and reveals as strong solute-solvent interaction, over the solute-solute and solvent-solvent interactions. Optimum energies with the optimised geometries of molecular assembly for (BTEACl+SBz), (BTEACl+Scyt), (BTMACl+SBz) and (BTMACl+Scyt) systems were calculated from Ab-initio quantum chemical calculations using Gaussian 09W quantum chemical package which found supportive to the practical outcomes.

Chapter IX: This chapter includes the concluding remarks about the research works done in this thesis.

TABLE OF CONTENTS

LIST OF TABLES

LIST OF FIGURES

LIST OF SCHEMES

APPENDIX A

LIST OF PUBLICATIONS

1. Study to Probe Subsistence of Host-Guest Inclusion Complexes of α and β-Cyclodextrins with Biologically Potent Drugs for Safety Regulatory Dischargement

   Scientific Reports | (2018) 8:13031

   Included in the Thesis

2. Minimization of the dosage of food preservatives mixing with ionic liquids for controlling risky effect in human body: Physicochemical, antimicrobial and computational study

   Journal of Molecular Liquids 282 (2019) 415–427

   Included in the Thesis

3. Study to Explore Host Guest Inclusion Complexes of Vitamin B1 with CD Molecules for Enhancing Stability and Innovative Application in Biological System

   Journal of Molecular Liquids 298 (2020) 111952

   Included in the Thesis

4. Evidences for Inclusion and Encapsulation of an Ionic liquid with β-CD and 18-C-6 in Aqueous Environments by Physicochemical Investigation

J. Phys. Chem. B 2018, 122, 5, 1679-1694

5. Synthesis, characterization of 1-butyl-4-methylpyridinium lauryl sulfate and its inclusion phenomenon with β-cyclodextrin for enhanced applications

Colloids and Surfaces A 548 (2018) 206-217

6. Exploring inclusion complexes of ionic liquids with α and β-cyclodextrin by NMR, IR, mass, density, viscosity, surface tension and conductance study

Journal of Molecular Structure 1159 (2018) 205-215

7. Studies of solvation behaviour of LiI prevailing in diverse solvent systems conductometrically and spectrometrically supported by ab initio technique

Chemical Physics Letters 671 (2017) 7–14

8. Assorted interactions of amino acids prevailing in aqueous vitamin C solutions probed by physicochemical and ab-initio contrivances

Chemical Physics Letters 687 (2017) 209–221

APPENDIX B

List of Seminar/Conference/Workshop attended

1. SERB sponsored National Conference on "Green Chemistry: An Alternative of Conventional Chemistry" Organised by: Department of Chemistry, CBPBU, Cooch Behar, West Bengal, 20th – 21st September 2019. ***(Presented a poster)***

2. International Seminar on "The history of Science & Technology – A Journey from Metal Age to E-Age, Organised by: Department of Chemistry & IQAC, Alipurduar College, Alipurduar in Collaboration with: College of Science and Technology, Royal University of Bhutan, Rinchending, Bhutan. ***(Presented a poster)***

3. International Seminar on "Frontiers in Chemistry 2018" Organised by: Department of Chemistry, University of North Bengal & CRSI North Bengal Local Chapter. ***(Presented a poster)***

4. International Seminar on "Frontiers in Chemistry 2017– 2018" Sponsored by: University Grants Commission, New Delhi; Organised by: Department of Chemistry, University of North Bengal. ***(Presented a poster)***

5. National Conference on Recent Trends in Chemistry (RTC – 2017), February 17 – 18, 2017, Sikkim Manipal Institute of Technology, Majitar, Rangpo, Sikkim. ***(Oral presentation)***

6. International Seminar on "International Year of the Periodic Table of Chemical Elements – 2019" 22nd – 23rd November 2019, Organised by: Department of Chemistry, University of North Bengal.

7. National Seminar on "Frontiers in Chemistry – 2019" Organised by: Department of Chemistry, University of North Bengal & CRSI North Bengal Local Chapter.

8. International Seminar on Recent Trends in Chemistry (RTC – 2019) January 03, 2019, Organised by: Department of Chemistry, P.D. Women's College, Jalpaiguri – in association of Indian Chemical Society, Kolkata.

9. National Seminar on "Frontiers in Chemistry – 2017", Funded by: University Grants Commission and SAP (DRS-III), Organised by: Department of Chemistry, University of North Bengal.

10. Science Academies Lecture Workshop on "Frontiers in Chemical and Material Sciences: Theory and Practice", Organised by: Department of Chemistry, University of North Bengal.

11. National Seminar on "Frontiers in Chemistry 2017-18", Funded by: University Grants Commission and SAP (DRS-III), Organised by: Department of Chemistry, University of North Bengal.

12. Science Academies' Lecture Workshop on "Recent Developments on the Theoretical and Experimental Aspects of Advanced Materials" (September 18-19, 2015), Department of Chemistry, University of North Bengal.

13. One-day seminar on "Recent Trends on Chemistry and Biology Interface" Organised by: Chemical Research Society of India, NBU-Local Chapter, Department of Chemistry, University of North Bengal (Darjeeling) (August 28, 2015).

14. Frontiers in Chemistry-2015, Funded by: University Grants Commission and SAP (DRS-III), Organised by: Department of Chemistry, University of North Bengal.

15. Science Academies' Lecture Workshop on "Spectroscopy of Emerging Materials", November 26-27, 2014, Organised by: Department of Chemistry, University of North Bengal.

16. Science Academies' Lecture Workshop on "Fascinating Chemistry" January 20-21, 2014, Organised by: Department of Chemistry, Malda College, Malda, West Bengal.

17. Government of India, Directorate of Field Publicity, Ministry of information & Broadcasting, Malda and Malda Gaur Banga Press Club, Malda, September 20, 2007

CHAPTER I

NECESSITY OF THE RESEARCH WORK

I.1. OBJECT, SCOPE AND APPLICATIONS

Research gathers information and investigates phenomena allowing us to test the theories and make prediction-solving problems. Research creates new knowledge and understanding. It reduces the chances of making poor or dangerous choices protecting us from false ideas and risky beliefs. Basic research leads to applied research in unusual ways. That why research is the force behind everything that we do, such as phones we use, medicine we take, power we consume. It is time for us all to embrace Research to find the evidence, to back up beliefs, to test out hunches and to discover better ways of doing things. We human beings are doing research as the development of the world made. The world made up of matters and living organisms, so most of the research work confined into the group exploring matter – living organism interactions.

The supramolecular chemistry discovered by Cramer, Pedersen, Cram, and Lehn, achieved the mountain high success and gained an enormous momentum in the last eras, with sometimes around 20,000 corresponding papers per year.[1-4] A vast applications regarding the host-guest supramolecular chemistry, e.g., sensing, separation, drug delivery, catalytic, and biomedical technologies strongly paved the first step of this field. It introduces the noncovalent interactions in an unprecedented way. [5-8] Beside the calculation of binding energy, designing of the supramolecular systems and their applications are also of fundamental interest. These make able to understand biologically important association, techniques of complexation and designing a new host structure. Modern synthetic tool also helps to construct a suitable host structure, which can exert an extra potential for a particular guest compound. The interactions that results inclusion complexation can be identified and explained, based on the interactions their structures can also be elucidated. It has a great thermodynamics that can be determined quite accurately using binding constants of the inclusion complexes. A particular advantage of supramolecular

complexes is that they allow elucidation of the existence and the limitation of additivity of binding energies, which is inherently assumed in most applications, e.g., for rational drug design. Another advantage is that, in typical supramolecular complexes, several interactions contribute, and the loss of entropy of translation for any intermolecular association is already paid by a single association step. Several non-covalent forces stabilizes the inclusion complexes, which are (a) Van der waals forces of interactions (b) Short range repulsion (c) Electrostatic interactions (d) Hydrogen Bonding interaction (e) Interactions of Dipolar substances.

Macrocyclic host molecules are of immense importance in ICs, as their cyclized and constrained conformations offer the benefit of molecular selectivity.[9] The cyclodextrins (CDs) are particularly interesting in this regard because of their amphiphilic nature.[9,10] The interest in amphiphiles arises from their self-assembly in aqueous systems to form well-defined structures, such as micelles, nanotubes, nanorods, nanosheets, and vesicles, that can be applied in several fields ranging from nanodevices to drug delivery and cell imaging.[11-13] In recent times, cyclodextrin-modified nanoparticles have been the focus of great attention because they appreciably improve the characteristics of the resulting assemblies, such as the electronic, conductance, thermal, fluorescence, and catalytic properties, improving the potential applications of these assemblies as nanosensors and drug delivery vehicles.[14,15] Various sophisticated probes have been designed for this purpose for applications in the manufacture of molecular switches, molecular machines, supramolecular polymers, chemosensors, transmembrane channels, moleculebased logic gates, and other interesting host–guest systems.[16-18]

Oligosaccharides, specially cyclodextrins (CDs) regarding host-guest inclusion complexation have very significant importance in food industries[19-21] pharmaceuticals[22] and consumer goods due to their unique conical-shaped cyclic structures. Cyclodextrins and their derivatives are commercially available and differ because of the presence of different glucopyranose residues. Cyclodextrins have their distinctive biphasic layers possessing hydrophilic outer and hydrophobic inner surfaces. The inner region allows incorporating hydrophobic surface of different guest or segment(s) of guest molecules into the cavity of a suitable and stable geometrical sized CDs through various kinds of non-covalent interactions.[23] Herein, α

and β-cyclodextrins bearing 6 and 7 glucopyranose units, respectively, have taken as host molecules. Due to high inclusion efficiency, fitting cavity dimensions, low price, and negligible toxicity.[24] The CDs have found widespread application in pharmaceuticals, food industries, cosmetics[25], tissue engineering, bio-medical devices. Inclusion complexation within the non-polar cavity of CDs is employed for protecting the hydrophobic part of different bioactive molecules, enzymes, drugs, volatile organic compounds, flavors, essential oils, taxols, flavonoids, vitamins[26], and etc. to extend their light, air and thermal stability, enhancement of water solubility, bioavailability and shielding side effects.

The stabilisation and the controlled release of the drugs now days, are of great concern in pharmacology. To guard drug molecules from environmental effects and to reduce the side effects for their controlled release it is vital to investigate whether they can be encapsulated into the cyclodextrin molecule. Thus to complete such aim, the inclusion complex formation of drug molecules such as synephrine, phenylephrine hydrochloride, Vitamin B_1, alverine citrate, hexabromocyclododecane and with alpha and beta cyclodextrin have been studied to achieve the goal.

Structural characterization of Host-Guest inclusion complexes of α-CD and β-CD with two bio-active molecules, synephrine (SNP) and phenylephrine hydrochloride (PEH) were done over here in terms of geometry and structural preferences by means of a variety of physical and spectroscopic methods in solid state and solution phase. Phenylephrine hydrochloride is a selective α_1-adrenergic receptor agonist of the phenethylamine class used primarily in cold and flu conditions as an antipyretic, analgesic drug to relief pain.[27] In the United States PEH is used as nasal decongestant. Phenylpropanolamine, pseudoephedrine and ephedrine are also used as nasal decongestant as the substitute of PEH.[28,29] However, due to serious side effect (hemorrhagic stroke) phenylpropanolamine was withdrawn from market.[30] Alkaloid synephrine are used as bronchial muscle reluctant, increases blood pressure in the patients suffering from low blood pressure. Lipolytic stimulation by synephrine increases thermogenesis which leads to the increase in metabolic rate and fat oxidation.[31-34] In weight loss products as well as in the dietary supplement “ephedra free” synephrine is frequently used and starts to earn enormous attention after the banned product ephedrine.[35,36] Most of the cases patients suffering from obesity are

often found to suffer from type-2 diabetes and hence synephrine in weight loss products frequently becomes beneficial to the diabetic patients.[37] Cyclodextrins, mostly α-cyclodextrin, are found to form complexes with the dietary fat which are stable enough to undergo enzymatic hydrolysis by lipase. This restrains accumulation of fat in human body.[38] Hence, inclusion complex of SNP and cyclodextrins can be of a great deal for the weight loss/weight management dietary food supplement for sportsman or obese person.[39]

The inclusion of THC has been aimed within the cavity of α and β-CD separately in both solution and solid states to explore their formation of inclusion complex (IC) for enhancing the stability of THC. Regular release without any chemical alteration of THC in the presence of HSA from the cavity of α and β-CD develops the drug delivery system. The B vitamins and their derivatives are a class of water-soluble vitamins and naturally found in food substances. These have significant role in cell metabolism.[40] They have major importance for food processing and biological activities such as transferring the alkyl group, fitting carbon dioxide, decarboxylation and transamination of amino acids, lipids and sugars.[41,42] Among all the B vitamins and their derivatives, one of the most common is thiamine (vitamin B1) chloro hydrochloride (THC, Figure 1), which is usually used as a component of single vitamin B complex and multivitamin preparations, food supplement, antioxidant, prooxidant, pharmaceutical industries and biological fluids. THC is used to treat in appetence and dermatophytosis. Moreover, it is also helpful to metabolize in human body.[43,44] Due to the lack of thiamine hydrochloride, neurotransmission in human body can be affected. Deficiency of THC leads to the occurrence of various malfunctions inside the human body such as beriberi, confabulation and an irreversible dementia; even extreme deficiency may lead to heart failure and death.[45] Thus thiamine hydrochloride is extensively used in human body; moreover, it can be utilized as feed in agriculture and synthetic intermediates in industry. But THC is very sensitive to light and high temperature processing and also has tend to get oxidize easily in the presence of oxygen which limits their applications to a great extent in different fields. Chemical degradation is very common with vitamin B1 and the main route of the degradation is its reduction which is caused in the presence of food preservatives

such as sodium meta-bisulfite, with very low concentrations (~1 mmol/L). Moreover, it can degrade by some of cell surface enzymes and plant thiamine antagonists[46]

1,2,5,6,9,10-hexabromocyclododecane(HBCDD) is mainly globally used as fire retardant additives for producing extruded or expanded polystyrene foam materials in bulk amount and has been widely manufactured from 19601. Moreover, it is used as an additive to manufacture various things such as upholstered furniture, automobile interior textiles, car cushions, electric and electronic equipment etc[47,48]. In recent past decades it is one of the major environmental concern pollutant due to its persistent, toxic, bio-accumulative and biomagnifying or bio-transformative nature in environment.[49] For these reasons this cyclic aliphatic brominated compound is very harmful to aquatic life. Global market demand of HBCDD was 22000 tons per year in 20038. The major portion of HBCDD was used in Europe, which was estimated at 11,000 tons in 2006, of which about 96% were used in expanded and extruded polymer9. Recently, it is included in Annex A of the Stockholm Convention on Persistent Organic Pollutants (POP), 2009 and in 2013 for elimination with restricted uses.[50] Due to all of the adverse effects on environment it is restricted in Japan in2014 and in Republic of Korea (South Korea) in 2015 permanently till the advanced substituted one upto 2020.[51] In recent years, the bromine industry has taken important steps to reduce discharges from manufacture and use of HBCDD and other fire retardants, notably its production is closed in HBCDD manufacturing site Newton Aycliffenearly NE coast of England. Because of its dramatically negative environmental impact, the development of efficient HBCDD removal technologies has increasingly become a significant environmental concern. The bio-accumulative and biomagnifying nature of HBCDD is critically threaten to the sustainable development of our planet as influence of HBCDD on the environment is long-term and difficult to repair. Some traditional methods had applied to remove this HBCDD from water for example, debromination technique, adsorption technique etc. and also some micro biodegradation technique etc. had applied to degrade it.[52-54] Here we approach a new novel way to remove this POP via making an encapsulation complex with β-cyclodextrin (β-CD) and hydroxypropyl-β-cyclodextrin (HP-β-CD) respectively. As HBCDD is a hydrophobic molecule,it may be inserted into the hydrophobic cavity of

cyclodextrin forming inclusion complex, its solubility in water increases enhancing bioavailability and faster biodegradability of HBCDD by microorganisms.

Irritable bowel syndrome (IBS), a gastrointestinal disorder is a most commonly diagnosed gastroenterological problem in medical sciences. Patients suffering from IBS are found to suffer frequently from various gastrointestinal disorder like, abdominal pain or dis-comfort, altered bowel habit, bloating[55] associated with the symptoms, incomplete bowel movement, urgency and tenesmus.[56] Thus, irritable bowel syndrome is a functional gastrointestinal disorder showing a lot of abnormalities. Hyper-reactive intestinal motility and visceral hypersensitivity are also found in patients suffering from IBS. Alverine citrate (ALVC) belonging from a class of antispasmodic drugs used to treat irritable bowel syndrome and diverticular disease. Alverine citrate acts as a muscle relaxant and relieves abdominal pain, constipation or diarrhoea caused by the abnormal activity of the gut muscle. It also relaxes the muscle in the womb which is caused by the muscle spasms in uterus. Voltage-gated calcium channels are the main transducers of membrane potential changes into intracellular Ca^{2+} transients such a way they intervene smooth muscle contraction and activate endocrine to release hormone.[57,58] The supramolecular interaction between ALVC and cyclodextrins (CDs) to form inclusion complex was justified satisfactorily by the improvement of two novel aspects - (a) solubility of the ALVC into water for bioavailability, (b) drug delivery through HSA assisted controlled release from inclusion complexes.

A drug to show greater therapeutic effectiveness needs its bioavailability and solubility to a large scale. Pharmacological response to be shown by a drug a minimum concentration of it must be achieved, in this connection aqueous solubility of the drug to a desired level is significant. Solubility of a molecule may be defined qualitatively as the spontaneous interaction of two or more substances to form a homogeneous molecular dispersion. It is found that ALVC-CDs inclusion complexes enhances the aqueous solubility of drug making it more bioavailable. Encapsulation of the hydrophobic part of the guest (ALVC) molecule into the hydrophobic cavity of suitable dimension of CDs makes it to increase aqueous solubility. The cavity dimension of the CDs should be moderate to reduce the contact between water and

the nonpolar regions of host and guest molecule. Among the CDs, α and β-cyclodextrins were used for the dimensional suitability of their cavity size.

As the organism – environment interaction is essential for its survival, on the molecular level small molecule like drug – protein/drug – gene product interaction is also essential that underlie the organism's ability to adapt to environmental changes and include those that bind, transport, and metabolize small molecules. Human serum albumin, the most abundant protein in blood plasma found to act as a carrier protein for vitamin, nutrients, hormone, steroid, drug like small molecule of low water solubility and binding ability of these molecules to HSA constitute a vibrant matter in pharmacokinetics.[59-61] Here, binding property of ALVC to the HSA had been studied spectrofluorimetrically. Thus, HSA assists the drug ALVC to release from the inclusion complexes and makes its transportation to the affective area where adsorption of the drug molecule to be needed. Our study to form inclusion complexes of ALVC thus become moralised by the solubility enhancement and HSA assisted transformation and controlled release of the drug in human body.

An analysis on the diverse molecular interactions of implausible food preservatives, Sodium benzoate (SBz), Sodium salicylate (Scyt) in the aqueous solutions of Benzyltriethylammoniun chloride (BTEACl), Benzyltrimethylammoniun chloride (BTMACl) having durable anti-bacterial effect have been explored thoroughly. According to our knowledge, it is well known to all, there is so much of food productions all over the world but because of the process of spoilage, a large proportion of these is lost. So, it requires a great attention to preserve foods, produced industrially and even at home. There are so many preservatives known, that utterly prevents spoilage of foods, but having some sort of side effects, usedness of these is an inherent threat to the world health. Now, use of these in minimal amount i.e. below the MIC (Minimal Inhibitory Concentration) in food would overcome the threat. The challenge was accepted and reveals that, two well-known food preservatives (FPs), sodium benzoate and sodium salicylate works properly against various fungus as well as gram-positive and gram-negative bacteria below their MIC in the presence of negligible amount of two ammonium based ionic liquids (ILs) benzyltriethylammoniun chloride (BTEACl) and benzyltrimethylammonium

chloride (BTMACl), as a consequence reduces the unnecessary consumption of hazardous food preservative.

I.2. Choice of Biologically Active Molecule, Host Molecules, Ionic Liquids, Food Preservatives and Solvents Used in the Research Work

Names of the Biologically Active Molecule, Host Molecules, Ionic Liquids, Food Preservatives and Solvent molecules are listed below

Biologically Active Molecule:

- Synephrine
- Phenylephrine hydrochloride
- Thiamine hydrochloride
- Alverine citrate
- 1,2,5,6,9,10-hexabromocyclododecane

Host Molecules:

- α-Cyclodextrin
- β-Cyclodextrin
- 18-Crown-6 ether

Ionic Liquids:

- Benzyltriethylammoniun chloride
- Benzyltrimethylammonium chloride

Food Preservatives:

- Sodium benzoate
- Sodium salicylate

Solvents:

- Water
- Dimethyl sulfoxide

I.3. Methods of Investigations Used in the Research Work

Names of the Investigation Methods are listed below:

- UV-vis spectroscopy
- Fluorescence spectroscopy
- Differential Scanning Calorimetry (DSC)
- Powder X-Ray Diffraction (PXRD)
- Scanning Electron Microscopy (SEM)
- FTIR spectroscopy
- ^{1}H NMR spectroscopy
- 2D ROESY
- Surface tension study
- Conductivity study
- Density study
- Viscosity study
- Refractive Index study
- Antimicrobial activity

CHAPTER II

REVIEW OF THE EARLIER WORKS AND THEORY OF INVESTIGATION

II.1. Review of the Earlier Works:

In supramolecular chemistry, host–guest chemistry describes complexes that are composed of two or more molecules or ions that are held together in unique structural relationships by forces other than those of full covalent bonds.[1,2] Host–guest chemistry encompasses the idea of molecular recognition and interactions through non-covalent bonding. Non-covalent bonding is critical in maintaining the 3D structure of large molecules, such as proteins and is involved in many biological processes in which large molecules bind specifically but transiently to one another. Although non-covalent interactions could be roughly divided into those with more electrostatic or dispersive contributions, there are few commonly mentioned types of non-covalent interaction, ionic bonding, hydrogen bonds, van der Waals forces - Keesom force (dipole - dipole) - Debye (dipole - induced dipole), hydrophobic interactions.

Important concepts advanced by supramolecular chemistry include molecular self-assembly, molecular folding, molecular recognition, host–guest chemistry, mechanically-interlocked molecular architectures, and dynamic covalent chemistry. The study of non-covalent interactions is crucial to understanding many biological processes that rely on these forces for structure and function. Biological systems are often the inspiration for supramolecular research. The "host" component can be considered the larger molecule, and it encompasses the smaller, "guest", molecule. In biological systems, the analogous terms of host and guest are commonly referred to as enzyme and substrate respectively.

In order to design synthetic systems that perform specific functions and tasks, it is very important to understand the thermodynamics of binding between host and guest. Chemists are focusing on the energy exchange of different binding interactions and trying to develop scientific experiments to quantify the fundamental origins of these non-covalent interactions by utilizing various techniques such as NMR spectroscopy, UV/visible spectroscopy and isothermal titration calorimetry,.[3] Quantitative analysis of binding constant values provides useful thermodynamic information. The

thermodynamic benefits of host–guest chemistry are derived from the idea that there is a lower overall Gibbs free energy due to the interaction between host and guest molecules. Chemists are exhaustively trying to measure the energy and thermodynamic properties of these non-covalent interactions found throughout supramolecular chemistry; and by doing so hope to gain further insight into the combinatorial outcome of these many, small, non-covalent forces that are used to generate an overall effect on the supramolecular structure. Thus, thermodynamics is an important tool to design, control, and study supramolecular chemistry. Perhaps the most striking example is that of warm-blooded biological systems, which entirely cease to operate outside a very narrow temperature range.

S. Giuffrida et al. described small and stable platinum nanoparticles can be easily obtained in one step through visible light irradiation of a host–guest inclusion complex between â-cyclodextrin and platinum acetylacetonate in a water solution. The exclusive control of the reaction by an external trigger, the removal of the undesired reaction products without any manipulation of the sample, and the absence of ionic repulsions between the metal nanoparticles represent the main remarkable advantages offered by this synthetic methodology.[4]

V. Crupi et al. presented Inclusion complexes of cyclodextrins with nonpolar drugs are a topic of current interest in pharmaceutical science, because they increase the aqueous solubility, chemical stability and bioavailability of poorly water-soluble drugs.[5]

Y. X. Sun et al. describes a facile and targeted gene delivery system was prepared by conjugating β-cyclodextrin modified polyethylenimine (PEI-CD) and adamantyl peptide (AdGRGDS) based on host–guest interaction. With the rational design between PEI-CD and AdGRGDS, the PEI-CD/AdGRGDS gene delivery system showed excellent DNA binding capability and exhibited good ability to compact DNA into uniform spherical nanoparticles.[6]

W. C. E. Schofield et al. presented β-cyclodextrin barrels can be tethered to solid surfaces using the Williamson ether synthesis reaction via an intermediate pulsed plasma deposited poly(4-vinylbenzyl chloride) linker layer. The loading and release of

perfume molecules through hostguest inclusion complex formation with surface tethered β-cyclodextrin.[7]

S. Goswami et al. describes the interaction of a painkiller Isoxicam, belonging to the oxicam group of nonsteroidal anti-inflammatory drugs (NSAIDs) and its copper complex with different cyclodextrins (β-CD, γ-CD, HPβCD, and HPγCD), has been investigated in both solution and the solid state.[8]

M. Gangopadhyay et al. describes that a newly synthesized triphenylamine derivative shows significant differences in inclusion complex formation with two different macrocyclic hosts, cucurbit[7]uril and β-cyclodextrin.[9]

D. Patra et al. presented a supramolecular approach to the fabrication of self-powered micropumps based on "host-guest" molecular recognition between R- and β-cyclodextrin and transazobenzene. Both hydrogels and surface coatings based on host-guest partners were used as scaffolds to devise the micropumps. These soft micropumps are dual stimuli-responsive and can be actuated either by light or by introducing guest molecules. Furthermore, the micropumps can be recharged through reversible hostguest interaction.[10]

Z. Du et al. describes about the controlled self-assembly of multiple-responsive SAP based on a selective host–guest inclusion of β-cyclodextrin with a modified poly(ethylene glycol) consisting of a ferrocene end group, a C_{11} alkyl chain, an azobenzene block, and a poly(ethylene glycol)methyl ether chain.[11]

M. Gupta et al. presented a supramolecular strategy to improve the fluorescence intensity of coumarin dye through its interaction with the relatively new host cucurbit[7]uril (CB[7]). The virtually nonfluorescent coumarin was converted into a highly fluorescent entity in water upon addition of the nonfluorescent host CB[7].[12]

II.2. Theory of Investigations:

II.2.1. Hydrophobic Interactions:

The tendency that leads nonpolar substances to undergo aggregation in an aqueous solution ignoring water molecules is termed as hydrophobic effect. Simply, it means "water-hating", and describes the segregation of water and nonpolar substances, which maximizes hydrogen bonding interaction between molecules of water, as a result water - nonpolar molecules contact area get reduced. Thermodynamically, the change in free energy of water molecules surrounding a solute is the hydrophobic effect. A positive free energy change of the surrounding solvent designates hydrophobicity, whereas a negative free energy change entails hydrophilicity.

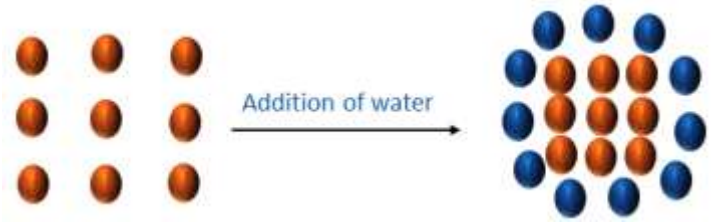

Figure 1: Hydrophobic interaction brings the interacting molecules closer

The hydrophobic effect controls various biological functions like, cell membrane and vesicle formation, insertion of membrane proteins into the nonpolar lipid environment, protein folding and protein-small molecule associations. Applying the concept of hydrophobicity sometimes, we can make two non-interacting molecules to undergo reactions by means of reducing the inter-molecular distance adding water to the system.

II.2.2. Van der Waals Forces:

According to van der Waals, van der Waals force is a distance-dependent interaction between atoms or molecules. These attractions are not like that of covalent bond resulting from a chemical electronic bond. The van der Waals force are relatively weak and quickly vanishes as the distances between interacting molecules gone large. The magnitude of van der Waals force depends on the surface area of the molecule and the magnitude of the force increases with increasing surface area.

Van der Waals force shows an ultimate part in fields as diverse as supramolecular chemistry, polymer science, structural biology, surface science and

nanotechnology. It also explains many properties of organic compounds and the formation of molecular solids, as well as the driving force that causes a solute molecule to undergo solvolysis in polar and non-polar media. The term van der Waals force is sometimes includes all intermolecular forces as well as the London dispersion force between instantaneously induced dipoles.

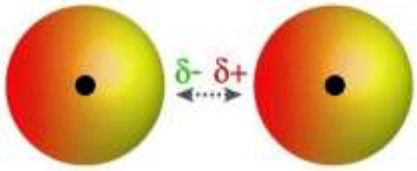

Figure 2: Van der Waals forces acting between molecules

The distance between atoms at which the force becomes repulsive rather than attractive as the atoms approach one another is termed as the van der Waals contact distance; the mutual repulsion between the atoms' electron clouds develops this phenomenon.

II.2.3. Hydrogen bonds:

A hydrogen bond is a partial intermolecular bonding interaction between a lone pair on an electron rich donor atom, particularly the elements nitrogen (N), oxygen (O) or fluorine (F) and hydrogen (H) atom.

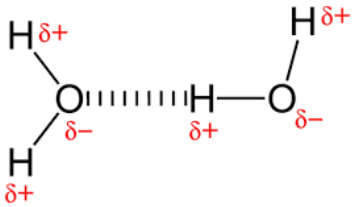

Figure 3: Hydrogen bonding in water molecules

There are two distinct types of Hydrogen bonds, intermolecular Hydrogen bond, bonding interaction between two separate molecule and intramolecular Hydrogen bond, bonding interaction between parts of same molecule. The bonding energy may vary from 1 to 40 kcal/mol and Depends on their geometry, the nature of the donor and acceptor atoms which constitute the bond and environment. This makes them to some extent stronger than a van der Waals interaction, but remains weaker than fully covalent or ionic bonds. This type of bond is found to occur in inorganic molecules such

as water and in organic molecules like DNA and proteins. Hydrogen bonding between the water molecules enhances the boiling point of water to 100 ^{0}c and makes difference in boiling point from other group 16 hydrides. Intramolecular hydrogen bonding is also responsible for the secondary and tertiary structures of proteins and nucleic acids. It also plays a vital role in the structure of polymers, both synthetic and natural.

II.2.4. Electrostatic Forces:

Electrostatic force governed from the Coulomb's law and it is defined as the as the amount of force between two stationary, electrically charged particles. The electrical force imparting between two charged bodies at rest is conventionally called electrostatic force or Coulomb force. Coulomb's law always describes the quantity of electrostatic force between stationary charges.

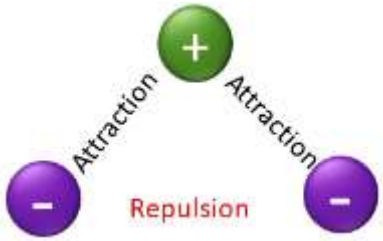

Figure 4: Electrostatic force working between charged species

The magnitude of the electrostatic force is directly proportional to the product of the magnitudes of charges and inversely proportional to the square of the distance between them and works along the direction of bond. The same charges repels each other whereas the opposite charges attracts each other.

II.2.5. Ion-Dipolar Attractions:

An electrostatic interaction between a charged ion and a dipolar molecule is termed as the ion-dipolar interaction. It is basically, an attractive force that is generally found to govern in solutions, exclusively ionic compounds when undergoes dissolution in polar liquids. A cation or an anion attracts the counter part of a polar molecule. Ion-dipole attractions become stronger with the increase in charge on the ion or as the magnitude of the dipole of the polar molecule increases. These interactions becomes very important issues in many chemical circumstances.

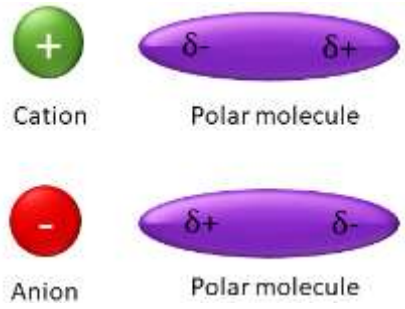

Figure 5: Ion–Dipolar attraction between the ion and polar molecules

II.2.6. Dipole-Dipole Attractions:

Dipole-dipole forces can be define as the attractive forces between the positive end of one polar molecule and the negative end of another polar molecule. Dipole-dipole forces have strengths that ranges from 5 kJ to 20 kJ per mole. Being weaker than ionic or covalent bonds in strength have a substantial effect only when the molecules involved are close together.

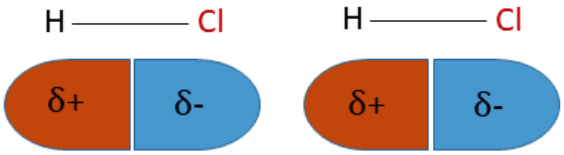

Figure 6: Dipole-Dipole attraction between the polar molecules

II.2.7. Solute-Solvent Interactions:

Chemistry of a solution is the study of a homogeneous mixture composed of two or more substances. The little quantity of substance that undergo dissolution to the another substance present in large quantity is termed as the solute and the substance presenting in large quantity determines the ultimate phase of the solution is known as the solvent. In the preparation of a solution, the solute-solvent interaction is one of the most accountable factors in solution chemistry. A profound solute-solvent interaction allows a solute, to undergo dissolution in a particular solvent molecule. Concentration of a solution is one of the important parameters, which is a measure of the amount of solute present in a given amount of solution or solvent. When the solvent is water then it is termed as the aqueous solution.

II.2.8. ^{1}H NMR Spectroscopy:

Among all of the spectroscopic techniques, Nuclear magnetic resonance spectroscopy, i.e. NMR spectroscopy is the most reliable method to characterize an organic molecule. It gives us information about the local magnetic environment around the atomic nuclei distinguishing number of total hydrogen atoms with magnetically different environment. Beside this, it also enriched us with the information that number of hydrogen atoms present in all the magnetically different environment.

The sample is placed in a magnetic field and the NMR signal is produced by excitation of the nuclei sample with radio waves into nuclear magnetic resonance, which is detected with sensitive radio receivers. The intramolecular magnetic field around an atom in a molecule changes the resonance frequency, thus giving access to details of the electronic structure of a molecule and its individual functional groups. As the fields are unique or highly characteristic to individual compounds, in modern organic chemistry practice, NMR spectroscopy is the definitive method to identify monomolecular organic compounds. Similarly, biochemists use NMR to identify proteins and other complex molecules. Besides identification, NMR spectroscopy provides detailed information about the structure, reaction state, dynamics and chemical environment of molecules. The most common types of NMR are proton and carbon-13 NMR spectroscopy, but it is applicable to the sample that contains nuclei possessing spin.

Long timescale of NMR does not allows for observing fast phenomena, therefore produces an averaged spectrum. Samples having a large extent of impurities unable show on an NMR spectrum. So, higher external magnetic field strength may be used for higher sensitivity.

Integrals and integration

With the help of software we can analyse peak intensity and the number of protons of different types. Integrating the peak area, we can easily measure the signal intensity and hence the number of hydrogen atoms presents in that area i.e. the number of protons is only proportional to the intensity or the integral, of the NMR signal in the very simplest NMR experiments. In case of carbon-13 NMR spectra, the integral of the signals also depends on the scalar and dipolar coupling constants and the relaxation

rate of the nucleus. But, lack of information about that, difficulties remains to have integrals of complicated systems.

Chemical Shift

Depending upon the nature of magnetic environments, protons with different magnetic environments registers their signals at different positions in ^{1}H NMR spectrum. Although strength of the external magnetic field may alter the position of the signals in the spectrum. A reference signal is usually used to report a NMR signal, usually that of TMS (tetramethylsilane). Electron density around a nucleus also generate a local magnetic field and as opposition to the external magnetic field shielding the nucleus from the external magnetic field. Then it undergoes upfield shifting in the ^{1}H NMR spectrum. Now, an electronegative atom nearby to proton atoms withdraws electron density from the proton and experiences the external magnetic field more resulting downfield shift of that proton in the ^{1}H NMR spectrum. The chemical shifts for heavier nuclei are strongly influenced by other factors including excited states.

In this research work, the interacting protons from both the host and guest molecules undergo shifting while the formation of inclusion complexes, suggesting diamagnetic or paramagnetic shielding host and guest protons.

II.2.9. 2D ROESY:

When two protons originating from same or different molecules somehow come closer in 0.4 nm range through space even if they are non-bonded will show a correlation through space registering an off diagonal cross peak in 2D ROESY spectrum. Thus, it provides vital information about the special proximity between two molecules through space. It can also detect chemical and conformational exchange. A ROESY spectrum exhibits a diagonal and cross peaks signals. The diagonals consist of the 1D spectrum. The cross peaks obtained owing to the presence of protons those are close to each other. So, 2D ROESY spectroscopy provides vital confirmation about the spatial closeness of the interacting atoms of the host and the guest by observing the intermolecular dipolar cross-correlations.

Consistent with the structure of α and β-CD, inclusion complexation inside into cyclodextrin cavity can be shown by the appearance of NOE cross-peaks between the protons of cyclodextrin and the protons of the aromatic guest identifying their spatial

proximity. To prove this, 2D ROESY spectra of the inclusion complexes with α and β-CD in D2O, were recorded, which shows significant correlation of aromatic protons of guest molecule with the H_3 and H_5 protons of α and β-CD, establishing the aromatic ring was encapsulated inside both the cyclodextrin cavities.

II.2.10. FTIR Spectroscopy:

Infrared (IR) spectroscopy, however, provides a direct way of observing these functional groups because it detects the stretching and bending of bonds rather than any property of the atoms themselves. It is particularly good at detecting the stretching of unsymmetrical bonds of the kind found in functional groups such as OH, C=O, NH_2, NO_2 etc. and for this reason IR spectroscopy complements NMR beautifully as a method for structural analysis.

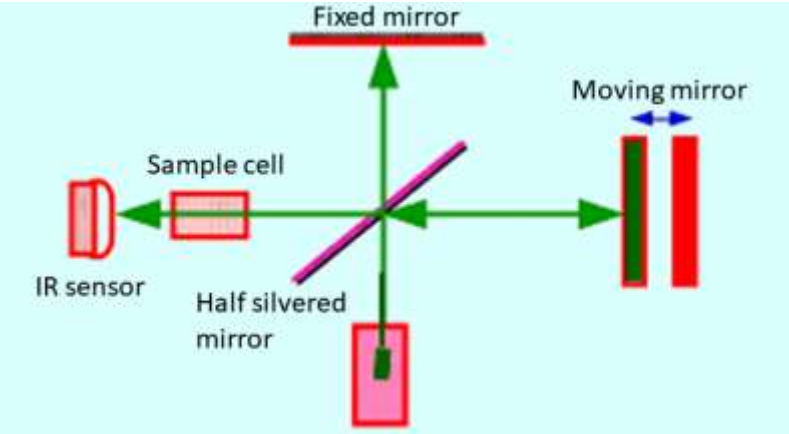

Figure 7: Diagrammatic representation of working principle of FTIR

The bonds between the two atoms are considered as a spring, which undergoes vibration like a simple harmonic oscillator. The frequency of vibration depends on the strength of the bond (force constant K) and the masses of the atoms, m_1, m_2 which are held together by the bond. According to the Hook's law frequency of vibration can be expressed as follows-

$$\bar{\nu} = \frac{1}{2\pi c}\sqrt{\frac{K}{\mu}} \qquad \text{(II.1)}$$

Where, μ is the reduced mass of the molecular system and can be expressed as follows-

$$\mu = \frac{m_1 m_2}{m_1 + m_2} \qquad \text{(II.2)}$$

The force constant K signifies the bond strength.

Preparation of Samples:

We recorded all the FTIR spectra in the solid state by preparing a palette of a minute quantity of sample mixing with a large quantity of dried KBr.

Elucidation of the Infrared spectroscopic data of the ICs as well as the pure Host and Guest molecules also reveals the veracity about the way by which the ICs are formed and supports the circumstances of host – guest interaction.

II.2.11. UV-Visible Spectroscopy:

Molecules containing various electronic energy levels can undergo transition from the lower energy state to the higher energy level showing a broad peak in the UV-Visible spectrum. Different energy levels, in terms of bonding and non-bonding electrons can absorb energy in the form of ultraviolet or visible light to excite these electrons to higher anti-bonding molecular orbitals. Lower the energy gap between the HOMO and the LUMO more easily the molecule get excited in the longer the wavelength of light. The possible four types of transitions are π–π*, n–π*, σ–σ* having the order of energy gap σ–σ* > n–σ* > π–π* > n–π*

According to the Lambert-Beers law, UV-Visible spectrometer shows absorbance of a sample and records the spectrum.

$A = \log(I_0/I) = \varepsilon c l$, for a given wavelength

A = Absorbance

I_0 = Intensity of incident light

I = Intensity of the light leaving sample

ε = Molar absorptivity

c = Molar concentration of solution containing sample

l = Length of cuvette containing sample

In this thesis, the UV-Visible spectroscopic data were fitted to the Benesi-Hildebrand equation for the calculation of the binding constants of the inclusion complexes formed by the cyclodextrin host with various guest molecules. The stoichiometries of the inclusion complexes were also determined with the data obtainable from the UV-Visible spectroscopy.

II.2.12. Fluorescence Spectroscopy:

Fluorescence spectra is an emission spectra originating by the transition from the higher energy levels to the lower energy level. Molecules having different electronic energy levels simultaneously have vibrational energy levels and can show fluorescence spectra. In fluorescence, a photon first excited the species from its ground electronic state to one of the various vibrational states in the excited electronic state. The excited molecule then undergoes deactivation through collisions with other molecules. it causes the excited molecule to lose vibrational energy until it reaches the lowest vibrational state from the excited electronic state according to the Jablonski diagram. Finally, the molecules drops down to one of the various vibrational levels of the ground electronic state again as a result photons gets emitted the process showing fluorescence. Since the vibrational energy levels of the ground electronic state have different energies, the energies of the emitted photons will have different energies by which we can determine the structure of the different vibrational levels.

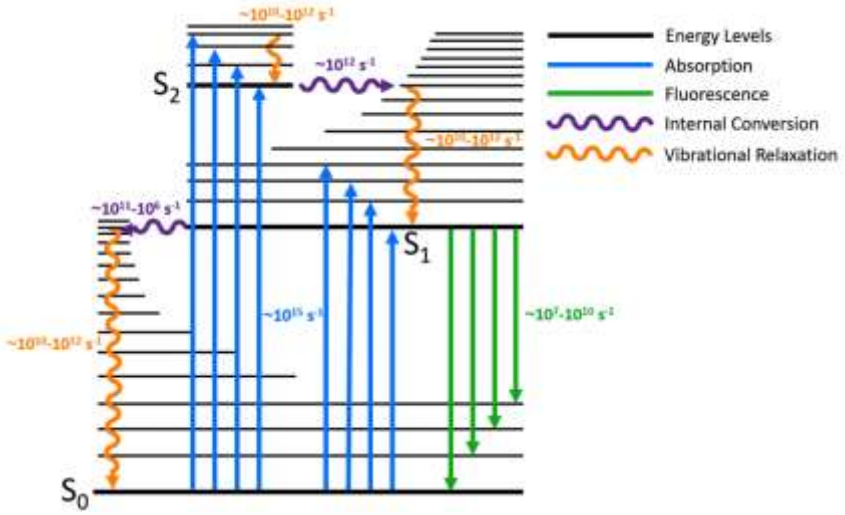

Figure 8: Jablonski Diagram

Fluorescence Spectroscopic measurement was employed for the further verification of the association constants obtained from the UV-Visible spectroscopic measurements.

Data obtained here with were fed to the modified Benesi-Hildebrand as well as the Stern-Volmer equation for the determination of association constants of the inclusion complexes and the guest – HSA binding interactions.

II.2.13. Differential Scanning Calorimetry (DSC):

DSC is a significant instrument by which we can analyse the heat change in a sample with the variation of temperature. Sometimes it helps us to observe the presence of impurities or change in crystal structure by studying the change in melting point registering a peak other than the melting temperature in the DSC thermograms. Various thermodynamic parameter can also obtained from this saying about the thermal stability of the sample under experiment.

There are two types of DSC, Heat Flux Type and Power Compensation Type. Heat Flux DSC includes the sample and reference holder, the heat sink, the heat resistor and the heater. The heater is supplies heat to the sample and the reference through heat sink and heat resistor. There is a proportional relationship between heat flow the heat difference of heat sink and holders. Heat sink has the greater heat capacity than the sample. Heat sink compensate the endothermic or exothermic phenomena of sample. It helps to keep constant temperature difference between the sample and the reference. The difference the amount of heat supplied to the sample and the reference is proportional to the temperature difference of both holders. Calibration of the standard material, allows measuring unknown sample quantitatively.

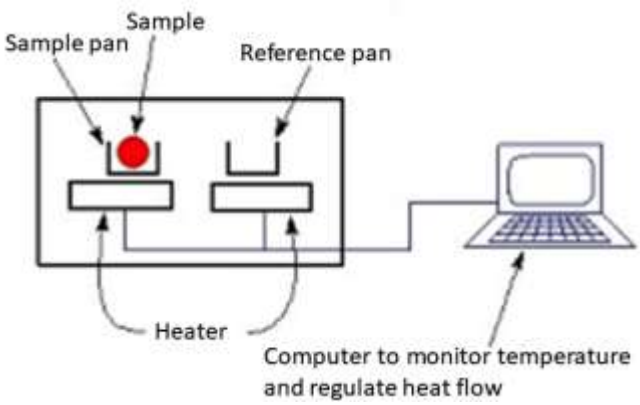

Figure 9: Diagrammatic representation of working principle of DSC

In this thesis, we gather both the qualitative and quantitative insight about the physicochemical state of the drug while encapsulated into the cavity of CDs. Generally,

the shifting of an endothermic peak to a different temperature or absence of an endothermic peak for the pure guest molecule in the inclusion complexes are found in DSC thermograms which indicates a change in melting point, crystal lattice or sublimation point due to inclusion complexation.

II.2.14. Powder X-Ray Diffraction (PXRD):

PXRD is a quick analytical method mostly used for phase identification of a crystalline material and can provide information on unit cell dimensions. The material which, is analysed, be finely ground, homogenized and average bulk composition is determined.

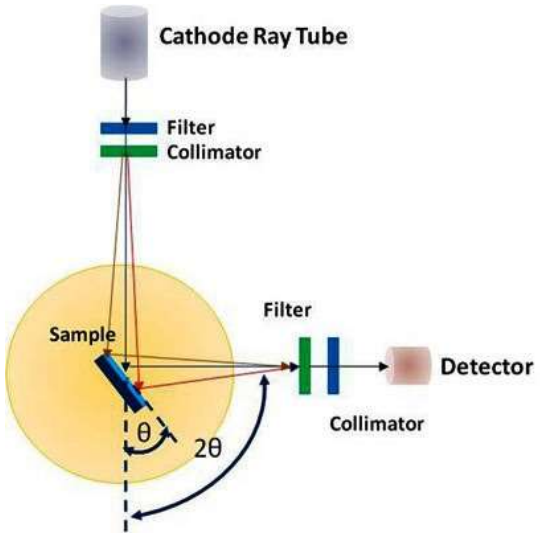

Figure 10: Diagrammatic representation of working principle of PXRD

It was revealed that, crystalline materials functions as three-dimensional diffraction grating for X- ray and the spacing of planes in crystal lattice comparable to wavelength of X-Ray. XRD is now a general practice for the determination of atomic spacing and crystal structures. Diffractions arise whilst light is scattered by a periodic array with long-range order, producing constructive interference at specific angle. The wavelengths of X-ray are related to the distance between two atoms; monitoring this principle crystalline character of a substance can be explained. The interactions of the incident rays with the sample makes constructive interference whilst satisfy the condition of the Bragg's Law-

$$n\lambda = 2d\sin\theta \qquad \text{(II.3)}$$

Where, n = Order of diffraction, d = inter-planar spacing, Θ = Glancing angle, λ = Wavelength of X-Ray used.

X-rays produced from the X-ray tube have been directed at the sample and diffracted X-rays are then recognized, processed and counted. Data were recorded throughout a range of 2θ angles.

II.2.15. Scanning Electron Microscopy (SEM):

In the Scanning Electron Microscope (SEM) a focused beam of high-energy electrons is used to produce a high-energy resolution image of the sample. After getting accelerated primary electrons hit the sample forming secondary electrons (SE).

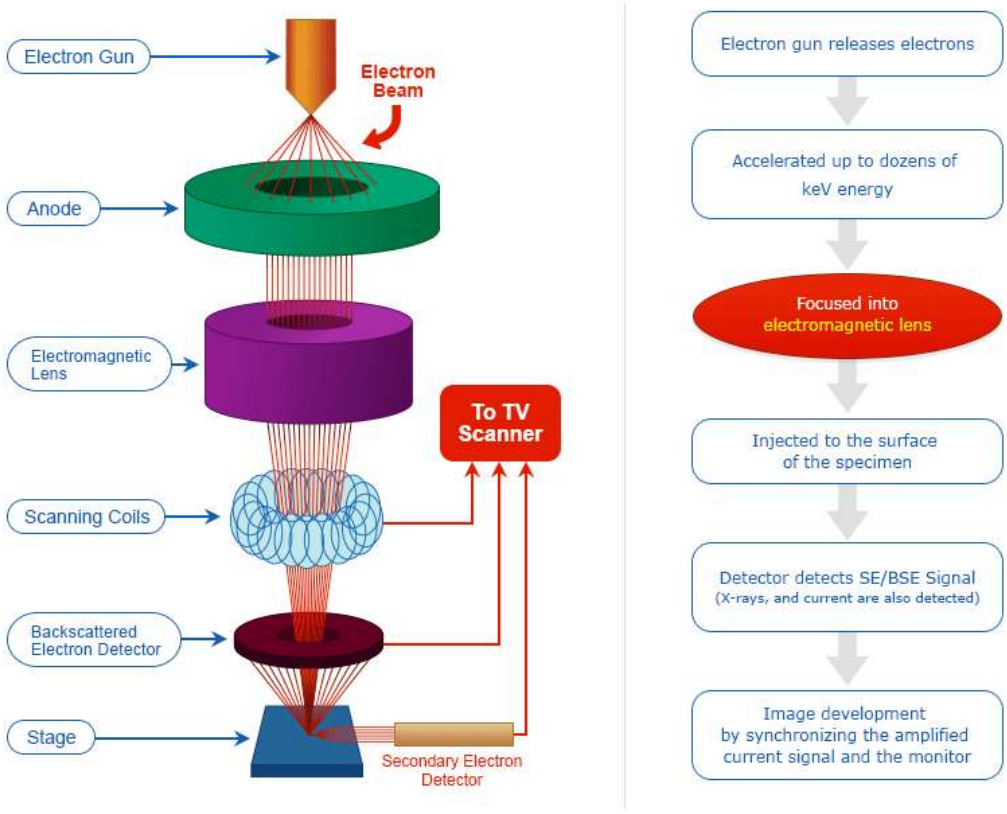

Figure 11: Diagrammatic representation of working principle of SEM

A positively charged electron detector composes these secondary electrons, which in turns provide 3D image of the sample. The signals developing from electron-sample interactions make known information concerning the sample along with the external morphology, crystalline structure, chemical composition and orientations of substances making up the sample. SEM scanning can image areas ranging from about 1cm to 5 microns width. The SEM is also able to perform analyses of chosen point of locations on the sample.

II.2.16. Mass Spectrometry:

Mass spectrometry, the most accurate analytical method, is used in different fields to establish the elemental composition. Here, molecules are bombarded with a beam of energised electrons to split and ionize the fragments. Specific kind of ions has a definite mass to charge ratio (i.e. m/z ratio). The m/z ratio is equal to the molecular mass for most of the ions as the ions mostly contain single charge. A parent ion or a molecular ion is formed when single electron is removed from the molecule.

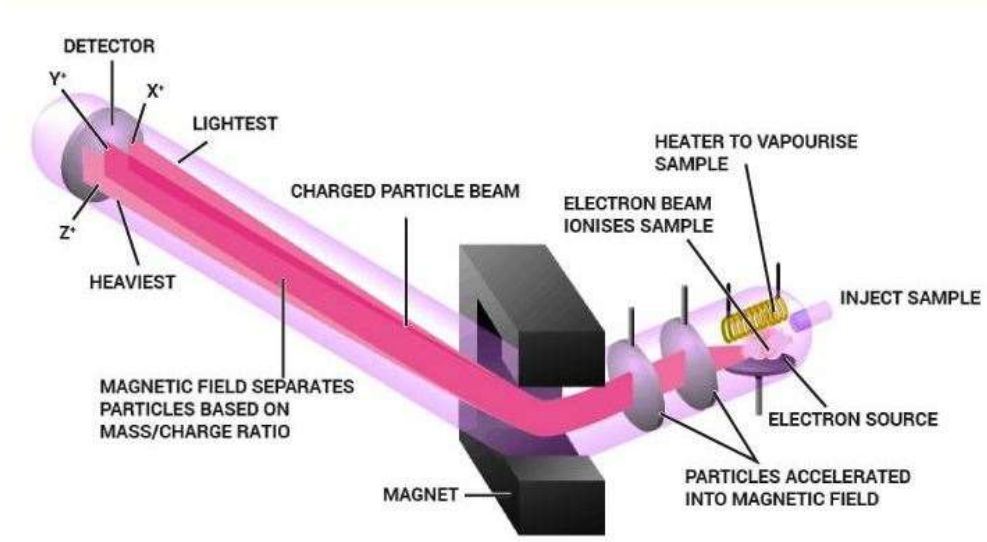

Figure 12: Diagrammatic representation of working principle of HRMS

$$M + e^- \text{ ----------> } M^+ + 2e^-$$

In case of the parent ion the m/z value is the molecular mass of the compound. Sometimes, the parent ion peak becomes the base peak that can be easily recognized but in most of the cases, molecular ion peak does not appear as base and is often of insignificant abundance. In the process of inclusion complexation there is no bond formation or breaking and hence the m/z ratio of inclusion complex should be equal to the sum of the masses of host and the guest molecules or it may add with proton or certain impurities such as sodium. Thus From the mass spectrometric analysis formation of the inclusion complex can be confirmed. The stoichiometry of inclusion complex can also be discussed.

II.2.17. Density measurements:

The volumetric information includes 'Density' as a function of weight, volume and mole fraction and excess volumes of mixing. It is a well-recognized method to the analyse molecular interactions in fluids. Depending upon the nature of solvent molar volume of the solute molecules changes. So, calculating apparent molar volume of a solution system, we can track about the nature of interaction taking place between solute and solvent in solution. The volumetric information may have immense importance in this regard.

Apparent molar volumes

Apparent molar volume of a substance in solution can be defined as the sum of the geometric volume of the two solute molecules while undergo solvation through solute-solvent interaction with the co-solvent. Density data can be used for the calculation of molar volume of a pure substance. However, the volume contributed to a solvent by the addition of one mole of an ion is difficult to determine. This is so because, upon entry into the solvent, the ions change the volume of the solution due to a breakup of the solvent structure near the ions and the compression of the solvent under the influence of the ion's electric field, i.e., electrostriction. Electrostriction takes place when there are electric fields of the order of 109-1010 V m^{-1}, the compression of ions and molecules is likely to be significant. The effective volume of an ion in solution, the partial molar volume, can be determined from a directly obtainable quantity- apparent molar volume (ϕ_v). The apparent molar volumes, (ϕ_v), of the solutes can be calculated by using the following relation.

$$\phi_v = \frac{M}{\rho} - \frac{1000(\rho - \rho_0)}{m\rho\rho_0} \qquad \text{(II.4)}$$

Where, M is the molar mass of the solute; m is the molality of the solution; ρ and ρ0 represents the densities of the solution and solvent respectively.

Limiting apparent molar volumes

Apparent molar volume at infinite dilution is termed as the limiting molar apparent volume (ϕ_v^0). Least squares fitting of linear plots of (ϕ_v) against the square root of

molar concentrations ($m^{1/2}$) using the Masson equation gives the values of limiting molar apparent volume (ϕ_v^0) and experimental slopes (S_v^*).

$$\phi_v = \phi_v^0 + S_v^*.\sqrt{m} \qquad \text{(II.5)}$$

Generally, the values of limiting molar apparent volume (ϕ_v^0) are always positive in all the cases and signifies the solute-solvent interaction taking place in the solution. On the other hand experimental slopes (S_v^*) suggests the solute-solute interaction in solution. Greatness the values between limiting molar apparent volume (ϕ_v^0) and experimental slopes (S_v^*) suggests the respective interaction in the solution as the profound interaction.

In this research work, I have found that, values of the experimental slope, (S_v^*) assigning the extent of ion-ion interaction in the solution has negative values indicating the presence of less ion-ion interaction in the medium. Quantitative comparison shows, greater the magnitude of (ϕ_v^0) than (S_v^*) recommends the ion-solvent interactions dominants over ion-ion interactions.

Structure making/structure breaking interaction

The solute – solvent interaction studied so far may be of two types, structure breaking or synergistic structure making interaction. The way developed by Hepler is helpful to analyse the nature of the solute – solvent interaction taking place in the solution phase.

In this connection, the limiting apparent molar volumes of solutions were calculated and the data obtained were fitted with the following polynomial equation-

$$\phi_v^0 = a_o + a_1 T + a_2 T^2 \qquad \text{(II.6)}$$

Where, a_0, a_1 and a_2 are the empirical coefficients depending on the nature of solute, mass fraction (W) of co-solvent. T represents temperature in Kelvin scale.

First derivative of equation ( ) gives the values of limiting apparent molar expansibilities (ϕ_E^0) which have been calculated for various temperatures.

$$\phi_E^0 = (\delta\phi_v^0/\delta T)_P = a_1 + 2a_2T \qquad \text{(II.7)}$$

Positive values of limiting apparent molar expansibilities (ϕ_E^0) suggests the absence of caging or packing effect in the solutions.

According to Hepler, values of $(\delta\phi_E^0/\delta T)_P$ in the expression given below, determines whether, it is structure breaker or structure maker interaction

$$(\delta\phi_E^0/\delta T)_P = (\delta^2\phi_v^0/\delta T^2)_P = 2a_2 \qquad \text{(II.8)}$$

Generally, positive or small negative values of strongly suggests structure making rather than structure breaking interaction. In this research work, I got structure making type of interaction in all the cases.

II.2.18. Refractive Index Measurements:

Optical data (refractive index) of electrolyte mixtures provide interesting information related to molecular interactions and structure of the solutions, as well as complementary data on practical procedures, such as concentration measurement or estimation of other properties.

Index of Refraction (n_D) for a substance is defined as the ratio of the speed of light in a vacuum to the speed of light in another medium.

$$\text{Refractive Index } (\text{n}_\text{D}) \text{ of substance } = \frac{\text{Speed of light in vacuum}}{\text{Speed of light in substance}}$$

Light changes its speed when it crosses a boundary from one medium into another, its path of travel also changes that is refraction occurred. The relationship between speed of light in the two mediums (V_A and V_B), the angles of incidence ($\sin\theta_A$), refraction ($\sin\theta_B$) and the refractive indexes of the two mediums (n_A and n_B) is shown below-

$$\frac{V_A}{V_B} = \frac{\sin\theta_A}{\sin\theta_B} = \frac{n_B}{n_A} \qquad \text{(II.9)}$$

Refractive index can be determined without measuring the speed of light of a sample. It is possible to establish the refractive index of the sample moderately accurately as a substitute, by measuring the angle of refraction, and knowing the index of refraction of the layer, which is in get in touch with the sample.

The refractive index of mixing can be correlated by the application of a composition-dependent polynomial equation. Molar refractivity, was obtained from the Lorentz- Lorenz relation by using n_D, experimental data according to the following expression-

$$R_M = \frac{(n_D^2 - 1)}{(n_D^2 + 2)}\left(\frac{M}{\rho}\right) \qquad \text{(II.10)}$$

Where, R_M, n_D, M and ρ represents molar refraction, refractive index, molar mass and density of solution respectively.

The limiting molar refraction, ( ) listed in Table S can be calculated using the following equation-

$$R_M = R_M^0 + R_S\sqrt{m} \qquad \text{(II.11)}$$

Where, 'm' is the molality of solution and is the limiting molar refraction that signifies solute – solvent interaction. Therefore, this measurement operates as an expensive tool for studying the molecular interaction in solution.

II.2.19. Viscosity measurement:

The viscosity relationships of electrolytic solutions are multifarious. Because ion-ion and ion-solvent interactions are occurring in the solution and separation of the related forces is a difficult task. But, from careful analysis, vivid and valid conclusions can be drawn regarding the structure and the nature of the solvation of the particular system. As viscosity is a measure of the friction between adjacent, relatively moving parallel planes of the liquid, anything that increases or decreases the interaction between the planes will raise or lower the friction resulting increase or decrease the viscosity. Therefore, monitoring the viscosities of the solution, simultaneously we deals with various interactions between solute and solvents taking place in solution.

Viscosity A- and B- coefficients

If a large sphere is placed in the liquid, the planes will be keyed together in increasing the viscosity. Similarly, increase in the average degree of hydrogen bonding between the planes will increase the friction between the planes, thereby viscosity. An ion with a large rigid co-sphere for a structure-promoting ion will behave as a rigid sphere placed in the liquid and increase the inter-planar friction. Similarly, an ion increasing the degree of hydrogen bonding or the degree of correlation among the adjacent solvent molecules will increase the viscosity. Conversely, ions destroying correlation would decrease the viscosity. In 1905, Grüneisen performed the first systematic measurement of viscosities of a number of electrolytic solutions over a wide range of concentrations. He noted non-linearity and negative curvature in the viscosity concentration curves irrespective of low or high concentrations. In 1929, Jones and Dole suggested an empirical equation quantitatively correlating the relative viscosities of the electrolytes with molar concentrations (c)-

$$\frac{\eta}{\eta_o} = \eta_r = 1 + A\sqrt{c} + Bc \qquad \text{(II.12)}$$

The above equation can be rearranged as-

$$\frac{\eta_r - 1}{\sqrt{c}} = A + B\sqrt{c} \qquad \text{(II.13)}$$

Where, A and B are constants specific to ion-ion and ion-solvent interactions. The equation is applicable equally to aqueous and non-aqueous solvent systems where there is no ionic association and has been used extensively. The term A√c, originally ascribed to Grüneisen effect, arose from the long-range columbic forces between the ions. The significance of the term had since then been realized due to the development Debye-Hückel theory of inter-ionic attractions in 1923. The A -coefficient depends on the ion-ion interactions, can be calculated from interionic attraction theory and is given by the Falkenhagen Vernon equation-

$$A_{Theo} = \frac{0.2577\Lambda_o}{\eta_o(\varepsilon T)^{0.5}\lambda_+^o\lambda_-^o}\left[1 - 0.6863\left(\frac{\lambda_+^o\lambda_-^o}{\Lambda_o}\right)^2\right] \qquad \text{(II.14)}$$

Where, the symbols have their usual significance.

The plots of $(\eta/\eta_0 -1)/\sqrt{c}$ against $\sqrt{c}$ for the electrolytes should give the value of A- and B-coefficient. But, sometimes, the values come out to be negative or considerably scatter and also deviation from linearity occur. Thus, instead of determining A - coefficient from the plots or by the least square method, the A - coefficient are generally calculated using Falkenhagen-Vernon equation. A-coefficient should be zero for non-electrolytes. According to Jones and Dole, the A - coefficient probably represents the stiffening effect on the solution of the electric forces between the ions, which tend to maintain a space-lattice structure.

The viscosity B - coefficient may be either positive or negative, that represents the ion-solvent interaction parameter. The B – coefficients are obtained as slopes of the straight lines using the least square method and intercepts equal to the A values.

The factors influencing viscosity B - coefficients

(1) The effect of ionic solvation and the action of the field of the ion in producing long-range order in solvent molecules, increases η or B - value.

(2) The destruction of the three-dimensional structure of solvent molecules (i.e., structure breaking effect decreases η values.

(3) High molal volume and low dielectric constant, which yield high B-values for similar solvents.

(4) Reduced B-values are obtained when the primary solution of ions is sterically hindered in high molal volume solvents or if either ion of a binary electrolyte cannot be specifically solvated.

Temperature dependence of viscosity B-coefficient

Regularity in the behaviour of B and dB/dT, has been observed in both aqueous and non-aqueous solvents and useful generalizations have been made by Kaminsky. He observed that (i) within a group of the periodic table the B -ion values decrease as the crystal ionic radii increase, (ii) within a group of periodic system, the temperature co-

efficient of B_{Ion} values increase as the ionic radius. The results can be summarized as follows-

(i) A and dA /dT >0

(ii) $B_{Ion} < 0$ and $dB_{Ion} / dT > 0$, characteristic of the structure breaking ions.

(iii) $B_{Ion} > 0$ and $dB_{Ion} / dT < 0$, characteristic of the structure making ions.

First derivative of viscosity B-coefficient over temperature is an upgradation of viscosity B coefficient in predicting the nature of solute – solvent interaction as structure maker or structure breaker. The value of dB/dT is a measure of activation energy required for the viscous flow in solution. This is the reason, why the measure of dB/dT is indicative towards the structure making or structure breaking ability than sign or magnitude of the B-coefficient. The negative small positive value of dB/dT signifies structure-making (kosmotropic) whereas the larger positive value identifies it as structure-breaking (chaotropic).

II.2.20. Conductivity measurement:

Conductivity (or specific conductance) of an electrolyte solution is a measure of its ability to conduct electricity. The SI unit of conductivity is Siemens per meter (S/m). Conductivity measurements are used routinely in many industrial and environmental applications as a fast, inexpensive and reliable way of measuring the ionic content in a solution. For example, the measurement of product conductivity is a typical way to monitor and continuously trend the performance of water purification systems.

Conductimetric study is also another approach, which makes us able to conclude about the supramolecular Host-guest interaction between the guest and CDs and their stoichiometric ratio in the ICs. However, guest molecules studied in regarding this thesis are organic compound, aqueous solution of guest molecules shows appreciable conductivity. Gradual increase in concentration of CDs leads to the decrease in conductivity (κ), of the aqueous guest solutions. The fruit full explanation for this observation comes through the decrease in the mobility of the conducting species in the solution due to molecular encapsulation of guest into the hydrophobic

cavity of the CDs. After a certain point there is no change in conductivity was observed generating a single break point behind that supports the 1:1 stoichiometries of the inclusion complexes.

II.2.21. Surface Tension measurement:

The attractive force exerted upon the surface molecules of a liquid by the molecules beneath that tends to draw the surface molecules into the bulk of the liquid and makes the liquid assume the shape having the least surface area.

The guest molecules used in this research work, having a hydrophobic part, aqueous solutions of the guest molecules shows an appreciable surface activity lowering the surface tension value less than pure water. On the addition of aqueous cyclodextrin solution surface tension of the solution rises, this is due to the migration of the guest molecules from the surface to the bulk of the solution by means of encapsulation of the guest molecules into the cavity of cyclodextrin. After reaching a certain concentration of cyclodextrin, no change in surface tension was observed showing a single break point in the surface tension vs concentration of cyclodextrin plot, suggesting the 1:1 stoichiometry of the inclusion complexes. Thus, the study of surface tension supports the inclusion phenomenon and the stoichiometry of the inclusion complexes.

CHAPTER III

EXPERIMENTAL SECTION

III.1. NAME, STRUCTURE, PHYSICAL AND CHEMICAL PROPERTIES, PURIFICATION AND APPLICATIONS OF THE CHEMICALS USED IN THE RESEARCH WORK

III.1.1. Biologically active molecules:

Synephrine: Alkaloid synephrine, occurring naturally in some animals, plants and in approved drugs products. Its m-substituted derivative is known as neo-synephrine. m-synephrine and p-Synephrine are known for their longer acting adrenergic effects compared to norepinephrine. This substance is found to various foodstuff at low concentration.[1,2]

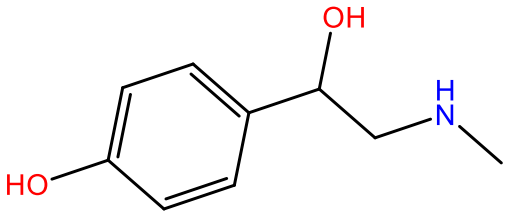

Synephrine

CAS Number	94-07-5
Chemical Formula	$C_9H_{13}NO_2$
Molar mass	167.21 g/mol
Appearance	Colourless solid
Melting Point	187 °C
Solubility in water	soluble

Source: Sigma Aldrich, Germany

Purification: Used as purchased. The purity of the chemical is ≥ 98%

Application: A number of studies of the effects of synephrine in humans, most of them focusing on its cardiovascular properties, have been performed since its introduction as a synthetic drug around 1930. Stockton and co-workers describes the effects of racemic synephrine in humans. Thus, it was shown by these investigators that intramuscular injections (average effective dose = 200 mg) of the drug produced an increase in systolic blood pressure and pulse rate, without affecting the diastolic pressure. However, the topical application of 1–3% solutions of the drug to the nasal mucosa of patients with sinusitis did produce a beneficial constriction without local irritation.

Phenylephrine hydrochloride: Phenylephrine is a medication primarily used as a decongestant, to dilate the pupil, to increase blood pressure, and to relieve haemorrhoids. However, it is used as a decongestant also recommended for hay fever. It can be taken by orally, by injection into muscle or applied to the skin.[3]

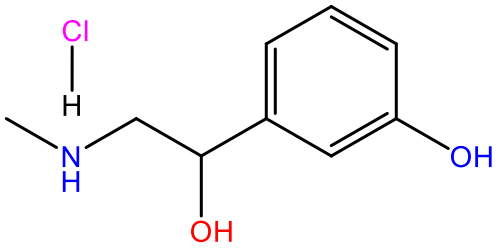

Phenylephrine hydrochloride

CAS Number	61-76-7
Chemical Formula	$C_9H_{13}NO_2.HCl$
Molar mass	203.67 g·mol^{-1}
Appearance	Solid powder
Melting Point	144 to 147°C
Solubility in water	soluble

Source: Sigma Aldrich, Germany

Purification: Used as purchased. The purity of the chemical is 98.0%

Application: Phenylephrine is used as a nasal spray. In the United States, it is recommended as ingredient over-the-counter decongestants. Other decongestants

include oxymetazoline and pseudoephedrine. Phenylephrine is an alternate option for pseudoephedrine in decongestant medicines. But, it is not as much efficient as placebo for relieving sinus congestion.

Thiamine hydrochloride (Vitamin B_1): Thiamine Hydrochloride is a vitamin essential for cell growth, aerobic metabolism and acetylcholine synthesis. Upon hydrolysis, it gives active thiamine pyrophosphate (TPP). TPP is a coenzyme that controls enzymatic activities involving amino acid, fatty acid and carbohydrate metabolism.[4]

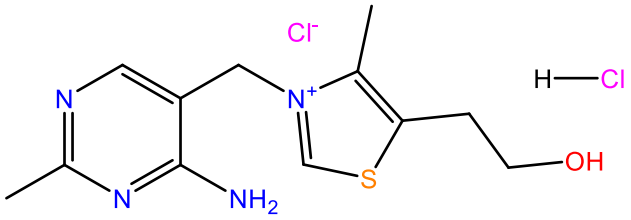

Thiamine hydrochloride (Vitamin B_1)

CAS Number	67-03-8
Chemical Formula	$C_{12}H_{17}ClN_4OS{\cdot}HCl$
Molar mass	$337.27 g{\cdot}mol^{-1}$
Appearance	Solid powder
Melting Point	164°C
Solubility in water	soluble

Source: Sigma Aldrich, Germany

Purification: Used as purchased without further purification. The purity of the chemical is > 99.0%

Application: Thiamine (vitamin B_1) is used to prevent or treat low levels of vitamin B_1 in people who do not get enough of the vitamin from their diets. Most people taking normal diet do not need to have extra vitamin B_1. However, alcoholism causes low levels of vitamin B_1. It maintains the health of the nerves and the heart. Deficiency of vitamin B_1 may cause nerve problems.

Alverine citrate: Alverine citrate is the citrate salt of alverine, resulting from the reaction of equimolar amounts of alvarine and citric acid. It acts directly on intestinal and uterine smooth muscle, treating irritable bowel syndrome. It also plays a role as a cholinergic antagonist drug. It is a citrate salt and an organo-ammonium salt.[5]

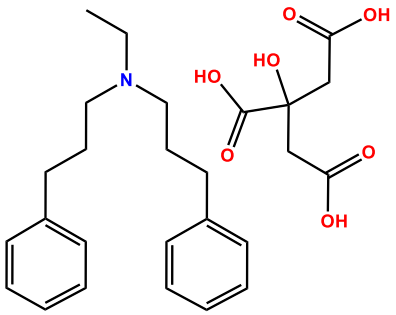

Alverine citrate

CAS Number	5560-59-8
Chemical Formula	$C_{20}H_{27}N{\cdot}C_6H_8O_7$
Molar mass	473.56 $g{\cdot}mol^{-1}$
Appearance	Solid powder
Melting Point	100 to 102°C
Solubility in water	soluble

Source: Sigma Aldrich, Germany

Purification: Used as purchased. The purity of the chemical is > 99.0%

Application: Alverine acts directly on the muscle in the gut, causing it to relax. This helps us to get rid of the muscle spasms, which occur in the gut in conditions such as diverticular disease and irritable bowel syndrome. Diverticular disease cause the formation of small pouches in the gut lining. Foods undergo trapping into these pouches and become inflamed and painful. The muscle spasms result in symptoms such as abdominal pain and bloating, constipation or diarrhoea. Alverine citrate relaxes the gut muscles, smooth muscle in the womb and relieves the pain. Therefore, it also treats painful menstruation, causing by muscle spasms in the uterus.

III.1.2. Water pollutant molecule:

1,2,5,6,9,10-Hexabromocyclododecane (HBCDD): HBCDD, the water pollutant, being present in biological samples undergoes long-range environmental transportation. So, it is classified as Persistent, Bio accumulative and Toxic (PBT). All the 16 possible stereoisomers of HBCDD has different biological activities. HBCDD generally, found to contain three main diastereomers namely alpha (α-HBCDD), beta (β- HBCDD) and gamma (γ- HBCDD) with traces of others.[6,7]

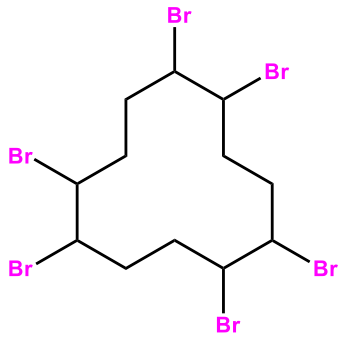

1,2,5,6,9,10-Hexabromocyclododecane

CAS Number	3194-55-6
Chemical Formula	$C_{12}H_{18}Br_6$
Molar mass	641.70 g·mol^{-1}
Appearance	Solid powder
Melting Point	186°C
Solubility in water	3.4 µg/L

Source: Sigma Aldrich, Germany

Purification: Used as purchased. The purity of the chemical is > 99.0%

Application: Hexabromocyclododecane (HBCD or HBCDD) is a brominated flame retardant. Its major application is in expanded (EPS) and extruded (XPS) polystyrene foam. Other uses are, automobile interior textiles, upholstered furniture and insulation blocks in packaging material, trucks, videocassette recorder, housing and electronic equipment.

III.1.3. Cyclodextrins:

α-Cyclodextrin (α-CD): α-cyclodextrin is a cyclic oligosaccharide composed of 6 glucose groups. This is white amorphous solid with a cylinder like molecular structure. Its versatility due to its structural arrangement. The properties are widely used in industry for various purposes.

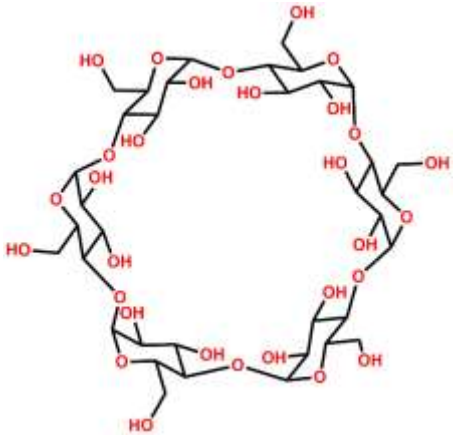

α-Cyclodextrin

CAS Number	10016-20-3
Chemical Formula	$C_{36}H_{60}O_{30}$
Molar mass	972.84 g·mol^{-1}
Appearance	white powder
Solubility in water	145 g/L
Number of glucose unit	6
Internal diameter (Å)	4.7-5.2
Depth	6.7

Source: Sigma Aldrich, Germany.

Purification: Used as parched. The purity is 99.98%.

Application: α-Cyclodextrin is a new substance with high solubility in water and which has wide application in medicinal chemistry, food-processing industry. Moreover, it is extensively used in modification of cosmetics, foodstuffs etc.; whose function is to improve stability, solubility and good smell. In the production of medicine, it can strengthen the stability of medicine without being oxidized and resolving. On the other hand, it can improve the solubility and the effect on living of

medicine, lower the toxic and side-effect of medicine and cover the strange and bad smell. In the food industry, it is used to cover strange and bad smell of food, improve the stability of perfume and the condiment and keep food dry or wet at will. α-CD with a cavity diameter of 4.7-5.3Å, is of the good interest because it is easily available in market and its cavity size allows to encapsulate many common guest moieties like hormones, vitamins, and many compounds. This capability has also been of assistance for different applications in medicines, cosmetics, food technology, pharmaceutical, and chemical industries as well as in agriculture and environmental engineering.

β-Cyclodextrin (β-CD): β-Cyclodextrinis white amorphous solid compound composed of 7 glucose groups having a cylinder like molecular structure. The function of β-Cyclodextrin depends on its molecular structure which can be easy to integrate other materials. That feature is applied widely in industry.

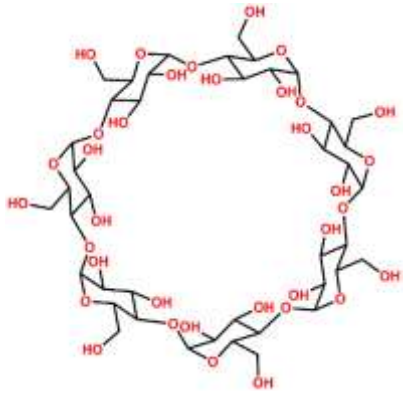

β-Cyclodextrin

CAS Number	7585-39-9
Chemical Formula	$C_{42}H_{70}O_{35}$
Molar mass	1134.98 g·mol^{-1}
Appearance	white powder
Solubility in water	18.5 g/L
Number of glucose unit	7
Internal diameter (Å)	6.4 – 7.5
Depth	6.7

Source: Sigma Aldrich, Germany.

Purification: Used as parched. The purity is 99.98%.

Application: β-Cyclodextrin is a new stuff which can be widely applied in production of medicine and food. And the effect on living of medicine, lower the toxic and side-effect of medicine and cover the strange and bad smell. In the production of food, it can mainly cover strange and bad smell of food, improve the stability of perfume and condiment and keep food dry or wet at will. β-CD with a cavity diameter of 6.4-7.5 Å, is the most interest because its cavity size allows for the best special fit for many common guest moieties. For this reason, β-cyclodextrin is widely used as host in the host-guest chemistry with various biologically active molecules such as hormones, vitamins, drug molecules and various compounds commonly used in tissue and cell-culture applications. This capability has also been of assistance for different applications in medicines, cosmetics, food technology, pharmaceutical, and chemical industries as well as in agriculture and environmental engineering as an encapsulating agent to protect sensitive molecules in hostile environment.

(2-Hydroxypropyl)-β-Cyclodextrin (HP-β-CD): HP-β-CD is a 2-hydroxypropyl beta-cyclodextrin which is highly soluble derivative of beta-cyclodextrin. (HP-β-CD) exists as a mixture of isomers having various degrees and pattern of hydroxyl propylation. (2-hydroxypropyl) beta-cyclodextrin (HP-β-CD) is a highly soluble derivative of beta-cyclodextrin. That's why, it is used as stabilizer and solubilizer for oral and parenteral formulations.

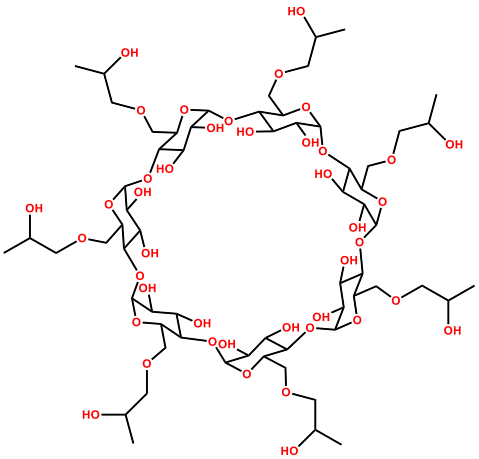

(2-Hydroxypropyl)-β-Cyclodextrin

CAS Number	128446-35-5
Chemical Formula	$C_{63}H_{112}O_{42}$

Molar mass	1541.5 g·mol^{-1}
Appearance	white powder
Solubility in water	soluble

Source: Sigma Aldrich, Germany.

Purification: Used as parched. The purity is 99.98%.

Application: It has enhanced solubility and less toxicity. Recently, its pharmacological activity has been documented in several diseases. The increasing applications need a closer gaze to the structure-activity relationship. Recently, the anticancer effect of HP-β-CD has been discovered and proved in vivo in mouse model of leukemia.

III.1.4. Food preservative molecules:

Sodium benzoate: Sodium benzoate is an extensively used food preservative. Reaction of benzoic acid with sodium hydroxide produces sodium benzoate, i.e. sodium salt of benzoic acid.[8,9]

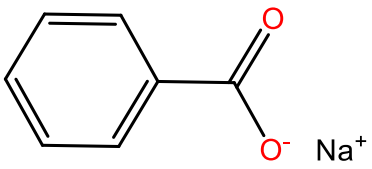

Sodium benzoate

CAS Number	532-32-1
Chemical Formula	$C_7H_5NaO_2$
Molar mass	144.10 g·mol^{-1}
Appearance	white crystalline powder
Melting Point	410 °C
Solubility in water	62.87 g/100mL at 30 °C

Source: Sigma Aldrich, Germany.

Purification: Used as parched. The purity is 99.98%.

Application: Sodium benzoate is a preservative and widely used in acidic foods such as carbonated drinks, salad dressings, jams, pickles and fruit juices, condiments and frogurt toppings. It is also preserves cosmetics and medicines. due to its poor water solubility is not used directly. Potassium sorbate is used in the majority of soft drinks in place of sodium benzoate. Sodium benzoate able to bind with amino acid and it is used to treat urea cycle disorders.

Sodium salicylate: Sodium salicylate is the sodium salt of salicylic acid. It can be prepared from carbon dioxide and sodium phenolate under higher temperature and pressure. It has been synthesized in presence of excess of sodium hydroxide by refluxing methyl salicylate.[10,11]

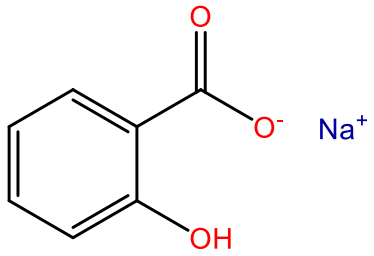

Sodium salicylate

CAS Number	54-21-7
Chemical Formula	$C_7H_5NaO_3$
Molar mass	160.10 g·mol^{-1}
Appearance	white crystalline powder
Melting Point	200°C
Solubility in water	124.6 g/100g at (25 °C)

Source: Sigma Aldrich, Germany.

Purification: Used as parched. The purity is 99.98%.

Application: Sodium salicylate is of the salicylate group and this compound is known to cause Reye's Syndrome in adults and children, generally following a viral infection such as chicken pox or influenza. It is used in medicine as an antipyretic and analgesic. Sodium salicylate also acts as NSAID and brings necrosis and apoptosis in

cancer cells.[12] It is also a potential replacement for aspirin for people sensitive to it. It may also be used as a phosphor for the detection of vacuum ultraviolet radiation and electrons.

III.1.5. Ionic liquids:

Benzyltrimethylammoniun chloride (BTMACl): Benzyltrimethylammoniun chloride is a quaternary ammonium based ionic liquid. It can execute some sort of anti-microbial effects for instance positive charge on the Nitrogen atom of these ionic liquids attracts naturally the negatively charged species, such as bacterial proteins and consequently disorganization in the protein chain makes it denature.[13]

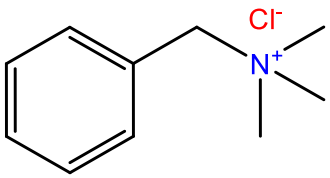

Benzyltrimethylammoniun chloride

CAS Number	56-93-9
Chemical Formula	$C_{10}H_{16}ClN$
Molar mass	185.69 g/mol
Appearance	Crystalline solid
Melting Point	239^0C
Solubility in water	soluble

Source: Sigma Aldrich, Germany.

Purification: Used as purchased. The purity is 97.0%.

Benzyltriethylammoniun chloride (BTEACl): Ionic liquids, benztltriethylammonim chloride is also a quaternary ammonium based ionic liquid and shows anti-microbial activity when used along with the food preservatives.[13]

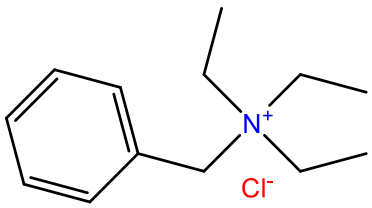

Benzyltriethylammoniun chloride

CAS Number	56-37-1
Chemical Formula	$C_{13}H_{22}ClN$
Molar mass	227.77 g/mol
Appearance	Crystalline solid
Melting Point	190 to 192°C
Solubility in water	soluble

Source: Sigma Aldrich, Germany.

Purification: Used as purchased. The purity is 99.0%.

III.1.6. Solvents:

Water: Water is the basis of life as life arose from water. Water is a universal chemical substance is made up of hydrogen and oxygen and is crucial for all well-known forms of life. In distinctive treatment, water refers only to its liquid form or state, but the matter also exists as solid state or gaseous state e.g. ice and steam respectively. Water is a high quality solvent and is frequently referred to as the Universal Solvent.[14]

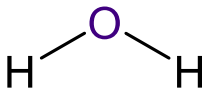

Water

CAS Number	7732-18-5
Chemical Formula	H_2O
Molar mass	18.015 g/mol
Appearance	Almost colourless, transparent, with a slight hint of blue liquid
Melting Point	273.15 K
Boiling point	373.13 K
pKa	13.995

Density	0.9998396 g/mL at 0°C 0.9970474 g/mL at 25°C
Refractive Index	1.3330 at 20°C
Viscosity	0.891 cP
Dipole moment	1.8546 D
Specific heat capacity	75.375 ± 0.05 J/mol K

Source: Distilled water, distilled from fractional distillation method in Laboratory.

Purification: Water was first deionised and then distilled in an all glass distilling set along with alkaline $KMnO_4$ solution to remove any organic matter therein. The doubly distilled water was finally distilled using an all glass distilling set. Precautions were taken to prevent contamination from CO_2 and other impurities. The triply distilled water had specific conductance less than 1×10^{-6} $S \cdot cm^{-1}$.

Application: Water is extensively used in chemical reactions as a solvent or reactant and less usually as a solute or catalyst. In inorganic reactions, water is a ordinary solvent, dissolving many ionic compounds. Supercritical water has newly been an important topic of research work. Oxygen saturated supercritical water combusts organic pollutants powerfully. It with no trouble forms hydrogen bond with other molecules and has appropriate polarity to freeze a numerous number of molecules and hence, it is said the universal solvent. Water is the most important constituent of life in the earth. Not only an elevated percentage of living substances, both plants and animals are set up in water, all forms of life on earth is consideration to have arisen from water and the biochemic bodies of all living organisms are composed mainly of water. About 70 to 92 percent of all organic matter is water. The biochemical reactions in all plants and animals that sustain life take place occur in water medium. Water not only gives the medium to create these life-satisfying reactions plausible, but water itself is often an essential reactant or product of all these reactions. In short, Biochemistry i.e. the 'Chemistry of life' is nothing but the "chemistry of water" in living bodies.[15,16]

Dimethyl solfoxide: Dimethyl sulfoxide (DMSO) is an organosulfur compound with the formula $(CH_3)_2SO$. This colorless liquid is an significant polar aprotic solvent and

able to dissolves both nonpolar and polar compounds and it has a great miscibility in a wide range of organic solvents as well as water. It has a comparatively high boiling point. DMSO has the unfamiliar property that many entities observe a garlic-like taste in the mouth.[17]

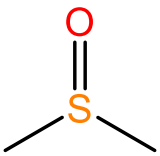

Dimethyl sulfoxide

CAS Number	67-68-5
Chemical Formula	C_2H_6OS
Molar mass	78.13 g/mol
Appearance	Colourless liquid
Melting Point	19°C
Boiling point	189°C
pKa	35
Density	1.1004 g/cm^3
Refractive Index	1.479
Viscosity	1.996 cP at 20°C
Solubility in water	Miscible

Source: Sigma Aldrich, Germany.

Purification: Used as purchased. The purity is 99.0%.

Application: DMSO is an aprotic polar solvent and is less toxic than other members of this class, such as dimethylacetamide, dimethylformamide, HMPA and N-methyl-2-pyrrolidone. DMSO is regularly used as a solvent for chemical reactions concerning salts, most remarkably nucleophilic substitutions and Finkelstein reactions. It is also comprehensively used as an extractant in cell biology and biochemistry. At normal atmospheric DMSO evaporates slowly due to its high boiling point, 189 °C. After dissolution in DMSO the samples cannot be easily recovered compared to other

solvents since, it is very hard to remove all traces of DMSO by orthodox rotary evaporation.[18-20]

III.2. EXPERIMENTAL METHODS

III.2.1. Preparation of solutions:

A stock solution for each salt was equipped (digital electronic analytical balance, Mettler Toledo, AG 285, Switzerland) by mass, and the functioning solutions were obtained by mass dilution. The doubt of molarity of dissimilar salt solutions was evaluated to be ± 0.0003 mol·dm^{-3}.

Solvent mixtures are prepared from pure components which were taken independently in glass stoppered bottles and thermostated at the needed temperature for adequate time. When the thermal equilibrium was ensured, the requisite volumes of each component were transferred in a dissimilar bottle which was already cleaned and dried methodically. Translation of essential mass of the relevant solvents to volume was skilled by using experimental densities of the solvents at experimental temperature. It was then Stoppard and the mixed contents were shaken well before use. While preparing different solvent mixtures care was taken to ensure that the same process was adopted right through the whole work. The physical properties of diverse pure and mixed solvents have been offered in the relevant chapters.

III.2.2. Preparation of multicomponent liquid mixtures:

The double and polycomponent liquid mixtures can be equipped by any one of the procedure discussed below:

(i) Mole fraction

(ii) Mass fraction

(iii) Volume fraction

(i) Mole fraction: The mole fraction (x_i) of the polycomponent liquid mixtures can be equipped using the following relation:

$$x_i = \frac{(w_i / M_i)}{\sum_{i=1}^{n}(w_i / M_i)}$$

Where, w_i, and M_i are mass and molecular mass of i^{th} component, correspondingly. The values of i depends on the number of components implicated in the development of a mixture.

(ii) Mass fraction: The mole fraction (w_i) of the polycomponent liquid mixtures can be equipped using the following relation:

$$w_i = \frac{(x_i / M_i)}{\sum_{i=1}^{n}(x_i M_i)}$$

(iii) Volume fraction: The volume fraction (ϕ_i) of the poly component liquid mixtures can be equipped by following employing three methods:

(a) ***Using volume:*** The volume fraction (ϕ_i) of the polycomponent liquid mixtures can be prepared by following relation

$$\phi_i = \frac{V_i}{\sum_{i=1}^{n} V_i}$$

Where, V_i, is the volume of pure liquid i.

(b) ***Using molar volume:*** The volume fraction (ϕ_i^l) of the polycomponent liquid mixtures can be equipped by following relation

$$\phi_i^l = \frac{x_i V_{mi}}{\sum_{i=1}^{n}(x_i V_{mi})}$$

Where, V_{mi} is the molar volume of pure liquid i.

(c) ***Using excess volume:*** The volume fraction (ϕ_i^{ex}) of the polycomponent liquid mixtures can be equipped by following relation

$$\phi_i^{ex} = \frac{x_i V_i}{\sum_{i=1}^{n} (x_i V_i) + V^E}$$

Where, V^E is the excess volume of the liquid mixture.

III.2.3. Preparation of Inclusion Complexes:

At first, 20 mL 1.0 (mM) solutions of α and β-CD were prepared separately with triply distilled, deionized and degassed water which, allowed to stir for several hours on a magnetic stirrer. Then, 20 mL 1.0 (mM) aqueous solutions of guest molecules were added drop wise to the previously prepared aqueous solution of α-CD or β-CD making the ultimate equimolar mixture and were continued to stir for 48-72 hours at 55-60°C. The suspensions obtained after cooling the mixture to 5 °C were filtered to obtain white crystalline powder, which were then dried in air and preserved in vacuum desiccators.

III.3. DETAILS OF THE INSTRUMENTS INVOLVED IN THE RESEARCH WORK:

III.3.1. Measurement of mass:

Digital electronic analytical balance Mettler Toledo, AG 285, Switzerland, was employed to measure mass.

It can determine mass with a excessive precision and accuracy. The weighing pot is of elevated accuracy and precision (0.0001g) is kept inside a glass enclosed space with sliding doors to save from harm from dust and air currents.

III.3.2. Water distiller:

Distillation of water was made by using glass distillation unit, Bionics Scientific Technologies (P). Ltd.

A water distillation system is designed to purify water quickly, cheaply and effectively. To distil water, we actually need a condenser and a heat source. Since water has a lower boiling point than contaminants and minerals like salt, bacteria, heavy metals, calcium and phosphorus, when untreated water is boiled, the water turns into vapour and leaves everything else behind. We heated water to the required minimum temperature to boil the water such that the undesirable elements cannot undergo vaporization along with water. The water vapour is routed through the condensing coil where reverts back to liquid form while the undesirable elements stay in the boiling tank

III.3.3. Thermostat:

Temperature of experimental solutions were controlled using Brookfield TC-550 thermostatic water bath with an accuracy of ± 0.01 K of the desired temperature.

Laboratory water bath has a vessel containing the material to be heated is placed into the one containing water that heats it. It has digital control with greater temperature uniformity, durability, heat retention and recovery.

III.3.4. Magnetic stirrer:

Magnetic stirrer cum hot plate made by IKA was used for the preparation of solutions and the solid inclusion complexes.

III.3.5. Density Measurement:

The solvent as well as the solution densities were measured with vibrating-tube density meter (Anton Paar, DMA 4500M), maintained at 298.15 to 318.15 K. Calibration of the instrument was done with doubly distilled water and dry air. The uncertainty in density was estimated to be ±0.00001 g cm^{-3}.

The sample is introduced into a U-shaped tube made from borosilicate glass that is excited to oscillate at its characteristic frequency which is directly related to the density of the sample. Getting a stable oscillation, then switched off the excitation and the oscillation gets fade out freely. This fade-out sequence and excitation is recurring continuously. After evaluation this pattern, we obtain a highly precise density.

III.3.6. Viscosity Measurement:

Brookfield DV-III Ultra Programmable Rheometer with fitted spindle size-42 was employed to measure viscosities of the solutions. The viscosities were obtained using following programmed equation

$$\eta = (100/RPM) \times TK \times torque \times SMC$$

Where SMC (0.327), RPM, TK (0.09373) stands for spindle multiplier constant, speed, viscometer torque constant respectively. Calibration of the instrument before starting experiment was done with provided standard viscosity samples, water and aqueous $CaCl_2$ solutions.

III.3.7. Refractive Index Measurement:

Refractive index can be measured with the help of Digital Refractometer (Mettler Toledo 30GS). The refractometer was calibrated by measuring the refractive indices of double-distilled water, cyclohexane, toluene and carbon tetrachloride at defined temperature. The accuracy of the instrument is +/- 0.0005. 2-3 drops of the sample was put onto the measurement cell and the reading was taken. During measurement,

refractometer determines the temperature and then corrects the refractive index to a temperature as desired by the user.

III.3.8. Conductivity Measurement:

METTLER-TOLEDO Seven Multi conductivity meter was employed to have specific conductivity values with an uncertainty of ±1.0 μS m^{-1}.

Temperature during the experiment was kept constant at the specific value with an auto-thermostatic water bath. HPLC-grade water having a specific conductance of 6.0 μS m^{-1} was used for conductivity measurement. Freshly prepared aqueous 0.01 M KCl solution was utilized for the calibration of the Systronics Type CD – 30 conductivity cell.

III.3.9. Surface Tension Measurement:

Surface tension of experimental solutions with the accuracy of ±0.1 mN m^{-1} were obtained by employing K9 digital TENSIOMETER (Krüss GmbH, Hamburg, Germany) which uses the platinum ring detachment technique.

The tensiometer is a precision instrument which will only perform reliably on a solid and vibration-free base. It places the same demands on its surroundings as a laboratory balance with a resolution of 0.1 mg. In addition surface tension measurements require a clean and dust-free atmosphere as atmospheric pollutants could directly falsify the results.

III.3.10. FT-IR Spectra Measurement:

With the help of Perkin-Elmer FTIR spectrometer FTIR data were collected in the scanning range of 4000–400 cm^{-1}. KBr disks were made in 1:100 ratios of sample and KBr according to the KBr disk method.

III.3.11. UV-Visible Spectra Measurement:

Compounds that absorb Ultraviolet and/or visible light have characteristic absorbance curves as a function of wavelength. Absorbance of altered wavelengths of light arises as the molecules moves to higher energy state. Utilizing JASCO V-530 and Agilent 8453 UV-Visible Spectrophotometer, UV−visible spectra were recorded with a wavelength accuracy of ±0.5 nm. Cell temperature during the experiment was controlled from 298.15K to 308.15K with a digital thermostat.

Agilent 8453 UV-Visible Spectrophotometer

Both the spectrophotometers uses two light sources, a deuterium lamp for ultraviolet light and a tungsten lamp for visible light. JASCO V-530 is a double beam spectrophotometer, one the beams passes through the reference cuvette containing solvent and the another beam goes through the cuvette containing experimental solution. On the other hand Agilent 8453 is a single beam spectrophotometer.

III.3.12. ^{1}H NMR and 2D ROESY Spectroscopic Measurement:

2D ROESY as well as ^{1}H NMR spectra were recorded in D_2O solvent at 400 MHz in Bruker Avance instrument at 298.15 K. The chemical shifts data, δ values are presented in parts per million (ppm) where, the residual protonated signal (HDO, δ 4.79 ppm) was used as internal standard.

Nuclear magnetic resonance spectroscopy, generally known as NMR spectroscopy, is a spectroscopic technique to understand local magnetic fields around atomic nuclei. After placing the sample in a magnetic field, the NMR signals were recorded by excitation of the nuclei sample with radio waves into nuclear magnetic resonance, which is spotted with sensitive radio receivers. Intramolecular magnetic field around an atom in a molecule has an influence on the resonance frequency that gives details of the electronic structure of a molecule and the different functional groups. As the

fields are exclusive or extremely characteristic to different compounds, in modern organic chemistry practice, NMR spectroscopy is the decisive method to detect monomolecular organic compounds. Similarly, biochemists use NMR to identify proteins and other complex molecules. Besides identification, NMR spectroscopy provides detailed information about the dynamics, structure, reaction state, and chemical environment of molecules.

III.3.13. Fluorescence Spectra Measurement:

The Bench top spectrofluorimeter from photon technologies International (Quantamaster-40, USA) was used to record fluorescence spectra at room temperature. Hellma quartz cuvette having optical path length 1.0 cm was also used. Fluorescence is the momentary absorption of electromagnetic wavelengths from the visible light spectrum by fluorescent molecules, and the subsequent emission of light from the higher to the lower energy level. Fluorescence of a molecule takes place, when an orbital electron, nanostructure, relaxes to its ground state by emitting a photon from an excited singlet state. Different competing pathways relax a molecule in S_1. It can get relaxed through non-radiative relaxation releasing heat (vibrations) to the solvent. It can also undergo relaxation via conversion to a triplet state, i.e. via phosphorescence.

A second molecule can relax an excited molecule through fluorescence quenching. The triplet state of the molecular oxygen is a tremendously efficient quencher of fluorescence.

III.3.14. Differential Scanning Calorimetry (DSC):

The DSC thermograms of the samples were recorded with the help of Perkin-Elmer DSC-6 differential scanning calorimeter at the heating rates of 10°C min^{-1}. The thermograms were taken by heating near about 1 mg of samples in aluminium-crimped pans under nitrogen gas flow.

To undergo a physical transformation like, phase transitions, the more or less heat will necessary to flow to it than the reference to keep both at the same temperature. Whether more or less heat flows to the sample depends on whether the process is endothermic or exothermic. For example, when a solid sample melts to a liquid, it will need more heat flowing to the sample to increase its temperature at the same rate as that of the reference. This is due to the absorption of heat by the sample as it undergoes the endothermic phase transition from solid to liquid.

III.3.15. Powder X-Ray Diffraction (PXRD):

Powdered X-Ray Diffraction (PXRD) patterns of the pure compound and ProC were recorded by using Cu-Kα radiation (D8 Advance Bruker).

The waves produced by a diffractometer at a known frequency that is governed by their source. The source is frequently x-rays, as they are the only kind of energy with the correct frequency for inter-atomic-scale diffraction. Nevertheless, the common sources are neutrons and electrons, where, the frequency can be determined by the de Broglie wavelength. After reached to the sample, the incoming beam is either reflected or can enter the lattice and get diffracted by the atoms present in the sample. To get constructive interference the atoms must be arranged symmetrically such that the path-length difference $2d\sin\theta$ is equal to an integral multiple of the wavelength, producing a diffraction maximum in accordance with Bragg's Law.

III.3.16. Scanning Electron Microscopy (SEM):

The Scanning Electron Microscope (SEM), JEOL JSM IT 100 was used to determine the surface topography of the samples at various resolutions. Samples were prepared on a small piece of double adhesive carbon-coated tape attached to brass stubs and then a coating of ultra-thin layer of gold ions was put in a gold-ionization chamber.

SEM samples should be small enough to adequate in the specimen stage, and special preparation is required to increase their electrical conductivity and to stabilize them, so that they can resist the high-energy beam of electrons and high vacuum conditions. Samples are commonly attached strictly on a specimen holder or stubbed by conductive adhesive. SEM is used widely for defect analysis of semiconductor wafers, and the instruments made by the manufacturer can be examined any part of a 300 mm semiconductor wafer. There are instruments that have chambers can tilt an object of that size to 45° and provide continuous 360° rotation.

III.3.17. High Resolution Mass Spectrometric Measurement:

Quadrupole time-of-flight (Q-TOF) high-resolution instrument with positive-mode electrospray ionization was employed to have HRMS spectra of the solid ICs, taking the methanol solution of the solid ICs.

The ion source ionizes the material under analysis (the analyte). The high voltage maintained by magnetic or electric fields makes the ions to undergo transportation to the mass analyzer. Depending on the types of samples under analysis, different mass spectrometric techniques should be used. Chemical ionization and electron ionization are used for vapours and gases.

CHAPTER IV

Study to Probe Subsistence of Host-Guest Inclusion Complexes of α and β-Cyclodextrins with Biologically Potent Drugs for Safety Regulatory Dischargement

Abstract: Host-guest interaction of two significant drugs, phenylephrine hydrochloride and synephrine with α and β-cyclodextrins were studied systematically. Initially two simple but reliable physicochemical techniques namely conductance and surface tension were employed to find out saturation concentration for the inclusion and its stoichiometry. The obtained 1:1 stoichiometry was further confirmed by two spectrometric methods, UV-Vis study and spectrofluorimetry. Significant shifts in IR stretching frequency also support the inclusion process. Relative stabilities of the inclusion complexes were established by the association constants obtained from UV-Vis spectroscopic measurements, program based mathematical calculation of conductivity data. Calculations of the thermodynamic parameters dictates thermodynamic feasibility of the inclusion process. Spectrofluorometric measurement scaffolds the UV-Vis spectroscopic measurement validating stability of the ICs once again. Mass spectroscopic measurement gives the molecular ion peaks corresponding to the inclusion complex of 1:1 molar ratio of host and guest molecules. The mechanism of inclusion was drawn by ^{1}H-NMR and 2D ROESY spectroscopic analysis. Surface texture of the inclusion complexes was studied by SEM. Finally, the cytotoxic activities of the inclusion complexes were analyzed and found, Cell viability also balances for non-toxic behavior of the ICs. Moreover, all the studies reveal the formation of inclusion complexes of two ephedra free, alternatively emerging drugs (after their banned product having ephedra) SNP, PEH with α and β-CD which enriches the drug delivery system with their regulatory release without any chemical modification.

Keywords: Phenylephrine hydrochloride; Synephrine; Drug delivery; Inclusion Complex.

1. Introduction:

In supramolecular chemistry of cyclodextrins various guest molecules having hydrophobic part, influenced by non-covalent interaction, can be inserted into the hydrophobic cavity of cyclodextrin molecules. Cyclodextrins (α-CD, β-CD, γ-CD) having six, seven and eight numbers of glucopyranose units respectively, (**Figure 1**) produced from starch by the enzymatic conversion, have different cavity sizes. Inclusion complexes (ICs) with structures of higher complexity in the solid state and solution phase can increase the aqueous solubility of various drugs cum bio-active molecules of merely water solubility which leads to the development of drug delivery systems.[1,2] Chiral Separation of molecules using cyclodextrins as chiral additives are also possible by applying capillary electrophoresis (CE) and electrochemical detection (ED) method.[3, 4,5,6] Structural characterization of Host-Guest inclusion complexes of α-CD and β-CD with two bio-active molecules, PEH and SNP were done over here in terms of geometry and structural preferences by means of a variety of physical and spectroscopic methods in solid state and solution phase.

Phenylephrine hydrochloride (PEH) (**Figure 1**) is a selective α_1-adrenergic receptor agonist of the phenethylamine class used primarily in cold and flu conditions as an antipyretic, analgesic drug to relief pain.[7] In the United States PEH is used as nasal decongestant. Phenylpropanolamine, pseudoephedrine and ephedrine are also used as nasal decongestant as the substitute of PEH.[8,9] However, due to serious side effect (hemorrhagic stroke) phenylpropanolamine was withdrawn from market.[10] Now it is imperative to find out the suitability of PEH as the same done by the Phenylpropanolamine, pseudoephedrine and ephedrine for the treatment of nasal or sinus congestion and to find out the way of delivery with biocompatibility.

Alkaloid synephrine (SNP) (**Figure 1**) was first extracted as a natural product from the leaves of various citrus trees are used as bronchial muscle reluctant, increases blood pressure in the patients suffering from low blood pressure. Its presence and positive retort as a bio-marker makes the orange juice like soft drinks authentic.[11] Lipolytic stimulation by synephrine increases thermogenesis which leads to the increase in metabolic rate and fat oxidation.[12,13,14,15,16] In weight loss products as well as in the dietary supplement “ephedra free” synephrine is frequently used and starts to earn enormous attention after the banned product ephedrine.[17,18] Most of the cases

patients suffering from obesity are often found to suffer from type-2 diabetes and hence synephrine in weight loss products frequently becomes beneficial to the diabetic patients.[19,20]

Cyclodextrins, mostly α-cyclodextrin, are found to form complexes with the dietary fat which are stable enough to undergo enzymatic hydrolysis by lipase. This restrains accumulation of fat in human body.[21,22] Hence, inclusion complex of SNP and cyclodextrins can be of a great deal for the weight loss/weight management dietary food supplement for sportsman or obese person.[23]

2. EXPERIMENTAL SECTION

2.1. Materials

Phenylephrine hydrochloride, Synephrine, α and β-cyclodextrin of puris grade of purity ≥98.0% were purchased from Sigma-Aldrich and were kept in a refrigerator as received and used right away.

2.2. Apparatus

Utilizing JASCO V-530 UV–Vis spectrophotometer, UV–visible spectra were recorded with a wavelength accuracy of ±0.5 nm. Cell temperature during the experiment was controlled from 298.15K to 308.15K with a digital thermostat.

Studies on surface tension at the experimental temperatures with the accuracy of ±0.1 mN m^{-1} were done by employing K9 digital TENSIOMETER (Krüss GmbH, Hamburg, Germany) which uses the platinum ring detachment technique. The temperature of the experimental solutions was kept constant at 298.15K by circulating thermostat water through a double-walled glass vessel holding solution.

Proper instrumentation of METTLER-TOLEDO Seven Multi conductivity meter provides specific conductivity values with an uncertainty of ±1.0 μS m^{-1}.Constancy in temperature at the specific value of the solutions under experiment was maintained with an auto-thermostatic water bath. HPLC-grade water with a specific conductance of 6.0 μS m^{-1} was utilized for conductivity measurement. Calibration of the Systronics Type CD – 30 conductivity cell was done using 0.01 M freshly prepared aqueous solution of KCl.

Fluorescence spectra were noted via JASCO V-530 UV/VIS Spectrophotometer, at 25°C in a Hellma quartz cuvette (250-400 nm spectral range, 2.0 mL volume, 10 mm path length) equipped with a magnetic stir bar. To a solution of [SNP/PEH] (100μM, 1 mL) in deionized water (Millipore, 18.2 MΩ. Cm) was prepared with α-CD and β-CD. (200 μM) in the stock fluorescence spectra were recorded after 1 hr of mixing time. The output range of the machine was nearly about 2 analogs (+/- 10 volts).

2D ROESY as well as 1H NMR spectra were recorded in D_2O solvent at 400 MHz in Bruker Avance instrument at 298.15 K. The residual protonated signal (HDO, δ 4.79 ppm) was used as an internal standard. The chemical shifts data, δ values are presented in parts per million.

HRMS spectra of the solid ICs were recorded on a quadrupole time-of-flight (Q-TOF) high-resolution instrument with positive-mode electrospray ionization taking the methanol solution of the solid ICs.

FTIR spectral analysis was performed on a Perkin-Elmer FTIR spectrometer in the scanning range of 4000−400 cm^{-1}. According to the KBr disk method the disks were made in 1:100 ratios of sample and KBr. Studies were carried out at room temperature and at a humidity of 45%.

SEM: Scanning Electron Microscope (JSM-6360) was aided to perform the analysis and obtain the data's. It also discusses about the morphological patterns and particle size of the Inclusion Complex.

Antimicrobial activity assay: In this experiment (gram negative E. coli*)*, (gram positive B. subtilis*)* were considered as model organism. This test was done according to the Agar cup method. In brief, spread plate technique was applied to inoculate the organisms in Muller-Hinton agar and the compounds were applied in agar cup at 1mg/ml concentration in separate plates and incubated at 37°C for 24 hrs. Double distilled water was used as the control. Antimicrobial activity was determined by

means of the zone of inhibition surroundings agar cup. Each of the experiments was done in triplicate.

Cell viability assay: In this experiment pure sample as well as ICs, SNP+α-CD, SNP+β-CD, PEH+α-CD and PEH+β-CD were added in the nutrient agar broth and E. coli and B. subtilis were inoculated. After 24 hrs of incubation at 37°C cells were plated, and colony count was completed. Growth in nutrient broth without the ICs was taken as the control. All the experiment was done in triplicate. Level of significance (p) for all experiment was set to 0.05.

2.3. Procedure

All the solutions under experiment were prepared after checking the solubility of the PEH, SNP and CDs in triply distilled, deionized and degassed water. METTLER TOLEDO AG-285 analytical balance with an uncertainty of ±0.1 mg at 298.15K was used to weigh all the experimental materials. Loss of materials caused by evaporation during mixing and working with the solutions was minimized by taking sufficient precautions. For the preparation of the solid inclusion complexes, 20 mL 1.0 (mM) solutions of α and β-CD were prepared separately with triply distilled, deionized and degassed water which, allowed to stir for 6 hours on a magnetic stirrer. Then,20 mL 1.0 (mM) aqueous solutions of SNP/PEH were added drop wise to the previously prepared aqueous solution of α-CD or β-CD making the ultimate equimolar mixture and were continued to stir for 48 hours at 55-60°C. The suspensions obtained after cooling the mixture to 5 °C were filtered to obtain white crystalline powder, which were then dried in air and preserved in vacuum desiccators for further use.

3. Result and discussion

3.1 Job plot: Stoichiometry of inter molecular association between guest and host:

The stoichiometry of the host-guest inclusion complexes was determined by employing the well-established Jobs method.[24] UV-Vis spectroscopic data were used in this technique to determine the stoichiometry of inclusion complexation. Absorption spectra of a set of solutions, prepared by mixing aqueous SNP/PEH solution with the aqueous α-CD/β-CD solution in the sort of 0 – 1 mole fraction, were recorded at 298.15

K of temperature. Absorbance of the prepared set of the solutions were taken at λ_{max} = 209 nm for SNP and λ_{max} = 219 nm for PEH **(Figure 2).** Jobs plots of (SNP + α-CD, SNP + β-CD, PEH + α-CD, PEH + β-CD) were obtained by plotting a graph, ΔA×R vs R. Where, ΔA is the deference in absorbance between the pure SNP/PEH and the solutions of the set, prepared with CDs (**Table S1, S2, S3, S4 and Figure 2**). R signifies [PEH]/([PEH] + [CD]) and [SNP]/([SNP] + [CD]). The corresponding fractional value of R at maxima of the Jobs plot indicates the stoichiometry of the inclusion complex formed and it is well known that, R = 0.33, 0.5, 0.66 and so on, evidently recommends 1:2, 1:1 and 2:1, Guest:Host stoichiometry of the inclusion complex respectively[25] (**Figure 3**). Ulatowski et al. and Hibbert et al. showed that Job plot may be used in case of 1:1 complexes, but for other stoichiometries various mathematical models are widely employed [26, 27]. In the experimental analysis of the present work, it is found that, for all the four systems (SNP + α-CD) and (SNP + β-CD), (PEH + α-CD), (PEH+ β-CD) the value of R = 0.5, clearly indicating the 1:1, Guest:Host stoichiometry of the ICs[28] (**Figure 4**).

3.2 Surface tension: An idea to the Host-Guest molecular association and their stoichiometry in the inclusion complex:

Sufficiently lower surface tension(γ) value of the aqueous solutions of SNP/PEH than the triply distilled pure water, suggests SNP and PEH to have surface activity. This may be due to the simultaneous presence of phenyl ring as well as the $-CH(OH)CH_2NHCH_3$ group to the opposite terminals of the same molecule. Study on the surface tension of diverse surface-active Guest molecules with cyclodextrins strongly supports the inclusion phenomenon and the stoichiometry of the ICs.[29, 30, 31, 32] In this work, surface tension of a fixed quantity of aqueous SNP/PEH solutions was studied at 298.15 K with the step wise addition of CDs solutions in same quantity (**Table S5, S6, Figure 5**). Whereas, according to literature as well as practically it is found that, there is an extremely slight change in the surface tension (γ) of CDs over a wide range of concentration in aqueous medium at 298.15 K.[33,34] It signifies all the changes in the value of surface tension (γ) are associated with the SNP/PEH. Being a surface phenomenon, more the number of surface active molecules in the surface of a solution, decreases more the surface tension of that solution. But permanent migration of surface active molecules from the surface to the bulk of the solution by means of solvation or many other stabilizing factors leads to the increase in surface tension (γ)

of that solution. This is exactly the trend, what we observed in our experiment during step wise addition of CDs in the aqueous SNP/PEH solution (**Table S5, S6, Figure 5**). This is obviously; there is migration of surface active SNP/PEH molecules from the surface to the bulk of the solution by means of encapsulation of the SNP/PEH into the hydrophobic cavity of the CDs forming host-guest ICs[30, 31, 35] (**Figure 6**). After a certain concentration of CDs, the surface tension (γ) becomes steady and consequently lefts a sharp break point behind it, in the plot of surface tension (γ) vs concentration of CDs (**Table 1, Figure 5**). Accordingly, surface chemistry confers the inclusion phenomenon and appearance of sharp, single break point at the 1:1 molar concentration ratio of Host and Guest molecules for all the cases (SNP + α-CD, SNP + β-CD, PEH + α-CD, PEH + β-CD) establishes the 1:1 stoichiometry of Host-Guest ICs.[36, 37, 38, 39]

3.3 Conductance: Molecular recognition of guest into host molecules and their stoichiometric ratio in ICs:

Conductimetric study is also another approach, which makes us able to conclude about the supramolecular Host-guest interaction between the SNP/PEH and CDs and their stoichiometric ratio in the ICs.[40,37] Though, both the SNP and PEH are organic molecules, 10 (mM) aqueous solution of SNP and PEH shows appreciable conductivity. Being a hydrochloride salt, PEH shows higher conductivity than SNP for the same concentration. In the present work, conductivity of SNP and PEH were measured with the step wise increasing concentration of CDs, at three different temperatures from 298.15K to 308.15 K with the interval of 5K of temperature (**Table S5, S6 and Figure 7**). It was found that, gradual increase in concentration of CDs leads to the decrease in conductivity (κ), of the aqueous SNP/PEH solutions (**Figure 7**). The fruit full explanation for this observation comes through the decrease in the mobility of the conducting species in the solution due to molecular encapsulation of SNP/PEH into the hydrophobic cavity of the CDs[36,41] (**Figure 6**). Generation of a single break point in the conductivity curves after reaching a certain concentration of CDs, suggests, the molecular encapsulation of SNP/PEH into the cavity of CDs is 1:1[31,41] (**Figure 7**). Corresponding concentration of SNP/PEH and CDs at the break points of the conductivity curve are listed in (**Table 2**). The near about equimolar concentration of SNP/PEH and CDs at the break points of the conductivity curve suggests the 1:1 stoichiometric ratio of the SNP/PEH into CDs of the ICs[36, 37] (**Figure 3**).

3.4 Ultraviolet Spectroscopy: The association constants (Ka) and Stability of the of the ICs:

The binding ability of the Guest into the Host molecule and the stability of the inclusion complexes formed were explored by measuring the association constants (Ka) of the ICs. The UV-vis spectroscopic study enables us to determine the association constant (Ka) of the ICs in the solution phase.[31] Molar extinction coefficient (Δε) of SNP/PEH, depending upon the solvent polarity, should change while going from polar aqueous media to the apolar hydrophobic cavity of the CDs to form ICs.[41,42] To determine association constant (Ka), the changes in absorbances (ΔA) of SNP/PEH were measured with increasing concentration of CDs at the temperature range 298.15 K to 308.15 K. (**Table S7, S8**, **S9**, **S10**) The λ_{max} = 209 nm for SNP and λ_{max} = 219 nm for PEH were considered to determine the association constant (Ka) in this case (**Table 3**). According to the Benesi-Hildebrand method to determine the association constant for the 1:1 host-guest inclusion complex, the double reciprocal plot was obtained by using the following equation[31, 43, 44, 45].

$$\frac{1}{\Delta A} = \frac{1}{\Delta\varepsilon[DGs]K_a}\frac{1}{[CD]} + \frac{1}{\Delta\varepsilon[DGs]} \qquad (1)$$

Where, ΔA represents the difference in absorbances of PEH or SNP without CDs to the absorbances of the same with the CDs. [DGs] refers to the concentration of the PEH and SNP. The association constants(K_a) of the inclusion complexes, listed in the (**Table 3**) were obtained by dividing the slope by the intercept of the plot given in the **Figure S1, S2**.

UV-vis spectroscopic data were also used in a nonlinear program that practices the changes in absorbance of SNP/PEH due to its molecular recognition into the apolar cavities of CDs and the association constants (K_a^{θ}) were obtained.[31,46] There should be an equilibrium between host and the guest molecules to the formation of 1:1 ICs.[47,48]

$$[DGs]_f + [CD]_f \overset{K_a^{\theta}}{\leftrightharpoons} [IC] \qquad (2)$$

The expression for the association constant (K_a^{θ}) can be obtained from the above equation as follows-

$$K_a^{\theta} = \frac{[IC]}{[DGs]_f [CD]_f} \quad (3)$$

Where, [IC], $[DGs]_f$ and $[CD]_f$ represents the concentration of inclusion complex, free SNP/PEHand cyclodextrin respectively at the equilibrium of the reaction. The equation for the association constant (K_a^{θ}) can also be expressed as the absorbances of the host and the guest molecules as follows-

$$K_a^{\theta} = \frac{[IC]}{[DGs]_f [CD]_f} = \frac{(A_{obs} - A_0)}{(A - A_{obs})[CD]_f} \quad (4)$$

Here,

$$[CD]_f = [CD]_x - \frac{[DGs]_x (A_{obs} - A_0)}{(A - A_{obs})} \quad \textbf{(5)}$$

Where, A_0 is the absorbance of SNP/PEH molecules in the initial state, A_{obs} denotes the absorbances of the same during the gradual addition of CDs and A refers to the final concentration of SNP/PEH molecules. $[CD]_x$ and $[DGs]_x$ is the concentration of cyclodextrins added and SNP/PEH molecules respectively. The association constants (K_a^{θ}), obtained from the binding isotherm with the application non-linear program are listed in the **Table** 3.

3.5 Conductance: Program based mathematical calculation of non-linear changes in the conductivity data and association constants (K_a^C):

Non-linear changes in the conductivity data at the temperature ranging from 298.15 K to 308.15 K were utilized in the mathematical program and the association constants (K_a^c) for 1:1 DGs-CDs ICs, listed in the **Table 3** are frequently obtained.[49, 50, 51] The complexation reaction between DGs and CDs to produce ICs is supposed to proceed via the following chemical equilibrium

$$[DGs]_f + [CD]_f \overset{K_a^C}{\leftrightharpoons} [IC] \quad (6)$$

The above equation can be reduced to the following form to find out the association constant (K_a^c)

$$K_a^c = \frac{[IC]}{[DGs]_f[CD]_f} \quad (7)$$

Here, $[IC]$ is the equilibrium concentration of inclusion complexes, $[DGs]_f$ and $[CD]_f$ refers to the concentration of SNP/PEH and CDs in the free state.

The association constant (K_a^c) can be calculated in terms of conductivities from the various non-linear isotherm as follows- [50, 51]

$$K_a^c = \frac{[IC]}{[DGs]_f[CD]_f} = \frac{(\kappa_{obs} - \kappa_0)}{(\kappa - \kappa_{obs})[CD]_f} \quad (8)$$

Where,

$$[CD]_f = [CD]_{ad} - \frac{[DGs]_{ad}(\kappa_{obs} - \kappa_0)}{(\kappa - \kappa_0)} \quad (9)$$

Here, κ_0, κ_{obs} and κ corresponds to the conductivities of DGs at initial state, during addition of CDs and the final state respectively. Instantaneous concentration of DGs while addition of CDs is represented by $[DGs]_{ad}$ and $[CD]_{ad}$ is the concentration of the added CDs.

3.6 Fluorescence: Modified Benesi-Hildebrand equation and association constants:

The association constants (K_a^F) of the ICs in the solution phase were also determined using the spectrofluorometric data and the association constants, determined are found in good agreement with the data obtained from all the previously described methodology[52, 53, 54] (**Table 3, Table S11-S14**). An enhancement of the intensities of the spectral lines accompanied by the slight hypsochromic shift were observed with the step wise increase in concentration of the CDs (α and β-cyclodextrins) solutions (**Figure S3, S4**). The observations enriched us with the knowledge that, a change in the molar extinction coefficient i.e. polarity of the environment, surrounding the chromophore, leaded by the encapsulation of the chromophore of the guest molecules (SNP and PEH) from the polar aqueous environment to the apolar hydrophobic cavity

of the cyclodextrins. Sometimes, the enhancement in the intensities of the spectral lines are experienced due to the shielding of the excited singlet species of the chromophores from quenching and non-radiative decay with the protective microenvironment created by the hollow-circular, apolar cavity of the CDs.[55,56] The spectrofluorometric data were analyzed and run with the modified Benesi-Hildebrand equation to generate the double reciprocal plots, (**Figure S5, S6**) and the association constants (K_a^F) of the ICs were obtained as the ratio of the intercept to slope of the plots.

$$\frac{1}{I - I_0} = \frac{1}{[I' - I_0]K_a^F}\frac{1}{[CD]} + \frac{1}{I' - I_0} \qquad (10)$$

Where, I and I_0 represents the fluorescence intensities of SNP/PEH in the presence and absence of the CDs respectively, I' are the intensities of the SNP/PEH while all the guest molecules for a particular system are complexed with CDs. [CD] represents the concentration of the cyclodextrins (α and β-CD).

3.7 UV-vis spectroscopy, Non-linear program based mathematical calculation, Fluorescence and Conductance: Association constants and the thermodynamic parameters:

According to the Van't Hoff equation (11) the various thermodynamic parameters for the formation of the inclusion complexes were derived from the ready available association constants (K_a, K_a^θ, K_a^C) obtained from Benesi-Hildebrand equation, nonlinear methods and non-linear changes in the conductivity data.[31, 37, 41] (**Table 4, Table S15-S20, Figure S7-S12**)

$$\ln K_a = -\frac{\Delta H^0}{RT} + \frac{\Delta S^0}{R} \qquad (11)$$

Calculation on the thermodynamic parameters of the formation of ICs, it is found that, both the changes in entropy and enthalpy of formation appears to be negative, suggesting an exothermic and entropy restricted rather than entropy driven process (**Table 4**). The explanation on the decrease in entropy during inclusion complexation comes from the molecular association of the host and guest molecules to form inclusion complexes in the solution. Though the process is entropy restricted, the negative value

of the enthalpy ($\Delta H^0, \Delta H^{\theta 0}, \Delta H^{C0}$) makes the overall energy negative i.e. negative ΔG^0 and finds its spontaneity in the formation of ICs (**Table 4**).

3.8 ^{1}H NMR and 2D ROESY NMR spectra analysis:

Inclusion of a molecule inside into the cavity of cyclodextrin consequences in the chemical shift of the interacting protons of both the guest and cyclodextrin in ^{1}H NMR spectra, due to their mutual shielding through space.[57] Encapsulation of aromatic guest molecule results the diamagnetic shielding of the interacting protons of cyclodextrin by the aromatic moiety[58] (**Table S21**). Cyclodextrin molecule has H3 and H5 hydrogens at inside of the conical cavity, specially, the H3 are located near the wider rim while H5 are positioned near the narrower rim and the other H1, H2 and H4 hydrogens are situated at the exterior of the cyclodextrin molecule (**Figure 1**).[59] In this work the molecular inclusions have been studied with the help of ^{1}H NMR spectra. The ^{1}H NMR spectra of the pure α-CD, β-CD, SNP+α-CD, SNP+β-CD, PEH+α-CD and PEH+β-CD systems are shown in **Figure S13-S18** respectively, where the aromatic as well as signals of H3 and H5 protons of cyclodextrins may be observed with corresponding chemical shift (δ) values. The ^{1}H NMR spectra of the complexes reveal that the signals of interior H3 and H5 of α and β-CD plus that of the interacting aromatic protons of SNP/PEH showed substantial upfield shift confirming the formation of inclusion complexes[60] **(Figure S13-S18).**

2D ROESY NMR spectroscopy provides decisive evidence about the spatial closeness of the interacting atoms of the host and the guest by observing the intermolecular dipolar cross-correlations.[61,62] The protons which are situated within 0.4 nm in space may produce a rotating-frame NOE spectroscopy (ROESY).[63] According to structure of α and β-CD, inclusion phenomenon inside into cyclodextrin cavity can be shown by the appearance of NOE cross-peaks between the protons of cyclodextrin and the protons of the aromatic guest identifying their spatial proximity.[64,65] To prove this, 2D ROESY spectra of the complexes of SNP and PEH with α and β-CD in D_2O, were recorded, which shows significant correlation of aromatic protons of SNP and PEH with the H3 and H5 protons of α and β-CD, establishing the aromatic ring was encapsulated inside both the cyclodextrin cavities[66] (**Figure 8-11**). It may be detected that the H-6

protons of cyclodextrins were not influenced by the inclusion processes, suggesting that the SNP/PEH molecule was incorporated into the cyclodextrin cavity via the wider rim, not through the narrower rim as otherwise cross-peaks between the H6 and the guest would have been observed in the ROESY spectra[67] (**Figure 6**).

3.9 HRMS Analysis of Inclusion complexes:

Mass spectroscopic study of the solid inclusion complexes of SNP/PEH with α and β-CD were done after the dissolution of the ICs in methanol. The spectra are shown in the **Figure 12** and **Table S22.** enlists the m/z values for the corresponding fragmentations added to the molecular ion peak. The appearance of peaks at the m/z 1140.42 and 1162.40 corresponds to the $[SNP/PEH+\alpha\text{-}CD+H]^+$ and $[SNP/PEH+\alpha\text{-}CD+Na]^+$ respectively and the peaks at 1302.47 and 1324.45 corresponding to the $[SNP+\beta\text{-}CD+H]^+$ and $[SNP+\beta\text{-}CD+Na]^+$ respectively. The tangible existence of the peaks in the spectra mentioned above approves the formation of the inclusion complexes i.e.[PEH+α-CD], [PEH+β-CD], [SNP+α-CD] and [SNP+β-CD] and their host – guest stoichiometric ratio should be 1:1 (**Figure 3**).[68,69]

3.10 FTIR spectroscopy:

Interpretation of the Infra-red spectroscopic data of the ICs as well as the pure Host and Guest molecules also reveals the veracity about the way by which the ICs are formed and supports the same circumstances of host – guest interaction as obtained from the 2D ROESY NMR spectroscopic study.[70,71] All the FTIR spectra of the solid inclusion complexes and the pure host and guest molecules were recorded by preparing KBr disk. The changes in the Significant peak values in the IR spectra on going from the pure host and guest molecules to the inclusion complexes which are shown in the **Figure 13-16**, suggests the formation of ICs exploring the binding mode of the guests to the host molecules.[72,60] The IR stretching frequencies (cm^{-1}) of noteworthy responsible for the corresponding chemical bonds are listed in the **Table S23**.

Analysis of the FTIR spectra for the [SNP+α-CD] along with the spectra of pure α-CD and SNP: (i) The -O-H stretching frequency of the α-CD and the -O-H and -N-H

stretching frequencies of SNP were observed at 3408.25 and 2992.46 to 2960.13 cm^{-1} respectively, which appears as a broad peak at 3374.08 cm^{-1} in case of the IC. The responsible fact for this shifting in frequencies is the formation of H-bond between SNP and α-CD. (ii) The peaks at 1054.12 and 1264.11 cm^{-1} responsible for the -C-O stretching for secondary and phenolic -C-OH group of SNP respectively are shifted to 1030.23 and 1154.27 cm^{-1} correspondingly for the [SNP+α-CD] IC. Thus, weakening of -C-O bond proposes the formation of H-bond via the phenolic as well as the secondary -OH group of the SNP molecule. (iii) The stretching and bending frequencies for the -C-H bond of the α-CD was at 2932.12 and 1406.17 cm^{-1} and -C-H the out-of-plane bending frequencies for SNP were at 782.42 and 640.37 cm^{-1}. But in case of IC their existence is observed at 2929.30, 1333.02, 707.25 and 583.26 cm^{-1}, suggesting the various interactions taking place between SNP and α-CD (**Figure 13**).

Innumerable interactions of the SNP and β-CD in the [SNP+β-CD] IC were analyzed as follows- (i) The signal for -O-H stretching of β-CD was at 3370.21 $cm^{-1}$and the -O-H and -N-H stretching frequencies of SNP were at 3288.34 cm^{-1} and the region of 2992.46 to 2960.13 cm^{-1} respectively, whereas in the IC these signals shifted to 3320.14 and 2933.18 cm^{-1} correspondingly. This is possibly due to the formation of H-bonding between SNP and β-CD. (ii) The peaks for -C-O (secondary and phenolic -C-OH group) of SNP were at 1054.12 and 1264.11 cm^{-1}, which shifted to 1032.29 and 1158.08 cm^{-1} respectively. This is probably owing to the formation of H-bond between SNP and β-CD. (iii) The signals at 2916.35 cm^{-1} and 1412.27 cm^{-1} corresponding to -C-H stretching and -C-H bending of β-CD, shifted to 2932.18 cm^{-1} and 1336.35 cm^{-1} respectively. On the other hand, -C-H out-of-plane bending for SNP molecule were observed at 782.42 cm^{-1} and 640.37 cm^{-1}, which shifted to 754.36 cm^{-1} and 582.13 cm^{-1} correspondingly. This may because of the various interactions taking place while the formation of the supramolecular assembly between SNP and β-CD (**Figure 14**).

The various interactions that may cause the following spectroscopic changes in the [PEH+α-CD] IC are: (i)The peak for -O-H of α-CD was at 3408.25 cm^{-1} and the phenolic -O-H and -N-H stretching frequencies of PEH appeared as a broad peak at 3028.17 to 3396.45 cm^{-1}. But, in case of IC it is shifted to 3370.14 cm^{-1} indicating the formation of H-bond between PEH and CD.(ii) The -C-O stretching frequencies of PEH was at 1070.06 cm^{-1} (secondary alcohol) and 1272.59 cm^{-1} (phenol) where as these are shifted to 1029.13 $cm^{-1}$and 1152.24 cm^{-1} respectively in case of IC, suggesting the

formation of H-bond through the secondary and phenolic H-atom of the PEH molecule.(iii) The signal of the -C-H stretching and -C-H bending mode of the α-CD were at 2932.12 and 1406.17 cm^{-1} respectively and the aromatic out-of-plane -C-H bending of PEH were at 792.26 and 700.15 cm^{-1} respectively, which appeared in case of the IC at the frequencies 2930.31, 1398.21, 716.19 and 690.20 cm^{-1} respectively, shifting of these signals leads to the ready explanation that, the close proximity of the -C-H of the α-CD with the aromatic -C-H of the PEH as obtainable from the 2D ROESY spectra.(**Figure 15**)

The shifting of the following IR signals satisfactorily explicates the formation of [PEH+β-CD] IC. (i) The -O-H signal for β-CD was at 3370.21 cm^{-1} and the phenolic -O-H and -N-H were at 3028.17 to 3396.45 cm^{-1} which are shifted to 3356.19 cm^{-1} for IC. This is probably the formation of the H-bond of PEH with β-CD. (ii) The peaks at the 1070.06 cm^{-1} (-C-O, secondary alcohol) and 1272.59 cm^{-1} (-C-O, phenolic) for the PEH were shifted to the frequencies 1030.34 cm^{-1} and 1156.31 cm^{-1}, validates the participation of secondary and phenolic -O-H group of PEH towards the formation of H-bond with β-CD. (iii) The -C-H stretching and bending mode of frequencies of β-CD were at 2918.35 and 1412.27 cm^{-1} respectively and peaks for the aromatic out-of-plane -C-H bending frequencies for PEH were at792.26 and 700.15 cm^{-1} respectively, are now shifted to 2926.32, 1376.12,756.39 and 685.11 cm^{-1} respectively. Thus, FTIR spectral analysis also indorses the same as obtained from the 2D ROESY spectra (**Figure 16**).

There is no sign of chemical reaction taking place while the formation of all the inclusion complexes, exemplified by the no appearance of additional signal in the IR spectra suggesting, all the shifting in signals appearing are responsible for the formation of ICs.

3.11 Scanning Electron Microscope (SEM):

Scanning Electron Microscopy (SEM) is an exceedingly well-known technique for analyzing the surface texture and particle size of solid materials. The surface morphological structures of α-CD, (SNP+α-CD) physical mixture, (SNP+α-CD) inclusion complex, β-CD, (SNP+β-CD) physical mixture, (SNP+β-CD) inclusion complex are shown in **Figure 17** respectively. From **Figure 17** it is clear, that the morphological structures that they are totally different from each other. Similarly, the surface morphological structures of α-CD, (PEH+α-CD) physical mixture, (PEH+α-CD)

inclusion complex, β-CD, (PEH+β-CD) physical mixture, (PEH+β-CD) inclusion complex are shown in **Figure 18** respectively. From **Figure 18** it is clear, that the morphological structures that they are totally different from each other. Moreover, as the complexation by α-CD and β-CD can be viewed distinctly. This is an additional evidence about the formation of inclusion complexes of SNP/PEH with α and β-CD, may support the same evident from 2D ROESY NMR analysis.

3.12 Cytotoxic activity of the Inclusion complexes:

No zone of inhibition was observed in case of both the gram-positive and gram-negative organisms.[73,74] Here was no growth inhibition compared to control. These results suggest that ICs doesn't have any antimicrobial activity. So, it can be said that it is non-toxic for the cells. After that cell viability assay was finished. Here we have found that cell viability of E. coli was 4.6% and 9% increase in presence of [SNP+β-CD, SNP+α-CD] and [PEH+β-CD, PEH+α-CD] respectively whereas the cell viability of B. subtilis was 3.2% and 8% increase in the presence of [SNP+β-CD, SNP+α-CD] and [PEH+β-CD, PEH+α-CD] correspondingly (**Figure 19, 20**). These consequences indicated that cell viability was positively regulated in occurrence of these ICs (**Figure 19, 20**). But there was very significant increase in growth when the samples were treated with (SNP+β-CD). So, this (SNP+β-CD) is more suitable for pharmaceutically active compounds**.** The outcome showed that both inclusion complexes increased the capability of SNP inhibiting cell growth rather than PEH. Particularly, SNP, complexed with beta-cyclodextrin (β-CD) showed the highest cytotoxic activity resting on E. coli and B. subtilis; with alpha-cyclodextrin (α-CD) the cytotoxic activity was rather low.

4. Conclusions:

The suggestion obtained from surface tension and conductometric study for the formation of 1:1 host-guest inclusion complexes of SNP and PEH with α and β-cyclodextrins are established by UV-vis spectroscopy, spectrofluorimetry, 2D ROESY NMR spectrometry and SEM technique by analyzing surface texture of the solid inclusion complexes. The association constants obtained from all the well-established techniques dictates the stability of inclusion complexes formed and the thermodynamic parameters reveals truth about the feasibility of their formation.

Removal of water molecules from the cavity of the CDs to make room for the guest molecule for accommodation while formation of inclusion complex, increases entropy of the process. Dimensional suitability being, one of the major stabilizing factor, the larger cavity size of β-CD (0.70 nm, diameter) compared to α-CD (0.56 nm, diameter), explains for the greater value of association constants and stability of the inclusion complexes formed with β-CD. The association constants, hence stability of the inclusion complexes of SNP with CDs were found more than that of the PEH. Because, -O-H group of SNP, being oriented to the para position may exert H-bonding interaction with CDs to some greater extent than that of the PEH, in which –OH group, being oriented at the meta – position can't travel the minimum distance for the formation H-bond with the CDs. The hydrophobic and H-bonding interactions thus stabilizes the ICs. The Cytotoxicity and Cell viability also balances for non-toxic behavior of the ICs. Thus, inclusion complexes of the recently emerging two drugs, SNP and PEH (after their banned alternatives) stabilizes SNP and PEH from their chemical modification and conveys a new approach for regulatory release to the targeted site reducing overdoses.

Author contributions: BR designed, performed the experiments and wrote the article, [a]SS designed and performed the experiments, KD designed and performed the experiments, BKB designed and performed the experiments, [b]SS performed cytotoxic activity, AB performed cytotoxic activity, MNR supervised the entire work and corresponding author.

Conflicts of interest: There is no conflicts of interest.

Acknowledgements: Prof. M. N. Roy would like to acknowledge UGC, New Delhi, Government of India, for being awarded One Time Grant under Basic Scientific Research via the grant-in-Aid no. F.4-10/2010 (BSR). BR is thankful to the "State Fellowship" bearing reference No. 1743/R-2017 dated 18.04.2017 and UGC-SAP DRS-III, New Delhi (no. 540/6/DRS/2007, SAP-1) for providing instrumental facilities according the research. Mr. Goutam Sarkar, The H.O.D., USIC, University of North Bengal, Darjeeling is also highly acknowledged for executing SEM associated with this paper and his sincere co-operation.

TABLES

Table 1. Values of Surface Tension (γ^a) at the Break Point with Corresponding Concentrations of DGs and CDs at 298.15 K[a]

Guest	Host	Concentration of host (mM)	Concentration of guest (mM)	Surface tension (γ^a) mNm^{-1}
PEH	α-CD	4.9379	5.0621	70.1829
	β-CD	4.9276	5.0724	70.4886
SNP	α-CD	5.2152	4.7848	70.1487
	β-CD	5.1564	4.8436	70.4149

[a]Standard uncertainties (u): temperature u(T) = ± 0.01 K, surface tension: u(γ) = ± 0.1 mNm^{-1}

Table 2. Values of Conductivity (κ) at the Break Point with Corresponding Concentrations of DGs and CDs at 298.15 K[a] to 308.15 K[a]

Guest	Host	Temperature (K[a])	Concentration of host (mM)	Concentration of guest (mM)	Conductivity (κ^a) (mSm^{-1})
PEH	α - CD	298.15	5.34	4.65	5.29
		303.15	5.21	4.78	5.88
		308.15	4.54	5.45	6.78
	β - CD	298.15	5.21	4.78	5.17
		303.15	5.12	4.87	5.74
		308.15	5.21	4.78	6.20
SNP	α - CD	298.15	5.04	4.95	0.73
		303.15	5.04	4.95	0.84
		308.15	5.23	4.76	0.93
	β - CD	298.15	5.11	4.88	0.70
		303.15	4.94	5.05	0.80
		308.15	5.12	4.87	0.91

[a]Standard uncertainties (u): temperature u(T) = ± 0.01 K, conductivity: u(κ) = ± 0.01 mSm^{-1}

Table 3. Association Constant obtained from Benesi-Hildebrand method (K_a), Association Constant obtained from the Nonlinear Program (K_a^{θ}), Association Constant obtained from Program based mathematical calculation of non-linear

changes in the conductivity data (K_a^C), Association Constant obtained from Benesi-Hildebrand equation, using the spectrofluorometric data (K_a^F) at 298.15 to 308.15 K[a].

Guest	Host	Temperature (K[a])	K_a (×10^{-3})	K_a^θ (×10^{-3})	K_a^C (×10^{-3})	K_a^F (×10^{-3})
PEH	α - CD	303.15	2.14	2.07	2.05	2.21
		308.15	1.79	1.74	1.72	
		313.15	1.48	1.40	1.38	
	β - CD	303.15	2.97	2.71	2.75	2.91
		308.15	2.26	2.10	2.12	
		313.15	1.79	1.70	1.68	
SNP	α - CD	303.15	2.84	2.82	2.80	2.87
		308.15	2.26	2.15	2.18	
		313.15	1.74	1.63	1.66	
	β - CD	303.15	3.82	3.41	3.35	3.73
		308.15	2.88	2.46	2.42	
		313.15	2.28	1.85	1.85	

[a]Standard uncertainty in temperature, u, are u(T) = ± 0.01 K

Table 4. Thermodynamic parameters (ΔH^0, ΔS^0, ΔG^0) calculated, using the association constants (K_a, K_a^θ, K_a^C) obtained from Benesi-Hildebrand method, nonlinear Program, program based mathematical calculation of non-linear changes in the conductivity data respectively.

Inclusion Complexes (ICs)	Application of (K_a) to Van't Hoff equation		Application of (K_a^θ) to Van't Hoff equation		Application of (K_a^C) to Van't Hoff equation	
PEH + α-CD	ΔH^0 (KJ mol^{-1})	-28.93	$\Delta H^{0\theta}$ (KJ mol^{-1})	-30.85	ΔH^{0C} (KJ mol^{-1})	-31.22
	ΔS^0 (J mol^{-1} K^{-1})	-31.69	$\Delta S^{0\theta}$ (J mol^{-1} K^{-1})	-38.20	ΔS^{0C} (J mol^{-1} K^{-1})	-39.50
	ΔG^0 (KJ mol^{-1})	-19.49	$\Delta G^{0\theta}$ (KJ mol^{-1})	-19.46	ΔG^{0C} (KJ mol^{-1})	-19.44
PEH + β-CD	ΔH^0 (KJ mol^{-1})	-40.15	$\Delta H^{0\theta}$ (KJ mol^{-1})	-36.82	ΔH^{0C} (KJ mol^{-1})	-38.91
	ΔS^0 (J mol^{-1} K^{-1})	-66.01	$\Delta S^{0\theta}$ (J mol^{-1} K^{-1})	-55.79	ΔS^{0C} (J mol^{-1} K^{-1})	-62.52
	ΔG^0 (KJ mol^{-1})	-20.47	$\Delta G^{0\theta}$ (KJ mol^{-1})	-20.19	ΔG^{0C} (KJ mol^{-1})	-20.27
SNP + α-CD	ΔH^0 (KJ mol^{-1})	-38.72	$\Delta H^{0\theta}$ (KJ mol^{-1})	-43.26	ΔH^{0C} (KJ mol^{-1})	-41.25
	ΔS^0 (J mol^{-1} K^{-1})	-61.54	$\Delta S^{0\theta}$ (J mol^{-1} K^{-1})	-76.63	ΔS^{0C} (J mol^{-1} K^{-1})	-70.04
	ΔG^0 (KJ mol^{-1})	-20.37	$\Delta G^{0\theta}$ (KJ mol^{-1})	-20.41	ΔG^{0C} (KJ mol^{-1})	-20.37
SNP + β-CD	ΔH^0 (KJ mol^{-1})	-40.81	$\Delta H^{0\theta}$ (KJ mol^{-1})	-48.37	ΔH^{0C} (KJ mol^{-1})	-46.89
	ΔS^0 (J mol^{-1} K^{-1})	-66.11	$\Delta S^{0\theta}$ (J mol^{-1} K^{-1})	-91.96	ΔS^{0C} (J mol^{-1} K^{-1})	-87.24

	ΔG^0 (KJ mol^{-1})	-21.10	$\Delta G^{0\theta}$ (KJ mol^{-1})	-20.95	ΔG^{0C} (KJ mol^{-1})	-20.88

Mean errors in variables are as follows: ΔH^0=±0.01 kJ mol^{-1}; ΔS^0 =±0.01 J $mol^{-1}K^{-1}$; ΔG^0 = ±0.01 kJ mol^{-1}; $\Delta H^{0\theta}$= ±0.01 kJ mol^{-1}; $\Delta S^{0\theta}$ = ±0.01 J $mol^{-1}K^{-1}$; $\Delta G^{0\theta}$ = ±0.01 kJ mol^{-1}; ΔH^{0C}= ±0.01 kJ mol^{-1}; ΔS^{0C} = ±0.01 J $mol^{-1}K^{-1}$; ΔG^{0C} = ±0.01 kJ mol^{-1}.

Table S5. Data for surface tension of aqueous (SNP+α-CD) and (SNP+β-CD) systems at 298.15 K[a].

SNP+α-CD				SNP+β-CD			
SNP (mL)	α-CD (mL)	Concentration of α-CD (mM)	Surface tension (mNm^{-1})	SNP (mL)	β-CD (mL)	Concentration of β-CD (mM)	Surface tension (mNm^{-1})
10	0	0.0000	62.2	10	0	0.0000	62.2
10	1	0.9091	63.2	10	1	0.9091	63.5
10	2	1.6667	64.4	10	2	1.6667	64.7
10	3	2.3077	65.3	10	3	2.3077	65.7
10	4	2.8571	66.2	10	4	2.8571	66.5
10	5	3.3333	66.9	10	5	3.3333	67.3
10	6	3.7500	67.8	10	6	3.7500	68.1
10	7	4.1176	68.5	10	7	4.1176	68.8
10	8	4.4444	69.0	10	8	4.4444	69.3
10	9	4.7368	69.5	10	9	4.7368	69.8
10	10	5.0000	70.0	10	10	5.0000	70.3
10	11	5.2381	70.2	10	11	5.2381	70.5
10	12	5.4545	70.3	10	12	5.4545	70.6
10	13	5.6522	70.4	10	13	5.6522	70.7
10	14	5.8333	70.5	10	14	5.8333	70.8
10	15	6.0000	70.6	10	15	6.0000	70.9

Table S6. Data for surface tension of aqueous (PEH+α-CD) and (PEH+β-CD) systems at 298.15 K[a]

PEH+α-CD				PEH+β-CD			
PEH (mL)	α-CD (mL)	Concentration of α-CD (mM)	Surface tension (mNm^{-1})	PEH (mL)	β-CD (mL)	Concentration of β-CD (mM)	Surface tension (mNm^{-1})
10	0	0.0000	52.6	10	0	0.0000	52.6
10	1	0.9091	55.6	10	1	0.9091	55.9
10	2	1.6667	58.4	10	2	1.6667	58.7
10	3	2.3077	60.9	10	3	2.3077	61.2
10	4	2.8571	62.7	10	4	2.8571	63.1
10	5	3.3333	64.6	10	5	3.3333	64.9
10	6	3.7500	65.9	10	6	3.7500	66.2
10	7	4.1176	67.3	10	7	4.1176	67.6
10	8	4.4444	68.4	10	8	4.4444	68.7
10	9	4.7368	69.5	10	9	4.7368	69.8
10	10	5.0000	70.3	10	10	5.0000	70.6
10	11	5.2381	70.4	10	11	5.2381	70.7
10	12	5.4545	70.5	10	12	5.4545	70.8
10	13	5.6522	70.6	10	13	5.6522	70.9
10	14	5.8333	70.7	10	14	5.8333	71.0
10	15	6.0000	70.8	10	15	6.0000	71.1

Table S7. UV-vis spectroscopic data for the Benesi-Hildebrand double reciprocal plot of (SNP+α-CD) system at 298.15 to 308.15 K[a].

Temp (K[a])	SNP (μM)	α-CD (μM)	Ao	A	ΔA	1/[α-CD] (M^{-1})	1/ΔA	Intercept	Slope	Ka ($M^{-1}\times10^{-3}$)
	50	20		0.3659	0.0135	0.0500	74.3494			
	50	30		0.3715	0.0191	0.0333	52.4384			
	50	40		0.3763	0.0238	0.0250	41.9639			
298.15	50	50	0.3524	0.3829	0.0304	0.0200	32.8515	4.0631	1429.4	2.84
	50	60		0.3875	0.0351	0.0167	28.5063			
	50	70		0.3953	0.0429	0.0143	23.3209			
	50	80		0.4011	0.0487	0.0125	20.5550			
	50	20		0.3651	0.0127	0.0500	78.9889			
	50	30		0.3704	0.0180	0.0333	55.6793			
	50	40		0.3751	0.0227	0.0250	44.1112			
303.15	50	50	0.3524	0.3815	0.0291	0.0200	34.4234	3.4735	1536.2	2.26
	50	60		0.3867	0.0343	0.0167	29.1545			
	50	70		0.3938	0.0414	0.0143	24.1501			
	50	80		0.3985	0.0461	0.0125	21.7004			
	50	20		0.3645	0.0121	0.0500	82.9187			
	50	30		0.3694	0.0170	0.0333	58.9623			
	50	40		0.3745	0.0221	0.0250	45.3104			
308.15	50	50	0.3524	0.3807	0.0283	0.0200	35.3982	2.8374	1630.9	1.74
	50	60		0.3858	0.0334	0.0167	29.9401			
	50	70		0.3927	0.0403	0.0143	24.8092			
	50	80		0.3965	0.0441	0.0125	22.6850			

[a]Standard uncertainties in temperature *u* are: *u*(T) = ±0.01 K.

Table S8. UV-vis spectroscopic data for the Benesi-Hildebrand double reciprocal plot of (SNP+β-CD) systems at 298.15 to 308.15 K[a].

Temp (K[a])	SNP (μM)	β-CD (μM)	Ao	A	ΔA	1/[β-CD] (M^{-1})	1/ΔA	Intercept	Slope	Ka ($M^{-1}\times10^{-3}$)
	50	20		0.3666	0.0142	0.0500	70.6714			
	50	30		0.3723	0.0199	0.0333	50.3018			
	50	40		0.3775	0.0251	0.0250	39.8724			
298.15	50	50	0.3524	0.3840	0.0315	0.0200	31.7158	4.6812	1341.6	3.82
	50	60		0.3889	0.0365	0.0167	27.4198			
	50	70		0.3961	0.0437	0.0143	22.8833			
	50	80		0.4015	0.0491	0.0125	20.3666			
	50	20		0.3656	0.0131	0.0500	76.0514			
	50	30		0.3712	0.0188	0.0333	53.3049			
	50	40		0.3762	0.0238	0.0250	42.0698			
303.15	50	50	0.3524	0.3826	0.0302	0.0200	33.1675	4.188	1453.5	2.88
	50	60		0.3878	0.0354	0.0167	28.2486			
	50	70		0.3938	0.0414	0.0143	24.1721			
	50	80		0.3979	0.0455	0.0125	21.9925			
	50	20		0.3651	0.0127	0.0500	78.9889			
	50	30		0.3707	0.0183	0.0333	54.7645			
	50	40		0.3755	0.0231	0.0250	43.3463			
308.15	50	50	0.3524	0.3817	0.0293	0.0200	34.1880	3.6968	1520.5	2.28
	50	60		0.3869	0.0345	0.0167	28.9855			
	50	70		0.3931	0.0407	0.0143	24.5654			
	50	80		0.3974	0.0450	0.0125	22.2311			

[a]Standard uncertainties in temperature *u* are: *u*(T) = ±0.01 K.

Table S9. UV-vis spectroscopic data for the Benesi-Hildebrand double reciprocal plot of (PEH+α-CD) system at 298.15 to 308.15 K[a].

Temp (K[a])	PEH (μM)	α-CD (μM)	Ao	A	ΔA	1/[α-CD] (M^{-1})	1/ΔA	Intercept	Slope	Ka ($M^{-1}\times10^{-3}$)
	50	20		0.3437	0.0134	0.0500	74.9064			
	50	30		0.3491	0.0188	0.0333	53.135			
	50	40		0.3555	0.0252	0.0250	39.7456			
298.15	50	50	0.3303	0.3618	0.0315	0.0200	31.746	3.1053	1453.1	2.14
	50	60		0.3676	0.0373	0.0167	26.8312			
	50	70		0.3720	0.0417	0.0143	23.9866			
	50	80		0.3779	0.0476	0.0125	21.0128			
	50	20		0.3430	0.0127	0.0500	79.0514			
	50	30		0.3481	0.0178	0.0333	56.1167			
	50	40		0.3542	0.0239	0.0250	41.9111			
303.15	50	50	0.3303	0.3603	0.0300	0.0200	33.3333	2.7682	1546.3	1.79
	50	60		0.3661	0.0358	0.0167	27.9564			
	50	70		0.3704	0.0401	0.0143	24.9439			
	50	80		0.3764	0.0461	0.0125	21.6967			
	50	20		0.3423	0.0120	0.0500	83.682			
	50	30		0.3471	0.0168	0.0333	59.453			
	50	40		0.3531	0.0228	0.0250	43.9367			
308.15	50	50	0.3303	0.3589	0.0286	0.0200	34.965	2.4393	1647.2	1.48
	50	60		0.3646	0.0343	0.0167	29.18			
	50	70		0.3688	0.0385	0.0143	25.9808			
	50	80		0.3741	0.0438	0.0125	22.8363			

[a]Standard uncertainties in temperature *u* are: *u*(T) = ±0.01 K.

Table S10. UV-vis spectroscopic data for the Benesi-Hildebrand double reciprocal plot of (PEH+β-CD) systems at 298.15 to 308.15 K[a].

Temp (K[a])	PEH (μM)	β-CD (μM)	Ao	A	ΔA	1/[β-CD] (M^{-1})	1/ΔA	Intercept	Slope	Ka ($M^{-1}\times10^{-3}$)
298.15	50	20	0.3303	0.3444	0.0141	0.0500	71.1744	4.037	1360.8	2.97
	50	30		0.3499	0.0196	0.0333	50.9684			
	50	40		0.3563	0.0260	0.0250	38.5208			
	50	50		0.3626	0.0323	0.0200	30.9598			
	50	60		0.3686	0.0383	0.0167	26.1301			
	50	70		0.3729	0.0426	0.0143	23.4797			
	50	80		0.3784	0.0481	0.0125	20.7943			
303.15	50	20	0.3303	0.3434	0.0131	0.0500	76.6284	3.3425	1481.7	2.26
	50	30		0.3487	0.0184	0.0333	54.2888			
	50	40		0.3549	0.0246	0.0250	40.7166			
	50	50		0.3611	0.0308	0.0200	32.4675			
	50	60		0.3667	0.0364	0.0167	27.4801			
	50	70		0.3716	0.0413	0.0143	24.2189			
	50	80		0.3755	0.0452	0.0125	22.1288			
308.15	50	20	0.3303	0.3428	0.0125	0.0500	80.3213	2.8083	1573.5	1.79
	50	30		0.3477	0.0174	0.0333	57.4053			
	50	40		0.3539	0.0236	0.0250	42.4448			
	50	50		0.3597	0.0294	0.0200	34.0136			
	50	60		0.3655	0.0352	0.0167	28.4333			
	50	70		0.3702	0.0399	0.0143	25.0689			
	50	80		0.3752	0.0449	0.0125	22.2767			

[a]Standard uncertainties in temperature *u* are: *u*(T) = ±0.01 K.

Table S11. Spectro-fluorimetric data for the Benesi-Hildebrand double reciprocal plot of (SNP+α-CD) system at 298.15 K[a].

SNP (μM)	α-CD (μM)	I_0	I	I-I_0	1/[α-CD] (M^{-1})	1/ΔI ($\times10^5$)	Intercept ($\times10^6$)	Slope ($\times10^{10}$)	Ka ($M^{-1}\times10^{-3}$)
50	20		1021722.0	31879.4	0.0500	3.1368			
50	30		1036798.0	46955.4	0.0333	2.1297			
50	40		1049428.0	59585.4	0.0250	1.6783			
50	50	989842.6	1064623.0	74780.4	0.0200	1.3372	1.70	5.93	2.87
50	60		1073962.6	84120.0	0.0167	1.1888			
50	70		1088841.6	98999.0	0.0143	1.0101			
50	80		1101249.0	111406.4	0.0125	0.8976			

[a]Standard uncertainties in temperature *u* are: *u*(T) = ±0.01 K.

Table S12. Spectro-fluorimetric data for the Benesi-Hildebrand double reciprocal plot of (SNP+β-CD) system at 298.15 K[a].

SNP (μM)	β-CD (μM)	I_0	I	I-I_0	1/[β-CD] (M^{-1})	1/ΔI ($\times10^5$)	Intercept ($\times10^6$)	Slope ($\times10^{10}$)	Ka ($M^{-1}\times10^{-3}$)
50	20		1032096	42253.4	0.0500	2.3667			
50	30		1050436	60593.4	0.0333	1.6503			
50	40		1071194	81351.4	0.0250	1.2292			
50	50	989842.6	1086066	96223.4	0.0200	1.0392	1.64	4.40	3.73
50	60		1102000	112157.4	0.0167	0.8916			
50	70		1115745	125902.4	0.0143	0.7943			
50	80		1125567	135724.4	0.0125	0.7368			

[a]Standard uncertainties in temperature *u* are: *u*(T) = ±0.01 K.

Table S13. Spectro-fluorimetric data for the Benesi-Hildebrand double reciprocal plot of (PEH+α-CD) system at 298.15 K[a].

PEH (μM)	α-CD (μM)	I_0	I	$I-I_0$	1/[α-CD] (M^{-1})	1/ΔI ($\times10^5$)	Intercept ($\times10^6$)	Slope ($\times10^{10}$)	Ka ($M^{-1}\times10^{-3}$)
50	20		1333970	30740	0.0500	3.2531			
50	30		1349246	46016	0.0333	2.1732			
50	40		1360816	57586	0.0250	1.7365			
50	50	1303230	1374011	70781	0.0200	1.4128	1.38	6.23	2.21
50	60		1387350	84120	0.0167	1.1888			
50	70		1402229	98999	0.0143	1.0101			
50	80		1416037	112807	0.0125	0.8865			

[a]Standard uncertainties in temperature *u* are: *u*(T) = ±0.01 K.

Table S14. Spectro-fluorimetric data for the Benesi-Hildebrand double reciprocal plot of (PEH+β-CD) system at 298.15 K[a].

PEH (μM)	β-CD (μM)	I_0	I	$I-I_0$	1/[β-CD] (M^{-1})	1/ΔI ($\times10^5$)	Intercept ($\times10^6$)	Slope ($\times10^{10}$)	Ka ($M^{-1}\times10^{-3}$)
50	20		1340002	36772	0.0500	2.7195			
50	30		1358291	55061	0.0333	1.8162			
50	40		1375178	71948	0.0250	1.3899			
50	50	1303230	1391725	88495	0.0200	1.1300	1.48	5.09	2.91
50	60		1399947	96717	0.0167	1.0339			
50	70		1416229	112999	0.0143	0.8850			
50	80		1428037	124807	0.0125	0.8012			

[a]Standard uncertainties in temperature *u* are: *u*(T) = ±0.01 K.

Table S15. Data of the van't Hoff equation for calculation of thermodynamic parameters ΔH^o, ΔS^o and ΔG^0 of different (SNP+α-CD) and (SNP+β-CD) inclusion complexes.

HOST	T(K[a])	1/T	Ka ($M^{-1}\times10^{-3}$)	lnKa	Slope	Intercept	ΔH^0 (KJ mol^{-1})	ΔS^0 (J mol^{-1} K^{-1})	ΔG^0 (KJ mol^{-1})
	303.15	0.0033	2.84	7.9527					
α-CD	308.15	0.0032	2.26	7.7236	4657.0	-7.4026	-38.72	-61.55	-20.37
	313.15	0.0032	1.74	7.4619					
	303.15	0.0033	3.82	8.2469					
β-CD	308.15	0.0032	2.88	7.9663	4908.7	-7.9513	-40.81	-66.11	-21.1
	313.15	0.0032	2.28	7.7300					

Table S16. Data of the van't Hoff equation for calculation of thermodynamic parameters ΔH^o, ΔS^o and ΔG^0 of different (PEH+α-CD) and (PEH+β-CD) inclusion complexes.

HOST	T(K[a])	1/T	Ka ($M^{-1}\times10^{-3}$)	lnKa	Slope	Intercept	ΔH^0 (KJ mol^{-1})	ΔS^0 (J mol^{-1} K^{-1})	ΔG^0 (KJ mol^{-1})
	303.15	0.0033	2.14	7.6671					
α-CD	308.15	0.0032	1.79	7.4902	3480.6	-3.8114	-28.94	-31.69	-19.49
	313.15	0.0032	1.48	3.3004					
	303.15	0.0033	2.97	7.9958					
β-CD	308.15	0.0032	2.26	7.7216	4829.2	-7.9393	-40.15	-66.01	-20.47
	313.15	0.0032	1.79	7.4872					

Table S17. Data of the van't Hoff equation for calculation of thermodynamic parameters $\Delta H^{\theta 0}$, $\Delta S^{\theta 0}$ and $\Delta G^{\theta 0}$ of different (SNP+α-CD) and (SNP+β-CD) inclusion complexes.

HOST	T(K[a])	1/T	K_a^θ ($M^{-1}\times10^{-3}$)	$\ln K_a^\theta$	Slope	Intercept	$\Delta H^{\theta 0}$ (KJ mol^{-1})	$\Delta S^{\theta 0}$ (J mol^{-1} K^{-1})	$\Delta G^{\theta 0}$ (KJ mol^{-1})
	303.15	0.0033	2.82	7.9445					
α-CD	308.15	0.0032	2.15	7.6732	5203.0	-9.2162	-43.26	-76.63	-20.41
	313.15	0.0032	1.63	7.3963					
	303.15	0.0033	3.41	8.1345					
β-CD	308.15	0.0032	2.46	7.8079	5817.1	-11.06	-48.37	-91.96	-20.95
	313.15	0.0032	1.85	7.5219					

Table S18. Data of the van't Hoff equation for calculation of thermodynamic parameters $\Delta H^{\theta 0}$, $\Delta S^{\theta 0}$ and $\Delta G^{\theta 0}$ of different (PEH+α-CD) and (PEH+β-CD) inclusion complexes.

HOST	T(K^a)	1/T	K_a^{θ} ($M^{-1}\times10^{-3}$)	$\ln K_a^{\theta}$	Slope	Intercept	$\Delta H^{\theta 0}$ (KJ mol^{-1})	$\Delta S^{\theta 0}$ (J mol^{-1} K^{-1})	$\Delta G^{\theta 0}$ (KJ mol^{-1})
	303.15	0.0033	2.07	7.6353					
α-CD	308.15	0.0032	1.74	7.4616	3,710.0	-4.5946	-30.85	-38.20	-19.46
	313.15	0.0032	1.40	7.2442					
	303.15	0.0033	2.71	7.9047					
β-CD	308.15	0.0032	2.10	7.6497	4,428.7	-6.7102	-36.82	-55.79	-20.19
	313.15	0.0032	1.70	7.4384					

Table S19. Data of the van't Hoff equation for calculation of thermodynamic parameters ΔH^{C0}, ΔS^{C0} and $\Delta G^{C0}$of different (SNP+α-CD) and (SNP+β-CD) inclusion complexes.

HOST	T(K^a)	1/T	K_a^{C0} ($M^{-1}\times10^{-3}$)	$\ln K_a^{C0}$	Slope	Intercept	ΔH^{C0} (KJ mol^{-1})	ΔS^{C0} (J mol^{-1} K^{-1})	ΔG^{C0} (KJ mol^{-1})
	303.15	0.0033	2.80	7.9374					
α-CD	308.15	0.0032	2.18	7.6871	4961.5	-8.4239	-41.25	-70.04	-20.37
	313.15	0.0032	1.66	7.4146					
	303.15	0.0033	3.35	8.1167					
β-CD	308.15	0.0032	2.42	7.7915	5639.2	-10.493	-46.89	-87.24	-20.88
	313.15	0.0032	1.85	7.5229					

Table S20. Data of the van't Hoff equation for calculation of thermodynamic parameters ΔH^{C0}, ΔS^{C0} and $\Delta G^{C0}$of different (PEH+α-CD) and (PEH+β-CD) inclusion complexes.

HOST	T(K^a)	1/T	K_a^{C0} ($M^{-1}\times10^{-3}$)	$\ln K_a^{C0}$	Slope	Intercept	ΔH^{C0} (KJ mol^{-1})	ΔS^{C0} (J mol^{-1} K^{-1})	ΔG^{C0} (KJ mol^{-1})
	303.15	0.0033	2.05	7.6256					
α-CD	308.15	0.0032	1.72	7.4501	3,754.3	-4.7505	-31.22	-39.50	-19.44
	313.15	0.0032	1.38	7.2298					
β-CD	303.15	0.0033	2.75	7.9194	4,679.3	-7.5194	-38.91	-62.52	-20.27

308.15	0.0032	2.12	7.6592
313.15	0.0032	1.68	7.4265

Table S21. ^{1}H NMR data of the pure α-Cyclodextrin, β-Cyclodextrin and the solid inclusion complexes.

α-Cyclodextrin (400 MHz, Solvent: D_2O), δ/ppm	β-Cyclodextrin (400 MHz, Solvent: D_2O), δ/ppm
3.49-3.51 (6H, t, =8.00 Hz), 3.53-3.57 (6H, dd, J = 3.00, 10.00 Hz), 3.74-3.83 (18H, m), 3.87-3.91 (6H, t, J = 8Hz), 4.95-4.96 (6H, d, J = 4.00 Hz)	3.49-3.54 (7H, t, J = 10.00 Hz), 3.56-3.60 (7H, dd, J = 9.6 Hz, 3.2 Hz), 3.79-3.85 (21H, m), 3.87-3.92 (7H, t, J = 9.2 Hz), 5.01-5.020 (7H, d, J = 3.6 Hz)
SNP+α-CD inclusion complex (400 MHz, Solvent: D_2O), δ/ppm)	SNP+β-CD inclusion complex (400 MHz, Solvent: D_2O), δ/ppm)
2.439-2.447 (3H, d, J = 2.8 Hz), 2.887-2.981 (1H, m), 2.991-3.012 (2H, dd, J = 3.2, 8.4 Hz), 3.40-3.48 (12H, m), 3.686-3.743 (6H, m), 3.769-3.823 (18H, m), 4.894-4.893 (6H, d, J = 4.0 Hz), 6.617-6.649 (2H, d, J = 12.8 Hz), 7.05-7.079 (2H, d, J = 11.6 Hz)	2.409-2.418 (3H, d, J = 3.6 Hz), 2.778-2.877 (1H, m), 2.891-2.922 (2H, dd, J = 5.6, 8.8 Hz), 3.38-3.49 (14H, m), 3.56-3.60 (7H, m), 3.65 3.77 (21H, m), 4.881-4.890 (7H, d, J = 3.6 Hz), 6.570-6.592 (2H, d, J = 8.8 Hz, 7.034-7.055 (2H, d, J = 8.4 Hz)
PEH+α-CD inclusion complex (400 MHz, Solvent: D_2O), δ/ppm)	PEH+β-CD inclusion complex (400 MHz, Solvent: D_2O), δ/ppm)
2.594-2.602 (3H, d, J = 3.2 Hz), 3.086-3.139 (1H, m), 3.145-3.166 (2H, dd, J = 3.2, 8.4 Hz), 3.39-3.476 (12H, m), 3.680-3.735 (6H, m), 3.761-3.821 (18H, m), 4.83-4.88 (6H, m), 6.754-6.777 (2H, d, J = 9.2 Hz), 7.16-7.18 (2H, d, J = 8 Hz)	2.633-2.641 (3H, d, J = 3.2 Hz), 3.015-3.070 (1H, m), 3.094-3.135 (2H, dd, J = 3.6, 12.8 Hz), 3.40-3.50 (14H, m), 3.61-3.635 (7H, m), 3.692-3.774 (21H, m), 4.929-4.895 (7H, m), 6.69-6.713 (2H, d, J = 9.2 Hz), 7.108-7.129 (2H, d, J = 8.4 Hz)

Table S22. The observed peaks at different m/z with corresponding ions for the solid inclusion complexes.

SNP-α-CD inclusion complex		PEH-α-CD inclusion complex		SNP-β-CD inclusion complex		PEH-β-CD inclusion complex	
m/z	Ion	m/z	Ion	m/z	Ion	m/z	Ion
168.10	$[SNP+H]^+$	168.10	$[PEH+H]^+$	168.10	$[SNP+H]^+$	168.10	$[PEH+H]^+$
190.08	$[SNP+Na]^+$	190.08	$[PEH+Na]^+$	190.08	$[SNP+Na]^+$	190.08	$[PEH+Na]^+$
973.32	$[\alpha\text{-CD}+H]^+$	973.32	$[\alpha\text{-CD}+H]^+$	1135.38	$[\beta\text{-CD}+H]^+$	1135.38	$[\beta\text{-CD}+H]^+$
995.31	$[\alpha\text{-CD}+Na]^+$	995.31	$[\alpha\text{-CD}+Na]^+$	1157.36	$[\beta\text{-CD}+Na]^+$	1157.36	$[\beta\text{-CD}+Na]^+$
1140.42	$[SNP+\alpha\text{-CD}+H]^+$	1140.42	$[PEH+\alpha\text{-CD}+H]^+$	1302.47	$[SNP+\beta\text{-CD}+H]^+$	1302.47	$[PEH+\beta\text{-CD}+H]^+$
1162.40	$[SNP+\alpha\text{-CD}+Na]^+$	1162.40	$[PEH+\alpha\text{-CD}+Na]^+$	1324.45	$[SNP+\beta\text{-CD}+Na]^+$	1324.45	$[PEH+\beta\text{-CD}+Na]^+$

Table S23. Frequencies at FTIR spectra ofα-CD, β-CD, SNP, PEH and solid inclusion complexes.

α-cyclodextrin (α-CD)		β-cyclodextrin (β-CD)	
Wavenumber (cm^{-1})	Group	Wavenumber (cm^{-1})	Group
3408.25	-O-H stretching	3370.21	-O-H stretching
2932.12	-C-H stretching	2916.35	-C-H stretching
1406.17	-C-H and -O-H bending	1412.27	-C-H and -O-H bending
1154.26	C-O-C bending	1158.14	C-O-C bending
1030.19	C-C-O stretching	1026.52	C-C-O stretching

978.23	skeletal vibration involving α-1,4linkage	938.08	skeletal vibration involving α-1,4linkage

Synephrine (SNP)		Phenylephrine hydrochloride (PEH)	
Wavenumber (cm^{-1})	Group	Wavenumber (cm^{-1})	Group
3288.34	-O-H stretching/N-H stretching	3396.45	-O-H stretching/N-H stretching
2878.21	-C-H stretching	2806.31	-C-H stretching
1610.31	C=C stretching	1602.37	C=C stretching
1508.17	Aromatic C=C bending/N-H bending	1458.51	-C-H bending (methyl/methylene)
1264.11	-C-O stretching (phenol)	1272.59	-C-O stretching (phenol)
1096.11	-C-N stretching	1172.23	-C-N stretching
1054.12	-C-O stretching (secondary alcohol)	1070.13	-C-O stretching (secondary alcohol)
782.42	Aromatic -C-H out-of-plane bending	792.26	Aromatic -C-H out-of-plane bending
640.37	Aromatic -C-H out-of-plane bending	700.15	Aromatic -C-H out-of-plane bending
SNP+α-CD		SNP+β-CD	
Wavenumber (cm^{-1})	Group	Wavenumber (cm^{-1})	Group
3374.08	-O-H stretching/N-H stretching	3320.19	-O-H stretching/N-H stretching
2929.29	-C-H stretching	2932.18	-C-H stretching
1628.35	C=C stretching	1604.08	C=C stretching
1333.45	-C-N stretching	1336.35	-C-N stretching

1154.27	-C-O stretching (phenol)	1158.08	-C-O stretching (phenol)
1030.23	-C-O stretching (secondary alcohol)	1032.29	-C-O stretching (secondary alcohol)
707.25	Aromatic -C-H out-of-plane bending	754.36	Aromatic -C-H out-of-plane bending
583.26	Aromatic -C-H out-of-plane bending	582.13	Aromatic -C-H out-of-plane bending

PEH+α-CD		PEH+β-CD	
Wavenumber (cm^{-1})	Group	Wavenumber (cm^{-1})	Group
3370.14	-O-H stretching/N-H stretching	3356.19	-O-H stretching/N-H stretching
2930.31	-C-H stretching	2926.32	-C-H stretching
1616.21	C=C stretching	1618.14	C=C stretching
1398.21	-C-N stretching	1370.35	-C-N stretching
1152.24	-C-O stretching (phenol)	1156.26	-C-O stretching (phenol)
1029.13	-C-O stretching (secondary alcohol)	1030.31	-C-O stretching (secondary alcohol)
716.19	Aromatic -C-H out-of-plane bending	756.39	Aromatic -C-H out-of-plane bending
705.20	Aromatic -C-H out-of-plane bending	685.11	Aromatic -C-H out-of-plane bending

FIGURES

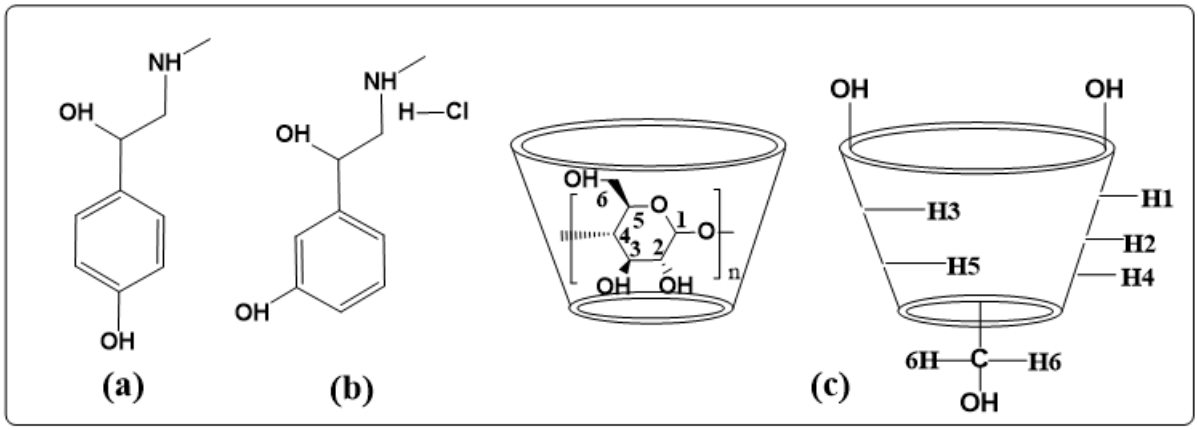

Figure 1. Molecular structures of (a) SNP, (b) PEH, (c) Cyclodextrins, showing the exterior and the interior protons, here, n = 6 to 8 for the α, β and ϒ-cyclodextrins respectively.

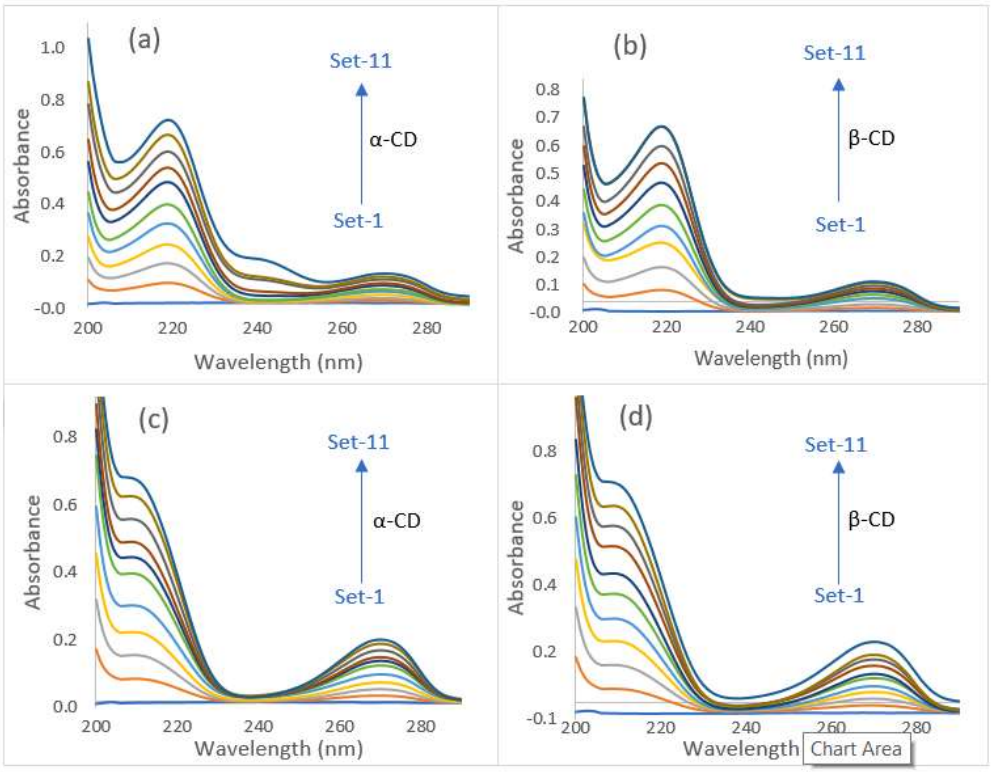

Figure 2. (a,b,c,d) UV-Vis spectra for the generation of Job plots of (a) SNP+α-CD and (b) SNP+β-CD systems at λ_{max} = 209 nm, and (c) PEH+α-CD and (d) PEH+β-CD systems at λ_{max} = 219 nm.

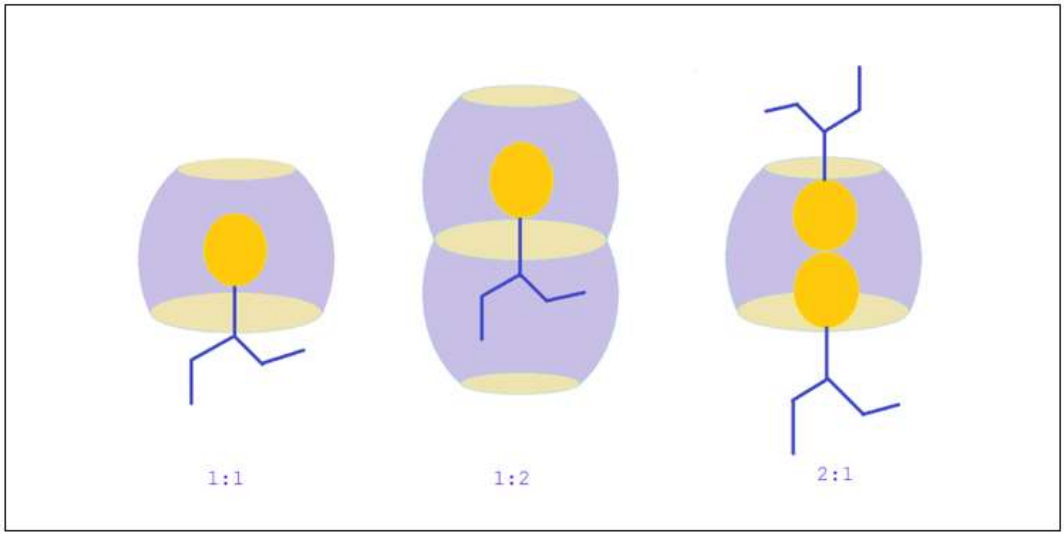

Figure 3. Probable host:guest stoichiometric ratio of the inclusion complexes.

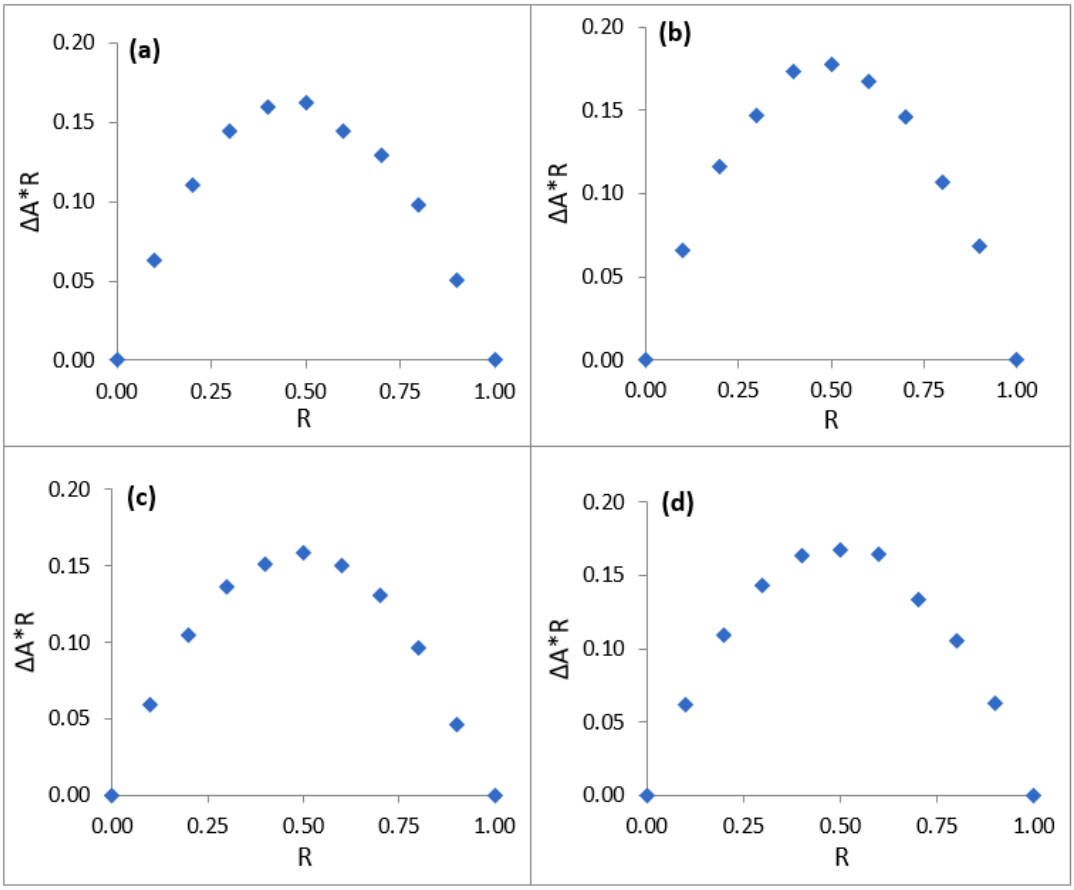

Figure 4. (a,b,c,d) Job plots of the (a) SNP+α-CD and (b) SNP+β-CD systems at λ_{max} = 209 nm and (c) PEH+α-CD and (d) PEH+β-CD systems at λ_{max} = 219 nm, at 298.15K. Δ A = absorbance difference of SNP/PEH without and with CD, R = [DGs]/([DGs] + [CD]).

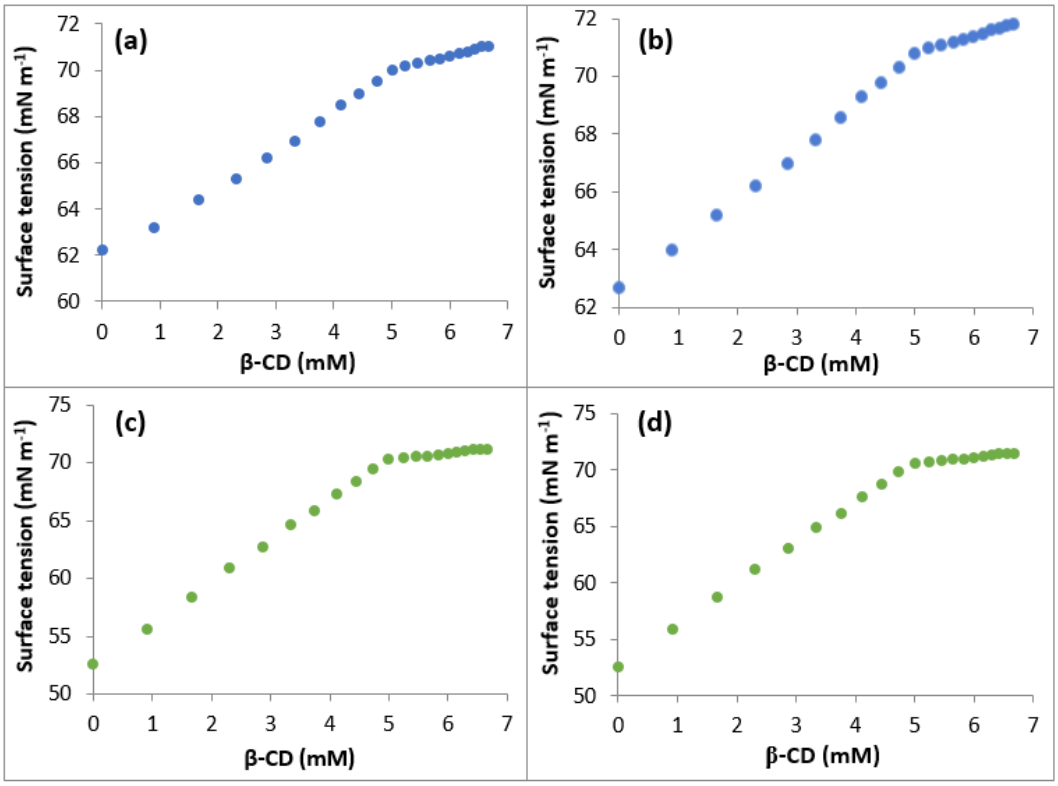

Figure 5. (a,b,c,d) Variations in the surface tension of aqueous SNP with increasing concentration of (a) α-CD, (b) β-CD and the variations in the same of aqueous PEH with increasing concentration of (c) α-CD, (d) β-CD at 298.15 K.

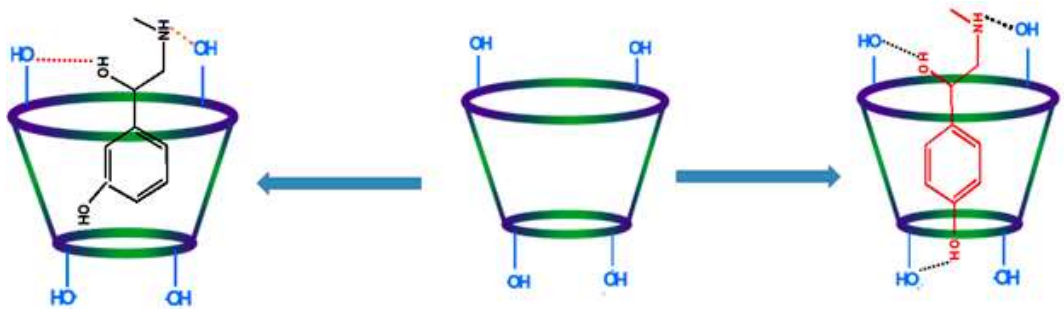

Figure 6. Schematic representation of the host:guest inclusion complexation through the more favorable wider rim of the cyclodextrin molecules.

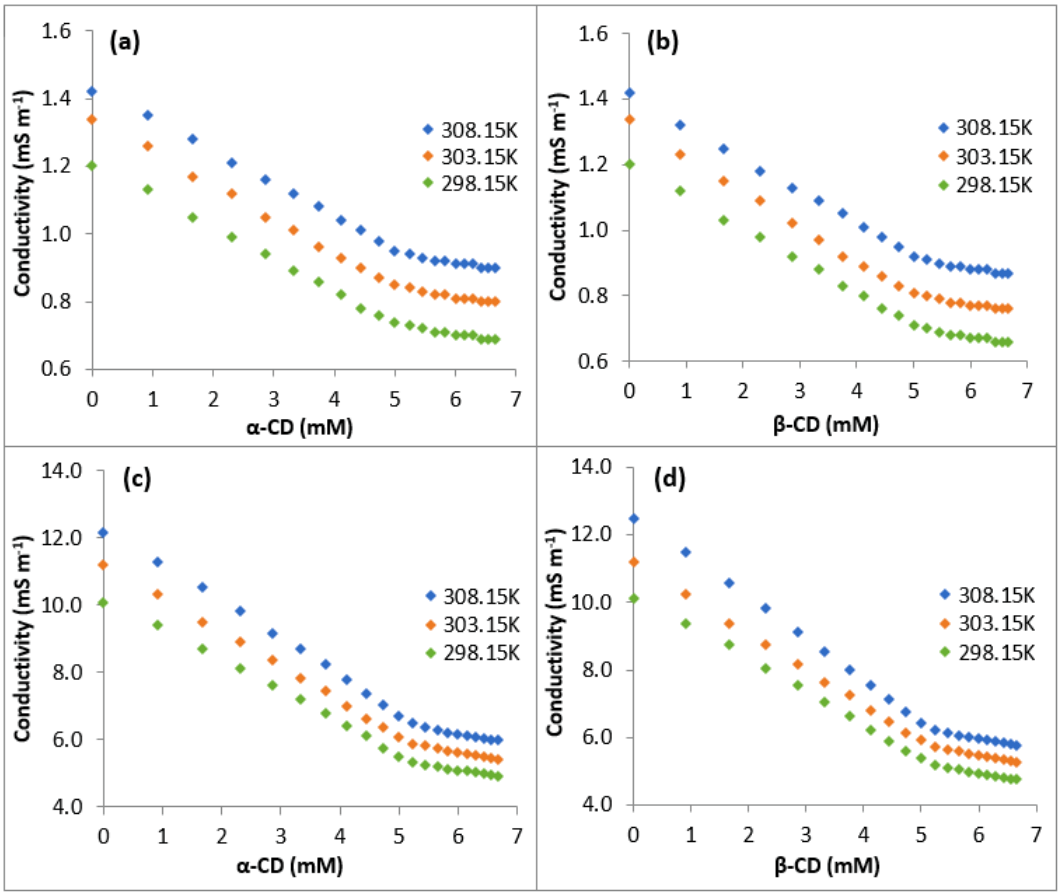

Figure 7. (a,b,c,d) Variations in the conductivity of aqueous SNP with increasing concentration of (a) α-CD, (b) β-CD and the variations in the same of aqueous PEH with increasing concentration of (c) α-CD, (d) β-CD at 298.15 to 308.15 K.

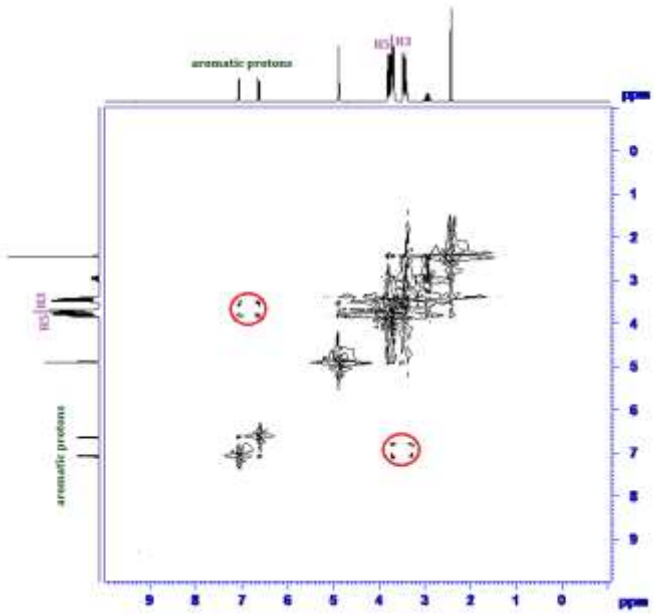

Figure 8. 2D ROESY NMR spectra of the solid (SNP+α-CD) system.

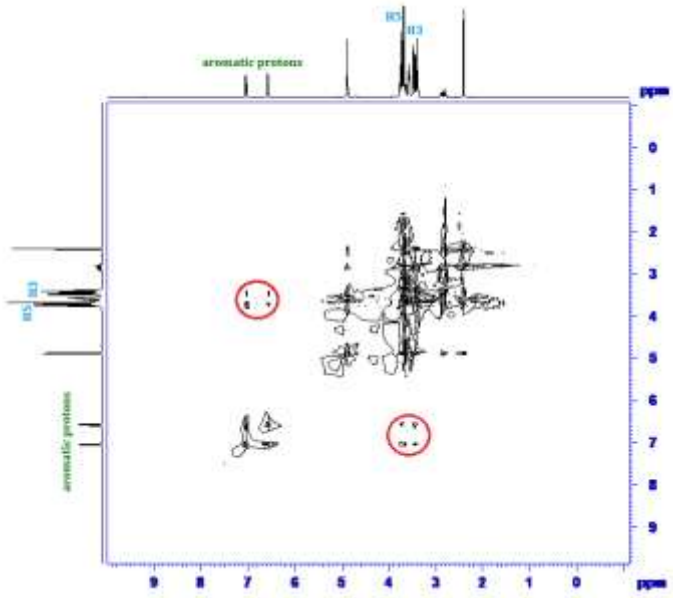

Figure 9. 2D ROESY NMR spectra of the solid (SNP+β-CD) system.

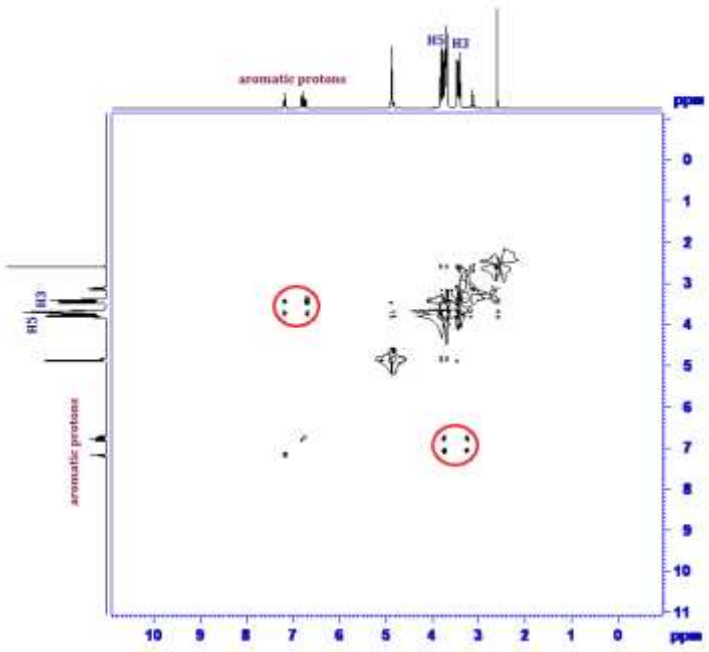

Figure 10. 2D ROESY NMR spectra of the solid (PEH+α-CD) system.

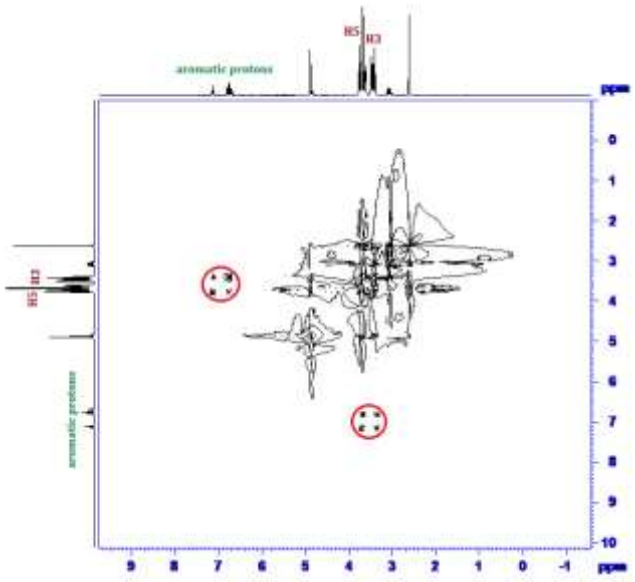

Figure 11. 2D ROESY NMR spectra of the solid (PEH+β-CD) system.

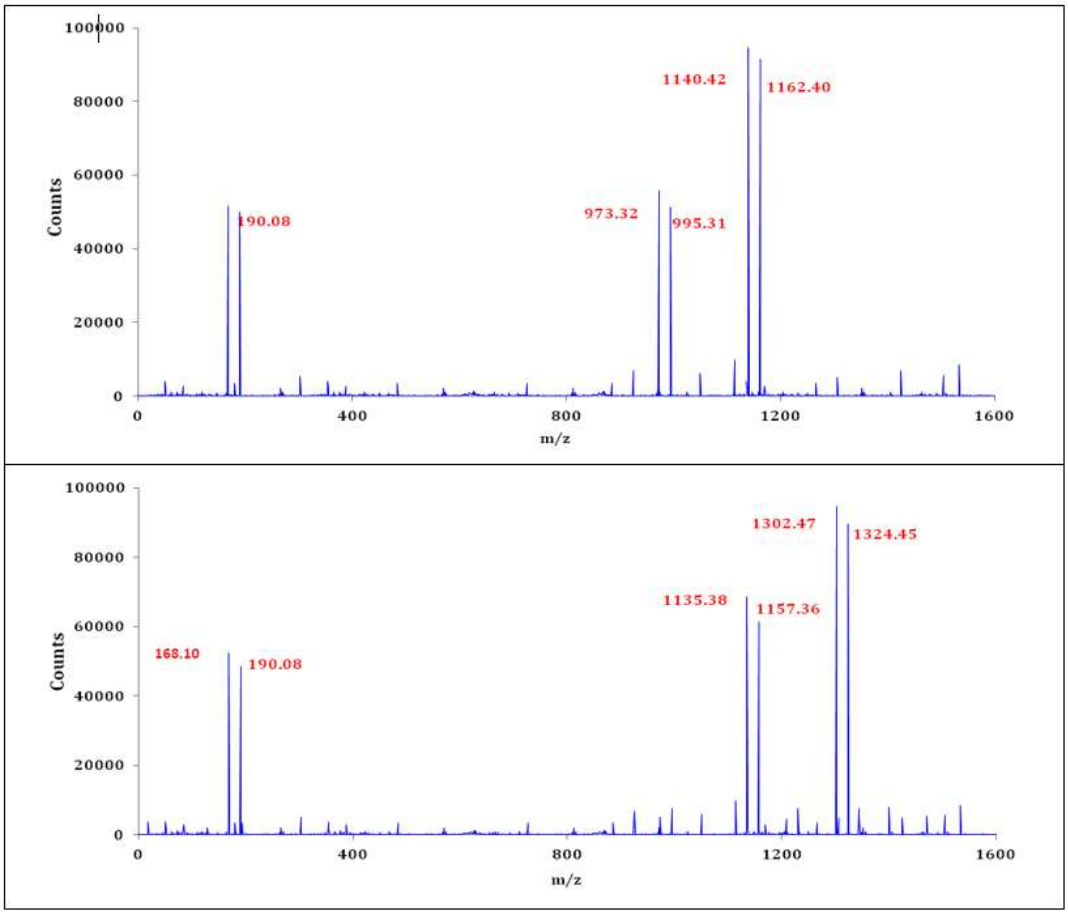

Figure 12. (a,b) HRMS spectra of the (a) SNP+α-CD, PEH+α-CD and (b) SNP+β-CD, PEH+β-CD ICs.

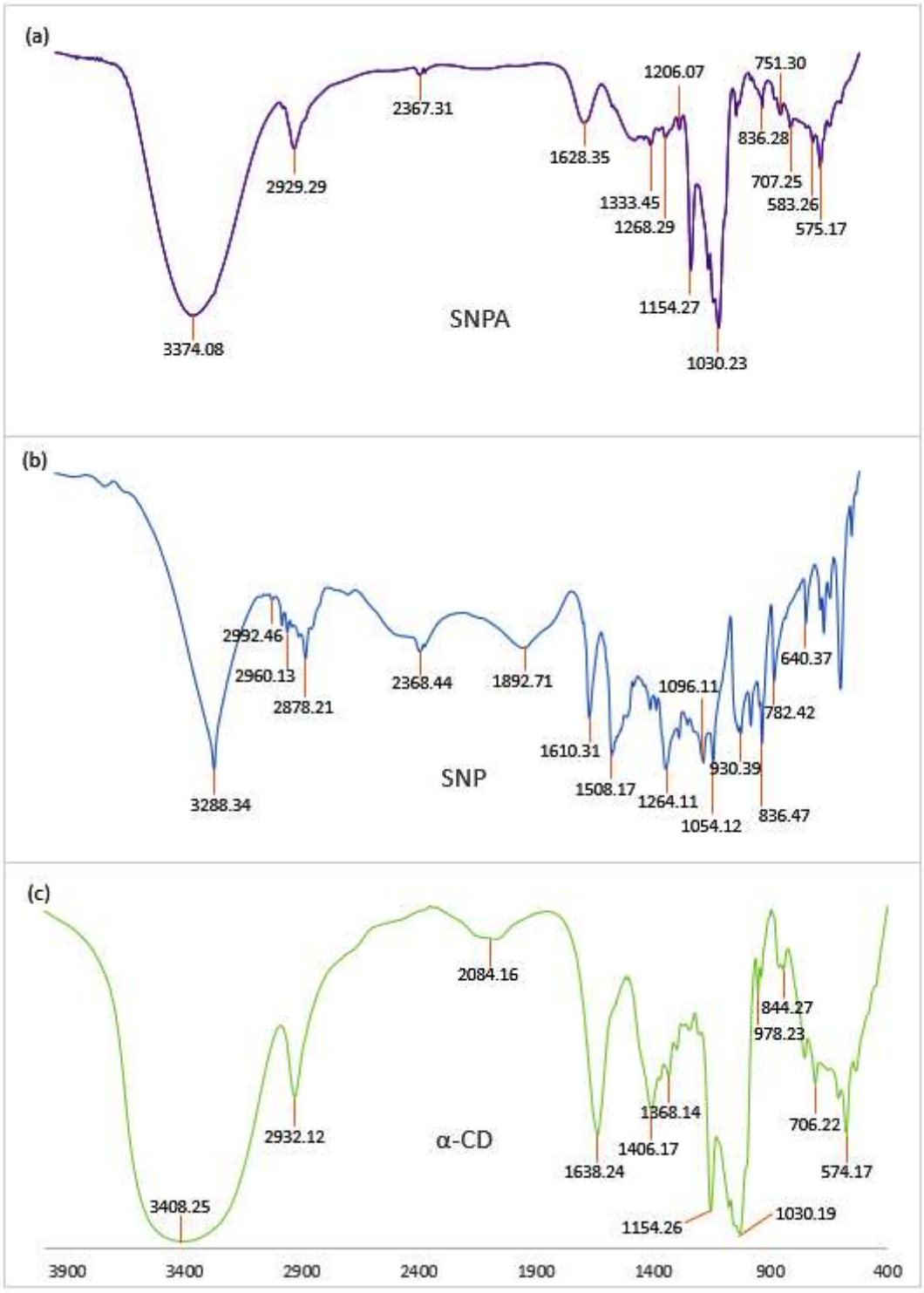

Figure 13. (a,b,c) FTIR spectra of (a) SNP+α-CD, (b) SNP, (c) α-CD.

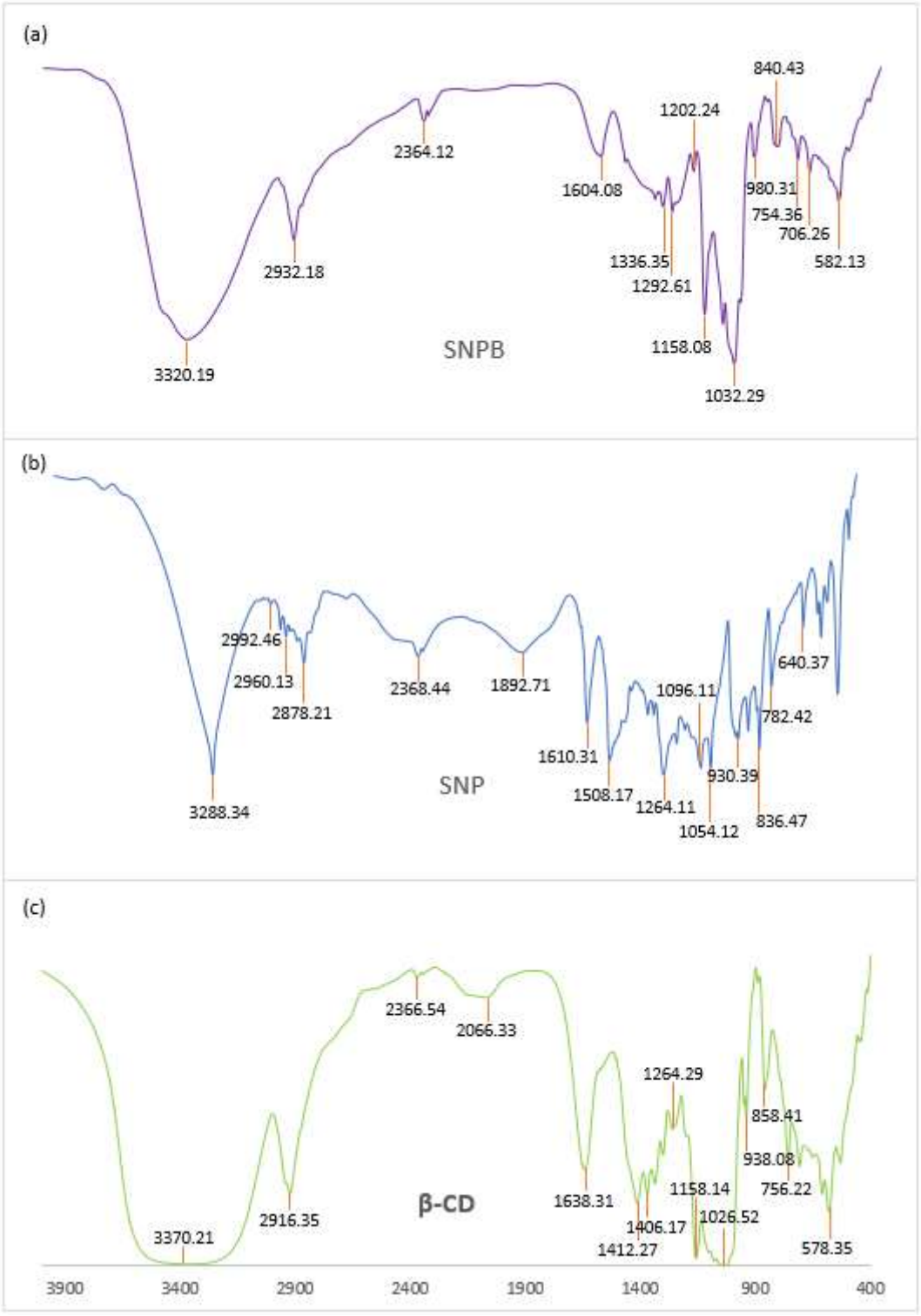

Figure 14. (a,b,c) FTIR spectra of (a) SNP+β-CD, (b) SNP, (c) β-CD.

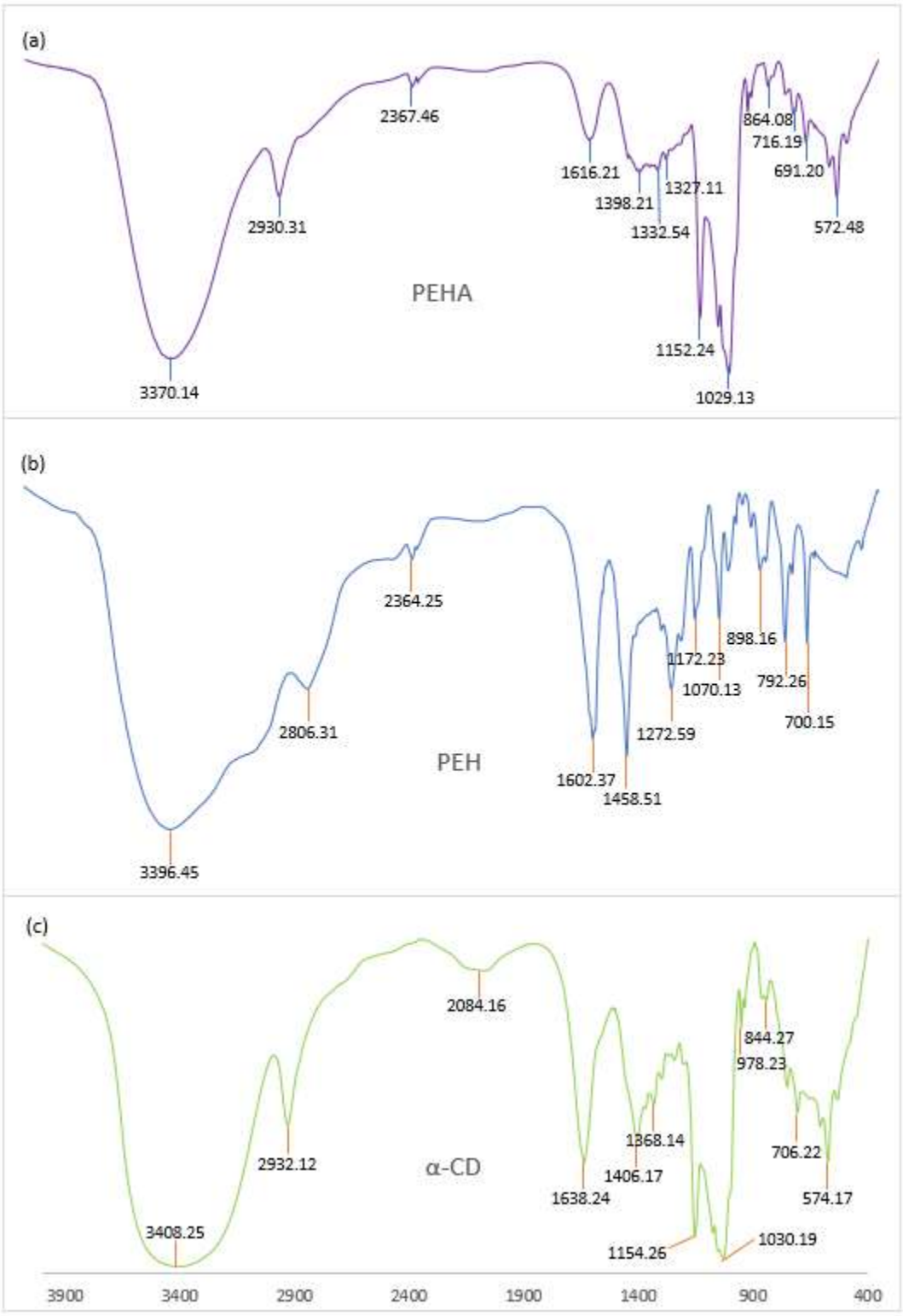

Figure 15. (a,b,c) FTIR spectra of (a) PEH+α-CD, (b) PEH, (c) α-CD.

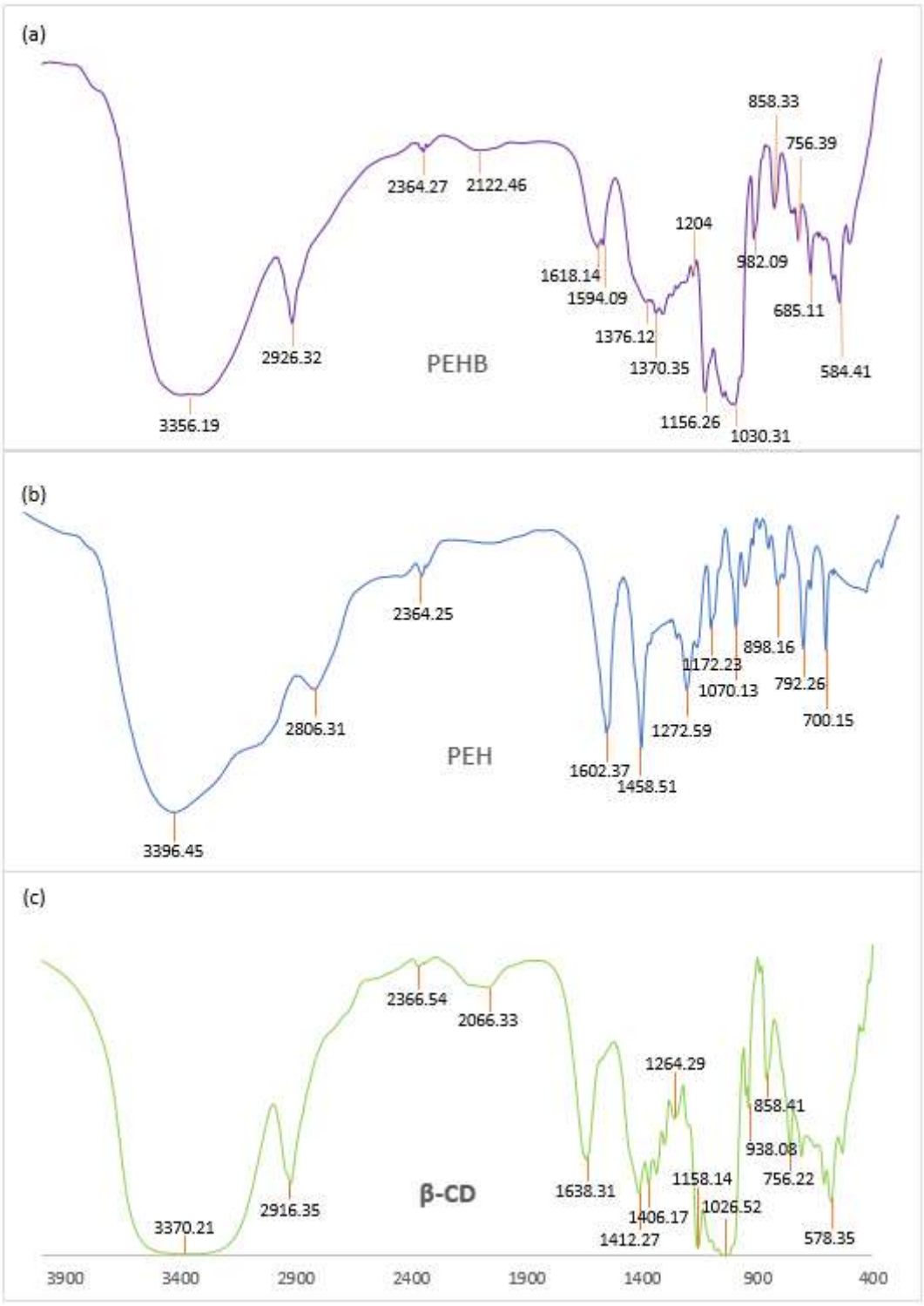

Figure 16. (a,b,c) FTIR spectra of (a) PEH+β-CD, (b) PEH, (c) β-CD.

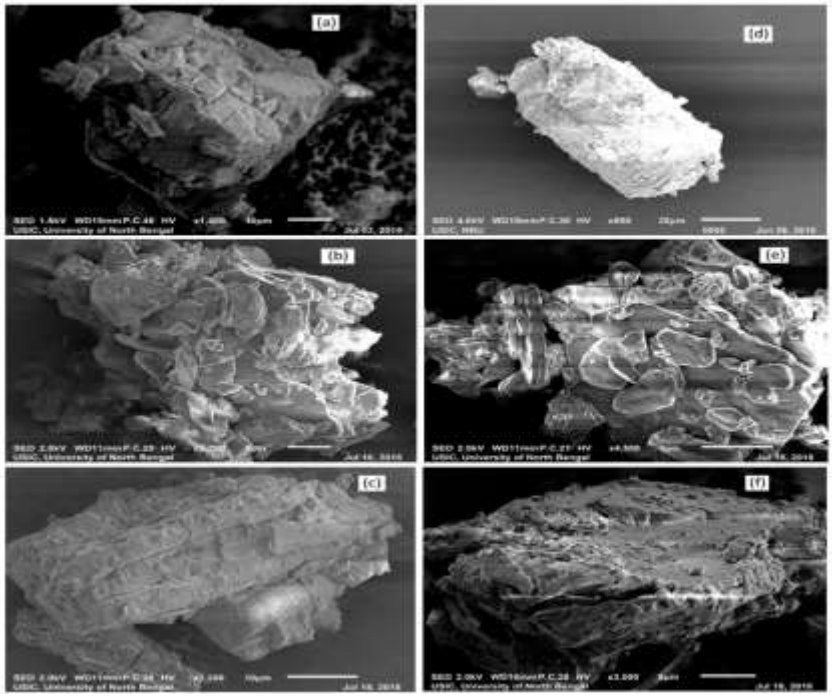

Figure 17. (a,b,c,d,e,f) SEM images of (a) α-CD, (b) (SNP+α-CD) physical mixture, (c) (SNP+α-CD) inclusion complex (d) β-CD, (e) (SNP+ β -CD) physical mixture, (f) (SNP+ β-CD) inclusion complex.

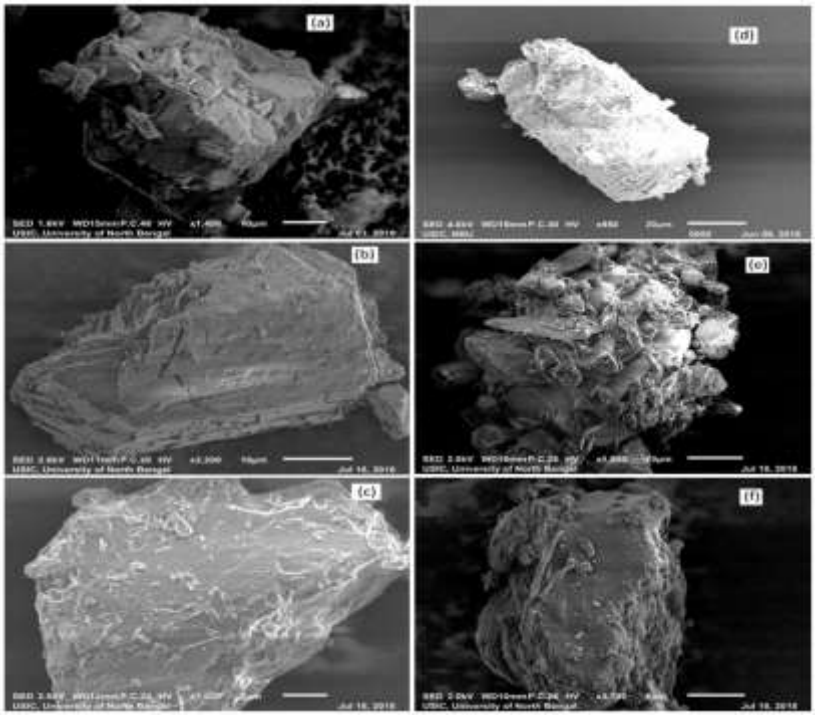

Figure 18. (a,b,c,d,e,f) SEM images of (a) α-CD, (b) (PEH+α-CD) physical mixture, (c) (PEH+α-CD) inclusion complex (d) β-CD, (e) (PEH+β-CD) physical mixture, (f) (PEH+β-CD) inclusion complex.

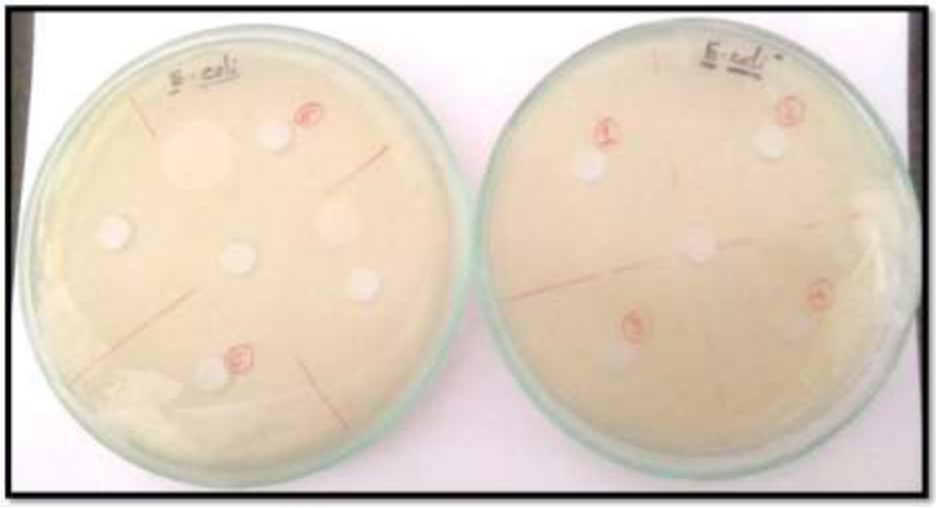

Figure 19. Antimicrobial activity analysis α-CD, β-CD on Gram-negative E. coli by Agar Cup method. No zone of inhibition was observed. Double distilled water was taken as the control. [Marker points (red) for the verified samples taken in the plates (1. SNP, 2. PEHB, 3. PEHA, 4. SNPA, 5. PEH, 6. SNPB) and Marker points (black) for the model organism taken in the plates]

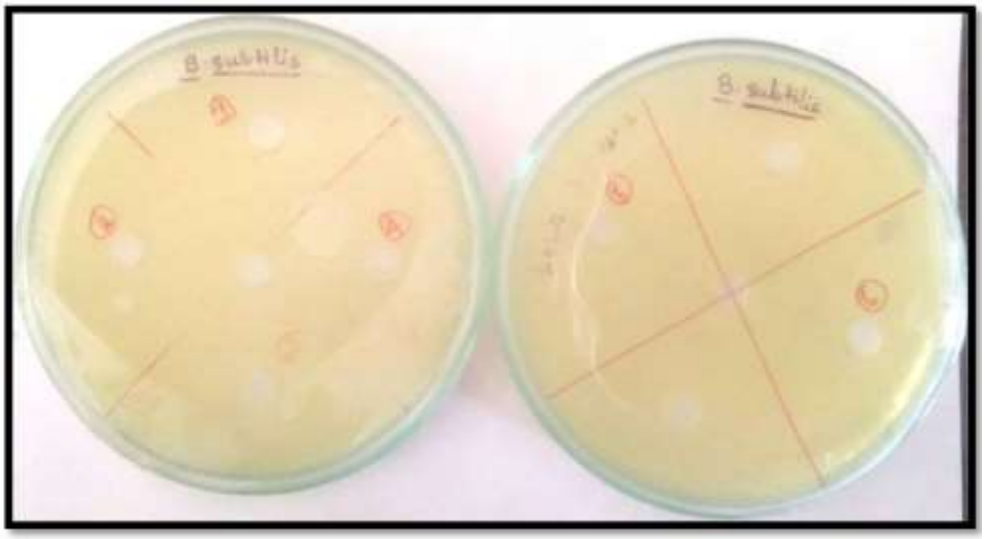

Figure 20. Antimicrobial activity analysis α-CD, β-CD on Gram-positive B. subtilis by Agar Cup method. No zone of inhibition was observed. Double distilled water was taken as the control. [Marker points (red) for the verified samples taken in the plates (1. SNP, 2. PEHB, 3. PEHA, 4. SNPA, 5. PEH, 6. SNPB) and Marker points (black) for the model organism taken in the plates]

CHAPTER V

Study to Explore Host Guest Inclusion Complexes of Vitamin B_1 with CD Molecules for Enhancing Stability and Innovative Application in Biological System

Abstract: In this article the host-guest inclusion of thiamine hydrochloride (guest) within the hydrophobic cavity of α and β-cyclodextrin molecules (hosts) have been studied scientifically in the solid and solution phases respectively. Various modern spectroscopic techniques had been used to establish the outcome of this work. The UV-Vis study supported the 1:1 stoichiometry of the inclusion complexes and also used to evaluate the association constants along with thermodynamic parameters with high accuracy for the determination of the feasibility of this inclusion process. From the mass spectrometric study,1:1 stoichiometry of the inclusion complexes had been confirmed in their solid state. Differential scanning calorimetric and infrared studies also supported this fact.^{1}H-NMR and 2D ROESY spectroscopic analysis had given the mechanism of inclusion process, and the SEM study exposed their surface structures. Finally, the sustained oozing of the guest molecule from the hydrophobic cavity of the respective cyclodextrin molecules separately had been studied in the presence of human serum albumin in their aqueous buffer solutions with the help of fluorescence spectroscopic technique. This study has a truly intense effect to the stabilization of the respective guest molecule from the external hazardous, such as photolytic degradation, oxidation-reduction, thermal cleavage etc., and also predicts the releasing behavior of thiamine hydrochloride in the presence of human serum albumin without any chemical modification.

Keywords: Thiamine hydrochloride, Oligosaccharide, inclusion complexes, Human serum albumin, releasing behavior.

1. Introduction:

Oligosaccharides, specially cyclodextrins (CDs) regarding host-guest inclusion complexation have very significant importance in food industries[1],[2],[3] pharmaceuticals[4, 5]and consumer goods[6] due to their unique conical-shaped[7]cyclic structures. Cyclodextrins and their derivatives are commercially available and differ because of the presence of different glucopyranose residues. Cyclodextrins have their distinctive biphasic layers possessing hydrophilic outer and hydrophobic inner surfaces. The inner region allows incorporating hydrophobic surface of different guest or segment(s) of guest molecules into the cavity of a suitable and stable geometrical sized CDs through various kinds of non-covalent interactions[8],[9]. Herein, α and β-cyclodextrins bearing 6 and 7 glucopyranose units, respectively, have taken as host molecules. Due to high inclusion efficiency, fitting cavity dimensions, low price, and negligible toxicity[10, 11].The CDs have found widespread application in pharmaceuticals[12], food industries[13], cosmetics[14], tissue engineering[15], bio-medical devices.[12, 16]Inclusion complexation within the non-polar cavity of CDs (**Figure 1**) is employed for protecting the hydrophobic part of different bioactive molecules[17],enzymes[18, 19], drugs[20], volatile organic compounds, flavors[21], essential oils [22, 23], taxols [24], flavonoids [25], vitamins[26], and etc. to extend their light, air and thermal stability, enhancement of water solubility, bioavailability and shielding side effects.

The B vitamins and their derivatives are a class of water-soluble vitamins and naturally found in food substances. These have significant role in cell metabolism[27]. They have major importance for food processing and biological activities such as transferring the alkyl group, fitting carbon dioxide, decarboxylation and transamination of amino acids, lipids and sugars[28-31]. Fruit juices are one of the main sources of vitamins and the quality of fruit juices in industry is maintained by different techniques including pasteurization, which led to the degradation of vitamins along with other valuable food nutrients. Day to day Consumer's realization about food nutritional value is throwing a challenge to the companies for healthier foods without any change in their chemical properties[32, 33]. Among all the B vitamins and their derivatives, one of the

most common is thiamine (vitamin B_1) chloro hydrochloride (THC, **Figure 1**), which is usually used as a component of single vitamin B complex and multivitamin preparations, food supplement, antioxidant, prooxidant, pharmaceutical industries and biological fluids. THC is used to treat in appetence and dermatophytosis. Moreover, it is also helpful to metabolize in human body.[34],[32, 35-37]Due to the lack of thiamine hydrochloride, neurotransmission in human body can be affected. Deficiency of THC leads to the occurrence of various malfunctions inside the human body such as beriberi, Wernicke-Korsakoff syndrome, confabulation and an irreversible dementia; even extreme deficiency may lead to heart failure and death[38],[39],[40]. Thus thiamine hydrochloride is extensively used in human body; moreover, it can be utilized as feed in agriculture and synthetic intermediates in industry[41].But THC is very sensitive to light and high temperature processing and also has tend to get oxidize easily in the presence of oxygen which limits their applications to a great extent in different fields. Chemical degradation is very common with vitamin B1 and the main route of the degradation is its reduction which is caused in the presence of food preservatives such as sodium meta-bisulfite, with very low concentrations (~1 mmol/L). Moreover, it can degrade by some of cell surface enzymes and plant thiamine antagonists[31, 33, 42].

Based on molecular recognition, inclusion of THC into CDs offers potential advantages in delivery without changing its chemical characteristics. In order to overcome all of these above mentioned foremost problems, we have attempted inclusion of THC within the hydrophobic cavity of α- and β-CD to improve stability and natural characteristics involving preservation for a long existence of time. Several studies have been done to find out the stability of THC within the cavity of CDs against the aforementioned adverse effect.

Human serum albumin (HSA) is one of the most abundant and popular protein in blood-plasma having 585 amino acid sequences. HSA consists of long chain polypeptides. It has tertiary structure consisting of three domains named I, II and III respectively. HSA has only one tryptophan residue (Trp-214) which is located in the sub-domain IIA. HSA plays a very important role for the maintenance of life systems.[43],[44-46]According to the two scientists Helms et al. and EI-Kemary et.al., serum proteins can take up many

conformations from the range of close compact to relaxed form. In recent years, there is an ongoing interest and a large field to investigate of plasma proteins with smaller molecules such as drugs, vitamins, hormones and other different kinds of bioactive molecules. The metabolism, distribution, free concentration can change significantly due to binding of HSA[44, 47],[48],[49],[50],[51]. In the other side, high intake of THC causes several effects such as developing cataracts, kidney disease and dysmenorrheal [52-54]. So, regular dischargement of THC at the targeted site for long term effectively is very important. In this work to get an idea about the regular releasing behavior of THC from the CDs cavity separately in the human body, HSA has taken which will help to formulate THC in pharmaceuticals and food industries.

In this novel work, the inclusion of THC has been aimed within the cavity of α and β-CD separately in both solution and solid states to explore their formation of inclusion complex (IC) for enhancing the stability of THC. Regular release without any chemical alteration of THC in the presence of HSA from the cavity of α and β-CD separately have been monitored with the help of fluorescence spectroscopy. Formation of inclusion complexes have been well characterized by various reliable techniques like 2D ROESY and ^{1}H NMR, IR, UV-Visible spectroscopy, Fluorescence spectroscopy, DSC, ESI-MS, SEM study has been done to get an idea about the surface nature of the corresponding two inclusion complexes. Association parameters, thermodynamic parameters, and stoichiometry have been evaluated to get a clear and quantitative idea about the formation of these ICs.

Hence, this present work mainly approaches towards the stability and regular release of THC inside the body and helps to execute the proposed utilization in the field of food chemistry and pharmaceutical science.

2. EXPERIMENTAL SECTION

2.1. Materials:

Thiamine hydrochloride having purity ≥98.0% was purchased from TOKYO CHEMICAL INDUSTRY CO., LTD while human serum albumin, α- and β-cyclodextrins of high purity

grade ≥97.0% and≥98.0% respectively were purchased from Sigma-Aldrich, Germany. All of these samples were kept in the refrigerator as received and used during the following experiments without further any alteration.

2.2. Apparatus:

UV-Visible spectra were recorded with the help of Agilent 8453 UV-Visible Spectrophotometer with an uncertainty of wavelength accuracy of ±0.5 nm and an automated digital thermostat was used to control the temperature of the cell during performing the experiments.

^{1}H-NMR and 2D ROESY spectra were recorded in D_2O solvent at 400 MHz in Bruker Avance instrument at 298.15 K. All the signals are shown in terms of δ values (in ppm) by using residual protonated solvent signal (HDO: δ 4.79 ppm) as internal standard and all the data are represented in the form of chemical shift (δ) values.

The DSC thermograms of the samples were recorded with the help of Perkin-Elmer DSC-6 differential scanning calorimeter at the heating rates of 10°C min^{-1}. The thermogram was taken by heating 1 mg of samples in aluminum crimped pans under nitrogen gas flow within the temperature range 30–300 °C.

ESI-MS analyses were performed by Q-TOF high resolution are shown with positive mode electro-spray ionization taking the methanol solution of the solid ICs.

According to KBr disk method, FTIR spectra were recorded on a Perkin-Elmer spectrometer within 4000-400 cm^{-1} scanning range at room temperature. All KBr disks were made in 1:100 ratios of sample to KBr and during the experimental studies humidity was at 45%.

SEM images had been recorded with the help of JEOL JSM IT 100 Scanning Electron Microscope (SEM) to determine surface morphology. Samples were prepared on a small

piece of double adhesive carbon-coated tape attached to brass stubs and then a coating of ultra-thin layer of gold ions was put in a gold-ionization chamber. SEM images were recorded at various resolutions.

Fluorescence spectra were recorded with the help of Bench top spectrofluorimeter from photon technologies International (Quantamaster-40, USA) at room temperature. Data were recorded by taking solutions into Hellma quartz cuvette having optical path length 1.0 cm while excitation and emission slit widths fixed at 5.0 nm and 5.0 nm, respectively.

2.3. Procedure:

Solubility of all the required compounds was specifically checked in triply distilled and de-ionized water. Mettler Toledo AG-285 having uncertainty±0.0003 g was used to prepare all the solutions of THC, HSA, α-and β-CD by mass at room temperature. All the stock solutions were prepared by mass dilution and freshly prepared solutions were used during each experiment in phosphate buffer aqueous solution of pH 7.4. Sufficient precautions had been taken during measuring weights, preparing solutions and performing all the respective experiments. Two solid ICs, THC+ α-CD and THC + β-CD had been prepared in 1:1 molar ratio of THC and CD. 1.0 mM of α-and β-CD were each separately mixed with water and stirred for 4 hours. After that the aqueous solution of 1.0 mM of THC was added drop wise to the respective solutions of CD and left for stirring near about 36 hours at 50-55 °C to prepare the corresponding two ICs. Just after filtration of the hot solutions, it is allowed to cool down to 5°C and kept for 12 hours without any disturbing. The obtained suspension was then filtered and washed with ethanol and dried in air to get white polycrystalline powder.

3. Result and Discussion

3.1. Job plot: Stoichiometry of the host-guest inclusion complex

The well-established Job's method, usually known as continuous variation method is used to find out the stoichiometry of host-guest inclusion complex[55].For this UV-Visible study, a set of solutions of THC had been taken along with host α and β-CD separately varying mole fractions within the range of 0-1**(Table S1-S4)** in aqueous

solution and experiment was done at 298.15 K. The THC has absorbance with respect to two λmax's regarding Π–Π* transitions, λmax = 236 nm for pyrimidine ring and = 263 nm for thiazole ring. Hence, the absorbance of THC had been taken at λmax = 236 nm and 263 nm respectively **(Figure 2)** for the set of prepared solutions. ΔA × R vs. R were plotted **(Figure 3)** of THC+α-CD and THC + β-CD for the graph of Job's plot separately where, ΔA is the difference in absorbance of THC without and with CDs and "R" refers to the mole fraction of THC, i.e. [THC]/ ([THC] + [CD]). The Y-axis in the Job's plot represents physical property (ΔA × R), that functions as a proxy for the concentration of inclusion complex. From the value of R at the maxima of the plots , the stoichiometry of inclusion complex can be obtained for example if the value of R is 0.33, 0.5 or 0.66 then the stoichiometry of host-guest inclusion complex is 1:2, 1:1 or 2:1 respectively[56]. In this experimental study the value of R had been obtained ~0.5 from the four plots at λmax = 236 and 263 nm for α and β-CD correspondingly which clearly indicates the host-guest inclusion stoichiometry 1:1 for both the cases [57]**(Figure 3)** that means both the pyrimidine and thiazole ring form 1:1 inclusion complexes with the respective CDs separately. So, it can be concluded that there is a high probability of formation of a dynamic equilibrium among the pyrimidine and thiazole part of THC with the respective CDs separately in the aqueous solution phase.

3.2. Ultraviolet spectroscopy for the determination of association constants of the ICs:

The non-covalent binding capability of the guest molecule within the cavity of host supra-molecules and the binding strength of the respective inclusion complexes had been explored by the evaluated association constants (Ka) of the ICs in the solution state with the help of UV-Visible spectroscopy[20]. The molar extinction co-efficient (ε) of the chromophore of THC was changed on the basis of the solvent polarity as it was changing its environment from polar aqueous medium to apolar cavity of CDs via non-covalent interactions to form host-guest inclusion complexes[58]. For the determination of Ka, the change in absorbance (ΔA) of THC at λmax = 236 and 263 nm for pyrimidine ring and thiazole ring respectively was measured with gradual increasing the concentrations of α- and β-CD separately by varying temperature within the range of 298.15 to 308.15 K

(Table S5-S8). The double reciprocal plots **(Figure S1-S2)** were drawn with the help of Benesi–Hildebrand method[59],[60],[61]for 1:1 host - guest complexation and the corresponding equation is given as follows

$$\frac{1}{\Delta A} = \frac{1}{\Delta\varepsilon[THC]K_a}\frac{1}{[CD]} + \frac{1}{\Delta\varepsilon[THC]} \qquad (1)$$

Where ΔA is the change in absorbance of THC (at λmax = 236 and 263nm) and Δε is the change in molar extinction co-efficient of THC from polar environment to apolar environment. The resulting plots are straight line and the Ka for the ICs are evaluated from the intercept to slope of the straight line of the double reciprocal plot **(Table 1).**

K_a's for the respective IC's were also determined with the help of non-linear programmed by the UV-visible study owing to the encapsulation of THC within the hydrophobic cavity of α-CD and β-CD separately. As a result of formation of 1:1 IC in the solution phase, there should be an equilibrium established between host and guest molecules[58, 62, 63].

$$[THC]_f + [CD]_f \overset{K_a^\tau}{\leftrightharpoons} [IC] \qquad (2)$$

The association constant (K_a^τ) for the above equation can be expressed as follows

$$K_a^\tau = \frac{[IC]}{[THC]_f[CD]_f} \qquad (3)$$

Where [IC], $[THC]_f$ and $[CD]_f$ refer the equilibrium concentrations of IC, free THC and free CD respectively for the above mentioned reaction equation. According to the binding isotherm, the (K_a^τ) for the for the formation of ICs can be written in terms of their absorbance as follows

$$[CD]_f = [CD]_x - \frac{[THC]_x(A_{obs} - A_0)}{(A - A_{obs})} \qquad (4)$$

Here, A_0 is the initial absorbance for THC molecule, A_{obs} is the absorbance of the THC in the time of ongoing addition of CDs and A denotes the final concentration of THC molecules. $[THC]_x$ and $[CD]_x$ are the concentrations of cyclodextrin and THC molecules respectively. The obtained (K_a^r) values the respective ICs at both λmax values are listed in the **(Table 1)** with the help of non-linear programmed.

The association constants of the IC's define the binding ability of the guest into the host as well as their stability as IC. The greater values of the association constants for IC's describes the greatness of their stability. From the Table 1, it is clear pyrimidine part of the THC binds more strongly than that of the thiazole part of THC. The IC's formed with β-CD were found more stable than that of the IC's formed with α-CD. With increasing temperature, the thermal stability of IC's decreases as the encapsulation of the guest into host cavity leads to the decrease in enthalpy **(Table 2)**.

3.3 UV-Visible spectroscopy, Non-linear program based mathematical calculation to determine the thermodynamic parameters:

Thermodynamic parameters were calculated basing on the association constants(K_a, K_a^r) obtained from a variety of isotherms by the above mentioned linear and non-linear methods with the help of van't Hoff equation[20, 64, 65]**(Figure S3-S4,Table S9-S10 and Figure S5-S6, Table S11-S12)**.

$$\ln K_a = -\frac{\Delta H^0}{RT} + \frac{\Delta S^0}{R} \qquad (5)$$

$$\Delta G^0 = \Delta H^0 - T\Delta S^0 \qquad (6)$$

where Δ Ho, Δ So, R and T carry their usual meanings. The calculating value of Δ Ho and ΔSo for the formation of ICs were suggesting that the entire inclusion complex formation process in the solution phase are exothermic and entropy restricted means the process is unfavorable in terms entropy **(Table 2)**. From these results it can be concluded that the entire inclusion complex formation process in solution phase is thermodynamically

spontaneous but entropically unfavorable as molecular recognition takes place and is highly diminished by the greater value of change in enthalpy($\Delta H^0, \Delta H^{\theta 0}$) hence makes the overall process thermodynamically favorable. Thus the Gibbs free energy ΔG^0 becomes negative directing spontaneity in the formation of the ICs

3.4 ^{1}H NMR and 2D ROESY NMR spectra analysis of solid inclusion complexes

In order to explain the mechanism of the inclusion complexation of THC with the respective cyclodextrin molecules, ^{1}H-NMR and 2D-ROESY spectra were recorded. The ^{1}H-NMR spectra and the chemical shift (δ) values of THC, α-CD, β-CD and their inclusion complexes are shown in the **Figure S7-S11** and in **Table S13** respectively. As a result of mutual shielding through space among the interacting protons of THC with that of the cyclodextrin molecules, there is a change in their NMR spectra in their corresponding inclusion complexes. Here, change of the chemical shift values of protons of cyclodextrin supramolecules occurs through diamagnetic shielding mainly by the aromatic segments of THC molecule. From the structure of CD **(Figure 1)**, it can be seen that H3 protons and H5 protons are situated at the wider and narrower rim sides respectively while the rest of protons are at the exterior area of the CD conical shaped molecule. From the **Figure S7-S11** of NMR spectra it is clearly seen that there is a upfield shift of H3 and H5 protons of α and β-CD correspondingly which confirms the formation of inclusion complexes with the THC molecule.

To get the clear idea about the mode of interactions of the protons of THC molecule with that of the CD molecules in their inclusion complexes 2D ROESY NMR had been performed and the spectra are shown in **Figure 4 & 5.** There are some diagonal and off-diagonal peaks are observed in the spectra in ROESY NMR for the THC-CD complexes if protons are situated within 0.4 nm in space. Off-diagonal peaks are due to the inter cross correlation of the protons of THC with the interior protons i.e. H3 and H5 of CD molecules. In the **Figure 4 & 5**, there are three off-diagonal peaks are observed due to the inter molecular dipolar cross correlation between H-6 proton of THC with the H3 and H5 of α and β-CD while H-1 and H-7of THC with H3 and H5 of α and β-CD molecule

respectively suggesting that the pyrimidine part of THC strongly interacts with the interior protons of CD molecules and resides inside the CD cavity but there is a weak interaction between the thiazole moiety of THC with the CDs probably that positive charge on the N atom of thiazole moiety resists it to stay within CD hydrophobic cavity. As there is no such significant peaks with the H6 protons of CD with that of the THC molecule, it can be concluded that the inclusion occurs through wider rim side **(Figure 6)** for both α and β -CD otherwise some changes will be observed as H6 protons reside near narrower side of the rim.

3.5 Differential scanning calorimetric (DSC) study

The thermal characterization of the inclusion complexes had been done with the help of DSC technique[66]. Each pure compound has its own characteristic boiling, melting or sublimation point which frequently disappears or shifts to the different temperature due to the formation of inclusion complexes[67],[68],[69].The DSC thermograms of THC and its ICs are shown in the **Figure 7**. The DSC thermogram of THC showed a sharp endothermic peak at 252.28 °C corresponds to its melting point. In the ICs a characteristic peak with large shifting in comparison with the THC to the different temperatures were observed. Initially endothermic peaks at 67.81 °C and 140.50 °C for IC-1 could be attributed to the loss of water due the evaporation. Similarly, endothermic peak at 62.67 °C for IC-2 is due to the loss of water molecules owe to the evaporation. Both the peak at 228.81°Cfor IC-1 and at 226.17°C for IC-2 indicate the loss of crystalline nature of THC molecule and also suggesting that there is a strong interaction of THC molecule with β-CD compare to α-CD.

3.6 ESI-mass spectrometric analysis of inclusion complexes

The ICs of THC with α-CD and β-CD separately were further investigated in their solid state with the help of ESI-mass spectrometry by dissolving in methanol. The observed spectra are shown in **Figure 8**. The peaks at m/z 1238.44 and 1260.42correspond to the $[THC+ α\text{-}CD+H]^+$ and $[THC+α\text{-}CD+Na]^+$ respectively and the peaks at m/z 1400.49 and 1422.47 correspond to $[THC+β\text{-}CD+H]^+$ and $[THC+β\text{-}CD+Na]^+$ respectively. From all of this values, it can be concluded that the ICs of THC with α-CD and β-CD separately have

been formed in the solid state and the obtained stoichiometric ratio is 1:1 for the host to guest molecule[70].

3.7 FT-IR spectra of solid inclusion complexes

The formation of inclusion complexes are also well explained with the help of infrared spectroscopic technique[71], [72], [73]. KBr disk method had been used to get the IR spectra of the pure THC, α-CD, β-CD and their respective IC's which are shown in the **Figure 9**. The noteworthy signals which are shifted sufficiently have been listed in the **Table S14**.

For IC-1 means (α-CD+THC) system, the following spectral changes are obtained due the host-guest interactions. (i) The broad signal at 3436.04$cm^{-1}$of THC generally found due to the merging of the two signals respective to -NH_2 and –OH groups together and this peak is found to shift at 3420.09 cm^{-1}in IC-1 while 3410.09cm^{-1} is observed for –OH groups in α-CD. (ii) The signal of 2361.26 cm^{-1} for ($C^{sp3}H_2$) bending of THC is shifted to 2365.21 cm^{-1} in the complex. (iii) The peak at 1636.35 cm^{-1} for N-H (NH_2) bending of THC is obtained at 1632.02 cm^{-1} while complexed with α-CD. (iv) The peaks from 519.08 cm^{-1} to 1380.15 cm^{-1} of THC are almost completely masked in its complex with α-CD.

For IC-2 means (β-CD+THC) system, the following changes in their spectra are observed owe to the various non-covalent interactions of THC with β–CD. (i) The signal at 3424.05 cm^{-1} for –OH stretching of β-CD is changed to 3401.23cm^{-1} in IC-2. (ii) The peak at 2361.26 $cm^{-1}$for ($C^{sp3}H_2$) bending of THC is shifted to 2363.29 in its complex with β–CD. (iii) The peak at 1636.35 $cm^{-1}$for N-H (NH_2) bending of THC is now changed to 1632.27 cm^{-1}. (iv) The signals in the range of 519.08 $cm^{-1}$to 1380.15 cm^{-1} are also just as IC-1 masked significantly in IC-2.

Thus, from the above discussions along with the **Figure 9** and **Table S14**, it was seen that, there is no significant appearance of new signals which clearly indicate the absence of formation new chemical bonds between THC and CDs. So, it can be clearly said that the slight shifting of some significant IR signals that may signify hydrophobic-

hydrophobic as well as non-covalent interaction of thiazole and pyrimidine ring of THC with CDs causing random weakening and strengthening of the interacting bonds while formation of IC's.

3.8 Scanning Electron microscopic (SEM) study to exhibit the surface structures:

Scanning electron microscopy (SEM) is a well-established technique to analyze the surface morphology and the particle size of the solid substances[9, 59, 74]. The surface morphology of the pure guest THC, pure hosts α and β-CD separately, their respective ICs and their corresponding physical mixtures have been shown in the **Figure 10 & 11.** From the SEM images, it is clear that the surface morphology of the ICs is totally different from their raw materials which indicates the formation of new morphology probably indicating the formation of host-guest inclusion complexes as evident from the above mentioned different experimental studies.

3.9. Steady-state fluorescence: Association constants from Modified Benesi-Hildebrand equation and association constants.

The association constants of THC molecule with and without the presence of CD molecule had been derived from the modified Benesi-Hildebrand equation by using spectrofluorimetric method [75], [76], [77].

$$\frac{1}{I - I_0} = \frac{1}{[I' - I_0]K_a^{\phi}}\frac{1}{[THC]} + \frac{1}{I' - I_0} \qquad (7)$$

Where, I and I_0 represents the fluorescence intensities of HSA in the presence and absence of the THC respectively, I' are the intensities of the HSA while all the guest molecules for a particular system are complexed with THC. [THC] represents the concentration of the Thiamine hydrochloride.

From the above discussions it is clear that there is a formation of 1:1 inclusion complex of THC with CDs. All the fluorescence spectra are taken by exciting the HSA at λ_{max} 280 nm by keeping constant the volume and concentration of HSA and CDs in the

respective aqueous solution mixtures while the concentration of THC was varied. The whole experiment was done at phosphate buffer aqueous solutions by maintaining pH 7.4 at 298.15 K. From the plots **(Figure S12)** drawn by using the above mentioned equation, association constants are evaluated which are shown in **Table S15-S17**, suggesting the stability of the newly formed complexes in the solution phase at room temperature. The Gibbs free energy value **(Table 3)** suggesting the spontaneity of the whole complexation processes.

3.10. Binding interaction of the THC molecule in the presence of human serum albumin with and without CDs: The process of dischargement of guest from the cavity of CDs

Fluorescence spectroscopy is a very useful and highly sensitive technique to inspect the change in the microenvironment around the fluorophore depending on the binding with quencher[78],[79].

Thus from this study lots of different kind of useful information can be obtained with respect to the binding mechanism[47, 48, 80]. The release of THC from the inclusion complexes was determined with the help of fluorescence emission spectroscopy by observing the binding interaction of HSA with THC in the presence and absence of CDs in aqueous medium. The intrinsic fluorescence of HSA is due to Trp 214 (hydrophobic moiety) alone having λ_{max} of 280 nm.

For all the set of solutions, excitation had been done at 280 nm to investigate the shift of λ_{max} and the intensity of the HSA molecule with and without the presence of CD molecules, the corresponding spectra was shown in the **Figure 12**. From these figures, hypochromic shift i.e. a regular decrease in the intensity of the spectra with increasing the concentrations of THC separately in the aqueous buffered solutions of HSA along with respective CDs, was clearly observed probably as a result of strong non-covalent interactions of fluorophore moiety of HSA molecule with the THC molecule. The binding constants of THC:HSA in the presence of CD molecule are $3.03 \times 10^3$and 2.49×10^3 M^{-1} for α and β-CD respectively ,where 4.21×10^3 M^{-1} for THC: HSA without CDs suggesting there

is a less association of THC with HSA molecule in the presence of CDs as inclusion of THC with CDs decreases the strength of their binding by blocking the non-covalent interactions existing between them . So, HSA strongly competes with CDs to bind THC and in this way it helps in effective delivery of vitamins. Accordingly, it enhances the availability of free THC in blood plasma resulting effective therapeutic effect at the target site. This study also proves the formation of inclusion complexes of THC with both α and β-CD respectively in solution phase.

Hence from this experimental study we can conclude that there is a regularity in the oozing of the guest molecule from the cavity of CDs into the aqueous solution in the presence of HSA molecule.

4. Conclusion

1:1 host-guest inclusion complexes of THC within the cavity of α and β-CD are well established by the various techniques in solution phase as well as in the solid state. The entire inclusion process is thermodynamically feasible process as obtained from the calculated thermodynamic parameters and evaluated association constants reveal the stability of the formation of ICs. Molecular recognition due to the dimensional suitability is the major stabilizing factor. The positive entropy factor is also responsible for the formation of ICs via non-covalent interactions such as hydrogen bonding and other hydrophobic interactions as more number of water molecules compare to that of THC molecule are released from the cavity of the CDs for making the free suitable space for the incoming THC molecule. Formation of inclusion complexes enhances the photochemical stability of THC, protect it from thermal degradation and retain its property without any kind of chemical transformation. Moreover, the regulatory dischargement of THC molecule at pH 7.4 from the hydrophobic cavity to the polar aqueous media has been clearly explained in the presence of HSA molecule. So, there is a strong probability to show similar kind of binding behavior of THC with HSA in the human body and successfully will be delivered to the targeted area as per required amount of it. Hence the study for the formation of inclusion complex and the regulatory dischargement of THC from the hydrophobic cavity of CDs into the aqueous solution approach a novel way for the versatile uses and formulation in food, medicinal and

pharmaceutical industries without any chemical modification. In conclusion, this article demands far reaching effects by dint of innovative applications in pharmaceutical science.

Acknowledgement

Prof. M. N. Roy would like to acknowledge UGC, New Delhi, Government of India, for being awarded One Time Grant under Basic Scientific Research via the grant-in-Aid no. F.4-10/2010 (BSR). BR is thankful to the "State Fellowship" bearing reference No. 1743/R-2017 dated 18.04.2017. Mr. Goutam Sarkar, The H.O.D., USIC, University of North Bengal, Darjeeling is also highly acknowledged for executing SEM associated with this paper.

Disclosure of interest

The authors declare no conflicts of interest.

TABLES

Table 1: Association Constants derived from Benesi-Hildebrand method (K_a) and also from the Nonlinear Program (K_a^{τ}) using UV-Visible spectroscopic data at 236 to 263 nm in the temperature range 298.15 to 308 K.

Host	λ_{max} (nm)	Temperature (K[a])	K_a (×10³)	K_a^{τ} (×10³)
α-CD	236	298.15	1.28	1.30
		303.15	1.12	1.10
		308.15	0.86	0.87
	263	298.15	1.12	1.22
		303.15	0.85	0.81
		308.15	0.62	0.64
β-CD	236	298.15	1.90	2.10
		303.15	1.62	1.52
		308.15	1.33	1.23
	263	298.15	1.67	1.47
		303.15	1.50	1.20

		308.15	1.13	0.93

[a]Standard uncertainty in temperature, u, are u(T) = ± 0.01 K

Table 2: Thermodynamic parameters (ΔH^0, ΔS^0, ΔG^0) and ($\Delta H^{0\tau}$, $\Delta S^{0\tau}$, $\Delta G^{0\tau}$) calculated, using the association constants (K_a, K_a^{τ}) obtained from Benesi-Hildebrand method, Nonlinear Program for λ_{max}=236 nm and 263 nm.

Inclusion Complexes (ICs)	λ_{max} (nm)	Application of (K_a) to Van't Hoff equation		Application of (K_a^{τ}) to Van't Hoff equation	
THC + α-CD	236	ΔH^0 (KJ mol^{-1})	-30.07	$\Delta H^{0\tau}$ (KJ mol^{-1})	-30.32
		ΔS^0 (J mol^{-1} K^{-1})	-41.20	$\Delta S^{0\tau}$ (J mol^{-1} K^{-1})	-41.98
		ΔG^0 (KJ mol^{-1})	-17.79	$\Delta G^{0\tau}$ (KJ mol^{-1})	-17.80
	263	ΔH^0 (KJ mol^{-1})	-44.77	$\Delta H^{0\tau}$ (KJ mol^{-1})	-48.97
		ΔS^0 (J mol^{-1} K^{-1})	-91.69	$\Delta S^{0\tau}$ (J mol^{-1} K^{-1})	-105.35
		ΔG^0 (KJ mol^{-1})	-17.43	$\Delta G^{0\tau}$ (KJ mol^{-1})	-17.56
THC + β-CD	236	ΔH^0 (KJ mol^{-1})	-27.11	$\Delta H^{0\tau}$ (KJ mol^{-1})	-40.81
		ΔS^0 (J mol^{-1} K^{-1})	-28.11	$\Delta S^{0\tau}$ (J mol^{-1} K^{-1})	-73.42
		ΔG^0 (KJ mol^{-1})	-18.73	$\Delta G^{0\tau}$ (KJ mol^{-1})	-18.92
	263	ΔH^0 (KJ mol^{-1})	-29.59	$\Delta H^{0\tau}$ (KJ mol^{-1})	-29.59
		ΔS^0 (J mol^{-1} K^{-1})	-37.28	$\Delta S^{0\tau}$ (J mol^{-1} K^{-1})	-37.28
		ΔG^0 (KJ mol^{-1})	-18.47	$\Delta G^{0\tau}$ (KJ mol^{-1})	-18.47

Mean errors in variables are as follows: ΔH^0=±0.01 kJ mol^{-1}; ΔS^0 =±0.01 J mol^{-1}K^{-1}; $^{\Delta G^{0\tau}}$ = ±0.01 kJ mol^{-1}; $^{\Delta H^{0\tau}}$ = ±0.01 kJ mol^{-1}; $^{\Delta S^{0\tau}}$ = ±0.01 J mol^{-1}K^{-1}

Table 3. Association constants (K_a^{Φ}) and standard free energy changes for (HSA +THC), (HSA+THC+α-CD) and (HSA+THC+β-CD) systems at 298.15 K.

System	HSA+THC	HSA+THC+α-CD	HSA+THC+β-CD
K_a^{Φ} ×10^3(M^{-1})	4.21	3.03	2.49
$\Delta G^{\Phi 0}$ (KJ mol^{-1})	-20.24	-19.44	-18.97

Table S1. UV-Vis spectroscopic data for the generation of Job plots of aqueous THC+α-CD system at 298.15 K[a] and 236 nm.

THC + ALPHA – CYCLODEXTRIN							
THC (mL)	α-CD (mL)	THC (μM)	α-CD (μM)	$\frac{[THC]}{[THC]+[\alpha-CD]}$	Absorbance (A)	ΔA	$\frac{\Delta A \times [THC]}{[THC]+[\alpha-CD]}$
0	3	0	100	0	0.0000	1.1139	0.0000
0.3	2.7	10	90	0.1	0.1360	0.9779	0.0978
0.6	2.4	20	80	0.2	0.2421	0.8718	0.1744
0.9	2.1	30	70	0.3	0.3396	0.7743	0.2323
1.2	1.8	40	60	0.4	0.4380	0.6759	0.2703
1.5	1.5	50	50	0.5	0.5460	0.5679	0.2839
1.8	1.2	60	40	0.6	0.6365	0.4774	0.2864
2.1	0.9	70	30	0.7	0.7857	0.3281	0.2297
2.4	0.6	80	20	0.8	0.9233	0.1905	0.1524
2.7	0.3	90	10	0.9	1.0359	0.0780	0.0702
3	0	100	0	1	1.1139	0.0000	0.0000

[a]Standard uncertainties in temperature u are: u(T) = ±0.01 K.

Table S2. UV-Vis spectroscopic data for the generation of Job plots of aqueous THC+α-CD system at 298.15 K[a] and 263 nm.

THC + ALPHA – CYCLODEXTRIN							
THC (mL)	α-CD (mL)	THC (μM)	α-CD (μM)	$\frac{[THC]}{[THC]+[\alpha-CD]}$	Absorbance (A)	ΔA	$\frac{\Delta A \times [THC]}{[THC]+[\alpha-CD]}$
0	3	0	100	0	0.0000	1.0006	0.0000
0.3	2.7	10	90	0.1	0.1069	0.8937	0.0894
0.6	2.4	20	80	0.2	0.1901	0.8105	0.1621
0.9	2.1	30	70	0.3	0.2736	0.7270	0.2181
1.2	1.8	40	60	0.4	0.3602	0.6404	0.2562
1.5	1.5	50	50	0.5	0.4603	0.5403	0.2701
1.8	1.2	60	40	0.6	0.5545	0.4461	0.2677
2.1	0.9	70	30	0.7	0.6906	0.3100	0.2170
2.4	0.6	80	20	0.8	0.8073	0.1933	0.1547
2.7	0.3	90	10	0.9	0.9063	0.0943	0.0849
3	0	100	0	1	1.0006	0.0000	0.0000

Table S3. UV-Vis spectroscopic data for the generation of Job plots of aqueous THC+β-CD system at 298.15 K[a] and 236 nm.

THC+BETA – CYCLODEXTRIN							
THC (mL)	β-CD (mL)	THC (μM)	β-CD (μM)	$\frac{[THC]}{[THC]+[\beta-CD]}$	Absorbance (A)	ΔA	$\frac{\Delta A \times [THC]}{[THC]+[\beta-CD]}$
0	3	0	100	0	0.0000	1.0698	0.0000
0.3	2.7	10	90	0.1	0.1188	0.9510	0.0951
0.6	2.4	20	80	0.2	0.2082	0.8616	0.1723
0.9	2.1	30	70	0.3	0.3368	0.7330	0.2199
1.2	1.8	40	60	0.4	0.4364	0.6334	0.2534
1.5	1.5	50	50	0.5	0.5505	0.5192	0.2596
1.8	1.2	60	40	0.6	0.6621	0.4077	0.2446
2.1	0.9	70	30	0.7	0.7480	0.3217	0.2252
2.4	0.6	80	20	0.8	0.8576	0.2122	0.1698
2.7	0.3	90	10	0.9	0.9648	0.1049	0.0944
3	0	100	0	1	1.0698	0.0000	0.0000

Table S4. UV-Vis spectroscopic data for the generation of Job plots of aqueous THC+β-CD system at 298.15 K[a] and 263 nm.

THC+ BETA - CYCLODEXTRIN							
THC (mL)	β-CD (mL)	THC (μM)	β-CD (μM)	$\frac{[THC]}{[THC]+[\beta-CD]}$	Absorbance (A)	ΔA	$\frac{\Delta A \times [THC]}{[THC]+[\beta-CD]}$
0	3	0	100	0	0.0000	0.9661	0.0000
0.3	2.7	10	90	0.1	0.0913	0.8748	0.0875
0.6	2.4	20	80	0.2	0.1621	0.8040	0.1608
0.9	2.1	30	70	0.3	0.2759	0.6902	0.2071
1.2	1.8	40	60	0.4	0.3559	0.6103	0.2441
1.5	1.5	50	50	0.5	0.4633	0.5028	0.2514
1.8	1.2	60	40	0.6	0.5568	0.4093	0.2456
2.1	0.9	70	30	0.7	0.6437	0.3224	0.2257
2.4	0.6	80	20	0.8	0.7421	0.2240	0.1792
2.7	0.3	90	10	0.9	0.8463	0.1198	0.1078
3	0	100	0	1	0.9661	0.0000	0.0000

[a]Standard uncertainties in temperature *u* are: *u*(T) = ±0.01 K.

Table S5. UV-vis spectroscopic data for the Benesi-Hildebrand double reciprocal plot of (THC+α-CD) system at 298.15 to 308.15 K[a] and 236 nm.

Temp (K[a])	THC (μM)	α-CD (μM)	Ao	A	ΔA	1/[α-CD] (M^{-1})	1/ΔA	Intercept	Slope	Ka ($M^{-1}\times10^{-3}$)
298.15	50	30	0.4994	0.5337	0.0343	0.0333	29.1698	1.0717	839.4	1.28
	50	40		0.5455	0.0461	0.0250	21.6693			
	50	50		0.5541	0.0547	0.0200	18.2715			
	50	60		0.5666	0.0672	0.0167	14.8702			
	50	70		0.5757	0.0763	0.0143	13.1116			
303.15	50	30	0.4986	0.5326	0.0340	0.0333	29.4273	0.966	859.1	1.12
	50	40		0.5426	0.0440	0.0250	22.7024			
	50	50		0.5527	0.0541	0.0200	18.4740			
	50	60		0.5664	0.0678	0.0167	14.7387			
	50	70		0.5734	0.0748	0.0143	13.3747			
308.15	50	30	0.4977	0.5314	0.0336	0.0333	29.7191	0.7515	873.27	0.86
	50	40		0.5417	0.0440	0.0250	22.7197			
	50	50		0.5512	0.0535	0.0200	18.6928			
	50	60		0.5658	0.0681	0.0167	14.6811			
	50	70		0.5725	0.0747	0.0143	13.3807			

Table S6. UV-vis spectroscopic data for the Benesi-Hildebrand double reciprocal plot of (THC+α-CD) system at 298.15 to 308.15 K[a] and 263 nm.

Temp (K[a])	THC (µM)	α-CD (µM)	Ao	A	ΔA	1/[α-CD] (M^{-1})	1/ΔA	Intercept	Slope	Ka ($M^{-1}\times10^{-3}$)
298.15	50	30	0.4138	0.4422	0.0284	0.0333	35.2033	1.1361	1011.9	1.12
	50	40		0.4542	0.0404	0.0250	24.7547			
	50	50		0.4559	0.0421	0.0200	23.7804			
	50	60		0.4723	0.0585	0.0167	17.0961			
	50	70		0.4786	0.0648	0.0143	15.4353			
303.15	50	30	0.4357	0.4616	0.0258	0.0333	38.7174	0.9986	1168.8	0.85
	50	40		0.4667	0.0310	0.0250	32.2933			
	50	50		0.4756	0.0398	0.0200	25.1165			
	50	60		0.4875	0.0518	0.0167	19.3059			
	50	70		0.4936	0.0578	0.0143	17.2966			
308.15	50	30	0.4254	0.4505	0.0252	0.0333	39.7079	0.7447	1192.2	0.62
	50	40		0.4584	0.0330	0.0250	30.2706			
	50	50		0.4604	0.0351	0.0200	28.5016			
	50	60		0.4789	0.0535	0.0167	18.6870			
	50	70		0.4847	0.0594	0.0143	16.8451			

Table S7. UV-vis spectroscopic data for the Benesi-Hildebrand double reciprocal plot of (THC+β -CD) system at 298.15 to 308.15 K[a] and 236 nm.

Temp (K[a])	THC (µM)	α-CD (µM)	Ao	A	ΔA	1/[α-CD] (M^{-1})	1/ΔA	Intercept	Slope	Ka ($M^{-1}\times10^{-3}$)
298.15	50	30	0.4994	0.5351	0.0357	0.0333	28.0253	1.5026	792.53	1.90
	50	40		0.5471	0.0477	0.0250	20.9432			
	50	50		0.5559	0.0565	0.0200	17.6897			
	50	60		0.5672	0.0678	0.0167	14.7387			
	50	70		0.5780	0.0786	0.0143	12.7278			
303.15	50	30	0.4986	0.5342	0.0356	0.0333	28.1041	1.3224	815.43	1.62
	50	40		0.5432	0.0446	0.0250	22.3973			
	50	50		0.5543	0.0557	0.0200	17.9436			
	50	60		0.5687	0.0701	0.0167	14.2555			
	50	70		0.5754	0.0768	0.0143	13.0262			
308.15	50	30	0.4977	0.5329	0.0351	0.0333	28.4508	1.0958	824.43	1.33
	50	40		0.5436	0.0459	0.0250	21.7795			
	50	50		0.5527	0.0550	0.0200	18.1830			
	50	60		0.5687	0.0710	0.0167	14.0816			
	50	70		0.5742	0.0764	0.0143	13.0831			

Table S8. UV-vis spectroscopic data for the Benesi-Hildebrand double reciprocal plot of (THC+β -CD) system at 298.15 to 308.15 K[a] and 263 nm.

Temp (K[a])	THC (µM)	α-CD (µM)	Ao	A	ΔA	1/[α-CD] (M^{-1})	1/ΔA	Intercept	Slope	Ka ($M^{-1}\times10^{-3}$)
298.15	50	30	0.4138	0.4547	0.0409	0.0333	24.4383	1.1691	698.68	1.67
	50	40		0.4684	0.0546	0.0250	18.3205			
	50	50		0.4772	0.0634	0.0200	15.7846			
	50	60		0.4916	0.0778	0.0167	12.8543			
	50	70		0.5064	0.0926	0.0143	10.8034			
303.15	50	30	0.4357	0.4691	0.0334	0.0333	29.9619	1.2649	845.09	1.50
	50	40		0.4833	0.0475	0.0250	21.0437			
	50	50		0.4876	0.0519	0.0200	19.2762			
	50	60		0.5045	0.0688	0.0167	14.5341			
	50	70		0.5079	0.0721	0.0143	13.8643			
308.15	50	30	0.4254	0.4469	0.0215	0.0333	46.4261	1.5487	1364.6	1.13
	50	40		0.4532	0.0279	0.0250	35.8995			
	50	50		0.4577	0.0324	0.0200	30.8866			
	50	60		0.4685	0.0431	0.0167	23.1797			
	50	70		0.4742	0.0488	0.0143	20.4792			

Table S9. Data of the van't Hoff equation for calculation of thermodynamic parameters ΔH^o, ΔS^o and ΔG^0 of different (THC+α-CD) inclusion complexes at λ_{max} = 236 and 263 nm.

λ_{max} (nm)	T (K^a)	1/T	Ka ($M^{-1}\times10^{-3}$)	lnKa	Slope	Intercept	ΔH^0 (KJ mol^{-1})	ΔS^0 (J mol^{-1} K^{-1})	ΔG^0 (KJ mol^{-1})
236	298.15	0.00335	1.28	7.1521	3,616.90	-4.9551	-30.07	-41.20	-17.79
	303.15	0.00330	1.12	7.0250					
	308.15	0.00325	0.86	6.7576					
263	298.15	0.00335	1.12	7.0235	5,384.50	-11.028	-44.77	-91.69	-17.43
	303.15	0.00330	0.85	6.7504					
	308.15	0.00325	0.62	6.4372					

Table S10. Data of the van't Hoff equation for calculation of thermodynamic parameters ΔH^o, ΔS^o and ΔG^0 of different (THC+β-CD) inclusion complexes at λ_{max} = 236 and 263 nm.

λ_{max} (nm)	T (K^a)	1/T	Ka ($M^{-1}\times10^{-3}$)	lnKa	Slope	Intercept	ΔH^0 (KJ mol^{-1})	ΔS^0 (J mol^{-1} K^{-1})	ΔG^0 (KJ mol^{-1})
236	298.15	0.00335	1.90	7.5475	3,260.70	-3.381	-27.11	-28.11	-18.73
	303.15	0.00330	1.62	7.3912					
	308.15	0.00325	1.33	7.1923					
263	298.15	0.00335	1.67	7.4226	3,558.30	-4.4839	-29.59	-37.28	-18.47
	303.15	0.00330	1.50	7.3111					
	308.15	0.00325	1.13	7.0343					

Table S11. Data of the van't Hoff equation for calculation of thermodynamic parameters $\Delta H^{\tau 0}, \Delta S^{\tau 0}$ and $\Delta G^{\tau 0}$ of different (THC+α-CD) inclusion complexes at λ_{max} = 236 and 263 nm.

λ_{max} (nm)	T (K[a])	1/T	K_a^{τ} ($M^{-1}\times10^{-3}$)	$\ln K_a^{\tau}$	Slope	Intercept	$\Delta H^{\tau 0}$ (KJ mol^{-1})	$\Delta S^{\tau 0}$ (J mol^{-1} K^{-1})	$\Delta G^{\tau 0}$ (KJ mol^{-1})
236	298.15	0.00335	1.30	7.1676	3,646.30	-5.0485	-30.32	-41.98	-17.80
	303.15	0.00330	1.10	7.0071					
	308.15	0.00325	0.87	6.7703					
263	298.15	0.00335	1.22	7.1088	5,889.60	-12.671	-48.97	-105.35	-17.56
	303.15	0.00330	0.81	6.7024					
	308.15	0.00325	0.64	6.4687					

Table S12. Data of the van't Hoff equation for calculation of thermodynamic parameters $\Delta H^{\tau 0}, \Delta S^{\tau 0}$ and $\Delta G^{\tau 0}$ of different (THC+β-CD) inclusion complexes at λ_{max} = 236 and 263 nm.

λ_{max} (nm)	T (K[a])	1/T	K_a^{τ} ($M^{-1}\times10^{-3}$)	$\ln K_a^{\tau}$	Slope	Intercept	$\Delta H^{\tau 0}$ (KJ mol^{-1})	$\Delta S^{\tau 0}$ (J mol^{-1} K^{-1})	$\Delta G^{\tau 0}$ (KJ mol^{-1})
236	298.15	0.00335	2.10	7.6478	4,908.10	-8.8301	-40.81	-73.42	-18.92
	303.15	0.00330	1.52	7.3276					
	308.15	0.00325	1.23	7.1141					
263	298.15	0.00335	1.47	7.2953	3,558.30	-4.4839	-29.59	-37.28	-18.47
	303.15	0.00330	1.20	7.0874					
	308.15	0.00325	0.93	6.8405					

Table S13. ^{1}H NMR data of the pure thiamine hydrochloride, pure α-Cyclodextrin, β-Cyclodextrin and the respective inclusion complexes.

α-Cyclodextrin (400 MHz, Solvent: D_2O), δ/ppm	**β-Cyclodextrin (400 MHz, Solvent: D_2O), δ/ppm**
3.161-3.207 (6H, t, J =18.400 Hz), 3.217-3.250 (6H, dd, J = 5.200, 13.200Hz), 3.436-3.562 (18H, m), 3.585-3.609 (6H, t, J = 9.600Hz), 4.659-4.650 (6H, d, J = 3.600 Hz)	3.399-3.444 (7H, t, J = 18.000 Hz), 3.472-3.506 (7H, dd, J = 6.400 Hz, 13.6 Hz), 3.692-3.751 (21H, m), 3.776-3.823 (7H, t, J = 18.800 Hz), 4.904-4.913 (7H, d, J = 3.600 Hz)
Thiamine hydrochloride (400 MHz, Solvent: D_2O), δ/ppm	
2.386(3H, s), 2.472(3H, s), 3.018-3.047(2H, t, J=5.600Hz), 3.710-3.739(2H, t, J=6.00Hz), ``5.412(2H, s), 7.868(1H, s), 9.509(1H, s)	
THC+α-CD inclusion complex (400 MHz, Solvent: D_2O), δ/ppm)	**THC+β-CD inclusion complex (400 MHz, Solvent: D_2O), δ/ppm)**
2.406(3H, s), 2.493(3H,s), 3.055-3.082(2H, t, J=5.4), 3.451-3.513(14H, m), 3.707-3.870(24H,m), 4.922-4.932(6H, d, J=4.0), 5.430(2H, s),7.876(1H, s), 9.523(1H, s)	2.444(3H, s), 2.531(3H, s),3.075-3.105(2H, t, J=6.000Hz),3.486-3.567(16H, m), 3.780-3.883(28H, m), 4.976-4.996(7H,d, J=8Hz), 5.467(2H, s),7.917(1H, s),9.550(1H,s)

Table S14. Frequencies of FTIR spectra of α-CD, β-CD, THC and two solid inclusion complexes

α-cyclodextrin (α-CD)		**β-cyclodextrin (β-CD)**	
Wavenumber (cm^{-1})	**Group**	**Wavenumber (cm^{-1})**	**Group**
3410.09	-O-H stretching	3424.05	-O-H stretching
2927.18	-C-H stretching	2927.31	-C-H stretching
1363.21	-C-H and -O-H bending	1398.37	-C-H and -O-H bending
1152.27	C-O-C bending	1160.32	C-O-C bending
1033.25	C-C-O stretching	1030.39	C-C-O stretching
950.32	skeletal vibration involving α-1,4linkage	940.29	skeletal vibration involving α-1,4linkage
Thiamine hydrochloride (THC)			
Wavenumber (cm^{-1})		**Group**	
3436.05		Broad band of merged spectra due to the presence of NH_2 and -OH stretching	
2361.26		-CH_2 out of plane bending	
1636.35		Bend N-H (NH_2) stretching	
1000.03		Deformation N-H (NH_2)	
1614.02-1380.15		Pyrimidine ring stretching vibration	
1360.25		C-CH_3 group	
1223.15		Stretching C-CH_2 bridge of pyrimidine ring	
519.08		S-C-N and S-C-C out of plane deformation of thiazole ring	

(IC - 1) THC + α-CD		(IC – 2) THC + β-CD	
Wavenumber (cm^{-1})	**Group**	**Wavenumber (cm^{-1})**	**Group**
3420.09	-O-H stretching	3405.23	-O-H stretching
2914.19	-C-H stretching	2906.16	-C-H stretching
2365.21	$-CH_2$ bending	2363.29	$-CH_2$ bending
1632.02	C-O-C bending	1632.27	C-O-C bending
1153.25	Stretching C-CH_2 bridge of pyrimidine ring	1157.33	Stretching C-CH_2 bridge of pyrimidine ring
1029.13	C-C-O stretching	1027.11	C-C-O stretching

Table S15. Spectro-fluorimetric data for the Benesi-Hildebrand double reciprocal plot of (HSA+THC) system at 298.15 K[a].

HSA (g/L)	THC (μM)	I_0	I	$I-I_0$	1/[THC] (M^{-1})	1/ΔI ($\times10^6$)	Intercept ($\times10^7$)	Slope ($\times10^{10}$)	K_a^{ϕ} ($M^{-1}\times10^{-3}$)
0.1	20	3373138.75	3194777	178362.0	0.0500	5.6066	4.2954	1.0213	4.21
0.1	30		3101683	271455.5	0.0333	3.6838			
0.1	40		3034246	338893.3	0.0250	2.9508			
0.1	50		2987936	385202.8	0.0200	2.5960			
0.1	60		2901248	471891.3	0.0167	2.1191			

[a]Standard uncertainties in temperature *u* are: *u*(T) = ±0.01 K.

Table S16. Spectro-fluorimetric data for the Benesi-Hildebrand double reciprocal plot of (HSA+THC) system in presence of fixed amount of α-CD at 298.15 K[a].

HSA (g/L)	THC (μM)	I_0	I	I-I_0	1/[THC] (M^{-1})	1/ΔI (×10^6)	Intercept (×10^7)	Slope (×10^{10})	K_a^{ϕ} (M^{-1}×10^{-3})
0.1	20	3373138.75	3201177	171962.0	0.0500	0.5815	3.3303	1.1004	3.03
0.1	30		3121683	251455.5	0.0333	0.3977			
0.1	40		3066246	306893.3	0.0250	0.3258			
0.1	50		2958936	414202.8	0.0200	0.2414			
0.1	60		2909248	463891.3	0.0167	0.2156			

Table S17. Spectro-fluorimetric data for the Benesi-Hildebrand double reciprocal plot of (HSA+THC) system in presence of fixed amount of β-CD at 298.15 K[a].

HSA (g/L)	THC (μM)	I_0	I	I-I_0	1/[THC] (M^{-1})	1/ΔI (×10^6)	Intercept (×10^7)	Slope (×10^{10})	K_a^{ϕ} (M^{-1}×10^{-3})
0.1	20	3373138.75	3211177	161962.0	0.0500	0.6174	2.9210	1.1743	2.49
0.1	30		3138683	234455.5	0.0333	0.4265			
0.1	40		3047246	325893.3	0.0250	0.3068			
0.1	50		2993936	379202.8	0.0200	0.2637			

0.1	60		2946248	426891.3	0.0167	0.2343			

FIGURE

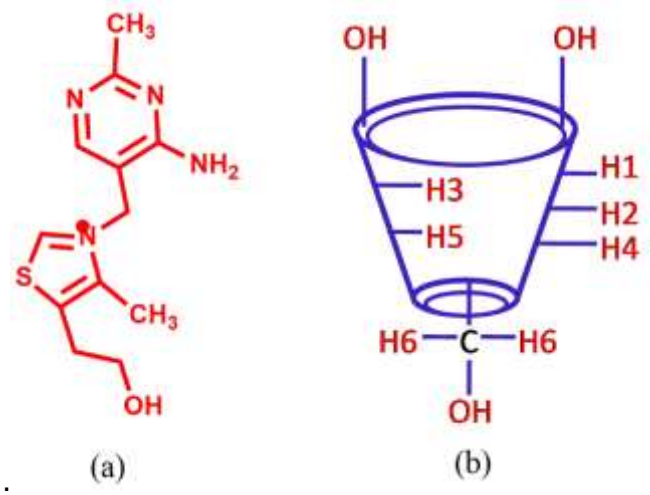

Figure 1: Molecular structures of (a) thiamine hydrochloride, (b) cyclodextrin

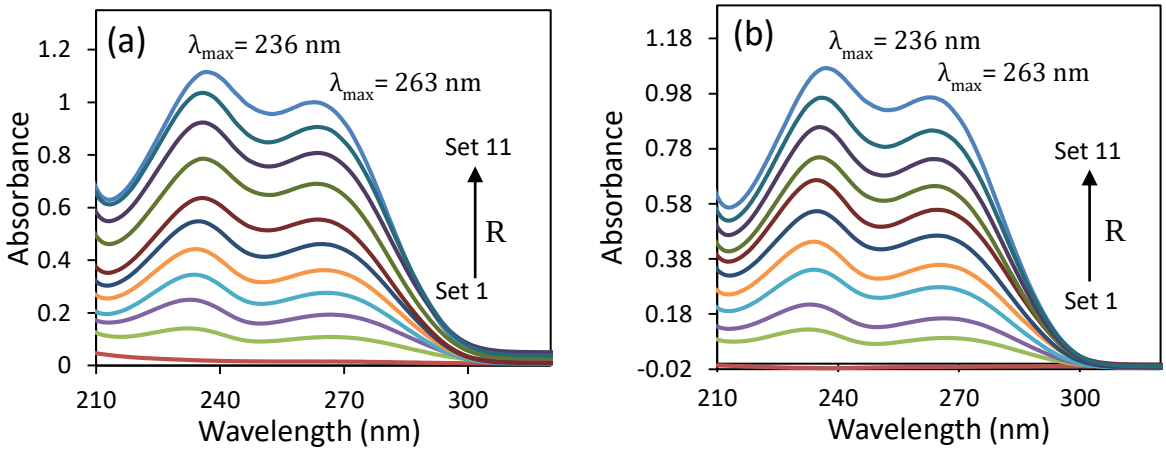

Figure 2(a,b): Spectra for the generation of Job plot of (a) THC+α-CD and (b) THC+β-CD systems at 236 and 263 nm.

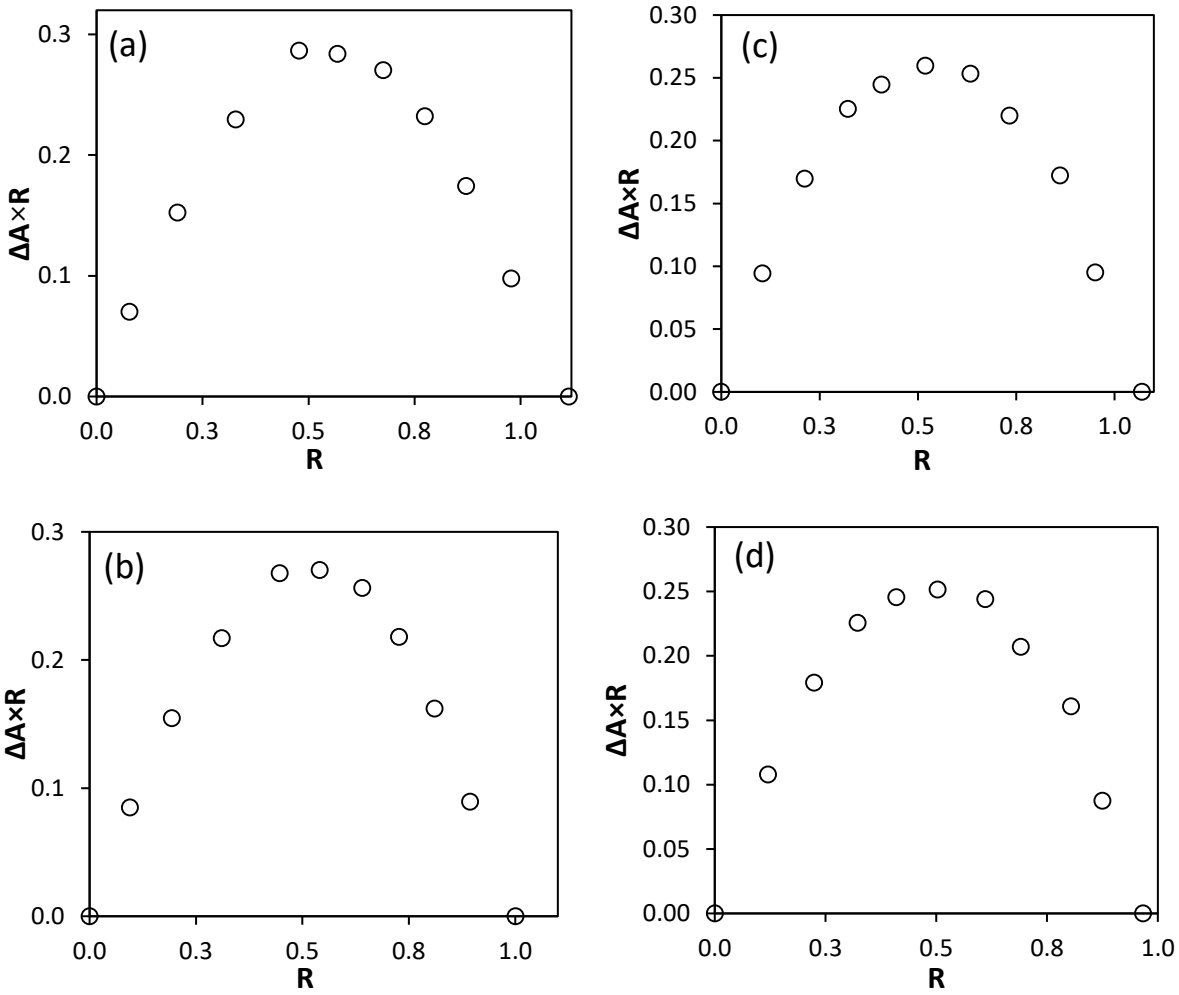

Figure 3(a,b,c,d): Job plots of the THC+α-CD system at (a) λ_{max}=236 nm, (b) λ_{max}=263 nm and THC+β-CD system at (c) λ_{max}=236 nm, (d) λ_{max}=263 nm

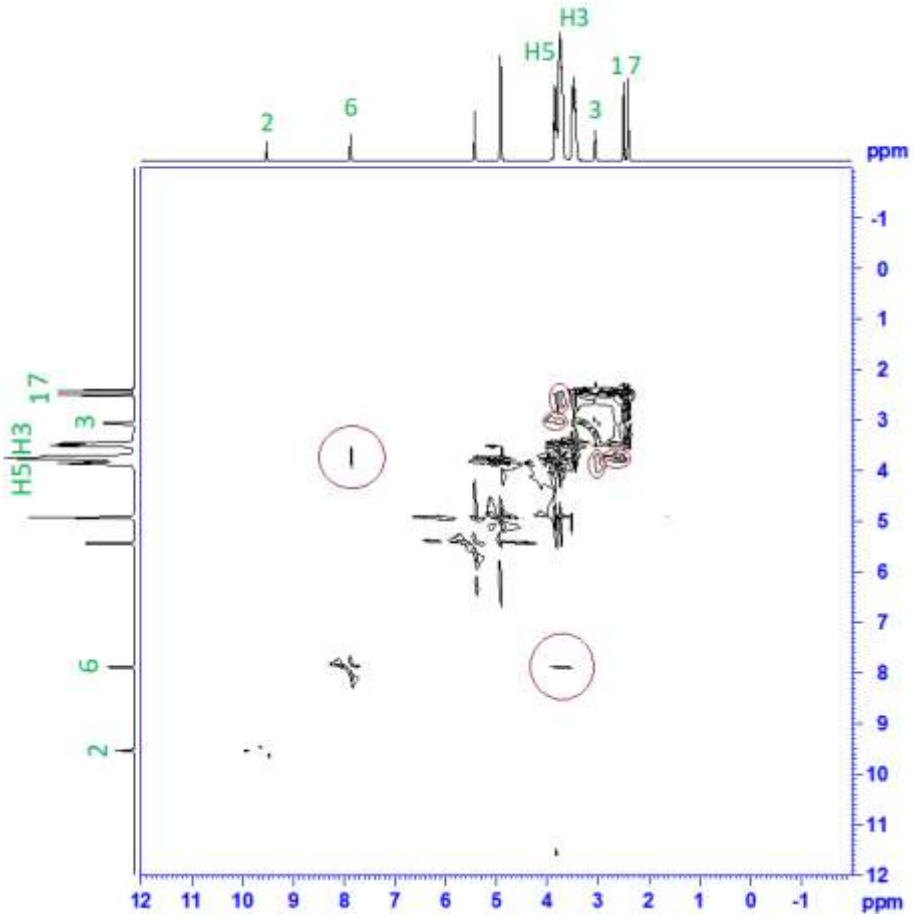

Figure 4. 2D ROESY NMR spectra of IC-1 (THC+α-CD)

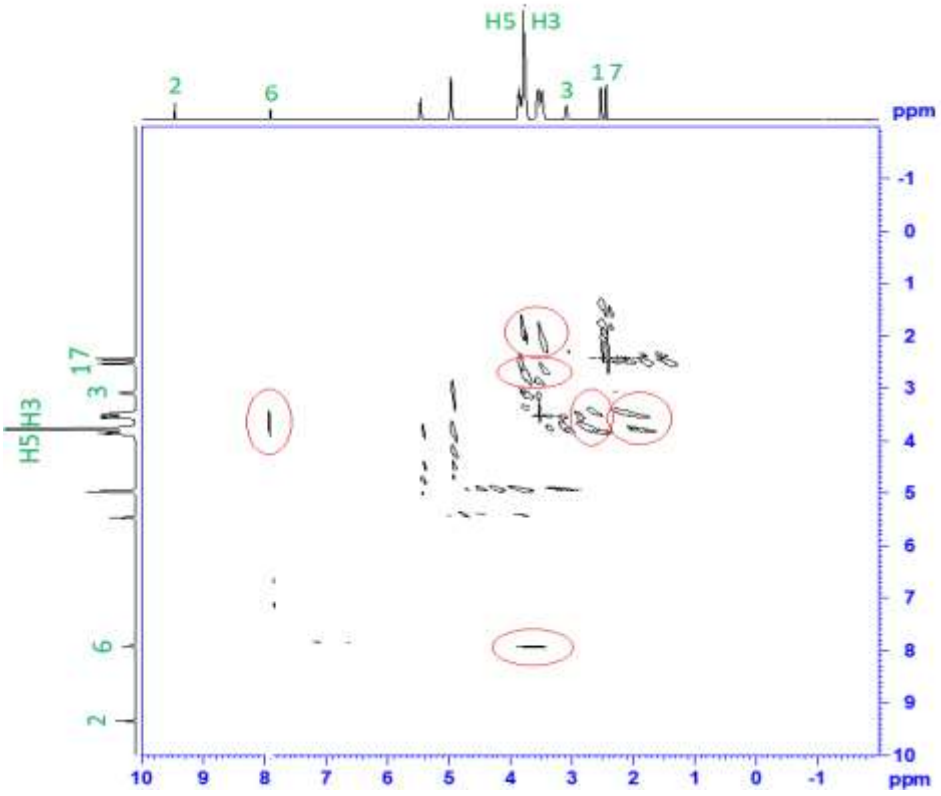

Figure 5. 2D ROESY NMR spectra of IC-2 (THC+β-CD)

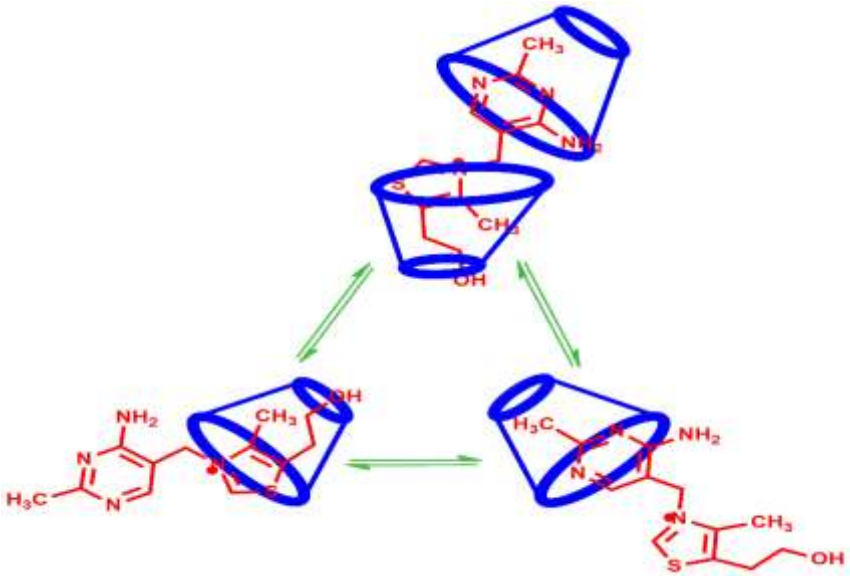

Figure 6: Plausible mechanism of inclusion complexation through wider rim of cyclodextrin.

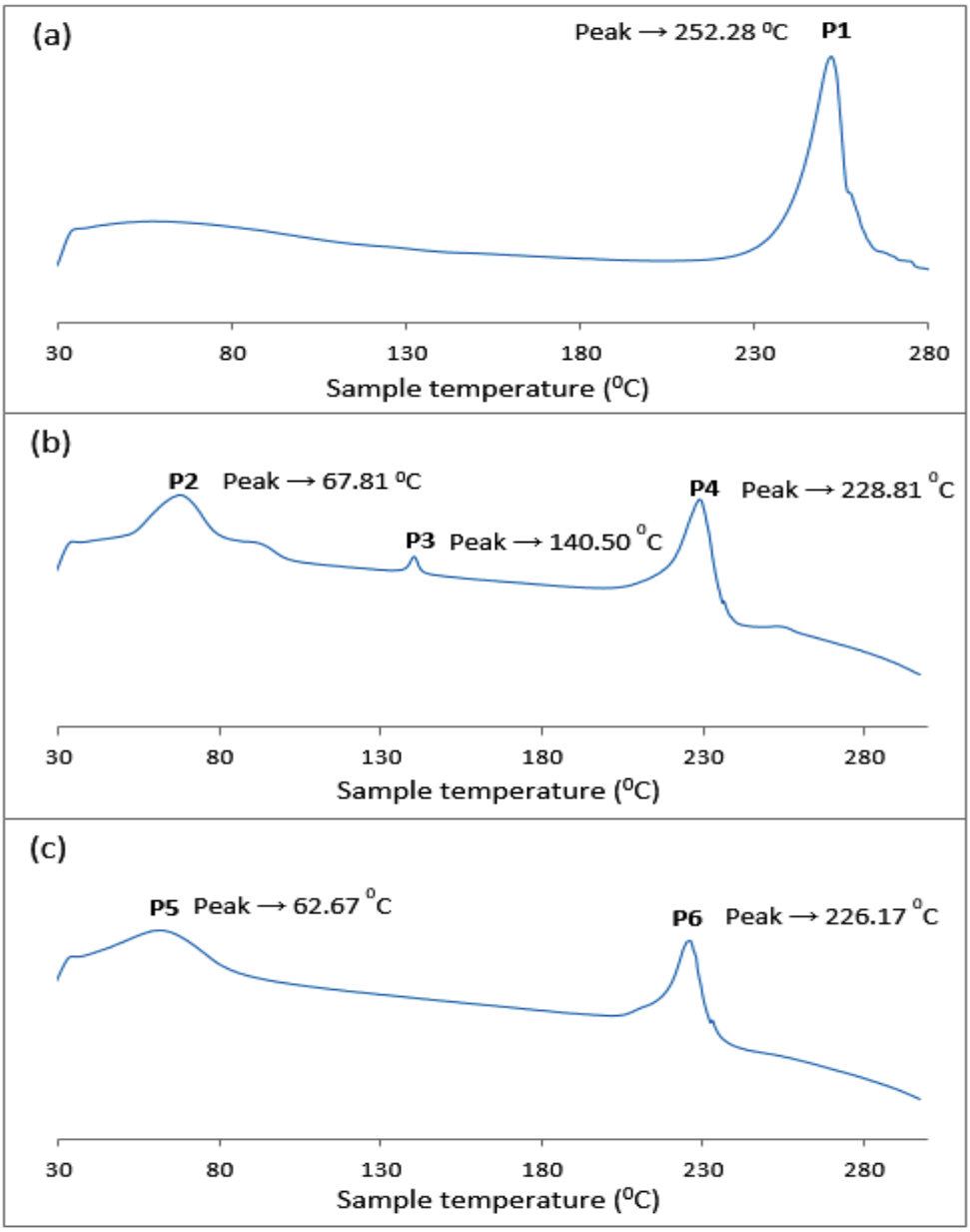

Figure 7(a,b,c):DSC thermos-gram of (a) THC, (b) THC+α-CD, (c) THC+β-CD

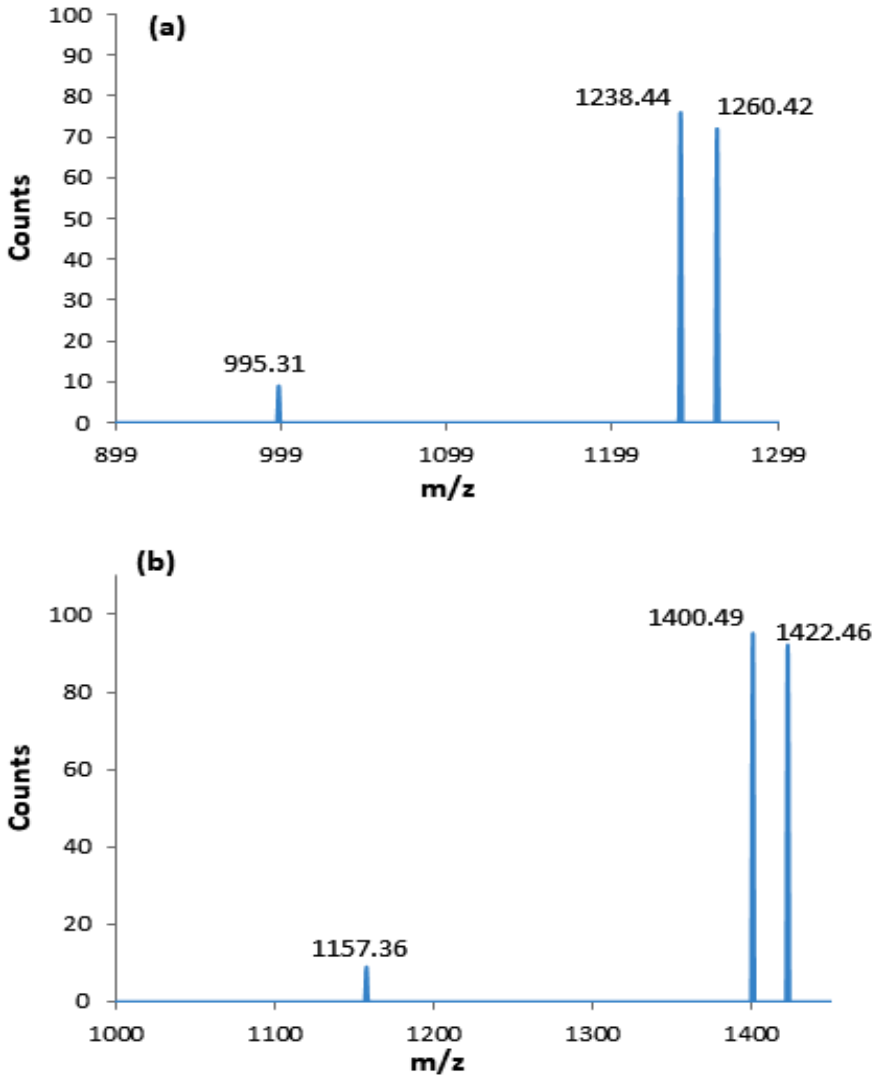

Figure 8(a,b): ESI- Mass spectra of (a) IC-1 (THC+α-CD), (b) IC-2 (THC+β-CD)

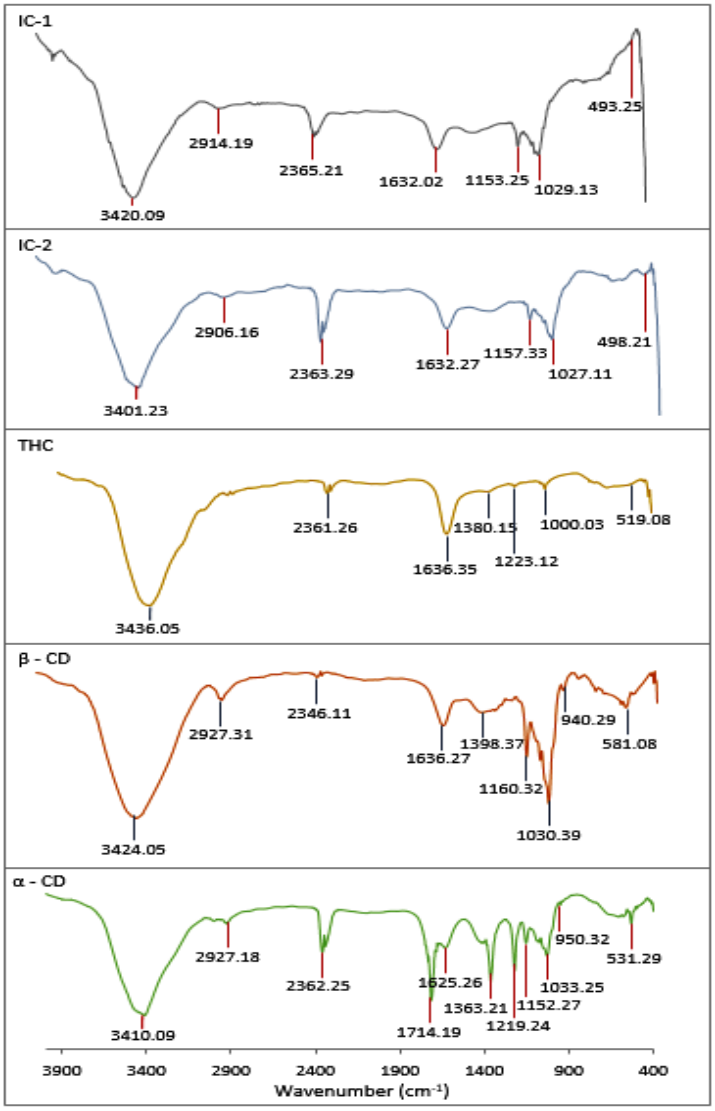

Figure 9(a,b,c):FTIR spectra of IC-1 (THC+α-CD), IC-2(THC+β-CD), THC, β-CD and α-CD

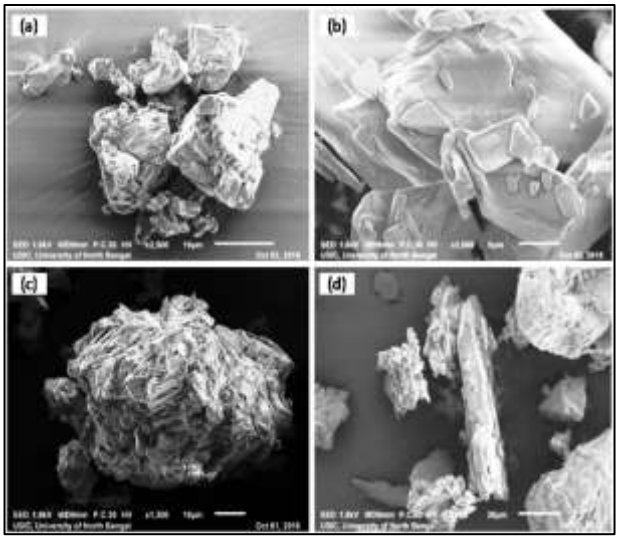

Figure 10(a,b,c,d):SEM images of (a) α-CD, (b) THC, (c) (THC+α-CD) IC and (d) (THC+α-CD) physical mixture.

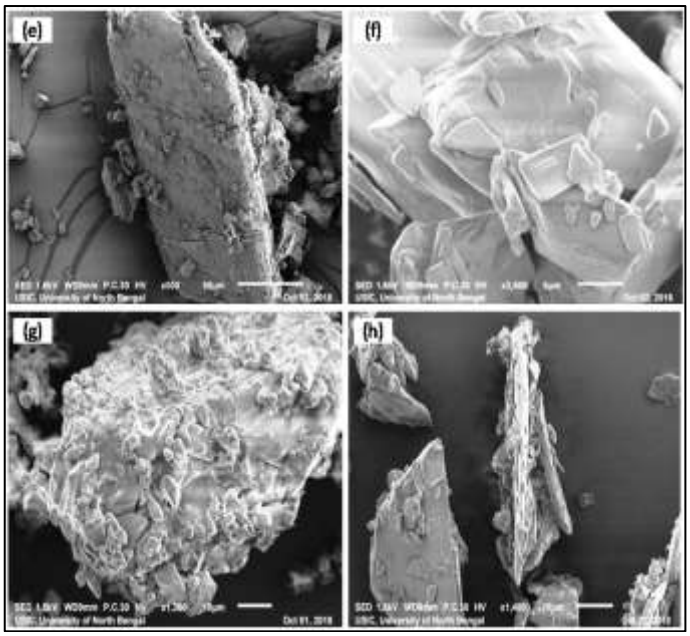

Figure 11(e,f,g,h):SEM images of (e) α-CD, (f) THC, (g) (THC+α-CD) IC and (h) (THC+α-CD) physical mixture.

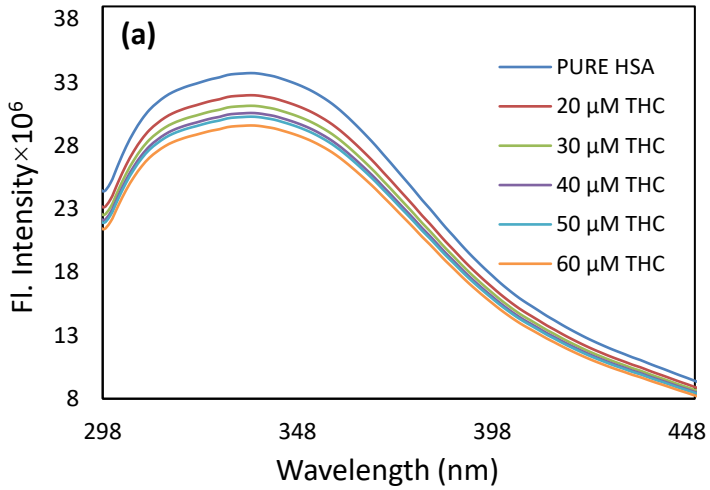

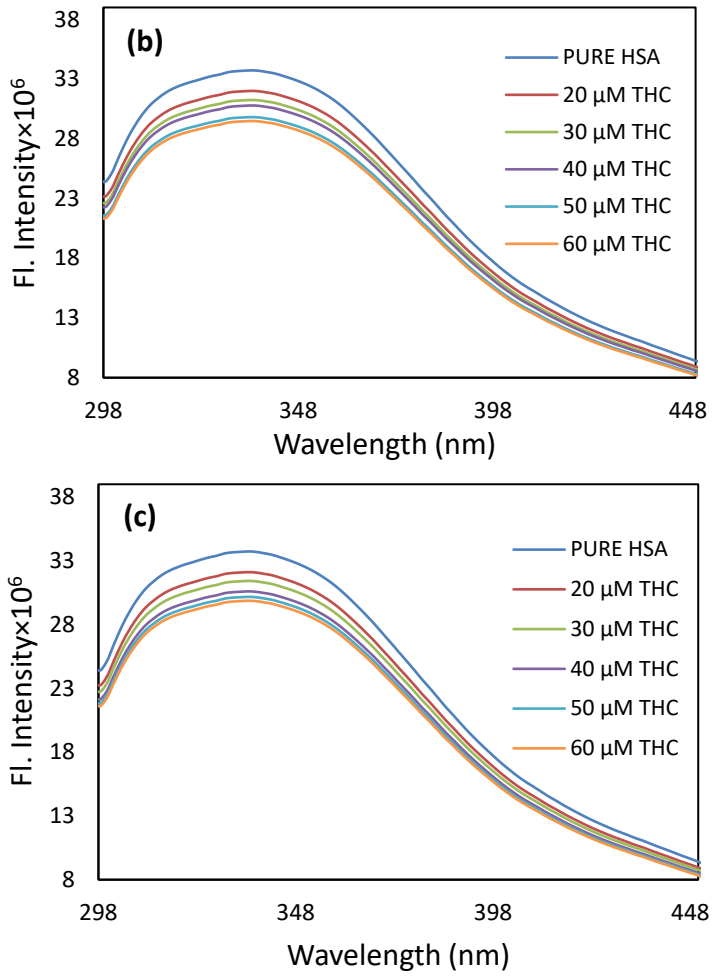

Figure 12(a, b, c): Fluorescence spectra of HSA molecule in presence of (a) THC, (b) THC along with β-CD (c) THC along with α-CD at the various concentrations.

CHAPTER VI

Enhancement of Fire Resistivity & Conversion into Bio-Degradable Pollutant to Minimize Environmental Pollution Explored by Physicochemical Contrivance

Abstract: Inclusion complexation of a non-biodegradable pollutant in hydrophobic cavity of β-cyclodextrin and hydroxypropyl-β-cyclodextrin were synthesized and characterized to retain its fire resistance property and converted it into bio-degradable molecule. ^{1}H NMR, 2D ROESY, HRMS, SEM, surface tension, etc. studies have been executed to establish this fact. The stoichiometry of the two complexes has been obtained as 1:1. The inclusion has been established by ^{1}H-NMR and 2D ROESY spectroscopic analysis. Substantial shifts in IR stretching frequency support the inclusion process. HRMS measurement gives the molecular ion peaks corresponding to the inclusion complex of 1:1 molar ratio of host and guest molecules. Surface texture properties of the inclusion complexes were studied by SEM and the presence of bromine were proved by EDXS. Thermal stabilities of the inclusion complexes were illustrated by DSC and melting point analysis. The aqueous solubility of the inclusion complexes demonstrate that these are more bio-available to the microorganism making them biodegradable in nature. The biodegradability study confirms the conversion of non-biodegradable HBCDD into biodegradable material by encapsulating in the two cyclodextrins.

1. Introduction

1,2,5,6,9,10-hexabromocyclododecane(HBCDD) is mainly globally used as fire retardant additives for producing extruded or expanded polystyrene foam materials in bulk amount and has been widely manufactured from 1960[1](Figure 1). Moreover, it is used as an additive to manufacture various things such as upholstered furniture, automobile interior textiles, car cushions, electric and electronic equipment etc[2-5]. In recent past decades it is one of the major environmental concern pollutant due to its persistent, toxic, bio-accumulative and biomagnifying or bio-transformative nature in environment[4,6,7]. For these reasons this cyclic aliphatic brominated compound is very harmful to aquatic life. Global market demand of HBCDD was 22000 tons per year in 2003[8].The major portion of HBCDD was used in Europe which was estimated at

11,000 tons in 2006,of which about 96% were used in expanded and extruded polymer[9]. Recently, it is included in Annex A of the Stockholm Convention on Persistent Organic Pollutants (POP),2009 and in 2013 for elimination with restricted uses[5,8,10]. Due to all of the adverse effects on environment it is restricted in Japan in2014 and in Republic of Korea(South Korea) in 2015 permanently till the advanced substituted one upto 2020[11,12].In recent years, the bromine industry has taken important steps to reduce discharges from manufacture and use of HBCDD and other fire retardants, notably its production is closed in HBCDD manufacturing site Newton Aycliffenearly NE coast of England. According to Newton EU risk assessment, "it was the largest single source of emissions of HBCDD to the environment"[13]. But unfortunately brominated compounds are still manufactured in huge extent and used in customer's product in both developed and developing countries resulting environmental contamination and highly exposure to wildlife and human beings to a great extent[11,12]. HBCDD has been found in different environment samples for example residential dust, pooled milk, human breast milk, geographic polar areas, sediments and marine food, marine animals i.e. Harbor porpoises and Fishes, Birds, Bird eggs, water, mounting and sealant foam, oriented strand board and other composite woods, etc.[6,8,14-16]. Among different adverse toxicological and environmental effects on biota, the most crucial effect is on the mammalian nervous system. Lowest observable effects at very low μM concentrations about 1000-20,000 ng g^{-1} of HBCDD are observed in vitro exposures and in vivo exposures[1].

Because of its dramatically negative environmental impact, the development of efficient HBCDD removal technologies has increasingly become a significant environmental concern. The bio-accumulative and biomagnifying nature of HBCDD is critically threaten to the sustainable development of our planet as influence of HBCDD on the environment is long-term and difficult to repair. Some traditional methods had applied to remove this HBCDD from water for example, debromination technique, UV-irradiation technique, adsorption technique etc. and also some micro biodegradation technique etc. had applied to degrade it[17-21]. Here we approach a new novel way to remove this POP via making an encapsulation complex with β-cyclodextrin (β-CD) and hydroxypropyl-β-cyclodextrin (HP-β-CD) respectively. These supramolecular cyclodextrin compounds have been chosen as host moiety due to

their unique bi-phasic catalytic structural features i.e. hydrophobic interior and hydrophilic exterior and having an interesting internal capacity for undergoing reversible capture and release of molecular guest species[22,23]. Cyclodextrins are well established oligosaccharide of glucose units in multiple area of science for last few decades. As HBCDD is a hydrophobic molecule,it may be inserted into the hydrophobic cavity of cyclodextrin giant molecule. Cyclodextrin molecules have wide range of applications in different area of science for example trapping of different chemicals, chemo-sensors solubility enhancement, molecular switches, selective transport of compounds, molecule-based logic gates, controlled drug delivery, perfume release,chromatography, molecular machines,transmembrane channels, supramolecular polymers, transmembrane channels etc.[24-28].

Here, we have attempted to make inclusion complexes of HBCDD within the apolar cavity of β-CD and HP-β-CD respectively. The structure of inclusion complexes has been characterized by several reliable spectroscopic techniques such as ^{1}H NMR,2D ROESY,HRMS, SEM, DSC and FTIR spectra.This novel work moves toward the removal of HBCDD organic pollutant from environment via formation of inclusion complexes with water soluble cyclodextrin supra-molecules. The aim of this novel work is to enhance the water solubility and bioavailability of HBCDD towards microorganisms for its faster biodegradability.

2. Experimental

2.1. Materials

1,2,5,6,9,10-hexabromocyclododecane and β-CD of purity grade were bought from Sigma-Aldrich and Hydroxypropyl-β cyclodextrin was purchased from Tokyo Chemical Industry and also used as received.The purity of all these compounds were ≥95%,97% and98% respectively.

2.2. Apparatus

^{1}H NMR spectroscopy were done in DMSO-d^{6} at 300 MHz in Bruker Avance 300 MHz apparatus at 298 K and 2DROESY experiment was performed in Bruker Avance 400 MHz apparatus at 298 K.Theelaborated ^{1}H NMR and 2D ROESY spectra have been shown in Figure 2 and S1-S5.All the data are represented in terms of

chemical shift andthe signals were taken as δ values in ppm byDMSO-d^6 atδ = 2.50 ppm as internal standard.

Fourier transform infrared spectra were done in a Perkin Elmer FT-IR spectrometer as per KBr disk technique. KBr disks were prepared in 1:100 ratio of sample to KBr.At room temperature 4000-400 cm^{-1} scanning range had taken during the FTIR studying.

Mass spectrometry was performed by Q-TOF apparatus with positive mode ionization using methanol solution of the inclusion compounds.

Surface tension data were obtained by platinum ring detachment method using digital tensiometer K9, KRÜSS. Temperature was kept at 298.15 K by circulating thermostatic water through a double walled glass vessel holding the solution.

The surface morphology of HBCDD, β-CD, HP-β-CD and their inclusion complexes was studied by JEOL JSM IT 100 Scanning Electron Microscope (SEM) using different accelerating voltage. Dry samples were spread onto carbon tapes (double adhesive carbon-coated tape) adhered to aluminum stubs which were then coated with a thin layer of gold ions in gold -ionization chamber. Then samples were scanned by SEM and images were taken under different resolutions.

Melting points of HBCDD and the two inclusion complexes were determined with the help of capillary tube by Thiele tube method.

2.3. Procedure of formation of solid inclusion complexes

All the experimental samples were accurately weighed in desired proper quantities with the help of METTLER TOLEDO AG-285 analytical balance having uncertainty of ±0.1 mg at 298.15K. Adequateprotectionwas taken to reduce the loss of solvent caused by evaporation throughout working with the solutions. The solid inclusion complexes have been prepared with 0.3mM of β-CD and HP-β-CD separately in two clean and dried beakers with triply distilled and deionized water which were allowed to stir for 6 hours on a magnetic stirrer at room temperature. Then 0.3 mM solution of HBCDD was prepared in a beaker with HPLC grade absolute ethanol and allowed to stir for 6 hours. After that, the prepared HBCDD solution was added

dropwise to those respective host solutionsseparately making the ultimate equimolar solutions. After completion of 48 hours stirringmaintaining the temperature at 50-55°C, the solutions were taken off from the hot-top (Tarsons Digital Spinot) in order to cool down at room temperature. Suspensions appeared after cooling were filtered off and stored in vacuum desiccator after drying in air.[29]

2.4. Procedure for biodegradation study

10 mM solution of the two inclusion complexes and pure HBCDD in DMSO were separately incubated at 37^{o}C in a medium of 1.0 g of glucose, 5.0 g of polypeptone, 5.0 g of yeast extract, and 10 g of NaCl per liter, pH 7.0 with and without Pseudomonas sp. bacteria in 100 ml conical flask for 7 days. 2 mL solution was taken out from each incubated media and subjected to centrifuge in orbital incubator at 10,000 rpm speed for 10 minutes. Then the soup was extracted after being thoroughly mixed with equal volume of ethyl acetate (EAA) for each case and with the solution in EAA, TLC was performed with 10% EAAin n-hexane solution media. The respective TLC spots were observed in a closed glass chamber which was completely saturated with iodine vapour.

3. Result and discussion

3.1. ^{1}H NMR and 2D ROESY spectra analysis of the inclusion complexes

Encapsulation of any molecule inside the hydrophobic cavity of β and HP-β-CD results the change in the chemical shift of the interacting protons of the guest along with CD in ^{1}H NMR spectrabecause of the mutual shielding via space.CD has H3 and H5 hydrogenatoms inside the torus cavity, specially, the H3 protons are located near the wider rim while H5 protons are positioned close to the narrower rim while the other H1, H2 and H4 protons are located at the outer surface of the CD molecule[22,29-31]. The ^{1}H NMR spectra ofHBCDD,β-CD, HP-β-CD and their two ICs areshown in FigureS1-S5, where the hydrogens of HBCDD as well as signals for H3 and H5 hydrogens of cyclodextrin is appeared with shifted chemical shift (δ) values. The ^{1}H NMR spectra for all of these newly formed complexes reveal considerable upfield shift confirming the construction of inclusion complexes.[32-34]

2D ROESY NMR spectroscopy offersconvincingsupport about the spatial close proximity of the interacting atoms of the guest with the host molecules by detecting the off-diagonal cross-correlations[35,36].The hydrogens which are placed within 0.4 nm in gap may generate a rotating-frame NOE spectroscopy (ROESY)[37].2D ROESY spectra of HBCDD with β and HP-β-CDwere recordedin DMSO-d^6which show noteworthy correlation of the hydrogens of HBCDD with the respective H3 and H5 protons of both CD molecules establishing that the HBCDD molecule was encapsulated into the both cyclodextrin cavities (Figure2)[38,39]. It may be noticed that the H-6 protons of cyclodextrins did not interact with the protons of HBCDD by the inclusion processes, suggesting that the pollutant molecule was inserted into the cyclodextrin cavity via the wider rim and not from the side of the narrower rim otherwise off-diagonal cross-peaks could be observed for the interaction of H6 with the guest molecule in the respective ROESY spectra[40,41].

3.2. FTIR spectra of solid inclusion complexes

Infra-red spectroscopic analysis of IC's along with the pure host and guest molecules also unveils the reliability about the way by which the IC's are formed and found to mimic the mode of host – guest interaction as obtained from the 2D ROESY NMR spectroscopic study[42-44]. KBr disk of the samples were prepared separately and the spectra obtained are reported in Figure 3, 4. The significant peaks of corresponding chemical bonds that undergo shift by wavelength while complexations are listed in table 1 and S1.

The following spectral changes (Table 1), taking place in the (HBCDD+β-CD) system may enable us to recognize it as an inclusion complex. (i) The signal for (C^{sp3}-Br) stretching of HBCDD usually appears in the range between 718.02-538.17 cm^{-1}, but most of the signals in this span of wavelength were found to be masked leaving a broad signal at 604.28 cm^{-1} while complexed with β-CD. (ii) The peak at 1442.06 cm^{-1} responsible for ($C^{sp3}H_2$) bending of HBCDD is now shifted to 1380.34 cm^{-1} making a large wavenumber shift of 61.72 cm^{-1}. (iii) (C^{sp3}-H) stretching frequency of HBCDD appearing at 2930.25 cm^{-1}, shifted to 2915.05 cm^{-1} during its complexation with β-CD. (iv) A frequency shift of 13.25 cm^{-1} is also observed for (O-H) stretching of β-CD for

which, signal of (O-H) stretching at free and complexed state were noted as 3436.28 and 3423.03 cm^{-1} respectively.

The formation of (HBCDD + HP β-CD) inclusion complex and various interactions developed thereby were analyzed by the following spectral changes – (i) The peaks for (C^{sp3}-Br) stretching of HBCDD were observed in the range of 718.02-538.17cm^{-1}, shifted to the wavelength range of 701.15-529.11 cm^{-1} in case of inclusion complex. Beside shifting (12.955 cm^{-1}) masking of various significant is also observed in this region. (ii) The signal responsible for ($C^{sp3}H_2$) bending mode of HBCDD appearing at 1442.06 cm^{-1}, shifted to 1419.23 cm^{-1} while formation of inclusion complex with HP β-CD. (iii) The (C^{sp3}-H) stretching frequency of HBCDD was observed at 2930.25 cm^{-1}, in case of inclusion complex it was found to appear in the range 2940.07-2895.12 cm^{-1} making a significant shift of 15.155 cm^{-1}. (iv) The (O-H) stretching frequency of HP β-CD also made to be shifted from 3419.25 to 3405.05 cm^{-1} owing to the supramolecular host – guest interaction.

This is hardly to detect the appearance of additional signals in the infra-red spectrum of studied ICs suggests there is no sign of chemical reaction which may be taken place during complexation. Now, it is easy to say that, the spectral changes, observed in case of inclusion complexes responsible for supramolecular interaction.

3.3. High resolution mass spectrometric (HRMS) analysis of inclusion complexes

The formation of two inclusion complexes i.e., IC-1 and IC-2 may be confirmed with the help of ESI-MS study. Figure 5 shows mass spectra of two ICs, which show the intense peaks at m/z 1798.27 and 2183.88 respectivelyindicating the formation of $[HBCDD+\beta\text{-}CD+Na]^+$and $[HBCDD+HP\text{-}\beta\text{-}CD+H]^+$inclusion complexes and their corresponding host-guest stoichiometric ratio is 1:1 (Table 2). It is noted that no other peaks around those values are observed in mass-spectrometry[45,46].

3.4 Surface tension and stoichiometry in the inclusion complex

Surface tension (ST) data provides the stoichiometry of the host-guest inclusion complex. The ST is plotted against the mole ratio of β-CD and HP-β-CD respectively with HBCDD. Figure 6 explains the variation of ST, where in both cases

there were progressively rising trend of ST with increasing concentration of cyclodextrins as a result of encapsulation of the HBCDD molecule from the surface of the solution into the hydrophobic cavity of cyclodextrins forming host-guest inclusion complexes. Most importantly both the plots demonstrate that there are single clear breaks in each curve (figure 6), which not only reveal the formation but also specify the 1:1 stoichiometric ratio for each of the inclusion complexes formed [47] [48] [29] [49].

3.5. Scanning electron microscopic (SEM) analysis of the inclusion complexes

Scanning electron microscopy is a qualitative method to determine surface topographical aspect of the raw materials and corresponding products formed by complexation with cyclodextrins[50]. Figure 7 shows the micro-photographs of HBCDD, β-CD, HP-β-CD, IC-1 and IC-2 respectively. From these images it is cleared to see that the original individual characteristic morphology of each raw materialwas completely lost in their respective products i.e. IC-1 and IC-2. The irregular characteristic amorphous natured HBCDD, irregular and parallelogram shaped β-CD and cavity with spherical shaped HP-β-CDwere completely changed in their respective ICs[51]. Here,IC-1 showed more compactness from its individual raw materials but still some amorphous character was present in it and IC-2 appeared as smooth, homogeneous, even, regular and plate-like shape. But it is clear that it was not possible to differentiate between two individual components in their respective binary systems(IC-1 and IC-2).

Thus, the reason behind the formation of these new surfaced products (IC-1 and IC-2) is possibly due to the strong complexing interaction of HBCDD with β-CD and HP β-CD accordingly, which is further supported by Energy-Dispersive X-ray Spectroscopy (EDXS) analysis[52].

EDXS is an analytic technique used for elemental analysis of a sample. From Figure 8 it is shown that, in pure β-CD and HP-β-CD there is no Br atoms at all but in their ICs with guest HBCDD, we can see the appearance of Br atoms which also supported the fact drawn from the SEM studies.

3.5. DSC thermogram

The differential scanning calorimetry (DSC) is a suitable method for the investigation of thermal properties of CD based inclusion complexes as both the qualitative and quantitative insights about the physicochemical state of the drug can be gathered while encapsulated into the cavity of CDs. Normally, the shifting of an endothermic peak in DSC thermogram indicates a change in melting point, crystal lattice or sublimation point due to inclusion complexation[53,54]. DSC thermograms of inclusion complexes, pure host and pure HBCDD have been depicted in figure 9, which is evident that the peak at 139^0C of pure HBCDD is absent in the HBCDD-β-CD and HBCDD-HP-β-CD inclusion complexes respectively. This indicates the higher stability and more fire resistivity of the inclusion complexes than the pure HBCDD.

3.7. Melting point and aqueous solubility of the solid inclusion complexes

Melting points for both the ICs including pure HBCDD were determined with the help of capillary method. From Table 3,it can be seen that the melting points of HBCDD, IC-1 and IC-2 differ significantly from each other[55]. The melting point for HBCDD is 195.0^0C, for IC-1 209.5^0C and for IC-2 210.5^0C. The higher melting point of the inclusion complexes compare to its parent compound, namely, HBCDD are because of the fact that extra amount of heat is required for that compound to come out from the corresponding cyclodextrins (β-CD and HP-β-CD respectively) cavity and also these higher values of melting point i.e. 209.5^0C and 210.5^0C clearly indicate the formation of two new inclusion complexes i.e. IC-1 and IC-2 respectively[55].

The aqueous solubility of HBCDD is very low in a wide range of temperature. But, the inclusion complexes were found to be fairly soluble in water at room temperature (Figure 10 and Table 4)[56-58]. This is the indication of a molecule to be bio-available and also bio-degradable by the microorganisms. Thus the pollutant HBCDD which was a non-bio-degradable in nature, now has been converted into a bio-degradable material through the newly formed inclusion complexes with β and HP-β-CD respectively**.**

3.8. Bio-degradability study of the inclusion complexes

The two inclusion complexes and pure HBCDD were exposed to Pseudomonas sp. bacteria in a medium (1.0 g of glucose, 5.0 g of polypeptone,5.0 g of yeast extract,

and 10 g of NaCl per liter, pH 7.0) in 100 ml conical flask for 7 days to explore the degradation of HBCDD in the IC-1 and IC-2.[59,60,61]Interesting results were found after incubation at 37^{o}C. The IC-2 was found to be fully degraded at this condition and IC-1 was found partially degraded by the Pseudomonas sp. bacteria, while incubation of pure HBCDD with Pseudomonas sp. bacteria under identical condition causes no degradation of the pollutant as found from the spots in TLC plates.

TLC of the incubated inclusion complexes are shown in figure 11, which confirm the use of HP-β-CD andβ-CD as the encapsulating agent for HBCDD to make the pollutant bio-available and bio-degradable.

The TLC plates I and II show the degradation study of IC-1 and IC-2 respectively. Spot I-a is for the incubated solution of IC-1 with bacteria, I-b for incubated solution of IC-1 without bacteria, I-c for IC-1 and I-d for HBCDD. Similarly for the second TLC Spot II-a is for the incubated solution of IC-2 with bacteria, II-b for incubated solution of IC-2 without bacteria, II-c for IC-2 and II-d for HBCDD. After incubation no spot was found for IC-2, clearly indicating the decomposition of HBCDD while encapsulated byHP-β-CD. The HBCDD was decomposed partially while encapsulated by β-CD as found from the faint spot on TLC plate. This study evidently reveals that the non-biodegradable pollutant HBCDD has been converted to biodegradable by making inclusion complexes with HP-β-CD and β-CD.

4. Conclusion

In this novel study the inclusion complexation of a non-biodegradable pollutant (HBCDD) with β-CD and HP-β-CD were synthesized and characterized to retain its fire resistance property and to convert it into bio-degradable molecule. Various spectroscopic studieshave been performed to establish this fact. The stoichiometry of the two complexes has been foundas 1:1 molar ratio of host and guest molecules. Surface texture properties of the inclusion complexes were studied by SEM and the presence of bromine in the complexes were evidenced by EDXS. The melting point analysis indicates that the inclusion complexes are more stable than HBCDD and hence ICs are preferred to HBCDD. The aqueous solubility of the inclusion complexes demonstrates that the inclusion complexes are more bio-available to the microorganism and thus evidently inclusion complexation of HBCDD converts it into

bio-degradable material making them eco-friendly in nature and minimizes the environmental pollution.

Acknowledgement

BM is thankful to the Department of Chemistry, NBU for providing the instrumental facilities to conduct the research work. Prof. M. N. Roy would like to acknowledge UGC, New Delhi, Government of India, for being awarded One Time Grant under Basic Scientific Research via the grant-in-Aid no. F.4-10/2010 (BSR). The SAIF, NEHU, Shillong; Mr. Subhasis Dey, IIT Guwahati and Mr. Goutam Sarkar are also highly acknowledged for executing NMR, HRMS and SEM respectively. Ms Khusboo Lepcha, Head, Department of Microbiology, NBU is highly acknowledged for executing the biodegradable essay associated with this paper.

Author contribution

BM, SS and BR: designed, performed the experiments and wrote the article, DR: performed the experiments, RG: designed the experiments, SB provided the theme of the work, designed and assisted to write the article and MNR: corresponding author, supervised the entire work.

Additional Information

The authors do not have any competing financial and non-financial interests.

TABLES

Table 1. FTIR frequency of some significant groups of β-CD, HP β-CD, HBCDD observed at free and complexed state showing corresponding shift

Group	Free state/cm^{-1}	Complexed state/cm^{-1}	Shift/cm^{-1}
HBCDD + β-CD			
$(O\text{-}H)_{str}$ of β-CD	3436.28	3423.03	13.25
$(C^{sp3}\text{-}H)_{str}$ of HBCDD	2930.25	2915.05	15.20
$(C^{sp3}H_2)_{bend}$ of	1442.06	1380.34	61.72

HBCDD			
$(C^{sp3}\text{-}Br)_{str}$ of HBCDD	718.02-538.17	604.28	23.815
HBCDD + HPβ-CD			
$(O\text{-}H)_{str}$ of HP β-CD	3419.25	3405.05	14.20
$(C^{sp3}\text{-}H)_{str}$ of HBCDD	2930.25	2940.07-2895.12	15.155
$(C^{sp3}H_2)_{bend}$ of HBCDD	1442.06	1419.23	22.83
$(C^{sp3}\text{-}Br)_{str}$ of HBCDD	718.02-538.17	701.15-529.11	12.955

Table 2. Exact mass and the observed m/z values of the two inclusion complexes

Inclusion complex	Exact mass	m/z
IC-1	1799.00	1798.27
IC-2	2184.25	2183.88

Table 3. Melting points of HBCDD, IC-1 and IC-2

	Melting point /^{0}C
HBCDD	**195.0**
IC-1	**209.5**
IC-2	**210.5**

Table 4. Aqueous solubility of HBCDD, IC-1 and IC-2 at 298 K

	Solubility /mM mL^{-1}
HBCDD	5.3×10^{-9}
IC-1	2.9×10^{-3}
IC-2	3.7×10^{-3}

Table S1. Frequencies of FTIR spectra ofβ-CD, HP-β-CD, HBCDDand two solid inclusion complexes

β-cyclodextrin (β-CD)		**Hydroxy-propyl β-cyclodextrin (HP β-CD)**	
Wavenumber (cm^{-1})	**Group**	**Wavenumber (cm^{-1})**	**Group**
3436.28	-O-H stretching	3419.25	-O-H stretching
2923.07	-C-H stretching	2917.19	-C-H stretching
1377.14	-C-H and -O-H bending	1369.19	-C-H and -O-H bending
1157.11	C-O-C bending	1157.16	C-O-C bending
1029.13	C-C-O stretching	1028.27	C-C-O stretching
940.12	skeletal vibration involving α-1,4linkage	951.25	skeletal vibration involving α-1,4linkage
Hexabromocyclododecane (HBCDD)			
Wavenumber (cm^{-1})		**Group**	
2930.25		-C-H stretching	
1442.06		$-CH_2$ out of plane bending	
718.02-538.17		C-Br stretching	

HBCDD + β-CD		**HBCDD + HP-β-CD**	
Wavenumber (cm^{-1})	**Group**	**Wavenumber (cm^{-1})**	**Group**
3423.03	-O-H stretching	3405.05	-O-H stretching
2915.05	-C-H stretching	2940.07-2895.12	-C-H stretching
1380.34	$-CH_2$ bending	1419.23	$-CH_2$ bending

1156.01	C-O-C bending	1157.18	C-O-C bending
1029.01	C-C-O stretching	1033.31	C-C-O stretching
604.28	C-Br stretching	720.15-583.11	C-Br stretching

FIGURES

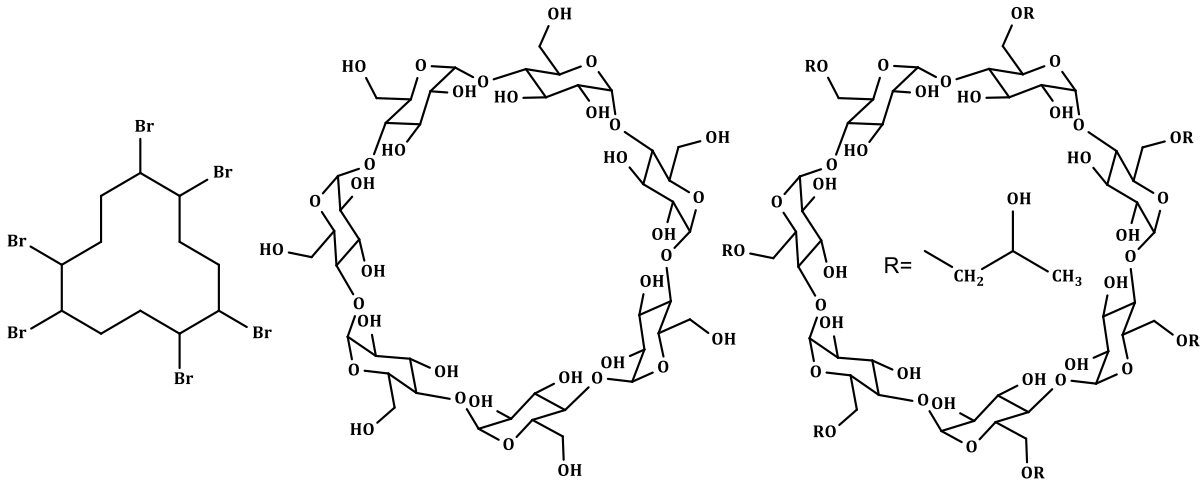

(a) **(b)** **(c)**

Figure 1. Molecular structures of (a) 1,2,5,6,9,10-hexabromocyclododecane (b) β-cyclodextrin and (c) hydroxypropyl-β-cyclodextrin.

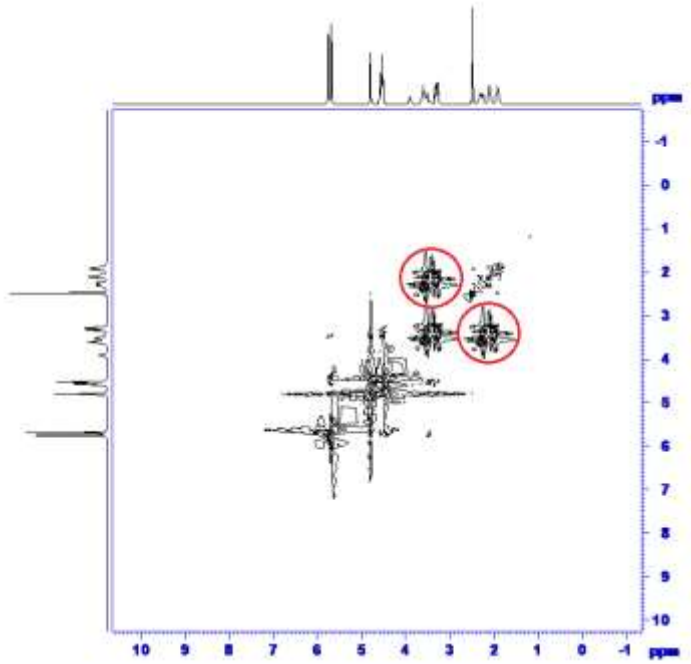

(a)

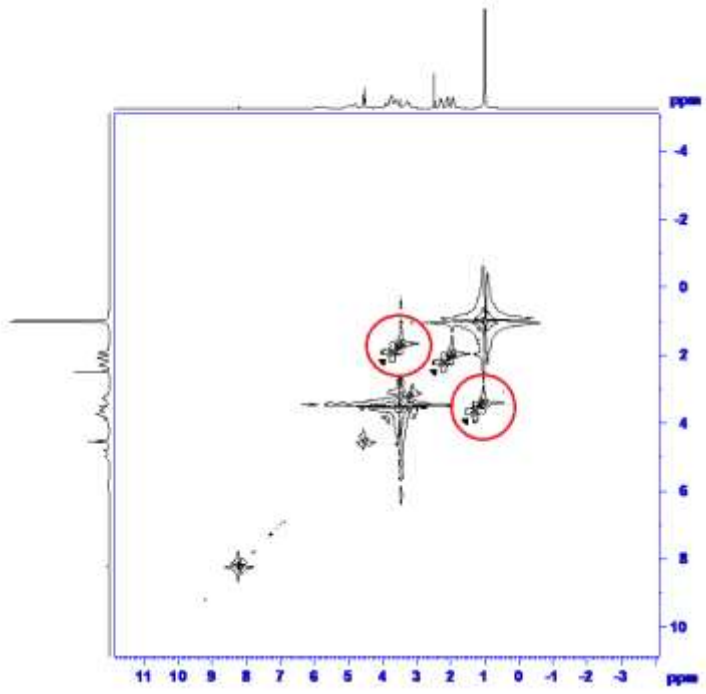

(b)

Figure 2. (a) 2D ROESY spectra of inclusion complex of HBCDD and β-CD in DMSO-d^6(correlation signals are marked by red circles) (b) 2D ROESY spectra of inclusion complex of HBCDD and HP-β-CD in DMSO-d^6(correlation signals are marked by red circles).

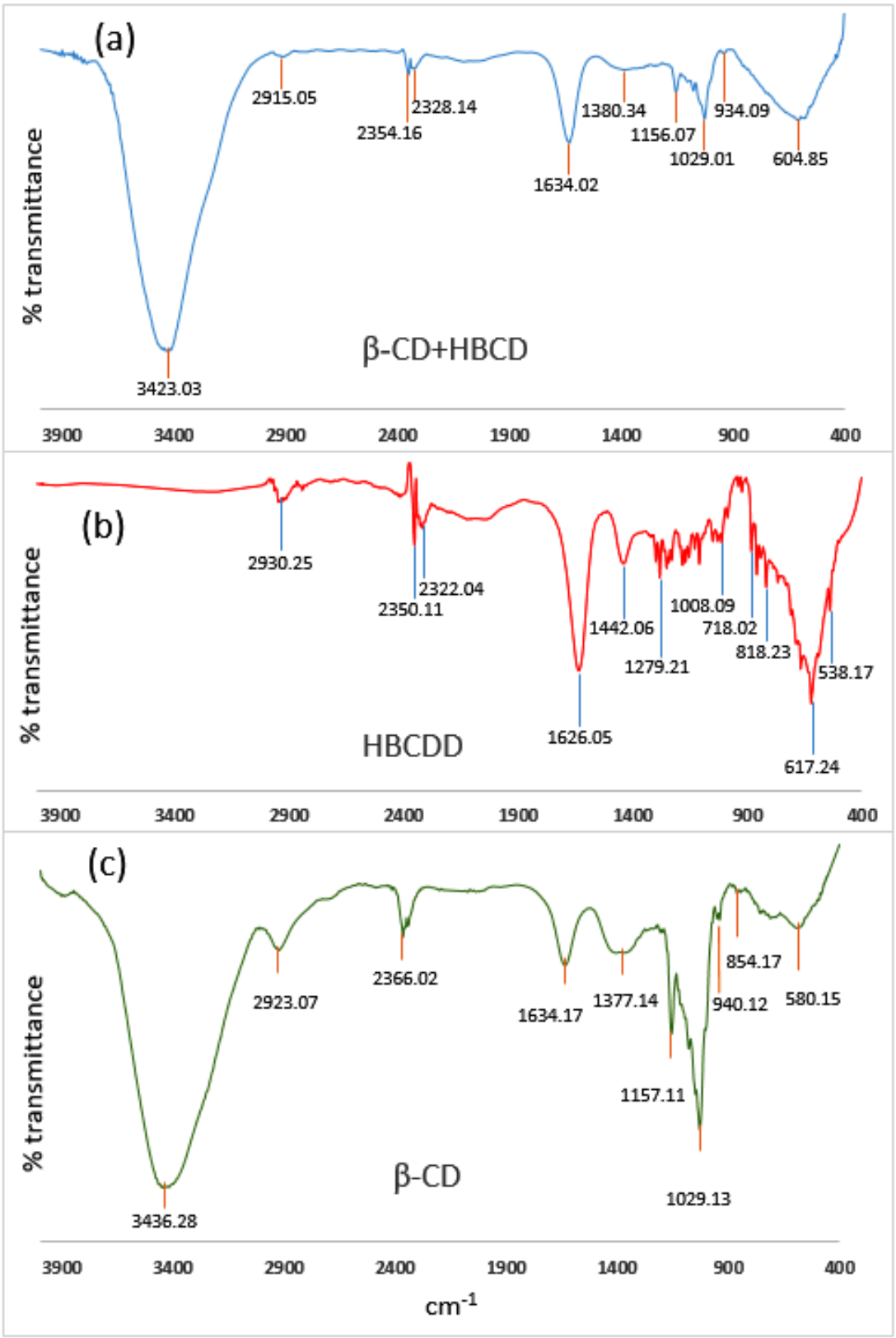

Figure 3(a, b, c): FTIR spectra of (a) (HBCDD+β-CD) inclusion complex, (b) HBCDD, (c) β-CD.

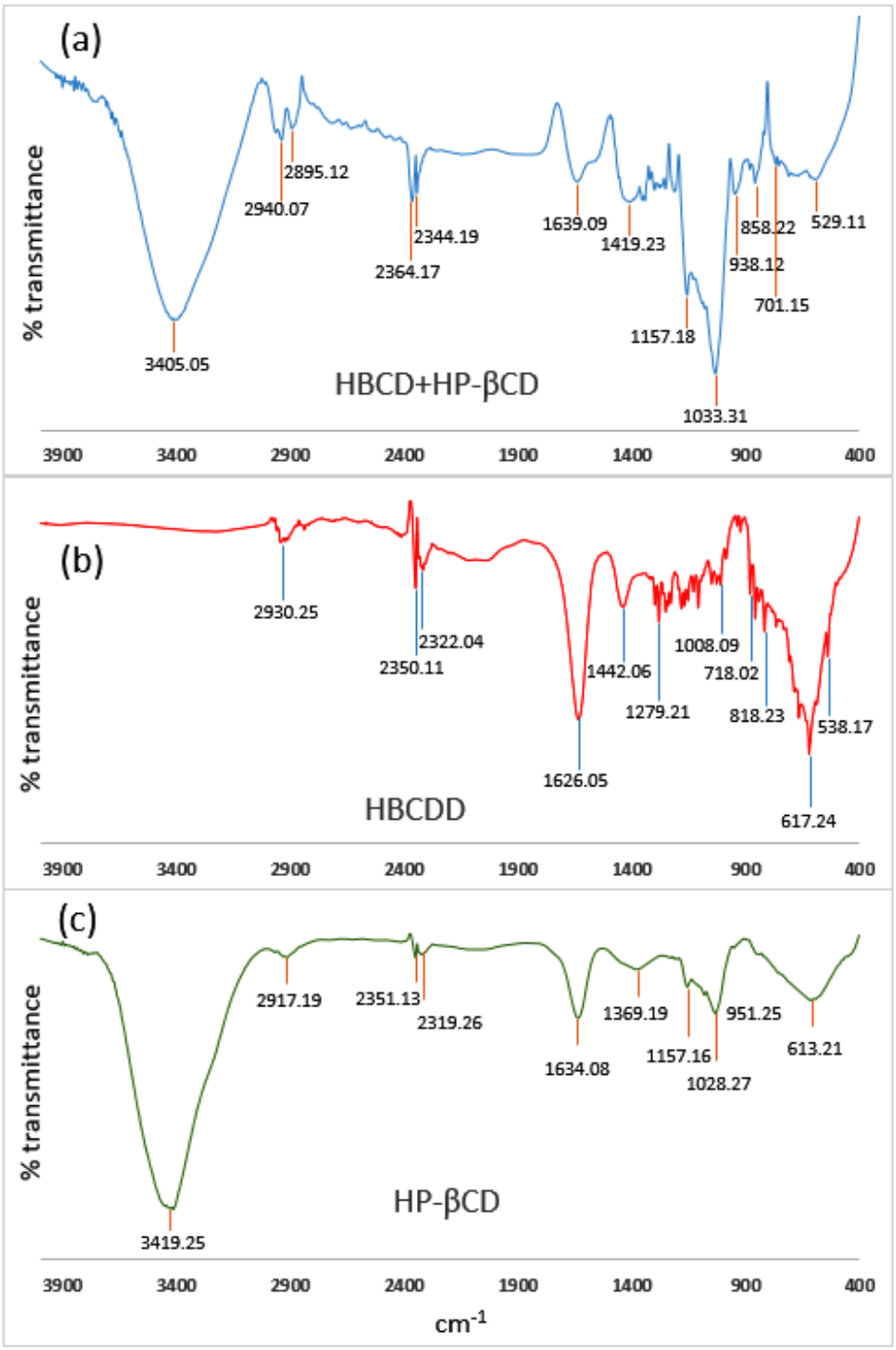

Figure 4(a, b, c): FTIR spectra of (a) (HBCDD+HP β-CD) inclusion complex, (b) HBCDD, (c) HP β-CD

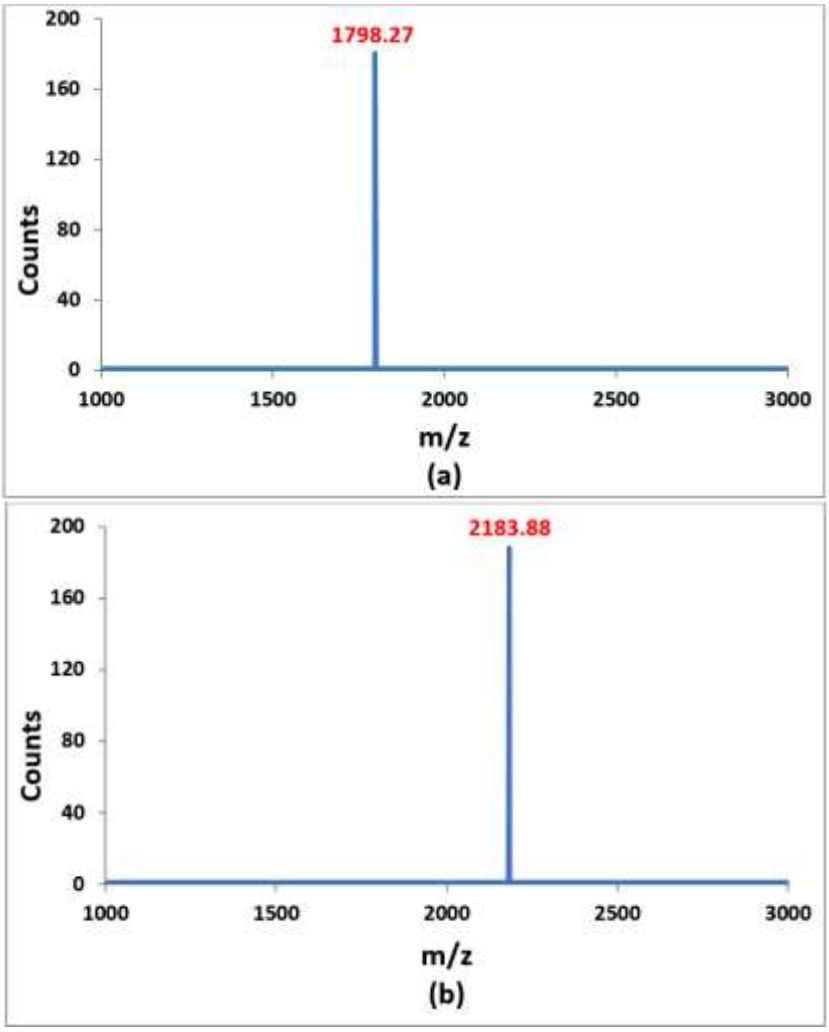

Figure 5. HRMS spectra of (a) HBCDD-β-CD inclusion complex and (b) HBCDD-HP-β-CD inclusion complex.

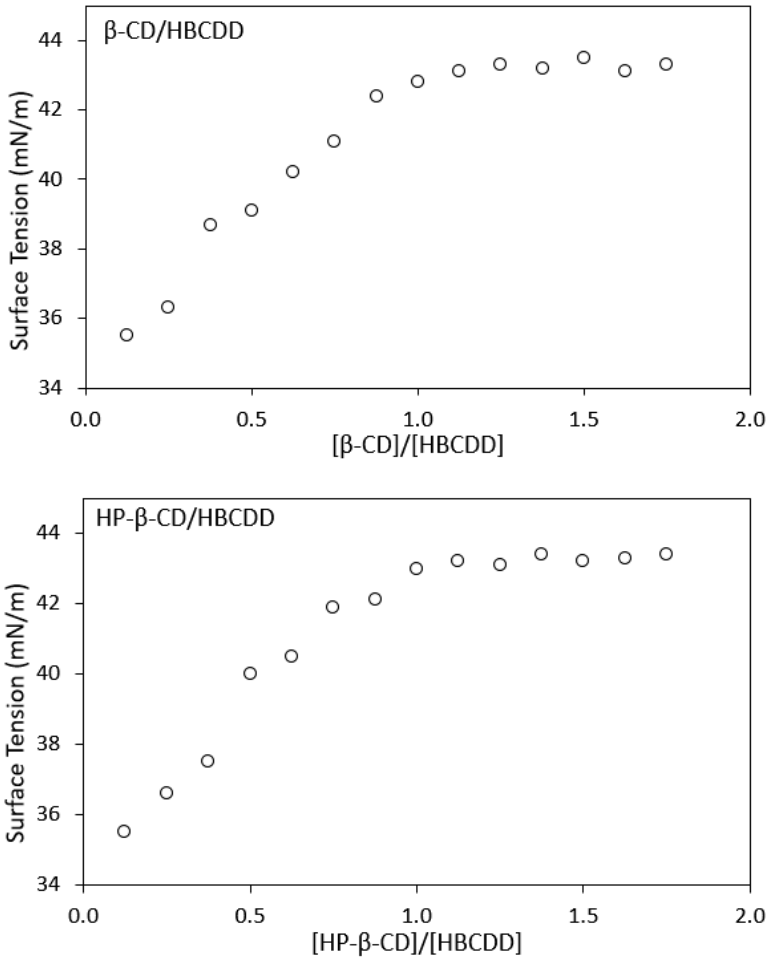

Figure 6. Variation of surface tension with mole ratio of β-CD and HP-β-CD respectively.

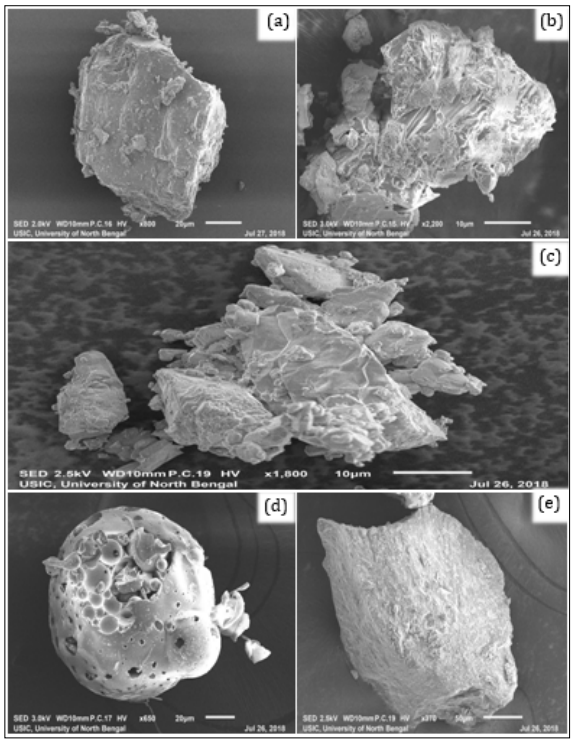

Figure 7. SEM images of (a) β-CD, (b) IC-1, (c) HBCDD, (d) HP-β-CD and (e) IC-2.

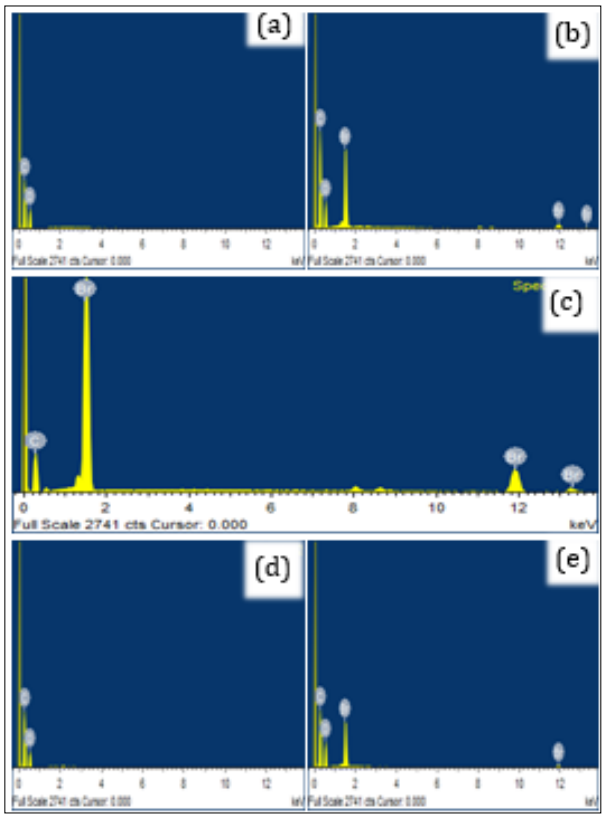

Figure 8. EDX images of (a) β-CD, (b) IC-1, (c)HBCDD, (d) HP-β-CD and (e) IC-2

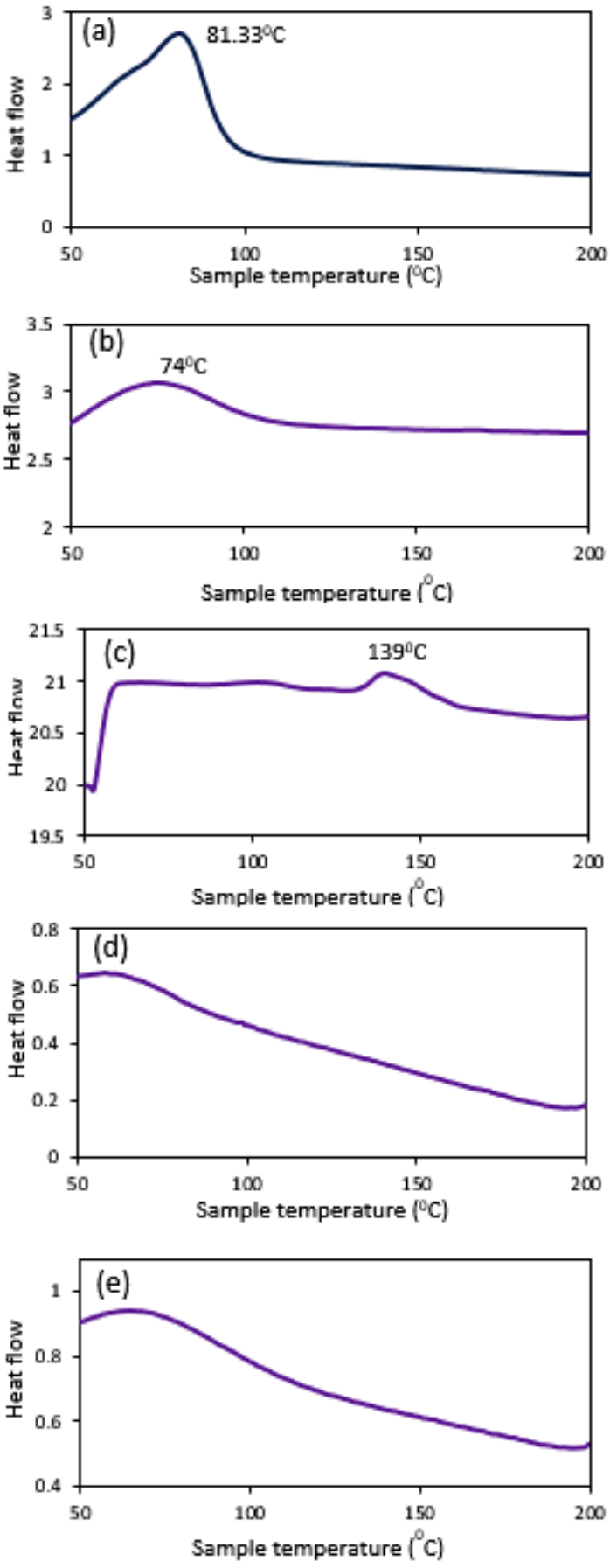

Figure 9: DSC thermograms of (a) β-CD, (b) HP-β-CD, (c) HBCDD, (e) IC-1, (d) IC-2.

Figure 10. Solubility of (a) HBCDD, (b) HBCDD-β-CD inclusion complex and (c) HBCDD-HP-β-CD inclusion complex in water.

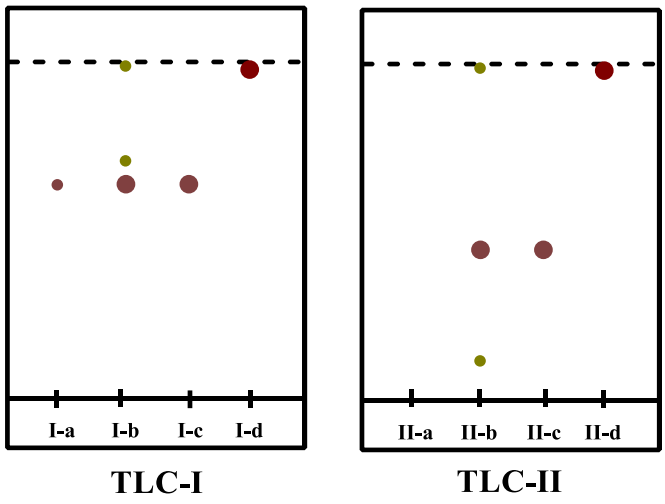

Figure 11. Representative TLC plats for degradation studies of IC-1 and IC-2.

TLC-I: R_f (I-a): 0.77; R_f (I-b): 0.77, 0.86, 0.96; R_f (I-c): 0.77; R_f (I-d): 0.98.

TLC-II: R_f (II-b): 0.21, 0.60, 0.96; R_f (II-c): 0.60; R_f (II-d): 0.98.

Figure S1. ^{1}H NMR spectra of HBCD in DMSO-d^{6} at 298.15 K

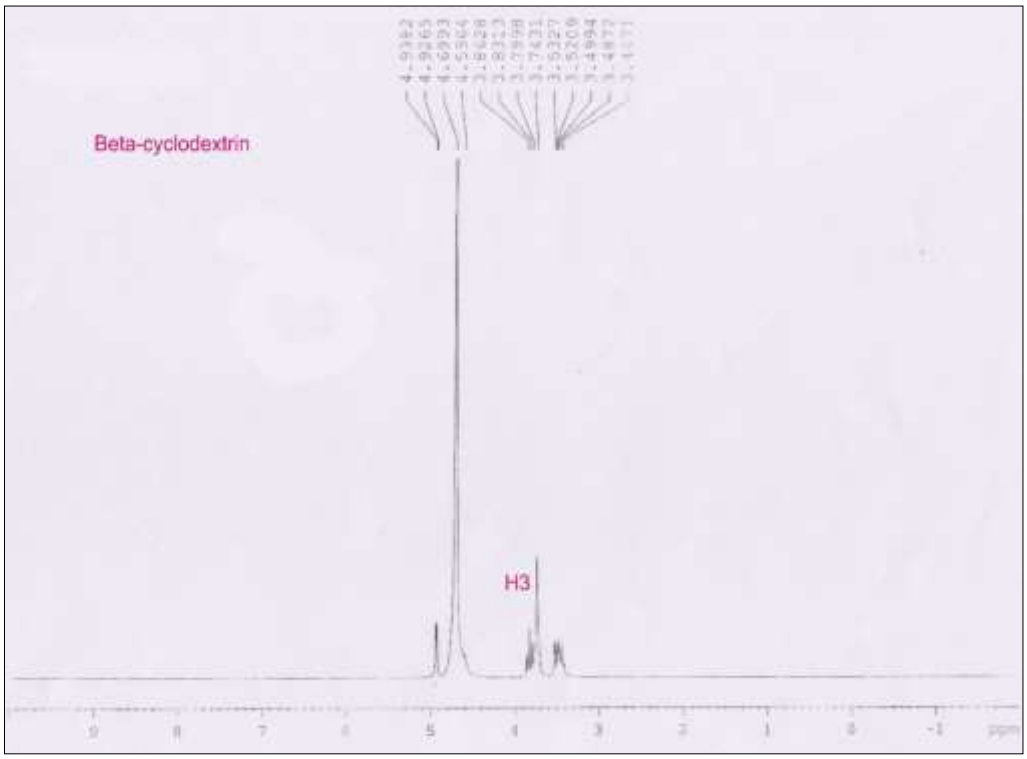

Figure S2. ^{1}H NMR spectra of β-cyclodextrin in DMSO-d^{6} at 298.15 K

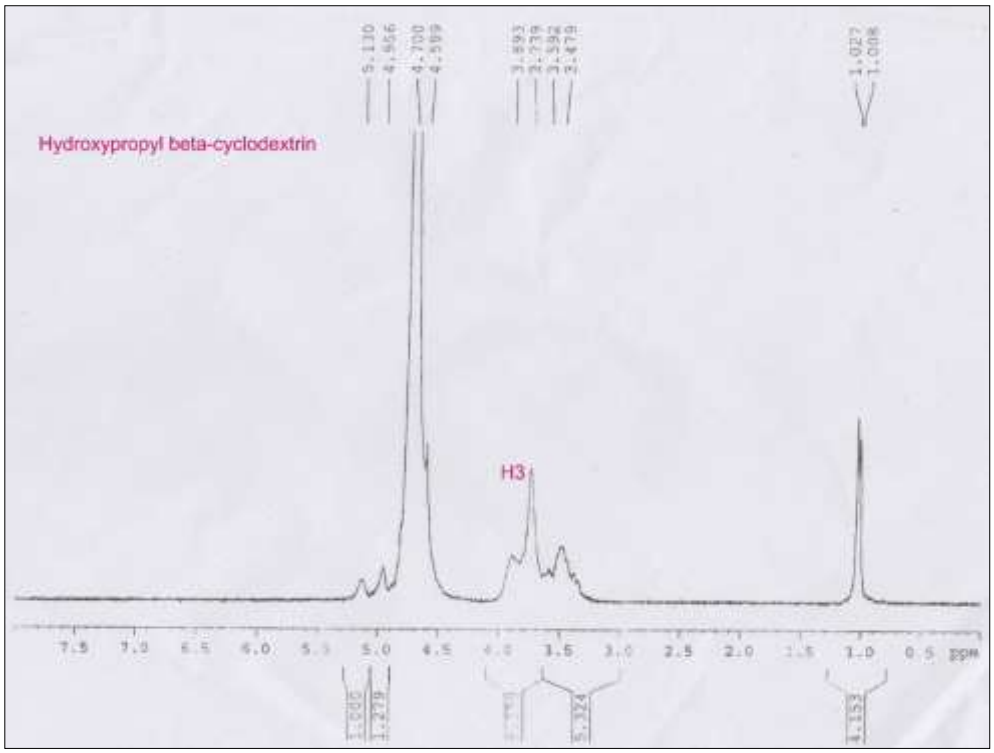

Figure S3. ^{1}H NMR spectra of HP-β-cyclodextrin in DMSO-d^{6} at 298.15 K

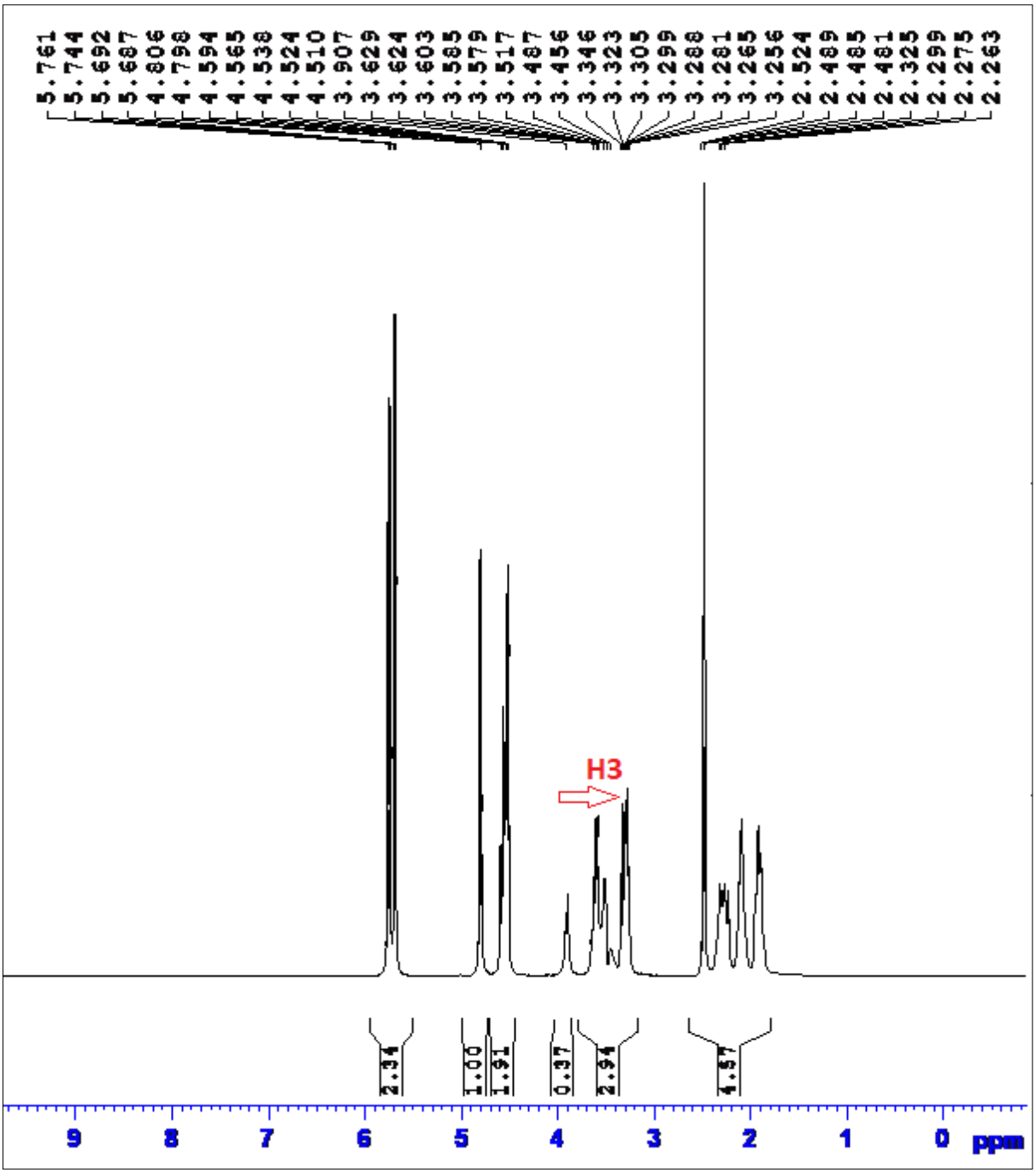

Figure S4. ^{1}H NMR spectra of IC-1 in DMSO-d^{6} at 298.15 K

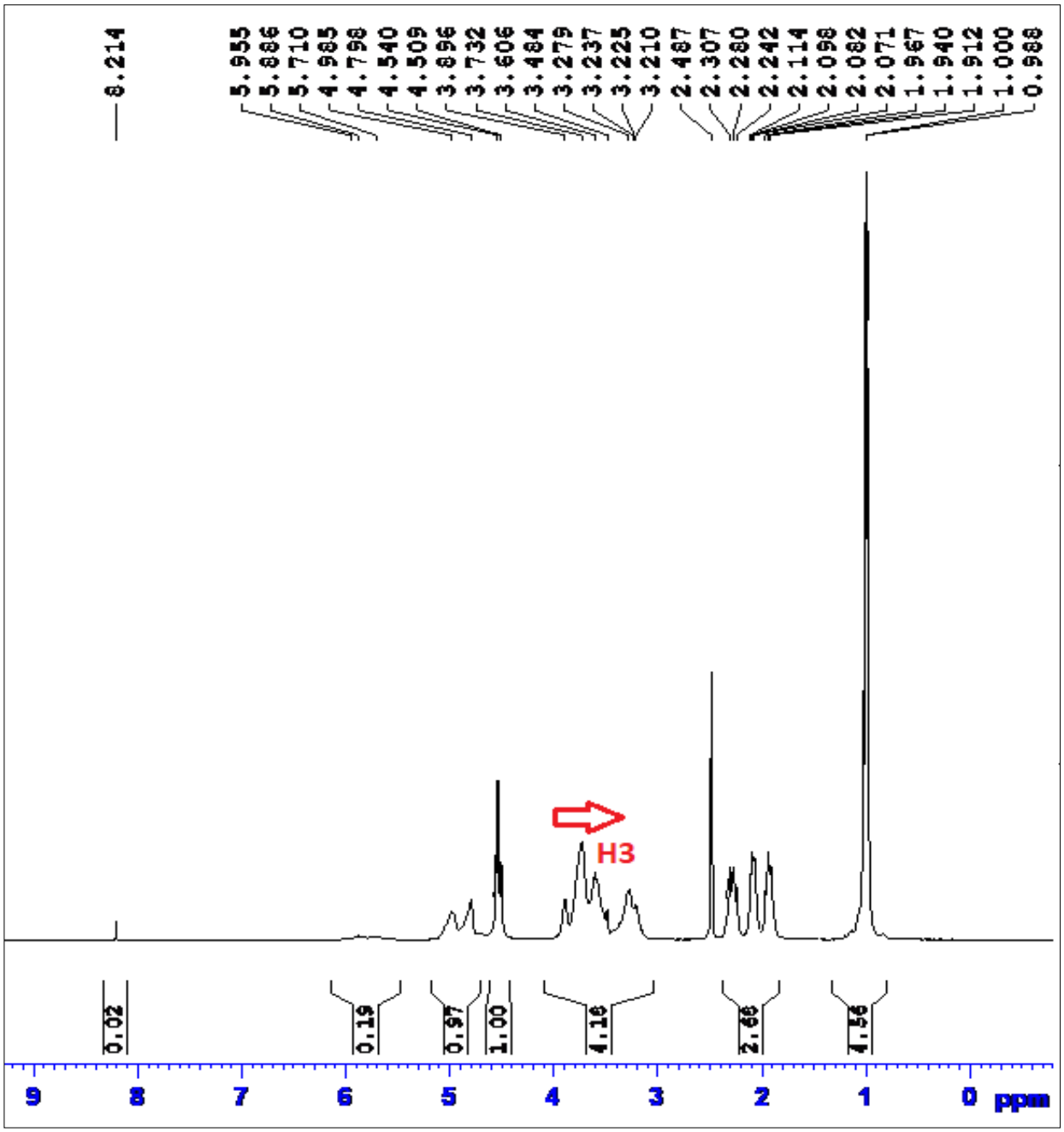

Figure S5. ^{1}H NMR spectra of IC-2 in DMSO-d^{6} at 298.15 K.

CHAPTER VII

Synthesis, Characterization and Innovative Applications in Pharmaceutical Sciences of 2:1 Host Guest Inclusion Complexes assembled of Cyclic Oligo-Saccharides with Antispasmodics

Abstract: Solubility development of supramolecular host-guest interaction between Alverine citrate with αand β-cyclodextrins were studied throughout the article. 2:1 host to guest stoichiometry of the inclusion complexation in the solution phase were confirmed by the Job's plot and further confirmation about the stoichiometry was also obtained from the mass spectra of the inclusion complexes. IR, DSC, SEM and PXRD data turn out to be supportive about the phenomenon, inclusion complexation. Association constants and thermodynamic parameters of the inclusion complexes were obtained using UV-vis and spectrofluorometric measurement. The mechanism of inclusion complexation was explored by 1H and 2D ROESY NMR spectroscopy. Binding ability of the drug molecule, Alverine citrate with the HSA and the controlled release of the drug molecule from inclusion complexes were studied at PH-7.4 by spectrofluorimetricaly. Studied phenomenon thus develops the solubility of merely soluble drug into water, consequently makes bioavailable and enriches the drug delivery system.

Keywords: Alverine citrate; HSA; Controlled Drug delivery; Inclusion Complex; Solubility enhancement

1.Introduction:

Irritable bowel syndrome (IBS), a gastrointestinal disorder is a most commonly diagnosed gastroenterological problem in medical sciences. Patients suffering from IBS are found to suffer frequently from various gastrointestinal disorder like, abdominal pain or dis-comfort, altered bowel habit, bloating[1,2] associated with the symptoms, incomplete bowel movement, urgency and tenesmus[3, 4]. Thus, irritable bowel syndrome is a functional gastrointestinal disorder showing a lot of

abnormalities. Hyper-reactive intestinal motility[5] and visceral hypersensitivity are also found in patients suffering from IBS.

Alverine citrate (ALVC) **(Scheme 1)** belonging from a class of antispasmodic drugs used to treat irritable bowel syndrome and diverticular disease. Alverine citrate acts as a muscle relaxant and relieves abdominal pain, constipation or diarrhoea caused by the abnormal activity of the gut muscle. It also relaxes the muscle in the womb which is caused by the muscle spasms in uterus. Voltage-gated calcium channels are the main transducers of membrane potential changes into intracellular Ca^{2+} transients such a way they intervene smooth muscle contraction and activate endocrine to release hormone[6, 7, 8]. The visceral pronociceptive effect of 5-HTcan be reduced as ALVC binds with 5-HT1A acting as an antagonist. ALVC when combined with simethicone, found to act more effectively in the treatment of abdominal pain in IBS. It is marketed commercially by the name Spasmonal® Forte in the form of hard capsule (Alverine citrate 60/120 mg) and soft capsule (60 mg Alverine citrate/300 mg simethicone). ALVC ultimately metabolised to two secondary metabolites through the conversion of its primary active metabolite, para hydroxy alverine (PHA)[9].

The supramolecular interaction between ALVC and cyclodextrins (CDs) to form inclusion complex was justified satisfactorily by the improvement of two novel aspects - (a) solubility of the ALVC into water for bioavailability, (b) drug delivery through HSA assisted controlled release from inclusion complexes.

A drug to show greater therapeutic effectiveness needs its bioavailability and solubility to a large scale. Pharmacological response to be shown by a drug a minimum concentration of it must be achieved, in this connection aqueous solubility of the drug to a desired level is significant. Solubility of a molecule may be defined qualitatively as the spontaneous interaction of two or more substances to form a homogeneous molecular dispersion. It is found that ALVC-CDs inclusion complexes enhances the aqueous solubility of drug making it more bioavailable. Encapsulation of the hydrophobic part of the guest (ALVC) molecule into the hydrophobic cavity of suitable dimension of CDs makes it to increase aqueous solubility. The cavity dimension of the CDs should be moderate to reduce the contact between water and the nonpolar regions of host and guest molecule. Among the CDs, α and β-

cyclodextrins were used for the dimensional suitability of their cavity size **(Scheme 1)**.

As the organism – environment interaction is essential for its survival, on the molecular level small molecule like drug – protein/drug – gene product interaction is also essential that underlie the organism's ability to adapt to environmental changes and include those that bind, transport, and metabolize small molecules. Human serum albumin, the most abundant protein in blood plasma found to act as a carrier protein for vitamin, nutrients, hormone, steroid, drug like small molecule of low water solubility and binding ability of these molecules to HSA constitute a vibrant matter in pharmacokinetics[10, 11, 12, 13]. Here, binding property of ALVC to the HSA had been studied spectrofluorimetrically. Thus, HSA assists the drug ALVC to release from the inclusion complexes and makes its transportation to the affective area where adsorption of the drug molecule to be needed. Our study to form inclusion complexes of ALVC thus become moralised by the solubility enhancement and HSA assisted transformation and controlled release of the drug in human body.

2. EXPERIMENTAL SECTION

2.1. Materials

Alverine citrate, α and β-cyclodextrin, purity ≥98.0% and ≥97.0% were purchased from Sigma-Aldrich and were conserved in a refrigerator as received.

2.2. Apparatus

The Agilent 8453 UV-Visible Spectrophotometer was performed to record UV-vis spectra with an uncertainty of wavelength accuracy of ±0.5 nm. An automated digital thermostat, Julabo was used to control the cell temperature during experiments.

HRMS spectra of the solid ICs were recorded on a quadrupole time-of-flight (Q-TOF) high-resolution instrument with positive-mode electrospray ionization taking the methanol solution of the solid ICs.

2D ROESY as well as 1H NMR spectra were recorded in D_2O solvent at 400 MHz in Bruker Avance instrument at 298.15 K. The chemical shifts data, δ values are

presented in parts per million where, the residual protonated signal (HDO, δ 4.79 ppm) was used as internal standard.

With the help of Perkin-Elmer FTIR spectrometer the FTIR spectra of the solid ICs as well as the pure compounds were recorded in the scanning range of 4000−400 cm^{-1}at room temperature. KBr disk of the samples were prepared in the suitable ratio of sample to KBr to minimise noise.

Powdered X-Ray Diffraction (PXRD) patterns of the pure compound and ProC were recorded by using Cu-Kαradiation (D8 Advance Bruker)

The DSC thermograms of the samples were recorded with the help of Perkin-Elmer DSC-6 differential scanning calorimeter at the heating rates of 10°C min^{-1}. The thermograms were taken by heating near about 1 mg of samples in aluminium crimped pans under nitrogen gas flow.

The Scanning Electron Microscope (SEM), JEOL JSM IT 100 was used to determine the surface topography of the samples at various resolutions. Samples were prepared on a small piece of double adhesive carbon-coated tape attached to brass stubs and then a coating of ultra-thin layer of gold ions was put in a gold-ionization chamber.

The Bench top spectrofluorimeter from photon technologies International (Quantamaster-40, USA) was used to record fluorescence spectra at room temperature. Hellma quartz cuvette having optical path length 1.0 cm was also used.

2.3. Procedure

Solubility of ALVC and CDs were checked and the solutions were prepared with triply distilled water. A digital analytical balance METTLER TOLEDO AG-285 was used weigh with an uncertainty of ±0.1 mg taking sufficient precautions to avoid loss of materials. The aqueous solution of ALVC and CDs were prepared separately in the same molarity. The aqueous solution of CDs in a beaker then placed on a hot top of a magnetic stirrer for stirring. After that, aqueous ALVC solution was added dropwise to the solution of CDs placed on magnetic stirrer and the equimolar mixture of ALVC and CD solutions were allowed to stir for 8 hours keeping temperature at 40-45°C.

The suspensions obtained after cooling the mixture to 5 °C were filtered to obtain white crystalline powder, which were then dried in air and preserved in vacuum desiccators.

3. Result and discussion

3.1 Job plot: Stoichiometry of inter molecular association between guest and host:

According to the well-established Job's method the stoichiometry of the host-guest inclusion complexes was determined using the UV-vis spectroscopic data[14, 15]. A set of solutions in the range of 0 – 1 mole fraction were prepared by mixing aqueous ALVC and CDs in the calculated proportion and recorded the spectra at 298.15 K of temperature. Absorbances of the set of solutions at λ_{max} = 258 nm were considered for the calculation to obtain the Job's plot **(Figure 1).** Plotting ΔA×R vs R generates the Job's plot and value of R corresponding to the maxima of Job's plot signifies the stoichiometry of inclusion complexes. Where, ΔA represents the differences in absorbance between pure ALVC and each of the solutions of the set **(Table S1, S2 and Figure 1)**. R indicates [CDs]/[ALVC]+[CDs] and its value of R = 0.33, 0.5, 0.66 corresponding to the maxima recommends strongly the 1:2, 1:1 and 2:1 host to guest stoichiometry in the inclusion complexes[16]. In the present work we have found R = 0.66 suggesting 2:1 host to guest stoichiometry[17, 18]**(Scheme 2)**.

3.2 HRMS Analysis of Inclusion complexes:

Further confirmation about the formation inclusion complexes of stoichiometry 2:1 was obtained from the mass spectroscopic study of the solid inclusion complexes. After dissolving the inclusion complexes in methanol the spectra were recorded which are shown in the **Figure 2.** According to the spectra the peaks at the m/z 2226.86and 2551.97 corresponds to the $[ALVC+2\alpha\text{-}CD+H]^+$ and $[ALVC+2\beta\text{-}CD+H]^+$respectively**(Table S3)**.The appearance of the peaks in the spectra showing appreciable abundance simply implies the formation of the [ALVC+2α-CD] and [ALVC+2β-CD]inclusion complexes of 2:1 host to guest stoichiometry[19, 20](**Scheme 2**).

3.3 ^{1}H NMR and 2D ROESY NMR spectra analysis:

The mechanism of inclusion complexation with the identification of part of the guest molecule that undergoes insertion into the hydrophobic cavity of cyclodextrin was achieved and concluded by 1H NMR as well as 2D ROESY NMR spectroscopic study. Cyclodextrins having the truncated structure H3 and H5 protons are oriented inside the cavity whereas H1, H2 and H4 protons are exposed to the outer side of CDs[21](**Scheme 1**). So, the molecule that undergo insertion into the cavity must interact with H3 and H5 protons of CDs to show chemical shift in 1H NMR spectrum owing to their mutual shielding through space[22]. Encapsulation of aromatic guest molecule ring current of the aromatic moiety exerts diamagnetic shielding to the H3 and H5 protons of the CDs[23](**Table S4**). 1H NMR spectra of pure α-CD, β-CD, ALVC as well as the inclusion complexes are shown in **Figure S1-S5**respectively. From the 1H NMR spectra it was observed, there are considerable upfield shift of the H3, H5 protons of CDs and the interacting protons of the guest molecule that confirms the formation of inclusion complexes[24]**(Figure S1-S5**.)

2D ROESY NMR spectroscopy brings pivotal confirmation about the spatial closeness of the interacting protons by observing the intermolecular dipolar cross-correlations.[25,26] The protons within 0.4 nm in space may exert a rotating-frame NOE spectroscopy (ROESY) and produce off diagonal cross peak in the 2D NMR spectra of inclusion complexes.[27] Thus NOE cross peaks between interacting protons of host and guest in spectra helps us to identifying the special part of the guest molecule that undergoes encapsulation into the cavity of CDs. In this case significant correlation between aromatic protons of ALVC and the H3, H5 protons of cyclodextrin were identified in 2D ROESY spectra of inclusion complexes establishing the aromatic ring was encapsulated inside both the cyclodextrin cavities[28] (**Figure 3-4**). The H-6 protons situated in the narrower rim of cyclodextrins were found not to influenced by the inclusion processes, this may lead to the conclusion that incorporation of the guest molecule into the cavity of CDs takes place through the more favourable wider rim of CDs.[29] (**Scheme 2**).

3.4 FTIR spectroscopy:

Encapsulation of the guest molecule into the cyclodextrin cavity may lead to the shifting in vibrational frequencies of the interacting bonds of host and guest molecules. Considerable shifting in the vibrational frequencies of the interacting

bonds in the FTIR spectra of inclusion complexes compared to the frequencies of the pure ALVC and CDs suggests the formation of inclusion complexes and simultaneously, it makes us possible to identify the encapsulated part of the guest molecule as obtained from the 2D ROESY NMR spectroscopic study.[30,31] FTIR spectra of all the samples in this regard, recorded by preparing KBr disk are shown in **Figure 5** and some signals responsible for significant bond vibration are listed in **Table S5**.

Innumerable interactions of the ALVC and α-CD in the [ALVC+α-CD] inclusion complex were analysed as follows- (i) The signal at 2936.05 cm^{-1} for aromatic –C-H stretching of ALVC was found to shifted to 2925.26 cm^{-1} in the inclusion complex. (ii) the aromatic C-C stretching of ALVC was at 1397.17- 1598.11 cm^{-1}, whereas for inclusion complex it is appeared at 1402.23-1613.22 cm^{-1}. (iii) the peaks at 1024.25 cm^{-1} responsible for aromatic in plane –C-H bending for ALVC shifted to 1028.41 cm^{-1} in case of inclusion complex. (iv) the signals at 702.14-884.27 cm^{-1} appearing for aromatic out-of-plane –C-H bending were found to appear at 715.21-849.27 cm^{-1} in case of inclusion complex. This may be due to the various interaction taking place during encapsulation of ALVC. (**Figure 5**)

The shifting of the IR signals that adequately clarifies the formation of [ALVC+β-CD] inclusion complex. (i)The signal for aromatic –C-H stretching of ALVC was at 2936.05 cm^{-1} found to appear at 2927.09 cm^{-1} in the inclusion complex. (ii) the signals responsible for aromatic C-C stretching of ALVC was at 1397.17- 1598.11 cm^{-1}, but it is shifted to 1406.11-1615.12cm^{-1} for inclusion complex. (iii) the peaks at 1024.25 cm^{-1} for aromatic in plane –C-H bending for ALVC shifted to 1031.19 cm^{-1} in case of inclusion complex. (iv) the signals at 702.14-884.27 cm^{-1} appearing for aromatic out-of-plane –C-H bending were found to appear at 710.12-860.17 cm^{-1} in case of inclusion complex (**Figure 5**). Thus, FTIR spectral analysis also suggests the same outcomes as obtained from the 2D ROESY spectral analysis.

Appearance of no any other additional peaks in the FTIR spectra suggests there is no chemical reaction taking place during encapsulation and all the spectral changes happened responsible for inclusion complex formation.

3.5 XRD:

For the elucidation of various physicochemical properties of inclusion complexes, pure ALVC and CDs, X-ray diffraction data would come helpful in this case which are shown in **Figure 6**. The pure ALVC shows distinctive sharp, highly intense and less diffused diffraction peaks at angles of 2θ values of 3.85^0, 7.65^0 and 15.2^0. α-cyclodextrin registered its characteristics intense diffraction peaks at 2θ values of 5.35^0, 9.95^0, 13.65^0, 14.4^0 and 21.75^0. According to the diffractogram of β-cyclodextrin the intense peaks were recognised at the 2θ values of 4.7^0, 12.8^0, 17.15^0 and 28.8^0. Analysing the diffractogram of ALVC-α-CD inclusion complex, it was found that, all the characteristic peak of the ALVC get disappeared registering a new diffuse peak of low intensity at 2θ angle of 20.05^0. Similarly, in the case of ALVC-β-CD inclusion complex the peak position responsible for ALVC get shifted to 3.95^0, 7.4^0 and 15.65^0 respectively. Thus, disappearance of significant guest peaks, decrease of peak intensity with slight shifting of peak position and importantly, appearance of new characteristic peak in the diffractogram of inclusion complexes supports the inclusion phenomenon as discussed herewith.[32, 33, 34]

3.6 DSC thermogram:

The differential scanning calorimetry (DSC) is a very convenient technique for the exploration of thermal properties of CD based inclusion complexes because, we can gather both the qualitative and quantitative insight about the physicochemical state of the drug while encapsulated into the cavity of CDs. Generally, the shifting of an endothermic peak to a different temperature or absence of an endothermic peak for the pure guest molecule in the inclusion complexes are found in DSC thermogram which indicates a change in melting point, crystal lattice or sublimation point due to inclusion complexation[35, 36, 37, 38]. DSC thermograms of inclusion complexes and pure ALVC are depicted in **Figure 7**. From the **Figure 7** it is evident that an endothermic peak at 104.98^0C corresponding to the melting point of pure ALVC get shifted with the reduction of peak intensity to 102.80^0C and 102.84^0C for ALVC-α-CD and ALVC-β-CD inclusion complexes respectively. The intensity of the another peak at 189.86^0C get reduced drastically while going from pure ALVC to inclusion complexes. This indicates reduction of drug crystallinity through amorphization by ALVC-CDs inclusion complex formation.

3.7 Scanning Electron Microscope (SEM):

Scanning Electron Microscope (SEM) is a type of electron microscope that produces images of the sample that enable us to about the surface morphology, surface texture and particle size of solid materials[38, 39, 40, 41].The SEM images describing the surface morphology of inclusion complexes, ALVC-CDs physical mixture, pure ALVC and CDs are shown in **Figure 8**. It is evident from the analysis of the microscopic images of the inclusion complexes, ALVC-CDs physical mixture, pure ALVC and CDs, the surface morphologies are different from each of the categories. The may be possibly for the formation of inclusion complexes. Thus, it appears to an additional evidence about the formation of inclusion complexes along with 2D ROESY NMR analysis.

3.8 UV and solubility:

Well-known Higuchi and Connor method was employed to study the phase solubility of the ALVC in CDs[38, 42, 43]. A set of aqueous solution of CDs were prepared separately in the concentration range 0 to 10 mM. The pH of the prepared solutions was maintained to 7.4 using phosphate buffer solution. An excess amount of ALVC were added to each of the solutions of set prepared previously with CDs. The solutions were then allowed to stir for 24 hours at 25^0C on a magnetic stirrer. Then, the solutions were filtered and diluted properly to determine the amount of contained ALVC through dissolution in the solution UV-vis spectroscopically using 1 cm quartz cuvette. Apparent water solubilities were measured by plotting a solubility curve as a function of CDs concentration **(Figure S6-S7)**. The amount of ALVC contained by the solution are shown in **Table 1**.

We also calculated the association constant (K_a) using the following equation-

$$K_a = \frac{Slope}{S_0(1-Slope)} \qquad (1)$$

Where, S_0 represents the inherent water solubility of ALVC in water and the Slope is according to the slope of the phase solubility plot. With the known value of K_a, the complexation efficiency (CE) was determined as follows-

$$CE = \frac{Slope}{1-Slope} = K_a \times S_0 \qquad (2)$$

Where, K_a, S_0 and slope represents the same as mentioned above. The association constants (K_a) of the inclusion complexes and complexation efficiencies (CE) are listed in **Table 2**. The enhancement of solubility thus simply suggests the formation of inclusion complexes[44].

3.9 Ultraviolet Spectroscopy: The association constants (Ka) of the Inclusion Complexes:

The capability of the Guest to bind into the Host's hydrophobic cavity and the association constants (Ka) representing the extent of stability of the ICs were calculated using the Benesi-Hildebrand equation[41, 45, 46]. The UV-vis spectroscopic data were used to determine the association constant (Ka) of the ICs in the solution phase.[47] As the molar extinction coefficient (Δε) depends upon the solvent polarity, the absorbance of the guest molecule must change while going from polar aqueous media to the apolar hydrophobic cavity of the CDs to form ICs.[48,49] The data obtainable from the UV-vis spectroscopic measurement are listed in the **Table S6-S7**. The Benesi-Hildebrand method uses the following equation[45, 47, 50, 51]to determine the association constant of the ICs.

$$\frac{1}{\Delta A} = \frac{1}{\Delta\varepsilon[DGs]K_a}\frac{1}{[CD]^n} + \frac{1}{\Delta\varepsilon[DGs]} \qquad (3)$$

Where, ΔA is the difference in absorbances of ALVC without CDs and with the CDs. [DGs] represents the concentration of ALVC. The value of (n) says about the stoichiometry of the ICs. When the linearity of the double reciprocal plot fits by putting n=1 in the above equation then it suggests 1:1 stoichiometry of the ICs. But, when n=2 suggests the 2:1 inclusion complex of the Host to the Guest. Here, we observed no linear relationship of the Benesi-Hildebrand double reciprocal plot indicating the composition of complex was not 1:1. On the other hand the linearity of the plot best fits when n=2 suggesting the 2:1 stoichiometry of the ICs[15] as obtained from the Job's plot.

$$\frac{1}{\Delta A} = \frac{1}{\Delta\varepsilon[DGs]K_a}\frac{1}{[CD]^2} + \frac{1}{\Delta\varepsilon[DGs]} \qquad (4)$$

The value of slope and intercept of the double reciprocal plot **(Figure S7-S8)** enable us to calculate the association constants (K_a) of the inclusion complexes and listed in the T**able 3**.

With knowledge of the association constants (K_a) of the ICs at various temperature the thermodynamic parameters of the ICs were calculated using the Van't Hoff equation-

$$\ln K_a = -\frac{\Delta H^0}{RT} + \frac{\Delta S^0}{R} \qquad (5)$$

The thermodynamic parameters of the formation of ICs obtained from a linear plot **(Figure S9)** of Van't Hoff equation, listed in the **Table 3** it was found that, enthalpy change of formation is negative and entropy increases while formation of ICs, suggesting an exothermic and entropically driven process making the process spontaneous which is reflected from the free energy change of the process.

3.10 Fluorescence and binding of Guest to HSA:

The ALVC-HSA interaction and the quenching in fluorescence intensity caused by the changes in the environment surrounding ALVC. The fluorescence spectra were recorded at a fixed concentration of HSA exciting at 295 nm. Fluorescence spectra of HSA were recorded for a set of solutions containing varying amount of ALVC in the solutions and results were fed to Stern-Volmer equation[52] to calculate the binding constant of the ALVC to HSA.

$$F_0/F = 1 + K_{sv}[Q] = 1 + K_q\tau_0[Q] \qquad (6)$$

Where, F_0 and F represents the fluorescence intensities of HSA in the absence and presence of ALVC respectively, K_{sv} is the linear Stern Volmer constant and [Q] is the concentration of ALVC i.e. the concentration of the quencher. The Stern-Volmer quenching constant (K_{sv}), is the measure of efficiency of quenching. K_q indicates the bimolecular quenching rate constant and τ_0 represents the average fluorescent life time of protein without quencher, which is 5.6×10^{-9}s[53]. The value of binding constant was calculated using the following logarithm equation,

$$\log[(F_0 - F/F)] = \log K_b + n\log[Q] \quad (7)$$

Where, F_0 and F represents the fluorescence intensities of the HSA in the absence and presence of different concentration of ALVC and n is the number of binding sites. The values of binding constant (Kb) obtained from the slope of the linear plot[54] **(Figure 9)** of $\log(F\text{-}F_0)/F$ versus log[Q] and are listed in the **Table 4**.

4. Conclusions:

All the experiments suggest the successful formation of inclusion complex with 2:1 stoichiometry. The association constants of the inclusion complexes of ALVC formed with β-cyclodextrin were found greater than that of the inclusion complexes formed with the α-cyclodextrin and hence more stable, this is may be due to the better fitness of the guest molecule into the larger hydrophobic cavity of β-cyclodextrin compared to the α-cyclodextrin. The ready availability of the association constants enables us to calculate the thermodynamic parameters of the inclusion process which makes the thermodynamic background of the process and recognise it as a thermodynamically feasible process. When the guest molecule gets encapsulated into the hydrophobic cavity of cyclodextrin molecule, the water molecules removed from the hydrophobic cavity of cyclodextrin molecule increases the entropy of the process. Thus, the hydrophobic-hydrophobic interaction and entropy factor would become the driving forces for the formation of inclusion complexes. The binding constant of ALVC to the HSA become appreciable showing an affinity of HSA towards the drug molecule. Thus, it is expected that, the drug molecule gets released from the inclusion complex and binds successfully with the HSA which then get transported to the targeted site promoting regulatory release consequently reduces overdoses without any chemical modification.

Conflicts of interest: There is no conflicts of interest.

Acknowledgements: Prof. M. N. Roy would like to acknowledge UGC, New Delhi, Government of India, for being awarded One Time Grant under Basic Scientific Research via the grant-in-Aid no. F.4-10/2010 (BSR). BR is thankful to the "State

Fellowship" bearing reference No. 1743/R-2017 dated 18.04.2017 and Mr. Goutam Sarkar, The H.O.D., USIC, University of North Bengal, Darjeeling is also highly acknowledged for executing SEM associated with this paper and his sincere co-operation.

TABLES

Table 1: The association constant (K_a) and complexation efficiency of the inclusion complexes at 298.15 K.

Guest	Host	Temperature (K[a])	K_a (×10^{-3})	CE
ALVC	α– CD	298.15	861.43	2.58
	β – CD	298.15	871.75	2.62

Table 2: The solubility of ALVC (moles/litre) in the aqueous solution of cyclodextrins of concentration ranging from 0.002 to 0.01 (M).

α-CD (M)	Solubility of ALVC (moles/litre)	β-CD (M)	Solubility of ALVC (moles/litre)
0.002	0.0166	0.002	0.0179
0.004	0.0218	0.004	0.0221
0.006	0.0250	0.006	0.0259
0.008	0.0276	0.008	0.0282
0.01	0.0300	0.01	0.0310

Table 3. Association Constant obtained from Benesi-Hildebrand method (K_a) using the UV-vis spectroscopic data at 293.15 to 303.15 K and the thermodynamic parameters calculated using Van't Hoff equation.

Guest	Host	Temperature (K[a])	K_a (×10^{-6}) /M^{-2}	ΔH^0 (KJ mol^{-1})	ΔS^0 (J mol^{-1} K^{-1})	ΔG^0 (KJ mol^{-1})
ALVC	α– CD	293.15	919	-8.16	143.71	-51.01
		298.15	856			
		303.15	823			
	β – CD	293.15	921	-7.85	144.85	-51.04
		298.15	877			
		303.15	829			

[a]Standard uncertainty in temperature, u, are u(T) = ± 0.01 K

Table 4: HSA-ALVC binding constant and number of binding site.

Binding constant (K_b)×10^{-3}/M^{-1}	Number of binding site
1.03	0.86

Table S1. UV-Vis spectroscopic data for the generation of Job plots of aqueous ALVC+α-CD system at 298.15 K[a].

ALVC + ALPHA - CYCLODEXTRIN							
ALVC (mL)	α-CD (mL)	ALVC (μM)	α-CD (μM)	$\frac{[\mathbf{ALVC}]}{[\mathbf{ALVC}]+[\alpha-\mathbf{CD}]}$	Absorbance (A)	ΔA	$\frac{\Delta\mathbf{A}\times[\mathbf{ALVC}]}{[\boldsymbol{ALVC}]+[\alpha-\mathbf{CD}]}$
0	3	0	100	0	0.0087	0.0598	0.0000
0.3	2.7	10	90	0.1	0.0390	0.0295	0.0030
0.6	2.4	20	80	0.2	0.0401	0.0284	0.0057
0.9	2.1	30	70	0.3	0.0441	0.0245	0.0073
1.2	1.8	40	60	0.4	0.0456	0.0229	0.0092
1.5	1.5	50	50	0.5	0.0447	0.0238	0.0119
1.8	1.2	60	40	0.6	0.0451	0.0234	0.0141
2.1	0.9	70	30	0.7	0.0501	0.0185	0.0129
2.4	0.6	80	20	0.8	0.0544	0.0141	0.0113
2.7	0.3	90	10	0.9	0.0635	0.0050	0.0045
3	0	100	0	1	0.0685	0.0000	0.0000

Table S2. UV-Vis spectroscopic data for the generation of Job plots of aqueous ALVC+β-CD system at 298.15 K[a].

ALVC + BETA - CYCLODEXTRIN							
ALVC (mL)	β-CD (mL)	ALVC (μM)	β-CD (μM)	$\frac{[ALVC]}{[ALVC]+[\beta-CD]}$	Absorbance (A)	ΔA	$\frac{\Delta A \times [ALVC]}{[ALVC]+[\beta-CD]}$
0	3	0	100	0	0.0091	0.0607	0.0000
0.3	2.7	10	90	0.1	0.0385	0.0313	0.0031
0.6	2.4	20	80	0.2	0.0336	0.0362	0.0072
0.9	2.1	30	70	0.3	0.0431	0.0267	0.0080
1.2	1.8	40	60	0.4	0.0459	0.0239	0.0096
1.5	1.5	50	50	0.5	0.0472	0.0226	0.0113
1.8	1.2	60	40	0.6	0.0466	0.0232	0.0139
2.1	0.9	70	30	0.7	0.0518	0.0181	0.0126
2.4	0.6	80	20	0.8	0.0567	0.0131	0.0105
2.7	0.3	90	10	0.9	0.0648	0.0050	0.0045
3	0	100	0	1	0.0698	0.0000	0.0000

Table S3. Mass spectrometric data showing the molecular ion peak corresponding to the 2:1 Host –Guest inclusion complexes.

ALVC+α-CD inclusion complex (IC_1)		ALVC+β-CD inclusion complex (IC_2)	
m/z	Ion	m/z	Ion
2226.86	$[ALVC+ 2\ \alpha\text{-CD}]^+$	2551.97	$[ALVC+ 2\ \beta\text{-CD}]^+$

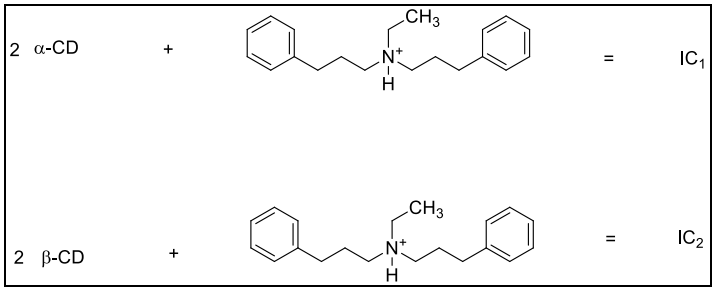

Table S4. ^{1}H NMR data of the pure α-Cyclodextrin, β-Cyclodextrin, alverine citrate and the solid inclusion complexes.

α-Cyclodextrin (400 MHz, Solvent: D2O), δ/ppm	**β-Cyclodextrin (400 MHz, Solvent: D2O), δ/ppm**
3.43 (6H, t, J = 8 Hz), 3.50 (6H, dd, J = 3.00, 10.00 Hz), 3.73 (18H, m), 3.84 (6H, t, J = 8Hz), 4.91 (6H, d, J = 4.00 Hz)	3.44 (7H, t, J = 8.00 Hz), 3.50 (7H, dd, J = 8 Hz, 4 Hz), 3.72 (21H, m), 3.82 (7H, t, J = 8 Hz), 4.92 (7H, d, J = 4 Hz)
Alverine citrate (400 MHz, Solvent: D2O), δ/ppm)	
1.04 (3H, t), 1.77 (4H, m), 2.53 (4H, m), 2.67 (4H, t), 2.92 (4H, t), 3.01 (2H, q), 7.18 (10H, m)	
ALVC+α-CD inclusion complex (400 MHz, Solvent: D2O), δ/ppm)	**ALVC+β-CD inclusion complex (400 MHz, Solvent: D2O), δ/ppm)**
1.04 (3H, t), 1.78 (4H, m), 2.54 (4H, t), 2.68 (4H, t), 2.92 (4H, t), 3.02 (2H, q), 3.42 (6H, t), 3.49 (6H, dd), 3.72 (18H, m), 3.79 (6H, d), 7.19 (10H, m)	1.03 (3H, t), 1.74 (4H, m), 2.53 (4H, t), 2.67 (4H, t), 2.92 (4H, t), 3.01 (2H, q), 3.44 (7H, t), 3.56 (7H, dd), 3.70 (21H, m), 7.16 (10H, m)

Table S5. Frequencies at FTIR spectra of α-CD, β-CD, 18-Crown-6, ALVC and solid inclusion complexes.

α-cyclodextrin (α-CD)		**β-cyclodextrin (β-CD)**	
Wavenumber (cm^{-1})	**Group**	**Wavenumber (cm^{-1})**	**Group**
3408.25	-O-H stretching	3370.21	-O-H stretching
2932.12	-C-H stretching	2916.35	-C-H stretching
1406.17	-C-H and -O-H bending	1412.27	-C-H and -O-H bending
1154.26	C-O-C bending	1158.14	C-O-C bending
1030.19	C-C-O stretching	1026.52	C-C-O stretching
978.23	skeletal vibration involving α-1,4linkage	938.08	skeletal vibration involving α-1,4linkage

Alverine citrate (ALVC)			
Wavenumber (cm^{-1})		**Group**	
3396.45		-O-H stretching/N-H stretching	
2806.31		-C-H stretching	
1602.37		C=C stretching	
1458.51		-C-H bending (methyl/methylene)	
1272.59		-C-O stretching (phenol)	
1172.23		-C-N stretching	
1070.13		-C-O stretching (secondary alcohol)	
792.26		Aromatic -C-H out-of-plane bending	
700.15		Aromatic -C-H out-of-plane bending	
ALVC+α-CD		**ALVC+β-CD**	
Wavenumber (cm^{-1})	**Group**	**Wavenumber (cm^{-1})**	**Group**
3374.08	-O-H stretching/N-H stretching	3320.19	-O-H stretching/N-H stretching
2929.29	-C-H stretching	2932.18	-C-H stretching
1628.35	C=C stretching	1604.08	C=C stretching
1333.45	-C-N stretching	1336.35	-C-N stretching
1154.27	-C-O stretching (phenol)	1158.08	-C-O stretching (phenol)
1030.23	-C-O stretching (secondary alcohol)	1032.29	-C-O stretching (secondary alcohol)
707.25	Aromatic -C-H out-of-plane bending	754.36	Aromatic -C-H out-of-plane bending
583.26	Aromatic -C-H out-of-plane bending	582.13	Aromatic -C-H out-of-plane bending

Table S6. UV-vis spectroscopic data for the Benesi-Hildebrand double reciprocal plot of (ALVC+α-CD) system at 293.15 to 303.15 K[a].

Temp (K[a])	ALVC (μM)	α-CD (μM)	Ao	A	ΔA	1/[α-CD]^2 (M^{-2})	1/ΔA	Intercept	Slope	Ka ($M^{-2}\times10^{-6}$)
293.15	80	20	0.0614	0.0923	0.0309	0.0025	32.3948	8.7231	9494.8	919
	80	50		0.1409	0.0795	0.0004	12.5798			
	80	80		0.1464	0.0850	0.0002	11.7659			
	80	110		0.1759	0.1145	0.0001	8.7374			
	80	140		0.1801	0.1187	0.0001	8.4254			
298.15	80	20	0.0624	0.0929	0.0305	0.0025	32.8201	8.3936	9806.9	856
	80	50		0.1405	0.0781	0.0004	12.8053			
	80	80		0.1570	0.0946	0.0002	10.5718			
	80	110		0.1775	0.1151	0.0001	8.6918			
	80	140		0.1820	0.1196	0.0001	8.3620			
303.15	80	20	0.0631	0.0934	0.0303	0.0025	33.0369	8.1871	9951.3	823
	80	50		0.1449	0.0818	0.0004	12.2261			
	80	80		0.1604	0.0973	0.0002	10.2784			
	80	110		0.1771	0.1140	0.0001	8.7757			
	80	140		0.1827	0.1196	0.0001	8.3620			

Table S7. UV-vis spectroscopic data for the Benesi-Hildebrand double reciprocal plot of (ALVC+β-CD) system at 293.15 to 303.15 K[a].

Temp (K[a])	ALVC (μM)	β-CD (μM)	Ao	A	ΔA	1/[β-CD]^2 (M^{-2})	1/ΔA	Intercept	Slope	Ka ($M^{-2}\times10^{-6}$)
293.15	80	20	0.0616	0.0930	0.0301	0.0025	33.2566	8.7447	9485.1	921
	80	50		0.1416	0.0787	0.0004	12.7077			
	80	80		0.1471	0.0842	0.0002	11.8777			
	80	110		0.1756	0.1127	0.0001	8.8770			
	80	140		0.1808	0.1179	0.0001	8.4826			
298.15	80	20	0.0621	0.0943	0.0322	0.0025	31.0374	8.0806	9211.3	877
	80	50		0.1429	0.0808	0.0004	12.3774			
	80	80		0.1714	0.1093	0.0002	9.1499			
	80	110		0.1752	0.1131	0.0001	8.8456			
	80	140		0.1815	0.1194	0.0001	8.3760			
303.15	80	20	0.0627	0.0949	0.0322	0.0025	31.0857	7.7624	9367.3	829
	80	50		0.1441	0.0814	0.0004	12.2861			
	80	80		0.1766	0.1139	0.0002	8.7803			
	80	110		0.1764	0.1137	0.0001	8.7989			
	80	140		0.1919	0.1292	0.0001	7.7418			

Table S8. Data of the van't Hoff equation for calculation of thermodynamic parameters ΔH^o, ΔS^o and ΔG^0 of different (ALVC+α-CD) and (ALVC+β-CD) inclusion complexes.

HOST	T (K[a])	1/T	Ka ($M^{-2}\times10^{-6}$)	lnKa	Slope	Intercept	ΔH^0 (KJ mol^{-1})	ΔS^0 (J mol^{-1} K^{-1})	ΔG^0 (KJ mol^{-1})
	293.15	0.00341	919	20.6388					
α-CD	298.15	0.00335	856	20.5678	981.97	17.284	-8.16	143.71	-51.01
	303.15	0.00330	823	20.5285					
	293.15	0.00341	921	20.6421					
β-CD	298.15	0.00335	877	20.5920	944.50	17.241	-7.85	144.85	-51.04
	303.15	0.00330	829	20.5357					

FIGURES

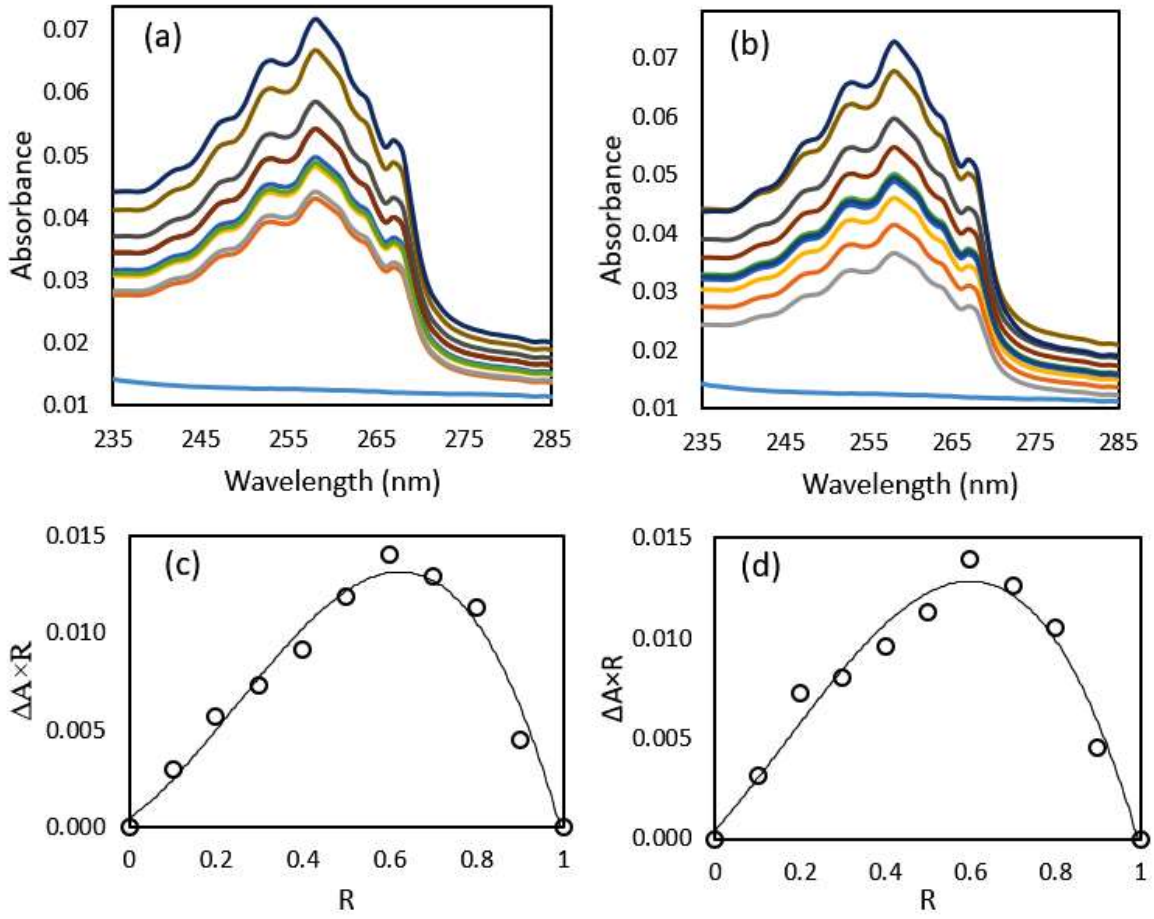

Figure 1: UV-vis spectra for the generation of Job's plot (a,c) ALVC-α-CD inclusion complexes and (b,d) ALVC-β-CD inclusion complexes.

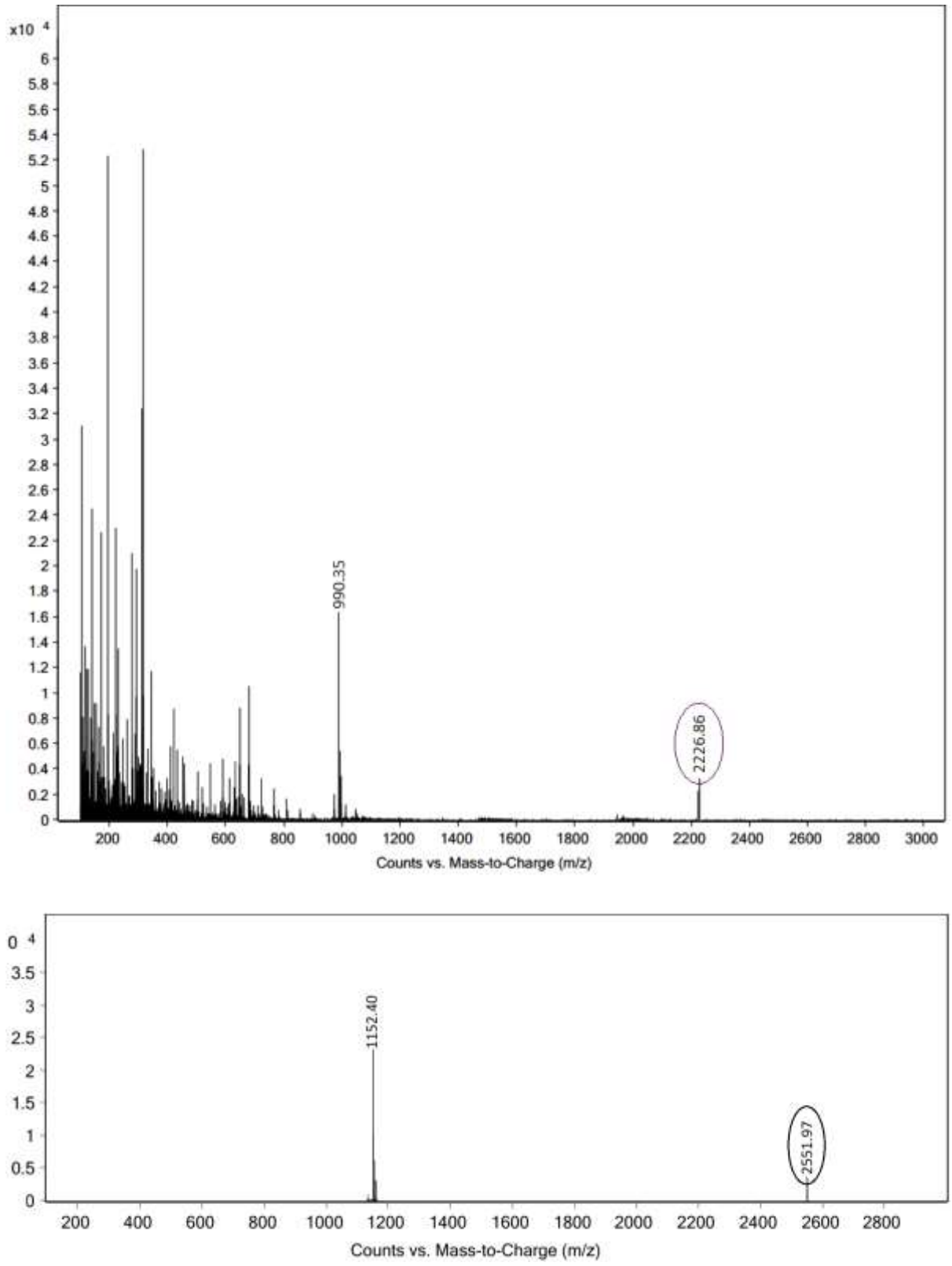

Figure 2: Mass spectra of (a) ALVC/α-CD inclusion complex, (b) ALVC/β-CD inclusion complex.

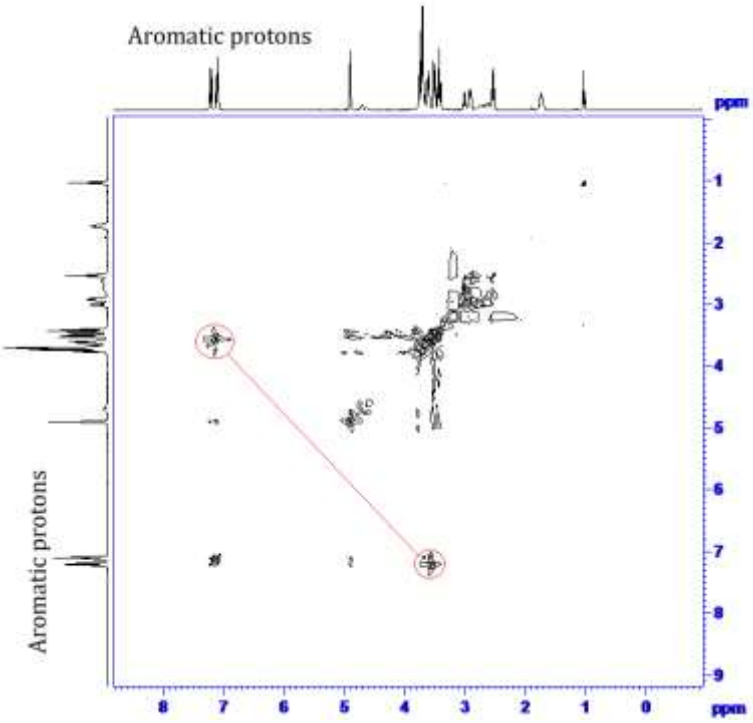

Figure 3: 2D ROESY NMR spectra of ALVC/α-CD inclusion complex.

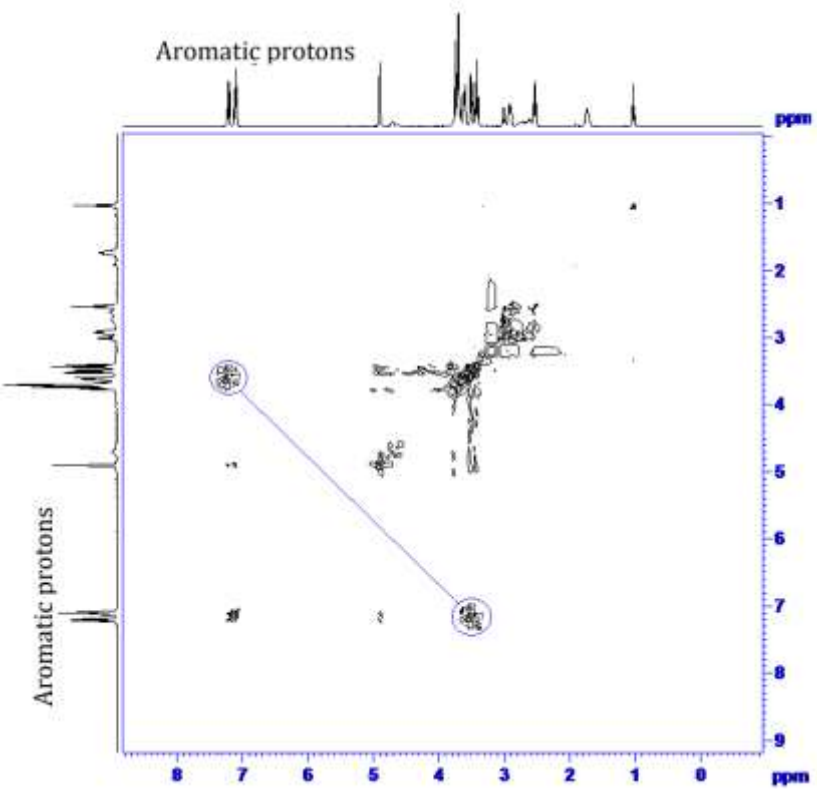

Figure 4: 2D ROESY NMR spectra of ALVC/β-CD inclusion complex.

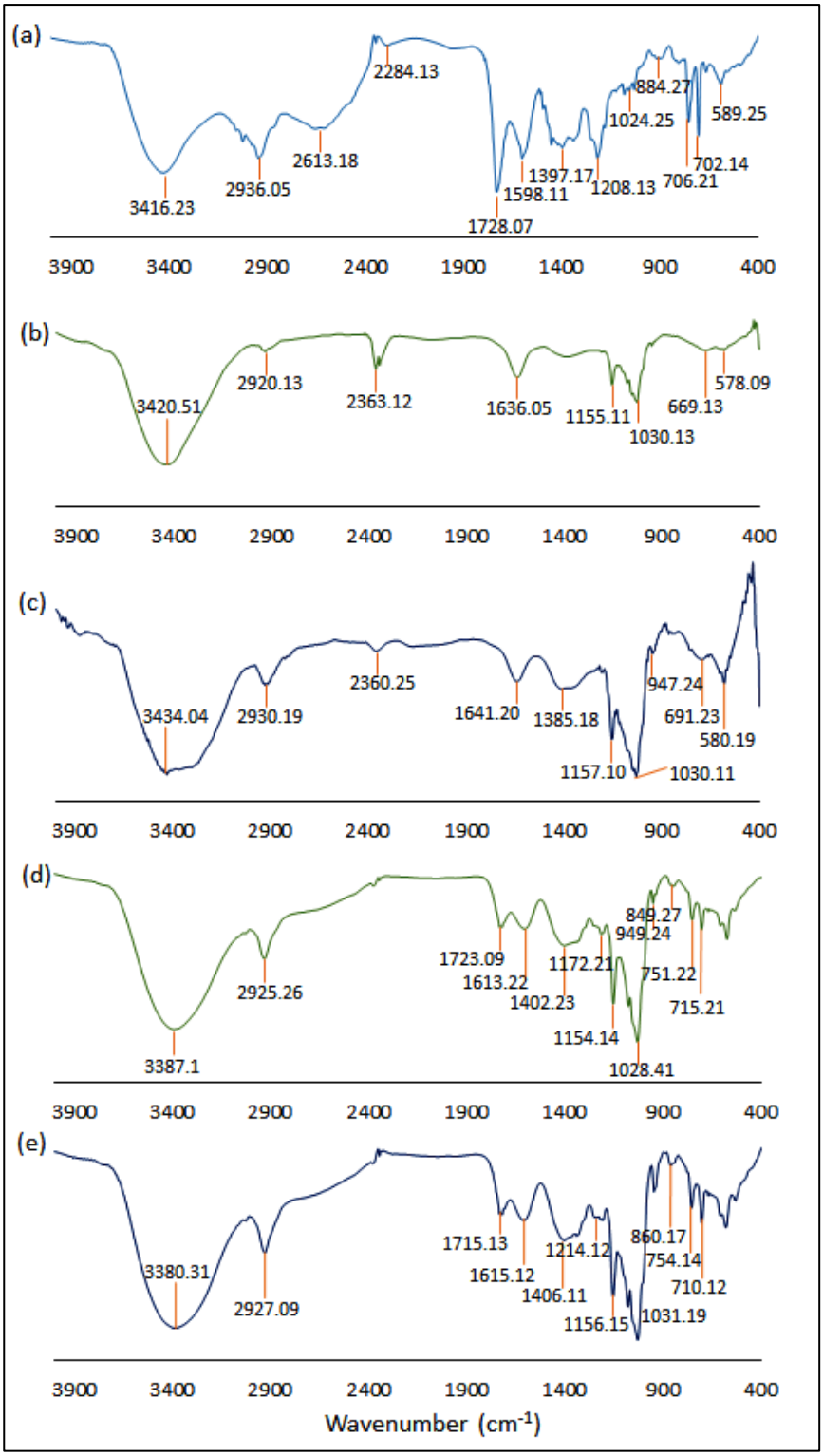

Figure 5(a, b, c, d, e): IR frequencies of (a) ALVC, (b) α-CD, (c) β-CD, (d) ALVC/α-CD inclusion complex, (e) ALVC/β-CD inclusion complex.

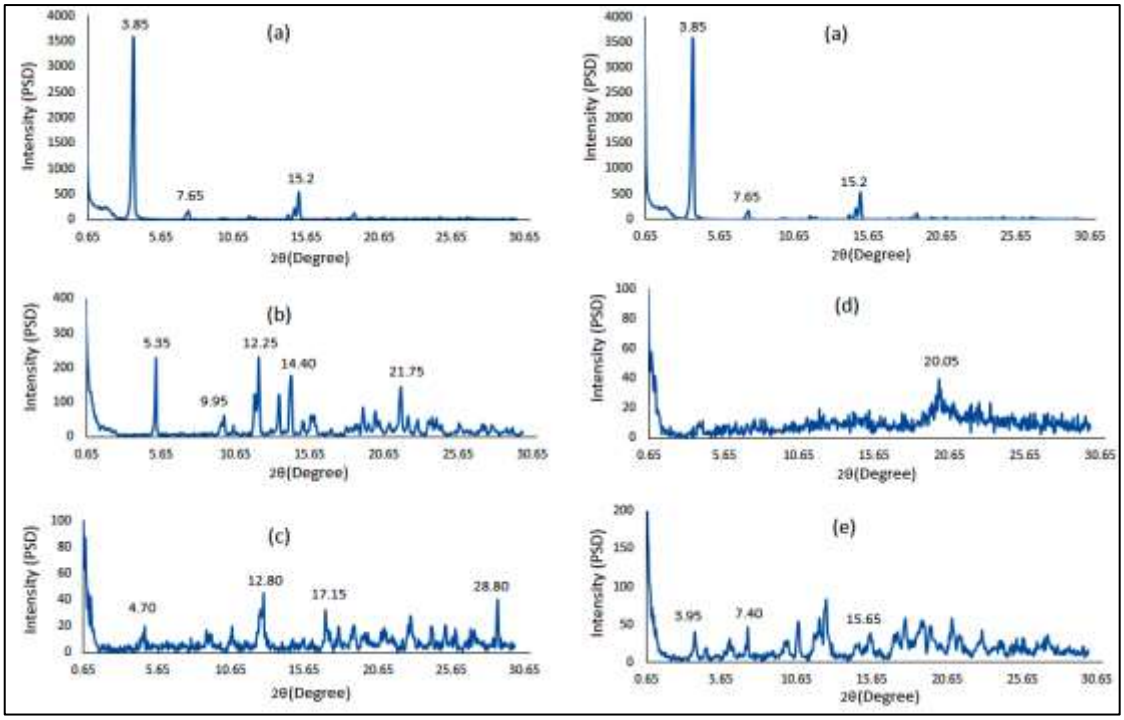

Figure 6(a, b, c, d, e): PXRD spectra of (a) ALVC, (b) α-CD, (c) β-CD, (d) ALVC/α-CD inclusion complex, (e) ALVC/β-CD inclusion complex.

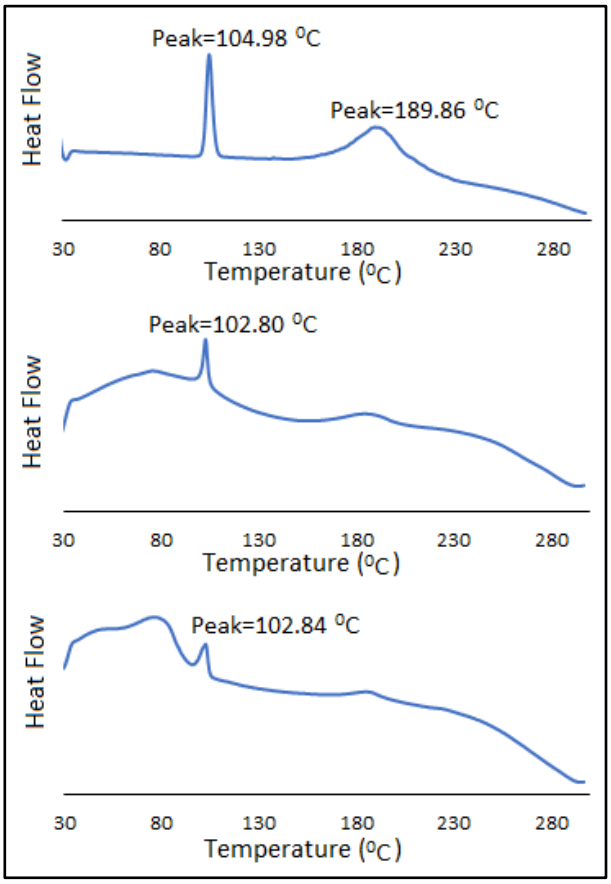

Figure 7(a, b, c): DSC thermogram of the (a) ALVC, (b) ALVC/α-CD inclusion complex, (c) ALVC/β-CD inclusion complex.

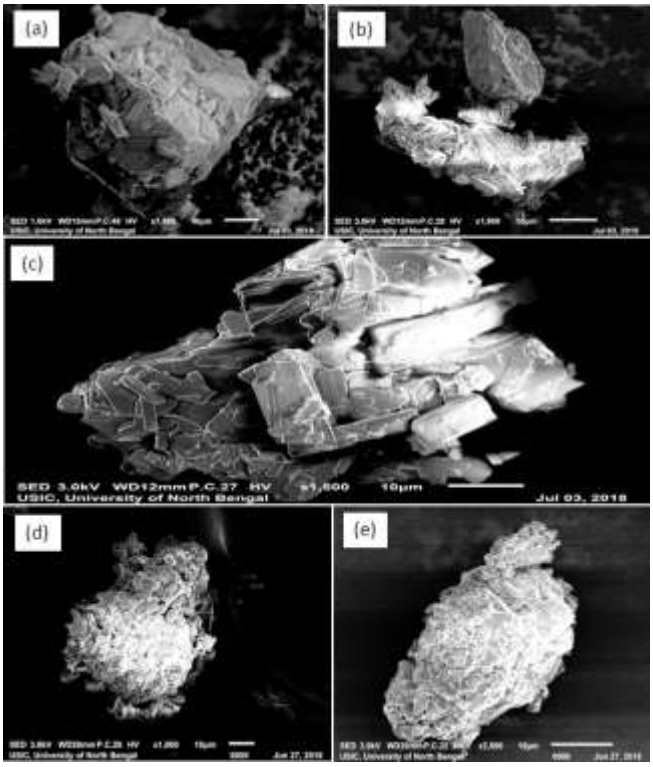

Figure 8(a, b, c, d, e): SEM images of (a) α-CD, (b) β-CD, (c) ALVC, (d) ALVC/ α-CD inclusion complex, (e) ALVC/ β-CD inclusion complex.

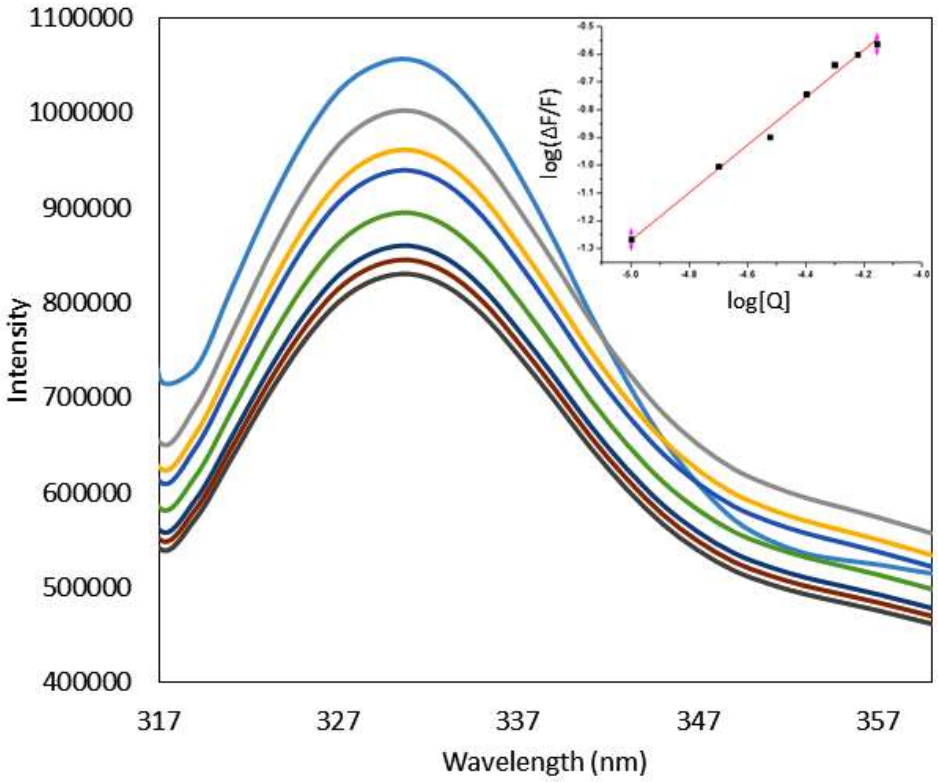

Figure 9: Fluorescence spectra and plot for obtaining binding constant.

SCHEMES

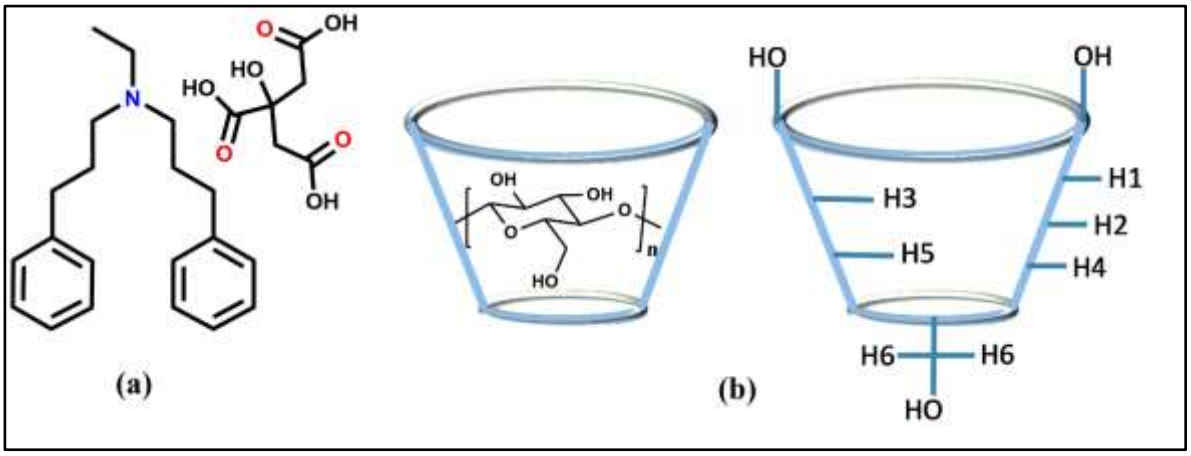

Scheme 1: Molecular structure of (a) alverine citrate, (b) α, β-cyclodextrins where, n=5 to 6 respectively.

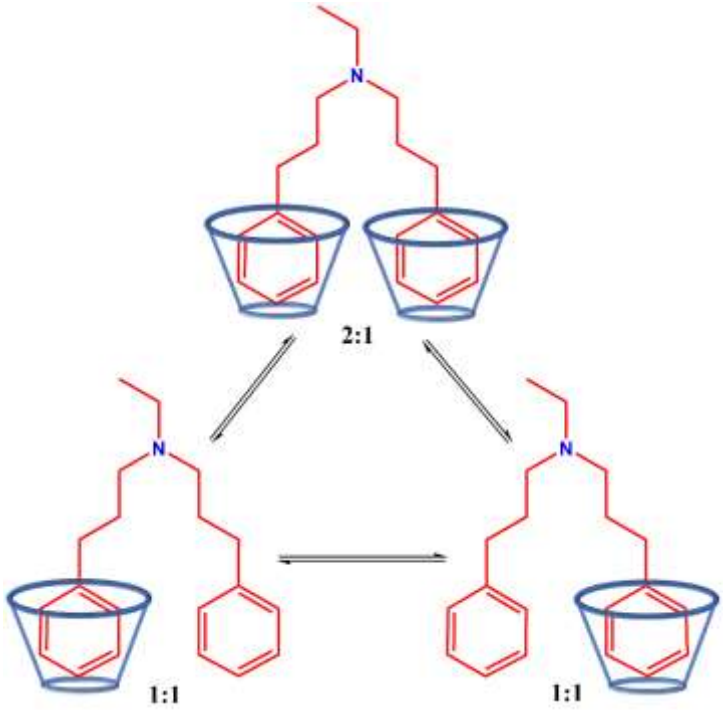

Scheme 2: Schematic representation of the formation of Inclusion Complex.

CHAPTER VIII

Minimization of the Dosage of Food Preservatives Mixing with Ionic Liquids for Controlling Risky Effect in Human Body: Physicochemical, Antimicrobial and Computational Study

Abstract: An analysis on the diverse molecular interactions of implausible food preservatives, Sodium benzoate (SBz), Sodium salicylate (Scyt) in the aqueous solutions of Benzyltriethylammoniun chloride (BTEACl), Benzyltrimethylammoniun chloride (BTMACl) having durable anti-bacterial effect have been explored thoroughly by various physicochemical methodologies such as Density, Refractive index, Viscosity, Electrical conductivity, at five different temperatures ranging from 298.15 K to 318.15 K. Anti-bacterial as well as the anti-fungal effects of the ternary mixtures, (BTEACl+SBz+H_2O), (BTEACl+Scyt+H_2O), (BTMACl+SBz+H_2O) and (BTMACl+Scyt+H_2O) were further analysed for better results and found to act synergistically below the MIC of both the food preservative, thus minimises the hazardous threat, caused by unnecessarily excessive consumption of food preservatives. Association constants governed by diverse intermolecular interactions in the solution phase were studied by UV-vis spectroscopy. Construction of thermodynamic background caused by innumerable interactions taking place in the ternary mixtures were explored by calculating the free energies of various molecular associations. The genesis of diverse interactions was exposed by measurement of the apparent molar volume (ϕ_v), limiting apparent molar volume (ϕ_v^0), molar refraction (R_M), limiting molar refraction (R_M^0) viscosity B coefficients and reveals as strong solute-solvent interaction, over the solute-solute and solvent-solvent interactions. Optimum energies with the optimised geometries of molecular assembly for (BTEACl+SBz), (BTEACl+Scyt), (BTMACl+SBz) and (BTMACl+Scyt) systems were calculated from Ab-initio quantum chemical calculations using Gaussian 09W quantum chemical package which found supportive to the practical outcomes.

Keywords: Benzyltriethylammoniun chloride, Benzyltrimethylammoniun chloride, Sodium benzoate, Sodium salicylate, Solute-Solvent interaction, anti-microbial activity.

1. INTRODUCTION

According to our knowledge, it is well known to all, there is so much of food productions all over the world but because of the process of spoilage a large proportion of these is lost. So, it requires a great attention to preserve foods, produced industrially and even at home. There are so many preservatives known, that utterly prevents spoilage of foods, but having some sort of side effects, usedness of these is an inherent threat to the world health. Now, use of these in minimal amount i.e. below the MIC (Minimal Inhibitory Concentration) in food would overcome the threat. The challenge was accepted and reveals that, two well-known food preservatives (FPs), sodium benzoate and sodium salicylate works properly against various fungus as well as gram-positive and gram-negative bacteria below their MIC in the presence of negligible amount of two ammonium based ionic liquids (ILs) benzyltriethylammoniun chloride (BTEACl) and benzyltrimethylammonium chloride (BTMACl).

Sodium benzoate (SBz) **(Scheme 1)** having inhibitory effect on the microbial growth is strongly recommended as a food preservative and commonly used in foods like soda, fruit juice and a variety of products, such as cosmetics and pharmaceuticals. In acidic medium SBz works better on yeasts, molds, bacterial growth and prevent spoilage[1],[2],[3],[4],[5]. In patients with acute hyper-ammonaemia, who were born with urea cycle disorders[6],[7] SBz acts as a therapeutic agent and also treats dental carries, blocks D-dopa in the hemi-parkinsonian rat[8]. Beside these bio-medical and pharmaceutical applications SBz have some antagonistic effect, it can damage parts of the DNA affecting the future generations[9]. The acceptable daily intake (ADI) levels of SB should be 5 mg/kg body weight[10], as strictly recommended by Joint Food and Agriculture Organization of the United Nations/World Health Organization expert committee on food additives, otherwise SBz may be toxic and imperils human health[11]. Research on interaction of antimicrobials shows that, a pair of antimicrobials acting synergistically can show satisfactory result and better microbial control could be achieved[12]. In this connection SBz and chitosan found synergistic against spoilage yeast in saline solution[13].

Sodium salicylate (Scyt) **(Scheme 1)** is a significant antibacterial agent, also enhances the activities of certain antibiotics[14],[15],[16],[17]. The bacterial strains, Salmonella, Shigella including Escherichia coli that causes diarrhoea used to inhibited

by bismuth subsalicylate efficiently[18]. Being an active anti-inflammatory compound Scyt have been used as anti-inflammatory, analgesic and anti-pyretic agent[19] still it has gastric bleeding like serious disadvantage[20]. Scyt acts synergistically with vancomycin and enhances anti-staphylococcal activity significantly. The presence of salicylate in 5 mM concentration, vancomycin prevents biofilm formation and kill bacteria effectively below its MIC[17]. In vitro CPS production can be reduced to 80% or more by Scyt, the major metabolite of aspirin. Scyt also increases synergistic activity of amikacin and imipenem[21].

Quaternary ammonium based ionic liquids also execute some sort of anti-microbial effects for instance positive charge on the Nitrogen atom of these ionic liquids attracts naturally the negatively charged species, such as bacterial proteins and consequently disorganization in the protein chain makes it denature. Ionic liquids, benztltriethylammonim chloride, benztltrimethylammonim chloride **(Scheme 1)** were used herewith in all four possible combinations to the illustrious food preservative SBz and Scyt. Anti-microbial activities of the set of four combinations were studied warily at concentrations below their MIC and found synergistic to each other.

In this article the synergism activity between the above mentioned food preservatives and ionic liquids against micro-organisms were studied such that, their combination can act properly below their MICs (Minimal Inhibitory Concentration) and as a consequence reduces the unnecessary consumption of hazardous food preservative. In this connection anti-bacterial and anti-fungal activities of both the food preservatives, SBz and Scyt were studied in the presence of trace amount of ionic liquids. Then, volumetric and viscometric analysis as well as refractive index and conductimetric measurement defines the cause of synergism between FPs and ILs.

2. EXPERIMENTAL SECTION

2.1. Materials

All the chemicals, sodium benzoate (purity ≥ 99.5%), sodium salicylate (purity ≥ 99.5%), benzyltriethylammoniun chloride (purity 99.0%), benzyltrimethylammonium chloride (purity 97%) were purchased from Sigma Aldrich Germany and used as received taking sufficient precautions.

2.2. Apparatus

All the experimental solutions were prepared by transferring required amount of weighed materials to a volumetric flask and then filled with the solvents upto the mark. The uncertainty in molality of the prepared solutions evaluated as ±0.0001 mol kg^{-3}. Different sets of solutions with various concentration were prepared by proper dilution of the mother solution. The quantity of samples for the preparation of the mother solutions were weighed precociously by Mettler Toledo AG-285 with uncertainty ±0.0003 g.

The molality of the solution which has been calculated from the molar concentration data using the relation[22]

$$m = \frac{1}{[\rho/c - M/1000]} \qquad (1)$$

Where, m is the molality of the solutions, ρ and c refer to densities and concentration of the solutions respectively, M stands for relative molar mass of the materials used.

The antimicrobial activities of SBz and Scyt were tested in relation to the bacteria *Bacillus subtilis* and *Escherichia coli* by well diffusion assay[23]. Briefly, the bacterial cultures were grown overnight in Nutrient Broth and uniformly spread on the surface of Muller Hington agar plates using sterile cotton swabs. Wells of diameter 8 mm was made using sterile cork borers and SBz, Scyt, BTEACl and BTMACl were used singly and in combinations at concentrations of 3mg/ml and 6mg/ml. The plates were incubated overnight at 37^0C and observed for formation of inhibition zones. The "diameter of the inhibition" for positive results was recorded as diameter of zone of inhibition – diameter of the well (8 mm). The diameter of inhibition when no zone was observed was kept at zero.

The solvent as well as the solution densities were measured with vibrating-tube density meter (Anton Paar, DMA 4500M), maintained at 298.15 to 318.15 K. Calibration of the instrument was done with doubly distilled water and dry air. The uncertainty in density was estimated to be ±0.00001 g cm^{-3}.

Digital Refractometer Mettler Toledo was used to measure refractive index. Refractive indices of experimental solutions were measured after rectifying twice the refractometer by distilled water. During measurement calibration of the instrument

was done after each few measurements. Temperature of the solutions under measurement were maintained in a Brookfield Digital TC-500 thermostat water bath.

Brookfield DV-III Ultra Programmable Rheometer with fitted spindle size-42 was employed to measure viscosities of the solutions. The viscosities were obtained using following programmed equation

$$\eta = (100/RPM) \times TK \times torque \times SMC \qquad (2)$$

where SMC (0.327), RPM, TK (0.09373) stands for spindle multiplier constant, speed, viscometer torque constant respectively. Calibration of the instrument before starting experiment was done with provided standard viscosity samples, water and aqueous $CaCl_2$ solutions. Temperature of the solution was maintained with Brookfield Digital TC-500 thermostat bath.

The conductivity of the experimental solutions was measured in aSystronics-308 conductivity bridge using a dip-type immersion conductivity cell, CD-10, having a cell constant of approximately 0.1 ± 0.001 cm^{-1} of accuracy ±0.01%. Calibration of the conductivity cell was done according the method proposed by Lind et al[24]. The cell constant was measured using freshly prepared 0.01 M aqueous KCl solution and it was maintained within the range 0.09-1.00 cm^{-1} during experiment. Temperature during experiment was monitored and controlled to the experimental temperature using Brookfield Digital TC-500 thermostat bath. HPLC-grade water with a specific conductance of 6.0 μS m^{-1} was used for conductivity measurement. The conductance data were reported at the accuracy of±0.3%.

UV−visible spectra were recorded utilizing JASCO V-530 UV−Vis spectrophotometer, with a wavelength accuracy of ±0.5 nm. Cell temperature during the experiment was controlled from 298.15K to 318.15K with a digital thermostat.

Theoretical i.e. Ab-initio calculations were executed through Gaussian 09Wquantum chemical package[25].

3. RESULT AND DISCUSSION

3.1 Antimicrobial effects of SBz and Scyt in combination with BTEACl and BTMACl reveals synergistic:

The results clearly indicated the enhancement of antimicrobial effects of SBz and Scyt when used in combination with ionic liquids BTEACl and BTMACl.

In case of gram positive *B.subtilis* both BTEACl and BTMACl enhanced antimicrobial activity of SBz and Scyt with the effect being comparatively more profound in SBz in combination with BTEACl. The idea of lowering the concentrations to 3 mg was to check the enhancement when SBz and BTEACl individually showed minimal or no zone of inhibition. As expected 3 mg of SBz showed no zone of inhibition and 3 mg BTEACl showed minimal diameter of 2 mm which was enhanced to 8mm when used in combination indicating enhanced antimicrobial activity. In case of gram negative *E.coli* no susceptibility was observed in case of SBz alone or in combination with ILs. However, E. coli showed enhanced susceptibility to Scyt when used in combination with BTEACl and BTMACl **(Figure 1, 2, 3)**.

The differences in the structure of their cell walls can be accounted for the differences in susceptibility of *Bacillus subtilis* and *E.coli*, with *E.coli* having an outer lipid layer which acts as a molecular filter for hydrophilic compounds[26]. This lipid layer might have reduced the ability of the hydrophilic components to penetrate into the cells and hence exert their potential inhibitory action. The zero antimicrobial effects of SBz and Scyt at concentrations of 3 mg and 6 mg may be because of their concentration being lower than the reported microbial inhibitory concentrations (MIC) of around 10 mg/mL[27]. BTEACl has also showed inhibitory action when used alone which might be due to the presence of quaternary ammonium with ethyl group whereas BTMACl has shown no inhibitory effect when used singly.

The outcome of this study is that SBz and Scyt can exert antimicrobial effects when used with ionic liquids such as BTEACl and BTMACl even at minimal concentrations which normally do not exert antimicrobial effects when used alone. However, the chances of ILs exerting cytotoxic effects on human cell lines will have to be ruled out before its proper application in industries.

3.2 Density and volumetric measurements:

Here, we present information concerning the chemistry of food preservative–ionic liquid interactions in aqueous solutions that have been acquired from the apparent molar volume (ϕ_v), limiting apparent molar volume (ϕ_v^0) and (S_v^*) of food preservatives in aqueous solutions of ionic liquids meanwhile all these three

parameters evidently be governed by the solvent environment surrounding the solute species and known to cover information belong to the structural penalties of solute–solvent interactions[28]. Apparent molar volume of a substance in solution can be defined as the sum of the geometric volume of the two solute molecules while undergo solvation through solute-solvent interaction with the co-solvent. Densities of the co-solvents of various mass fractions, made by two ionic liquids BTEACl and BTMACl separately with water, were measured at temperature range 298.15 to 318.15K are listed in **(Table S1)**. The values of (ϕ_v) for the (BTEACl+SBz+H_2O), (BTEACl+Scyt+H_2O) systems **(Table S8, S9, S10)** and the same for (BTMACl+SBz+H_2O), (BTMACl+Scyt+H_2O) systems **(Table S11, S12, S13)** were calculated by means of density (ρ) data **(Table S2-S4)** and **(Table S5-S7)** through the following equation[29],[30],[31],[32]

$$\phi_v = \frac{M}{\rho} - \frac{1000(\rho - \rho_0)}{m\rho\rho_0} \qquad (3)$$

Where M is the molar mass of the solute; m is the molality of the solution; ρ and $\rho_0$represents the densities of the solution and solvent respectively. Apparent molar volume at infinite dilution, i.e. limiting molar apparent volume (ϕ_v^0) and experimental slopes (S_v^*) were determined using least squares fitting of linear plots of (ϕ_v) against the square root of molar concentrations ($m^{1/2}$) using the Masson equation[33],[25].

$$\phi_v = \phi_v^0 + S_v^* . \sqrt{m} \qquad (4)$$

The experimental plots, generated from Masson equation and corresponding values of (ϕ_v^0) and (S_v^*) of each plot are shown in **(Figure S1, S2)** and **(Table1, 2)**. The values of (ϕ_v^0) are found positive for all the systems and is greatest for (BTMACl+Scyt) system, suggesting the presence of stronger solute-solvent interactions in this case than that of the other systems and found to follow the order,(BTMACl+Scyt)>(BTMACl+SBz)>(BTEACl+Scyt)>(BTEACl+Scyt) as represented in **(Scheme 2)**. The dipole–dipole interaction taking place in the solutions explains the truth behind the above mentioned order of solute-solvent interactions since greater the dipole-dipole interaction smaller will be the values of (ϕ_v) as well as (ϕ_v^0)[34]. The

dipole moment of SBz, Scyt, BTEACl and BTMACl were calculated theoretically with the help of Gaussian 09W quantum chemical package, are listed in the **(Table 7)**.

Increasing trend in the (ϕ_v^0) values with rise in temperature and mass fraction of BTEACl and BTMACl, suggests the rising trend of solute-solvent interaction as well. This is probably due to the release of a number of the solvent molecules from loose solvation layers during the solute-solvent interactions. The phenomenon drawn above also reflected in the molar conductivity data as discussed in this article. Values of the experimental slope, (S_v^*) assign the extent of ion-ion interaction in the solution, and the negative values indicate the presence of less ion-ion interaction in the medium. Quantitative comparison shows, greater the magnitude of (ϕ_v^0) than (S_v^*) recommends the ion-solvent interactions dominants over ion-ion interactions[35].

Temperature dependency of the limiting apparent molar volume(ϕ_v^0) were studied between the temperature range 298.15 to 318.15K at the interval of 5K of temperature and the results obtained were found to follow the following polynomial equation[36]

$$\phi_v^0 = a_o + a_1 T + a_2 T^2 \qquad (5)$$

Where, a_0, a_1 and a_2 are the empirical coefficients depending on the nature of solute, mass fraction (W) of co-solvent are listed in **(Table 3)**. T represents temperature in Kelvin scale. The values of these coefficients of the above equation. First derivative of equation (5) gives the values of limiting apparent molar expansibilities (ϕ_E^0) which have been calculated for various temperature and listed in **(Table 4)**.

$$\phi_E^0 = (\delta\phi_v^0 / \delta T)_P = a_1 + 2a_2 T \qquad (6)$$

Limiting apparent molar expansibilities (ϕ_E^0) for all the systems are found positive signifying the absence of caging or packing effect in the solutions of all the four different systems.

The solute – solvent interaction studied so far is now at a state that, it may be structure breaker or synergistic structure maker interaction. In this connection Hepler developed a way to examine the nature of the solute – solvent interaction taking place

in the solution phase[37]. According to Hepler, values of $(\delta\phi_E^0/\delta T)_P$ in the expression given below, determines whether, it is structure breaker or structure maker interaction[38].

$$(\delta\phi_E^0/\delta T)_P = (\delta^2\phi_v^0/\delta T^2)_P = 2a_2 \quad (7)$$

Generally, positive or small negative values of $(\delta\phi_E^0/\delta T)_P$ strongly suggests structure making rather than structure breaking interaction. Here, positive and small negative values of $(\delta\phi_E^0/\delta T)_P$ listed in **(Table 4)** confirms the mode of solute – solvent interaction is structure making.

3.3 Refractive index:

Optical data of refractive index of the two studied heterogeneous systems has provided interesting information allied to molecular interactions, structure of solutions in these assay. The refractive index of mixing can be interconnected by the application of a composition-dependent polynomial equation and molar refraction, R_M in solution thus can be estimated from Lorentz-Lorenz relation[39],[40]

$$R_M = \frac{(n_D^2 - 1)}{(n_D^2 + 2)}\left(\frac{M}{\rho}\right) \quad (8)$$

Where, R_M, n_D, M and ρ represents molar refraction, refractive index, molar mass and density of solution respectively.

Generally, refractive index of a system is the ability to refract light and hence it can simultaneously measure the compactness of that system. The refractive indices (n_D) of (BTEACl+SBz+H_2O), (BTEACl+Scyt+H_2O) systems are reported in **(Table S2-S4)** and for(BTMACl+SBz+H_2O), (BTMACl+Scyt+H_2O) systems in **(Table S5-S7).** The molar refraction (R_M) of the studied solutions were calculated and listed in the **(Table S8 – S10)** for (BTEACl+SBz+H_2O), (BTEACl+Scyt+H_2O) systems and **(Table S11 – S13)** for (BTMACl+SBz+H_2O), (BTMACl+Scyt+H_2O) systems. Analysis of these data enable us to draw the following sequence of compactness of the various (food preservative – ionic liquid) systems in solution phase.

(BTMACl+Scyt)>(BTMACl+SBz)>(BTEACl+Scyt)>(BTEACl+Scyt)

The limiting molar refraction, (R_M^0) listed in Table S can be calculated using the following equation-

$$R_M = R_M^0 + R_S\sqrt{m} \quad (9)$$

Where, 'm' is the molality of solution and R_M^0 is the limiting molar refraction that signifies solute – solvent interaction. So, this measurement operates as an expensive tool for studying the molecular interaction in solution. Gradual increase in the values of R_M and R_M^0 **(Table 1, 2 and Figure 4, S3)** with rise in mass fraction of co-solvent also signifies that, solute – solvent interaction predominant over ion-ion interactions as obtained from density measurement.

3.4 Viscosity measurement:

In aqueous electrolytic solutions the extent of ionic hydration[41] and structural interactions[42],[43],[44] within the ionic hydration co-spheres[45] can be explored easily by studying viscosity coefficient with varying concentration and temperature of the aqueous solution. Experimental values of viscosities for all the food preservative – ionic liquid systems, taken at various concentration and temperature are listed in **(Table S2-S4)** and **(Table S5-S7)**. Viscosity data so obtained were analysed with the help of Jones-Dole equation[46]-

$$\eta_r = \frac{\eta}{\eta_0} = 1 + A\sqrt{c} + Bc \quad (10)$$

Where, η and η_0 are viscosities of solution and solvent respectively, c is the concentration of solution in molality.

Rearrangement of the above equation (8) gives following-

$$\frac{\eta_r - 1}{\sqrt{c}} = A + B\sqrt{c} \quad (11)$$

Here, viscosity A coefficient is a constant, also known as Falken hagen coefficient[47], stands for long-range coulombic forces, so represents the solute-solute/ion-ion interaction in solution, while B coefficient is an adjustable parameter, which is the

measure of the effective hydrodynamic volume, reflects the solute-solvent interaction. Magnitude of viscosity B coefficient depends on the shape, size and partial molar entropies of the ions. According to the Jones-Dole equation from the plots of $(\eta_r - 1)/\sqrt{c}$ vs. $\sqrt{c}$ **(Figure S4, S5)** viscosity A and B coefficients were obtained by linear least-square analysis, are reported in **(Table 1, 2).** Obtained viscosity A and B coefficients are actually the intercept and experimental slopes of the plots **(Figure S4, S5)** respectively. An observation and deep investigation on the change in viscosity B coefficient of the various food preservative-ionic liquid systems at a given temperature and mass fraction of co-solvent, enable us to conclude the following sequences of solute-solvent interaction [48],[43],[49] - (BTMACl + Scyt) > (BTMACl + SBz) > (BTEACl+Scyt) > (BTEACl+Scyt) **(Scheme 2)**. Having near about the same shape and size of both the ionic liquids, size and structural properties of BTEACl and BTMACl can't differentiate the change in viscosity B coefficient, rather it seems to be controlled indirectly by the ion-ion interaction i.e. (SBz-SBz) and (Scyt-Scyt) interaction taking place in SBz and Scyt solution. Lower the ion-ion interaction can enhance dissolution of a solute in solvent through solvation of ions and thereby developing solute-solvent interaction. Now, an inspection on the **(Table 1, 2)** shows lower viscosity A coefficient for (Scyt-ionic liquid) than that of (SBz-ionic liquid) systems. This can be accounted by the fact that, benzoate ions originating from SBz in solution can undergo dimerization, whereas dimerization of salicylate ions gets disturbed by the intra-molecular H-bonding in Scyt. The innumerable interactions governed in solution which are also responsible for developing solute-solvent interaction can be explained on the basis of the interaction of $R_4N^{\oplus}$ from ionic liquid with the COO^{-} and OH group originating from food preservative as follows- (i) Lower effective charge accumulation on nitrogen atom of $R_4N^{\oplus}$ in BTEACl than that of BTMACl, caused by greater +I (positive inductive) effect of (–CH_2-CH_3) rather than (–CH_3) group operating in case of BTEACl. (ii) COO^{-} and OH group of Scyt interacts with $R_4N^{\oplus}$ in Scyt-ionic liquid systems, while the COO^{-} interacts alone with $R_4N^{\oplus}$ in case of SBz-ionic liquid systems. On the other hand, at a given temperature, if we deal with a particular food preservative-ionic liquid system viscosity B coefficient found to increase with increasing mass fraction of co-solvent made of ionic liquids in water. The above observation has a ready explanation that,

replacement of water molecules by more co-solvent molecules (BTEACl or BTMACl) from the solvation sphere of food preservatives (SBz or Scyt) that, brings solute and co-solvent closer thereby increasing viscosity B coefficients and accounts for the higher solute-solvent interaction. The overall viscometric studies shows that, viscosity B coefficients are positive and greater than viscosity A coefficient, suggesting solute–solvent interaction predominant over the solute-solute interaction.

Extensive study of the viscosity B coefficient such that, its first derivative over temperature is an upgradation of viscosity B coefficient in predicting the nature of solute – solvent interaction as structure maker or structure breaker. The value of dB/dT **(Table 5)** is a measure of activation energy required for the viscous flow in solution. This is the reason, why the measure of dB/dT is indicative towards the structure making or structure breaking ability than sign or magnitude of the B-coefficient[50],[51],[52],[53]. The small positive or negative value of dB/dT signifies structure-making (kosmotropic) whereas the larger positive value identifies it as structure-breaking (chaotropic). The variation of dB/dT with the mass fraction of co-solvents have shown in **(Figure 5).**

3.5 Conductimetric study

The conductance study of the interaction (solute – solvent) between Scyt and SBz with the aqueous solution of ILs, BTMACl and BTEACl has been performed at five different temperatures. Advantage of this study is that this measurement provides information about the interaction and transport phenomena of the (Scyt + ILs + H_2O) and (SBz + ILs + H_2O) ternary systems[54].

The molar conductivities[55] (Λ) of aqueous BTEACl and BTMACl has been monitored with increasing the concentration of Scyt and SBz respectively at five different temperatures and have been listed in **(Table S14, S17)**. The **Figure S6 and S7,** shows the resulting plots of (BTMACl + SBz + H_2O), (BTMACl + Scyt + H_2O), (BTEACl + SBz + H_2O) and (BTEACl + Scyt + H_2O) respectively. For every system it has been observed that Λ values increase with increase in temperature and gradual addition of either Scyt or SBz to ILs solution causes a continuous decrease in molar conductance. The mobility of the ionic species in solution playing the leading role, in spite of growing number of ionic species with added aqueous SBz or Scyt solution in step, the molar conductivity decreases[56]. It may be due to the development of solute-solvent interaction governed by the dipole-dipole as well

as the pπ –pπ and hydrophobic – hydrophobic interaction in solution mixtures between the solute and solvent molecules. The formation of molecular assembly thus forces the ionic species to lose their independent movement making the ionic species less mobile to show conductivity in solution. The intra-molecular H-bonding of Scyt as discussed in viscosity context also inhibits dimerization between Scyt molecules and makes it available for exerting solute – solvent interaction with ILs more than that of SBz in solution. Conductimetric study thus supports the volumetric, refractometric and viscometric study and echoes the same observation as well.

3.6 UV-Vis spectroscopic analysis: The association constants

The stability of the molecular association developed in solution mixtures by the manifestation of solute-solvent interaction were explored by measuring the association constants (K_a). The UV-vis spectroscopic data for the various mixtures of solutions were recorded and employed to determine the association constant (K_a). To determine association constant (K_a), the changes in absorbances (ΔA) of SBz and Scyt at λ_{max} = 220 nm and λ_{max} = 292 nm were measured with increasing concentration of BTEACl/BTMACl at 298.15 K **(Table S18 – S21)**. According to the Benesi-Hildebrand method[57], the double reciprocal plots obtained from (equation 10) were found linear that, usually says about the solute : solvent ratio in solution[57],[58].

$$\frac{1}{\Delta A} = \frac{1}{\Delta\varepsilon[FPs]K_a}\frac{1}{[ILs]} + \frac{1}{\Delta\varepsilon[FPs]} \qquad (12)$$

Where, ΔA refers to the difference in absorbances of SBz or Scyt without ILs to the absorbances of the same with the ILs. [FPs] represents the concentration of the SBz and Scyt. For the calculation of the association constants (K_a), listed in the **(Table 6)**, we divide slope by the intercept obtainable from the Benesi-Hildebrand double reciprocal plots[59],[60] **(Figure 6, 7)**.

The well-known association constant – free energy relationship enables us to calculate the free energy change for the molecular association taking place between the respective molecules by the following equation-

$$\Delta G = -RT\ln K_a \qquad (13)$$

Where, ΔG is the change in free energy, K_a stands for association constant, R and T refers to the universal gas constant and temperature in Kelvin respectively. The change in free energies for various (FPs –ILs) systems are listed in **(Table 6)** and depicts the sequence of interaction as obtained from the previous studies in article.

3.7 Gaussian 09W quantum chemical calculation: Theoretical basis of the interaction

This field is of immense theoretical interest. Here is no use of sequence alignments and no straight use of known structures. Basic idea is to erect empirical function that replicates real physical forces and potentials of chemical contacts. In this manuscript, numerical calculations have been performed using UB3LYP functional. Diffused basis functions have repeatedly been found to be effective in describing weak interaction amid atoms. Therefore, we use 6-31G(d) basis set for an accurate description of weak interactions which may prevail in the transition structures.

These calculations are implemented through Gaussian 09W quantum chemical package. The quantum chemical calculations estimate that the O···N···O···, C=O···H-O, H···O-H, weak H-bond interactions in SBz/Scyt clusters in the solvent sphere of aqueous ILs[61] **(Scheme 2)**. The formation of the weak hydrogen bond is an interaction, cohesive interaction[61],[62]. Under definite conditions an atom of hydrogen is attracted by rather strong forces to two atoms instead of only one, so that it may be considered to be acting as a bond between them[27]. The aforementioned statements were well thought-out in our present work. We have depicted the existence of SBz···ILs and SCyt···ILs complexes as clusters through quantum chemical calculations and we hereby compared and calculated values with the experimental values in order to verify sequence of interaction as obtained theoretically.

Several approximate properties of varied systems of aqueous SBz - ILs and SCyt - ILs clusters are summarized in **(Table 7)**. The availability of the optimisation energy (E) of pure as well as the molecular assembly makes it possible to calculate the extent of stabilisation (E) while, formation of molecular assembly assorted by solute – solvent interaction between FPs and ILs in solution. Stabilization energy of molecular assembly i.e. the value of *E*, the optimization energy, which approaches to a minimal value with growing possibility of solute-solvent interactions. From the **(Table 7)** it is clear that

stabilisation through solute – solvent interaction found prominent in case of (BTMACl+Scyt+H_2O) system over the other systems discussed herewith. Specifically, the optimum geometry **(Figure 8)** would involve central FPs surrounded by aqueous ILs molecules via weaker non-covalent interactions which can be explained on the basis of solution thermodynamics[63] in addition to solute-solvent interactions.

Conclusion: The motive to reduce unnecessarily-excessive use of food preservative in the preservation of food is reached, since antimicrobial activity of SBz and Scyt studied herewith, in all possible combination with the BTEACl and BTMACl reveal synergistic to kill micro-organisms and found to act properly below their reported MICs. The physico-chemical methodologies, density, viscosity, refractive index and conductance study describes the mode of interaction between the FPs and ILs in solution. Calculation of apparent molar volume, limiting apparent molar volume, molar refraction, limiting molar refraction and viscosity B coefficient makes possible to identify the interaction as predominant solute – solvent interaction. The values of $(\delta\phi_E^0/\delta T)_P$ and (dB/dT) have been calculated to provide the information that, the solute – solvent interaction is structure making. Association constants, optimisation energy and free energy changes for the molecular assembly grown in solution assorted by structure making solute – solvent interaction dictate their stability in solution and consequently, the order of synergism between them. Thus, solution chemistry for all the possible combinations explores the chemistry behind the synergism. This makes one easy to choose a mixture of compounds such that their combination would arise synergistic. Nevertheless, the synergistic combination of food preservatives reduces the level of hazardous food preservative which is used to stop spoilage of foods produced worldwide and makes the world health, safe. So, the study of microbial activity along with solution chemistry would be a great interest in the field of food chemistry for their preservation.

Conflicts of interest: There is no conflicts of interest.

Acknowledgements: Prof. M. N. Roy would like to acknowledge UGC, New Delhi, Government of India, for being awarded One Time Grant under Basic Scientific Research via the grant-in-Aid no. F.4-10/2010 (BSR). BR is thankful to the "State

Fellowship" bearing reference No. 1743/R-2017 dated 18.04.2017 and UGC-SAP DRS-III, New Delhi (no. 540/6/DRS/2007, SAP-1) for providing instrumental facilities according the research.

TABLES

Table 1. Apparent molar volume (Φ_V^0), Molar Refraction (R_M^0) and viscosity A and viscosity B co-efficient of (BTEACl+SBz+H_2O), (BTEACl+SCyt+H_2O) systems in solution of BTEACl of mass fractions W_1=0.001, W_2=0.003, W_3=0.005, at 298.15K, 303.15K, 308.15K, 313.15K and 318.15 K.

Temperature T(K^b)	$\Phi_v^0 \times 10^6$ /m^3mol^{-1}	$S_v^* \times 10^6$ /$m^3mol^{-3/2}$ $kg^{1/2}$	R_M^0 /m^3mol^{-1}	A /$dm^{3/2}$ $mol^{-1/2}$	B /dm^3 mol^{-1}
W_1=0.001[a]	(BTEACl+SBz+H_2O) System				
298.15	99.02	-56.68	29.42	0.034	0.508
303.15	103.60	-62.40	29.46	0.022	0.523
308.15	108.80	-73.10	29.49	0.014	0.544
313.15	112.32	-77.21	29.52	0.0024	0.551
318.15	116.95	-89.10	29.56	0.0019	0.570
W_1=0.003[a]	(BTEACl+SBz+H_2O) System				
298.15	111.50	-79.40	29.45	0.027	0.515
303.15	116.20	-91.88	29.47	0.017	0.531
308.15	122.10	-100.88	29.49	0.010	0.551
313.15	126.51	-108.52	29.53	0.009	0.565
318.15	128.00	-107.77	29.55	0.004	0.587
W_1=0.005[a]	(BTEACl+SBz+H_2O) System				
298.15	124.20	-105.81	29.48	0.020	0.520
303.15	128.70	-115.14	29.51	0.011	0.537
308.15	133.40	-120.07	29.54	0.006	0.559
313.15	137.22	-126.81	29.56	0.0005	0.581
318.15	142.75	-133.20	29.60	0.0014	0.595
W_1=0.001[a]	(BTEACl+SCyt+H_2O) System				
298.15	114.30	-62.17	32.72	0.042	0.513
303.15	118.10	-68.17	32.76	0.030	0.533
308.15	123.50	-78.97	32.81	0.021	0.546
313.15	127.01	-82.35	32.86	0.016	0.570
318.15	131.87	-92.17	32.90	0.006	0.588
W_1=0.003[a]	(BTEACl+SCyt+H_2O) System				
298.15	121.90	-81.64	32.76	0.037	0.520
303.15	125.00	-86.36	32.80	0.027	0.538
308.15	131.90	-98.03	32.83	0.015	0.552
313.15	136.80	-105.63	32.87	0.028	0.583

318.15	139.19	-107.08	32.91	0.014	0.599
W_1=0.005[a]	(BTEACl+SCyt+H_2O) System				
298.15	129.60	-97.46	32.79	0.029	0.526
303.15	135.50	-110.58	32.82	0.018	0.545
308.15	139.40	-109.83	32.84	0.009	0.558
313.15	144.18	-119.02	32.86	0.017	0.595
318.15	147.20	-130.68	32.89	0.005	0.595

[a]Standard uncertainties in mass fraction u(W) = $\pm$0.0001 mol Kg^{-1}; [b]Standard uncertainties in temperature u(T) = $\pm$0.01 K

Table 2. Apparent molar volume (Φ_V^0), Molar Refraction (R_M^0) and viscosity A and viscosity B co-efficient of (BTMACl+SBz+H_2O), (BTMACl+SCyt+H_2O) systems in solution of BTMACl of mass fractions W_1=0.001, W_2=0.003, W_3=0.005, at 298.15K, 303.15K, 308.15K, 313.15K and 318.15 K.

Temperature T(K[b])	$\Phi_v^0 \times 10^6$ /m^3mol^{-1}	$S_v^* \times 10^6$ /$m^3mol^{-3/2}$ $kg^{1/2}$	R_M^0 /m^3mol^{-1}	A /$dm^{3/2}$ $mol^{-1/2}$	B /dm^3 mol^{-1}
W_1=0.001[a]	(BTMACl+SBz+H_2O) System				
298.15	105.45	-99.91	29.47	0.035	0.513
303.15	109.89	-110.76	29.51	0.032	0.526
308.15	114.06	-118.33	29.54	0.017	0.549
313.15	116.16	-120.51	29.59	0.006	0.550
318.15	121.60	-130.61	29.63	0.003	0.560
W_1=0.003[a]	(BTMACl+SBz+H_2O) System				
298.15	119.81	-146.67	29.51	0.041	0.519
303.15	123.25	-157.20	29.56	0.036	0.531
308.15	126.03	-157.09	29.60	0.010	0.551
313.15	130.21	-160.23	29.67	0.008	0.556
318.15	134.43	-169.08	29.70	0.001	0.568
W_1=0.005[a]	(BTMACl+SBz+H_2O) System				
298.15	130.37	-166.42	29.55	0.037	0.523
303.15	134.28	-168.25	29.57	0.030	0.535
308.15	138.21	-176.01	29.62	0.026	0.555
313.15	144.46	-185.85	29.70	0.019	0.561
318.15	145.29	-182.24	29.75	0.013	0.574
W_1=0.001[a]	(BTMACl+SCyt+H_2O) System				
298.15	118.97	-82.80	32.75	0.045	0.518
303.15	123.36	-96.41	32.79	0.042	0.539
308.15	128.20	-108.95	32.85	0.037	0.550
313.15	134.03	-122.95	32.90	0.029	0.563
318.15	135.95	-130.35	32.93	0.014	0.570
W_1=0.003[a]	(BTMACl+SCyt+H_2O) System				

298.15	124.06	-95.93	32.77	0.041	0.521
303.15	128.90	-106.88	32.82	0.040	0.533
308.15	135.11	-121.50	32.87	0.035	0.554
313.15	140.30	-136.26	32.93	0.025	0.567
318.15	144.74	-142.63	32.97	0.022	0.578
W_1=0.005[a]	(BTMACl+SCyt+H_2O) System				
298.15	133.83	-121.38	32.84	0.038	0.525
303.15	138.44	-131.90	32.88	0.032	0.536
308.15	143.53	-141.79	32.93	0.029	0.557
313.15	146.48	-150.48	32.93	0.026	0.571
318.15	150.08	-154.30	33.02	0.020	0.581

[a]Standard uncertainties in mass fraction u(W) = ±0.0001 mol Kg^{-1}; [b]Standard uncertainties in temperature u(T) = ± 0.01 K

Table 3: Values of empirical coefficients (a_0, a_1, and a_2) of Eq. 5for aqueous (BTEACl+SBz), (BTEACl+SCyt), (BTMACl+SBz), (BTMACl+SCyt) systems in different mass fraction of aqueous BTEACl/BTMACl solution at 298.15 to 318.15 K.

BTEACl+SBz				BTEACl+SCyt		
Mass fraction (W^a)	$a_0\times10^6$ /m^3 mol^{-1}	$a_1\times10^6$ /m^3 mol^{-1} K^{-1}	$a_2\times10^6$ /m^3 mol^{-1} K^{-2}	$a_0\times10^6$ /m^3 mol^{-1}	$a_1\times10^6$ /m^3 mol^{-1} K^{-1}	$a_2\times10^6$ /m^3 mol^{-1} K^{-2}
0.001	-595.04	3.6738	-0.0045	-86.16	0.476	0.0007
0.003	-2290.90	14.7950	-0.0226	-1082.30	6.949	-0.0098
0.005	172.07	-1.1654	0.0034	-1454.50	9.471	-0.0139
BTMACl+SBz				BTMACl+SCyt		
0.001	-143.26	0.8947	-0.0002	-1218.00	7.848	-0.0113
0.003	706.28	-4.4881	0.0085	-684.10	4.260	-0.0052
0.005	-1149.40	7.5621	-0.0110	-1235.40	8.136	-0.0119

[a]Standard uncertainties in mass fraction u(W) = ± 0.0001 mol Kg^{-1}

Table 4. Values of limiting apparent molar expansibilities (Φ_E^0) of aqueous (BTEACl+SBz), (BTEACl+SCyt), (BTMACl+SBz), (BTMACl+SCyt) systems in different mass fraction of aqueous BTEACl/BTMACl solution at 298.15 to 318.15 K.

(BTEACl+SBz) System	$\Phi_E^0\times10^6$/m^3 mol^{-1} K^{-1}					$(\frac{\partial\Phi_E^0}{\partial T})_P\times10^6$ /m^3 mol^{-1} K^{-2}
Mass fraction (W^a)	298.15	303.15	308.15	313.15	318.15	
0.001	0.9905	0.9455	0.9005	0.8555	0.8105	-0.0090
0.003	1.3186	1.0926	0.8666	0.6406	0.4146	-0.0452
0.005	0.8620	0.8960	0.9300	0.9640	0.9980	0.0068

(BTEACl+SCyt) System						
0.001	0.8934	0.9004	0.9074	0.9144	0.9214	0.0014
0.003	1.1053	1.0073	0.9093	0.8113	0.7133	-0.0196
0.005	1.1820	1.0430	0.9040	0.7650	0.6260	-0.0278
(BTMACl+SBz) System						
0.001	0.7754	0.7734	0.7714	0.7694	0.7674	-0.0004
0.003	0.5805	0.6655	0.7505	0.8355	0.9205	0.0170
0.005	1.0028	0.8928	0.7828	0.6728	0.5628	-0.0220
(BTMACl+SCyt) System						
0.001	1.1098	0.9968	0.8838	0.7708	0.6578	-0.0226
0.003	1.1592	1.1072	1.0552	1.0032	0.9512	-0.0104
0.005	1.0400	0.9210	0.8020	0.6830	0.5640	-0.0238

[a]Standard uncertainties in mass fraction u(W) = $\pm$ 0.0001 mol Kg^{-1}

Table 5. Values of dB/dT for aqueous (BTEACl+SBz), (BTEACl+SCyt), (BTMACl+SBz), (BTMACl+SCyt) systems in different mass fraction of aqueous BTEACl/BTMACl solution at 298.15 to 318.15 K.

Mass fraction (W)	$(\frac{dB}{dT})$/ dm^3 mol^{-1}/K^{-1}			
	BTEACl+SBz	BTEACl+Scyt	BTMACl+SBz	BTMACl+Scyt
0.001	0.0030	0.0037	0.0024	0.0026
0.003	0.0036	0.0041	0.0025	0.0030
0.005	0.0039	0.0038	0.0026	0.0029

Table 6. Association constant and Gibb's free energy of (BTEACl+SBz), (BTEACl+SCyt), (BTMACl+SBz) and (BTMACl+SCyt) systems at 298.15 K.

System	(BTEACl+SBz)	(BTEACl+SCyt)	(BTMACl+SBz)	(BTMACl+SCyt)
K_a /M^{-1} (×10^{-3})	2.70	3.31	3.05	3.68
ΔG /KJ mol^{-1}	-19.6	-20.1	-19.9	-20.4

Table 7. Optimisation energies of pure BTEACl, BTMACl, SBz, SCyt and (BTEACl+SBz), (BTEACl+SCyt), (BTMACl+SBz), (BTMACl+SCyt) systems using UB3LYP methodology and 6-31G(d) basis set.

System	Calculation Method	Basis Set	Optimisation energy (a.u.)	Dipole moment (Debye)
SBz	UB3LYP	6-31G(d)	-582.58203318	5.6642
SCyt	UB3LYP	6-31G(d)	-657.78951762	4.4047

BTEACl	UB3LYP	6-31G(d)	-1023.56406394	11.6512
BTMACl	UB3LYP	6-31G(d)	-905.62574200	13.5905
(BTEACl+SBz)	UB3LYP	6-31G(d)	-865.63204549	12.5596
(BTEACl+SCyt)	UB3LYP	6-31G(d)	-940.83809561	11.2236
(BTMACl+SBz)	UB3LYP	6-31G(d)	-983.56112523	12.6819
(BTMACl+SCyt)	UB3LYP	6-31G(d)	-1058.76749759	11.1263

Table S1. Density (ρ), Refractive index (n_D), Viscosity (η) of aqueous pure BTEACl and BTMACl solutions of mass fractions W = 0.001, 0.003, 0.005 at temperatures 298.15 K, 303.15 K, 308.15 K, 313.15 K and 318.15 K.

BTEACl+H_2O				
Mass fraction (W[a])	Temperature (K[b])	Density (ρ[c]) ×10^{-3} Kg.m^{-3}	Refractive index (n_D^d)	Viscosity (η[e]) mPa.S
0.001	298.15	0.9973	1.3303	0.8929
	303.15	0.9948	1.3306	0.7989
	308.15	0.9924	1.3303	0.7209
	313.15	0.9868	1.3302	0.6322
	318.15	0.9843	1.3301	0.5462
0.003	298.15	0.9974	1.3306	0.8948
	303.15	0.9952	1.3308	0.8015
	308.15	0.9931	1.3305	0.7259
	313.15	0.9909	1.3306	0.6354
	318.15	0.9888	1.3307	0.5509
0.005	298.15	0.9975	1.3311	0.8991
	303.15	0.9955	1.3310	0.8041
	308.15	0.9935	1.3307	0.7284
	313.15	0.9915	1.3305	0.6358
	318.15	0.9895	1.3308	0.5520
BTMACl+H_2O				
0.001	298.15	0.9973	1.3308	0.8948
	303.15	0.9948	1.3305	0.8055
	308.15	0.9924	1.3307	0.7231
	313.15	0.9868	1.3306	0.6267
	318.15	0.9843	1.3304	0.5407
0.003	298.15	0.9975	1.3314	0.8971
	303.15	0.9952	1.3304	0.8081
	308.15	0.9927	1.3308	0.7256
	313.15	0.9840	1.3309	0.6231
	318.15	0.9815	1.3310	0.5371
0.005	298.15	0.9977	1.3316	0.9012
	303.15	0.9956	1.3309	0.8128
	308.15	0.9931	1.3310	0.7304

CHAPTER VIII

Minimization of the Dosage of Food Preservatives Mixing with Ionic Liquids for Controlling Risky Effect in Human Body: Physicochemical, Antimicrobial and Computational Study

Abstract: An analysis on the diverse molecular interactions of implausible food preservatives, Sodium benzoate (SBz), Sodium salicylate (Scyt) in the aqueous solutions of Benzyltriethylammoniun chloride (BTEACl), Benzyltrimethylammoniun chloride (BTMACl) having durable anti-bacterial effect have been explored thoroughly by various physicochemical methodologies such as Density, Refractive index, Viscosity, Electrical conductivity, at five different temperatures ranging from 298.15 K to 318.15 K. Anti-bacterial as well as the anti-fungal effects of the ternary mixtures, (BTEACl+SBz+H_2O), (BTEACl+Scyt+H_2O), (BTMACl+SBz+H_2O) and (BTMACl+Scyt+H_2O) were further analysed for better results and found to act synergistically below the MIC of both the food preservative, thus minimises the hazardous threat, caused by unnecessarily excessive consumption of food preservatives. Association constants governed by diverse intermolecular interactions in the solution phase were studied by UV-vis spectroscopy. Construction of thermodynamic background caused by innumerable interactions taking place in the ternary mixtures were explored by calculating the free energies of various molecular associations. The genesis of diverse interactions was exposed by measurement of the apparent molar volume (ϕ_v), limiting apparent molar volume (ϕ_v^0), molar refraction (R_M), limiting molar refraction (R_M^0) viscosity B coefficients and reveals as strong solute-solvent interaction, over the solute-solute and solvent-solvent interactions. Optimum energies with the optimised geometries of molecular assembly for (BTEACl+SBz), (BTEACl+Scyt), (BTMACl+SBz) and (BTMACl+Scyt) systems were calculated from Ab-initio quantum chemical calculations using Gaussian 09W quantum chemical package which found supportive to the practical outcomes.

Keywords: Benzyltriethylammoniun chloride, Benzyltrimethylammoniun chloride, Sodium benzoate, Sodium salicylate, Solute-Solvent interaction, anti-microbial activity.

1. INTRODUCTION

According to our knowledge, it is well known to all, there is so much of food productions all over the world but because of the process of spoilage a large proportion of these is lost. So, it requires a great attention to preserve foods, produced industrially and even at home. There are so many preservatives known, that utterly prevents spoilage of foods, but having some sort of side effects, usedness of these is an inherent threat to the world health. Now, use of these in minimal amount i.e. below the MIC (Minimal Inhibitory Concentration) in food would overcome the threat. The challenge was accepted and reveals that, two well-known food preservatives (FPs), sodium benzoate and sodium salicylate works properly against various fungus as well as gram-positive and gram-negative bacteria below their MIC in the presence of negligible amount of two ammonium based ionic liquids (ILs) benzyltriethylammoniun chloride (BTEACl) and benzyltrimethylammonium chloride (BTMACl).

Sodium benzoate (SBz) **(Scheme 1)** having inhibitory effect on the microbial growth is strongly recommended as a food preservative and commonly used in foods like soda, fruit juice and a variety of products, such as cosmetics and pharmaceuticals. In acidic medium SBz works better on yeasts, molds, bacterial growth and prevent spoilage[1],[2],[3],[4],[5]. In patients with acute hyper-ammonaemia, who were born with urea cycle disorders[6],[7] SBz acts as a therapeutic agent and also treats dental carries, blocks D-dopa in the hemi-parkinsonian rat[8]. Beside these bio-medical and pharmaceutical applications SBz have some antagonistic effect, it can damage parts of the DNA affecting the future generations[9]. The acceptable daily intake (ADI) levels of SB should be 5 mg/kg body weight[10], as strictly recommended by Joint Food and Agriculture Organization of the United Nations/World Health Organization expert committee on food additives, otherwise SBz may be toxic and imperils human health[11]. Research on interaction of antimicrobials shows that, a pair of antimicrobials acting synergistically can show satisfactory result and better microbial control could be achieved[12]. In this connection SBz and chitosan found synergistic against spoilage yeast in saline solution[13].

Sodium salicylate (Scyt) **(Scheme 1)** is a significant antibacterial agent, also enhances the activities of certain antibiotics[14],[15],[16],[17]. The bacterial strains, Salmonella, Shigella including Escherichia coli that causes diarrhoea used to inhibited

by bismuth subsalicylate efficiently[18]. Being an active anti-inflammatory compound Scyt have been used as anti-inflammatory, analgesic and anti-pyretic agent[19] still it has gastric bleeding like serious disadvantage[20]. Scyt acts synergistically with vancomycin and enhances anti-staphylococcal activity significantly. The presence of salicylate in 5 mM concentration, vancomycin prevents biofilm formation and kill bacteria effectively below its MIC[17]. In vitro CPS production can be reduced to 80% or more by Scyt, the major metabolite of aspirin. Scyt also increases synergistic activity of amikacin and imipenem[21].

Quaternary ammonium based ionic liquids also execute some sort of anti-microbial effects for instance positive charge on the Nitrogen atom of these ionic liquids attracts naturally the negatively charged species, such as bacterial proteins and consequently disorganization in the protein chain makes it denature. Ionic liquids, benztltriethylammonim chloride, benztltrimethylammonim chloride **(Scheme 1)** were used herewith in all four possible combinations to the illustrious food preservative SBz and Scyt. Anti-microbial activities of the set of four combinations were studied warily at concentrations below their MIC and found synergistic to each other.

In this article the synergism activity between the above mentioned food preservatives and ionic liquids against micro-organisms were studied such that, their combination can act properly below their MICs (Minimal Inhibitory Concentration) and as a consequence reduces the unnecessary consumption of hazardous food preservative. In this connection anti-bacterial and anti-fungal activities of both the food preservatives, SBz and Scyt were studied in the presence of trace amount of ionic liquids. Then, volumetric and viscometric analysis as well as refractive index and conductimetric measurement defines the cause of synergism between FPs and ILs.

2. EXPERIMENTAL SECTION

2.1. Materials

All the chemicals, sodium benzoate (purity ≥ 99.5%), sodium salicylate (purity ≥ 99.5%), benzyltriethylammoniun chloride (purity 99.0%), benzyltrimethylammonium chloride (purity 97%) were purchased from Sigma Aldrich Germany and used as received taking sufficient precautions.

2.2. Apparatus

All the experimental solutions were prepared by transferring required amount of weighed materials to a volumetric flask and then filled with the solvents upto the mark. The uncertainty in molality of the prepared solutions evaluated as ±0.0001 mol kg^{-3}. Different sets of solutions with various concentration were prepared by proper dilution of the mother solution. The quantity of samples for the preparation of the mother solutions were weighed precociously by Mettler Toledo AG-285 with uncertainty ±0.0003 g.

The molality of the solution which has been calculated from the molar concentration data using the relation[22]

$$m = \frac{1}{[\rho/c - M/1000]} \qquad (1)$$

Where, m is the molality of the solutions, ρ and c refer to densities and concentration of the solutions respectively, M stands for relative molar mass of the materials used.

The antimicrobial activities of SBz and Scyt were tested in relation to the bacteria *Bacillus subtilis* and *Escherichia coli* by well diffusion assay[23]. Briefly, the bacterial cultures were grown overnight in Nutrient Broth and uniformly spread on the surface of Muller Hington agar plates using sterile cotton swabs. Wells of diameter 8 mm was made using sterile cork borers and SBz, Scyt, BTEACl and BTMACl were used singly and in combinations at concentrations of 3mg/ml and 6mg/ml. The plates were incubated overnight at 37^0C and observed for formation of inhibition zones. The "diameter of the inhibition" for positive results was recorded as diameter of zone of inhibition – diameter of the well (8 mm). The diameter of inhibition when no zone was observed was kept at zero.

The solvent as well as the solution densities were measured with vibrating-tube density meter (Anton Paar, DMA 4500M), maintained at 298.15 to 318.15 K. Calibration of the instrument was done with doubly distilled water and dry air. The uncertainty in density was estimated to be ±0.00001 g cm^{-3}.

Digital Refractometer Mettler Toledo was used to measure refractive index. Refractive indices of experimental solutions were measured after rectifying twice the refractometer by distilled water. During measurement calibration of the instrument

was done after each few measurements. Temperature of the solutions under measurement were maintained in a Brookfield Digital TC-500 thermostat water bath.

Brookfield DV-III Ultra Programmable Rheometer with fitted spindle size-42 was employed to measure viscosities of the solutions. The viscosities were obtained using following programmed equation

$$\eta = (100/RPM) \times TK \times torque \times SMC \qquad (2)$$

where SMC (0.327), RPM, TK (0.09373) stands for spindle multiplier constant, speed, viscometer torque constant respectively. Calibration of the instrument before starting experiment was done with provided standard viscosity samples, water and aqueous $CaCl_2$ solutions. Temperature of the solution was maintained with Brookfield Digital TC-500 thermostat bath.

The conductivity of the experimental solutions was measured in aSystronics-308 conductivity bridge using a dip-type immersion conductivity cell, CD-10, having a cell constant of approximately 0.1 ± 0.001 cm^{-1} of accuracy ±0.01%. Calibration of the conductivity cell was done according the method proposed by Lind et al[24]. The cell constant was measured using freshly prepared 0.01 M aqueous KCl solution and it was maintained within the range 0.09-1.00 cm^{-1} during experiment. Temperature during experiment was monitored and controlled to the experimental temperature using Brookfield Digital TC-500 thermostat bath. HPLC-grade water with a specific conductance of 6.0 μS m^{-1} was used for conductivity measurement. The conductance data were reported at the accuracy of±0.3%.

UV−visible spectra were recorded utilizing JASCO V-530 UV−Vis spectrophotometer, with a wavelength accuracy of ±0.5 nm. Cell temperature during the experiment was controlled from 298.15K to 318.15K with a digital thermostat.

Theoretical i.e. Ab-initio calculations were executed through Gaussian 09Wquantum chemical package[25].

3. RESULT AND DISCUSSION

3.1 Antimicrobial effects of SBz and Scyt in combination with BTEACl and BTMACl reveals synergistic:

The results clearly indicated the enhancement of antimicrobial effects of SBz and Scyt when used in combination with ionic liquids BTEACl and BTMACl.

In case of gram positive *B.subtilis* both BTEACl and BTMACl enhanced antimicrobial activity of SBz and Scyt with the effect being comparatively more profound in SBz in combination with BTEACl. The idea of lowering the concentrations to 3 mg was to check the enhancement when SBz and BTEACl individually showed minimal or no zone of inhibition. As expected 3 mg of SBz showed no zone of inhibition and 3 mg BTEACl showed minimal diameter of 2 mm which was enhanced to 8mm when used in combination indicating enhanced antimicrobial activity. In case of gram negative *E.coli* no susceptibility was observed in case of SBz alone or in combination with ILs. However, E. coli showed enhanced susceptibility to Scyt when used in combination with BTEACl and BTMACl **(Figure 1, 2, 3)**.

The differences in the structure of their cell walls can be accounted for the differences in susceptibility of *Bacillus subtilis* and *E.coli*, with *E.coli* having an outer lipid layer which acts as a molecular filter for hydrophilic compounds[26]. This lipid layer might have reduced the ability of the hydrophilic components to penetrate into the cells and hence exert their potential inhibitory action. The zero antimicrobial effects of SBz and Scyt at concentrations of 3 mg and 6 mg may be because of their concentration being lower than the reported microbial inhibitory concentrations (MIC) of around 10 mg/mL[27]. BTEACl has also showed inhibitory action when used alone which might be due to the presence of quaternary ammonium with ethyl group whereas BTMACl has shown no inhibitory effect when used singly.

The outcome of this study is that SBz and Scyt can exert antimicrobial effects when used with ionic liquids such as BTEACl and BTMACl even at minimal concentrations which normally do not exert antimicrobial effects when used alone. However, the chances of ILs exerting cytotoxic effects on human cell lines will have to be ruled out before its proper application in industries.

3.2 Density and volumetric measurements:

Here, we present information concerning the chemistry of food preservative–ionic liquid interactions in aqueous solutions that have been acquired from the apparent molar volume (ϕ_v), limiting apparent molar volume (ϕ_v^0) and (S_v^*) of food preservatives in aqueous solutions of ionic liquids meanwhile all these three

parameters evidently be governed by the solvent environment surrounding the solute species and known to cover information belong to the structural penalties of solute–solvent interactions[28]. Apparent molar volume of a substance in solution can be defined as the sum of the geometric volume of the two solute molecules while undergo solvation through solute-solvent interaction with the co-solvent. Densities of the co-solvents of various mass fractions, made by two ionic liquids BTEACl and BTMACl separately with water, were measured at temperature range 298.15 to 318.15K are listed in **(Table S1)**. The values of (ϕ_v) for the (BTEACl+SBz+H_2O), (BTEACl+Scyt+H_2O) systems **(Table S8, S9, S10)** and the same for (BTMACl+SBz+H_2O), (BTMACl+Scyt+H_2O) systems **(Table S11, S12, S13)** were calculated by means of density (ρ) data **(Table S2-S4)** and **(Table S5-S7)** through the following equation[29],[30],[31],[32]

$$\phi_v = \frac{M}{\rho} - \frac{1000(\rho - \rho_0)}{m\rho\rho_0} \qquad (3)$$

Where M is the molar mass of the solute; m is the molality of the solution; ρ and $\rho_0$represents the densities of the solution and solvent respectively. Apparent molar volume at infinite dilution, i.e. limiting molar apparent volume (ϕ_v^0) and experimental slopes (S_v^*) were determined using least squares fitting of linear plots of (ϕ_v) against the square root of molar concentrations ($m^{1/2}$) using the Masson equation[33],[25].

$$\phi_v = \phi_v^0 + S_v^* . \sqrt{m} \qquad (4)$$

The experimental plots, generated from Masson equation and corresponding values of (ϕ_v^0) and (S_v^*) of each plot are shown in **(Figure S1, S2)** and **(Table1, 2)**. The values of (ϕ_v^0) are found positive for all the systems and is greatest for (BTMACl+Scyt) system, suggesting the presence of stronger solute-solvent interactions in this case than that of the other systems and found to follow the order,(BTMACl+Scyt)>(BTMACl+SBz)>(BTEACl+Scyt)>(BTEACl+Scyt) as represented in **(Scheme 2)**. The dipole–dipole interaction taking place in the solutions explains the truth behind the above mentioned order of solute-solvent interactions since greater the dipole-dipole interaction smaller will be the values of (ϕ_v) as well as (ϕ_v^0)[34]. The

dipole moment of SBz, Scyt, BTEACl and BTMACl were calculated theoretically with the help of Gaussian 09W quantum chemical package, are listed in the **(Table 7)**.

Increasing trend in the (ϕ_v^0) values with rise in temperature and mass fraction of BTEACl and BTMACl, suggests the rising trend of solute-solvent interaction as well. This is probably due to the release of a number of the solvent molecules from loose solvation layers during the solute-solvent interactions. The phenomenon drawn above also reflected in the molar conductivity data as discussed in this article. Values of the experimental slope, (S_v^*) assign the extent of ion-ion interaction in the solution, and the negative values indicate the presence of less ion-ion interaction in the medium. Quantitative comparison shows, greater the magnitude of (ϕ_v^0) than (S_v^*) recommends the ion-solvent interactions dominants over ion-ion interactions[35].

Temperature dependency of the limiting apparent molar volume(ϕ_v^0) were studied between the temperature range 298.15 to 318.15K at the interval of 5K of temperature and the results obtained were found to follow the following polynomial equation[36]

$$\phi_v^0 = a_o + a_1 T + a_2 T^2 \qquad (5)$$

Where, a_0, a_1 and a_2 are the empirical coefficients depending on the nature of solute, mass fraction (W) of co-solvent are listed in **(Table 3)**. T represents temperature in Kelvin scale. The values of these coefficients of the above equation. First derivative of equation (5) gives the values of limiting apparent molar expansibilities (ϕ_E^0) which have been calculated for various temperature and listed in **(Table 4)**.

$$\phi_E^0 = (\delta\phi_v^0 / \delta T)_P = a_1 + 2a_2 T \qquad (6)$$

Limiting apparent molar expansibilities (ϕ_E^0) for all the systems are found positive signifying the absence of caging or packing effect in the solutions of all the four different systems.

The solute – solvent interaction studied so far is now at a state that, it may be structure breaker or synergistic structure maker interaction. In this connection Hepler developed a way to examine the nature of the solute – solvent interaction taking place

in the solution phase[37]. According to Hepler, values of $(\delta\phi_E^0/\delta T)_P$ in the expression given below, determines whether, it is structure breaker or structure maker interaction[38].

$$(\delta\phi_E^0/\delta T)_P = (\delta^2\phi_v^0/\delta T^2)_P = 2a_2 \quad (7)$$

Generally, positive or small negative values of $(\delta\phi_E^0/\delta T)_P$ strongly suggests structure making rather than structure breaking interaction. Here, positive and small negative values of $(\delta\phi_E^0/\delta T)_P$ listed in **(Table 4)** confirms the mode of solute – solvent interaction is structure making.

3.3 Refractive index:

Optical data of refractive index of the two studied heterogeneous systems has provided interesting information allied to molecular interactions, structure of solutions in these assay. The refractive index of mixing can be interconnected by the application of a composition-dependent polynomial equation and molar refraction, R_M in solution thus can be estimated from Lorentz-Lorenz relation[39],[40]

$$R_M = \frac{(n_D^2 - 1)}{(n_D^2 + 2)}\left(\frac{M}{\rho}\right) \quad (8)$$

Where, R_M, n_D, M and ρ represents molar refraction, refractive index, molar mass and density of solution respectively.

Generally, refractive index of a system is the ability to refract light and hence it can simultaneously measure the compactness of that system. The refractive indices (n_D) of (BTEACl+SBz+H_2O), (BTEACl+Scyt+H_2O) systems are reported in **(Table S2-S4)** and for(BTMACl+SBz+H_2O), (BTMACl+Scyt+H_2O) systems in **(Table S5-S7).** The molar refraction (R_M) of the studied solutions were calculated and listed in the **(Table S8 – S10)** for (BTEACl+SBz+H_2O), (BTEACl+Scyt+H_2O) systems and **(Table S11 – S13)** for (BTMACl+SBz+H_2O), (BTMACl+Scyt+H_2O) systems. Analysis of these data enable us to draw the following sequence of compactness of the various (food preservative – ionic liquid) systems in solution phase.

(BTMACl+Scyt)>(BTMACl+SBz)>(BTEACl+Scyt)>(BTEACl+Scyt)

The limiting molar refraction, (R_M^0) listed in Table S can be calculated using the following equation-

$$R_M = R_M^0 + R_S\sqrt{m} \quad (9)$$

Where, 'm' is the molality of solution and R_M^0 is the limiting molar refraction that signifies solute – solvent interaction. So, this measurement operates as an expensive tool for studying the molecular interaction in solution. Gradual increase in the values of R_M and R_M^0 **(Table 1, 2 and Figure 4, S3)** with rise in mass fraction of co-solvent also signifies that, solute – solvent interaction predominant over ion-ion interactions as obtained from density measurement.

3.4 Viscosity measurement:

In aqueous electrolytic solutions the extent of ionic hydration[41] and structural interactions[42],[43],[44] within the ionic hydration co-spheres[45] can be explored easily by studying viscosity coefficient with varying concentration and temperature of the aqueous solution. Experimental values of viscosities for all the food preservative – ionic liquid systems, taken at various concentration and temperature are listed in **(Table S2-S4)** and **(Table S5-S7)**. Viscosity data so obtained were analysed with the help of Jones-Dole equation[46]-

$$\eta_r = \frac{\eta}{\eta_0} = 1 + A\sqrt{c} + Bc \quad (10)$$

Where, η and η_0 are viscosities of solution and solvent respectively, c is the concentration of solution in molality.

Rearrangement of the above equation (8) gives following-

$$\frac{\eta_r - 1}{\sqrt{c}} = A + B\sqrt{c} \quad (11)$$

Here, viscosity A coefficient is a constant, also known as Falken hagen coefficient[47], stands for long-range coulombic forces, so represents the solute-solute/ion-ion interaction in solution, while B coefficient is an adjustable parameter, which is the

measure of the effective hydrodynamic volume, reflects the solute-solvent interaction. Magnitude of viscosity B coefficient depends on the shape, size and partial molar entropies of the ions. According to the Jones-Dole equation from the plots of $(\eta_r - 1)/\sqrt{c}$ vs. $\sqrt{c}$ **(Figure S4, S5)** viscosity A and B coefficients were obtained by linear least-square analysis, are reported in **(Table 1, 2).** Obtained viscosity A and B coefficients are actually the intercept and experimental slopes of the plots **(Figure S4, S5)** respectively. An observation and deep investigation on the change in viscosity B coefficient of the various food preservative-ionic liquid systems at a given temperature and mass fraction of co-solvent, enable us to conclude the following sequences of solute-solvent interaction [48],[43],[49] - (BTMACl + Scyt) > (BTMACl + SBz) > (BTEACl+Scyt) > (BTEACl+Scyt) **(Scheme 2)**. Having near about the same shape and size of both the ionic liquids, size and structural properties of BTEACl and BTMACl can't differentiate the change in viscosity B coefficient, rather it seems to be controlled indirectly by the ion-ion interaction i.e. (SBz-SBz) and (Scyt-Scyt) interaction taking place in SBz and Scyt solution. Lower the ion-ion interaction can enhance dissolution of a solute in solvent through solvation of ions and thereby developing solute-solvent interaction. Now, an inspection on the **(Table 1, 2)** shows lower viscosity A coefficient for (Scyt-ionic liquid) than that of (SBz-ionic liquid) systems. This can be accounted by the fact that, benzoate ions originating from SBz in solution can undergo dimerization, whereas dimerization of salicylate ions gets disturbed by the intra-molecular H-bonding in Scyt. The innumerable interactions governed in solution which are also responsible for developing solute-solvent interaction can be explained on the basis of the interaction of $R_4N^{\oplus}$ from ionic liquid with the COO^{-} and OH group originating from food preservative as follows- (i) Lower effective charge accumulation on nitrogen atom of $R_4N^{\oplus}$ in BTEACl than that of BTMACl, caused by greater +I (positive inductive) effect of (–CH_2-CH_3) rather than (–CH_3) group operating in case of BTEACl. (ii) COO^{-} and OH group of Scyt interacts with $R_4N^{\oplus}$ in Scyt-ionic liquid systems, while the COO^{-} interacts alone with $R_4N^{\oplus}$ in case of SBz-ionic liquid systems. On the other hand, at a given temperature, if we deal with a particular food preservative-ionic liquid system viscosity B coefficient found to increase with increasing mass fraction of co-solvent made of ionic liquids in water. The above observation has a ready explanation that,

replacement of water molecules by more co-solvent molecules (BTEACl or BTMACl) from the solvation sphere of food preservatives (SBz or Scyt) that, brings solute and co-solvent closer thereby increasing viscosity B coefficients and accounts for the higher solute-solvent interaction. The overall viscometric studies shows that, viscosity B coefficients are positive and greater than viscosity A coefficient, suggesting solute–solvent interaction predominant over the solute-solute interaction.

Extensive study of the viscosity B coefficient such that, its first derivative over temperature is an upgradation of viscosity B coefficient in predicting the nature of solute – solvent interaction as structure maker or structure breaker. The value of dB/dT **(Table 5)** is a measure of activation energy required for the viscous flow in solution. This is the reason, why the measure of dB/dT is indicative towards the structure making or structure breaking ability than sign or magnitude of the B-coefficient[50],[51],[52],[53]. The small positive or negative value of dB/dT signifies structure-making (kosmotropic) whereas the larger positive value identifies it as structure-breaking (chaotropic). The variation of dB/dT with the mass fraction of co-solvents have shown in **(Figure 5).**

3.5 Conductimetric study

The conductance study of the interaction (solute – solvent) between Scyt and SBz with the aqueous solution of ILs, BTMACl and BTEACl has been performed at five different temperatures. Advantage of this study is that this measurement provides information about the interaction and transport phenomena of the (Scyt + ILs + H_2O) and (SBz + ILs + H_2O) ternary systems[54].

The molar conductivities[55] (Λ) of aqueous BTEACl and BTMACl has been monitored with increasing the concentration of Scyt and SBz respectively at five different temperatures and have been listed in **(Table S14, S17)**. The **Figure S6 and S7,** shows the resulting plots of (BTMACl + SBz + H_2O), (BTMACl + Scyt + H_2O), (BTEACl + SBz + H_2O) and (BTEACl + Scyt + H_2O) respectively. For every system it has been observed that Λ values increase with increase in temperature and gradual addition of either Scyt or SBz to ILs solution causes a continuous decrease in molar conductance. The mobility of the ionic species in solution playing the leading role, in spite of growing number of ionic species with added aqueous SBz or Scyt solution in step, the molar conductivity decreases[56]. It may be due to the development of solute-solvent interaction governed by the dipole-dipole as well

as the pπ –pπ and hydrophobic – hydrophobic interaction in solution mixtures between the solute and solvent molecules. The formation of molecular assembly thus forces the ionic species to lose their independent movement making the ionic species less mobile to show conductivity in solution. The intra-molecular H-bonding of Scyt as discussed in viscosity context also inhibits dimerization between Scyt molecules and makes it available for exerting solute – solvent interaction with ILs more than that of SBz in solution. Conductimetric study thus supports the volumetric, refractometric and viscometric study and echoes the same observation as well.

3.6 UV-Vis spectroscopic analysis: The association constants

The stability of the molecular association developed in solution mixtures by the manifestation of solute-solvent interaction were explored by measuring the association constants (K_a). The UV-vis spectroscopic data for the various mixtures of solutions were recorded and employed to determine the association constant (K_a). To determine association constant (K_a), the changes in absorbances (ΔA) of SBz and Scyt at λ_{max} = 220 nm and λ_{max} = 292 nm were measured with increasing concentration of BTEACl/BTMACl at 298.15 K **(Table S18 – S21)**. According to the Benesi-Hildebrand method[57], the double reciprocal plots obtained from (equation 10) were found linear that, usually says about the solute : solvent ratio in solution[57],[58].

$$\frac{1}{\Delta A} = \frac{1}{\Delta\varepsilon[FPs]K_a}\frac{1}{[ILs]} + \frac{1}{\Delta\varepsilon[FPs]} \qquad (12)$$

Where, ΔA refers to the difference in absorbances of SBz or Scyt without ILs to the absorbances of the same with the ILs. [FPs] represents the concentration of the SBz and Scyt. For the calculation of the association constants (K_a), listed in the **(Table 6)**, we divide slope by the intercept obtainable from the Benesi-Hildebrand double reciprocal plots[59],[60] **(Figure 6, 7)**.

The well-known association constant – free energy relationship enables us to calculate the free energy change for the molecular association taking place between the respective molecules by the following equation-

$$\Delta G = -RT\ln K_a \qquad (13)$$

Where, ΔG is the change in free energy, K_a stands for association constant, R and T refers to the universal gas constant and temperature in Kelvin respectively. The change in free energies for various (FPs –ILs) systems are listed in **(Table 6)** and depicts the sequence of interaction as obtained from the previous studies in article.

3.7 Gaussian 09W quantum chemical calculation: Theoretical basis of the interaction

This field is of immense theoretical interest. Here is no use of sequence alignments and no straight use of known structures. Basic idea is to erect empirical function that replicates real physical forces and potentials of chemical contacts. In this manuscript, numerical calculations have been performed using UB3LYP functional. Diffused basis functions have repeatedly been found to be effective in describing weak interaction amid atoms. Therefore, we use 6-31G(d) basis set for an accurate description of weak interactions which may prevail in the transition structures.

These calculations are implemented through Gaussian 09W quantum chemical package. The quantum chemical calculations estimate that the O···N···O···, C=O···H-O, H···O-H, weak H-bond interactions in SBz/Scyt clusters in the solvent sphere of aqueous ILs[61] **(Scheme 2)**. The formation of the weak hydrogen bond is an interaction, cohesive interaction[61],[62]. Under definite conditions an atom of hydrogen is attracted by rather strong forces to two atoms instead of only one, so that it may be considered to be acting as a bond between them[27]. The aforementioned statements were well thought-out in our present work. We have depicted the existence of SBz···ILs and SCyt···ILs complexes as clusters through quantum chemical calculations and we hereby compared and calculated values with the experimental values in order to verify sequence of interaction as obtained theoretically.

Several approximate properties of varied systems of aqueous SBz - ILs and SCyt - ILs clusters are summarized in **(Table 7)**. The availability of the optimisation energy (E) of pure as well as the molecular assembly makes it possible to calculate the extent of stabilisation (E) while, formation of molecular assembly assorted by solute – solvent interaction between FPs and ILs in solution. Stabilization energy of molecular assembly i.e. the value of *E*, the optimization energy, which approaches to a minimal value with growing possibility of solute-solvent interactions. From the **(Table 7)** it is clear that

stabilisation through solute – solvent interaction found prominent in case of (BTMACl+Scyt+H_2O) system over the other systems discussed herewith. Specifically, the optimum geometry **(Figure 8)** would involve central FPs surrounded by aqueous ILs molecules via weaker non-covalent interactions which can be explained on the basis of solution thermodynamics[63] in addition to solute-solvent interactions.

Conclusion: The motive to reduce unnecessarily-excessive use of food preservative in the preservation of food is reached, since antimicrobial activity of SBz and Scyt studied herewith, in all possible combination with the BTEACl and BTMACl reveal synergistic to kill micro-organisms and found to act properly below their reported MICs. The physico-chemical methodologies, density, viscosity, refractive index and conductance study describes the mode of interaction between the FPs and ILs in solution. Calculation of apparent molar volume, limiting apparent molar volume, molar refraction, limiting molar refraction and viscosity B coefficient makes possible to identify the interaction as predominant solute – solvent interaction. The values of $(\delta\phi_E^0/\delta T)_P$ and (dB/dT) have been calculated to provide the information that, the solute – solvent interaction is structure making. Association constants, optimisation energy and free energy changes for the molecular assembly grown in solution assorted by structure making solute – solvent interaction dictate their stability in solution and consequently, the order of synergism between them. Thus, solution chemistry for all the possible combinations explores the chemistry behind the synergism. This makes one easy to choose a mixture of compounds such that their combination would arise synergistic. Nevertheless, the synergistic combination of food preservatives reduces the level of hazardous food preservative which is used to stop spoilage of foods produced worldwide and makes the world health, safe. So, the study of microbial activity along with solution chemistry would be a great interest in the field of food chemistry for their preservation.

Conflicts of interest: There is no conflicts of interest.

Acknowledgements: Prof. M. N. Roy would like to acknowledge UGC, New Delhi, Government of India, for being awarded One Time Grant under Basic Scientific Research via the grant-in-Aid no. F.4-10/2010 (BSR). BR is thankful to the "State

Fellowship" bearing reference No. 1743/R-2017 dated 18.04.2017 and UGC-SAP DRS-III, New Delhi (no. 540/6/DRS/2007, SAP-1) for providing instrumental facilities according the research.

TABLES

Table 1. Apparent molar volume (Φ_V^0), Molar Refraction (R_M^0) and viscosity A and viscosity B co-efficient of (BTEACl+SBz+H_2O), (BTEACl+SCyt+H_2O) systems in solution of BTEACl of mass fractions W_1=0.001, W_2=0.003, W_3=0.005, at 298.15K, 303.15K, 308.15K, 313.15K and 318.15 K.

Temperature T(K^b)	$\Phi_v^0 \times 10^6$ /m^3mol^{-1}	$S_v^* \times 10^6$ /$m^3mol^{-3/2}$ $kg^{1/2}$	R_M^0 /m^3mol^{-1}	A /$dm^{3/2}$ $mol^{-1/2}$	B /dm^3 mol^{-1}
W_1=0.001[a]	(BTEACl+SBz+H_2O) System				
298.15	99.02	-56.68	29.42	0.034	0.508
303.15	103.60	-62.40	29.46	0.022	0.523
308.15	108.80	-73.10	29.49	0.014	0.544
313.15	112.32	-77.21	29.52	0.0024	0.551
318.15	116.95	-89.10	29.56	0.0019	0.570
W_1=0.003[a]	(BTEACl+SBz+H_2O) System				
298.15	111.50	-79.40	29.45	0.027	0.515
303.15	116.20	-91.88	29.47	0.017	0.531
308.15	122.10	-100.88	29.49	0.010	0.551
313.15	126.51	-108.52	29.53	0.009	0.565
318.15	128.00	-107.77	29.55	0.004	0.587
W_1=0.005[a]	(BTEACl+SBz+H_2O) System				
298.15	124.20	-105.81	29.48	0.020	0.520
303.15	128.70	-115.14	29.51	0.011	0.537
308.15	133.40	-120.07	29.54	0.006	0.559
313.15	137.22	-126.81	29.56	0.0005	0.581
318.15	142.75	-133.20	29.60	0.0014	0.595
W_1=0.001[a]	(BTEACl+SCyt+H_2O) System				
298.15	114.30	-62.17	32.72	0.042	0.513
303.15	118.10	-68.17	32.76	0.030	0.533
308.15	123.50	-78.97	32.81	0.021	0.546
313.15	127.01	-82.35	32.86	0.016	0.570
318.15	131.87	-92.17	32.90	0.006	0.588
W_1=0.003[a]	(BTEACl+SCyt+H_2O) System				
298.15	121.90	-81.64	32.76	0.037	0.520
303.15	125.00	-86.36	32.80	0.027	0.538
308.15	131.90	-98.03	32.83	0.015	0.552
313.15	136.80	-105.63	32.87	0.028	0.583

318.15	139.19	-107.08	32.91	0.014	0.599
W_1=0.005[a]	(BTEACl+SCyt+H_2O) System				
298.15	129.60	-97.46	32.79	0.029	0.526
303.15	135.50	-110.58	32.82	0.018	0.545
308.15	139.40	-109.83	32.84	0.009	0.558
313.15	144.18	-119.02	32.86	0.017	0.595
318.15	147.20	-130.68	32.89	0.005	0.595

[a]Standard uncertainties in mass fraction u(W) = $\pm$0.0001 mol Kg^{-1}; [b]Standard uncertainties in temperature u(T) = $\pm$0.01 K

Table 2. Apparent molar volume (Φ_V^0), Molar Refraction (R_M^0) and viscosity A and viscosity B co-efficient of (BTMACl+SBz+H_2O), (BTMACl+SCyt+H_2O) systems in solution of BTMACl of mass fractions W_1=0.001, W_2=0.003, W_3=0.005, at 298.15K, 303.15K, 308.15K, 313.15K and 318.15 K.

Temperature T(K[b])	$\Phi_v^0 \times 10^6$ /m^3mol^{-1}	$S_v^* \times 10^6$ /$m^3mol^{-3/2}$ $kg^{1/2}$	R_M^0 /m^3mol^{-1}	A /$dm^{3/2}$ $mol^{-1/2}$	B /dm^3 mol^{-1}
W_1=0.001[a]	(BTMACl+SBz+H_2O) System				
298.15	105.45	-99.91	29.47	0.035	0.513
303.15	109.89	-110.76	29.51	0.032	0.526
308.15	114.06	-118.33	29.54	0.017	0.549
313.15	116.16	-120.51	29.59	0.006	0.550
318.15	121.60	-130.61	29.63	0.003	0.560
W_1=0.003[a]	(BTMACl+SBz+H_2O) System				
298.15	119.81	-146.67	29.51	0.041	0.519
303.15	123.25	-157.20	29.56	0.036	0.531
308.15	126.03	-157.09	29.60	0.010	0.551
313.15	130.21	-160.23	29.67	0.008	0.556
318.15	134.43	-169.08	29.70	0.001	0.568
W_1=0.005[a]	(BTMACl+SBz+H_2O) System				
298.15	130.37	-166.42	29.55	0.037	0.523
303.15	134.28	-168.25	29.57	0.030	0.535
308.15	138.21	-176.01	29.62	0.026	0.555
313.15	144.46	-185.85	29.70	0.019	0.561
318.15	145.29	-182.24	29.75	0.013	0.574
W_1=0.001[a]	(BTMACl+SCyt+H_2O) System				
298.15	118.97	-82.80	32.75	0.045	0.518
303.15	123.36	-96.41	32.79	0.042	0.539
308.15	128.20	-108.95	32.85	0.037	0.550
313.15	134.03	-122.95	32.90	0.029	0.563
318.15	135.95	-130.35	32.93	0.014	0.570
W_1=0.003[a]	(BTMACl+SCyt+H_2O) System				

298.15	124.06	-95.93	32.77	0.041	0.521
303.15	128.90	-106.88	32.82	0.040	0.533
308.15	135.11	-121.50	32.87	0.035	0.554
313.15	140.30	-136.26	32.93	0.025	0.567
318.15	144.74	-142.63	32.97	0.022	0.578
W_1=0.005[a]	(BTMACl+SCyt+H_2O) System				
298.15	133.83	-121.38	32.84	0.038	0.525
303.15	138.44	-131.90	32.88	0.032	0.536
308.15	143.53	-141.79	32.93	0.029	0.557
313.15	146.48	-150.48	32.93	0.026	0.571
318.15	150.08	-154.30	33.02	0.020	0.581

[a]Standard uncertainties in mass fraction u(W) = ±0.0001 mol Kg^{-1}; [b]Standard uncertainties in temperature u(T) = ± 0.01 K

Table 3: Values of empirical coefficients (a_0, a_1, and a_2) of Eq. 5for aqueous (BTEACl+SBz), (BTEACl+SCyt), (BTMACl+SBz), (BTMACl+SCyt) systems in different mass fraction of aqueous BTEACl/BTMACl solution at 298.15 to 318.15 K.

BTEACl+SBz				BTEACl+SCyt		
Mass fraction (W^a)	$a_0\times10^6$ /m^3 mol^{-1}	$a_1\times10^6$ /m^3 mol^{-1} K^{-1}	$a_2\times10^6$ /m^3 mol^{-1} K^{-2}	$a_0\times10^6$ /m^3 mol^{-1}	$a_1\times10^6$ /m^3 mol^{-1} K^{-1}	$a_2\times10^6$ /m^3 mol^{-1} K^{-2}
0.001	-595.04	3.6738	-0.0045	-86.16	0.476	0.0007
0.003	-2290.90	14.7950	-0.0226	-1082.30	6.949	-0.0098
0.005	172.07	-1.1654	0.0034	-1454.50	9.471	-0.0139
BTMACl+SBz				BTMACl+SCyt		
0.001	-143.26	0.8947	-0.0002	-1218.00	7.848	-0.0113
0.003	706.28	-4.4881	0.0085	-684.10	4.260	-0.0052
0.005	-1149.40	7.5621	-0.0110	-1235.40	8.136	-0.0119

[a]Standard uncertainties in mass fraction u(W) = ± 0.0001 mol Kg^{-1}

Table 4. Values of limiting apparent molar expansibilities (Φ_E^0) of aqueous (BTEACl+SBz), (BTEACl+SCyt), (BTMACl+SBz), (BTMACl+SCyt) systems in different mass fraction of aqueous BTEACl/BTMACl solution at 298.15 to 318.15 K.

(BTEACl+SBz) System	$\Phi_E^0\times10^6$/m^3 mol^{-1} K^{-1}					$(\frac{\partial\Phi_E^0}{\partial T})_P\times10^6$ /m^3 mol^{-1} K^{-2}
Mass fraction (W^a)	298.15	303.15	308.15	313.15	318.15	
0.001	0.9905	0.9455	0.9005	0.8555	0.8105	-0.0090
0.003	1.3186	1.0926	0.8666	0.6406	0.4146	-0.0452
0.005	0.8620	0.8960	0.9300	0.9640	0.9980	0.0068

(BTEACl+SCyt) System						
0.001	0.8934	0.9004	0.9074	0.9144	0.9214	0.0014
0.003	1.1053	1.0073	0.9093	0.8113	0.7133	-0.0196
0.005	1.1820	1.0430	0.9040	0.7650	0.6260	-0.0278
(BTMACl+SBz) System						
0.001	0.7754	0.7734	0.7714	0.7694	0.7674	-0.0004
0.003	0.5805	0.6655	0.7505	0.8355	0.9205	0.0170
0.005	1.0028	0.8928	0.7828	0.6728	0.5628	-0.0220
(BTMACl+SCyt) System						
0.001	1.1098	0.9968	0.8838	0.7708	0.6578	-0.0226
0.003	1.1592	1.1072	1.0552	1.0032	0.9512	-0.0104
0.005	1.0400	0.9210	0.8020	0.6830	0.5640	-0.0238

[a]Standard uncertainties in mass fraction u(W) = $\pm$ 0.0001 mol Kg^{-1}

Table 5. Values of dB/dT for aqueous (BTEACl+SBz), (BTEACl+SCyt), (BTMACl+SBz), (BTMACl+SCyt) systems in different mass fraction of aqueous BTEACl/BTMACl solution at 298.15 to 318.15 K.

Mass fraction (W)	$(\frac{dB}{dT})$/ dm^3 mol^{-1}/K^{-1}			
	BTEACl+SBz	BTEACl+Scyt	BTMACl+SBz	BTMACl+Scyt
0.001	0.0030	0.0037	0.0024	0.0026
0.003	0.0036	0.0041	0.0025	0.0030
0.005	0.0039	0.0038	0.0026	0.0029

Table 6. Association constant and Gibb's free energy of (BTEACl+SBz), (BTEACl+SCyt), (BTMACl+SBz) and (BTMACl+SCyt) systems at 298.15 K.

System	(BTEACl+SBz)	(BTEACl+SCyt)	(BTMACl+SBz)	(BTMACl+SCyt)
K_a /M^{-1} (×10^{-3})	2.70	3.31	3.05	3.68
ΔG /KJ mol^{-1}	-19.6	-20.1	-19.9	-20.4

Table 7. Optimisation energies of pure BTEACl, BTMACl, SBz, SCyt and (BTEACl+SBz), (BTEACl+SCyt), (BTMACl+SBz), (BTMACl+SCyt) systems using UB3LYP methodology and 6-31G(d) basis set.

System	Calculation Method	Basis Set	Optimisation energy (a.u.)	Dipole moment (Debye)
SBz	UB3LYP	6-31G(d)	-582.58203318	5.6642
SCyt	UB3LYP	6-31G(d)	-657.78951762	4.4047

BTEACl	UB3LYP	6-31G(d)	-1023.56406394	11.6512
BTMACl	UB3LYP	6-31G(d)	-905.62574200	13.5905
(BTEACl+SBz)	UB3LYP	6-31G(d)	-865.63204549	12.5596
(BTEACl+SCyt)	UB3LYP	6-31G(d)	-940.83809561	11.2236
(BTMACl+SBz)	UB3LYP	6-31G(d)	-983.56112523	12.6819
(BTMACl+SCyt)	UB3LYP	6-31G(d)	-1058.76749759	11.1263

Table S1. Density (ρ), Refractive index (n_D), Viscosity (η) of aqueous pure BTEACl and BTMACl solutions of mass fractions W = 0.001, 0.003, 0.005 at temperatures 298.15 K, 303.15 K, 308.15 K, 313.15 K and 318.15 K.

BTEACl+H_2O				
Mass fraction (W[a])	Temperature (K[b])	Density (ρ[c]) ×10^{-3} Kg.m^{-3}	Refractive index (n_D^d)	Viscosity (η[e]) mPa.S
0.001	298.15	0.9973	1.3303	0.8929
	303.15	0.9948	1.3306	0.7989
	308.15	0.9924	1.3303	0.7209
	313.15	0.9868	1.3302	0.6322
	318.15	0.9843	1.3301	0.5462
0.003	298.15	0.9974	1.3306	0.8948
	303.15	0.9952	1.3308	0.8015
	308.15	0.9931	1.3305	0.7259
	313.15	0.9909	1.3306	0.6354
	318.15	0.9888	1.3307	0.5509
0.005	298.15	0.9975	1.3311	0.8991
	303.15	0.9955	1.3310	0.8041
	308.15	0.9935	1.3307	0.7284
	313.15	0.9915	1.3305	0.6358
	318.15	0.9895	1.3308	0.5520
BTMACl+H_2O				
0.001	298.15	0.9973	1.3308	0.8948
	303.15	0.9948	1.3305	0.8055
	308.15	0.9924	1.3307	0.7231
	313.15	0.9868	1.3306	0.6267
	318.15	0.9843	1.3304	0.5407
0.003	298.15	0.9975	1.3314	0.8971
	303.15	0.9952	1.3304	0.8081
	308.15	0.9927	1.3308	0.7256
	313.15	0.9840	1.3309	0.6231
	318.15	0.9815	1.3310	0.5371
0.005	298.15	0.9977	1.3316	0.9012
	303.15	0.9956	1.3309	0.8128
	308.15	0.9931	1.3310	0.7304

	313.15	0.9783	1.3312	0.6377
	318.15	0.9758	1.3311	0.5522

[a]Standard uncertainties in mass fraction u(W) = ±0.0001 mol Kg^{-1}; [b]Standard uncertainties in temperature u(T) = ± 0.01 K; [c]Standard uncertainties in density u(ρ) = ± 0.00001 Kg m^{-3}; [d]Standard uncertainties in refractive indices u(n_D) = ± 0.0001; [d]Standard uncertainties in viscosity u(η) = ± 0.01 mPa.S

Table S2. Density (ρ), Refractive Index (n_D) and Viscosity (η) of (BTEACl+SBz+H_2O) and (BTEACl+SCyt+H_2O), systems in aqueous BTEACl solutions of mass fractions W_1=0.001, W_2=0.003, W_3=0.005, at 298.15K, 303.15K, 308.15K, 313.15K and 318.15 K.

(BTEACl+SBz+H_2O) system, W_1=0.001				(BTEACl+SCyt+H_2O) system, W_1=0.001		
Temperature – 298.15 K				Temperature – 298.15 K		
Molality (Mol/Kg)	Density (ρ) ×10^{-3} Kg.m^{-3}	Refractive Index (n_D)	Viscosity (η) mPa.S	Density (ρ) ×10^{-3} Kg.m^{-3}	Refractive Index (n_D)	Viscosity (η) mPa.S
0.0100	0.99780	1.3306	0.894	0.99781	1.3308	0.894
0.0251	0.99865	1.3315	0.899	0.99869	1.3317	0.899
0.0402	0.99958	1.3323	0.906	0.99964	1.3323	0.904
0.0554	1.00051	1.3331	0.911	1.00065	1.3331	0.909
0.0705	1.00152	1.3337	0.917	1.00165	1.3338	0.915
0.0858	1.00253	1.3343	0.923	1.00270	1.3344	0.922
Temperature – 303.15 K				Temperature – 303.15 K		
0.0100	0.99526	1.3302	0.801	0.99528	1.3304	0.800
0.0251	0.99606	1.3312	0.807	0.99612	1.3313	0.806
0.0402	0.99691	1.3319	0.812	0.99704	1.3320	0.812
0.0554	0.99785	1.3328	0.817	0.99802	1.3328	0.817
0.0705	0.99879	1.3334	0.824	0.99902	1.3334	0.822
0.0858	0.99980	1.3340	0.830	1.00003	1.3341	0.828
Temperature – 308.15 K				Temperature – 308.15 K		
0.0100	0.99284	1.3298	0.724	0.99286	1.3301	0.723
0.0251	0.99359	1.3308	0.729	0.99366	1.3310	0.728
0.0402	0.99441	1.3315	0.735	0.99453	1.3316	0.734
0.0554	0.99532	1.3325	0.740	0.99547	1.3325	0.739
0.0705	0.99627	1.3331	0.745	0.99650	1.3331	0.745
0.0858	0.99725	1.3337	0.752	0.99747	1.3338	0.749
Temperature – 313.15 K				Temperature – 313.15 K		
0.0100	0.98720	1.3281	0.635	0.98723	1.3286	0.635
0.0251	0.98792	1.3290	0.641	0.98796	1.3294	0.640
0.0402	0.98874	1.3298	0.646	0.98883	1.3303	0.645
0.0554	0.98955	1.3306	0.651	0.98970	1.3308	0.650
0.0705	0.99053	1.3312	0.657	0.99074	1.3316	0.655

	313.15	0.9783	1.3312	0.6377
	318.15	0.9758	1.3311	0.5522

[a]Standard uncertainties in mass fraction u(W) = ±0.0001 mol Kg^{-1}; [b]Standard uncertainties in temperature u(T) = ± 0.01 K; [c]Standard uncertainties in density u(ρ) = ± 0.00001 Kg m^{-3}; [d]Standard uncertainties in refractive indices u(n_D) = ± 0.0001; [d]Standard uncertainties in viscosity u(η) = ± 0.01 mPa.S

Table S2. Density (ρ), Refractive Index (n_D) and Viscosity (η) of (BTEACl+SBz+H_2O) and (BTEACl+SCyt+H_2O), systems in aqueous BTEACl solutions of mass fractions W_1=0.001, W_2=0.003, W_3=0.005, at 298.15K, 303.15K, 308.15K, 313.15K and 318.15 K.

(BTEACl+SBz+H_2O) system, W_1=0.001				(BTEACl+SCyt+H_2O) system, W_1=0.001		
Temperature – 298.15 K				Temperature – 298.15 K		
Molality (Mol/Kg)	Density (ρ) ×10^{-3} Kg.m^{-3}	Refractive Index (n_D)	Viscosity (η) mPa.S	Density (ρ) ×10^{-3} Kg.m^{-3}	Refractive Index (n_D)	Viscosity (η) mPa.S
0.0100	0.99780	1.3306	0.894	0.99781	1.3308	0.894
0.0251	0.99865	1.3315	0.899	0.99869	1.3317	0.899
0.0402	0.99958	1.3323	0.906	0.99964	1.3323	0.904
0.0554	1.00051	1.3331	0.911	1.00065	1.3331	0.909
0.0705	1.00152	1.3337	0.917	1.00165	1.3338	0.915
0.0858	1.00253	1.3343	0.923	1.00270	1.3344	0.922
Temperature – 303.15 K				Temperature – 303.15 K		
0.0100	0.99526	1.3302	0.801	0.99528	1.3304	0.800
0.0251	0.99606	1.3312	0.807	0.99612	1.3313	0.806
0.0402	0.99691	1.3319	0.812	0.99704	1.3320	0.812
0.0554	0.99785	1.3328	0.817	0.99802	1.3328	0.817
0.0705	0.99879	1.3334	0.824	0.99902	1.3334	0.822
0.0858	0.99980	1.3340	0.830	1.00003	1.3341	0.828
Temperature – 308.15 K				Temperature – 308.15 K		
0.0100	0.99284	1.3298	0.724	0.99286	1.3301	0.723
0.0251	0.99359	1.3308	0.729	0.99366	1.3310	0.728
0.0402	0.99441	1.3315	0.735	0.99453	1.3316	0.734
0.0554	0.99532	1.3325	0.740	0.99547	1.3325	0.739
0.0705	0.99627	1.3331	0.745	0.99650	1.3331	0.745
0.0858	0.99725	1.3337	0.752	0.99747	1.3338	0.749
Temperature – 313.15 K				Temperature – 313.15 K		
0.0100	0.98720	1.3281	0.635	0.98723	1.3286	0.635
0.0251	0.98792	1.3290	0.641	0.98796	1.3294	0.640
0.0402	0.98874	1.3298	0.646	0.98883	1.3303	0.645
0.0554	0.98955	1.3306	0.651	0.98970	1.3308	0.650
0.0705	0.99053	1.3312	0.657	0.99074	1.3316	0.655

0.0858	0.99145	1.3321	0.661	0.99171	1.3323	0.660
Temperature – 318.15 K				Temperature – 318.15 K		
0.0100	0.98467	1.3277	0.549	0.98470	1.3282	0.549
0.0251	0.98535	1.3286	0.554	0.98539	1.3290	0.554
0.0402	0.98614	1.3295	0.559	0.98618	1.3298	0.559
0.0554	0.98699	1.3301	0.563	0.98707	1.3306	0.564
0.0705	0.98794	1.3309	0.568	0.98810	1.3313	0.568
0.0858	0.98885	1.3317	0.573	0.98909	1.3320	0.572

Table S3. Density (ρ), Refractive Index (n_D) and Viscosity (η) of (BTEACl+SBz+H_2O) and (BTEACl+SCyt+H_2O), systems in aqueous BTEACl solutions of mass fractions W_1=0.001, W_2=0.003, W_3=0.005, at 298.15K, 303.15K, 308.15K, 313.15K and 318.15 K.

(BTEACl+SBz+H_2O) system, W_2=0.003				(BTEACl+SCyt+H_2O) system, W_2=0.003		
Temperature – 298.15 K				Temperature – 298.15 K		
Molality (Mol/Kg)	Density (ρ) $\times10^{-3}$ Kg.m^{-3}	Refractive Index (n_D)	Viscosity (η) mPa.S	Density (ρ) $\times10^{-3}$ Kg.m^{-3}	Refractive Index (n_D)	Viscosity (η) mPa.S
0.0100	0.99776	1.3309	0.897	0.99781	1.3312	0.896
0.0251	0.99848	1.3317	0.903	0.99863	1.3320	0.901
0.0402	0.99929	1.3325	0.909	0.99957	1.3326	0.907
0.0554	1.00016	1.3331	0.915	1.00052	1.3334	0.913
0.0705	1.00111	1.3338	0.920	1.00157	1.3340	0.919
0.0858	1.00216	1.3345	0.926	1.00259	1.3346	0.924
Temperature – 303.15 K				Temperature – 303.15 K		
0.0100	0.99555	1.3305	0.804	0.99561	1.3309	0.804
0.0251	0.99625	1.3313	0.810	0.99641	1.3316	0.809
0.0402	0.99705	1.3322	0.817	0.99729	1.3323	0.814
0.0554	0.99791	1.3328	0.823	0.99827	1.3331	0.821
0.0705	0.99885	1.3336	0.828	0.99926	1.3337	0.827
0.0858	0.99985	1.3343	0.833	1.00026	1.3343	0.831
Temperature – 308.15 K				Temperature – 308.15 K		
0.0100	0.99341	1.3301	0.729	0.99347	1.3305	0.729
0.0251	0.99403	1.3310	0.735	0.99419	1.3313	0.734
0.0402	0.99479	1.3319	0.741	0.99502	1.3320	0.740
0.0554	0.99559	1.3326	0.747	0.99588	1.3327	0.746
0.0705	0.99655	1.3333	0.752	0.99691	1.3335	0.751
0.0858	0.99750	1.3340	0.757	0.99796	1.3340	0.757
Temperature – 313.15 K				Temperature – 313.15 K		
0.0100	0.99120	1.3298	0.639	0.99126	1.3302	0.638
0.0251	0.99178	1.3307	0.643	0.99189	1.3309	0.642
0.0402	0.99248	1.3314	0.648	0.99272	1.3318	0.646

0.0554	0.99322	1.3321	0.654	0.99359	1.3324	0.653
0.0705	0.99425	1.3331	0.659	0.99448	1.3331	0.656
0.0858	0.99519	1.3337	0.665	0.99562	1.3337	0.662
Temperature – 318.15 K				Temperature – 318.15 K		
0.0100	0.98908	1.3294	0.554	0.98913	1.3298	0.554
0.0251	0.98964	1.3305	0.558	0.98979	1.3306	0.558
0.0402	0.99038	1.3312	0.563	0.99053	1.3315	0.562
0.0554	0.99112	1.3320	0.568	0.99136	1.3321	0.567
0.0705	0.99192	1.3329	0.573	0.99225	1.3328	0.572
0.0858	0.99293	1.3337	0.578	0.99336	1.3333	0.577

Table S4. Density (ρ), Refractive Index (n_D) and Viscosity (η) of (BTEACl+SBz+H_2O) and (BTEACl+SCyt+H_2O), systems in aqueous BTEACl solutions of mass fractions W_1=0.001, W_2=0.003, W_3=0.005, at 298.15K, 303.15K, 308.15K, 313.15K and 318.15 K.

(BTEACl+SBz+H_2O) system, W_3=0.005				(BTEACl+SCyt+H_2O) system, W_3=0.005		
Temperature – 298.15 K				Temperature – 298.15 K		
Molality (Mol/Kg)	Density (ρ) ×10^{-3} Kg.m^{-3}	Refractive Index (n_D)	Viscosity (η) mPa.S	Density (ρ) ×10^{-3} Kg.m^{-3}	Refractive Index (n_D)	Viscosity (η) mPa.S
0.0100	0.99782	1.3313	0.902	0.99792	1.3315	0.901
0.0251	0.99842	1.3320	0.908	0.99866	1.3323	0.907
0.0402	0.99916	1.3327	0.915	0.99952	1.3329	0.913
0.0554	1.00002	1.3333	0.921	1.00045	1.3336	0.920
0.0705	1.00088	1.3340	0.927	1.00145	1.3342	0.925
0.0858	1.00184	1.3347	0.933	1.00257	1.3348	0.932
Temperature – 303.15 K				Temperature – 303.15 K		
0.0100	0.99572	1.3310	0.807	0.99581	1.3311	0.807
0.0251	0.99630	1.3317	0.814	0.99651	1.3320	0.813
0.0402	0.99703	1.3324	0.820	0.99733	1.3326	0.819
0.0554	0.99780	1.3330	0.826	0.99829	1.3333	0.825
0.0705	0.99872	1.3337	0.831	0.99925	1.3339	0.831
0.0858	0.99959	1.3344	0.838	1.00029	1.3345	0.837
Temperature – 308.15 K				Temperature – 308.15 K		
0.0100	0.99376	1.3306	0.732	0.99385	1.3307	0.732
0.0251	0.99427	1.3315	0.738	0.99449	1.3316	0.738
0.0402	0.99491	1.3321	0.744	0.99523	1.3322	0.744
0.0554	0.99569	1.3327	0.750	0.99611	1.3330	0.750
0.0705	0.99655	1.3334	0.756	0.99702	1.3335	0.756
0.0858	0.99747	1.3341	0.762	0.99809	1.3342	0.760
Temperature – 313.15 K				Temperature – 313.15 K		
0.0100	0.99171	1.3303	0.639	0.99179	1.3304	0.639

0.0251	0.99217	1.3310	0.645	0.99239	1.3311	0.643
0.0402	0.99281	1.3317	0.651	0.99312	1.3320	0.648
0.0554	0.99361	1.3324	0.656	0.99391	1.3326	0.654
0.0705	0.99435	1.3332	0.662	0.99487	1.3334	0.660
0.0858	0.99529	1.3338	0.667	0.99589	1.3340	0.666
Temperature – 318.15 K				Temperature – 318.15 K		
0.0100	0.98967	1.3300	0.555	0.98976	1.3300	0.555
0.0251	0.99007	1.3307	0.560	0.99039	1.3307	0.560
0.0402	0.99061	1.3313	0.565	0.99112	1.3317	0.564
0.0554	0.99131	1.3321	0.570	0.99199	1.3322	0.569
0.0705	0.99214	1.3328	0.576	0.99287	1.3330	0.575
0.0858	0.99309	1.3335	0.580	0.99381	1.3336	0.580

Table S5. Density (ρ), Refractive Index (n_D) and Viscosity (η) of (BTMACl+SBz+H_2O) and (BTMACl+SCyt+H_2O) systems in aqueous BTMACl solutions of mass fractions W_1=0.001, W_2=0.003, W_3=0.005, at 298.15 K, 303.15 K, 308.15 K, 313.15 K and 318.15 K

(BTMACl+SBz+H_2O) system, W_1=0.001				(BTMACl+SCyt+H_2O) system, W_1=0.001		
Temperature – 298.15 K				Temperature – 298.15 K		
Molality (Mol/Kg)	Density (ρ) ×10^{-3} Kg.m^{-3}	Refractive Index (n_D)	Viscosity (η) mPa.S	Density (ρ) ×10^{-3} Kg.m^{-3}	Refractive Index (n_D)	Viscosity (η) mPa.S
0.0100	0.99781	1.3310	0.896	0.99782	1.3311	0.896
0.0251	0.99869	1.3319	0.901	0.99868	1.3320	0.900
0.0402	0.99968	1.3327	0.906	0.99965	1.3327	0.905
0.0554	1.00076	1.3334	0.913	1.00070	1.3333	0.910
0.0705	1.00191	1.3340	0.919	1.00173	1.3341	0.916
0.0858	1.00309	1.3346	0.924	1.00287	1.3347	0.924
Temperature – 303.15 K				Temperature – 303.15 K		
0.0100	0.99530	1.3306	0.807	0.99531	1.3307	0.807
0.0251	0.99614	1.3315	0.812	0.99614	1.3315	0.811
0.0402	0.99712	1.3323	0.817	0.99709	1.3322	0.816
0.0554	0.99819	1.3330	0.823	0.99813	1.3329	0.821
0.0705	0.99932	1.3336	0.829	0.99925	1.3335	0.827
0.0858	1.00049	1.3343	0.835	1.00036	1.3343	0.833
Temperature – 308.15 K				Temperature – 308.15 K		
0.0100	0.99280	1.3301	0.726	0.99280	1.3303	0.725
0.0251	0.99359	1.3312	0.731	0.99361	1.3312	0.729
0.0402	0.99453	1.3320	0.737	0.99457	1.3318	0.734
0.0554	0.99558	1.3327	0.742	0.99554	1.3325	0.739
0.0705	0.99669	1.3333	0.748	0.99667	1.3331	0.744
0.0858	0.99791	1.3340	0.753	0.99780	1.3338	0.750

Temperature – 313.15 K				Temperature – 313.15 K		
0.0100	0.98720	1.3285	0.629	0.98720	1.3287	0.629
0.0251	0.98799	1.3293	0.635	0.98793	1.3296	0.633
0.0402	0.98898	1.3299	0.640	0.98887	1.3303	0.637
0.0554	0.98998	1.3307	0.645	0.98984	1.3308	0.642
0.0705	0.99099	1.3312	0.650	0.99097	1.3316	0.648
0.0858	0.99211	1.3319	0.654	0.99215	1.3321	0.651
Temperature – 318.15 K				Temperature – 318.15 K		
0.0100	0.98467	1.3281	0.544	0.98468	1.3281	0.543
0.0251	0.98539	1.3290	0.548	0.98543	1.3290	0.547
0.0402	0.98628	1.3295	0.552	0.98637	1.3297	0.551
0.0554	0.98728	1.3303	0.558	0.98744	1.3303	0.557
0.0705	0.98839	1.3308	0.562	0.98847	1.3309	0.561
0.0858	0.98945	1.3316	0.566	0.98955	1.3315	0.564

Table S6. Density (ρ), Refractive Index (n_D) and Viscosity (η) of (BTMACl+SBz+H_2O) and (BTMACl+SCyt+H_2O) systems in aqueous BTMACl solutions of mass fractions W_1=0.001, W_2=0.003, W_3=0.005, at 298.15 K, 303.15 K, 308.15 K, 313.15 K and 318.15 K

(BTMACl+SBz+H_2O) system, W_2=0.003				(BTMACl+SCyt+H_2O) system, W_2=0.003		
Temperature – 298.15 K				Temperature – 298.15 K		
Molality (Mol/Kg)	Density (ρ) ×10^{-3} Kg.m^{-3}	Refractive Index (n_D)	Viscosity (η) mPa.S	Density (ρ) ×10^{-3} Kg.m^{-3}	Refractive Index (n_D)	Viscosity (η) mPa.S
0.0100	0.99785	1.3314	0.898	0.99796	1.3314	0.898
0.0251	0.99859	1.3321	0.902	0.99878	1.3321	0.903
0.0402	0.99949	1.3327	0.909	0.99974	1.3328	0.909
0.0554	1.00055	1.3334	0.915	1.00076	1.3336	0.915
0.0705	1.00167	1.3340	0.920	1.00182	1.3341	0.921
0.0858	1.00286	1.3347	0.927	1.00291	1.3349	0.926
Temperature – 303.15 K				Temperature – 303.15 K		
0.0100	0.99554	1.3311	0.812	0.99563	1.3311	0.809
0.0251	0.99625	1.3318	0.816	0.99641	1.3318	0.814
0.0402	0.99716	1.3324	0.821	0.99734	1.3324	0.819
0.0554	0.99819	1.3331	0.827	0.99834	1.3332	0.824
0.0705	0.99935	1.3337	0.833	0.99941	1.3338	0.830
0.0858	1.00054	1.3343	0.840	1.00050	1.3345	0.836
Temperature – 308.15 K				Temperature – 308.15 K		
0.0100	0.99304	1.3307	0.731	0.99311	1.3307	0.727
0.0251	0.99372	1.3315	0.735	0.99385	1.3315	0.732
0.0402	0.99461	1.3322	0.740	0.99474	1.3321	0.736

0.0554	0.99558	1.3328	0.747	0.99572	1.3328	0.742
0.0705	0.99666	1.3334	0.752	0.99678	1.3335	0.747
0.0858	0.99783	1.3340	0.758	0.99787	1.3342	0.753
Temperature – 313.15 K				Temperature – 313.15 K		
0.0100	0.98428	1.3284	0.626	0.98435	1.3281	0.625
0.0251	0.98492	1.3290	0.631	0.98505	1.3290	0.630
0.0402	0.98571	1.3298	0.637	0.98594	1.3296	0.635
0.0554	0.98658	1.3303	0.640	0.98692	1.3302	0.639
0.0705	0.98776	1.3310	0.647	0.98798	1.3310	0.644
0.0858	0.98893	1.3317	0.652	0.98910	1.3316	0.648
Temperature – 318.15 K				Temperature – 318.15 K		
0.0100	0.98176	1.3279	0.540	0.98182	1.3278	0.539
0.0251	0.98232	1.3287	0.544	0.98245	1.3288	0.544
0.0402	0.98311	1.3294	0.550	0.98334	1.3296	0.547
0.0554	0.98399	1.3300	0.554	0.98432	1.3302	0.552
0.0705	0.98516	1.3308	0.559	0.98516	1.3310	0.556
0.0858	0.98631	1.3313	0.562	0.98650	1.3316	0.560

Table S7. Density (ρ), Refractive Index (n_D) and Viscosity (η) of (BTMACl+SBz+H_2O) and (BTMACl+SCyt+H_2O) systems in aqueous BTMACl solutions of mass fractions W_1=0.001, W_2=0.003, W_3=0.005, at 298.15 K, 303.15 K, 308.15 K, 313.15 K and 318.15 K

(BTMACl+SBz+H_2O) system, W_3=0.005				(BTMACl+SCyt+H_2O) system, W_3=0.005		
Temperature – 298.15 K				Temperature – 298.15 K		
Molality (Mol/Kg)	Density (ρ) ×10^{-3} Kg.m^{-3}	Refractive Index (n_D)	Viscosity (η) mPa.S	Density (ρ) ×10^{-3} Kg.m^{-3}	Refractive Index (n_D)	Viscosity (η) mPa.S
0.0100	0.99731	1.3317	0.903	0.99743	1.3318	0.903
0.0251	0.99797	1.3323	0.908	0.99820	1.3325	0.907
0.0402	0.99880	1.3329	0.913	0.99910	1.3331	0.914
0.0554	0.99974	1.3335	0.919	1.00012	1.3337	0.919
0.0705	1.00086	1.3342	0.926	1.00113	1.3344	0.926
0.0858	1.00199	1.3348	0.932	1.00227	1.3350	0.932
Temperature – 303.15 K				Temperature – 303.15 K		
0.0100	0.99580	1.3314	0.815	0.99592	1.3316	0.815
0.0251	0.99638	1.3320	0.820	0.99665	1.3323	0.820
0.0402	0.99719	1.3326	0.826	0.99754	1.3328	0.825
0.0554	0.99809	1.3332	0.831	0.99851	1.3334	0.831
0.0705	0.99912	1.3339	0.837	0.99955	1.3340	0.836
0.0858	1.00024	1.3344	0.843	1.00065	1.3346	0.843
Temperature – 308.15 K				Temperature – 308.15 K		
0.0100	0.99330	1.3311	0.733	0.99341	1.3312	0.732

0.0251	0.99386	1.3317	0.737	0.99408	1.3321	0.737
0.0402	0.99465	1.3323	0.743	0.99493	1.3327	0.743
0.0554	0.99552	1.3329	0.748	0.99591	1.3333	0.748
0.0705	0.99652	1.3335	0.754	0.99693	1.3338	0.753
0.0858	0.99761	1.3342	0.760	0.99802	1.3344	0.759
Temperature – 313.15 K				Temperature – 313.15 K		
0.0100	0.97848	1.3266	0.640	0.97861	1.3264	0.640
0.0251	0.97896	1.3270	0.645	0.97928	1.3270	0.644
0.0402	0.97965	1.3276	0.649	0.98013	1.3276	0.648
0.0554	0.98052	1.3282	0.655	0.98101	1.3282	0.654
0.0705	0.98152	1.3288	0.660	0.98221	1.3288	0.659
0.0858	0.98271	1.3294	0.665	0.98322	1.3295	0.664
Temperature – 318.15 K				Temperature – 318.15 K		
0.0100	0.97596	1.3262	0.555	0.97609	1.3259	0.554
0.0251	0.97646	1.3267	0.559	0.97668	1.3266	0.558
0.0402	0.97715	1.3272	0.563	0.97753	1.3271	0.563
0.0554	0.97792	1.3278	0.569	0.97850	1.3278	0.568
0.0705	0.97882	1.3283	0.573	0.97942	1.3284	0.572
0.0858	0.98009	1.3290	0.577	0.98059	1.3290	0.577

Table S8. Apparent molar volume (φ_V), Molar Refraction (R_M) and $(\eta_r-1)/\sqrt{c}$ of (BTEACl+SBz+H_2O) and (BTEACl+SCyt+H_2O) systems in aqueous BTEACl solutions of mass fractions W_1=0.001, W_2=0.003, W_3=0.005, at 298.15 K, 303.15 K, 308.15 K, 313.15 K and 318.15 K.

(BTEACl+SBz+H_2O) system, W_1=0.001				(BTEACl+SCyt+H_2O) system, W1=0.001		
Temperature – 298.15 K				Temperature – 298.15 K		
Molality (Mol/Kg)	$\phi_V\times10^6$ (m^3 mol^{-1})	R_M m^3 mol^{-1}	$(\eta_r-1)/\sqrt{c}$ $dm^{3/2}$ $mol^{-1/2}$	$\phi_V\times10^6$ (m^3 mol^{-1})	R_M m^3 mol^{-1}	$(\eta_r-1)/\sqrt{c}$ $dm^{3/2}$ $mol^{-1/2}$
0.0100	93.5791	29.5116	0.0159	108.4914	32.8060	0.0083
0.0251	89.9963	29.5594	0.0449	104.4434	32.8582	0.0400
0.0402	87.1925	29.5966	0.0710	101.6234	32.8808	0.0614
0.0554	85.7699	29.6336	0.0859	99.2380	32.9194	0.0779
0.0705	83.9299	29.6523	0.1002	97.9519	32.9492	0.0919
0.0858	82.6490	29.6706	0.1133	96.6332	32.9685	0.1093
Temperature – 303.15 K				Temperature – 303.15 K		
0.0100	97.5212	29.5544	0.0305	111.6496	32.8533	0.0202
0.0251	93.6398	29.6118	0.0607	107.2026	32.9067	0.0556
0.0402	91.3463	29.6433	0.0834	104.3640	32.9397	0.0808
0.0554	88.7912	29.6884	0.0987	101.7061	32.9792	0.0944
0.0705	87.1808	29.7089	0.1182	99.9079	33.0000	0.1111
0.0858	85.4628	29.7275	0.1314	98.7283	33.0296	0.1237

Temperature – 308.15 K				Temperature – 308.15 K		
0.0100	101.4034	29.5937	0.0403	115.9365	32.9063	0.0294
0.0251	97.3867	29.6529	0.0723	110.6422	32.9611	0.0665
0.0402	94.4759	29.6853	0.0950	107.6894	32.9866	0.0921
0.0554	91.5512	29.7394	0.1138	104.8930	33.0365	0.1084
0.0705	89.3491	29.7599	0.1285	102.1157	33.0567	0.1235
0.0858	87.4655	29.7791	0.1468	100.9025	33.0873	0.1346
Temperature – 313.15 K				Temperature – 313.15 K		
0.0100	104.7186	29.6233	0.0511	118.3009	32.9572	0.0385
0.0251	100.0897	29.6756	0.0878	114.6334	33.0057	0.0768
0.0402	96.3004	29.7165	0.1081	110.2761	33.0586	0.1018
0.0554	94.7249	29.7575	0.1257	108.2166	33.0750	0.1197
0.0705	91.4293	29.7773	0.1472	104.5376	33.1129	0.1329
0.0858	89.9049	29.8229	0.1569	102.8952	33.1436	0.1504
Temperature – 318.15 K				Temperature – 318.15 K		
0.0100	107.9688	29.6665	0.0576	121.7619	33.0054	0.0484
0.0251	103.0556	29.7200	0.0856	117.8924	33.0554	0.0902
0.0402	98.9883	29.7702	0.1130	114.1492	33.1017	0.1148
0.0554	95.9558	29.7937	0.1299	110.7369	33.1448	0.1378
0.0705	92.8645	29.8308	0.1511	106.6795	33.1740	0.1503
0.0858	91.1978	29.8686	0.1662	104.4948	33.2043	0.1606

Table S9. Apparent molar volume (φ_V), Molar Refraction (R_M) and $(\eta_r-1)/\sqrt{c}$ of (BTEACl+SBz+H_2O) and (BTEACl+SCyt+H_2O) systems in aqueous BTEACl solutions of mass fractions W_1=0.001, W_2=0.003, W_3=0.005, at 298.15 K, 303.15 K, 308.15 K, 313.15 K and 318.15 K.

(BTEACl+SBz+H_2O) system, W_1=0.003				(BTEACl+SCyt+H_2O) system, W_1=0.003		
Temperature – 298.15 K				Temperature – 298.15 K		
Molality (Mol/Kg)	$\phi_V\times10^6$ (m^3 mol^{-1})	R_M m^3 mol^{-1}	$(\eta_r-1)/\sqrt{c}$ $dm^{3/2}$ $mol^{-1/2}$	$\phi_V\times10^6$ (m^3 mol^{-1})	R_M m^3 mol^{-1}	$(\eta_r-1)/\sqrt{c}$ $dm^{3/2}$ $mol^{-1/2}$
0.0100	103.2192	29.5370	0.0208	114.0241	32.8419	0.0150
0.0251	99.1509	29.5806	0.0556	109.2313	32.8871	0.0430
0.0402	95.8931	29.6214	0.0786	104.9742	32.9102	0.0689
0.0554	93.2593	29.6441	0.0978	102.6488	32.9505	0.0863
0.0705	90.6025	29.6725	0.1078	100.0053	32.9699	0.1029
0.0858	87.7216	29.6977	0.1199	98.6388	32.9900	0.1124
Temperature – 303.15 K				Temperature – 303.15 K		
0.0100	107.1809	29.5702	0.0330	116.9233	32.8875	0.0260
0.0251	101.5041	29.6143	0.0689	111.1073	32.9243	0.0589
0.0402	97.5395	29.6635	0.0939	107.6375	32.9584	0.0793
0.0554	94.6870	29.6866	0.1118	104.0811	32.9978	0.1016
0.0705	91.8367	29.7233	0.1246	101.9724	33.0190	0.1192

0.0858	89.3611	29.7502	0.1344	100.5672	33.0400	0.1269
Temperature – 308.15 K				Temperature – 308.15 K		
0.0100	111.6466	29.6013	0.0406	122.1166	32.9224	0.0397
0.0251	106.5032	29.6560	0.0788	116.3320	32.9708	0.0725
0.0402	101.8374	29.7066	0.1034	112.1208	33.0064	0.0953
0.0554	98.9561	29.7396	0.1209	109.5737	33.0409	0.1168
0.0705	94.8973	29.7677	0.1372	105.8013	33.0791	0.1306
0.0858	92.4191	29.7959	0.1459	103.0086	33.0890	0.1459
Temperature – 313.15 K				Temperature – 313.15 K		
0.0100	114.8911	29.6428	0.0509	125.3719	32.9685	0.0430
0.0251	109.5052	29.6988	0.0784	121.3735	33.0110	0.0684
0.0402	105.2974	29.7350	0.0997	115.3101	33.0648	0.0863
0.0554	102.5805	29.7699	0.1224	111.8415	33.0901	0.1151
0.0705	96.7373	29.8203	0.1399	109.5388	33.1238	0.1210
0.0858	94.0583	29.8407	0.1601	105.0174	33.1398	0.1429
Temperature – 318.15 K				Temperature – 318.15 K		
0.0100	117.1115	29.6735	0.0589	128.6664	33.0032	0.0517
0.0251	111.5217	29.7468	0.0860	121.5271	33.0538	0.0775
0.0402	105.4357	29.7817	0.1093	117.8136	33.1108	0.1003
0.0554	102.7074	29.8248	0.1311	114.3743	33.1374	0.1274
0.0705	100.1070	29.8739	0.1532	111.5369	33.1710	0.1470
0.0858	96.0641	29.9086	0.1710	107.0272	33.1790	0.1648

Table S10. Apparent molar volume (φ_V), Molar Refraction (R_M) and $(\eta_r-1)/\sqrt{c}$ of (BTEACl+SBz+H_2O) and (BTEACl+SCyt+H_2O) systems in aqueous BTEACl solutions of mass fractions W_1=0.001, W_2=0.003, W_3=0.005, at 298.15 K, 303.15 K, 308.15 K, 313.15 K and 318.15 K.

(BTEACl+SBz+H_2O) system, W_1=0.005				(BTEACl+SCyt+H_2O) system, W_1=0.005		
Temperature – 298.15 K				Temperature – 298.15 K		
Molality (Mol/Kg)	$\phi_V\times10^6$ (m^3 mol^{-1})	R_M m^3 mol^{-1}	$(\eta_r-1)/\sqrt{c}$ $dm^{3/2}$ $mol^{-1/2}$	$\phi_V\times10^6$ ($m^3.mol^{-1}$)	R_M m^3 mol^{-1}	$(\eta_r-1)/\sqrt{c}$ $dm^{3/2}$ $mol^{-1/2}$
0.0100	113.3305	29.5678	0.0287	119.6024	32.8656	0.0217
0.0251	108.0120	29.6067	0.0632	114.4212	32.9132	0.0540
0.0402	103.0900	29.6414	0.0870	110.0456	32.9387	0.0777
0.0554	98.7143	29.6644	0.1024	106.7787	32.9708	0.0981
0.0705	96.1658	29.6955	0.1169	103.8884	32.9916	0.1078
0.0858	93.3546	29.7234	0.1296	100.7541	33.0086	0.1235
Temperature – 303.15 K				Temperature – 303.15 K		
0.0100	117.6154	29.6057	0.0387	124.4448	32.8989	0.0341
0.0251	110.3994	29.6452	0.0754	118.1584	32.9571	0.0697
0.0402	104.9528	29.6803	0.1000	113.5591	32.9841	0.0925
0.0554	101.7472	29.7061	0.1169	108.8153	33.0152	0.1098

0.0705	97.7480	29.7355	0.1272	106.1567	33.0375	0.1242
0.0858	95.6633	29.7659	0.1447	103.4598	33.0570	0.1415
Temperature – 308.15 K				Temperature – 308.15 K		
0.0100	120.9155	29.6315	0.0480	128.1548	32.9278	0.0437
0.0251	114.6868	29.6895	0.0815	121.8591	32.9878	0.0791
0.0402	109.8921	29.7192	0.1075	118.0317	33.0176	0.1061
0.0554	105.2260	29.7448	0.1273	113.5072	33.0604	0.1252
0.0705	101.2003	29.7757	0.1407	110.4909	33.0752	0.1408
0.0858	98.0643	29.8050	0.1555	106.7351	33.1028	0.1486
Temperature – 313.15 K				Temperature – 313.15 K		
0.0100	124.0280	29.6683	0.0571	132.1614	32.9690	0.0492
0.0251	118.0063	29.7116	0.0913	125.1749	33.0123	0.0744
0.0402	112.0107	29.7495	0.1176	120.2613	33.0695	0.0941
0.0554	106.4438	29.7827	0.1351	116.9143	33.0975	0.1230
0.0705	103.8885	29.8253	0.1558	112.4909	33.1377	0.1410
0.0858	100.0513	29.8460	0.1678	108.9194	33.1578	0.1633
Temperature – 318.15 K				Temperature – 318.15 K		
0.0100	128.1950	29.7049	0.0624	135.4024	33.0002	0.0570
0.0251	122.2653	29.7501	0.0869	125.3544	33.0427	0.0867
0.0402	117.2622	29.7829	0.1181	120.4211	33.1090	0.1082
0.0554	112.1335	29.8273	0.1355	115.5803	33.1253	0.1301
0.0705	107.1876	29.8594	0.1604	112.6194	33.1683	0.1576
0.0858	102.5549	29.8877	0.1731	110.0430	33.1913	0.1717

Table S11. Apparent molar volume (φ_V), Molar Refraction (R_M) and $(\eta_r-1)/\sqrt{c}$ of (BTMACl+SBz+H_2O), (BTMACl+SCyt+H_2O) systems in aqueous BTMACl solutions of mass fractions W_1=0.001, W_2=0.003, W_3=0.005, at 298.15 K, 303.15 K, 308.15 K, 313.15 K and 318.15 K.

(BTMACl+SBz+H_2O) system, W_1=0.001				(BTMACl+SCyt+H_2O) system, W_1=0.001		
Temperature – 298.15 K				Temperature – 298.15 K		
Molality (Mol/Kg)	$\phi_V\times10^6$ ($m^3\ mol^{-1}$)	R_M $m^3\ mol^{-1}$	$(\eta_r-1)/\sqrt{c}$ $dm^{3/2}\ mol^{-1/2}$	$\phi_V\times10^6$ ($m^3\ mol^{-1}$)	R_M $m^3\ mol^{-1}$	$(\eta_r-1)/\sqrt{c}$ $dm^{3/2}\ mol^{-1/2}$
0.0100	95.3985	29.5437	0.0157	110.8669	32.8329	0.0086
0.0251	89.7838	29.5907	0.0455	105.9040	32.8854	0.0357
0.0402	85.3670	29.6259	0.0644	102.1328	32.9164	0.0577
0.0554	81.8872	29.6506	0.0878	98.9517	32.9358	0.0740
0.0705	78.6859	29.6647	0.1020	97.2213	32.9734	0.0908
0.0858	76.3954	29.6781	0.1126	94.9795	32.9897	0.1103
Temperature – 303.15 K				Temperature – 303.15 K		
0.0100	98.9057	29.5858	0.0235	113.4798	32.8794	0.0129
0.0251	92.5247	29.6339	0.0479	108.4202	32.9241	0.0421

0.0402	87.4032	29.6696	0.0701	104.2298	32.9559	0.0647
0.0554	83.4627	29.6944	0.0896	100.5262	32.9844	0.0841
0.0705	80.3688	29.7095	0.1091	97.3169	33.0014	0.1000
0.0858	77.8602	29.7311	0.1232	95.3946	33.0366	0.1172
Temperature – 308.15 K				Temperature – 308.15 K		
0.0100	101.8185	29.6195	0.0352	117.4887	32.9262	0.0200
0.0251	95.6783	29.6854	0.0710	110.9874	32.9808	0.0473
0.0402	90.6101	29.7226	0.0928	105.7195	33.0034	0.0731
0.0554	86.1741	29.7481	0.1133	102.8722	33.0342	0.0931
0.0705	82.6281	29.7634	0.1307	98.9958	33.0508	0.1083
0.0858	79.1627	29.7836	0.1394	96.5999	33.0766	0.1252
Temperature – 313.15 K				Temperature – 313.15 K		
0.0100	105.0695	29.6562	0.0430	120.8260	32.9672	0.0302
0.0251	97.1051	29.6980	0.0856	115.7712	33.0248	0.0586
0.0402	90.3062	29.7176	0.1082	109.2878	33.0573	0.0780
0.0554	86.8561	29.7530	0.1270	105.5108	33.0701	0.1021
0.0705	84.6147	29.7633	0.1395	101.0784	33.1050	0.1275
0.0858	81.9760	29.7867	0.1496	97.6610	33.1109	0.1336
Temperature – 318.15 K				Temperature – 318.15 K		
0.0100	105.0695	29.6995	0.0537	123.0874	32.9967	0.0420
0.0251	97.1051	29.7517	0.0865	115.9470	33.0538	0.0772
0.0402	90.3062	29.7661	0.1057	109.4308	33.0864	0.0965
0.0554	86.8561	29.8015	0.1322	103.7668	33.1050	0.1261
0.0705	84.6147	29.8088	0.1485	101.1800	33.1251	0.1416
0.0858	81.9760	29.8423	0.1590	98.9521	33.1435	0.1470

Table S12. Apparent molar volume (φ_V), Molar Refraction (R_M) and $(\eta_r-1)/\sqrt{c}$ of (BTMACl+SBz+H_2O), (BTMACl+SCyt+H_2O) systems in aqueous BTMACl solutions of mass fractions W_1=0.001, W_2=0.003, W_3=0.005, at 298.15 K, 303.15 K, 308.15 K, 313.15 K and 318.15 K.

(BTMACl+SBz+H_2O) system, W_1=0.003				(BTMACl+SCyt+H_2O) system, W_1=0.003		
Temperature – 298.15 K				Temperature – 298.15 K		
Molality (Mol/Kg)	$\phi_V\times10^6$ ($m^3\ mol^{-1}$)	R_M $m^3\ mol^{-1}$	$(\eta_r-1)/\sqrt{c}$ $dm^{3/2}\ mol^{-1/2}$	$\phi_V\times10^6$ ($m^3\ mol^{-1}$)	R_M $m^3\ mol^{-1}$	$(\eta_r-1)/\sqrt{c}$ $dm^{3/2}\ mol^{-1/2}$
0.0100	105.2179	29.5749	0.0135	114.7141	32.8553	0.0119
0.0251	96.5484	29.6096	0.0372	109.0736	32.8911	0.0383
0.0402	90.4968	29.6315	0.0635	104.3124	32.9225	0.0638
0.0554	84.8775	29.6568	0.0826	100.9365	32.9605	0.0825
0.0705	80.7097	29.6720	0.0957	98.5025	32.9705	0.0983
0.0858	77.2041	29.6930	0.1124	96.6076	33.0063	0.1098
Temperature – 303.15 K				Temperature – 303.15 K		

0.0100	107.3677	29.6193	0.0236	118.1824	32.9050	0.0160
0.0251	98.6995	29.6549	0.0434	112.3739	32.9424	0.0439
0.0402	91.6693	29.6766	0.0657	107.1847	32.9658	0.0644
0.0554	86.1212	29.7026	0.0871	103.3595	33.0045	0.0818
0.0705	81.1161	29.7166	0.1050	100.2991	33.0232	0.1033
0.0858	77.5387	29.7296	0.1253	98.0638	33.0500	0.1192
Temperature – 308.15 K				Temperature – 308.15 K		
0.0100	110.6005	29.6613	0.0364	123.0494	32.9522	0.0204
0.0251	101.3046	29.7061	0.0648	116.0938	33.0001	0.0520
0.0402	93.8037	29.7365	0.0830	110.3962	33.0246	0.0736
0.0554	88.7611	29.7561	0.1105	106.2273	33.0553	0.0956
0.0705	84.3986	29.7726	0.1271	102.6403	33.0832	0.1113
0.0858	80.4752	29.7862	0.1407	99.9975	33.1100	0.1271
Temperature – 313.15 K				Temperature – 313.15 K		
0.0100	113.8383	29.7360	0.0480	126.5002	33.0078	0.0272
0.0251	104.5056	29.7660	0.0800	119.3788	33.0666	0.0680
0.0402	98.4443	29.8080	0.1088	112.5818	33.0914	0.0912
0.0554	94.0243	29.8226	0.1168	107.8855	33.1133	0.1085
0.0705	87.0558	29.8444	0.1415	103.9764	33.1506	0.1274
0.0858	82.6337	29.8663	0.1565	100.7565	33.1676	0.1360
Temperature – 318.15 K				Temperature – 318.15 K		
0.0100	116.1272	29.7711	0.0559	129.8379	33.0654	0.0330
0.0251	108.8151	29.8201	0.0848	123.7133	33.1358	0.0756
0.0402	101.1681	29.8539	0.1185	115.3267	33.1789	0.0907
0.0554	95.8315	29.8764	0.1339	109.9002	33.2008	0.1155
0.0705	88.6118	29.9068	0.1523	108.8789	33.2456	0.1327
0.0858	84.1474	29.9129	0.1614	102.0699	33.2550	0.1455

Table S13. Apparent molar volume (φ_V), Molar Refraction (R_M) and $(\eta_r-1)/\sqrt{c}$ of (BTMACl+SBz+H_2O), (BTMACl+SCyt+H_2O) systems in aqueous BTMACl solutions of mass fractions W_1=0.001, W_2=0.003, W_3=0.005, at 298.15 K, 303.15 K, 308.15 K, 313.15 K and 318.15 K.

(BTMACl+SBz+H_2O) system, W_1=0.005				(BTMACl+SCyt+H_2O) system, W_1=0.005		
Temperature – 298.15 K				Temperature – 298.15 K		
Molality (Mol/Kg)	$\phi_V\times10^6$ (m^3 mol^{-1})	R_M m^3 mol^{-1}	$(\eta_r-1)/\sqrt{c}$ $dm^{3/2}$ $mol^{-1/2}$	$\phi_V\times10^6$ (m^3 mol^{-1})	R_M m^3 mol^{-1}	$(\eta_r-1)/\sqrt{c}$ $dm^{3/2}$ $mol^{-1/2}$
0.0100	114.2439	29.6154	0.0170	122.2504	32.9088	0.0155
0.0251	103.5095	29.6444	0.0451	114.3212	32.9464	0.0433
0.0402	96.5637	29.6683	0.0645	109.0697	32.9706	0.0687
0.0554	91.3922	29.6889	0.0839	104.4761	32.9908	0.0837
0.0705	85.8323	29.7122	0.1038	101.9521	33.0202	0.1018
0.0858	82.1614	29.7270	0.1172	98.8270	33.0364	0.1166

Temperature – 303.15 K				Temperature – 303.15 K		
0.0100	117.5442	29.6358	0.0244	125.8991	32.9406	0.0212
0.0251	107.9394	29.6672	0.0531	117.2609	32.9794	0.0524
0.0402	99.9138	29.6918	0.0782	111.2413	32.9951	0.0747
0.0554	94.5653	29.7136	0.0961	106.9603	33.0170	0.0929
0.0705	89.5645	29.7394	0.1120	103.4851	33.0365	0.1084
0.0858	85.3398	29.7465	0.1269	100.5203	33.0538	0.1257
Temperature – 308.15 K				Temperature – 308.15 K		
0.0100	121.1917	29.6861	0.0307	129.4122	32.9874	0.0278
0.0251	110.3198	29.7181	0.0602	121.4011	33.0466	0.0564
0.0402	101.7718	29.7432	0.0833	114.8900	33.0726	0.0830
0.0554	96.5448	29.7660	0.1019	109.3949	33.0940	0.1005
0.0705	91.5625	29.7847	0.1215	105.7932	33.1054	0.1181
0.0858	87.3466	29.8088	0.1378	102.5853	33.1232	0.1349
Temperature – 313.15 K				Temperature – 313.15 K		
0.0100	124.8639	29.7632	0.0391	131.7469	33.0451	0.0336
0.0251	115.7085	29.7816	0.0693	122.6501	33.0775	0.0653
0.0402	107.9295	29.8102	0.0888	115.9325	33.1040	0.0832
0.0554	101.1173	29.8335	0.1148	112.1591	33.1293	0.1112
0.0705	95.1697	29.8525	0.1324	105.3653	33.1441	0.1257
0.0858	89.0750	29.8659	0.1448	103.2482	33.1741	0.1434
Temperature – 318.15 K				Temperature – 318.15 K		
0.0100	127.2332	29.8068	0.0454	134.0989	33.0842	0.0396
0.0251	115.9343	29.8330	0.0782	127.0491	33.1286	0.0712
0.0402	108.1155	29.8533	0.0975	118.7240	33.1460	0.0961
0.0554	103.1705	29.8796	0.1281	112.5468	33.1775	0.1179
0.0705	98.2784	29.8935	0.1390	109.7590	33.2016	0.1320
0.0858	90.6384	29.9126	0.1545	104.9558	33.2172	0.1527

Table S14. Molar conductivities of (BTEACl+SBz+H_2O) and (BTEACl+SCyt+H_2O) systems in aqueous BTEACl solutions of mass fractions W_1=0.001, W_2=0.003, W_3=0.005, at 298.15 K, 303.15 K, 308.15 K, 313.15 K and 318.15 K.

(BTEACl+SBz+H_2O) system, W_1=0.001					
	Molar conductivities (S cm^2 mol^{-1})				
Molarity (moles/litre)	**298.15K**	**303.15K**	**308.15K**	**313.15K**	**318.15K**
0.0000	-	-	-	-	-
0.0103	92.82	106.80	117.48	128.16	134.95
0.0261	85.29	98.29	107.47	116.65	124.30
0.0378	82.61	93.20	101.68	110.15	118.09
0.0467	80.60	91.10	98.81	106.53	113.82
0.0567	78.20	88.97	95.50	102.03	108.03
0.0640	77.14	86.98	93.22	99.47	105.40

0.0713	76.54	85.79	91.54	97.28	102.75
0.0755	75.86	84.86	90.82	96.78	102.47
0.0809	75.00	84.27	89.83	95.39	100.71
0.0850	74.85	84.26	90.14	94.97	100.15
0.0881	75.35	84.43	89.53	94.64	99.18
0.0906	75.68	84.73	90.36	95.32	98.85
(BTEACl+SCyt+H_2O) system, W_1=0.001					
0.0000	-	-	-	-	-
0.0103	98.06	112.62	125.24	136.31	145.05
0.0261	86.05	96.00	105.18	113.75	121.39
0.0378	81.55	90.82	99.56	106.18	115.55
0.0467	79.95	88.31	96.24	103.83	110.90
0.0567	78.55	87.56	94.79	102.56	109.62
0.0640	78.08	87.60	95.57	101.81	108.37
0.0713	77.24	86.35	93.36	101.07	107.66
0.0755	77.18	85.53	93.60	101.47	106.71
0.0809	76.98	84.89	92.55	100.01	107.18
0.0850	76.49	84.97	93.20	99.44	107.09
0.0881	76.37	84.20	91.80	99.23	106.37
0.0906	76.02	84.29	92.34	99.40	107.13
(BTEACl+SBz+H_2O) system, W_1=0.003					
0.0000	-	-	-	-	-
0.0103	110.68	122.33	131.84	140.29	147.67
0.0261	90.64	101.35	111.22	120.67	129.69
0.0378	85.26	94.79	103.74	112.40	120.77
0.0467	83.17	91.53	99.41	106.75	114.16
0.0567	80.49	88.44	95.68	102.56	110.96
0.0640	77.76	85.73	92.76	100.80	108.07
0.0713	76.68	85.51	92.24	100.37	106.68
0.0755	76.26	84.33	92.81	100.09	106.18
0.0809	75.62	84.27	90.82	98.98	106.02
0.0850	75.43	84.14	91.20	98.97	106.03
0.0881	74.78	84.54	90.90	98.95	105.42
0.0906	74.80	83.96	90.69	99.40	105.69

Table S15. Molar conductivities of (BTEACl+SBz+H_2O) and (BTEACl+SCyt+H_2O) systems in aqueous BTEACl solutions of mass fractions W_1=0.001, W_2=0.003, W_3=0.005, at 298.15 K, 303.15 K, 308.15 K, 313.15 K and 318.15 K.

(BTEACl+SCyt+H_2O) system, W_1=0.003					
	Molar conductivities ($S\ cm^2\ mol^{-1}$)				
Molarity (moles/litre)	**298.15K**	**303.15K**	**308.15K**	**313.15K**	**318.15K**
0.0000	-	-	-	-	-

0.0103	112.62	127.18	136.89	144.66	151.46
0.0261	91.79	101.74	110.53	118.56	126.21
0.0378	87.11	96.38	104.32	111.74	118.89
0.0467	84.88	93.24	100.96	108.25	115.32
0.0567	81.73	90.73	99.38	106.27	113.86
0.0640	80.42	89.95	97.75	105.25	112.59
0.0713	79.34	88.45	96.72	103.17	111.58
0.0755	79.44	87.78	95.32	102.60	109.75
0.0809	78.83	86.74	94.16	101.32	108.37
0.0850	78.26	86.73	93.44	99.91	106.27
0.0881	78.07	85.90	92.94	99.75	106.44
0.0906	77.67	85.94	92.23	98.96	105.47
(BTEACl+SBz+H_2O) system, W_1=0.005					
0.0000	-	-	-	-	-
0.0103	136.89	151.46	162.14	171.84	180.58
0.0261	100.97	112.83	118.56	123.92	128.89
0.0378	93.20	103.53	109.62	115.45	121.01
0.0467	88.74	97.74	105.25	110.82	117.46
0.0567	85.79	95.50	100.26	104.85	112.27
0.0640	83.85	92.29	99.16	104.31	110.40
0.0713	81.58	90.84	97.14	101.91	107.94
0.0755	80.63	90.95	96.12	101.15	106.05
0.0809	77.85	89.96	94.53	98.98	103.30
0.0850	78.61	89.20	93.67	98.03	102.27
0.0881	78.19	88.74	93.28	97.71	102.02
0.0906	78.22	87.71	92.89	97.20	101.94
(BTEACl+SCyt+H_2O) system, W_1=0.005					
0.0000	-	-	-	-	-
0.0103	137.86	148.54	159.22	168.93	177.67
0.0261	103.65	109.77	120.86	131.57	141.89
0.0378	93.73	101.15	112.27	121.27	130.54
0.0467	90.46	97.96	106.75	115.32	123.68
0.0567	87.56	94.26	103.97	112.62	121.09
0.0640	85.26	92.76	101.19	109.46	117.58
0.0713	83.69	91.40	100.37	108.22	116.63
0.0755	82.08	90.42	98.63	106.71	114.65
0.0809	81.92	89.46	97.74	105.90	113.93
0.0850	81.44	88.61	97.09	105.44	113.68
0.0881	81.02	88.51	96.91	105.19	113.37
0.0906	80.76	87.93	95.98	104.48	112.75

Table S16. Molar conductivities of (BTMACl+SBz+H_2O) and (BTMACl+SCyt+H_2O) systems in aqueous BTMACl solution of mass fractions W_1=0.001, W_2=0.003, W_3=0.005, at 298.15 K, 303.15 K, 308.15 K, 313.15 K and 318.15 K.

(BTMACl+SBz+H_2O) system, W_1=0.001					
	Molar conductivities (S cm^2 mol^{-1})				
Molarity (moles/litre)	298.15K	303.15K	308.15K	313.15K	318.15K
0.0000	-	-	-	-	-
0.0103	84.56	95.24	95.24	100.00	104.85
0.0261	80.32	90.64	90.64	95.23	99.44
0.0378	77.85	88.70	88.70	92.94	97.44
0.0467	76.52	87.45	87.45	92.17	96.67
0.0567	75.20	86.32	86.32	91.09	96.03
0.0640	74.33	85.42	85.42	90.73	95.72
0.0713	74.01	84.81	84.81	90.28	95.60
0.0755	73.74	84.73	84.73	90.03	95.19
0.0809	73.52	84.52	84.52	89.83	95.02
0.0850	73.55	84.26	84.26	89.44	94.73
0.0881	73.42	84.43	84.43	89.76	94.75
0.0906	73.48	84.29	84.29	89.36	94.44
(BTMACl+SCyt+H_2O) system, W_1=0.001					
0.0000	-	-	-	-	-
0.0103	96.12	106.80	116.50	125.24	133.98
0.0261	87.58	97.15	106.33	115.12	123.54
0.0378	83.94	93.73	103.27	112.00	121.01
0.0467	81.24	91.74	102.03	111.03	119.82
0.0567	79.61	89.85	99.91	109.62	118.45
0.0640	77.92	89.16	99.47	109.00	118.21
0.0713	77.24	87.89	98.41	107.80	117.47
0.0755	77.18	87.51	97.71	107.50	116.90
0.0809	76.24	86.37	96.38	106.27	116.03
0.0850	76.26	86.14	95.91	105.56	115.09
0.0881	75.80	85.79	95.66	105.42	115.07
0.0906	75.46	85.39	95.21	104.92	114.52
(BTMACl+SBz+H_2O) system, W_1=0.003					
0.0000	-	-	-	-	-
0.0103	113.59	118.50	122.43	127.18	131.94
0.0261	92.56	96.00	99.06	102.88	106.71
0.0378	87.11	90.56	93.73	96.38	99.02
0.0467	85.31	88.42	91.31	93.78	96.24
0.0567	82.44	86.14	89.67	91.97	94.26
0.0640	81.51	84.56	87.45	90.02	92.60
0.0713	79.76	83.20	86.49	89.50	92.52
0.0755	79.44	82.74	85.92	88.83	91.74
0.0809	78.83	82.36	85.75	88.90	92.05
0.0850	78.26	82.08	85.79	89.26	92.73
0.0881	77.85	81.59	85.22	88.63	92.03
0.0906	77.67	81.42	85.06	88.48	91.90

Table S17. Molar conductivities of (BTMACl+SBz+H_2O) and (BTMACl+SCyt+H_2O) systems in aqueous BTMACl solution of mass fractions W_1=0.001, W_2=0.003, W_3=0.005, at 298.15 K, 303.15 K, 308.15 K, 313.15 K and 318.15 K.

(BTMACl+SCyt+H_2O) system, W_1=0.003					
	Molar conductivities ($S\ cm^2\ mol^{-1}$)				
Molarity (moles/litre)	298.15K	303.15K	308.15K	313.15K	318.15K
0.0000	-	-	-	-	-
0.0103	117.48	130.10	141.75	152.33	162.70
0.0261	94.47	105.56	116.27	126.56	136.76
0.0378	88.97	99.03	108.83	118.33	127.78
0.0467	86.60	96.67	106.53	116.16	124.45
0.0567	84.38	94.62	104.68	113.49	122.33
0.0640	83.70	93.07	102.28	111.32	119.86
0.0713	82.43	91.54	100.51	109.33	118.11
0.0755	81.95	90.95	99.82	108.55	117.24
0.0809	81.68	89.96	98.11	106.13	114.86
0.0850	81.32	89.56	97.68	105.67	113.63
0.0881	81.14	89.08	96.91	104.62	112.30
0.0906	80.76	88.81	96.76	104.58	112.38
(BTMACl+SBz+H_2O) system, W_1=0.005					
0.0000	-	-	-	-	-
0.0103	130.10	146.60	162.14	176.60	189.92
0.0261	96.76	106.33	115.50	124.26	132.57
0.0378	88.97	96.38	103.53	110.39	116.93
0.0467	85.95	94.53	101.39	108.46	114.03
0.0567	82.61	91.09	99.38	106.09	112.44
0.0640	80.73	88.70	96.50	104.14	111.59
0.0713	78.92	86.63	94.20	102.05	110.04
0.0755	78.11	86.19	94.13	101.93	109.57
0.0809	77.85	85.63	93.29	100.82	108.20
0.0850	77.43	85.20	92.85	100.37	107.75
0.0881	76.48	84.20	91.80	99.28	106.63
0.0906	76.35	84.07	91.68	99.17	106.53
(BTMACl+SCyt+H_2O) system, W_1=0.005					
0.0000	-	-	-	-	-
0.0103	135.92	150.49	164.08	176.70	188.35
0.0261	100.97	112.83	124.30	135.39	146.10
0.0378	94.53	103.80	112.80	121.54	130.01
0.0467	91.10	100.10	108.89	117.46	125.82
0.0567	88.08	96.73	105.21	113.50	121.62
0.0640	86.98	94.63	102.13	111.65	119.15
0.0713	84.95	93.64	102.19	110.60	118.87
0.0755	84.20	92.81	101.28	109.62	117.83

0.0809	83.28	91.69	99.96	108.12	116.15
0.0850	83.08	91.32	99.44	107.44	115.33
0.0881	82.84	91.35	99.75	108.03	116.20
0.0906	82.52	90.80	98.96	107.02	114.96

Table S18. UV-vis spectroscopic data for the Benesi-Hildebrand double reciprocal plot of (BTEACl+SBz) system at 298.15 K[b].

BTEACl+SBz										
Temp (K[a])	[SBz] (μM)	BTEACl (μM)	Ao	A	ΔA	1/[BTEACl] (M^{-1})	1/ΔA	Intercept	Slope	Ka/ $M^{-1}\times10^{-3}$
298.15	50	10	0.3169	0.3313	0.0144	0.1000	69.6258	1.82	674.03	2.70
	50	20	0.3169	0.3453	0.0284	0.0500	35.1999			
	50	30	0.3169	0.3621	0.0451	0.0333	22.1537			
	50	40	0.3169	0.3651	0.0481	0.0250	20.7731			
	50	50	0.3169	0.3875	0.0706	0.0200	14.1725			
	50	60	0.3169	0.3927	0.0757	0.0167	13.2032			
	50	70	0.3169	0.3963	0.0794	0.0143	12.5994			
	50	80	0.3169	0.4145	0.0976	0.0125	10.2502			
	50	90	0.3169	0.4273	0.1104	0.0111	9.0605			

Table S19. UV-vis spectroscopic data for the Benesi-Hildebrand double reciprocal plot of (BTEACl+Scyt) system at 298.15 K[b].

BTEACl+Scyt										
Temp (Ka)	[SCyt] (μM)	BTEACl (μM)	Ao	A	ΔA	1/[BTEACl] (M^{-1})	1/ΔA	Intercept	Slope	Ka/ $M^{-1}\times10^{-3}$
298.15	50	10	0.1851	0.1959	0.0109	0.1000	92.1192	2.981	899.9	3.31
	50	20	0.1851	0.2049	0.0199	0.0500	50.3117			
	50	30	0.1851	0.2162	0.0312	0.0333	32.0935			
	50	40	0.1851	0.2256	0.0406	0.0250	24.6442			
	50	50	0.1851	0.2306	0.0455	0.0200	21.9599			
	50	60	0.1851	0.2345	0.0495	0.0167	20.2071			

	50	70	0.1851	0.2545	0.0695	0.0143	14.3911			
	50	80	0.1851	0.2591	0.0740	0.0125	13.5084			
	50	90	0.1851	0.2673	0.0822	0.0111	12.1601			

Table S20. UV-vis spectroscopic data for the Benesi-Hildebrand double reciprocal plot of (BTMACl+SBz) system at 298.15 K[b].

BTMACl+SBz										
Temp (Ka)	**[SBz] (μM)**	**BTMACl (μM)**	**Ao**	**A**	**ΔA**	**1/[BTMACl] (M^{-1})**	**1/ΔA**	**Intercept**	**Slope**	**Ka/ $M^{-1}\times10^{-3}$**
298.15	50	10	0.3169	0.3317	0.0148	0.1000	67.7392	2.02	661.15	3.05
	50	20	0.3169	0.3447	0.0278	0.0500	35.9594			
	50	30	0.3169	0.3569	0.0399	0.0333	25.0381			
	50	40	0.3169	0.3738	0.0568	0.0250	17.5966			
	50	50	0.3169	0.3883	0.0714	0.0200	14.0136			
	50	60	0.3169	0.3935	0.0765	0.0167	13.0652			
	50	70	0.3169	0.3971	0.0802	0.0143	12.4736			
	50	80	0.3169	0.4153	0.0984	0.0125	10.1668			
	50	90	0.3169	0.4261	0.1092	0.0111	9.1601			

Table S21. UV-vis spectroscopic data for the Benesi-Hildebrand double reciprocal plot of (BTMACl+Scyt) system at 298.15 K[b].

BTMACl+Scyt										
Temp (Ka)	**[SCyt] (μM)**	**BTMACl (μM)**	**Ao**	**A**	**ΔA**	**1/[BTMACl] (M^{-1})**	**1/ΔA**	**Intercept**	**Slope**	**Ka/ $M^{-1}\times10^{-3}$**
298.15	50	10	0.1851	0.1965	0.0114	0.1000	87.7262	3.1654	860.01	3.68
	50	20	0.1851	0.2050	0.0199	0.0500	50.1726			
	50	30	0.1851	0.2181	0.0331	0.0333	30.2556			
	50	40	0.1851	0.2268	0.0417	0.0250	23.9771			
	50	50	0.1851	0.2310	0.0460	0.0200	21.7533			

	50	60	0.1851	0.2366	0.0515	0.0167	19.4071			
	50	70	0.1851	0.2568	0.0717	0.0143	13.9475			
	50	80	0.1851	0.2623	0.0772	0.0125	12.9497			
	50	90	0.1851	0.2713	0.0863	0.0111	11.5940			

FIGURES

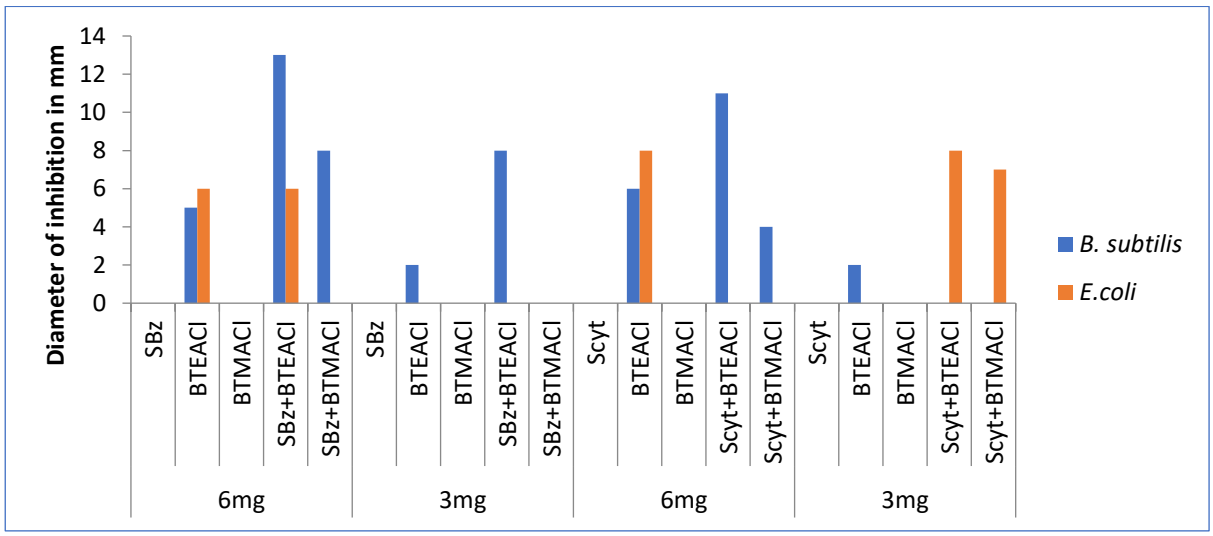

Figure 1: Graphical presentation of Well diffusion assay (Diameter of inhibition in mm) of Scyt and SBz, singly and in combination with IL1 (BTEACl) and IL2 (BTMACl) applied to B. subtilis and E. coli.

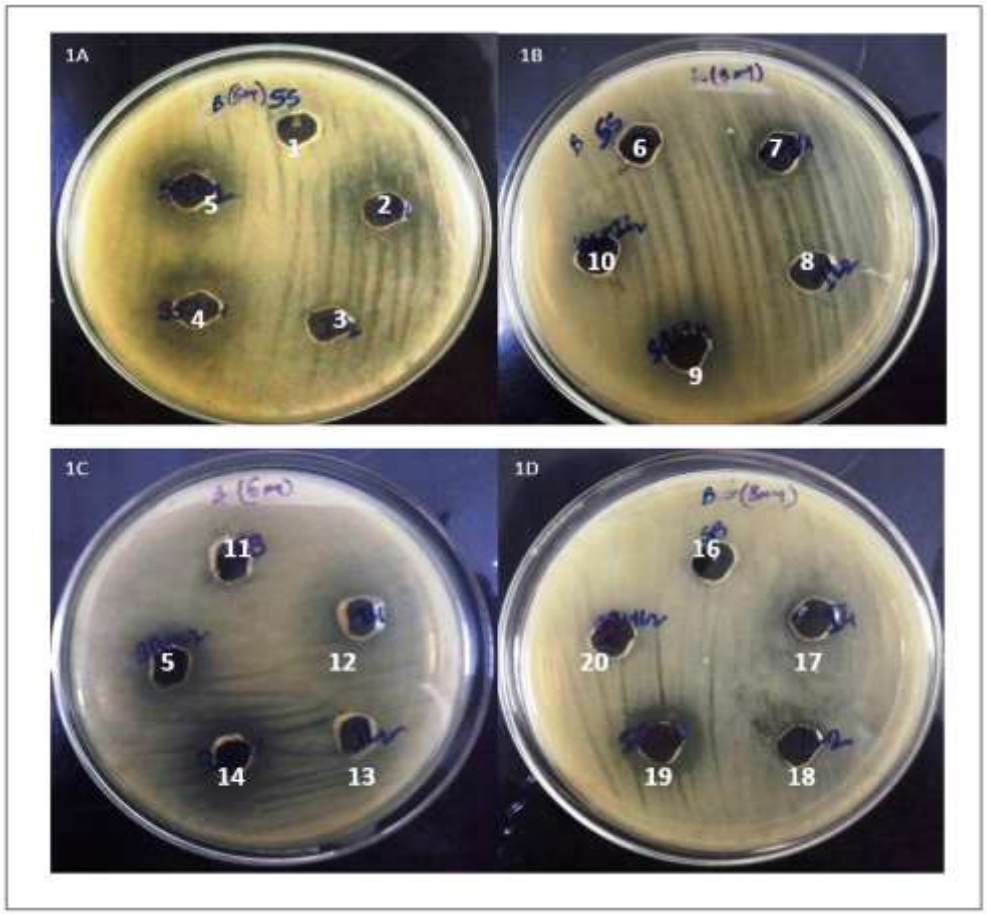

Figure 2: Well diffusion assay of Scyt and SBz, singly and in combination with IL1 (BTEACl) and IL2 (BTMACl).

Plate 1A-B shows susceptibility of *B. subtilis* towards Scyt in combination with IL1 (BTEACl) and IL2 (BTMACl) **where,** Well 1 contains 6 mg of SS (Scyt), Well 2 contains 6 mg IL1 (BTEACl), Well 3 contains 6mg IL2 (BTMACl), Well 4 contains 6mg SS (Scyt) and 6mg IL1 (BTEACl), Well 5 contains 6mg SS (Scyt) and 6mg IL2 (BTMACl), Well 6 contains 3 mg of SS (Scyt), Well 7 contains 3 mg IL1 (BTEACl), Well 8 contains 3 mg IL2 (BTMACl), Well 9 contains 3 mg SS (Scyt) and 3 mg IL1 (BTEACl), Well 10 contains 3mg SS (Scyt) and 3mg IL2 (BTMACl)

Plate 1C-D shows susceptibility of *B. subtilis* towards SBz in combination with IL1 (BTEACl) **and IL2 (BTMACl)where,** Well 11 contains 6 mg of SB (SBz), Well 12 contains 6 mg IL1 (BTEACl), Well 13 contains 6mg IL2 (BTMACl), Well 14 contains 6mg SB (SBz) and 6mg IL1 (BTEACl), Well 15 contains 6mg SB (SBz) and 6mg IL2 (BTMACl), Well 16 contains 3 mg of SB (SBz), Well 17 contains 3 mg IL1 (BTEACl), Well 18

contains 3 mg IL2 (BTMACl), Well 19 contains 3 mg SB (SBz) and 3 mg IL1 (BTEACl), Well 20 contains 3mg SB (SBz) and 3mg IL2 (BTMACl).

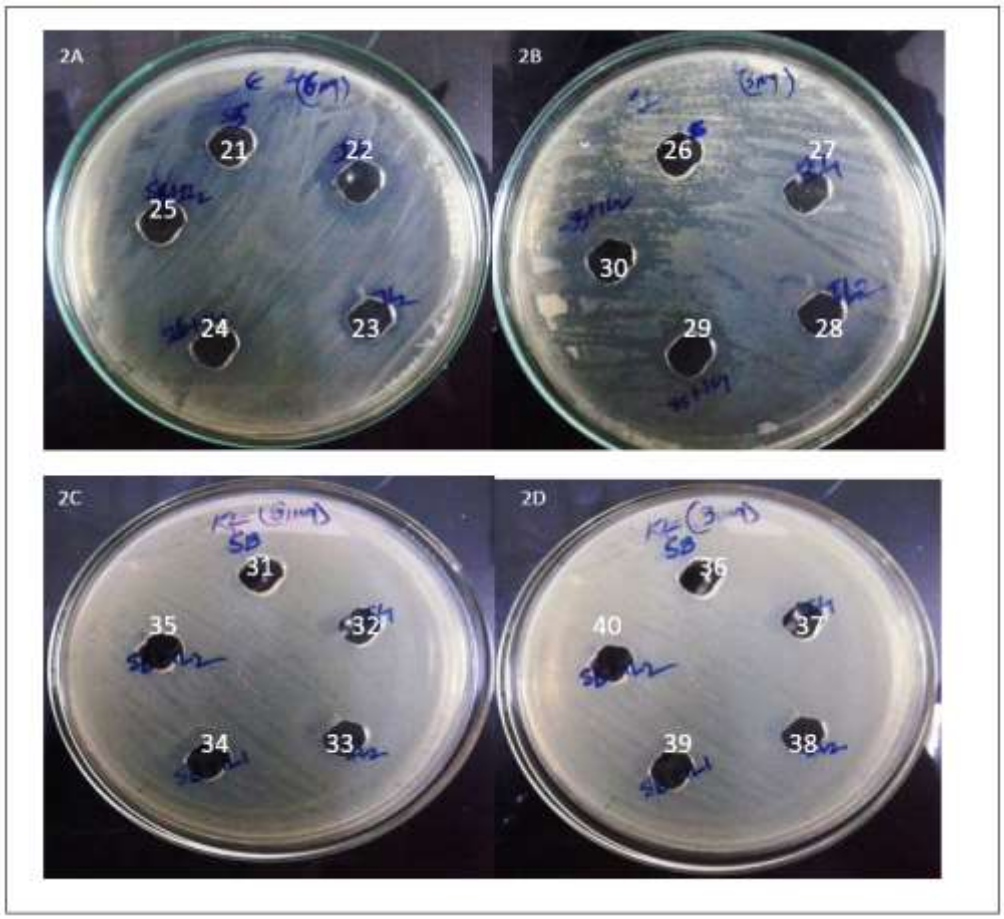

Figure 3: Well diffusion assay of Scyt and SBz, singly and in combination with IL1 (BTEACl) and IL2 (BTMACl).

Plate 2A-B shows susceptibility of *E. coli* towards Scyt in combination with IL1 (BTEACl) and IL2 (BTMACl)where, Well 21 contains 6 mg of SS (Scyt), Well 22 contains 6 mg IL1 (BTEACl), Well 23 contains 6mg IL2 (BTMACl), Well 24 contains 6mg SS (Scyt) and 6mg IL1 (BTEACl), Well 25 contains 6mg SS (Scyt) and 6mg IL2 (BTMACl), Well 26 contains 3 mg of SS (Scyt), Well 27 contains 3 mg IL1 (BTEACl), Well 28 contains 3 mg IL2 (BTMACl), Well 29 contains 3 mg SS (Scyt) and 3 mg IL1 (BTEACl), Well 30 contains 3mg SS (Scyt) and 3mg IL2 (BTMACl)

Plate 2C-D shows susceptibility of *E.coli* towards SBz in combination with IL1 (BTEACl) and IL2 (BTMACl) where, Well 31 contains 6 mg of SB (SBz), Well 32 contains 6 mg IL1 (BTEACl), Well 33 contains 6mg IL2 (BTMACl), Well 34 contains 6mg

SB (SBz) and 6mg IL1 (BTEACl), Well 35 contains 6mg SB (SBz) and 6mg IL2 (BTMACl), Well 36 contains 3 mg of SB (SBz), Well 37 contains 3 mg IL1 (BTEACl), Well 38 contains 3 mg IL2 (BTMACl), Well 39 contains 3 mg SB (SBz) and 3 mg IL1 (BTEACl), Well 40 contains 3mg SB (SBz) and 3mg IL2 (BTMACl).

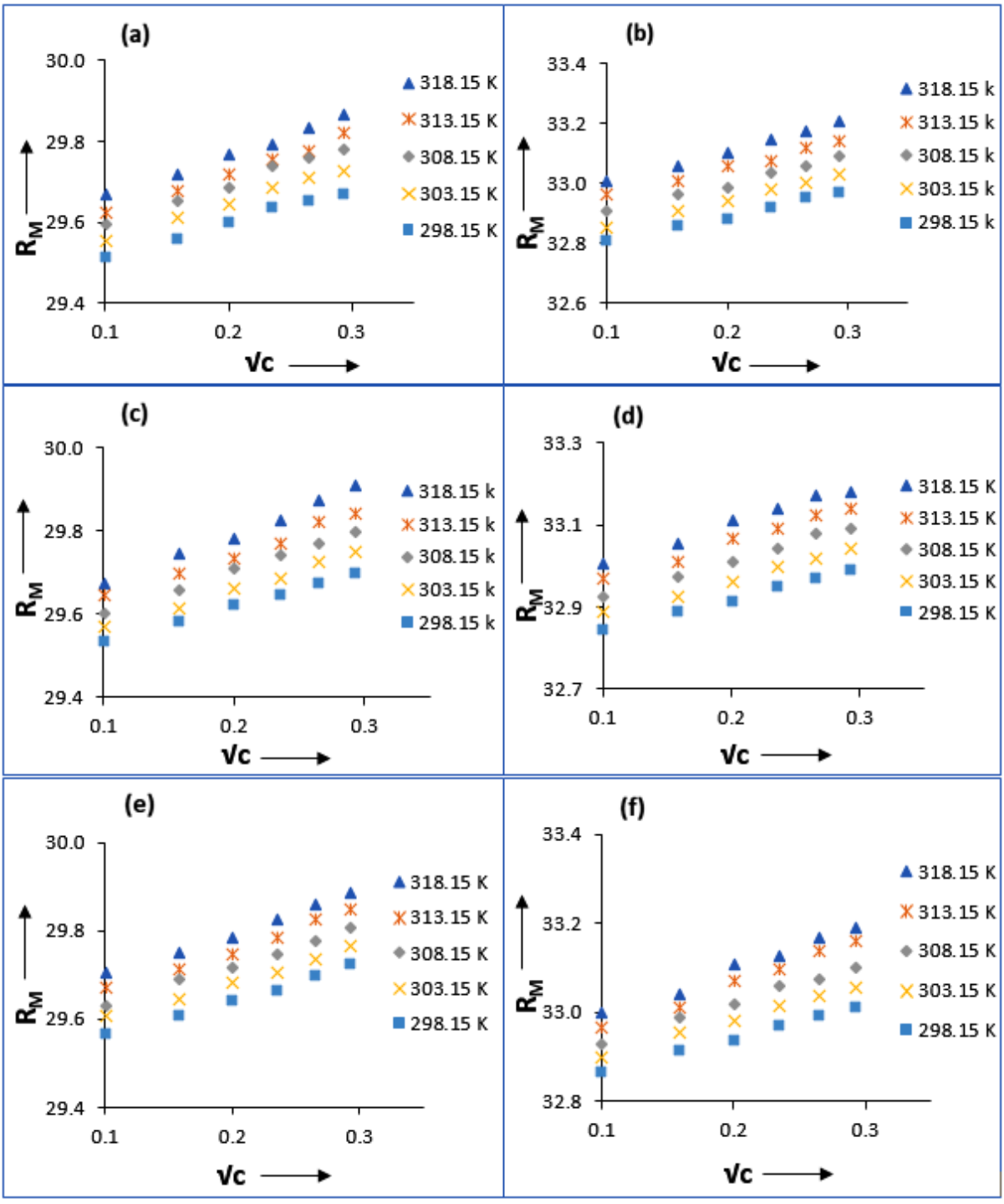

Figure 4. (a,b,c,d,e,f) Plot of (R_M) Vs √c for (BTEACl+SBz+H_2O), (BTEACl+SCyt+H_2O) systems in aqueous BTEACl solutions of mass fractions (a, b) W_1=0.001, (c, d)

W_2=0.003, (e, f) W_3=0.005respectively at 298.15 K, 303.15 K, 308.15 K, 313.15 K and 318.15 K.

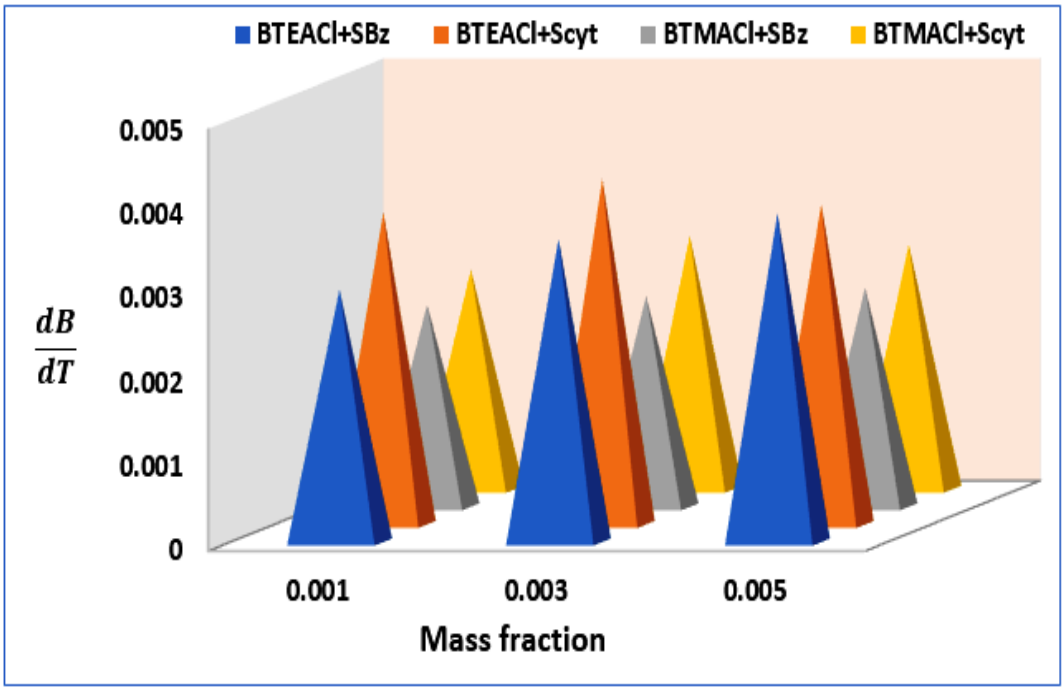

Figure 5. Variation of $\frac{dB}{dT}$ with the mass fraction of BTEACl and BTMACl separately at their four different combinations, BTEACl+SBz, BTEACl+Scyt, BTMACl+SBz, BTMACl+Scyt.

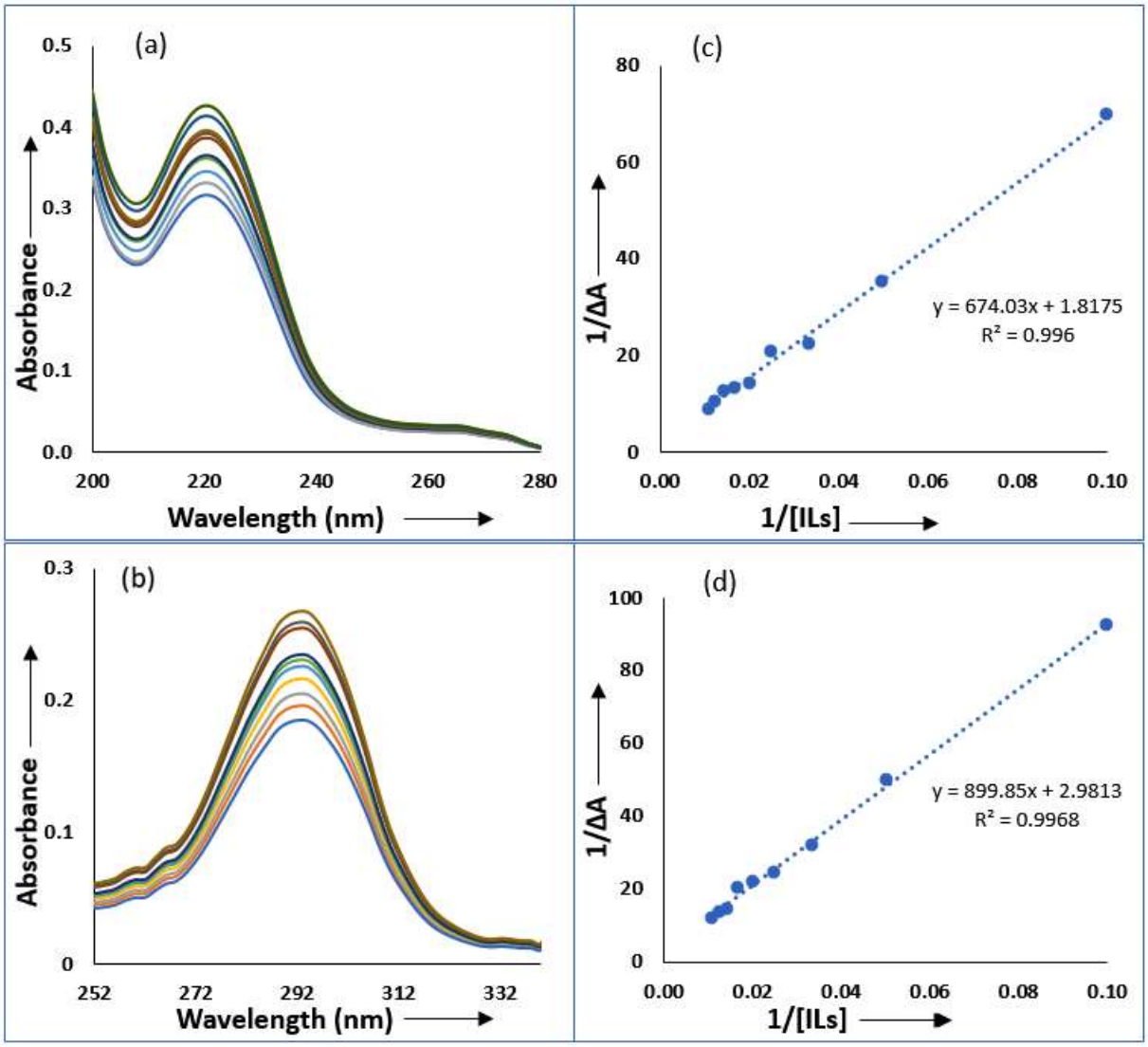

Figure 6 (a, b, c, d) Spectra for the generation of Benesi-Hildebrand double reciprocal plot of (a) BTEACl+SBz, (b) BTEACl+Scyt systems and corresponding Benesi-Hildebrand double reciprocal plot of (c) BTEACl+SBz, (d) BTEACl+Scyt systems.

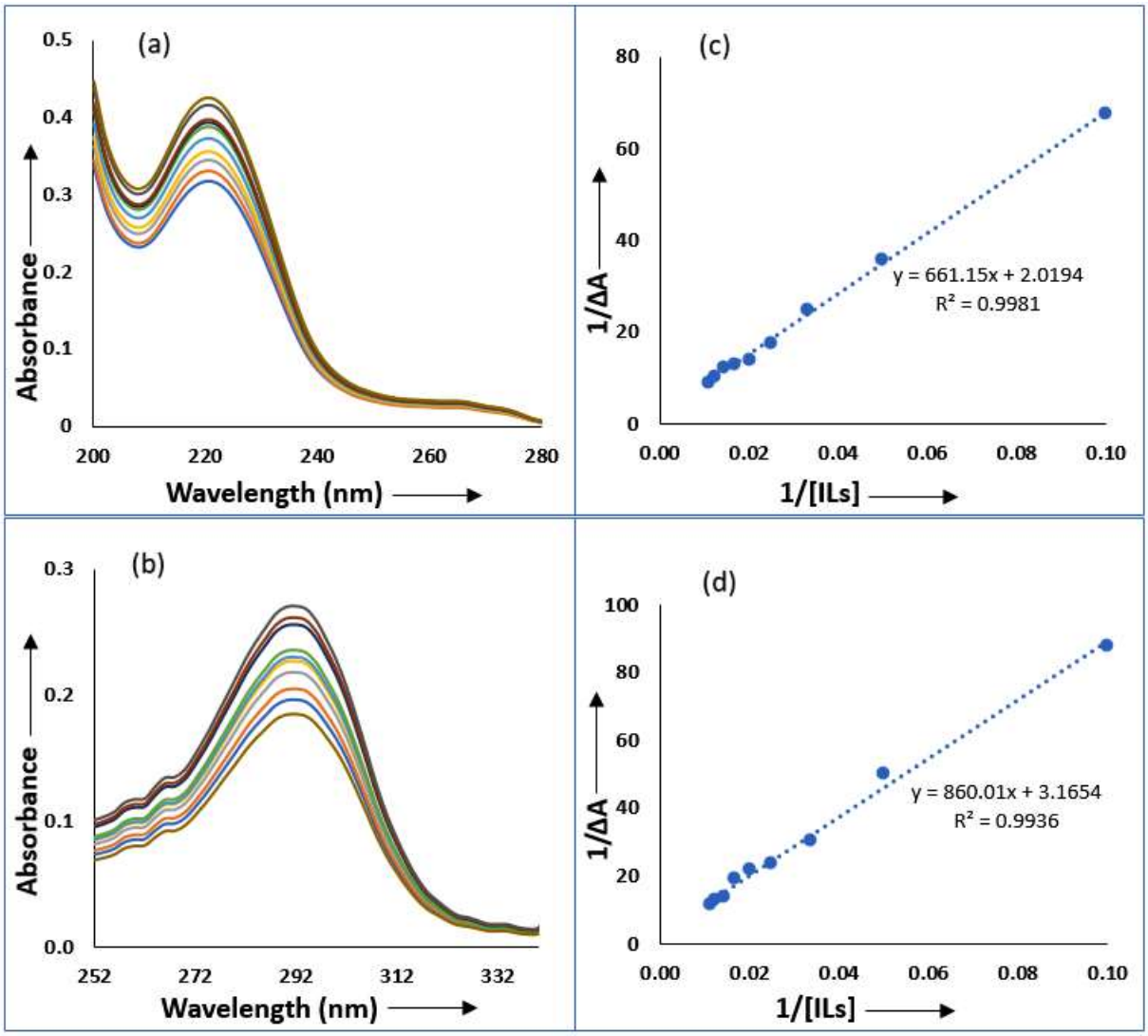

Figure 7 (a, b, c, d) Spectra for the generation of Benesi-Hildebrand double reciprocal plot of (a) BTMACl+SBz, (b) BTMACl+Scyt systems and corresponding Benesi-Hildebrand double reciprocal plot of (c) BTMACl+SBz, (d) BTMACl+Scyt systems.

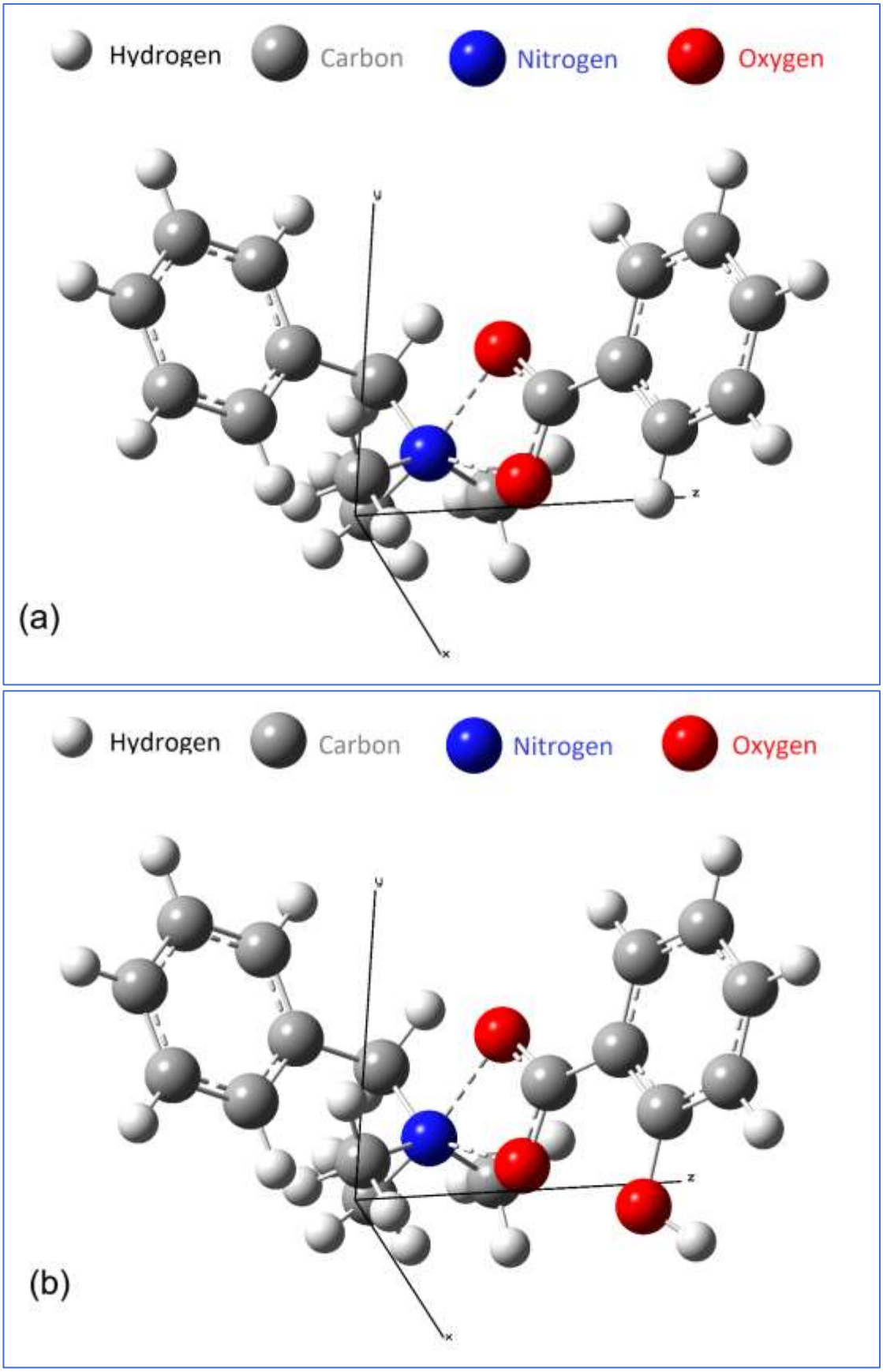

Figure 8 (a,b): Optimised geometry of (a) BTMACl+SBz and (b) BTMACl+Scyt systems.

SCHEMES

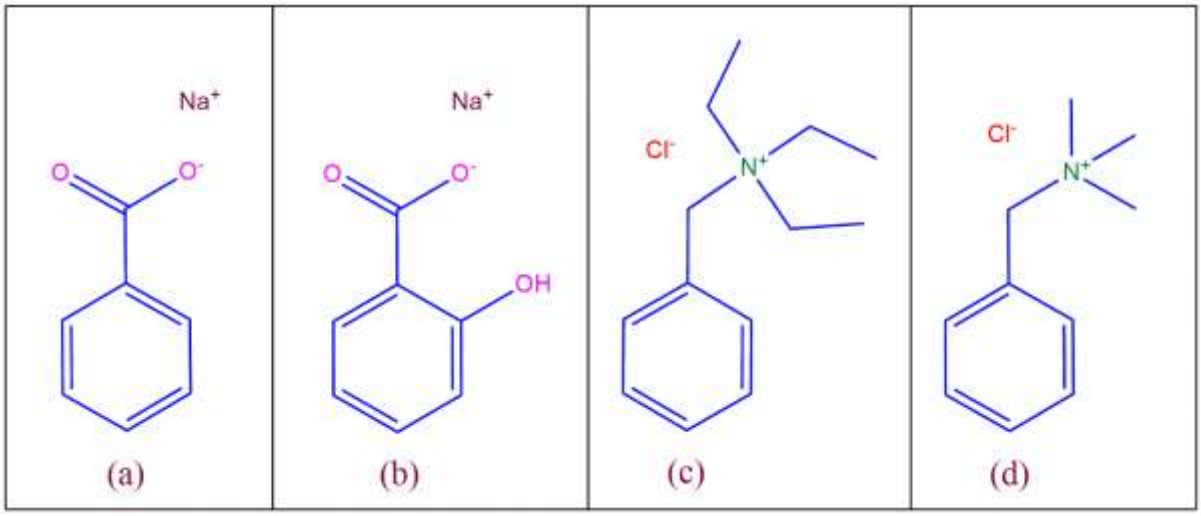

Scheme 1: The molecular structure of (a) Sodium benzoate, (b) Sodium salicylate, (c) Benzyltriethylammoniun chloride, (d) Benzyltrimethylammonium chloride.

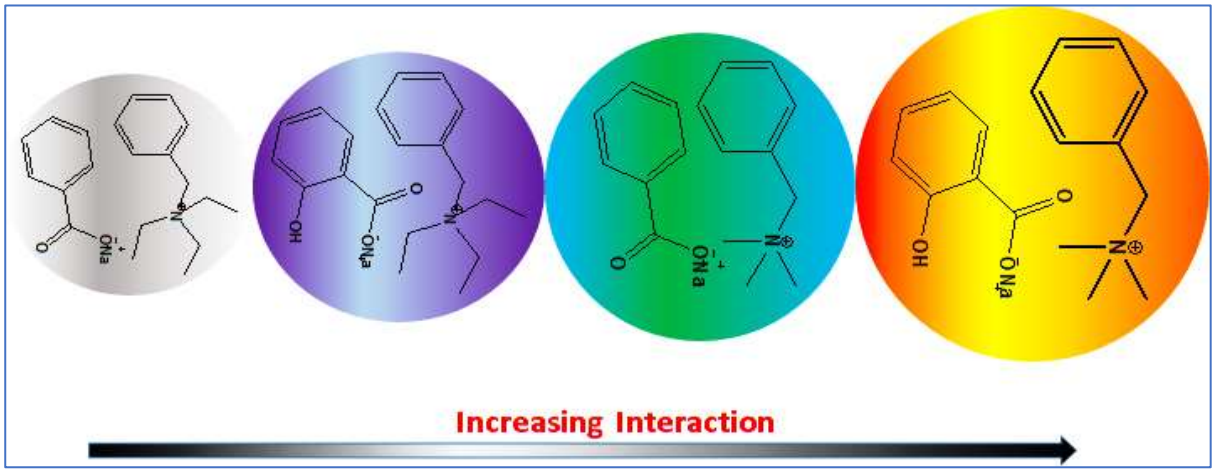

Scheme 2: Schematic representation of molecular interactions taking place between the FPs and ILs interaction in solution.

CHAPTER IX

CONCLUDING REMARKS

In this thesis I investigated the formation of host guest inclusion complexes of various biomolecules, vitamins, drugs, water pollutant with α and β-cyclodextrins exploring particularly towards their formation, stabilisation, solubility, bioavailability, bio degradability, fire resistivity and HSA assisted controlled release without chemical modification by various dependable methods like ^{1}H NMR, 2D ROESY, FTIR spectroscopy, UV-Visible spectroscopy, Fluorescence spectroscopy, Differential Scanning Calorimetry, Scanning Electron microscopy, Powder X-Ray Diffraction, High Resolution Mass Spectroscopy, Surface tension, Conductivity, which primarily focus on the encapsulation of the guest molecules into the cavity of cyclodextrins. The stoichiometry, association constant and thermodynamic parameters for the inclusion complexes have been determined to communicate a quantitative data regarding the encapsulation of the biomolecules inside into cyclodextrins.

This thesis also includes exploration of food preservatives-ionic liquids interactions in solution phase by means of various physicochemical parameters obtained from density, viscosity, Refractive index and conductivity studies. The antimicrobial activities of the mixture of the solutions were done with some gram-positive and gram-negative bacteria and the food preservatives-ionic liquids interactions were found synergistic towards the microbial activity

The findings are discussed chapter wise as follows –

Chapter IV: The suggestion obtained from surface tension and conductometric study for the formation of 1:1 host-guest inclusion complexes of SNP and PEH with α and β-cyclodextrins are established by UV-vis spectroscopy, spectrofluorimetry, 2D ROESY NMR spectrometry and SEM technique by analyzing surface texture of the solid inclusion complexes. The association constants obtained from all the well-established techniques dictates the stability of inclusion complexes formed and the thermodynamic parameters reveals truth about the feasibility of their formation. Removal of water molecules from the cavity of the CDs to make room for the guest molecule for accommodation while formation of inclusion complex, increases entropy of the process. Dimensional suitability being, one of the major stabilizing factor, the

larger cavity size of β-CD (0.70 nm, diameter) compared to α-CD (0.56 nm, diameter), explains for the greater value of association constants and stability of the inclusion complexes formed with β-CD. The association constants, hence stability of the inclusion complexes of SNP with CDs were found more than that of the PEH. Because, -O-H group of SNP, being oriented to the para position may exert H-bonding interaction with CDs to some greater extent than that of the PEH, in which –OH group, being oriented at the meta – position can't travel the minimum distance for the formation H-bond with the CDs. The hydrophobic and H-bonding interactions thus stabilizes the ICs. The Cytotoxicity and Cell viability also balances for non-toxic behavior of the ICs. Thus, inclusion complexes of the recently emerging two drugs, SNP and PEH (after their banned alternatives) stabilizes SNP and PEH from their chemical modification and conveys a new approach for regulatory release to the targeted site reducing overdoses.

Chapter V: 1:1 host-guest inclusion complexes of THC within the cavity of α and β-CD are well established by the various techniques in solution phase as well as in the solid state. The entire inclusion process is thermodynamically feasible process as obtained from the calculated thermodynamic parameters and evaluated association constants reveal the stability of the formation of ICs. Molecular recognition due to the dimensional suitability is the major stabilizing factor. The positive entropy factor is also responsible for the formation of ICs via non-covalent interactions such as hydrogen bonding and other hydrophobic interactions as more number of water molecules compare to that of THC molecule are released from the cavity of the CDs for making the free suitable space for the incoming THC molecule. Formation of inclusion complexes enhances the photochemical stability of THC, protect it from thermal degradation and retain its property without any kind of chemical transformation. Moreover, the regulatory dischargement of THC molecule at pH 7.4 from the hydrophobic cavity to the polar aqueous media has been clearly explained in the presence of HSA molecule. So, there is a strong probability to show similar kind of binding behavior of THC with HSA in the human body and successfully will be delivered to the targeted area as per required amount of it. Hence the study for the formation of inclusion complex and the regulatory dischargement of THC from the hydrophobic cavity of CDs into the aqueous solution approach a novel way for the versatile uses and formulation in food, medicinal and pharmaceutical industries without any chemical

modification. In conclusion, this article demands far reaching effects by dint of innovative applications in pharmaceutical science.

Chapter VI: In this novel study the inclusion complexation of a non-biodegradable pollutant (HBCDD) with β-CD and HP-β-CD were synthesized and characterized to retain its fire resistance property and to convert it into bio-degradable molecule. Various spectroscopic and thermal studies have been performed to establish this fact. The stoichiometry of the two complexes has been found as 1:1 molar ratio of host and guest molecules. Surface texture properties of the inclusion complexes were studied by SEM and the presence of bromine in the complexes were evidenced by EDXS. The melting point analysis indicates that the inclusion complexes are more stable than HBCDD and hence ICs are preferred to HBCDD. The aqueous solubility of the inclusion complexes demonstrates that the inclusion complexes are more bio-available to the microorganism and thus evidently inclusion complexation of HBCDD converts it into biodegradable material making them eco-friendly in nature and minimizes the environmental pollution.

Chapter VII: All the experiments suggest the successful formation of inclusion complex with 2:1 stoichiometry. The association constants of the inclusion complexes of ALVC formed with β-cyclodextrin were found greater than that of the inclusion complexes formed with the α-cyclodextrin and hence more stable, this is may be due to the better fitness of the guest molecule into the larger hydrophobic cavity of β-cyclodextrin compared to the α-cyclodextrin. The ready availability of the association constants enables us to calculate the thermodynamic parameters of the inclusion process which makes the thermodynamic background of the process and recognise it as a thermodynamically feasible process. When the guest molecule gets encapsulated into the hydrophobic cavity of cyclodextrin molecule, the water molecules removed from the hydrophobic cavity of cyclodextrin molecule increases the entropy of the process. Thus, the hydrophobic-hydrophobic interaction and entropy factor would become the driving forces for the formation of inclusion complexes. The binding constant of ALVC to the HSA become appreciable showing an affinity of HSA towards the drug molecule. Thus, it is expected that, the drug molecule gets released from the inclusion complex and binds successfully with the HSA which then get transported to the targeted site

promoting regulatory release consequently reduces overdoses without any chemical modification.

Chapter VIII: The motive to reduce unnecessarily-excessive use of food preservative in the preservation of food is reached, since antimicrobial activity of SBz and Scyt studied herewith, in all possible combination with the BTEACl and BTMACl reveal synergistic to kill micro-organisms and found to act properly below their reported MICs. The physico-chemical methodologies, describes the mode of interaction between the FPs and ILs in solution. Calculation of apparent molar volume, limiting apparent molar volume, molar refraction, limiting molar refraction and viscosity B coefficient makes possible to identify the interaction as predominant solute – solvent interaction. The values of $(\delta\phi_E^0/\delta T)_P$ and (dB/dT) have been calculated to provide the information that, the solute – solvent interaction is structure making. Association constants, optimisation energy and free energy changes for the molecular assembly grown in solution assorted by structure making solute – solvent interaction dictate their stability in solution and consequently, the order of synergism between them. Thus, solution chemistry for all the possible combinations explores the chemistry behind the synergism. This makes one easy to choose a mixture of compounds such that their combination would arise synergistic. Nevertheless, the synergistic combination of food preservatives reduces the level of hazardous food preservative, which is used to stop spoilage of foods produced worldwide and makes the world health, safe. So, the study of microbial activity along with solution chemistry would be a great interest in the field of food chemistry for their preservation.

My research may be justified by the following novel outcomes -

- All the studies supports successfully the formation of inclusion complexes.
- Van der waals forces gives the stability to the inclusion complexes. Sometimes H-bonding interaction gives the extra stability to the inclusion complexes.
- Enhances solubility, bio-avalability, fire returdacy and biodegradability of the inclusion complexes.
- HSA assists the guest molecules to come out form the inclusion complexes.
- Food preservatives-ionic liquids interactions were found synergistic towards antimicrobial effect.

BIBLIOGRAPHY

CHAPTER I

1 Friedman, S. H. Functional Synthetic Receptors Edited by Thomas Schrader (Philipps-Universität Marburg) and Andrew D. Hamilton (Yale University). Wiley-VCH Verlag GbH & Co. KgaA: Weinheim. 2005. xii + 428 pp. $180.00. ISBN 3-527-30655-2. *Journal of the American Chemical Society* **127**, 16747-16748, doi:10.1021/ja0597808 (2005).

2 Knill, C. J. & Kennedy, J. F. Principles and Methods in Supramolecular Chemistry: H.-J. Schneider and A.K. Yatsimirsky; John Wiley and Sons, Ltd, Chichester, 2000, xii+349 pages, ISBN 0-471-97253-3, £39-95. *Carbohydrate Polymers* **47**, 211, doi:https://doi.org/10.1016/S0144-8617(01)00282-X (2002).

3 Phlip, D. Supramolecular chemistry: Concepts and perspectives. By J.-M. Lehn, VCH, Weinheim 1995, x, 271 pp., softcover, DM 58.00, ISBN 3-527-2931 1-6. *Advanced Materials* **8**, 866-868, doi:10.1002/adma.19960081029 (1996).

4 Rotello, V. M. Core Concepts in Supramolecular Chemistry and Nanochemistry By Jonathan W. Steed (Durham University, U.K.), David R. Turner (Monash University, Australia), and Karl J. Wallace (University of Southern Mississippi). John Wiley & Sons, Ltd: Chichester. 2007. xii + 308 pp. $50. ISBN 978-0-470-85867-7. *Journal of the American Chemical Society* **129**, 14524-14524, doi:10.1021/ja0769853 (2007).

5 Persch, E., Dumele, O. & Diederich, F. Molecular recognition in chemical and biological systems. *Angew Chem Int Ed Engl* **54**, 3290-3327 (2015).

6 Schneider, H. J. Binding mechanisms in supramolecular complexes. *Angew Chem Int Ed Engl* **48**, 3924-3977 (2009).

7 Schmidtchen, F. P. Hosting anions. The energetic perspective. *Chemical Society Reviews* **39**, 3916-3935, doi:10.1039/c0cs00038h (2010).

8 Hunter, C. A. Quantifying intermolecular interactions: guidelines for the molecular recognition toolbox. *Angew Chem Int Ed Engl* **43**, 5310-5324 (2004).

9 Yu, G., Jie, K. & Huang, F. Supramolecular Amphiphiles Based on Host–Guest Molecular Recognition Motifs. *Chemical Reviews* **115**, 7240-7303, doi:10.1021/cr5005315 (2015).

10 Iglesias, E. Inclusion Complexation of Novocaine by β-Cyclodextrin in Aqueous Solutions. *The Journal of Organic Chemistry* **71**, 4383-4392, doi:10.1021/jo052666n (2006).

11 Liu, J., Hennink, W. E., van Steenbergen, M. J., Zhuo, R. & Jiang, X. Versatile Supramolecular Gene Vector Based on Host–Guest Interaction. *Bioconjugate Chemistry* **27**, 1143-1152, doi:10.1021/acs.bioconjchem.6b00094 (2016).

12 Aytac, Z. *et al.* Fast-Dissolving, Prolonged Release, and Antibacterial Cyclodextrin/Limonene-Inclusion Complex Nanofibrous Webs via Polymer-Free Electrospinning. *J Agric Food Chem* **64**, 7325-7334 (2016).

13 Chen, X. *et al.* Light-Induced Hydrogel Based on Tumor-Targeting Mesoporous Silica Nanoparticles as a Theranostic Platform for Sustained Cancer Treatment. *ACS Appl Mater Interfaces* **8**, 15857-15863 (2016).

14 Lin, N. & Dufresne, A. Supramolecular hydrogels from in situ host-guest inclusion between chemically modified cellulose nanocrystals and cyclodextrin. *Biomacromolecules* **14**, 871-880 (2013).

15 Kida, T., Iwamoto, T., Asahara, H., Hinoue, T. & Akashi, M. Chiral Recognition and Kinetic Resolution of Aromatic Amines via Supramolecular Chiral Nanocapsules in Nonpolar Solvents. *Journal of the American Chemical Society* **135**, 3371-3374, doi:10.1021/ja312367k (2013).

16 Shi, Z. Q., Cai, Y. T., Deng, J., Zhao, W. F. & Zhao, C. S. Host-Guest Self-Assembly Toward Reversible Thermoresponsive Switching for Bacteria Killing and Detachment. *ACS Appl Mater Interfaces* **8**, 23523-23532 (2016).

17 Zhu, W., Zhang, K., Chen, Y. & Xi, F. Simple, Clean Preparation Method for Cross-Linked α-Cyclodextrin Nanoparticles via Inclusion Complexation. *Langmuir* **29**, 5939-5943, doi:10.1021/la400478d (2013).

18 Li, H. *et al.* Visible light-driven water oxidation promoted by host-guest interaction between photosensitizer and catalyst with a high quantum efficiency. *J Am Chem Soc* **137**, 4332-4335 (2015).

19 Rodríguez-López, M. I. *et al.* Thorough characterization and stability of HP-β-cyclodextrin thymol inclusion complexes prepared by microwave technology: A required approach to a successful application in food industry. *Journal of the Science of Food and Agriculture* **99**, 1322-1333, doi:10.1002/jsfa.9307 (2019).

20 Kfoury, M., Geagea, C., Ruellan, S., Greige-Gerges, H. & Fourmentin, S. Effect of cyclodextrin and cosolvent on the solubility and antioxidant activity of caffeic acid. *Food Chem* **278**, 163-169, doi:https://doi.org/10.1016/j.foodchem.2018.11.055 (2019).

21 Mourtzinos, I. *et al.* Natural food colorants derived from onion wastes: Application in a yoghurt product. *ELECTROPHORESIS* **39**, 1975-1983, doi:10.1002/elps.201800073 (2018).

22 Bakirhan, N. K., Tok, T. T. & Ozkan, S. A. The redox mechanism investigation of non-small cell lung cancer drug: Erlotinib via theoretical and experimental techniques and its host–guest detection by β-Cyclodextrin nanoparticles modified glassy carbon electrode. *Sensors and Actuators B: Chemical* **278**, 172-180, doi:https://doi.org/10.1016/j.snb.2018.09.090 (2019).

23 Strokopytov, B. *et al.* X-ray Structure of Cyclodextrin Glycosyltransferase Complexed with Acarbose. Implications for the Catalytic Mechanism of Glycosidases. *Biochemistry* **34**, 2234-2240, doi:10.1021/bi00007a018 (1995).

24 Bellringer, M. E., Smith, T. G., Read, R., Gopinath, C. & Olivier, P. β-Cyclodextrin: 52-Week toxicity studies in the rat and dog. *Food and Chemical Toxicology* **33**, 367-376, doi:https://doi.org/10.1016/0278-6915(94)00149-I (1995).

25 Sayed, M., Gubbala, G. K. & Pal, H. Contrasting interactions of DNA-intercalating dye acridine orange with hydroxypropyl derivatives of β-cyclodextrin and γ-cyclodextrin hosts. *New Journal of Chemistry* **43**, 724-736, doi:10.1039/c8nj04067b (2019).

26 Ho, S., Thoo, Y. Y., Young, D. J. & Siow, L. F. Stability and recovery of cyclodextrin encapsulated catechin in various food matrices. *Food Chem* **275**, 594-599, doi:https://doi.org/10.1016/j.foodchem.2018.09.117 (2019).

27 de Oliveira, G. G. G. *et al.* Compatibility study of paracetamol, chlorpheniramine maleate and phenylephrine hydrochloride in physical mixtures. *Saudi Pharmaceutical Journal* **25**, 99-103, doi:https://doi.org/10.1016/j.jsps.2016.05.001 (2017).

28 Shah, H. N., Halquist, M. T. & Gerk, P. M. Direct detection of phenylephrine 3-O-sulfate in LS180 human intestinal cells using a novel hydrophilic interaction liquid chromatography (HILIC) assay. *Journal of Chromatography B* **1040**, 67-72, doi:https://doi.org/10.1016/j.jchromb.2016.11.018 (2017).

29 Kuan, Y.-C., Xu, Y.-B., Wang, W.-C. & Yang, M.-T. Enantioselective synthesis of (R)-phenylephrine by Serratia marcescens BCRC10948 cells that homologously express SM_SDR. *Enzyme and Microbial Technology* **110**, 14-19, doi:https://doi.org/10.1016/j.enzmictec.2017.12.001 (2018).

30 Kernan, W. N. *et al.* Phenylpropanolamine and the Risk of Hemorrhagic Stroke. *New England Journal of Medicine* **343**, 1826-1832, doi:10.1056/nejm200012213432501 (2000).

31 Tette, P. A. S., Guidi, L. R., Bastos, E. M. A. F., Fernandes, C. & Gloria, M. B. A. Synephrine - A potential biomarker for orange honey authenticity. *Food Chem* **229**, 527-533, doi:10.1016/j.foodchem.2017.02.108 (2017).

32 Arai, K., Jin, D., Kusu, F. & Takamura, K. Determination of p-hydroxymandelic acid enantiomers in urine by high-performance liquid chromatography with electrochemical detection. *Journal of Pharmaceutical and Biomedical Analysis* **15**, 1509-1514, doi:https://doi.org/10.1016/S0731-7085(97)00038-1 (1997).

33 Wheaton, T. A. & Stewart, I. Feruloylputrescine : Isolation and Identification from Citrus Leaves and Fruit. *Nature* **206**, 620, doi:10.1038/206620a0 (1965).

34 Vieira, S. M., Theodoro, K. H. & Glória, M. B. A. Profile and levels of bioactive amines in orange juice and orange soft drink. *Food Chem* **100**, 895-903, doi:https://doi.org/10.1016/j.foodchem.2005.10.050 (2007).

35 Gregory, P. J. Evaluation of the Stimulant Content of Dietary Supplements Marketed as "Ephedra-Free". *Journal of Herbal Pharmacotherapy* **7**, 65-72, doi:10.1080/J157v07n01_06 (2007).

36 Hallas, J., Bjerrum, L., Støvring, H. & Andersen, M. Use of a Prescribed Ephedrine/Caffeine Combination and the Risk of Serious Cardiovascular Events: A Registry-based Case-Crossover Study. *American Journal of Epidemiology* **168**, 966-973, doi:10.1093/aje/kwn191 (2008).

37 Dragull, K., Breksa Ap 3rd Fau - Cain, B. & Cain, B. Synephrine content of juice from Satsuma mandarins (Citrus unshiu Marcovitch).

38 Artiss, J. D., Brogan K Fau - Brucal, M., Brucal M Fau - Moghaddam, M., Moghaddam M Fau - Jen, K. L. C. & Jen, K. L. The effects of a new soluble dietary fiber on weight gain and selected blood parameters in rats.

39 Comerford, K. B., Artiss, J. D., Jen, K. L. & Karakas, S. E. The beneficial effects of alpha-cyclodextrin on blood lipids and weight loss in healthy humans. *Obesity* **19**, 1200-1204 (2011).

40 Gan, R.-Y. *et al.* in *Sprouted Grains* (eds Hao Feng, Boris Nemzer, & Jonathan W. DeVries) 191-246 (AACC International Press, 2019).

41 Yu, Y. *et al.* Saccharomyces-derived carbon dots for biosensing pH and vitamin B 12. *Talanta* **195**, 117-126, doi:https://doi.org/10.1016/j.talanta.2018.11.010 (2019).

42 Li, S. *et al.* Encapsulation of Vitamin B1 and Its Phosphate Derivatives by Cucurbit[7]uril: Tunability of the Binding Site and Affinity by the Presence of

Phosphate Groups. *The Journal of Organic Chemistry* **81**, 1300-1303, doi:10.1021/acs.joc.5b02666 (2016).

43 Abo Dena, A. S. & Ammar, A. A. H-point standard addition for simultaneous reagent-free spectrophotometric determination of B1 and B6 vitamins. *Spectrochimica Acta Part A: Molecular and Biomolecular Spectroscopy* **206**, 491-497, doi:https://doi.org/10.1016/j.saa.2018.08.047 (2019).

44 Aloysius, A., Ramanathan, R., Christy, A., Baskaran, S. & Antony, N. Experimental and theoretical studies on the corrosion inhibition of vitamins – Thiamine hydrochloride or biotin in corrosion of mild steel in aqueous chloride environment. *Egyptian Journal of Petroleum* **27**, 371-381, doi:https://doi.org/10.1016/j.ejpe.2017.06.003 (2018).

45 Abdou, E. & Hazell, A. S. Thiamine Deficiency: An Update of Pathophysiologic Mechanisms and Future Therapeutic Considerations. *Neurochemical Research* **40**, 353-361, doi:10.1007/s11064-014-1430-z (2015).

46 Voelker, A. L., Miller, J., Running, C. A., Taylor, L. S. & Mauer, L. J. Chemical stability and reaction kinetics of two thiamine salts (thiamine mononitrate and thiamine chloride hydrochloride) in solution. *Food Research International* **112**, 443-456, doi:https://doi.org/10.1016/j.foodres.2018.06.056 (2018).

47 Melymuk, L. *et al.* Challenges in the Analysis of Novel Flame Retardants in Indoor Dust: Results of the INTERFLAB 2 Interlaboratory Evaluation. *Environmental Science & Technology* **52**, 9295-9303, doi:10.1021/acs.est.8b02715 (2018).

48 Mitro, S. D. *et al.* Consumer Product Chemicals in Indoor Dust: A Quantitative Meta-analysis of U.S. Studies. *Environmental Science & Technology* **50**, 10661-10672, doi:10.1021/acs.est.6b02023 (2016).

49 Ruan, Y. *et al.* Stereoisomer-Specific Trophodynamics of the Chiral Brominated Flame Retardants HBCD and TBECH in a Marine Food Web, with Implications for Human Exposure. *Environmental Science & Technology* **52**, 8183-8193, doi:10.1021/acs.est.8b02206 (2018).

50 Arnot, J. A. *et al.* Toward a consistent evaluative framework for POP risk characterization. *Environ Sci Technol* **45**, 97-103 (2011).

51 Nguyen, T. N. T., Lee, H.-Y. & Choi, S.-D. in *Persistent Organic Chemicals in the Environment: Status and Trends in the Pacific Basin Countries I Contamination Status* Vol. 1243 *ACS Symposium Series* Ch. 9, 193-218 (American Chemical Society, 2016).

52 Zegers, B. N. *et al.* Levels of Hexabromocyclododecane in Harbor Porpoises and Common Dolphins from Western European Seas, with Evidence for Stereoisomer-Specific Biotransformation by Cytochrome P450. *Environmental Science & Technology* **39**, 2095-2100, doi:10.1021/es049209t (2005).

53 Peng, X., Wei, D., Huang, Q. & Jia, X. Debromination of Hexabromocyclododecane by Anaerobic Consortium and Characterization of Functional Bacteria. *Frontiers in Microbiology* **9**, doi:10.3389/fmicb.2018.01515 (2018).

54 Yan, X. *et al.* Disposal of hexabromocyclododecane (HBCD) by grinding assisted with sodium persulfate. *RSC Advances* **7**, 23313-23318, doi:10.1039/c7ra02689g (2017).

55 Annahazi, A., Roka, R., Rosztoczy, A. & Wittmann, T. Role of antispasmodics in the treatment of irritable bowel syndrome. *World J Gastroenterol* **20**, 6031-6043 (2014).

56 Martinez-Vazquez, M. A. *et al.* Effect of antispasmodic agents, alone or in combination, in the treatment of Irritable Bowel Syndrome: systematic review and meta-analysis. *Rev Gastroenterol Mex* **77**, 82-90 (2012).

57 Catterall, W. A. & Zheng, N. Deciphering voltage-gated Na⁺ and Ca²⁺ channels by studying prokaryotic ancestors. *Trends in Biochemical Sciences* **40**, 526-534, doi:10.1016/j.tibs.2015.07.002 (2015).

58 Wu, J. *et al.* Structure of the voltage-gated calcium channel Cav1.1 at 3.6 Å resolution. *Nature* **537**, 191, doi:10.1038/nature19321

https://www.nature.com/articles/nature19321#supplementary-information (2016).

59 Flarakos, J., Morand, K. L. & Vouros, P. High-Throughput Solution-Based Medicinal Library Screening against Human Serum Albumin. *Analytical Chemistry* **77**, 1345-1353, doi:10.1021/ac048685z (2005).

60 Zsila, F. Subdomain IB Is the Third Major Drug Binding Region of Human Serum Albumin: Toward the Three-Sites Model. *Molecular Pharmaceutics* **10**, 1668-1682, doi:10.1021/mp400027q (2013).

61 Dalvit, C., Fagerness, P. E., Hadden, D. T., Sarver, R. W. & Stockman, B. J. Fluorine-NMR experiments for high-throughput screening: theoretical aspects, practical considerations, and range of applicability. *J Am Chem Soc* **125**, 7696-7703 (2003).

CHAPTER II

1 Szejtli, J. Introduction and General Overview of Cyclodextrin Chemistry. *Chemical Reviews* **98**, 1743-1754, doi:10.1021/cr970022c (1998).

2 Cramer, F., Saenger, W. & Spatz, H. C. Inclusion Compounds. XIX.1a The Formation of Inclusion Compounds of α-Cyclodextrin in Aqueous Solutions. Thermodynamics and Kinetics. *Journal of the American Chemical Society* **89**, 14-20, doi:10.1021/ja00977a003 (1967).

3 Piñeiro, Á. *et al.* On the Characterization of Host–Guest Complexes: Surface Tension, Calorimetry, and Molecular Dynamics of Cyclodextrins with a Non-ionic Surfactant. *The Journal of Physical Chemistry B* **111**, 4383-4392, doi:10.1021/jp0688815 (2007).

4 Giuffrida, S., Ventimiglia, G., Petralia, S., Conoci, S. & Sortino, S. Facile Light-Triggered One-Step Synthesis of Small and Stable Platinum Nanoparticles in an Aqueous Medium from a β-Cyclodextrin Host–Guest Inclusion Complex. *Inorganic Chemistry* **45**, 508-510, doi:10.1021/ic0517366 (2006).

5 Crupi, V., Majolino, D., Paciaroni, A., Stancanelli, R. & Venuti, V. Influence of the "Host–Guest" Interactions on the Mobility of Genistein/β-Cyclodextrin

Inclusion Complex. *The Journal of Physical Chemistry B* **113**, 11032-11038, doi:10.1021/jp810546h (2009).

6 Sun, Y.-X. *et al.* Versatile Supermolecular Inclusion Complex Based on Host–Guest Interaction for Targeted Gene Delivery. *ACS Applied Materials & Interfaces* **9**, 42622-42632, doi:10.1021/acsami.7b14963 (2017).

7 Schofield, W. C. & Badyal, J. P. Controlled fragrant molecule release from surface-tethered cyclodextrin host-guest inclusion complexes. *ACS Appl Mater Interfaces* **3**, 2051-2056 (2011).

8 Goswami, S., Majumdar, A. & Sarkar, M. Painkiller Isoxicam and Its Copper Complex Can Form Inclusion Complexes with Different Cyclodextrins: A Fluorescence, Fourier Transform Infrared Spectroscopy, and Nuclear Magnetic Resonance Study. *The Journal of Physical Chemistry B* **121**, 8454-8466, doi:10.1021/acs.jpcb.7b05649 (2017).

9 Gangopadhyay, M. *et al.* Tuning Emission Responses of a Triphenylamine Derivative in Host–Guest Complexes and an Unusual Dynamic Inclusion Phenomenon. *The Journal of Organic Chemistry* **81**, 512-521, doi:10.1021/acs.joc.5b02353 (2016).

10 Patra, D., Zhang, H., Sengupta, S. & Sen, A. Dual Stimuli-Responsive, Rechargeable Micropumps via "Host–Guest" Interactions. *ACS Nano* **7**, 7674-7679, doi:10.1021/nn402173w (2013).

11 Du, Z., Ke, K., Chang, X., Dong, R. & Ren, B. Controlled Self-Assembly of Multiple-Responsive Superamphiphilc Polymers Based on Host–Guest Inclusions of a Modified PEG with β-Cyclodextrin. *Langmuir* **34**, 5606-5614, doi:10.1021/acs.langmuir.8b00470 (2018).

12 Gupta, M., Maity, D. K., Singh, M. K., Nayak, S. K. & Ray, A. K. Supramolecular Interaction of Coumarin 1 Dye with Cucurbit[7]uril as Host: Combined Experimental and Theoretical Study. *The Journal of Physical Chemistry B* **116**, 5551-5558, doi:10.1021/jp301266q (2012).

CHAPTER III

1 Li, C. *et al.* A green separation mode of synephrine from Citrus aurantium L. (Rutaceae) by nanofiltration technology. *Food Science & Nutrition* 7, 4014-4020, doi:10.1002/fsn3.1265 (2019).

2 Chin, E. L. *et al.* Longitudinal Transcriptomic, Proteomic, and Metabolomic Analyses of Citrus sinensis (L.) Osbeck Graft-Inoculated with "Candidatus Liberibacter asiaticus". *Journal of Proteome Research* 19, 719-732, doi:10.1021/acs.jproteome.9b00616 (2020).

3 Wasan, A. A.-U. DETERMINATION OF PHENYLEPHRINE HYDROCHLORIDE IN PHARMACEUTICAL PREPARATIONS USING SPECTROPHOTOMETRIC METHOD. *Asian Journal of Pharmaceutical and Clinical Research* 12, doi:10.22159/ajpcr.2019.v12i5.32339 (2019).

4 Kaur, K., Jindal, R. & Jindal, D. Controlled release of vitamin B1 and evaluation of biodegradation studies of chitosan and gelatin based hydrogels. *Int J Biol Macromol* 11, 223 (2019).

5 Vijayalakshmi, R., Naga Sri Ramya, Y. & Dhanaraju, M. D. METHOD DEVELOPMENT FOR QUANTIFICATION OF LORATIDINE AND ALVERINE CITRATE BY VISIBLE SPECTROPHOTOMETRY. *International Journal of Pharmaceutical Sciences and Drug Research* 8, doi:10.25004/ijpsdr.2016.080307 (2016).

6 Xie, X. *et al.* Exposure to HBCD promotes adipogenesis both in vitro and in vivo by interfering with Wnt6 expression. *Sci Total Environ* 705, 6 (2020).

7 Shah, S. B. Characterization of environmentally friendly degradation of hexabromocyclododecane by a Bacillus strain HBCD-sjtu. *International biodeterioration & biodegradation*, 2019, doi:10.1016/j.ibiod.2019.104794 (2019).

8 de Moraes, J. O., Hilton, S. T. & Moraru, C. I. The effect of Pulsed Light and starch films with antimicrobials on Listeria innocua and the quality of sliced cheddar

cheese during refrigerated storage. *Food Control* 112, 107134, doi:https://doi.org/10.1016/j.foodcont.2020.107134 (2020).

9 Xu, W. *et al.* Sodium Benzoate Attenuates Secondary Brain Injury by Inhibiting Neuronal Apoptosis and Reducing Mitochondria-Mediated Oxidative Stress in a Rat Model of Intracerebral Hemorrhage: Possible Involvement of DJ-1/Akt/IKK/NFκB Pathway. *Frontiers in Molecular Neuroscience* 12, doi:10.3389/fnmol.2019.00105 (2019).

10 Albakaa, A. R. M., ahmed, M. a., mohammed, B. t. & jabbar, z. a. Development Method for Determination of Aspirin as Sodium Salicylate by UV-VIS Spectroscopy. *IOP Conference Series: Materials Science and Engineering* 571, 012104, doi:10.1088/1757-899x/571/1/012104 (2019).

11 Cabello, M. C., Souza, G. A., Bello, L. V. & Baader, W. J. Mechanistic Studies on the Salicylate-Catalyzed Peroxyoxalate Chemiluminescence in Aqueous Medium. *Photochemistry and Photobiology* 96, 28-36, doi:10.1111/php.13180 (2020).

12 Klampfer, L., Cammenga, J. r., Wisniewski, H.-G. & Nimer, S. D. Sodium Salicylate Activates Caspases and Induces Apoptosis of Myeloid Leukemia Cell Lines. *Blood* 93, 2386-2394, doi:10.1182/blood.V93.7.2386 (1999).

13 Rajbanshi, B. *et al.* Minimization of the dosage of food preservatives mixing with ionic liquids for controlling risky effect in human body: Physicochemical, antimicrobial and computational study. *Journal of Molecular Liquids* 282, 415-427, doi:https://doi.org/10.1016/j.molliq.2019.03.034 (2019).

14 Mallamace, F., Corsaro, C. & Stanley, H. E. A singular thermodynamically consistent temperature at the origin of the anomalous behavior of liquid water. *Scientific Reports* 2, 993, doi:10.1038/srep00993 (2012).

15 Ball, P. Water — an enduring mystery. *Nature* 452, 291-292, doi:10.1038/452291a (2008).

16 Baroni, L., Cenci, L., Tettamanti, M. & Berati, M. Evaluating the environmental impact of various dietary patterns combined with different food production

systems. *European Journal of Clinical Nutrition* 61, 279-286, doi:10.1038/sj.ejcn.1602522 (2007).

17 Epstein, W. W. & Sweat, F. W. Dimethyl Sulfoxide Oxidations. *Chemical Reviews* 67, 247-260, doi:10.1021/cr60247a001 (1967).

18 Bordwell, F. G. Equilibrium acidities in dimethyl sulfoxide solution. *Accounts of Chemical Research* 21, 456-463, doi:10.1021/ar00156a004 (1988).

19 Chakrabarti, R. & Schutt, C. E. The enhancement of PCR amplification by low molecular-weight sulfones. *Gene* 274, 293-298, doi:https://doi.org/10.1016/S0378-1119(01)00621-7 (2001).

20 Pegg, D. E. in *Cryopreservation and Freeze-Drying Protocols* (eds John G. Day & Glyn N. Stacey) 39-57 (Humana Press, 2007).

CHAPTER IV

1. Bao L, Shu X, Yu M, Hou D, Cui L, Li C. Synthesis, structure, and host-guest properties of an anthracene-based macrocyclic arene. *Tetrahedron Letters* 59, 730-733 (2018).

2. Fang X, Gong F, Fang Y. Capillary Electrophoresis with Electrochemical Detection for Chiral Separation of Optical Isomers. *Analytical Chemistry* 70, 4030-4035 (1998).

3. Pal A, Gaba R, Soni S. Effect of presence of α-cyclodextrin and β-cyclodextrin on solution behavior of sulfathiazole at different temperatures: Thermodynamic and spectroscopic studies. *The Journal of Chemical Thermodynamics* 119, 102-113 (2018).

4. Tait RJ, Thompson DO, Stella VJ, Stobaugh JF. Sulfobutyl Ether .beta.-Cyclodextrin as a Chiral Discriminator for Use with Capillary Electrophoresis. *Analytical Chemistry* 66, 4013-4018 (1994).

5. Fanali S. Identification of chiral drug isomers by capillary electrophoresis. *Journal of Chromatography A* 735, 77-121 (1996).

6. Stalcup AM, Gahm KH. Application of Sulfated Cyclodextrins to Chiral Separations by Capillary Zone Electrophoresis. *Analytical Chemistry* 68, 1360-1368 (1996).

7. de Oliveira GGG, Feitosa A, Loureiro K, Fernandes AR, Souto EB, Severino P. Compatibility study of paracetamol, chlorpheniramine maleate and phenylephrine hydrochloride in physical mixtures. *Saudi Pharmaceutical Journal* 25, 99-103 (2017).

8. Shah HN, Halquist MT, Gerk PM. Direct detection of phenylephrine 3-O-sulfate in LS180 human intestinal cells using a novel hydrophilic interaction liquid chromatography (HILIC) assay. *Journal of Chromatography B* 1040, 67-72 (2017).

9. Kuan Y-C, Xu Y-B, Wang W-C, Yang M-T. Enantioselective synthesis of (R)-phenylephrine by Serratia marcescens BCRC10948 cells that homologously express SM_SDR. *Enzyme and Microbial Technology* 110, 14-19 (2018).

10. Kernan WN*, et al.* Phenylpropanolamine and the Risk of Hemorrhagic Stroke. *New England Journal of Medicine* 343, 1826-1832 (2000).

11. Wheaton TA, Stewart I. Biosynthesis of synephrine in citrus. *Phytochemistry* 8, 85-92 (1969).

12. Tette PAS, Guidi LR, Bastos EMAF, Fernandes C, Gloria MBA. Synephrine - A potential biomarker for orange honey authenticity. *Food Chem* 229, 527-533 (2017).

13. Arai K, Jin D, Kusu F, Takamura K. Determination of p-hydroxymandelic acid enantiomers in urine by high-performance liquid chromatography with electrochemical detection. *Journal of Pharmaceutical and Biomedical Analysis* 15, 1509-1514 (1997).

14. Wheaton TA, Stewart I. Feruloylputrescine : Isolation and Identification from Citrus Leaves and Fruit. *Nature* 206, 620 (1965).

15. M. Vieira S, H. Theodoro K, Gloria MBA. *Profile and levels of bioactive amines in orange juice and orange soft drink* (2007).

16. Vieira S, Calado R, Coelho H, Serôdio J. *Vieira et al 2009 MarBiol* (2012).

17. Gregory PJ. Evaluation of the Stimulant Content of Dietary Supplements Marketed as "Ephedra-Free". *Journal of Herbal Pharmacotherapy* 7, 65-72 (2007).

18. Hallas J, Bjerrum L, Støvring H, Andersen M. Use of a Prescribed Ephedrine/Caffeine Combination and the Risk of Serious Cardiovascular Events: A Registry-based Case-Crossover Study. *American Journal of Epidemiology* 168, 966-973 (2008).

19. Vatsavai LK, Kilari EK. Interaction of p-synephrine on the pharmacodynamics and pharmacokinetics of gliclazide in animal models. *Journal of Ayurveda and Integrative Medicine*, (2017).

20. Dragull K, Breksa Ap 3rd Fau - Cain B, Cain B. Synephrine content of juice from Satsuma mandarins (Citrus unshiu Marcovitch).

21. Venkata Giri Kumar P, Deshpande S, Joshi A, More P, Nagendra HR. Significance of arterial stiffness in Tridosha analysis: A pilot study. *Journal of Ayurveda and Integrative Medicine* 8, 252-256 (2017).

22. Artiss JD, Brogan K Fau - Brucal M, Brucal M Fau - Moghaddam M, Moghaddam M Fau - Jen KLC, Jen KL. The effects of a new soluble dietary fiber on weight gain and selected blood parameters in rats.

23. Comerford KB, Artiss JD, Jen KL, Karakas SE. The beneficial effects of alpha-cyclodextrin on blood lipids and weight loss in healthy humans. *Obesity* 19, 1200-1204 (2011).

24. Job P. *Formation and stability of inorganic complexes in solution* (1928).

25. Renny JS, Tomasevich LL, Tallmadge EH, Collum DB. Method of continuous variations: applications of job plots to the study of molecular associations in organometallic chemistry. *Angew Chem Int Ed Engl* 52, 11998-12013 (2013).

26. Brynn Hibbert D, Thordarson P. The death of the Job plot, transparency, open science and online tools, uncertainty estimation methods and other developments in supramolecular chemistry data analysis. *Chemical Communications* 52, 12792-12805 (2016).

27. Ulatowski F, Dąbrowa K, Bałakier T, Jurczak J. Recognizing the Limited Applicability of Job Plots in Studying Host–Guest Interactions in Supramolecular Chemistry. *The Journal of Organic Chemistry* 81, 1746-1756 (2016).

28. Caso JV*, et al.* Investigating the inclusion properties of aromatic amino acids complexing beta-cyclodextrins in model peptides.

29. Gao Y, Zhao X Fau - Dong B, Dong B Fau - Zheng L, Zheng L Fau - Li N, Li N Fau - Zhang S, Zhang S. Inclusion complexes of beta-cyclodextrin with ionic liquid surfactants.

30. Piñeiro Á*, et al.* On the Characterization of Host−Guest Complexes: Surface Tension, Calorimetry, and Molecular Dynamics of Cyclodextrins with a Non-ionic Surfactant. *The Journal of Physical Chemistry B* 111, 4383-4392 (2007).

31. Saha S, Roy A, Roy K, Roy MN. Study to explore the mechanism to form inclusion complexes of β-cyclodextrin with vitamin molecules. *Scientific Reports* 6, 35764 (2016).

32. Roy MN, Saha S, Barman S, Ekka D. Host-guest inclusion complexes of RNA nucleosides inside aqueous cyclodextrins explored by physicochemical and spectroscopic methods. *RSC Advances* 6, 8881-8891 (2016).

33. Roy MN, Ekka D, Saha S, Chandra Roy M. Host-guest inclusion complexes of [small alpha] and [small beta]-cyclodextrins with [small alpha]-amino acids. *RSC Advances* 4, 42383-42390 (2014).

34. Ghosh R, Ekka D, Rajbanshi B, Yasmin A, Roy MN. Synthesis,characterization of 1-butyl-4-methylpyridinium lauryl sulfate and its inclusion phenomenon with β-cyclodextrin for enhanced applications. *Colloids and Surfaces A: Physicochemical and Engineering Aspects* 548, 206-217 (2018).

35. Gao Y, Zhao X, Dong B, Zheng L, Li N, Zhang S. Inclusion complexes of beta-cyclodextrin with ionic liquid surfactants. *J Phys Chem B* 110, 8576-8581 (2006).

36. Roy A, Saha S, Datta B, Roy MN. Insertion behavior of imidazolium and pyrrolidinium based ionic liquids into [small alpha] and [small beta]-cyclodextrins: mechanism and factors leading to host-guest inclusion complexes. *RSC Advances* 6, 100016-100027 (2016).

37. Roy MN, Saha S, Kundu M, Saha BC, Barman S. Exploration of inclusion complexes of neurotransmitters with β-cyclodextrin by physicochemical techniques. *Chemical Physics Letters* 655-656, 43-50 (2016).

38. Roy MN, Roy A, Saha S. Probing inclusion complexes of cyclodextrins with amino acids by physicochemical approach. *Carbohydrate Polymers* 151, 458-466 (2016).

39. Saha S, Ray T, Basak S, Roy MN. NMR, surface tension and conductivity studies to determine the inclusion mechanism: thermodynamics of host-guest inclusion complexes of natural amino acids in aqueous cyclodextrins. *New Journal of Chemistry* 40, 651-661 (2016).

40. Barman BK, Rajbanshi B, Yasmin A, Roy MN. Exploring inclusion complexes of ionic liquids with α- and β- cyclodextrin by NMR, IR, mass, density, viscosity, surface tension and conductance study. *Journal of Molecular Structure* 1159, 205-215 (2018).

41. Roy PM, Saha S, Barman S, Ekka DD. *Host–guest inclusion complexes of RNA nucleosides inside aqueous cyclodextrins explored by physicochemical and spectroscopic methods* (2016).

42. Cramer F, Saenger W, Spatz HC. Inclusion Compounds. XIX.1a The Formation of Inclusion Compounds of α-Cyclodextrin in Aqueous Solutions. Thermodynamics and Kinetics. *Journal of the American Chemical Society* 89, 14-20 (1967).

43. Roy MN, Saha S, Barman S, Ekka D. Host–guest inclusion complexes of RNA nucleosides inside aqueous cyclodextrins explored by physicochemical and spectroscopic methods. *RSC Advances* 6, 8881-8891 (2016).

44. Benesi HA, Hildebrand JH. A Spectrophotometric Investigation of the Interaction of Iodine with Aromatic Hydrocarbons. *Journal of the American Chemical Society* 71, 2703-2707 (1949).

45. Caso JV*, et al.* Investigating the inclusion properties of aromatic amino acids complexing beta-cyclodextrins in model peptides. *Amino Acids* 47, 2215-2227 (2015).

46. Thordarson P. Determining association constants from titration experiments in supramolecular chemistry. *Chem Soc Rev* 40, 1305-1323 (2011).

47. Connors KA. The Stability of Cyclodextrin Complexes in Solution. *Chemical Reviews* 97, 1325-1358 (1997).

48. Szejtli J. Introduction and General Overview of Cyclodextrin Chemistry. *Chemical Reviews* 98, 1743-1754 (1998).

49. Evans DF, Matesich SMA. Ionic association in hydrogen-bonding solvents. *Journal of Solution Chemistry* 2, 193-216 (1973).

50. Khayatian G, Shariati S, Shamsipur M. Conductance Study of the Thermodynamics of Binding of Some Macrocyclic Polyethers with Tl+ Ion in Dimethylformamide-Acetonitrile Mixtures. *Journal of inclusion phenomena and macrocyclic chemistry* 45, 117-121 (2003).

51. de Namor AFD, Ritt M-C, Schwing-Weill M-J, Arnaud-Neu F, Lewis DFV. Solution thermodynamics of amino acid-18-crown-6 and amino acid-cryptand 222 complexes in methanol and ethanol. Linear enthalpy-entropy compensation

effect. *Journal of the Chemical Society, Faraday Transactions* 87, 3231-3239 (1991).

52. Prabu S, Swaminathan M, Sivakumar K, Rajamohan R. Preparation, characterization and molecular modeling studies of the inclusion complex of Caffeine with Beta-cyclodextrin. *Journal of Molecular Structure* 1099, 616-624 (2015).

53. Sanramé CN, de Rossi RH, Argüello GA. Effect of β-Cyclodextrin on the Excited State Properties of 3-Substituted Indole Derivatives. *The Journal of Physical Chemistry* 100, 8151-8156 (1996).

54. Oana M, Tintaru A, Gavriliu D, Maior O, Hillebrand M. Spectral Study and Molecular Modeling of the Inclusion Complexes of β-Cyclodextrin with Some Phenoxathiin Derivatives. *The Journal of Physical Chemistry B* 106, 257-263 (2002).

55. Zhang Q-F, Jiang Z-T, Guo Y-X, Li R. Complexation study of brilliant cresyl blue with β-cyclodextrin and its derivatives by UV–vis and fluorospectrometry. *Spectrochimica Acta Part A: Molecular and Biomolecular Spectroscopy* 69, 65-70 (2008).

56. Zhang M, Li J, Jia W, Chao J, Zhang L. Theoretical and experimental study of the inclusion complexes of ferulic acid with cyclodextrins. *Supramolecular Chemistry* 21, 597-602 (2009).

57. Sindelar V, Cejas Ma Fau - Raymo FM, Raymo Fm Fau - Chen W, Chen W Fau - Parker SE, Parker Se Fau - Kaifer AE, Kaifer AE. Supramolecular assembly of 2,7-dimethyldiazapyrenium and cucurbit[8]uril: a new fluorescent host for detection of catechol and dopamine.

58. Yang LJ*, et al.* Preparation and characterization of inclusion complexes of naringenin with beta-cyclodextrin or its derivative. *Carbohydr Polym* 98, 861-869 (2013).

59. Fernandes A*, et al.* Structural characterization of inclusion complexes between cyanidin-3-O-glucoside and β-cyclodextrin. *Carbohydrate Polymers* 102, 269-277 (2014).

60. Xiao CF*, et al.* Investigation of inclusion complex of epothilone A with cyclodextrins.

61. Yang B, Lin J, Chen Y, Liu Y. Artemether/hydroxypropyl-beta-cyclodextrin host-guest system: characterization, phase-solubility and inclusion mode. *Bioorg Med Chem* 17, 6311-6317 (2009).

62. Servais AC*, et al.* Capillary electrophoretic and nuclear magnetic resonance studies on the opposite affinity pattern of propranolol enantiomers towards various cyclodextrins.

63. Correia I, Bezzenine N, Ronzani N, Platzer N, Beloeil JC, Doan BT. Study of inclusion complexes of acridine with β- and (2,6-di-O-methyl)-β-cyclodextrin by use of solubility diagrams and NMR spectroscopy. *Journal of Physical Organic Chemistry* 15, 647-659 (2002).

64. Bednarek E, Bocian W, Poznanski J, Sitkowski J, Sadlej-Sosnowska N, Kozerski L. Complexation of steroid hormones: prednisolone, ethinyloestradiol and estriol with [small beta]-cyclodextrin. An aqueous 1H NMR study. *Journal of the Chemical Society, Perkin Transactions 2*, 999-1004 (2002).

65. Ishizu T, Hirata C, Yamamoto H, Harano K. Structure and intramolecular flexibility of β-cyclodextrin complex with (−)-epigallocatechin gallate in aqueous solvent. *Magnetic Resonance in Chemistry* 44, 776-783 (2006).

66. Kemelbekov U*, et al.* IR, UV and NMR studies of β-cyclodextrin inclusion complexes of kazcaine and prosidol bases. *Journal of inclusion phenomena and macrocyclic chemistry* 69, 181-190 (2011).

67. Stalin T, Srinivasan K, Sivakumar K, Radhakrishnan S. Preparation and characterizations of solid/aqueous phases inclusion complex of 2,4-dinitroaniline with beta-cyclodextrin.

68. Zhang JQ*, et al.* Novel water-soluble fisetin/cyclodextrins inclusion complexes: Preparation, characterization, molecular docking and bioavailability. *Carbohydr Res* 418, 20-28 (2015).

69. Okada Y, Ueyama K, Nishikawa J-i, Semma M, Ichikawa A. *Effect of 6-O-α-maltosyl-β cyclodextrin and its cholesterol inclusion complex on cellular cholesterol levels and ABCA1 and ABCG1 expression in mouse mastocytoma P-815 cells* (2012).

70. Sivakumar K, Ragi TR, Prema D, Stalin T. Experimental and theoretical investigation on the structural characterization and orientation preferences of 2-hydroxy-1-naphthoic acid/β-cyclodextrin host-guest inclusion complex. *Journal of Molecular Liquids* 218, 538-548 (2016).

71. Negi JS, Singh S. Spectroscopic investigation on the inclusion complex formation between amisulpride and gamma-cyclodextrin. *Carbohydr Polym* 92, 1835-1843 (2013).

72. Zhang W*, et al.* Investigation of water-soluble inclusion complex of hypericin with β-cyclodextrin polymer. *Carbohydrate Polymers* 95, 366-370 (2013).

73. Vesterdal J. The Agar Cup Method for the Estimation of Penicillin*). *Acta Pharmacologica et Toxicologica* 2, 9-21 (1946).

74. Di Donato C*, et al.* Alpha- and Beta-Cyclodextrin Inclusion Complexes with 5-Fluorouracil: Characterization and Cytotoxic Activity Evaluation. *Molecules* 21, (2016).

CHAPTER V

1 Rodríguez-López, M. I. *et al.* Thorough characterization and stability of HP-β-cyclodextrin thymol inclusion complexes prepared by microwave technology: A required approach to a successful application in food industry. *Journal of the Science of Food and Agriculture* 99, 1322-1333, doi:10.1002/jsfa.9307 (2019).

2 Kfoury, M., Geagea, C., Ruellan, S., Greige-Gerges, H. & Fourmentin, S. Effect of cyclodextrin and cosolvent on the solubility and antioxidant activity of caffeic acid. *Food Chemistry* 278, 163-169, doi:https://doi.org/10.1016/j.foodchem.2018.11.055 (2019).

3 Mourtzinos, I. *et al.* Natural food colorants derived from onion wastes: Application in a yoghurt product. *ELECTROPHORESIS* 39, 1975-1983, doi:10.1002/elps.201800073 (2018).

4 Bakirhan, N. K., Tok, T. T. & Ozkan, S. A. The redox mechanism investigation of non-small cell lung cancer drug: Erlotinib via theoretical and experimental techniques and its host–guest detection by β-Cyclodextrin nanoparticles modified glassy carbon electrode. *Sensors and Actuators B: Chemical* 278, 172-180, doi:https://doi.org/10.1016/j.snb.2018.09.090 (2019).

5 Saidman, E. *et al.* Inclusion complexes of β-cyclodextrin and polymorphs of mebendazole: Physicochemical characterization. *European Journal of Pharmaceutical Sciences* 127, 330-338, doi:https://doi.org/10.1016/j.ejps.2018.11.012 (2019).

6 Singh, N. & Sahu, O. in *The Impact and Prospects of Green Chemistry for Textile Technology* (eds Islam Shahid ul & B. S. Butola) 83-105 (Woodhead Publishing, 2019).

7 Cao, S. *et al.* A high efficient adsorbent for plant growth regulators based on ionic liquid and β-cyclodextrin functionalized magnetic graphene oxide. *Talanta* 194, 14-25, doi:https://doi.org/10.1016/j.talanta.2018.10.013 (2019).

8 Strokopytov, B. *et al.* X-ray Structure of Cyclodextrin Glycosyltransferase Complexed with Acarbose. Implications for the Catalytic Mechanism of Glycosidases. *Biochemistry* 34, 2234-2240, doi:10.1021/bi00007a018 (1995).

9 Cai, L., Jeremic, D., Lim, H. & Kim, Y. β-Cyclodextrins as sustained-release carriers for natural wood preservatives. *Industrial Crops and Products* 130, 42-48, doi:https://doi.org/10.1016/j.indcrop.2018.12.061 (2019).

10 Bardi, L., Mattei, A., Steffan, S. & Marzona, M. Hydrocarbon degradation by a soil microbial population with β-cyclodextrin as surfactant to enhance bioavailability. *Enzyme and Microbial Technology* 27, 709-713, doi:https://doi.org/10.1016/S0141-0229(00)00275-1 (2000).

11 Bellringer, M. E., Smith, T. G., Read, R., Gopinath, C. & Olivier, P. β-Cyclodextrin: 52-Week toxicity studies in the rat and dog. *Food and Chemical Toxicology* 33, 367-376, doi:https://doi.org/10.1016/0278-6915(94)00149-I (1995).

12 Jalalvandi, E. & Shavandi, A. Shear thinning/self-healing hydrogel based on natural polymers with secondary photocrosslinking for biomedical applications. *Journal of the Mechanical Behavior of Biomedical Materials* 90, 191-201, doi:https://doi.org/10.1016/j.jmbbm.2018.10.009 (2019).

13 Myszka, K., Leja, K. & Majcher, M. A current opinion on the antimicrobial importance of popular pepper essential oil and its application in food industry. *Journal of Essential Oil Research* 31, 1-18, doi:10.1080/10412905.2018.1511482 (2019).

14 Sayed, M., Gubbala, G. K. & Pal, H. Contrasting interactions of DNA-intercalating dye acridine orange with hydroxypropyl derivatives of β-cyclodextrin and γ-cyclodextrin hosts. *New Journal of Chemistry* 43, 724-736, doi:10.1039/c8nj04067b (2019).

15 Saekhor, K., Udomsinprasert, W., Honsawek, S. & Tachaboonyakiat, W. Preparation of an injectable modified chitosan-based hydrogel approaching for bone tissue engineering. *International Journal of Biological Macromolecules* 123, 167-173, doi:https://doi.org/10.1016/j.ijbiomac.2018.11.041 (2019).

16 van de Manakker, F., Vermonden, T., van Nostrum, C. F. & Hennink, W. E. Cyclodextrin-Based Polymeric Materials: Synthesis, Properties, and Pharmaceutical/Biomedical Applications. *Biomacromolecules* 10, 3157-3175, doi:10.1021/bm901065f (2009).

17 Mejías, F. J. R. *et al.* Provitamin supramolecular polymer micelle with pH responsiveness to control release, bioavailability enhancement and

potentiation of cytotoxic efficacy. *Colloids and Surfaces B: Biointerfaces* 173, 85-93, doi:https://doi.org/10.1016/j.colsurfb.2018.09.057 (2019).

18 Li, Y. *et al.* Digestion properties of corn starch modified by α-D-glucan branching enzyme and cyclodextrin glycosyltransferase. *Food Hydrocolloids* 89, 534-541, doi:https://doi.org/10.1016/j.foodhyd.2018.11.025 (2019).

19 Wang, P. *et al.* Effects of β-cyclodextrin on the enzymatic hydrolysis of hemp seed oil by lipase Candida sp.99–125. *Industrial Crops and Products* 129, 688-693, doi:https://doi.org/10.1016/j.indcrop.2018.11.046 (2019).

20 Rajbanshi, B. *et al.* Study to Probe Subsistence of Host-Guest Inclusion Complexes of α and β-Cyclodextrins with Biologically Potent Drugs for Safety Regulatory Dischargement. *Scientific Reports* 8, 13031, doi:10.1038/s41598-018-31373-x (2018).

21 Yin, Y. & Cadwallader, K. R. Spray-chilling encapsulation of 2-acetyl-1-pyrroline zinc chloride using hydrophobic materials: Storage stability and flavor application in food. *Food Chemistry* 278, 738-743, doi:https://doi.org/10.1016/j.foodchem.2018.11.122 (2019).

22 Zhang, G., Yuan, C. & Sun, Y. Effect of Selective Encapsulation of Hydroxypropyl-β-cyclodextrin on Components and Antibacterial Properties of Star Anise Essential Oil. *Molecules* 23, doi:10.3390/molecules23051126 (2018).

23 Beserra-Filho, J. I. A. *et al.* Eplingiella fruticosa leaf essential oil complexed with β-cyclodextrin produces a superior neuroprotective and behavioral profile in a mice model of Parkinson's disease. *Food and Chemical Toxicology* 124, 17-29, doi:https://doi.org/10.1016/j.fct.2018.11.056 (2019).

24 Chowdhury, P. *et al.* Tannic acid-inspired paclitaxel nanoparticles for enhanced anticancer effects in breast cancer cells. *Journal of Colloid and Interface Science* 535, 133-148, doi:https://doi.org/10.1016/j.jcis.2018.09.072 (2019).

25 Feng, T. *et al.* Associated-Extraction Efficiency of Six Cyclodextrins on Various Flavonoids in Puerariae Lobatae Radix. *Molecules* 24, doi:10.3390/molecules24010093 (2018).

26 Ho, S., Thoo, Y. Y., Young, D. J. & Siow, L. F. Stability and recovery of cyclodextrin encapsulated catechin in various food matrices. *Food Chemistry* 275, 594-599, doi:https://doi.org/10.1016/j.foodchem.2018.09.117 (2019).

27 Gan, R.-Y. *et al.* in *Sprouted Grains* (eds Hao Feng, Boris Nemzer, & Jonathan W. DeVries) 191-246 (AACC International Press, 2019).

28 Pinela, J. *et al.* Stability of total folates/vitamin B9 in irradiated watercress and buckler sorrel during refrigerated storage. *Food Chemistry* 274, 686-690, doi:https://doi.org/10.1016/j.foodchem.2018.09.042 (2019).

29 Yu, Y. *et al.* Saccharomyces-derived carbon dots for biosensing pH and vitamin B 12. *Talanta* 195, 117-126, doi:https://doi.org/10.1016/j.talanta.2018.11.010 (2019).

30 Oliveira, C. H. d. M., Assaid Simão, A. & Marcussi, S. Inhibitory effects of ascorbic acid, vitamin E, and vitamin B-complex on the biological activities induced by Bothrops venom. *Pharmaceutical Biology* 54, 845-852, doi:10.3109/13880209.2015.1087038 (2016).

31 Li, S. *et al.* Encapsulation of Vitamin B1 and Its Phosphate Derivatives by Cucurbit[7]uril: Tunability of the Binding Site and Affinity by the Presence of Phosphate Groups. *The Journal of Organic Chemistry* 81, 1300-1303, doi:10.1021/acs.joc.5b02666 (2016).

32 Li, X. *et al.* Measurement of Solubility of Thiamine Hydrochloride Hemihydrate in Three Binary Solvents and Mixing Properties of Solutions. *Journal of Chemical & Engineering Data* 61, 3665-3678, doi:10.1021/acs.jced.6b00613 (2016).

33 Islam, M. S. *et al.* Effect of UV Irradiation on the Nutritional Quality and Cytotoxicity of Apple Juice. *Journal of Agricultural and Food Chemistry* 64, 7812-7822, doi:10.1021/acs.jafc.6b02491 (2016).

34 Brasky, T. M., White, E. & Chen, C.-L. Long-Term, Supplemental, One-Carbon Metabolism–Related Vitamin B Use in Relation to Lung Cancer Risk in the Vitamins and Lifestyle (VITAL) Cohort. *Journal of Clinical Oncology* 35, 3440-3448, doi:10.1200/jco.2017.72.7735 (2017).

35 Abo Dena, A. S. & Ammar, A. A. H-point standard addition for simultaneous reagent-free spectrophotometric determination of B1 and B6 vitamins. *Spectrochimica Acta Part A: Molecular and Biomolecular Spectroscopy* 206, 491-497, doi:https://doi.org/10.1016/j.saa.2018.08.047 (2019).

36 Slawson, D. L., Fitzgerald, N. & Morgan, K. T. Position of the Academy of Nutrition and Dietetics: The Role of Nutrition in Health Promotion and Chronic Disease Prevention. *Journal of the Academy of Nutrition and Dietetics* 113, 972-979, doi:10.1016/j.jand.2013.05.005 (2013).

37 Aloysius, A., Ramanathan, R., Christy, A., Baskaran, S. & Antony, N. Experimental and theoretical studies on the corrosion inhibition of vitamins – Thiamine hydrochloride or biotin in corrosion of mild steel in aqueous chloride environment. *Egyptian Journal of Petroleum* 27, 371-381, doi:https://doi.org/10.1016/j.ejpe.2017.06.003 (2018).

38 Crook, M. A. in *Laboratory Assessment of Vitamin Status* (ed Dominic Harrington) 149-164 (Academic Press, 2019).

39 Nath, A., Tran, T., Shope, T. R. & Koch, T. R. Prevalence of clinical thiamine deficiency in individuals with medically complicated obesity. *Nutrition Research* 37, 29-36, doi:https://doi.org/10.1016/j.nutres.2016.11.012 (2017).

40 Abdou, E. & Hazell, A. S. Thiamine deficiency: an update of pathophysiologic mechanisms and future therapeutic considerations. *Neurochem Res* 40, 353-361 (2015).

41 Yang, Y., Han, D., Du, S., Wu, S. & Gong, J. Crystal morphology optimization of thiamine hydrochloride in solvent system: Experimental and molecular dynamics simulation studies. *Journal of Crystal Growth* 481, 48-55, doi:https://doi.org/10.1016/j.jcrysgro.2017.10.022 (2018).

42 Voelker, A. L., Miller, J., Running, C. A., Taylor, L. S. & Mauer, L. J. Chemical stability and reaction kinetics of two thiamine salts (thiamine mononitrate and thiamine chloride hydrochloride) in solution. *Food Research International* 112, 443-456, doi:https://doi.org/10.1016/j.foodres.2018.06.056 (2018).

43 Struch, N., Topić, F., Rissanen, K. & Lützen, A. Electron-deficient trifluoromethyl-substituted sub-components affect the properties of M4L4 tetrahedral cages. *Dalton Transactions* 46, 10809-10813, doi:10.1039/c7dt02182h (2017).

44 Zhu, T., Du, J., Cao, W., Fan, J. & Peng, X. Microenvironment-Sensitive Fluorescent Dyes for Recognition of Serum Albumin in Urine and Imaging in Living Cells. *Industrial & Engineering Chemistry Research* 55, 527-533, doi:10.1021/acs.iecr.5b04214 (2016).

45 Bolattin, M. B., Nandibewoor, S. T., Joshi, S. D., Dixit, S. R. & Chimatadar, S. A. Interaction of Hydralazine with Human Serum Albumin and Effect of β-Cyclodextrin on Binding: Insights from Spectroscopic and Molecular Docking Techniques. *Industrial & Engineering Chemistry Research* 55, 5454-5464, doi:10.1021/acs.iecr.6b00517 (2016).

46 Suryawanshi, V. D., Anbhule, P. V., Gore, A. H., Patil, S. R. & Kolekar, G. B. Spectroscopic Investigation on the Interaction of Pyrimidine Derivative, 2-Amino-6-hydroxy-4-(3,4-dimethoxyphenyl)-pyrimidine-5-carbonitrile with Human Serum Albumin: Mechanistic and Conformational Study. *Industrial & Engineering Chemistry Research* 51, 95-102, doi:10.1021/ie202005c (2012).

47 Weiss-Errico, M. J., Miksovska, J. & O'Shea, K. E. β-Cyclodextrin Reverses Binding of Perfluorooctanoic Acid to Human Serum Albumin. *Chemical Research in Toxicology* 31, 277-284, doi:10.1021/acs.chemrestox.8b00002 (2018).

48 Wang, L. *et al.* The influence of hydroxypropyl-β-cyclodextrin on the solubility, dissolution, cytotoxicity, and binding of riluzole with human serum albumin. *Journal of Pharmaceutical and Biomedical Analysis* 117, 453-463, doi:https://doi.org/10.1016/j.jpba.2015.09.033 (2016).

49 Sarbadhikary, P. & Dube, A. Spectroscopic investigations on the binding of an iodinated chlorin p6-copper complex to human serum albumin. *Photochemical & Photobiological Sciences* 16, 1762-1770, doi:10.1039/c7pp00197e (2017).

50 Martin, C., Cohen, B., Gaamoussi, I., Ijjaali, M. & Douhal, A. Ultrafast Dynamics of C30 in Solution and within CDs and HSA Protein. *The Journal of Physical Chemistry B* 118, 5760-5771, doi:10.1021/jp5026575 (2014).

51 Cohen, B., Martin Álvarez, C., Alarcos Carmona, N., Organero, J. A. & Douhal, A. Proton-Transfer Reaction Dynamics within the Human Serum Albumin Protein. *The Journal of Physical Chemistry B* 115, 7637-7647, doi:10.1021/jp200294q (2011).

52 Moulin, V., Grandoni, F., Castioni, J. & Lu, H. Pancytopenia in an adult patient with thiamine-responsive megaloblastic anaemia. *BMJ Case Reports* 2018, bcr-2018-225035, doi:10.1136/bcr-2018-225035 (2018).

53 Wrenn, K. D., Murphy, F. & Slovis, C. M. A toxicity study of parenteral thiamine hydrochloride. *Annals of Emergency Medicine* 18, 867-870, doi:https://doi.org/10.1016/S0196-0644(89)80215-X (1989).

54 Chern, C.-H., Chern, T.-L., Hu, S.-C., Lee, C.-H. & Deng, J.-F. Complete and partial response to flumazenil in patients with suspected benzodiazepine overdose. *The American Journal of Emergency Medicine* 13, 372-375, doi:https://doi.org/10.1016/0735-6757(95)90222-8 (1995).

55 Kumar, R. *et al.* Pyrene appended bis-triazolylated 1,4-dihydropyridine as a selective fluorogenic sensor for Cu2+. *Dyes and Pigments* 161, 162-171, doi:https://doi.org/10.1016/j.dyepig.2018.09.049 (2019).

56 Ulatowski, F., Dąbrowa, K., Bałakier, T. & Jurczak, J. Recognizing the Limited Applicability of Job Plots in Studying Host–Guest Interactions in Supramolecular Chemistry. *The Journal of Organic Chemistry* 81, 1746-1756, doi:10.1021/acs.joc.5b02909 (2016).

57 dos Santos, C. H., Uchiyama, N. M. & Bagatin, I. A. Selective azo dye-based colorimetric chemosensor for F−, CH3COO− and PO43−. *Spectrochimica Acta Part A: Molecular and Biomolecular Spectroscopy* 210, 355-361, doi:https://doi.org/10.1016/j.saa.2018.11.057 (2019).

58 Thordarson, P. Determining association constants from titration experiments in supramolecular chemistry. *Chemical Society Reviews* 40, 1305-1323, doi:10.1039/c0cs00062k (2011).

59 Yuan, L. *et al.* Studies on the preparation and photostability of avobenzone and (2-hydroxy)propyl-β-cyclodextrin inclusion complex. *Journal of Photochemistry and Photobiology A: Chemistry* 369, 174-180, doi:https://doi.org/10.1016/j.jphotochem.2018.09.036 (2019).

60 Bartolotta, M. & Buthelezi, M. T. Molecular polarity effect on the association constant of cyclodextrin-pyrimidine nucleobases in water. *Journal of Photochemistry and Photobiology A: Chemistry* 371, 382-386, doi:https://doi.org/10.1016/j.jphotochem.2018.11.037 (2019).

61 Moncada-Basualto, M. *et al.* Supramolecular hydrogels of β-cyclodextrin linked to calcium homopoly-l-guluronate for release of coumarins with trypanocidal activity. *Carbohydrate Polymers* 204, 170-181, doi:https://doi.org/10.1016/j.carbpol.2018.10.010 (2019).

62 KiranKumar, H. N., RohitKumar, H. G. & Advirao, G. M. Synthesis, DNA binding and cytotoxic activity of pyrimido[4′,5′:4,5]thieno(2,3-b)quinoline with 9-hydroxy-4-(3-diethylaminopropylamino) and 8-methoxy-4-(3-diethylaminopropylamino) substitutions. *Journal of Photochemistry and Photobiology B: Biology* 178, 1-9, doi:https://doi.org/10.1016/j.jphotobiol.2017.10.022 (2018).

63 Connors, K. A. & Pendergast, D. D. Microscopic binding constants in cyclodextrin systems: complexation of .alpha.-cyclodextrin with sym-1,4-disubstituted benzenes. *Journal of the American Chemical Society* 106, 7607-7614, doi:10.1021/ja00336a048 (1984).

64 Saha, S., Roy, A. & Roy, M. N. Mechanistic Investigation of Inclusion Complexes of a Sulfa Drug with α- and β-Cyclodextrins. *Industrial & Engineering Chemistry Research* 56, 11672-11683, doi:10.1021/acs.iecr.7b02619 (2017).

65 Saha, S., Roy, A., Roy, K. & Roy, M. N. Study to explore the mechanism to form inclusion complexes of β-cyclodextrin with vitamin molecules. *Scientific Reports* 6, 35764, doi:10.1038/srep35764

https://www.nature.com/articles/srep35764#supplementary-information (2016).

66 Geng, Q. *et al.* Preparation and Characterization of Butachlor/(2-Hydroxypropyl)-β-cyclodextrin Inclusion Complex: Improve Soil Mobility and Herbicidal Activity and Decrease Fish Toxicity. *Journal of Agricultural and Food Chemistry* 66, 12198-12205, doi:10.1021/acs.jafc.8b04812 (2018).

67 Sancho, M. I. *et al.* Physicochemical Characterization of 2-Hydroxybenzophenone with β-Cyclodextrin in Solution and Solid State. *The Journal of Physical Chemistry B* 119, 5918-5925, doi:10.1021/acs.jpcb.5b01742 (2015).

68 Sherje, A. P. *et al.* Inclusion Complexation of Etodolac with Hydroxypropyl-beta-cyclodextrin and Auxiliary Agents: Formulation Characterization and Molecular Modeling Studies. *Molecular Pharmaceutics* 14, 1231-1242, doi:10.1021/acs.molpharmaceut.6b01115 (2017).

69 do Nascimento Cavalcante, A. *et al.* Elaboration and characterization of the inclusion complex between β-cyclodextrin and the anticholinesterase 2-oleyl-1,3-dipalmitoyl-glycerol extracted from the seeds of Platonia insignis MART. *Journal of Molecular Structure* 1177, 286-301, doi:https://doi.org/10.1016/j.molstruc.2018.09.067 (2019).

70 Barman, B. K., Barman, S. & Roy, M. N. Inclusion complexation between tetrabutylphosphonium methanesulfonate as guest and α- and β-cyclodextrin as hosts investigated by physicochemical methodology. *Journal of Molecular Liquids* 264, 80-87, doi:https://doi.org/10.1016/j.molliq.2018.04.148 (2018).

71 Aytac, Z. *et al.* Fast-Dissolving, Prolonged Release, and Antibacterial Cyclodextrin/Limonene-Inclusion Complex Nanofibrous Webs via Polymer-Free Electrospinning. *Journal of Agricultural and Food Chemistry* 64, 7325-7334, doi:10.1021/acs.jafc.6b02632 (2016).

72 Guo, H. *et al.* Photoresponsive self-assembly of a β-cyclodextrin derivative with an azobenzene terminal group in water. *Dyes and Pigments* 149, 626-632, doi:https://doi.org/10.1016/j.dyepig.2017.11.035 (2018).

73 Celebioglu, A. & Uyar, T. Antioxidant Vitamin E/Cyclodextrin Inclusion Complex Electrospun Nanofibers: Enhanced Water Solubility, Prolonged Shelf Life, and Photostability of Vitamin E. *Journal of Agricultural and Food Chemistry* 65, 5404-5412, doi:10.1021/acs.jafc.7b01562 (2017).

74 Gong, L. *et al.* An inclusion complex of eugenol into β-cyclodextrin: Preparation, and physicochemical and antifungal characterization. *Food Chemistry* 196, 324-330, doi:https://doi.org/10.1016/j.foodchem.2015.09.052 (2016).

75 Ikeda, H. *et al.* Fluorescent Cyclodextrins for Molecule Sensing: Fluorescent Properties, NMR Characterization, and Inclusion Phenomena of N-Dansylleucine-Modified Cyclodextrins. *Journal of the American Chemical Society* 118, 10980-10988, doi:10.1021/ja960183i (1996).

76 Banerjee, A. & Sengupta, P. K. Encapsulation of 3-hydroxyflavone and fisetin in β-cyclodextrins: Excited state proton transfer fluorescence and molecular mechanics studies. *Chemical Physics Letters* 424, 379-386, doi:https://doi.org/10.1016/j.cplett.2006.05.006 (2006).

77 Chaudhuri, S., Chakraborty, S. & Sengupta, P. K. Encapsulation of serotonin in β-cyclodextrin nano-cavities: Fluorescence spectroscopic and molecular modeling studies. *Journal of Molecular Structure* 975, 160-165, doi:https://doi.org/10.1016/j.molstruc.2010.04.014 (2010).

78 Sharma, U. S., Balasubramanian, S. V. & Straubinger, R. M. Pharmaceutical and Physical Properties of Paclitaxel (Taxol †) Complexes with Cyclodextrins ‡.

Journal of Pharmaceutical Sciences 84, 1223-1230, doi:https://doi.org/10.1002/jps.2600841015 (1995).

79 Dsouza, R. N., Pischel, U. & Nau, W. M. Fluorescent Dyes and Their Supramolecular Host/Guest Complexes with Macrocycles in Aqueous Solution. *Chemical Reviews* 111, 7941-7980, doi:10.1021/cr200213s (2011).

80 Naik, R. S., Pawar, S. K., Tandel, R. D. & J, S. Insights in to the mechanism of interaction of a thrombin inhibitor, dabigatran etexilate with human serum albumin and influence of β-cyclodextrin on binding: Spectroscopic and computational approach. *Journal of Molecular Liquids* 251, 119-127, doi:https://doi.org/10.1016/j.molliq.2017.12.056 (2018).

CHAPTER VI

1 Marvin, C. H. *et al.* Hexabromocyclododecane: Current Understanding of Chemistry, Environmental Fate and Toxicology and Implications for Global Management. *Environmental Science & Technology* 45, 8613-8623, doi:10.1021/es201548c (2011).

2 Melymuk, L. *et al.* Challenges in the Analysis of Novel Flame Retardants in Indoor Dust: Results of the INTERFLAB 2 Interlaboratory Evaluation. *Environmental Science & Technology* 52, 9295-9303, doi:10.1021/acs.est.8b02715 (2018).

3 Mitro, S. D. *et al.* Consumer Product Chemicals in Indoor Dust: A Quantitative Meta-analysis of U.S. Studies. *Environmental Science & Technology* 50, 10661-10672, doi:10.1021/acs.est.6b02023 (2016).

4 Su, G., Letcher, R. J., McGoldrick, D. J. & Backus, S. M. Halogenated Flame Retardants in Predator and Prey Fish From the Laurentian Great Lakes: Age-Dependent Accumulation and Trophic Transfer. *Environmental Science & Technology* 51, 8432-8441, doi:10.1021/acs.est.7b02338 (2017).

5 Tay, J. H. *et al.* Human Exposure to Legacy and Emerging Halogenated Flame Retardants via Inhalation and Dust Ingestion in a Norwegian Cohort. *Environmental Science & Technology* 51, 8176-8184, doi:10.1021/acs.est.7b02114 (2017).

6 Ruan, Y. *et al.* Stereoisomer-Specific Trophodynamics of the Chiral Brominated Flame Retardants HBCD and TBECH in a Marine Food Web, with Implications for Human Exposure. *Environmental Science & Technology* 52, 8183-8193, doi:10.1021/acs.est.8b02206 (2018).

7 Nguyen, K.-H., Abou-Elwafa Abdallah, M., Moehring, T. & Harrad, S. Biotransformation of the Flame Retardant 1,2-Dibromo-4-(1,2-dibromoethyl)cyclohexane (TBECH) in Vitro by Human Liver Microsomes. *Environmental Science & Technology* 51, 10511-10518, doi:10.1021/acs.est.7b02834 (2017).

8 Rauert, C., Schuster, J. K., Eng, A. & Harner, T. Global Atmospheric Concentrations of Brominated and Chlorinated Flame Retardants and Organophosphate Esters. *Environmental Science & Technology* 52, 2777-2789, doi:10.1021/acs.est.7b06239 (2018).

9 Vorkamp, K., Falk, K., Møller, S., Rigét, F. F. & Sørensen, P. B. Regulated and Unregulated Halogenated Flame Retardants in Peregrine Falcon Eggs from Greenland. *Environmental Science & Technology* 52, 474-483, doi:10.1021/acs.est.7b04866 (2018).

10 Arnot, J. A. *et al.* Toward a Consistent Evaluative Framework for POP Risk Characterization. *Environmental Science & Technology* 45, 97-103, doi:10.1021/es102551d (2011).

11 Loganathan, B. in *Persistent Organic Chemicals in the Environment: Status and Trends in the Pacific Basin Countries I Contamination Status* Vol. 1243 *ACS Symposium Series* Ch. 1, 1-15 (American Chemical Society, 2016).

12 Masunaga, S., Loganathan, B. G., Khim, J. S. & Kodavanti, P. R. S. in *ACS Symposium Series* Vol. 1243 0 (American Chemical Society, 2016).

13 Law, R. J. *et al.* A Significant Downturn in Levels of Hexabromocyclododecane in the Blubber of Harbor Porpoises (Phocoena phocoena) Stranded or Bycaught in the UK: An Update to 2006. *Environmental Science & Technology* 42, 9104-9109, doi:10.1021/es8014309 (2008).

14 Su, G. *et al.* Isomer-Specific Hexabromocyclododecane (HBCDD) Levels in Top Predator Fish from Across Canada and 36-Year Temporal Trends in Lake Ontario. *Environmental Science & Technology* 52, 6197-6207, doi:10.1021/acs.est.8b01052 (2018).

15 Wang, Y. *et al.* Organophosphorus Flame Retardants and Plasticizers in Building and Decoration Materials and Their Potential Burdens in Newly Decorated Houses in China. *Environmental Science & Technology* 51, 10991-10999, doi:10.1021/acs.est.7b03367 (2017).

16 Dominguez-Romero, E. *et al.* Tissue Distribution and Transfer to Eggs of Ingested α-Hexabromocyclododecane (α-HBCDD) in Laying Hens (Gallus domesticus). *Journal of Agricultural and Food Chemistry* 64, 2112-2119, doi:10.1021/acs.jafc.5b05574 (2016).

17 Shi, Y. *et al.* Antioxidant gene expression and metabolic responses of earthworms (Eisenia fetida) after exposure to various concentrations of hexabromocyclododecane. *Environmental Pollution* 232, 245-251, doi:https://doi.org/10.1016/j.envpol.2017.09.039 (2018).

18 Peng, Y.-H., Chen, Y.-j., Chang, M. & Shih, Y.-h. The effect of zerovalent iron on the microbial degradation of hexabromocyclododecane. *Chemosphere* 200, 419-426, doi:https://doi.org/10.1016/j.chemosphere.2018.02.123 (2018).

19 Peng, X., Wei, D., Huang, Q. & Jia, X. Debromination of Hexabromocyclododecane by Anaerobic Consortium and Characterization of Functional Bacteria. *Frontiers in Microbiology* 9, doi:10.3389/fmicb.2018.01515 (2018).

20 Li, X. *et al.* Novel approach for removing brominated flame retardant from aquatic environments using Cu/Fe-based metal-organic frameworks: A case of

hexabromocyclododecane (HBCD). *Science of The Total Environment* 621, 1533-1541, doi:https://doi.org/10.1016/j.scitotenv.2017.10.075 (2018).

21 Yan, X. *et al.* Disposal of hexabromocyclododecane (HBCD) by grinding assisted with sodium persulfate. *RSC Advances* 7, 23313-23318, doi:10.1039/c7ra02689g (2017).

22 Rajbanshi, B. *et al.* Study to Probe Subsistence of Host-Guest Inclusion Complexes of α and β-Cyclodextrins with Biologically Potent Drugs for Safety Regulatory Dischargement. *Scientific Reports* 8, 13031, doi:10.1038/s41598-018-31373-x (2018).

23 Saha, S., Roy, A. & Roy, M. N. Mechanistic Investigation of Inclusion Complexes of a Sulfa Drug with α- and β-Cyclodextrins. *Industrial & Engineering Chemistry Research* 56, 11672-11683, doi:10.1021/acs.iecr.7b02619 (2017).

24 Zhou, H., Yamada, T. & Kimizuka, N. Supramolecular Thermo-Electrochemical Cells: Enhanced Thermoelectric Performance by Host–Guest Complexation and Salt-Induced Crystallization. *Journal of the American Chemical Society* 138, 10502-10507, doi:10.1021/jacs.6b04923 (2016).

25 Xue, M., Wei, W., Su, Y., Johnson, D. & Heath, J. R. Supramolecular Probes for Assessing Glutamine Uptake Enable Semi-Quantitative Metabolic Models in Single Cells. *Journal of the American Chemical Society* 138, 3085-3093, doi:10.1021/jacs.5b12187 (2016).

26 Ling, B. *et al.* Mechanism study on pH-responsive cyclodextrin capped mesoporous silica: effect of different stalk densities and the type of cyclodextrin. *Nanotechnology* 26, 165704 (2015).

27 Rajesh, K. G., Suzuki, R., Maeda, H., Murio, Y. & Sasaguri, S. 5-HT2 receptor blocker sarpogrelate prevents downregulation of antiapoptotic protein Bcl-2 and protects the heart against ischemia-reperfusion injury. *Life Sci* 79, 1749-1755, doi:10.1016/j.lfs.2006.06.026 (2006).

28 Li, H. *et al.* Viologen-mediated assembly of and sensing with carboxylatopillar[5]arene-modified gold nanoparticles. *J Am Chem Soc* 135, 1570-1576 (2013).

29 Saha, S., Roy, A., Roy, K. & Roy, M. N. Study to explore the mechanism to form inclusion complexes of β-cyclodextrin with vitamin molecules. *Scientific Reports* 6, 35764, doi:10.1038/srep35764

https://www.nature.com/articles/srep35764#supplementary-information (2016).

30 Roy, M. N., Roy, A. & Saha, S. Probing inclusion complexes of cyclodextrins with amino acids by physicochemical approach. *Carbohydrate Polymers* 151, 458-466, doi:10.1016/j.carbpol.2016.05.100 (2016).

31 Roy, M. N., Saha, S., Barman, S. & Ekka, D. Host-guest inclusion complexes of RNA nucleosides inside aqueous cyclodextrins explored by physicochemical and spectroscopic methods. *RSC Advances* 6, 8881-8891, doi:10.1039/c5ra24102b (2016).

32 Ji, H., Liu, F. & Sun, S. Study of the Counter Anions in the Host-Guest Chemistry of Cucurbit[8]uril and 1-Ethyl-1′-benzyl-4,4′-bipyridinium. *The Scientific World Journal* 2013, 452056, doi:10.1155/2013/452056 (2013).

33 Yang, L. J. *et al.* Preparation and characterization of inclusion complexes of naringenin with beta-cyclodextrin or its derivative. *Carbohydr Polym* 98, 861-869 (2013).

34 Fernandes, A. *et al.* Structural characterization of inclusion complexes between cyanidin-3-O-glucoside and β-cyclodextrin. *Carbohydrate Polymers* 102, 269-277, doi:https://doi.org/10.1016/j.carbpol.2013.11.037 (2014).

35 Yang, B., Lin, J., Chen, Y. & Liu, Y. Artemether/hydroxypropyl-beta-cyclodextrin host-guest system: characterization, phase-solubility and inclusion mode. *Bioorg Med Chem* 17, 6311-6317, doi:10.1016/j.bmc.2009.07.060 (2009).

36 Servais, A.-C. *et al.* Capillary electrophoretic and nuclear magnetic resonance studies on the opposite affinity pattern of propranolol enantiomers towards

various cyclodextrins. *Journal of Separation Science* 33, 1617-1624, doi:10.1002/jssc.201000040 (2010).

37 Correia, I. *et al.* Study of inclusion complexes of acridine with β- and (2,6-di-O-methyl)-β-cyclodextrin by use of solubility diagrams and NMR spectroscopy. *Journal of Physical Organic Chemistry* 15, 647-659, doi:10.1002/poc.528 (2002).

38 Bednarek, E. *et al.* Complexation of steroid hormones: prednisolone, ethinyloestradiol and estriol with [small beta]-cyclodextrin. An aqueous 1H NMR study. *Journal of the Chemical Society, Perkin Transactions 2*, 999-1004, doi:10.1039/b110435g (2002).

39 Ishizu, T., Hirata, C., Yamamoto, H. & Harano, K. Structure and intramolecular flexibility of β-cyclodextrin complex with (−)-epigallocatechin gallate in aqueous solvent. *Magnetic Resonance in Chemistry* 44, 776-783, doi:10.1002/mrc.1848 (2006).

40 Kemelbekov, U. *et al.* IR, UV and NMR studies of β-cyclodextrin inclusion complexes of kazcaine and prosidol bases. *Journal of inclusion phenomena and macrocyclic chemistry* 69, 181-190, doi:10.1007/s10847-010-9829-x (2011).

41 Stalin, T., Srinivasan, K., Sivakumar, K. & Radhakrishnan, S. Preparation and characterizations of solid/aqueous phases inclusion complex of 2,4-dinitroaniline with beta-cyclodextrin.

42 Sivakumar, K., Ragi, T. R., Prema, D. & Stalin, T. Experimental and theoretical investigation on the structural characterization and orientation preferences of 2-hydroxy-1-naphthoic acid/β-cyclodextrin host-guest inclusion complex. *Journal of Molecular Liquids* 218, 538-548, doi:https://doi.org/10.1016/j.molliq.2016.03.004 (2016).

43 Negi, J. S. & Singh, S. Spectroscopic investigation on the inclusion complex formation between amisulpride and gamma-cyclodextrin. *Carbohydr Polym* 92, 1835-1843 (2013).

44 Xiao, C. F. *et al.* Investigation of inclusion complex of epothilone A with cyclodextrins.

45 Zhang, J. Q. *et al.* Novel water-soluble fisetin/cyclodextrins inclusion complexes: Preparation, characterization, molecular docking and bioavailability. *Carbohydr Res* 418, 20-28 (2015).

46 Okada, Y., Ueyama, K., Nishikawa, J.-i., Semma, M. & Ichikawa, A. *Effect of 6-O-α-maltosyl-β cyclodextrin and its cholesterol inclusion complex on cellular cholesterol levels and ABCA1 and ABCG1 expression in mouse mastocytoma P-815 cells*. Vol. 357 (2012).

47 Keutner, C. *et al.* Photoemission Electron Microscopy and Scanning Electron Microscopy of Magnetospirillum magnetotacticum's Magnetosome Chains. *Analytical Chemistry* 86, 9590-9594, doi:10.1021/ac502050j (2014).

48 Tsiper, S. *et al.* Sparsity-Based Super Resolution for SEM Images. *Nano Letters* 17, 5437-5445, doi:10.1021/acs.nanolett.7b02091 (2017).

49 Piispanen, M. H. *et al.* A Comparative Study of Fly ash Characterization by LA-ICP-MS and SEM-EDS. *Energy & Fuels* 23, 3451-3456, doi:10.1021/ef801037a (2009).

50 Sifaoui, H. *et al.* Formation of β-cyclodextrin complexes in an anhydrous environment. *Journal of Molecular Modeling* 22, 207, doi:10.1007/s00894-016-3061-6 (2016).

51 Celebioglu, A. & Uyar, T. Antioxidant Vitamin E/Cyclodextrin Inclusion Complex Electrospun Nanofibers: Enhanced Water Solubility, Prolonged Shelf Life, and Photostability of Vitamin E. *Journal of Agricultural and Food Chemistry* 65, 5404-5412, doi:10.1021/acs.jafc.7b01562 (2017).

52 Yang, G.-F., Wang, H.-B., Yang, W.-C., Gao, D. & Zhan, C.-G. Bioactive Permethrin/β-Cyclodextrin Inclusion Complex. *The Journal of Physical Chemistry B* 110, 7044-7048, doi:10.1021/jp056809l (2006).

53 Păduraru, O. M., Bosînceanu, A., Ţântaru, G. & Vasile, C. Effect of Hydroxypropyl-β-Cyclodextrin on the Solubility of an Antiarrhythmic Agent. *Industrial & Engineering Chemistry Research* 52, 2174-2181, doi:10.1021/ie303440w (2013).

54 Takahama, Y. & Yamada, Y. Isolation of Pseudomonas sp. Strain HB01 Which Degrades the Persistent Brominated Flame Retardant γ-Hexabromocyclododecane AU - YAMADA, Takashi. *Bioscience, Biotechnology, and Biochemistry* 73, 1674-1678, doi:10.1271/bbb.90104 (2009).

55 Kamanavalli, C. M. & Ninnekar, H. Z. Biodegradation of DDT by a Pseudomonas Species. *Current Microbiology* 48, 10-13, doi:10.1007/s00284-003-4053-1 (2004).

56 Lin, Q. & Jianlong, W. Biodegradation characteristics of quinoline by Pseudomonas putida. *Bioresour Technol* 101, 7683-7686, doi:10.1016/j.biortech.2010.05.026 (2010).

CHAPTER VII

1 Annahazi, A., Roka, R., Rosztoczy, A. & Wittmann, T. Role of antispasmodics in the treatment of irritable bowel syndrome. *World J Gastroenterol* 20, 6031-6043 (2014).

2 Martinez-Vazquez, M. A. *et al.* Effect of antispasmodic agents, alone or in combination, in the treatment of Irritable Bowel Syndrome: systematic review and meta-analysis. *Rev Gastroenterol Mex* 77, 82-90 (2012).

3 Carmona-Sánchez, R. *et al.* Consenso mexicano sobre el síndrome de intestino irritable. *Revista de Gastroenterología de México* 81, 149-167, doi:https://doi.org/10.1016/j.rgmx.2016.01.004 (2016).

4 Remes-Troche, J. M. *et al.* Guía clínica para diagnóstico y tratamiento de la enfermedad celíaca en México. *Revista de Gastroenterología de México* 83, 434-450, doi:https://doi.org/10.1016/j.rgmx.2018.05.005 (2018).

5 Wittmann, T., Paradowski, L., Ducrotte, P., Bueno, L. & Andro Delestrain, M. C. Clinical trial: the efficacy of alverine citrate/simeticone combination on abdominal pain/discomfort in irritable bowel syndrome--a randomized, double-blind, placebo-controlled study. *Aliment Pharmacol Ther* 31, 615-624 (2010).

6 Catterall, W. A. Voltage-gated calcium channels. *Cold Spring Harbor perspectives in biology* 3, a003947-a003947, doi:10.1101/cshperspect.a003947.

7 Wu, J. *et al.* Structure of the voltage-gated calcium channel Cav1.1 at 3.6 Å resolution. *Nature* 537, 191, doi:10.1038/nature19321

https://www.nature.com/articles/nature19321#supplementary-information (2016).

8 Catterall, W. A. & Zheng, N. Deciphering voltage-gated Na⁺ and Ca²⁺ channels by studying prokaryotic ancestors. *Trends in Biochemical Sciences* 40, 526-534, doi:10.1016/j.tibs.2015.07.002 (2015).

9 Rathod, D. M. *et al.* An improved LC-MS/MS method for the quantification of alverine and para hydroxy alverine in human plasma for a bioequivalence study(☆). *Journal of pharmaceutical analysis* 7, 95-102, doi:10.1016/j.jpha.2016.11.003 (2017).

10 Flarakos, J., Morand, K. L. & Vouros, P. High-Throughput Solution-Based Medicinal Library Screening against Human Serum Albumin. *Analytical Chemistry* 77, 1345-1353, doi:10.1021/ac048685z (2005).

11 Vuignier, K., Veuthey, J. L., Carrupt, P. A. & Schappler, J. Global analytical strategy to measure drug-plasma protein interactions: from high-throughput to in-depth analysis. *Drug Discov Today* 18, 1030-1034 (2013).

12 Zsila, F. Subdomain IB Is the Third Major Drug Binding Region of Human Serum Albumin: Toward the Three-Sites Model. *Molecular Pharmaceutics* 10, 1668-1682, doi:10.1021/mp400027q (2013).

13 Dalvit, C., Fagerness, P. E., Hadden, D. T., Sarver, R. W. & Stockman, B. J. Fluorine-NMR experiments for high-throughput screening: theoretical aspects, practical

considerations, and range of applicability. *J Am Chem Soc* 125, 7696-7703 (2003).

14 Job, P. *Formation and stability of inorganic complexes in solution*. Vol. 10 (1928).

15 Kano, K., Nishiyabu, R., Asada, T. & Kuroda, Y. Static and Dynamic Behavior of 2:1 Inclusion Complexes of Cyclodextrins and Charged Porphyrins in Aqueous Organic Media. *Journal of the American Chemical Society* 124, 9937-9944, doi:10.1021/ja020253n (2002).

16 Renny, J. S., Tomasevich, L. L., Tallmadge, E. H. & Collum, D. B. Method of continuous variations: applications of job plots to the study of molecular associations in organometallic chemistry. *Angew Chem Int Ed Engl* 52, 11998-12013 (2013).

17 He, J., Deng, L. & Yang, S. Synthesis and characterization of beta-cyclodextrin inclusion complex containing di(8-hydroxyquinoline) magnesium. *Spectrochim Acta A Mol Biomol Spectrosc* 70, 878-883, doi:10.1016/j.saa.2007.10.004 (2008).

18 Liu, Y., Yang, Y.-W., Chen, Y. & Ding, F. Efficient fluorescent sensors of oligopeptides by dithiobis(2-benzoylamide)-bridged bis(beta-cyclodextrin)s: structure in solution, binding behavior, and thermodynamic origin. *Bioorg Med Chem* 13, 963-971, doi:10.1016/j.bmc.2004.11.042 (2005).

19 Zhang, J. Q. *et al.* Novel water-soluble fisetin/cyclodextrins inclusion complexes: Preparation, characterization, molecular docking and bioavailability. *Carbohydr Res* 418, 20-28 (2015).

20 Okada, Y., Ueyama, K., Nishikawa, J.-i., Semma, M. & Ichikawa, A. *Effect of 6-O-α-maltosyl-β cyclodextrin and its cholesterol inclusion complex on cellular cholesterol levels and ABCA1 and ABCG1 expression in mouse mastocytoma P-815 cells*. Vol. 357 (2012).

21 Sindelar, V. *et al.* Supramolecular assembly of 2,7-dimethyldiazapyrenium and cucurbit[8]uril: a new fluorescent host for detection of catechol and dopamine.

22 Yang, L. J. *et al.* Preparation and characterization of inclusion complexes of naringenin with beta-cyclodextrin or its derivative. *Carbohydr Polym* 98, 861-869 (2013).

23 Fernandes, A. *et al.* Structural characterization of inclusion complexes between cyanidin-3-O-glucoside and β-cyclodextrin. *Carbohydrate Polymers* 102, 269-277, doi:https://doi.org/10.1016/j.carbpol.2013.11.037 (2014).

24 Xiao, C. F. *et al.* Investigation of inclusion complex of epothilone A with cyclodextrins.

25 Yang, B., Lin, J., Chen, Y. & Liu, Y. Artemether/hydroxypropyl-beta-cyclodextrin host-guest system: characterization, phase-solubility and inclusion mode. *Bioorg Med Chem* 17, 6311-6317, doi:10.1016/j.bmc.2009.07.060 (2009).

26 Servais, A. C. *et al.* Capillary electrophoretic and nuclear magnetic resonance studies on the opposite affinity pattern of propranolol enantiomers towards various cyclodextrins.

27 Correia, I. *et al.* Study of inclusion complexes of acridine with β- and (2,6-di-O-methyl)-β-cyclodextrin by use of solubility diagrams and NMR spectroscopy. *Journal of Physical Organic Chemistry* 15, 647-659, doi:10.1002/poc.528 (2002).

28 Kemelbekov, U. *et al.* IR, UV and NMR studies of β-cyclodextrin inclusion complexes of kazcaine and prosidol bases. *Journal of inclusion phenomena and macrocyclic chemistry* 69, 181-190, doi:10.1007/s10847-010-9829-x (2011).

29 Stalin, T., Srinivasan, K., Sivakumar, K. & Radhakrishnan, S. Preparation and characterizations of solid/aqueous phases inclusion complex of 2,4-dinitroaniline with beta-cyclodextrin.

30 Sivakumar, K., Ragi, T. R., Prema, D. & Stalin, T. Experimental and theoretical investigation on the structural characterization and orientation preferences of 2-hydroxy-1-naphthoic acid/β-cyclodextrin host-guest inclusion complex. *Journal of Molecular Liquids* 218, 538-548, doi:https://doi.org/10.1016/j.molliq.2016.03.004 (2016).

31 Negi, J. S. & Singh, S. Spectroscopic investigation on the inclusion complex formation between amisulpride and gamma-cyclodextrin. *Carbohydr Polym* 92, 1835-1843 (2013).

32 Inoue, Y., Hirano, A., Murata, I., Kobata, K. & Kanamoto, I. *Assessment of the Physical Properties of Inclusion Complexes of Forchlorfenuron and γ-Cyclodextrin Derivatives and Their Promotion of Plant Growth*. Vol. 3 (2018).

33 Suzuki, R. *et al.* Preparation, characterization, and study of the antimicrobial activity of a Hinokitiol-copper(II)/γ-cyclodextrin ternary complex. *Journal of Molecular Structure* 1194, 19-27, doi:https://doi.org/10.1016/j.molstruc.2019.05.078 (2019).

34 Tanwar, S., Barbey, C. & Dupont, N. Experimental and theoretical studies of the inclusion complex of different linear aliphatic alcohols with cyclodextrins. *Carbohydrate Polymers* 217, 26-34, doi:https://doi.org/10.1016/j.carbpol.2019.04.052 (2019).

35 Yadav, V. R., Suresh, S., Devi, K. & Yadav, S. Effect of cyclodextrin complexation of curcumin on its solubility and antiangiogenic and anti-inflammatory activity in rat colitis model. *AAPS PharmSciTech* 10, 752-762 (2009).

36 Yao, Q. *et al.* Inclusion complexes of cypermethrin and permethrin with monochlorotriazinyl-beta-cyclodextrin: a combined spectroscopy, TG/DSC and DFT study. *Spectrochim Acta A Mol Biomol Spectrosc* 117, 576-586 (2014).

37 Li, J.-H., Zhang, N., Li, X.-T. & Wang, J.-Y. Thermal Stability and Decomposition Kinetics of the β-CD Cinnamic Aldehyde Inclusion Complex. *Journal of inclusion phenomena and molecular recognition in chemistry* 28, 95-103, doi:10.1023/a:1007991708832 (1997).

38 Jiang, L., Yang, J., Wang, Q., Ren, L. & Zhou, J. Physicochemical properties of catechin/β-cyclodextrin inclusion complex obtained via co-precipitation. *CyTA - Journal of Food* 17, 544-551, doi:10.1080/19476337.2019.1612948 (2019).

39 Yildiz, Z. I. & Uyar, T. Fast-dissolving electrospun nanofibrous films of paracetamol/cyclodextrin inclusion complexes. *Applied Surface Science* 492, 626-633, doi:https://doi.org/10.1016/j.apsusc.2019.06.220 (2019).

40 Qiu, N. *et al.* Inclusion complex of emodin with hydroxypropyl-β-cyclodextrin: Preparation, physicochemical and biological properties. *Journal of Molecular Liquids* 289, 111151, doi:https://doi.org/10.1016/j.molliq.2019.111151 (2019).

41 Rajbanshi, B. *et al.* Study to Probe Subsistence of Host-Guest Inclusion Complexes of α and β-Cyclodextrins with Biologically Potent Drugs for Safety Regulatory Dischargement. *Scientific Reports* 8, 13031, doi:10.1038/s41598-018-31373-x (2018).

42 Matencio, A., Hernández-García, S., García-Carmona, F. & López-Nicolás, M. J. A Way to Increase the Bioaccesibility and Photostability of Roflumilast, a COPD Treatment, by Cyclodextrin Monomers. *Polymers* 11, doi:10.3390/polym11050801 (2019).

43 Sursyakova, V. V., Levdansky, V. A. & Rubaylo, A. I. Thermodynamic parameters for the complexation of water-insoluble betulin derivatives with (2-hydroxypropyl)-γ-cyclodextrin determined by phase-solubility technique combined with capillary zone electrophoresis. *ELECTROPHORESIS* 40, 1656-1661, doi:10.1002/elps.201800516 (2019).

44 Loftsson, T., Hreinsdottir, D. & Masson, M. Evaluation of cyclodextrin solubilization of drugs. *Int J Pharm* 302, 18-28 (2005).

45 Benesi, H. A. & Hildebrand, J. H. A Spectrophotometric Investigation of the Interaction of Iodine with Aromatic Hydrocarbons. *Journal of the American Chemical Society* 71, 2703-2707, doi:10.1021/ja01176a030 (1949).

46 Das, K. *et al.* Physicochemical investigations of amino acid ionic liquid based inclusion complex probed by spectral and molecular docking techniques. *Journal of Molecular Liquids* 291, 111255, doi:https://doi.org/10.1016/j.molliq.2019.111255 (2019).

47 Saha, S., Roy, A., Roy, K. & Roy, M. N. Study to explore the mechanism to form inclusion complexes of β-cyclodextrin with vitamin molecules. *Scientific Reports* 6, 35764, doi:10.1038/srep35764

https://www.nature.com/articles/srep35764#supplementary-information (2016).

48 Roy, P. M., Saha, S., Barman, S. & Ekka, D. D. *Host–guest inclusion complexes of RNA nucleosides inside aqueous cyclodextrins explored by physicochemical and spectroscopic methods*. Vol. 6 (2016).

49 Cramer, F., Saenger, W. & Spatz, H. C. Inclusion Compounds. XIX.1a The Formation of Inclusion Compounds of α-Cyclodextrin in Aqueous Solutions. Thermodynamics and Kinetics. *Journal of the American Chemical Society* 89, 14-20, doi:10.1021/ja00977a003 (1967).

50 Roy, M. N., Saha, S., Barman, S. & Ekka, D. Host–guest inclusion complexes of RNA nucleosides inside aqueous cyclodextrins explored by physicochemical and spectroscopic methods. *RSC Advances* 6, 8881-8891, doi:10.1039/c5ra24102b (2016).

51 Caso, J. V. *et al.* Investigating the inclusion properties of aromatic amino acids complexing beta-cyclodextrins in model peptides. *Amino Acids* 47, 2215-2227 (2015).

52 Huang, B. *et al.* A low temperature and highly sensitive ethanol sensor based on Au modified In2O3 nanofibers by coaxial electrospinning. *Journal of Materials Chemistry C* 6, 10935-10943, doi:10.1039/c8tc03669a (2018).

53 Yeggoni, D. P., Rachamallu, A., Dubey, S., Mitra, A. & Subramanyam, R. Probing the interaction mechanism of menthol with blood plasma proteins and its cytotoxicity activities. *J Biomol Struct Dyn* 36, 465-474 (2018).

54 Jia, K. *et al.* Plasmon enhanced fluorescence of a bisphthalonitrile-based dye via a dopamine mediated interfacial crosslinking reaction on silver nanoparticles. *RSC Advances* 5, 71652-71657, doi:10.1039/c5ra12242b (2015).

CHAPTER VIII

1 Voigt, J. J. M. Jones: Food Safety. 453 Seiten, zahlr. Abb. und Tab. Eagan Press, St. Paul, Minnesota, 1992. Preis: 50,– $ (USA 42,– $). *Food / Nahrung* 36, 425-425, doi:10.1002/food.19920360440 (1992).

2 4: Final Report on the Safety Assessment of Sorbic Acid and Potassium Sorbate. *Journal of the American College of Toxicology* 7, 837-880, doi:10.3109/10915818809078711 (1988).

3 Puttemans, M. L., Branders, C., Dryon, L. & Massart, D. L. Extraction of organic acids by ion-pair formation with tri-n-octylamine. Part 6. Determination of sorbic acid, benzoic acid, and saccharin in yogurt. *J Assoc Off Anal Chem* 68, 80-82 (1985).

4 M, P. J. H. & T, G. M. Rapid high-performance liquid chromatography method for the analysis of sodium benzoate and potassium sorbate in foods. *Journal of chromatography. A : including electrophoresis and other separation methods* 883, 299-304 (2000).

5 Kubota, K. & Ishizaki, T. Dose-dependent pharmacokinetics of benzoic acid following oral administration of sodium benzoate to humans. *Eur J Clin Pharmacol* 41, 363-368 (1991).

6 Praphanphoj, V., Boyadjiev, S. A., Waber, L. J., Brusilow, S. W. & Geraghty, M. T. Three cases of intravenous sodium benzoate and sodium phenylacetate toxicity occurring in the treatment of acute hyperammonaemia. *J Inherit Metab Dis* 23, 129-136 (2000).

7 Wittke, P. & Walther, F. Cyclic Deformation Behavior of Friction Drilled Internal Threads in AlSi10Mg and AZ31 Profiles. *Procedia Structural Integrity* 2, 3264-3271, doi:https://doi.org/10.1016/j.prostr.2016.06.407 (2016).

8 Moses, J., Siddiqui, A. & Silverman, P. B. Sodium benzoate differentially blocks circling induced by D-and L-dopa in the hemi-parkinsonian rat. *Neurosci Lett* 218, 145-148, doi:10.1016/s0304-3940(96)13131-1 (1996).

9 Zengin, N., Yuzbasioglu, D., Unal, F., Yilmaz, S. & Aksoy, H. The evaluation of the genotoxicity of two food preservatives: sodium benzoate and potassium benzoate. *Food Chem Toxicol* 49, 763-769 (2011).

10 Lennerz, B. S. *et al.* Effects of sodium benzoate, a widely used food preservative, on glucose homeostasis and metabolic profiles in humans. *Mol Genet Metab* 114, 73-79 (2015).

11 Liu, D. *et al.* Microfibrillar Polysaccharide-Derived Biochars as Sodium Benzoate Adsorbents. *ACS Omega* 2, 2959-2966, doi:10.1021/acsomega.7b00404 (2017).

12 López-Malo, A., Barreto-Valdivieso, J., Palou, E. & Martín, F. S. Aspergillus flavus growth response to cinnamon extract and sodium benzoate mixtures. *Food Control* 18, 1358-1362, doi:https://doi.org/10.1016/j.foodcont.2006.04.010 (2007).

13 Sagoo, S. K., Board, R. & Roller, S. Chitosan potentiates the antimicrobial action of sodium benzoate on spoilage yeasts. *Lett Appl Microbiol* 34, 168-172 (2002).

14 Farber, B. F. & Wolff, A. G. The use of nonsteroidal antiinflammatory drugs to prevent adherence of Staphylococcus epidermidis to medical polymers. *J Infect Dis* 166, 861-865 (1992).

15 Muller, E., Al-Attar, J., Wolff, A. G. & Farber, B. F. Mechanism of salicylate-mediated inhibition of biofilm in Staphylococcus epidermidis. *J Infect Dis* 177, 501-503 (1998).

16 Domenico, P., Straus, D. C., Woods, D. E. & Cunha, B. A. Salicylate Potentiates Amikacin Therapy in Rodent Models of Klebsiella Pneumoniae Infection. *The Journal of Infectious Diseases* 168, 766-769 (1993).

17 Polonio, R. E., Mermel, L. A., Paquette, G. E. & Sperry, J. F. Eradication of Biofilm-Forming Staphylococcus epidermidis (RP62A) by a Combination of Sodium Salicylate and Vancomycin. *Antimicrobial Agents and Chemotherapy* 45, 3262 (2001).

18 Manhart, M. D. In vitro antimicrobial activity of bismuth subsalicylate and other bismuth salts. *Rev Infect Dis* 12, S11-15 (1990).

19 Vane, S. J. Aspirin and other anti-inflammatory drugs. *Thorax* 55, S3-S9, doi:10.1136/thorax.55.suppl_2.S3 (2000).

20 Awtry, E. H. & Loscalzo, J. Aspirin. *Circulation* 101, 1206-1218 (2000).

21 Domenico, P., Hopkins, T. & Cunha, B. A. The effect of sodium salicylate on antibiotic susceptibility and synergy in Klebsiella pneumoniae. *Journal of Antimicrobial Chemotherapy* 26, 343-351, doi:10.1093/jac/26.3.343 (1990).

22 Friberg, S. E. Interactions of Surfactants with Polymers and Proteins. E.D.Goddard and K.P. Ananthapadmanabhan (eds.), CRC Press, Boca Raton, FL, 1993, pp. 1-427, $169.95. *Journal of Dispersion Science and Technology* 15, 399-399, doi:10.1080/01932699408943565 (1994).

23 Balouiri, M., Sadiki, M. & Ibnsouda, S. K. Methods for in vitro evaluating antimicrobial activity: A review. *J Pharm Anal* 6, 71-79 (2016).

24 Lind, J. E., Zwolenik, J. J. & Fuoss, R. M. Calibration of Conductance Cells at 25° with Aqueous Solutions of Potassium Chloride1. *Journal of the American Chemical Society* 81, 1557-1559, doi:10.1021/ja01516a010 (1959).

25 Masson, D. O. XXVIII. Solute molecular volumes in relation to solvation and ionization. *The London, Edinburgh, and Dublin Philosophical Magazine and Journal of Science* 8, 218-235, doi:10.1080/14786440808564880 (1929).

26 Benz, R. & Bauer, K. Permeation of hydrophilic molecules through the outer membrane of gram-negative bacteria. Review on bacterial porins. *Eur J Biochem* 176, 1-19 (1988).

27 Sarkhel, S. & Desiraju, G. R. N-H...O, O-H...O, and C-H...O hydrogen bonds in protein-ligand complexes: strong and weak interactions in molecular recognition. *Proteins* 54, 247-259 (2004).

28 Roy, M. N., Chanda, R., Das, R. K. & Ekka, D. Densities and Viscosities of Citric Acid in Aqueous Cetrimonium Bromide Solutions with Reference to the Manifestation of Solvation. *Journal of Chemical & Engineering Data* 56, 3285-3290, doi:10.1021/je2000217 (2011).

29 Ayranci, E. Apparent Molar Volume and Viscosity of Compounds with Asymmetric Carbon Atoms. *Journal of Chemical & Engineering Data* 42, 934-937, doi:10.1021/je970055p (1997).

30 Yan, Z., Wang, J. & Lu, J. Apparent Molar Volumes and Viscosities of Some α-Amino Acids in Aqueous Sodium Butyrate Solutions at 298.15 K. *Journal of Chemical & Engineering Data* 46, 217-222, doi:10.1021/je000211j (2001).

31 Li, Y., Wang, X. & Wang, Y. Comparative Studies on Interactions of Bovine Serum Albumin with Cationic Gemini and Single-Chain Surfactants. *The Journal of Physical Chemistry B* 110, 8499-8505, doi:10.1021/jp060532n (2006).

32 Zafarani-Moattar, M. T., Shekaari, H. & Jafari, P. Thermodynamic study of aqueous two-phase systems containing biocompatible cholinium aminoate ionic-liquids and polyethylene glycol di-methyl ether 250 and their performances for bovine serum albumin separation. *The Journal of Chemical Thermodynamics* 130, 17-32, doi:https://doi.org/10.1016/j.jct.2018.10.001 (2019).

33 Kumar, K. & Chauhan, S. Surface tension and UV–visible investigations of aggregation and adsorption behavior of NaC and NaDC in water–amino acid mixtures. *Fluid Phase Equilibria* 394, 165-174, doi:https://doi.org/10.1016/j.fluid.2015.03.012 (2015).

34 Ravichandran, G., Lakshiminarayanan, G. & Ragouramane, D. Apparent molar volume and ultrasonic studies on some bile salts in water–aprotic solvent mixtures. *Fluid Phase Equilibria* 356, 256-263, doi:https://doi.org/10.1016/j.fluid.2013.07.041 (2013).

35 Ekka, D. & Roy, M. N. Molecular interactions of alpha-amino acids insight into aqueous beta-cyclodextrin systems. *Amino Acids* 45, 755-777 (2013).

36 Roy, M. N., Dakua, V. K. & Sinha, B. Partial Molar Volumes, Viscosity B-Coefficients, and Adiabatic Compressibilities of Sodium Molybdate in Aqueous 1,3-Dioxolane Mixtures from 303.15 to 323.15 K. *International Journal of Thermophysics* 28, 1275-1284, doi:10.1007/s10765-007-0220-0 (2007).

37 Zhang, Y. & Cremer, P. S. Interactions between macromolecules and ions: The Hofmeister series. *Curr Opin Chem Biol* 10, 658-663 (2006).

38 Yasmin, A., Barman, S., Barman, B. K. & Roy, M. N. Investigation of diverse interactions of amino acids (Asp and Glu) in aqueous Dopamine hydrochloride with the manifestation of the catecholamine molecule recognition tool in solution phase. *Journal of Molecular Liquids* 271, 715-729, doi:https://doi.org/10.1016/j.molliq.2018.08.114 (2018).

39 Tasic, A. Z., Djordjevic, B. D., Grozdanic, D. K. & Radojkovic, N. Use of mixing rules in predicting refractive indexes and specific refractivities for some binary liquid mixtures. *Journal of Chemical & Engineering Data* 37, 310-313, doi:10.1021/je00007a009 (1992).

40 The Chemistry of Macrocyclic Ligand Complexes L. F. Lindoy Cambridge: Cambridge University Press 1989, pp viii +269 £45.00. SUS 69.50 ISBN 0 521 25261 X. *Journal of Coordination Chemistry* 21, 87-87, doi:10.1080/00958979009408188 (1990).

41 Eisenberg, H. Chemical physics of ionic solutions. B. E. Conway and R. G. Barradas, Eds., Wiley, New York, 1966. 622 pp. $25.00. *Journal of Polymer Science Part A-2: Polymer Physics* 6, 1943-1943, doi:10.1002/pol.1968.160061111 (1968).

42 Banipal, P. K., Banipal, T. S., Ahluwalia, J. C. & Lark, B. S. Partial molar heat capacities and volumes of transfer of some saccharides from water to aqueous urea solutions atT= 298.15 K. *The Journal of Chemical Thermodynamics* 32, 1409-1432, doi:https://doi.org/10.1006/jcht.2000.0689 (2000).

43 Jenkins, H. D. B. & Marcus, Y. Viscosity B-Coefficients of Ions in Solution. *Chemical Reviews* 95, 2695-2724, doi:10.1021/cr00040a004 (1995).

44 Briscoe, H. T. & Rinehart, W. T. Studies of Relative Viscosity of Non-aqueous Solutions. *The Journal of Physical Chemistry* 46, 387-394, doi:10.1021/j150417a009 (1942).

45 Brady, G. W. & Krause, J. T. Structure in Ionic Solutions. I. *The Journal of Chemical Physics* 27, 304-308, doi:10.1063/1.1743691 (1957).

46 Jones, G. & Dole, M. THE VISCOSITY OF AQUEOUS SOLUTIONS OF STRONG ELECTROLYTES WITH SPECIAL REFERENCE TO BARIUM CHLORIDE. *Journal of the American Chemical Society* 51, 2950-2964, doi:10.1021/ja01385a012 (1929).

47 Ali, A., Hyder, S. & Akther, Y. *Viscometric studies of a –amino acid in aqueous NaCl and MgCl2 at 303 K*. Vol. 79 (2005).

48 Marcus, Y. ViscosityB-coefficients, structural entropies and heat capacities, and the effects of ions on the structure of water. *Journal of Solution Chemistry* 23, 831-848, doi:10.1007/bf00972677 (1994).

49 Friedman, H. L. & Krishnan, C. V. in *Aqueous Solutions of Simple Electrolytes* (ed Felix Franks) 1-118 (Springer US, 1973).

50 Devine, W. & M. Lowe, B. *Viscosity B-coefficients at 15 and 25 °C for glycine, ?-alanine, 4-amino-n-butyric acid, and 6-amino-n-hexanoic acid in aqueous solution*. (1971).

51 Sarma, T. S. & Ahluwalia, J. C. Experimental studies on the structures of aqueous solutions of hydrophobic solutes. *Chemical Society Reviews* 2, 203-232, doi:10.1039/cs9730200203 (1973).

52 Pitkänen, I., Suuronen, J. & Nurmi, J. Partial Molar Volume, Ionization, Viscosity and Structure of Glycine Betaine in Aqueous Solutions. *Journal of Solution Chemistry* 39, 1609-1626, doi:10.1007/s10953-010-9618-6 (2010).

53 Bhattacharyya, M. M. & Sengupta, M. Ion–Solvent Interaction of Amino Acids. The Role of the “Zwitterionic” and the “Ionic” Forms in the Modification of Water

Structure over the Temperature Range 25–45 °C. *Bulletin of the Chemical Society of Japan* 61, 4107-4112, doi:10.1246/bcsj.61.4107 (1988).

54 Ekka, D. & Roy, M. N. Conductance, a Contrivance To Explore Ion Association and Solvation Behavior of an Ionic Liquid (Tetrabutylphosphonium Tetrafluoroborate) in Acetonitrile, Tetrahydrofuran, 1,3-Dioxolane, and Their Binaries. *The Journal of Physical Chemistry B* 116, 11687-11694, doi:10.1021/jp302465s (2012).

55 Ekka, D., Ray, T., Roy, K. & Roy, M. N. Exploration of Solvation Consequence of Ionic Liquid [Bu4PCH3SO3] in Various Solvent Systems by Conductance and FTIR Study. *Journal of Chemical & Engineering Data* 61, 2187-2196, doi:10.1021/acs.jced.5b00670 (2016).

56 Shen, X. M., Zhang, F. & Dryhurst, G. Oxidation of dopamine in the presence of cysteine: characterization of new toxic products. *Chem Res Toxicol* 10, 147-155 (1997).

57 Benesi, H. A. & Hildebrand, J. H. A Spectrophotometric Investigation of the Interaction of Iodine with Aromatic Hydrocarbons. *Journal of the American Chemical Society* 71, 2703-2707, doi:10.1021/ja01176a030 (1949).

58 Rajbanshi, B. *et al.* Study to Probe Subsistence of Host-Guest Inclusion Complexes of α and β-Cyclodextrins with Biologically Potent Drugs for Safety Regulatory Dischargement. *Scientific Reports* 8, 13031, doi:10.1038/s41598-018-31373-x (2018).

59 Roy, M. N., Saha, S., Barman, S. & Ekka, D. Host–guest inclusion complexes of RNA nucleosides inside aqueous cyclodextrins explored by physicochemical and spectroscopic methods. *RSC Advances* 6, 8881-8891, doi:10.1039/c5ra24102b (2016).

60 Caso, J. V. *et al.* Investigating the inclusion properties of aromatic amino acids complexing beta-cyclodextrins in model peptides. *Amino Acids* 47, 2215-2227 (2015).

61 Das, K., Roy, M. C., Rajbanshi, B. & Roy, M. N. Assorted interactions of amino acids prevailing in aqueous vitamin C solutions probed by physicochemical and ab-initio contrivances. *Chemical Physics Letters* 687, 209-221, doi:https://doi.org/10.1016/j.cplett.2017.08.054 (2017).

62 Panigrahi, S. K. & Desiraju, G. R. Strong and weak hydrogen bonds in the protein-ligand interface. *Proteins* 67, 128-141 (2007).

63 Samadi, F., Eckelt, J., Wolf, B. A., Schüle, H. & Frey, H. Branched versus linear oligo(dimethylsiloxane): Differences in their thermodynamic interaction with solvents. *Journal of Polymer Science Part B: Polymer Physics* 48, 1309-1318, doi:10.1002/polb.22029 (2010).

INDEX

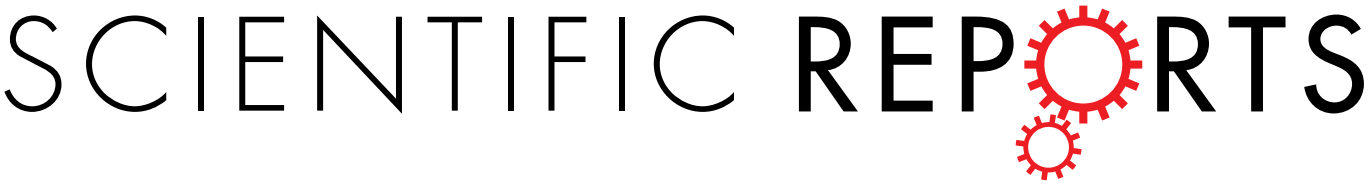

OPEN

Received: 6 June 2018
Accepted: 17 August 2018
Published online: 29 August 2018

Study to Probe Subsistence of Host-Guest Inclusion Complexes of α and β-Cyclodextrins with Biologically Potent Drugs for Safety Regulatory Dischargement

Biplab Rajbanshi[1], Subhadeep Saha[1], Koyeli Das[1], Biraj Kumar Barman[1], Swarnab Sengupta[2], Arindam Bhattacharjee[2] & Mahendra Nath Roy[1]

Host-guest interaction of two significant drugs, phenylephrine hydrochloride and synephrine with α and β-cyclodextrins were studied systematically. Initially two simple but reliable physicochemical techniques namely conductance and surface tension were employed to find out saturation concentration for the inclusion and its stoichiometry. The obtained 1:1 stoichiometry was further confirmed by two spectrometric methods, UV-Vis study and spectrofluorimetry. Significant shifts in IR stretching frequency also support the inclusion process. Relative stabilities of the inclusion complexes were established by the association constants obtained from UV-Vis spectroscopic measurements, program based mathematical calculation of conductivity data. Calculations of the thermodynamic parameters dictates thermodynamic feasibility of the inclusion process. Spectrofluorometric measurement scaffolds the UV-Vis spectroscopic measurement validating stability of the ICs once again. Mass spectroscopic measurement gives the molecular ion peaks corresponding to the inclusion complex of 1:1 molar ratio of host and guest molecules. The mechanism of inclusion was drawn by ^{1}H-NMR and 2D ROESY spectroscopic analysis. Surface texture of the inclusion complexes was studied by SEM. Finally, the cytotoxic activities of the inclusion complexes were analyzed and found, Cell viability also balances for non-toxic behavior of the ICs. Moreover, all the studies reveal the formation of inclusion complexes of two ephedra free, alternatively emerging drugs (after their banned product having ephedra) SNP, PEH with α and β-CD which enriches the drug delivery system with their regulatory release without any chemical modification.

In supramolecular chemistry of cyclodextrins various guest molecules having hydrophobic part, influenced by non-covalent interaction, can be inserted into the hydrophobic cavity of cyclodextrin molecules. Cyclodextrins (α-CD, β-CD, γ-CD) having six, seven and eight numbers of glucopyranose units respectively, (Fig. 1) produced from starch by the enzymatic conversion, have different cavity sizes. Inclusion complexes (ICs) with structures of higher complexity in the solid state and solution phase can increase the aqueous solubility of various drugs cum bio-active molecules of merely water solubility which leads to the development of drug delivery systems[1,2]. Chiral Separation of molecules using cyclodextrins as chiral additives are also possible by applying capillary electrophoresis (CE) and electrochemical detection (ED) method[3–6]. Structural characterization of Host-Guest inclusion complexes of α-CD and β-CD with two bio-active molecules, PEH and SNP were done over here in terms of geometry and structural preferences by means of a variety of physical and spectroscopic methods in solid state and solution phase.

Phenylephrine hydrochloride (PEH) (Fig. 1) is a selective α_1-adrenergic receptor agonist of the phenethylamine class used primarily in cold and flu conditions as an antipyretic, analgesic drug to relief pain[7]. In the

[1]Department of Chemistry, University of North Bengal, Darjeeling, 734013, India. [2]Department of Microbiology, University of North Bengal, Darjeeling, 734013, India. Correspondence and requests for materials should be addressed to M.N.R. (email: mahendraroy2002@yahoo.co.in)

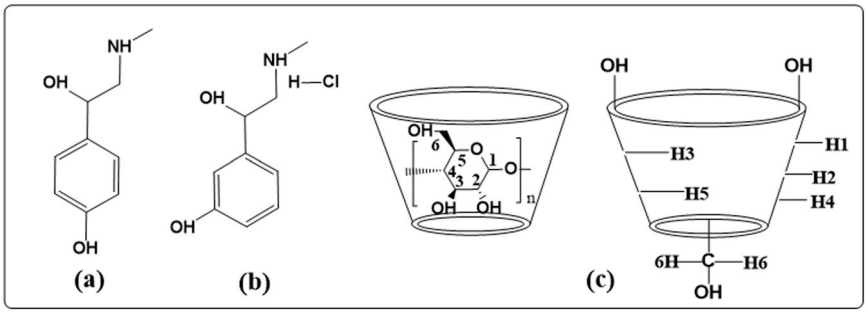

Figure 1. Molecular structures of **(a)** SNP, **(b)** PEH, **(c)** Cyclodextrins, showing the exterior and the interior protons, here, n = 6 to 8 for the α, β and ϒ-cyclodextrins respectively.

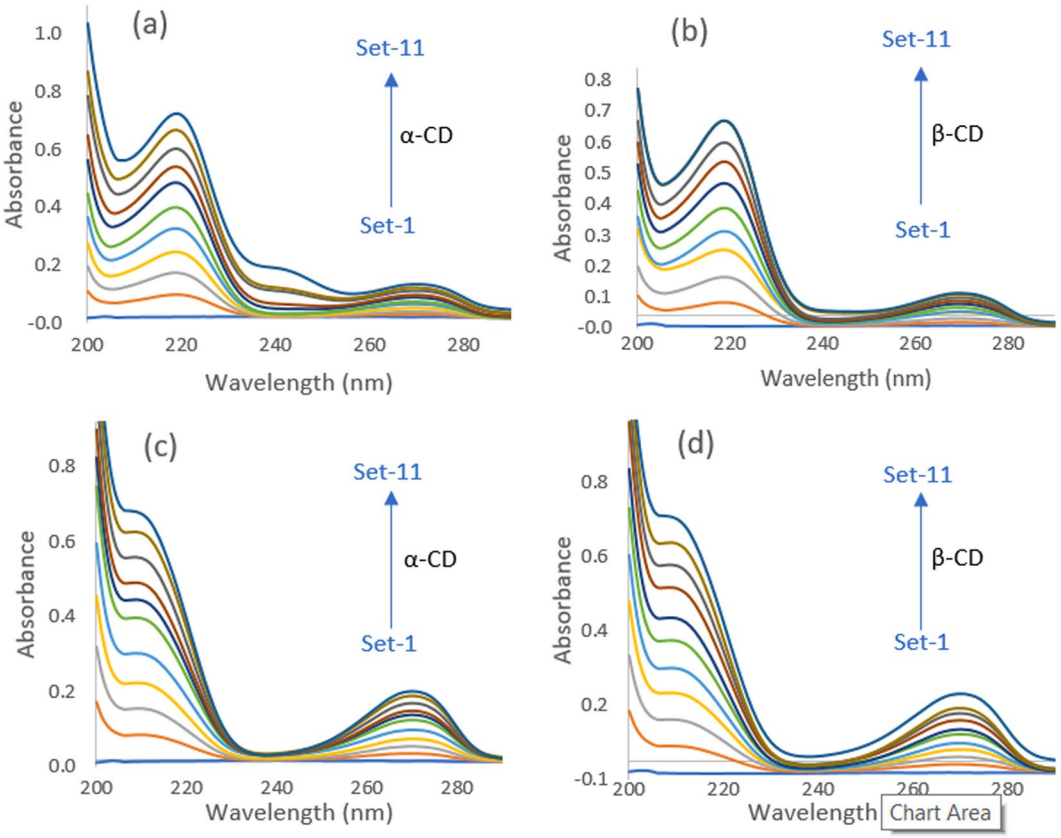

Figure 2. **(a**,**b**,**c**,**d)** UV-Vis spectra for the generation of Job plots of **(a)** SNP + α-CD and **(b)** SNP + β-CD systems at $\lambda_{max} = 209$ nm, and **(c)** PEH + α-CD and **(d)** PEH + β-CD systems at $\lambda_{max} = 219$ nm.

United States PEH is used as nasal decongestant. Phenylpropanolamine, pseudoephedrine and ephedrine are also used as nasal decongestant as the substitute of PEH[8,9]. However, due to serious side effect (hemorrhagic stroke) phenylpropanolamine was withdrawn from market[10]. Now it is imperative to find out the suitability of PEH as the same done by the Phenylpropanolamine, pseudoephedrine and ephedrine for the treatment of nasal or sinus congestion and to find out the way of delivery with biocompatibility.

Alkaloid synephrine (SNP) (Fig. 1) was first extracted as a natural product from the leaves of various citrus trees are used as bronchial muscle reluctant, increases blood pressure in the patients suffering from low blood pressure. Its presence and positive retort as a bio-marker makes the orange juice like soft drinks authentic[11]. Lipolytic stimulation by synephrine increases thermogenesis which leads to the increase in metabolic rate and fat oxidation[12–16]. In weight loss products as well as in the dietary supplement "ephedra free" synephrine is frequently used and starts to earn enormous attention after the banned product ephedrine[17,18]. Most of the cases patients suffering from obesity are often found to suffer from type-2 diabetes and hence synephrine in weight loss products frequently becomes beneficial to the diabetic patients[19,20].

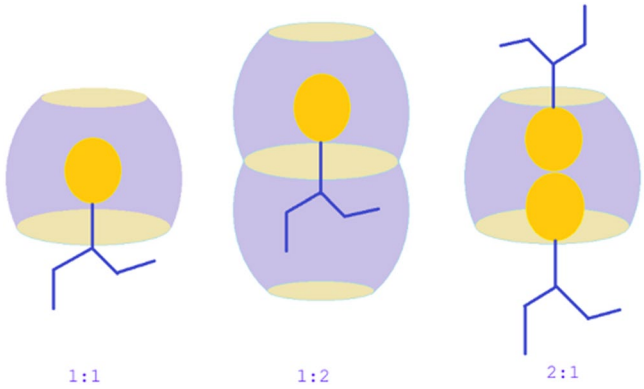

Figure 3. Probable host:guest stoichiometric ratio of the inclusion complexes.

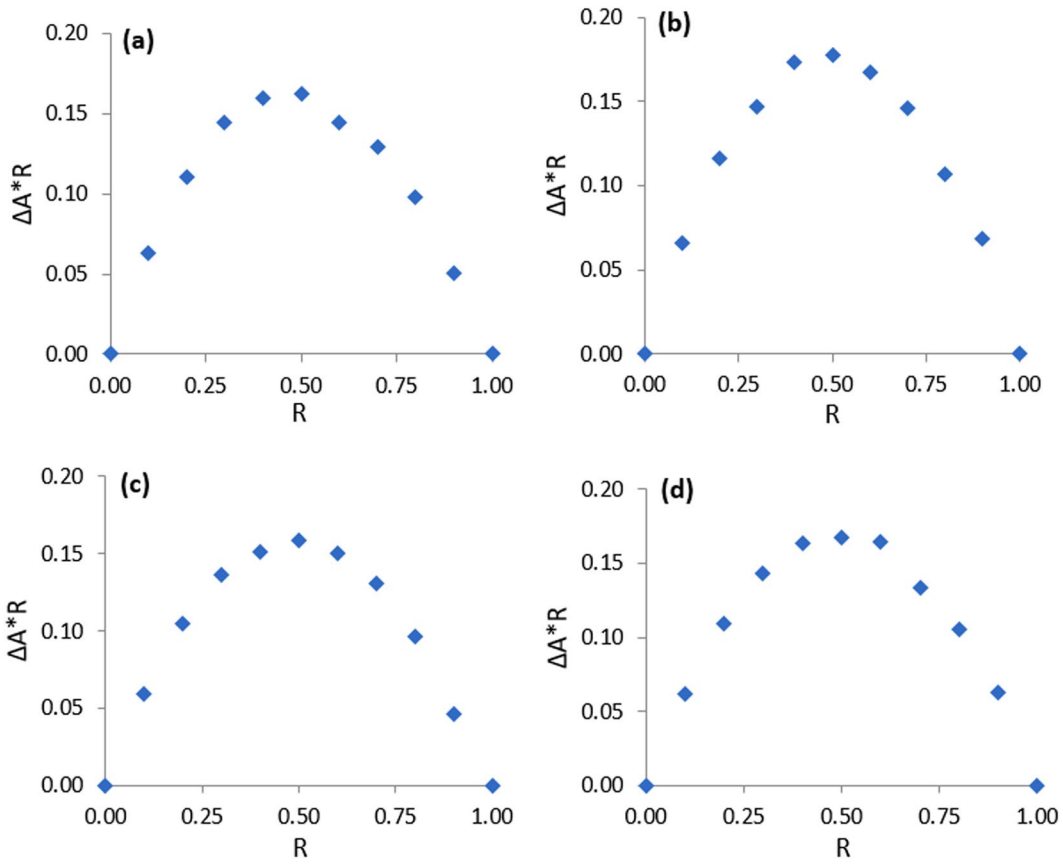

Figure 4. **(a**,**b**,**c**,**d)** Job plots of the **(a)** SNP + α-CD and **(b)** SNP + β-CD systems at $\lambda_{max} = 209$ nm and **(c)** PEH + α-CD and **(d)** PEH + β-CD systems at $\lambda_{max} = 219$ nm, at 298.15 K. ΔA = absorbance difference of SNP/PEH without and with CD, R = [DGs]/([DGs] + [CD]).

Cyclodextrins, mostly α-cyclodextrin, are found to form complexes with the dietary fat which are stable enough to undergo enzymatic hydrolysis by lipase. This restrains accumulation of fat in human body[21,22]. Hence, inclusion complex of SNP and cyclodextrins can be of a great deal for the weight loss/weight management dietary food supplement for sportsman or obese person[23].

Experimental Section

Materials. Phenylephrine hydrochloride, Synephrine, α and β-cyclodextrin of puris grade of purity ≥98.0% were purchased from Sigma-Aldrich and were kept in a refrigerator as received and used right away.

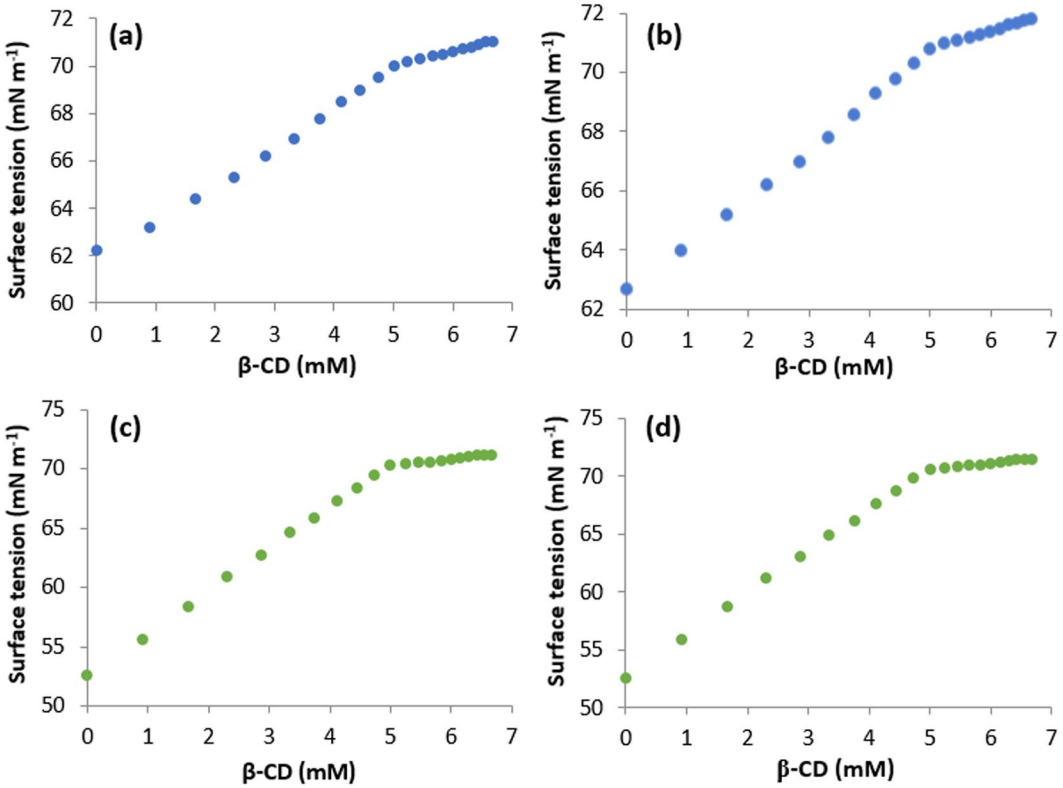

Figure 5. **(a**,**b**,**c**,**d)** Variations in the surface tension of aqueous SNP with increasing concentration of **(a)** α-CD, **(b)** β-CD and the variations in the same of aqueous PEH with increasing concentration of **(c)** α-CD, **(d)** β-CD at 298.15 K.

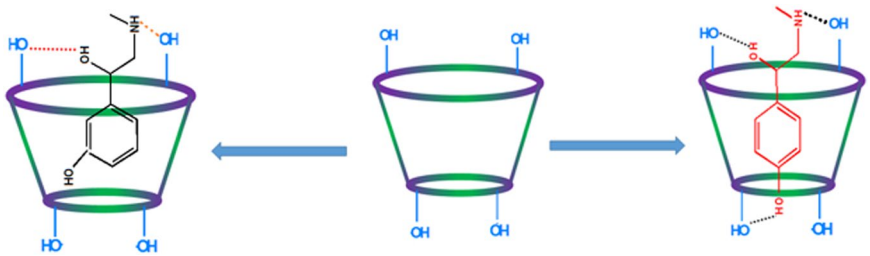

Figure 6. Schematic representation of the host:guest inclusion complexation through the more favorable wider rim of the cyclodextrin molecules.

Apparatus. Utilizing JASCO V-530 UV−Vis spectrophotometer, UV−visible spectra were recorded with a wavelength accuracy of ±0.5 nm. Cell temperature during the experiment was controlled from 298.15 K to 308.15 K with a digital thermostat.

Studies on surface tension at the experimental temperatures with the accuracy of ±0.1 mN m^{-1} were done by employing K9 digital TENSIOMETER (Krüss GmbH, Hamburg, Germany) which uses the platinum ring detachment technique. The temperature of the experimental solutions was kept constant at 298.15 K by circulating thermostat water through a double-walled glass vessel holding solution.

Proper instrumentation of METTLER-TOLEDO Seven Multi conductivity meter provides specific conductivity values with an uncertainty of ±1.0 μS m^{-1}. Constancy in temperature at the specific value of the solutions under experiment was maintained with an auto-thermostatic water bath. HPLC-grade water with a specific conductance of 6.0 μS m^{-1} was utilized for conductivity measurement. Calibration of the Systronics Type CD – 30 conductivity cell was done using 0.01 M freshly prepared aqueous solution of KCl.

Fluorescence spectra were noted via JASCO V-530 UV/VIS Spectrophotometer, at 25 °C in a Hellma quartz cuvette (250–400 nm spectral range, 2.0 mL volume, 10 mm path length) equipped with a magnetic stir bar. To a solution of [SNP/PEH] (100 μM, 1 mL) in deionized water (Millipore, 18.2 MΩ. Cm) was prepared with α-CD and β-CD. (200 μM) in the stock fluorescence spectra were recorded after 1 hr of mixing time. The output range of the machine was nearly about 2 analogs (+/−10 volts).

Guest	Host	Concentration of host (mM)	Concentration of guest (mM)	Surface tension (γ^a) mNm^{-1}
PEH	α-CD	4.9379	5.0621	70.1829
	β-CD	4.9276	5.0724	70.4886
SNP	α-CD	5.2152	4.7848	70.1487
	β-CD	5.1564	4.8436	70.4149

Table 1. Values of Surface Tension (γ^a) at the Break Point with Corresponding Concentrations of DGs and CDs at 298.15 K[a]. [a]Standard uncertainties (u): temperature $u(T) = \pm 0.01$ K, surface tension: $u(\gamma) = \pm 0.1$ mNm^{-1}.

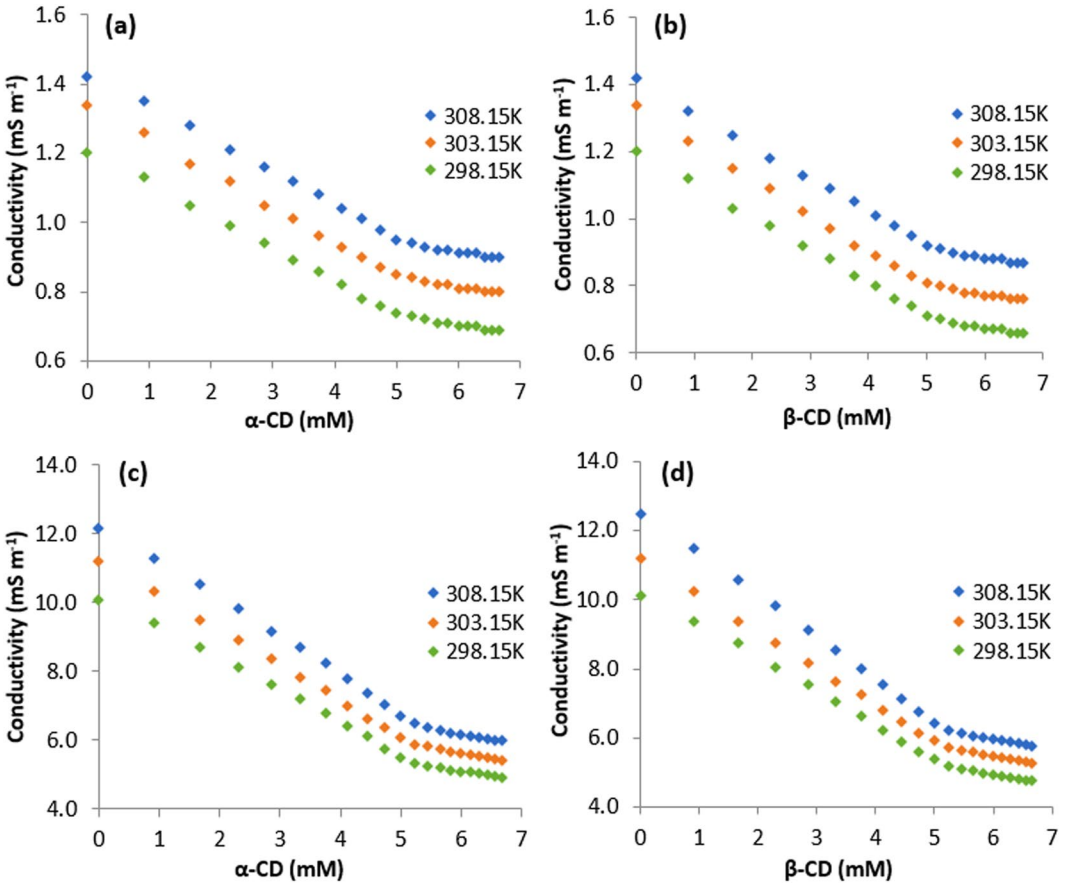

Figure 7. **(a**,**b**,**c**,**d)** Variations in the conductivity of aqueous SNP with increasing concentration of **(a)** α-CD, **(b)** β-CD and the variations in the same of aqueous PEH with increasing concentration of **(c)** α-CD, **(d)** β-CD at 298.15 to 308.15 K.

2D ROESY as well as 1 H NMR spectra were recorded in D_2O solvent at 400 MHz in Bruker Avance instrument at 298.15 K. The residual protonated signal (HDO, δ 4.79 ppm) was used as an internal standard. The chemical shifts data, δ values are presented in parts per million.

HRMS spectra of the solid ICs were recorded on a quadrupole time-of-flight (Q-TOF) high-resolution instrument with positive-mode electrospray ionization taking the methanol solution of the solid ICs.

FTIR spectral analysis was performed on a Perkin-Elmer FTIR spectrometer in the scanning range of $4000-400\,cm^{-1}$. According to the KBr disk method the disks were made in 1:100 ratios of sample and KBr. Studies were carried out at room temperature and at a humidity of 45%.

SEM: Scanning Electron Microscope (JSM-6360) was aided to perform the analysis and obtain the data's. It also discusses about the morphological patterns and particle size of the Inclusion Complex.

Antimicrobial activity assay: In this experiment (gram negative *E. coli*), (gram positive B. subtilis) were considered as model organism. This test was done according to the Agar cup method. In brief, spread plate technique was applied to inoculate the organisms in Muller-Hinton agar and the compounds were applied in agar cup at 1 mg/ml concentration in separate plates and incubated at 37 °C for 24 hrs. Double distilled water was used as the control. Antimicrobial activity was determined by means of the zone of inhibition surroundings agar cup. Each of the experiments was done in triplicate.

Guest	Host	Temperature (K^a)	Concentration of host (mM)	Concentration of guest (mM)	Conductivity (K^a) (mSm^{-1})
PEH	α-CD	298.15	5.34	4.65	5.29
		303.15	5.21	4.78	5.88
		308.15	4.54	5.45	6.78
	β-CD	298.15	5.21	4.78	5.17
		303.15	5.12	4.87	5.74
		308.15	5.21	4.78	6.20
SNP	α-CD	298.15	5.04	4.95	0.73
		303.15	5.04	4.95	0.84
		308.15	5.23	4.76	0.93
	β-CD	298.15	5.11	4.88	0.70
		303.15	4.94	5.05	0.80
		308.15	5.12	4.87	0.91

Table 2. Values of Conductivity (κ) at the Break Point with Corresponding Concentrations of DGs and CDs at 298.15 K^a to 308.15 K^a. [a]Standard uncertainties (u): temperature u(T) = ±0.01 K, conductivity: u(κ) = ±0.01 mSm^{-1}.

Guest	Host	Temperature (K^a)	$(K_a)(\times 10^{-3})$	$(K_a^{\theta})(\times 10^{-3})$	$(K_a^{C})(\times 10^{-3})$	$(K_a^{F})(\times 10^{-3})$
PEH	α-CD	303.15	2.14	2.07	2.05	2.21
		308.15	1.79	1.74	1.72	
		313.15	1.48	1.40	1.38	
	β-CD	303.15	2.97	2.71	2.75	2.91
		308.15	2.26	2.10	2.12	
		313.15	1.79	1.70	1.68	
SNP	α-CD	303.15	2.84	2.82	2.80	2.87
		308.15	2.26	2.15	2.18	
		313.15	1.74	1.63	1.66	
	β-CD	303.15	3.82	3.41	3.35	3.73
		308.15	2.88	2.46	2.42	
		313.15	2.28	1.85	1.85	

Table 3. Association Constant obtained from Benesi-Hildebrand method (K_a), Association Constant obtained from the Nonlinear Program (K_a^{θ}), Association Constant obtained from Program based mathematical calculation of non-linear changes in the conductivity data (K_a^{C}), Association Constant obtained from Benesi-Hildebrand equation, using the spectrofluorometric data (K_a^{F}) at 298.15 to 308.15 K^a. [a]Standard uncertainty in temperature, u, are u(T) = ±0.01 K^a.

Cell viability assay: In this experiment pure sample as well as ICs, SNP + α-CD, SNP + β-CD, PEH + α-CD and PEH + β-CD were added in the nutrient agar broth and *E. coli* and B. subtilis were inoculated. After 24 hrs of incubation at 37 °C cells were plated, and colony count was completed. Growth in nutrient broth without the ICs was taken as the control. All the experiment was done in triplicate. Level of significance (p) for all experiment was set to 0.05.

Procedure. All the solutions under experiment were prepared after checking the solubility of the PEH, SNP and CDs in triply distilled, deionized and degassed water. METTLER TOLEDO AG-285 analytical balance with an uncertainty of ±0.1 mg at 298.15 K was used to weigh all the experimental materials. Loss of materials caused by evaporation during mixing and working with the solutions was minimized by taking sufficient precautions. For the preparation of the solid inclusion complexes, 20 mL 1.0 (mM) solutions of α and β-CD were prepared separately with triply distilled, deionized and degassed water which, allowed to stir for 6 hours on a magnetic stirrer. Then, 20 mL 1.0 (mM) aqueous solutions of SNP/PEH were added drop wise to the previously prepared aqueous solution of α-CD or β-CD making the ultimate equimolar mixture and were continued to stir for 48 hours at 55–60 °C. The suspensions obtained after cooling the mixture to 5 °C were filtered to obtain white crystalline powder, which were then dried in air and preserved in vacuum desiccators for further use.

Result and Discussion

Job plot: Stoichiometry of inter molecular association between guest and host. The stoichiometry of the host-guest inclusion complexes was determined by employing the well-established Jobs method[24]. UV-Vis spectroscopic data were used in this technique to determine the stoichiometry of inclusion complexation. Absorption spectra of a set of solutions, prepared by mixing aqueous SNP/PEH solution with the aqueous

Inclusion Complexes (ICs)	Application of (K_a) to Van't Hoff equation		Application of (K_a^{θ}) to Van't Hoff equation		Application of (K_a^{C}) to Van't Hoff equation	
PEH + α-CD	ΔH° (KJ mol^{-1})	−28.93	$\Delta H^{0\theta}$ (KJ mol^{-1})	−30.85	ΔH^{0C} (KJ mol^{-1})	−31.22
	ΔS° (J mol^{-1} K^{-1})	−31.69	$\Delta S^{0\theta}$ (J mol^{-1} K^{-1})	−38.20	ΔS^{0C} (J mol^{-1} K^{-1})	−39.50
	ΔG° (KJ mol^{-1})	−19.49	$\Delta G^{0\theta}$ (KJ mol^{-1})	−19.46	ΔG^{0C} (KJ mol^{-1})	−19.44
PEH + β-CD	ΔH^{0} (KJ mol^{-1})	−40.15	$\Delta H^{0\theta}$ (KJ mol^{-1})	−36.82	ΔH^{0C} (KJ mol^{-1})	−38.91
	ΔS^{0} (J mol^{-1} K^{-1})	−66.01	$\Delta S^{0\theta}$ (J mol^{-1} K^{-1})	−55.79	ΔS^{0C} (J mol^{-1} K^{-1})	−62.52
	ΔG^{0} (KJ mol^{-1})	−20.47	$\Delta G^{0\theta}$ (KJ mol^{-1})	−20.19	ΔG^{0C} (KJ mol^{-1})	−20.27
SNP + α-CD	ΔH^{0} (KJ mol^{-1})	−38.72	$\Delta H^{0\theta}$ (KJ mol^{-1})	−43.26	ΔH^{0C} (KJ mol^{-1})	−41.25
	ΔS^{0} (J mol^{-1} K^{-1})	−61.54	$\Delta S^{0\theta}$ (J mol^{-1} K^{-1})	−76.63	ΔS^{0C} (J mol^{-1} K^{-1})	−70.04
	ΔG^{0} (KJ mol^{-1})	−20.37	$\Delta G^{0\theta}$ (KJ mol^{-1})	−20.41	ΔG^{0C} (KJ mol^{-1})	−20.37
SNP + β-CD	ΔH^{0} (KJ mol^{-1})	−40.81	$\Delta H^{0\theta}$ (KJ mol^{-1})	−48.37	ΔH^{0C} (KJ mol^{-1})	−46.89
	ΔS^{0} (J mol^{-1} K^{-1})	−66.11	$\Delta S^{0\theta}$ (J mol^{-1} K^{-1})	−91.96	ΔS^{0C} (J mol^{-1} K^{-1})	−87.24
	ΔG^{0} (KJ mol^{-1})	−21.10	$\Delta G^{0\theta}$ (KJ mol^{-1})	−20.95	ΔG^{0C} (KJ mol^{-1})	−20.88

Table 4. Thermodynamic parameters (ΔH°, ΔS°, ΔG°) calculated, using the association constants (K_a, K_a^{θ}, K_a^{C}) obtained from Benesi-Hildebrand method, nonlinear Program, program based mathematical calculation of non-linear changes in the conductivity data respectively. Mean errors in variables are as follows: $\Delta H^{0} = \pm 0.01$ kJ mol^{-1}; $\Delta S^{0} = \pm 0.01$ J mol^{-1}K^{-1}; $\Delta G^{0} = \pm 0.01$ kJ mol^{-1}; $\Delta H^{0\theta} = \pm 0.01$ kJ mol^{-1}; $\Delta S^{0\theta} = \pm 0.01$ J mol^{-1}K^{-1}; $\Delta G^{0\theta} = \pm 0.01$ kJ mol^{-1}; $\Delta H^{0C} = \pm 0.01$ kJ mol^{-1}; $\Delta S^{0C} = \pm 0.01$ J mol^{-1}K^{-1}; $\Delta G^{0C} = \pm 0.01$ kJ mol^{-1}.

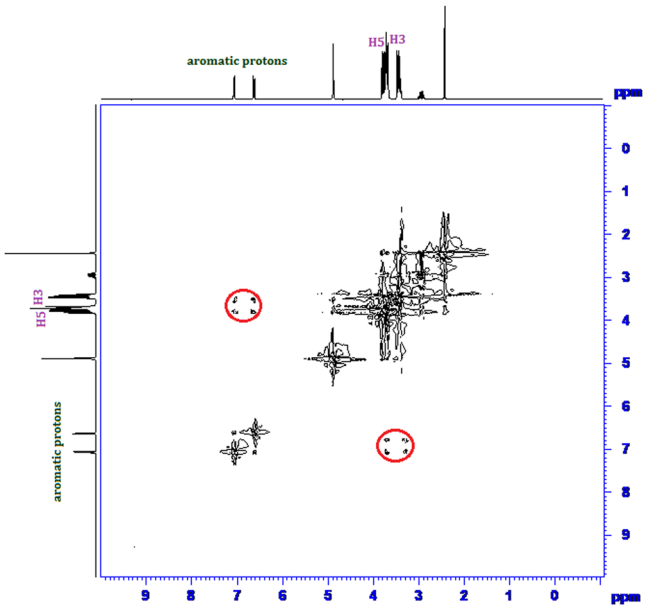

Figure 8. 2D ROESY NMR spectra of the solid (SNP + α-CD) system.

α-CD/β-CD solution in the sort of 0–1 mole fraction, were recorded at 298.15 K of temperature. Absorbance of the prepared set of the solutions were taken at $\lambda_{max} = 209$ nm for SNP and $\lambda_{max} = 219$ nm for PEH (Fig. 2). Jobs plots of (SNP + α-CD, SNP + β-CD, PEH + α-CD, PEH + β-CD) were obtained by plotting a graph, $\Delta A \times R$ vs R. Where, ΔA is the deference in absorbance between the pure SNP/PEH and the solutions of the set, prepared with CDs (Tables S1–S4 and Fig. 2). R signifies [PEH]/([PEH] + [CD]) and [SNP]/([SNP] + [CD]). The corresponding fractional value of R at maxima of the Jobs plot indicates the stoichiometry of the inclusion complex formed and it is well known that, R = 0.33, 0.5, 0.66 and so on, evidently recommends 1:2, 1:1 and 2:1, Guest:Host stoichiometry of the inclusion complex respectively[25] (Fig. 3). Ulatowski *et al.* and Hibbert *et al.* showed that Job plot may be used in case of 1:1 complexes, but for other stoichiometries various mathematical models are widely employed[26,27]. In the experimental analysis of the present work, it is found that, for all the four systems (SNP + α-CD) and (SNP + β-CD), (PEH + α-CD), (PEH + β-CD) the value of R = 0.5, clearly indicating the 1:1, Guest:Host stoichiometry of the ICs[28] (Fig. 4).

Surface tension: An idea to the Host-Guest molecular association and their stoichiometry in the inclusion complex. Sufficiently lower surface tension(γ) value of the aqueous solutions of SNP/PEH

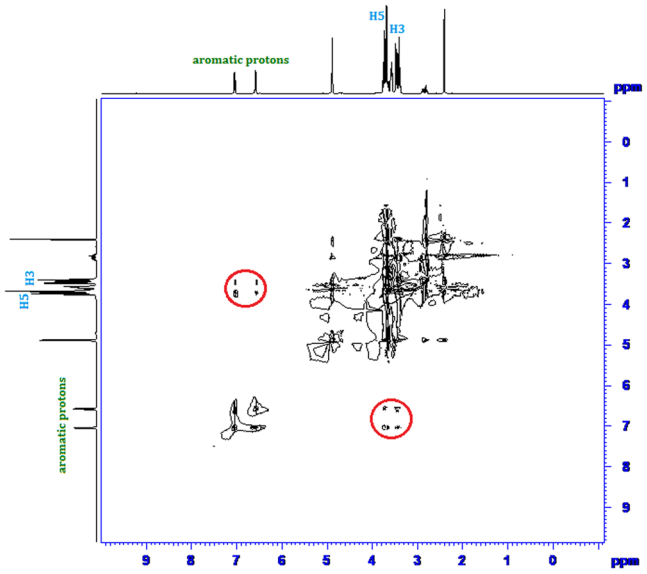

Figure 9. 2D ROESY NMR spectra of the solid (SNP + β-CD) system.

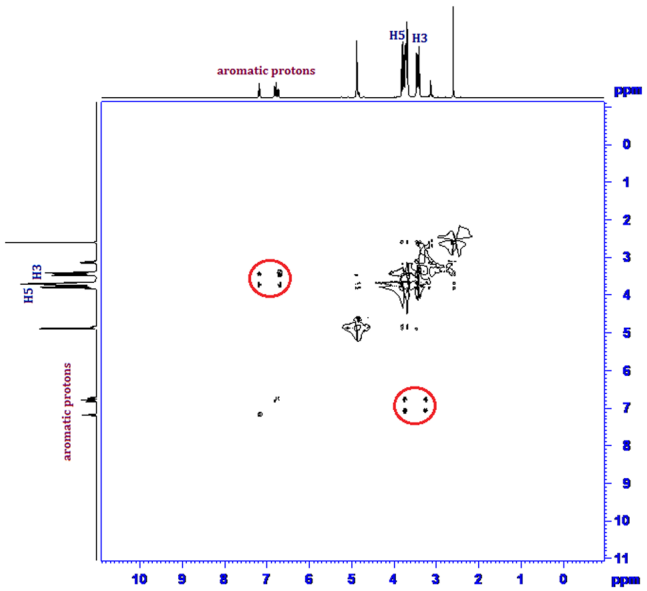

Figure 10. 2D ROESY NMR spectra of the solid (PEH + α-CD) system.

than the triply distilled pure water, suggests SNP and PEH to have surface activity. This may be due to the simultaneous presence of phenyl ring as well as the $-CH(OH)CH_2NHCH_3$ group to the opposite terminals of the same molecule. Study on the surface tension of diverse surface-active guest molecules with cyclodextrins strongly supports the inclusion phenomenon and the stoichiometry of the ICs[29–32]. In this work, surface tension of a fixed quantity of aqueous SNP/PEH solutions was studied at 298.15 K with the step wise addition of CDs solutions in same quantity (Tables S5, S6, Fig. 5). Whereas, according to literature as well as practically it is found that, there is an extremely slight change in the surface tension (γ) of CDs over a wide range of concentration in aqueous medium at 298.15 K[33,34]. It signifies all the changes in the value of surface tension (γ) are associated with the SNP/PEH. Being a surface phenomenon, more the number of surface active molecules in the surface of a solution, decreases more the surface tension of that solution. But permanent migration of surface active molecules from the surface to the bulk of the solution by means of solvation or many other stabilizing factors leads to the increase in surface tension (γ) of that solution. This is exactly the trend, what we observed in our experiment during step wise addition of CDs in the aqueous SNP/PEH solution (Tables S5, S6, Fig. 5). This is obviously; there is migration of surface active SNP/PEH molecules from the surface to the bulk of the solution by means of encapsulation of the SNP/PEH into the hydrophobic cavity of the CDs forming host-guest ICs[30,31,35] (Fig. 6). After a certain

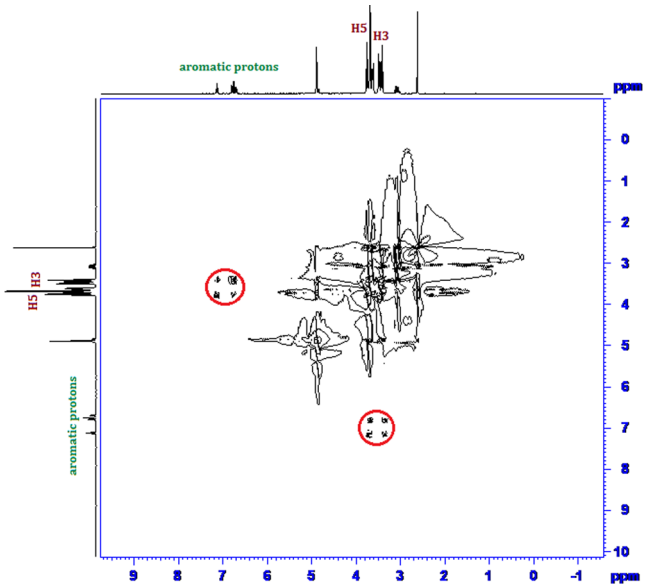

Figure 11. 2D ROESY NMR spectra of the solid (PEH + β-CD) system.

concentration of CDs, the surface tension (γ) becomes steady and consequently lefts a sharp break point behind it, in the plot of surface tension (γ) vs concentration of CDs (Table 1, Fig. 5). Accordingly, surface chemistry confers the inclusion phenomenon and appearance of sharp, single break point at the 1:1 molar concentration ratio of host and guest molecules for all the cases (SNP + α-CD, SNP + β-CD, PEH + α-CD, PEH + β-CD) establishes the 1:1 stoichiometry of host-guest ICs[36–39].

Conductance: Molecular recognition of guest into host molecules and their stoichiometric ratio in ICs. Conductimetric study is also another approach, which makes us able to conclude about the supramolecular host-guest interaction between the SNP/PEH and CDs and their stoichiometric ratio in the ICs[37,40]. Though, both the SNP and PEH are organic molecules, 10 (mM) aqueous solution of SNP and PEH shows appreciable conductivity. Being a hydrochloride salt, PEH shows higher conductivity than SNP for the same concentration. In the present work, conductivity of SNP and PEH were measured with the step wise increasing concentration of CDs, at three different temperatures from 298.15 K to 308.15 K with the interval of 5 K of temperature (Tables S5, S6 and Fig. 7). It was found that, gradual increase in concentration of CDs leads to the decrease in conductivity (κ), of the aqueous SNP/PEH solutions (Fig. 7). The fruit full explanation for this observation comes through the decrease in the mobility of the conducting species in the solution due to molecular encapsulation of SNP/PEH into the hydrophobic cavity of the CDs[36,41] (Fig. 6). Generation of a single break point in the conductivity curves after reaching a certain concentration of CDs, suggests, the molecular encapsulation of SNP/PEH into the cavity of CDs is 1:1[31,41] (Fig. 7). Corresponding concentration of SNP/PEH and CDs at the break points of the conductivity curve are listed in (Table 2). The near about equimolar concentration of SNP/PEH and CDs at the break points of the conductivity curve suggests the 1:1 stoichiometric ratio of the SNP/PEH into CDs of the ICs[36,37] (Fig. 3).

Ultraviolet Spectroscopy: The association constants (K_a) and Stability of the of the ICs. The binding ability of the guest into the host molecule and the stability of the inclusion complexes formed were explored by measuring the association constants (K_a) of the ICs. The UV-vis spectroscopic study enables us to determine the association constant (K_a) of the ICs in the solution phase[31]. Molar extinction coefficient (Δε) of SNP/PEH, depending upon the solvent polarity, should change while going from polar aqueous media to the apolar hydrophobic cavity of the CDs to form ICs[41,42]. To determine association constant (K_a), the changes in absorbances (ΔA) of SNP/PEH were measured with increasing concentration of CDs at the temperature range 298.15 K to 308.15 K. (Tables S7–S10) The $\lambda_{max} = 209$ nm for SNP and $\lambda_{max} = 219$ nm for PEH were considered to determine the association constant (K_a) in this case (Table 3). According to the Benesi-Hildebrand method to determine the association constant for the 1:1 host-guest inclusion complex, the double reciprocal plot was obtained by using the following equation[31,43–45].

$$\frac{1}{\Delta A} = \frac{1}{\Delta\varepsilon[DGs]K_a}\frac{1}{[CD]} + \frac{1}{\Delta\varepsilon[DGs]} \quad (1)$$

where, ΔA represents the difference in absorbances of PEH or SNP without CDs to the absorbances of the same with the CDs. [DGs] refers to the concentration of the PEH and SNP. The association constants(K_a) of the inclusion complexes, listed in the (Table 3) were obtained by dividing the slope by the intercept of the plot given in the Figs S1, S2.

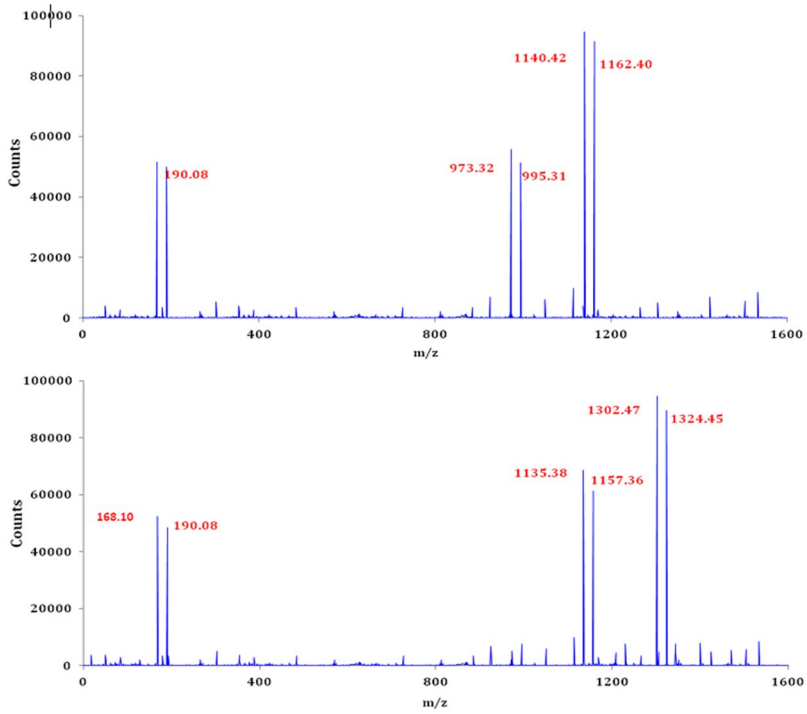

Figure 12. **(a**,**b)** HRMS spectra of the **(a)** SNP + α-CD, PEH + α-CD and **(b)** SNP + β-CD, PEH + β-CD ICs.

UV-vis spectroscopic data were also used in a nonlinear program that practices the changes in absorbance of SNP/PEH due to its molecular recognition into the apolar cavities of CDs and the association constants (K_a^θ) were obtained[31,46]. There should be an equilibrium between host and the guest molecules to the formation of 1:1 ICs[47,48].

$$[DGs]_f + [CD]_f \overset{K_a^\theta}{\rightleftharpoons} [IC] \tag{2}$$

The expression for the association constant (K_a^θ) can be obtained from the above equation as follows-

$$K_a^\theta = \frac{[IC]}{[DGs]_f\,[CD]_f} \tag{3}$$

where, [IC], $[DGs]_f$ and $[CD]_f$ represents the concentration of inclusion complex, free SNP/PEHand cyclodextrin respectively at the equilibrium of the reaction. The equation for the association constant (K_a^θ) can also be expressed as the absorbances of the host and the guest molecules as follows-

$$K_a^\theta = \frac{[IC]}{[DGs]_f\,[CD]_f} = \frac{(A_{obs} - A_0)}{(A - A_{obs})[CD]_f} \tag{4}$$

Here,

$$[CD]_f = [CD]_x - \frac{[DGs]_x(A_{obs} - A_0)}{(A - A_{obs})} \tag{5}$$

where, A_0 is the absorbance of SNP/PEH molecules in the initial state, A_{obs} denotes the absorbances of the same during the gradual addition of CDs and A refers to the final concentration of SNP/PEH molecules. $[CD]_x$ and $[DGs]_x$ is the concentration of cyclodextrins added and SNP/PEH molecules respectively. The association constants (K_a^θ), obtained from the binding isotherm with the application non-linear program are listed in the Table 3.

Conductance: Program based mathematical calculation of non-linear changes in the conductivity data and association constants (K_a^C). Non-linear changes in the conductivity data at the temperature ranging from 298.15 K to 308.15 K were utilized in the mathematical program and the association constants (K_a^c) for1:1 DGs-CDs ICs, listed in the Table 3 are frequently obtained[49–51]. The complexation reaction between DGs and CDs to produce ICs is supposed to proceed via the following chemical equilibrium

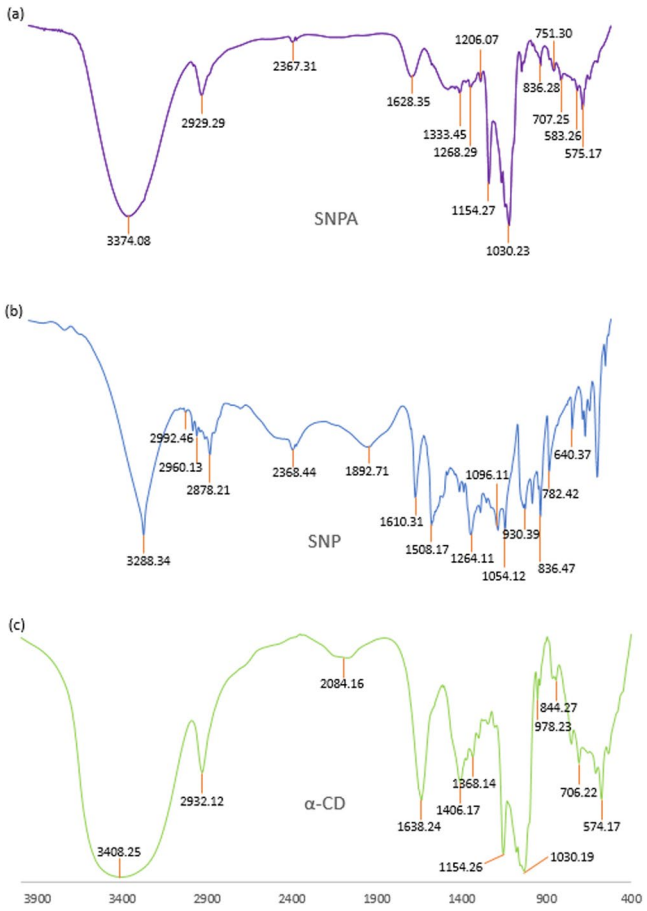

Figure 13. **(a**,**b**,**c)** FTIR spectra of **(a)** SNP + α-CD, **(b)** SNP, **(c)** α-CD.

$$[DGs]_f + [CD]_f \overset{K_a^C}{\rightleftharpoons} [IC] \tag{6}$$

The above equation can be reduced to the following form to find out the association constant K_a^c

$$K_a^c = \frac{[IC]}{[DGs]_f [CD]_f} \tag{7}$$

Here, $[IC]$ is the equilibrium concentration of inclusion complexes, $[DGs]_f$ and $[CD]_f$ refers to the concentration of SNP/PEH and CDs in the free state.

The association constant (K_a^c) can be calculated in terms of conductivities from the various non-linear isotherm as follows[50,51]-

$$K_a^c = \frac{[IC]}{[DGs]_f [CD]_f} = \frac{(\kappa_{obs} - \kappa_0)}{(\kappa - \kappa_{obs})[CD]_f} \tag{8}$$

Where,

$$[CD]_f = [CD]_{ad} - \frac{[DGs]_{ad}(\kappa_{obs} - \kappa_0)}{(\kappa - \kappa_0)} \tag{9}$$

Here, κ_0, κ_{obs} and κ corresponds to the conductivities of DGs at initial state, during addition of CDs and the final state respectively. Instantaneous concentration of DGs while addition of CDs is represented by $[DGs]_{ad}$ and $[CD]_{ad}$ is the concentration of the added CDs.

Fluorescence: Modified Benesi-Hildebrand equation and association constants. The association constants (K_a^F) of the ICs in the solution phase were also determined using the spectrofluorometric data and the association constants, determined are found in good agreement with the data obtained from all the previously described methodology[52–54] (Table 3, Tables S11–S14). An enhancement of the intensities of the spectral lines

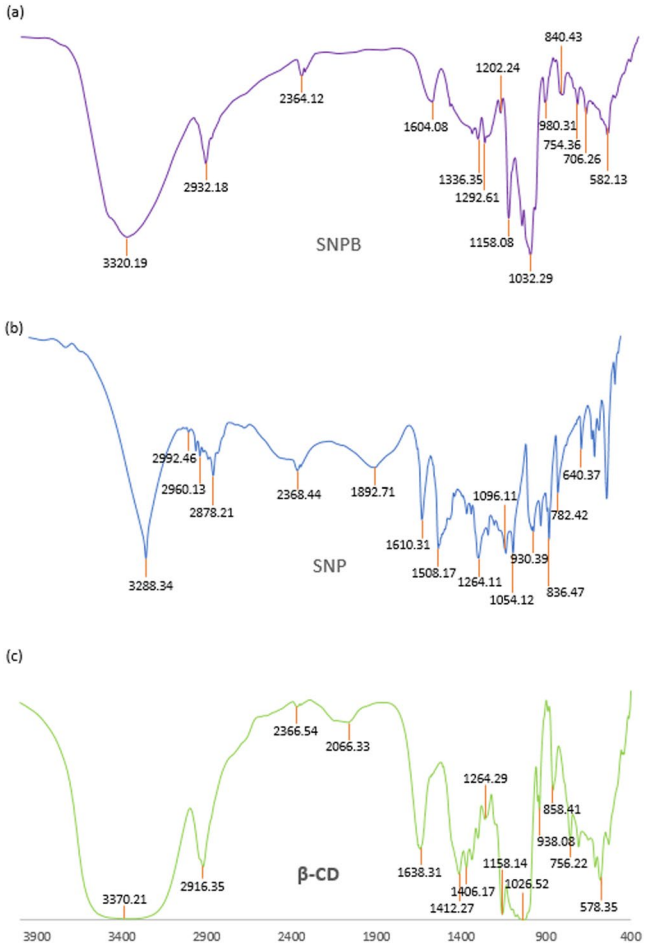

Figure 14. **(a**,**b**,**c)** FTIR spectra of **(a)** SNP + β-CD, **(b)** SNP, **(c)** β-CD.

accompanied by the slight hypsochromic shift were observed with the step wise increase in concentration of the CDs (α and β-cyclodextrins) solutions (Figs S3, S4). The observations enriched us with the knowledge that, a change in the molar extinction coefficient i.e. polarity of the environment, surrounding the chromophore, leaded by the encapsulation of the chromophore of the guest molecules (SNP and PEH) from the polar aqueous environment to the apolar hydrophobic cavity of the cyclodextrins. Sometimes, the enhancement in the intensities of the spectral lines are experienced due to the shielding of the excited singlet species of the chromophores from quenching and non-radiative decay with the protective microenvironment created by the hollow-circular, apolar cavity of the CDs[55,56]. The spectrofluorometric data were analyzed and run with the modified Benesi-Hildebrand equation to generate the double reciprocal plots, (Figs S5, S6) and the association constants (K_a^F) of the ICs were obtained as the ratio of the intercept to slope of the plots.

$$\frac{1}{I-I_0} = \frac{1}{[I'-I_0]K_a^F}\frac{1}{[CD]} + \frac{1}{I'-I_0} \tag{10}$$

where, I and I_0 represents the fluorescence intensities of SNP/PEH in the presence and absence of the CDs respectively, I' are the intensities of the SNP/PEH while all the guest molecules for a particular system are complexed with CDs. [CD] represents the concentration of the cyclodextrins (α and β-CD).

UV-vis spectroscopy, Non-linear program based mathematical calculation, Fluorescence and Conductance: Association constants and the thermodynamic parameters. According to the Van't Hoff Eq. (11) the various thermodynamic parameters for the formation of the inclusion complexes were derived from the ready available association constants (K_a, K_a^θ, K_a^C) obtained from Benesi-Hildebrand equation, nonlinear methods and non-linear changes in the conductivity data[31,37,41]. (Tables 4, S15–S20, Figs S7–S12)

$$\ln K_a = -\frac{\Delta H^0}{RT} + \frac{\Delta S^0}{R} \tag{11}$$

Calculation on the thermodynamic parameters of the formation of ICs, it is found that, both the changes in entropy and enthalpy of formation appears to be negative, suggesting an exothermic and entropy restricted rather

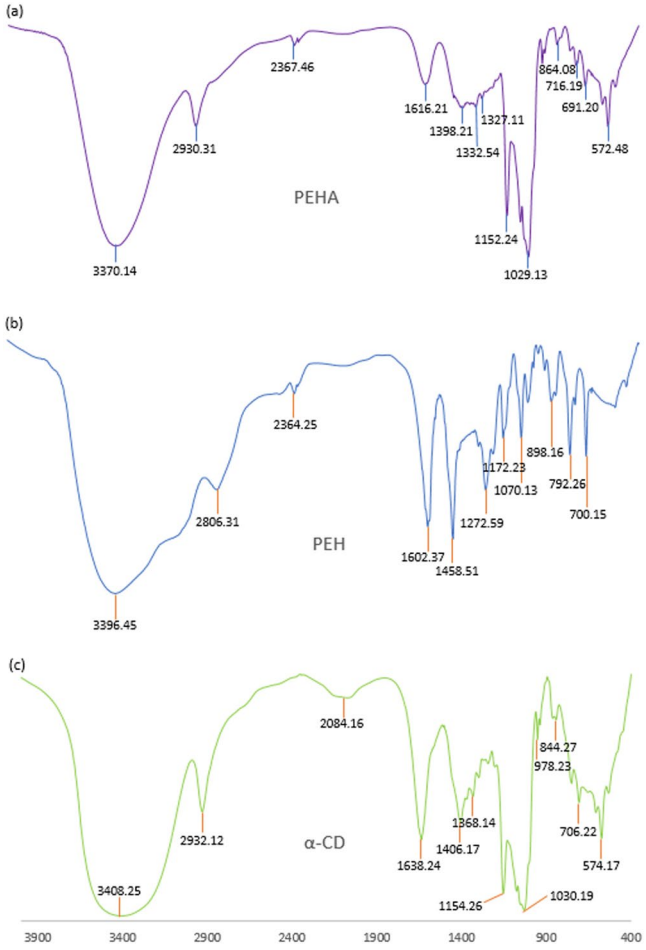

Figure 15. **(a**,**b**,**c)** FTIR spectra of **(a)** PEH + α-CD, **(b)** PEH, **(c)** α-CD.

than entropy driven process (Table 4). The explanation on the decrease in entropy during inclusion complexation comes from the molecular association of the host and guest molecules to form inclusion complexes in the solution. Though the process is entropy restricted, the negative value of the enthalpy (ΔH^0, $\Delta H^{\theta 0}$, ΔH^{C0}) makes the overall energy negative i.e. negative ΔG^0 and finds its spontaneity in the formation of ICs (Table 4).

^{1}H NMR and 2D ROESY NMR spectra analysis. Inclusion of a molecule inside into the cavity of cyclodextrin consequences in the chemical shift of the interacting protons of both the guest and cyclodextrin in ^{1}H NMR spectra, due to their mutual shielding through space[57]. Encapsulation of aromatic guest molecule results the diamagnetic shielding of the interacting protons of cyclodextrin by the aromatic moiety[58] (Table S21). Cyclodextrin molecule has H3 and H5 hydrogens at inside of the conical cavity, specially, the H3 are located near the wider rim while H5 are positioned near the narrower rim and the other H1, H2 and H4 hydrogens are situated at the exterior of the cyclodextrin molecule (Fig. 1)[59]. In this work the molecular inclusions have been studied with the help of ^{1}H NMR spectra. The ^{1}H NMR spectra of the pure α-CD, β-CD, SNP + α-CD, SNP + β-CD, PEH + α-CD and PEH + β-CD systems are shown in Figs S13–S18 respectively, where the aromatic as well as signals of H3 and H5 protons of cyclodextrins may be observed with corresponding chemical shift (δ) values. The ^{1}H NMR spectra of the complexes reveal that the signals of interior H3 and H5 of α and β-CD plus that of the interacting aromatic protons of SNP/PEH showed substantial upfield shift confirming the formation of inclusion complexes[60] (Figs S13–S18).

2D ROESY NMR spectroscopy provides decisive evidence about the spatial closeness of the interacting atoms of the host and the guest by observing the intermolecular dipolar cross-correlations[61,62]. The protons which are situated within 0.4 nm in space may produce a rotating-frame NOE spectroscopy (ROESY)[63]. According to structure of α and β-CD, inclusion phenomenon inside into cyclodextrin cavity can be shown by the appearance of NOE cross-peaks between the protons of cyclodextrin and the protons of the aromatic guest identifying their spatial proximity[64,65]. To prove this, 2D ROESY spectra of the complexes of SNP and PEH with α and β-CD in D_2O, were recorded, which shows significant correlation of aromatic protons of SNP and PEH with the H3 and H5 protons of α and β-CD, establishing the aromatic ring was encapsulated inside both the cyclodextrin cavities[66] (Figs 8–11). It may be detected that the H-6 protons of cyclodextrins were not influenced by the inclusion processes, suggesting that the SNP/PEH molecule was incorporated into the cyclodextrin cavity via the wider rim,

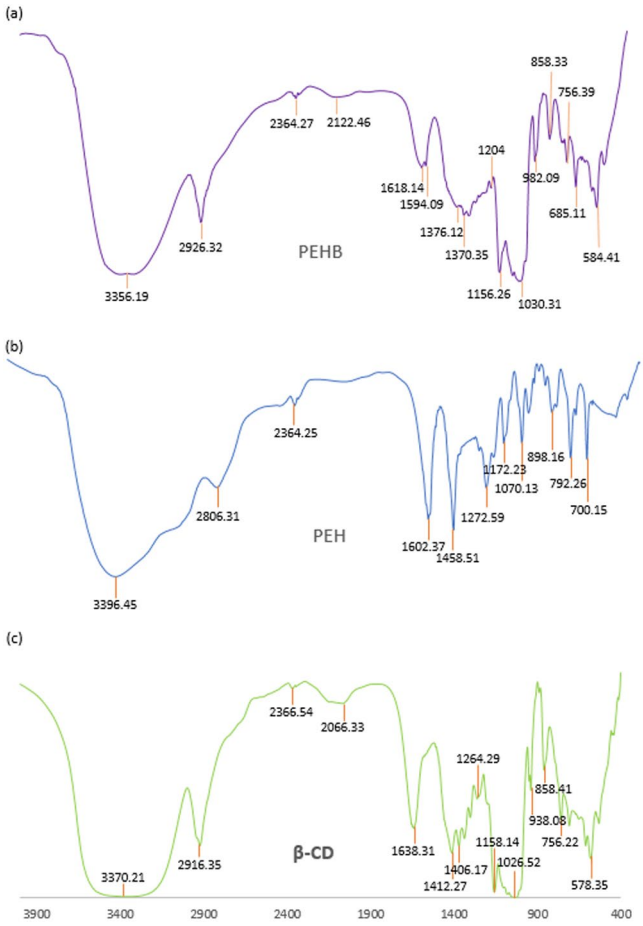

Figure 16. **(a**,**b**,**c)** FTIR spectra of **(a)** PEH + β-CD, **(b)** PEH, **(c)** β-CD.

not through the narrower rim as otherwise cross-peaks between the H6 and the guest would have been observed in the ROESY spectra[67] (Fig. 6).

HRMS Analysis of Inclusion complexes. Mass spectroscopic study of the solid inclusion complexes of SNP/PEH with α and β-CD were done after the dissolution of the ICs in methanol. The spectra are shown in the Fig. 12 and Table S22. enlists the m/z values for the corresponding fragmentations added to the molecular ion peak. The appearance of peaks at the m/z 1140.42 and 1162.40 corresponds to the $[SNP/PEH + \alpha\text{-CD} + H]^+$ and $[SNP/PEH + \alpha\text{-CD} + Na]^+$ respectively and the peaks at 1302.47 and 1324.45 corresponding to the $[SNP + \beta\text{-CD} + H]^+$ and $[SNP + \beta\text{-CD} + Na]^+$ respectively. The tangible existence of the peaks in the spectra mentioned above approves the formation of the inclusion complexes i.e. [PEH + α-CD], [PEH + β-CD], [SNP + α-CD] and [SNP + β-CD] and their host – guest stoichiometric ratio should be 1:1 (Fig. 3)[68,69].

FTIR spectroscopy. Interpretation of the Infra-red spectroscopic data of the ICs as well as the pure host and guest molecules also reveals the veracity about the way by which the ICs are formed and supports the same circumstances of host – guest interaction as obtained from the 2D ROESY NMR spectroscopic study[70,71]. All the FTIR spectra of the solid inclusion complexes and the pure host and guest molecules were recorded by preparing KBr disk. The changes in the significant peak values in the IR spectra on going from the pure host and guest molecules to the inclusion complexes which are shown in the Figs 13–16, suggests the formation of ICs exploring the binding mode of the guests to the host molecules[60,72]. The IR stretching frequencies (cm^{-1}) of noteworthy responsible for the corresponding chemical bonds are listed in the Table S23.

Analysis of the FTIR spectra for the [SNP + α-CD] along with the spectra of pure α-CD and SNP: (i) The -O-H stretching frequency of the α-CD and the -O-H and -N-H stretching frequencies of SNP were observed at 3408.25 and 2992.46 to 2960.13 cm^{-1} respectively, which appears as a broad peak at 3374.08 cm^{-1} in case of the IC. The responsible fact for this shifting in frequencies is the formation of H-bond between SNP and α-CD. (ii) The peaks at 1054.12 and 1264.11 cm^{-1} responsible for the -C-O stretching for secondary and phenolic -C-OH group of SNP respectively are shifted to 1030.23 and 1154.27 cm^{-1} correspondingly for the [SNP + α-CD] IC. Thus, weakening of -C-O bond proposes the formation of H-bond via the phenolic as well as the secondary -OH group of the SNP molecule. (iii) The stretching and bending frequencies for the -C-H bond of the α-CD was at 2932.12 and 1406.17 cm^{-1} and -C-H the out-of-plane bending frequencies for SNP were at 782.42 and

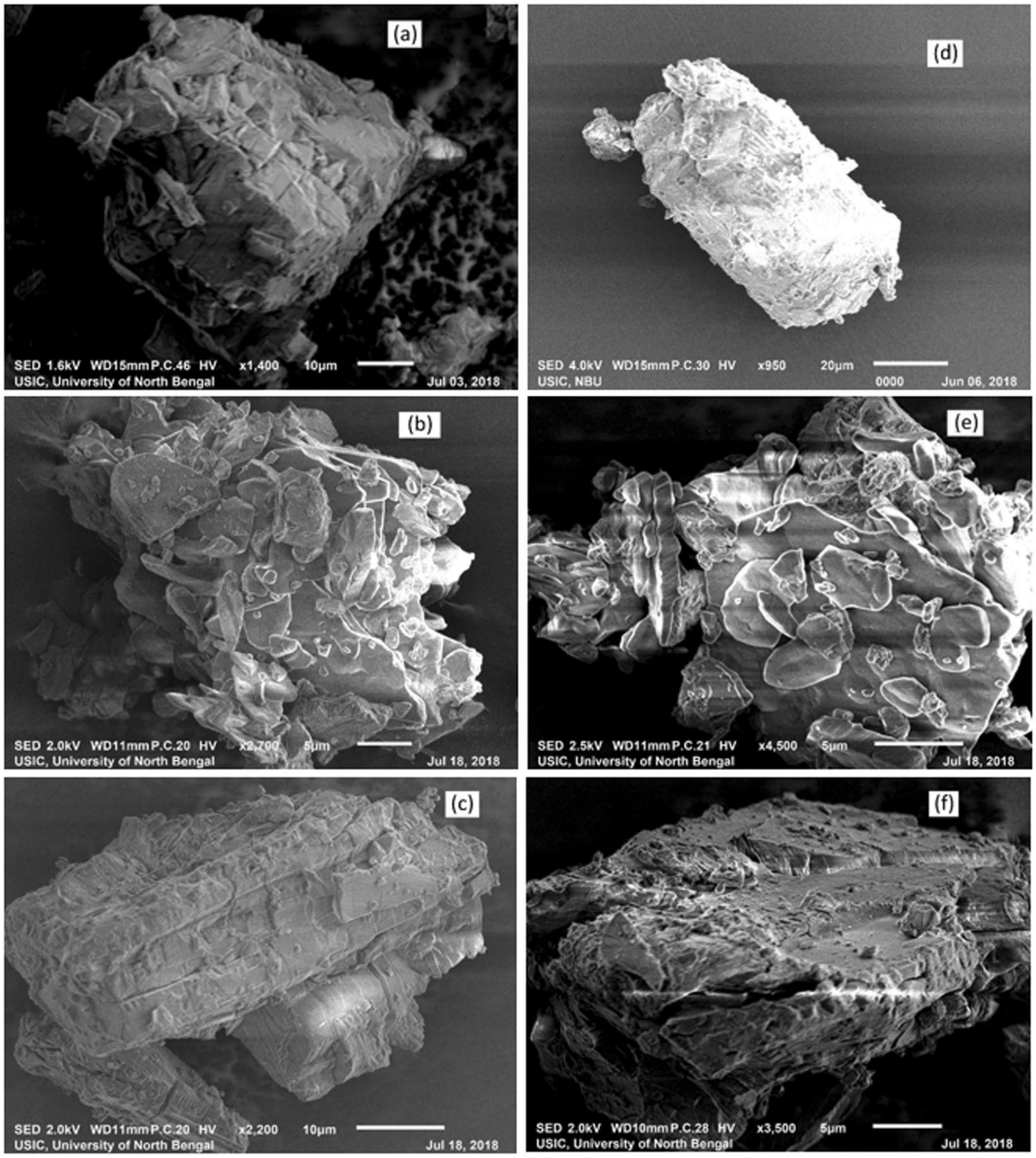

Figure 17. **(a**,**b**,**c**,**d**,**e**,**f)** SEM images of **(a)** α-CD, **(b)** (SNP + α-CD) physical mixture, **(c)** (SNP + α-CD) inclusion complex **(d)** β-CD, **(e)** (SNP + β -CD) physical mixture, **(f)** (SNP + β-CD) inclusion complex.

640.37 cm^{-1}. But in case of IC their existence is observed at 2929.30, 1333.02, 707.25 and 583.26 cm^{-1}, suggesting the various interactions taking place between SNP and α-CD (Fig. 13).

Innumerable interactions of the SNP and β-CD in the [SNP + β-CD] IC were analyzed as follows- (i) The signal for -O-H stretching of β-CD was at 3370.21 $cm^{-1}$and the -O-H and -N-H stretching frequencies of SNP were at 3288.34 cm^{-1} and the region of 2992.46 to 2960.13 cm^{-1} respectively, whereas in the IC these signals shifted to 3320.14 and 2933.18 cm^{-1} correspondingly. This is possibly due to the formation of H-bonding between SNP and β-CD. (ii) The peaks for -C-O (secondary and phenolic -C-OH group) of SNP were at 1054.12 and 1264.11 cm^{-1}, which shifted to 1032.29 and 1158.08 cm^{-1} respectively. This is probably owing to the formation of H-bond between SNP and β-CD. (iii) The signals at 2916.35 cm^{-1} and 1412.27 cm^{-1} corresponding to -C-H stretching and -C-H bending of β-CD, shifted to 2932.18 cm^{-1} and 1336.35 cm^{-1} respectively. On the other hand, -C-H out-of-plane bending for SNP molecule were observed at 782.42 cm^{-1} and 640.37 cm^{-1}, which shifted to 754.36 cm^{-1} and 582.13 cm^{-1} correspondingly. This may because of the various interactions taking place while the formation of the supramolecular assembly between SNP and β-CD (Fig. 14).

The various interactions that may cause the following spectroscopic changes in the [PEH + α-CD] IC are: (i) The peak for -O-H of α-CD was at 3408.25 cm^{-1} and the phenolic -O-H and -N-H stretching frequencies of PEH appeared as a broad peak at 3028.17 to 3396.45 cm^{-1}. But, in case of IC it is shifted to 3370.14 cm^{-1} indicating the formation of H-bond between PEH and CD. (ii) The -C-O stretching frequencies of PEH was at 1070.06 cm^{-1} (secondary alcohol) and 1272.59 cm^{-1} (phenol) where as these are shifted to 1029.13 $cm^{-1}$and 1152.24 cm^{-1} respectively in case of IC, suggesting the formation of H-bond through the secondary and phenolic H-atom of the

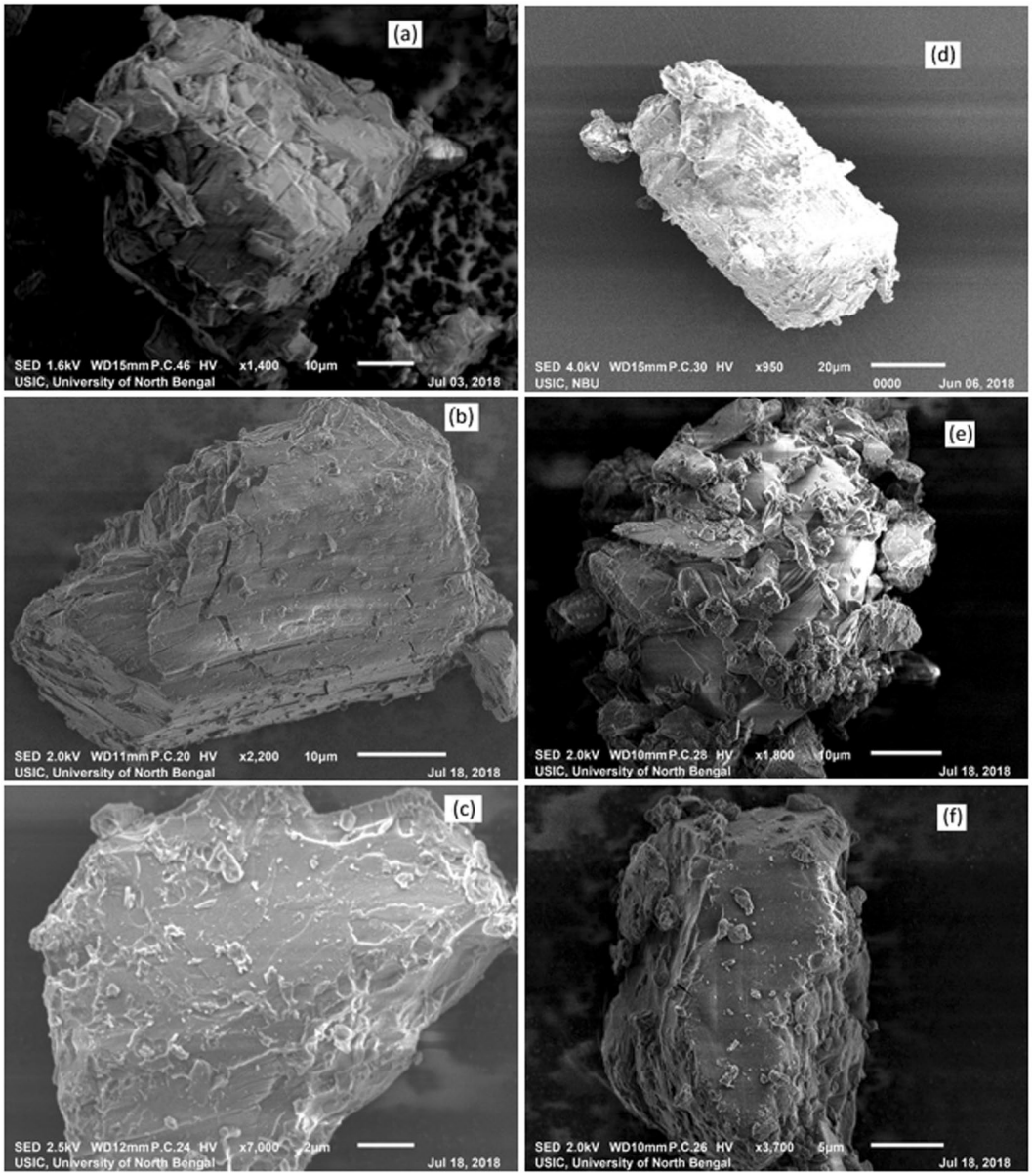

Figure 18. **(a**,**b**,**c**,**d**,**e**,**f)** SEM images of **(a)** α-CD, **(b)** (PEH + α-CD) physical mixture, **(c)** (PEH + α-CD) inclusion complex **(d)** β-CD, **(e)** (PEH + β-CD) physical mixture, **(f)** (PEH + β-CD) inclusion complex.

PEH molecule. (iii) The signal of the -C-H stretching and -C-H bending mode of the α-CD were at 2932.12 and 1406.17 cm^{-1} respectively and the aromatic out-of-plane -C-H bending of PEH were at 792.26 and 700.15 cm^{-1} respectively, which appeared in case of the IC at the frequencies 2930.31, 1398.21, 716.19 and 690.20 cm^{-1} respectively, shifting of these signals leads to the ready explanation that, the close proximity of the -C-H of the α-CD with the aromatic -C-H of the PEH as obtainable from the 2D ROESY spectra. (Fig. 15).

The shifting of the following IR signals satisfactorily explicates the formation of [PEH + β-CD] IC. (i) The -O-H signal for β-CD was at 3370.21 cm^{-1} and the phenolic -O-H and -N-H were at 3028.17 to 3396.45 cm^{-1} which are shifted to 3356.19 cm^{-1} for IC. This is probably the formation of the H-bond of PEH with β-CD. (ii) The peaks at the 1070.06 cm^{-1} (-C-O, secondary alcohol) and 1272.59 cm^{-1} (-C-O, phenolic) for the PEH were shifted to the frequencies 1030.34 cm^{-1} and 1156.31 cm^{-1}, validates the participation of secondary and phenolic -O-H group of PEH towards the formation of H-bond with β-CD. (iii) The -C-H stretching and bending mode of frequencies of β-CD were at 2918.35 and 1412.27 cm^{-1} respectively and peaks for the aromatic out-of-plane -C-H bending frequencies for PEH were at792.26 and 700.15 cm^{-1} respectively, are now shifted to 2926.32, 1376.12,756.39 and 685.11 cm^{-1} respectively. Thus, FTIR spectral analysis also indorses the same as obtained from the 2D ROESY spectra (Fig. 16).

There is no sign of chemical reaction taking place while the formation of all the inclusion complexes, exemplified by the no appearance of additional signal in the IR spectra suggesting, all the shifting in signals appearing are responsible for the formation of ICs.

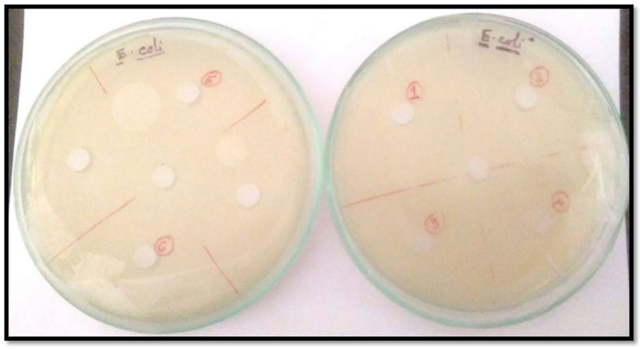

Figure 19. Antimicrobial activity analysis α-CD, β-CD on Gram-negative *E. coli* by Agar Cup method. No zone of inhibition is observed. Double distilled water is taken as the control. [Marker points (red) for the verified samples taken in the plates (1. SNP, 2. PEHB, 3. PEHA, 4. SNPA, 5. PEH, 6. SNPB) and Marker points (black) for the model organism taken in the plates].

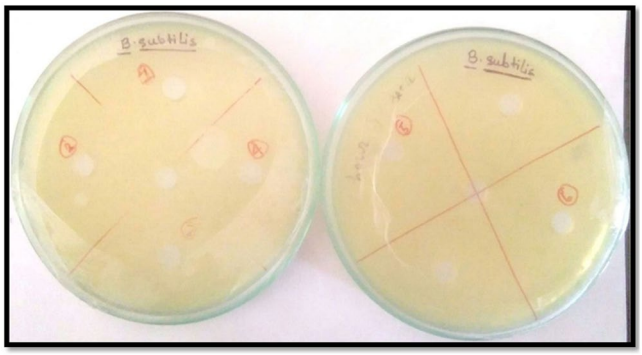

Figure 20. Antimicrobial activity analysis α-CD, β-CD on Gram-positive B. subtilis by Agar Cup method. No zone of inhibition is observed. Double distilled water is taken as the control. [Marker points (red) for the verified samples taken in the plates (1. SNP, 2. PEHB, 3. PEHA, 4. SNPA, 5. PEH, 6. SNPB) and Marker points (black) for the model organism taken in the plates].

Scanning Electron Microscope (SEM). Scanning Electron Microscopy (SEM) is an exceedingly well-known technique for analyzing the surface texture and particle size of solid materials. The surface morphological structures of α-CD, (SNP + α-CD) physical mixture, (SNP + α-CD) inclusion complex, β-CD, (SNP + β-CD) physical mixture, (SNP + β-CD) inclusion complex are shown in Fig. 17 respectively. From Fig. 17 it is clear, that the morphological structures that they are totally different from each other. Similarly, the surface morphological structures of α-CD, (PEH + α-CD) physical mixture, (PEH + α-CD) inclusion complex, β-CD, (PEH + β-CD) physical mixture, (PEH + β-CD) inclusion complex are shown in Fig. 18 respectively. From Fig. 18 it is clear, that the morphological structures that they are totally different from each other. Moreover, as the complexation by α-CD and β-CD can be viewed distinctly. This is an additional evidence about the formation of inclusion complexes of SNP/PEH with α and β-CD, may support the same evident from 2D ROESY NMR analysis.

Cytotoxic activity of the Inclusion complexes. No zone of inhibition is observed in case of both the gram-positive and gram-negative organisms[73,74]. There is no growth inhibition compared to control. These results suggest that ICs doesn't have any antimicrobial activity. So, it can be said that it is non-toxic for the cells. After that cell viability assay is finished. Here, we have found that cell viability of *E. coli* is 4.6% and 9% increase in presence of [SNP + β-CD, SNP + α-CD] and [PEH + β-CD, PEH + α-CD] respectively whereas the cell viability of B. subtilis is 3.2% and 8% increase in the presence of [SNP + β-CD, SNP + α-CD] and [PEH + β-CD, PEH + α-CD] correspondingly (Figs 19, 20). These consequences indicate that cell viability is positively regulated in occurrence of these ICs (Figs 19, 20). But there is very significant increase in growth when the samples are treated with (SNP + β-CD). So, this (SNP + β-CD) is more suitable for pharmaceutically active compounds. The outcome shows that both inclusion complexes have increased the capability of SNP inhibiting cell growth rather than PEH. Particularly, SNP, complexed with beta-cyclodextrin (β-CD) show the highest cytotoxic activity resting on *E. coli* and B. subtilis; with alpha-cyclodextrin (α-CD) the cytotoxic activity is found to be rather low.

Conclusions

The suggestion obtained from surface tension and conductometric study for the formation of 1:1 host-guest inclusion complexes of SNP and PEH with α and β-cyclodextrins are established by UV-Vis spectroscopy, spectrofluorimetry, 2D ROESY NMR spectrometry and SEM technique by analyzing surface texture of the solid inclusion complexes. The association constants obtained from all the well-established techniques dictates the stability of inclusion complexes formed and the thermodynamic parameters reveals truth about the feasibility of their formation. Removal of water molecules from the cavity of the CDs to make room for the guest molecule for accommodation while formation of inclusion complex, increases entropy of the process. Dimensional suitability being, one of the major stabilizing factor, the larger cavity size of β-CD (0.70 nm, diameter) compared to α-CD (0.56 nm, diameter), explains for the greater value of association constants and stability of the inclusion complexes formed with β-CD. The association constants, hence stability of the inclusion complexes of SNP with CDs were found more than that of the PEH. Because, -O-H group of SNP, being oriented to the para position may exert H-bonding interaction with CDs to some greater extent than that of the PEH, in which –OH group, being oriented at the meta – position can't travel the minimum distance for the formation of H-bond with the CDs. The hydrophobic and H-bonding interactions thus stabilizes the ICs. The Cytotoxicity and Cell viability also balances for non-toxic behavior of the ICs. Thus, inclusion complexes of the recently emerging two drugs, SNP and PEH (after their banned alternatives) stabilizes SNP and PEH from their chemical modification and conveys a new approach for regulatory release to the targeted site reducing overdoses.

References

1. Bao, L. *et al*. Synthesis, structure, and host-guest properties of an anthracene-based macrocyclic arene. *Tetrahedron Letters* **59**, 730–733 (2018).
2. Fang, X., Gong, F. & Fang, Y. Capillary Electrophoresis with Electrochemical Detection for Chiral Separation of Optical Isomers. *Analytical Chemistry* **70**, 4030–4035 (1998).
3. Pal, A., Gaba, R. & Soni, S. Effect of presence of α-cyclodextrin and β-cyclodextrin on solution behavior of sulfathiazole at different temperatures: Thermodynamic and spectroscopic studies. *The Journal of Chemical Thermodynamics* **119**, 102–113 (2018).
4. Tait, R. J., Thompson, D. O., Stella, V. J. & Stobaugh, J. F. Sulfobutyl Ether.beta.-Cyclodextrin as a Chiral Discriminator for Use with Capillary Electrophoresis. *Analytical Chemistry* **66**, 4013–4018 (1994).
5. Fanali, S. Identification of chiral drug isomers by capillary electrophoresis. *Journal of Chromatography A* **735**, 77–121 (1996).
6. Stalcup, A. M. & Gahm, K. H. Application of Sulfated Cyclodextrins to Chiral Separations by Capillary Zone Electrophoresis. *Analytical Chemistry* **68**, 1360–1368 (1996).
7. de Oliveira, G. G. G. *et al*. Compatibility study of paracetamol, chlorpheniramine maleate and phenylephrine hydrochloride in physical mixtures. *Saudi Pharmaceutical Journal* **25**, 99–103 (2017).
8. Shah, H. N., Halquist, M. T. & Gerk, P. M. Direct detection of phenylephrine 3-O-sulfate in LS180 human intestinal cells using a novel hydrophilic interaction liquid chromatography (HILIC) assay. *Journal of Chromatography B* **1040**, 67–72 (2017).
9. Kuan, Y.-C., Xu, Y.-B., Wang, W.-C. & Yang, M.-T. Enantioselective synthesis of (R)-phenylephrine by Serratia marcescens BCRC10948 cells that homologously express SM_SDR. *Enzyme and Microbial Technology* **110**, 14–19 (2018).
10. Kernan, W. N. *et al*. Phenylpropanolamine and the Risk of Hemorrhagic Stroke. *New England Journal of Medicine* **343**, 1826–1832 (2000).
11. Wheaton, T. A. & Stewart, I. Biosynthesis of synephrine in citrus. *Phytochemistry* **8**, 85–92 (1969).
12. Tette, P. A. S. & Guidi, L. R. Bastos EMAF, Fernandes C, Gloria MBA. Synephrine - A potential biomarker for orange honey authenticity. *Food Chem* **229**, 527–533 (2017).
13. Arai, K., Jin, D., Kusu, F. & Takamura, K. Determination of p-hydroxymandelic acid enantiomers in urine by high-performance liquid chromatography with electrochemical detection. *Journal of Pharmaceutical and Biomedical Analysis* **15**, 1509–1514 (1997).
14. Wheaton, T. A. & Stewart, I. Feruloylputrescine: Isolation and Identification from Citrus Leaves and Fruit. *Nature* **206**, 620 (1965).
15. Vieira, S. M., Theodoro, K. H. & Gloria, M. B. A. *Profile and levels of bioactive amines in orange juice and orange soft drink* (2007).
16. Vieira, S., Calado, R., Coelho, H. & Serôdio, J. *Vieira et al 2009 MarBiol* (2012).
17. Gregory, P. J. Evaluation of the Stimulant Content of Dietary Supplements Marketed as "Ephedra-Free". *Journal of Herbal Pharmacotherapy* **7**, 65–72 (2007).
18. Hallas, J., Bjerrum, L., Støvring, H. & Andersen, M. Use of a Prescribed Ephedrine/Caffeine Combination and the Risk of Serious Cardiovascular Events: A Registry-based Case-Crossover Study. *American Journal of Epidemiology* **168**, 966–973 (2008).
19. Vatsavai, L. K. & Kilari, E. K. Interaction of p-synephrine on the pharmacodynamics and pharmacokinetics of gliclazide in animal models. *Journal of Ayurveda and Integrative Medicine* (2017).
20. Dragull, K., Breksa, A. P. 3rd. & Cain, B. Synephrine content of juice from Satsuma mandarins (Citrus unshiu Marcovitch) *J Agric Food Chem* **56**(19), 74–8 (2008).
21. Venkata Giri Kumar, P., Deshpande, S., Joshi, A., More, P. & Nagendra, H. R. Significance of arterial stiffness in Tridosha analysis: A pilot study. *Journal of Ayurveda and Integrative Medicine* **8**, 252–256 (2017).
22. Artiss, J. D. *et al*. The effects of a new soluble dietary fiber on weight gain and selected blood parameters in rats. *Metabolism* **55**(2), 195–202 (2006).
23. Comerford, K. B., Artiss, J. D., Jen, K. L. & Karakas, S. E. The beneficial effects of alpha-cyclodextrin on blood lipids and weight loss in healthy humans. *Obesity* **19**, 1200–1204 (2011).
24. Job, P. Formation and stability of inorganic complexes in solution. *Annales de Chimie (France)* **9**, 113–203 (1928).
25. Renny, J. S., Tomasevich, L. L., Tallmadge, E. H. & Collum, D. B. Method of continuous variations: applications of job plots to the study of molecular associations in organometallic chemistry. *Angew Chem Int Ed Engl* **52**, 11998–12013 (2013).
26. Brynn Hibbert, D. & Thordarson, P. The death of the Job plot, transparency, open science and online tools, uncertainty estimation methods and other developments in supramolecular chemistry data analysis. *Chemical Communications* **52**, 12792–12805 (2016).
27. Ulatowski, F., Dąbrowa, K., Bałakier, T. & Jurczak, J. Recognizing the Limited Applicability of Job Plots in Studying Host–Guest Interactions in Supramolecular Chemistry. *The Journal of Organic Chemistry* **81**, 1746–1756 (2016).
28. Caso, J. V. *et al*. Investigating the inclusion properties of aromatic amino acids complexing beta-cyclodextrins in model peptides. *Amino Acids* **47**(10), 2215–27 (2015).
29. Gao, Y. *et al*. Inclusion complexes of beta-cyclodextrin with ionic liquid surfactants. *J Phys Chem B* **110**(17) 8576–81 (2006).
30. Piñeiro, Á. *et al*. On the Characterization of Host−Guest Complexes: Surface Tension, Calorimetry, and Molecular Dynamics of Cyclodextrins with a Non-ionic Surfactant. *The Journal of Physical Chemistry B* **111**, 4383–4392 (2007).
31. Saha, S., Roy, A., Roy, K. & Roy, M. N. Study to explore the mechanism to form inclusion complexes of β-cyclodextrin with vitamin molecules. *Scientific Reports* **6**, 35764 (2016).
32. Roy, M. N., Saha, S., Barman, S. & Ekka, D. Host-guest inclusion complexes of RNA nucleosides inside aqueous cyclodextrins explored by physicochemical and spectroscopic methods. *RSC Advances* **6**, 8881–8891 (2016).

33. Roy, M. N., Ekka, D., Saha, S. & Chandra Roy, M. Host-guest inclusion complexes of [small alpha] and [small beta]-cyclodextrins with [small alpha]-amino acids. *RSC Advances* **4**, 42383–42390 (2014).
34. Ghosh, R., Ekka, D., Rajbanshi, B., Yasmin, A. & Roy, M. N. Synthesis,characterization of 1-butyl-4-methylpyridinium lauryl sulfate and its inclusion phenomenon with β-cyclodextrin for enhanced applications. *Colloids and Surfaces A: Physicochemical and Engineering Aspects* **548**, 206–217 (2018).
35. Gao, Y. *et al*. Inclusion complexes of beta-cyclodextrin with ionic liquid surfactants. *J Phys Chem B* **110**, 8576–8581 (2006).
36. Roy, A., Saha, S., Datta, B. & Roy, M. N. Insertion behavior of imidazolium and pyrrolidinium based ionic liquids into [small alpha] and [small beta]-cyclodextrins: mechanism and factors leading to host-guest inclusion complexes. *RSC Advances* **6**, 100016–100027 (2016).
37. Roy, M. N., Saha, S., Kundu, M., Saha, B. C. & Barman, S. Exploration of inclusion complexes of neurotransmitters with β-cyclodextrin by physicochemical techniques. *Chemical Physics Letters* **655–656**, 43–50 (2016).
38. Roy, M. N., Roy, A. & Saha, S. Probing inclusion complexes of cyclodextrins with amino acids by physicochemical approach. *Carbohydrate Polymers* **151**, 458–466 (2016).
39. Saha, S., Ray, T., Basak, S. & Roy, M. N. NMR, surface tension and conductivity studies to determine the inclusion mechanism: thermodynamics of host-guest inclusion complexes of natural amino acids in aqueous cyclodextrins. *New Journal of Chemistry* **40**, 651–661 (2016).
40. Barman, B. K., Rajbanshi, B., Yasmin, A. & Roy, M. N. Exploring inclusion complexes of ionic liquids with α- and β- cyclodextrin by NMR, IR, mass, density, viscosity, surface tension and conductance study. *Journal of Molecular Structure* **1159**, 205–215 (2018).
41. Roy, P. M., Saha, S., Barman, S. & Ekka, D. D. *Host–guest inclusion complexes of RNA nucleosides inside aqueous cyclodextrins explored by physicochemical and spectroscopic methods* (2016).
42. Cramer, F., Saenger, W. & Spatz, H. C. Inclusion Compounds. XIX.1a The Formation of Inclusion Compounds of α-Cyclodextrin in Aqueous Solutions. Thermodynamics and Kinetics. *Journal of the American Chemical Society* **89**, 14–20 (1967).
43. Roy, M. N., Saha, S., Barman, S. & Ekka, D. Host–guest inclusion complexes of RNA nucleosides inside aqueous cyclodextrins explored by physicochemical and spectroscopic methods. *RSC Advances* **6**, 8881–8891 (2016).
44. Benesi, H. A. & Hildebrand, J. H. A Spectrophotometric Investigation of the Interaction of Iodine with Aromatic Hydrocarbons. *Journal of the American Chemical Society* **71**, 2703–2707 (1949).
45. Caso, J. V. *et al*. Investigating the inclusion properties of aromatic amino acids complexing beta-cyclodextrins in model peptides. *Amino Acids* **47**, 2215–2227 (2015).
46. Thordarson, P. Determining association constants from titration experiments in supramolecular chemistry. *Chem Soc Rev* **40**, 1305–1323 (2011).
47. Connors, K. A. The Stability of Cyclodextrin Complexes in Solution. *Chemical Reviews* **97**, 1325–1358 (1997).
48. Szejtli, J. Introduction and General Overview of Cyclodextrin Chemistry. *Chemical Reviews* **98**, 1743–1754 (1998).
49. Evans, D. F. & Matesich, S. M. A. Ionic association in hydrogen-bonding solvents. *Journal of Solution Chemistry* **2**, 193–216 (1973).
50. Khayatian, G., Shariati, S. & Shamsipur, M. Conductance Study of the Thermodynamics of Binding of Some Macrocyclic Polyethers with Tl+ Ion in Dimethylformamide-Acetonitrile Mixtures. *Journal of inclusion phenomena and macrocyclic chemistry* **45**, 117–121 (2003).
51. de Namor, A. F. D., Ritt, M.-C., Schwing-Weill, M.-J., Arnaud-Neu, F. & Lewis, D. F. V. Solution thermodynamics of amino acid-18-crown-6 and amino acid-cryptand 222 complexes in methanol and ethanol. Linear enthalpy-entropy compensation effect. *Journal of the Chemical Society, Faraday Transactions* **87**, 3231–3239 (1991).
52. Prabu, S., Swaminathan, M., Sivakumar, K. & Rajamohan, R. Preparation, characterization and molecular modeling studies of the inclusion complex of Caffeine with Beta-cyclodextrin. *Journal of Molecular Structure* **1099**, 616–624 (2015).
53. Sanramé, C. N., de Rossi, R. H. & Argüello, G. A. Effect of β-Cyclodextrin on the Excited State Properties of 3-Substituted Indole Derivatives. *The Journal of Physical Chemistry* **100**, 8151–8156 (1996).
54. Oana, M., Tintaru, A., Gavriliu, D., Maior, O. & Hillebrand, M. Spectral Study and Molecular Modeling of the Inclusion Complexes of β-Cyclodextrin with Some Phenoxathiin Derivatives. *The Journal of Physical Chemistry B* **106**, 257–263 (2002).
55. Zhang, Q.-F., Jiang, Z.-T., Guo, Y.-X. & Li, R. Complexation study of brilliant cresyl blue with β-cyclodextrin and its derivatives by UV–vis and fluorospectrometry. *Spectrochimica Acta Part A: Molecular and Biomolecular Spectroscopy* **69**, 65–70 (2008).
56. Zhang, M., Li, J., Jia, W., Chao, J. & Zhang, L. Theoretical and experimental study of the inclusion complexes of ferulic acid with cyclodextrins. *Supramolecular Chemistry* **21**, 597–602 (2009).
57. Sindelar, V. *et al*. Supramolecular assembly of 2,7-dimethyldiazapyrenium and cucurbit[8]uril: a new fluorescent host for detection of catechol and dopamine. *Chemistry* **11**(23), 7054–9 (2005).
58. Yang, L. J. *et al*. Preparation and characterization of inclusion complexes of naringenin with beta-cyclodextrin or its derivative. *Carbohydr Polym* **98**, 861–869 (2013).
59. Fernandes, A. *et al*. Structural characterization of inclusion complexes between cyanidin-3-O-glucoside and β-cyclodextrin. *Carbohydrate Polymers* **102**, 269–277 (2014).
60. Xiao, C. F. *et al*. Investigation of inclusion complex of epothilone A with cyclodextrins. *Carbohydr Polym* **102**, 297–305 (2014).
61. Yang, B., Lin, J., Chen, Y. & Liu, Y. Artemether/hydroxypropyl-beta-cyclodextrin host-guest system: characterization, phase-solubility and inclusion mode. *Bioorg Med Chem* **17**, 6311–6317 (2009).
62. Servais, A. C. *et al*. Capillary electrophoretic and nuclear magnetic resonance studies on the opposite affinity pattern of propranolol enantiomers towards various cyclodextrins. *J Sep Sci* **33**(11), 1617–24 (2010).
63. Correia, I. *et al*. Study of inclusion complexes of acridine with β- and (2,6-di-O-methyl)-β-cyclodextrin by use of solubility diagrams and NMR spectroscopy. *Journal of Physical Organic Chemistry* **15**, 647–659 (2002).
64. Bednarek, E. *et al*. Complexation of steroid hormones: prednisolone, ethinyloestradiol and estriol with [small beta]-cyclodextrin. An aqueous 1H NMR study. *Journal of the Chemical Society, Perkin Transactions* **2**, 999–1004 (2002).
65. Ishizu, T., Hirata, C., Yamamoto, H. & Harano, K. Structure and intramolecular flexibility of β-cyclodextrin complex with (−)-epigallocatechin gallate in aqueous solvent. *Magnetic Resonance in Chemistry* **44**, 776–783 (2006).
66. Kemelbekov, U. *et al*. IR, UV and NMR studies of β-cyclodextrin inclusion complexes of kazcaine and prosidol bases. *Journal of inclusion phenomena and macrocyclic chemistry* **69**, 181–190 (2011).
67. Stalin, T., Srinivasan, K., Sivakumar, K. & Radhakrishnan, S. Preparation and characterizations of solid/aqueous phases inclusion complex of 2,4-dinitroaniline with beta-cyclodextrin. *Carbohydr Polym* **107**, 72–84 (2014).
68. Zhang, J. Q. *et al*. Novel water-soluble fisetin/cyclodextrins inclusion complexes: Preparation, characterization, molecular docking and bioavailability. *Carbohydr Res* **418**, 20–28 (2015).
69. Okada, Y., Ueyama, K., Nishikawa J.-I., Semma M. & Ichikawa, A. *Effect of 6-O-α-maltosyl-β cyclodextrin and its cholesterol inclusion complex on cellular cholesterol levels and ABCA1 and ABCG1 expression in mouse mastocytoma P-815 cells* (2012).
70. Sivakumar, K., Ragi, T. R., Prema, D. & Stalin, T. Experimental and theoretical investigation on the structural characterization and orientation preferences of 2-hydroxy-1-naphthoic acid/β-cyclodextrin host-guest inclusion complex. *Journal of Molecular Liquids* **218**, 538–548 (2016).
71. Negi, J. S. & Singh, S. Spectroscopic investigation on the inclusion complex formation between amisulpride and gamma-cyclodextrin. *Carbohydr Polym* **92**, 1835–1843 (2013).
72. Zhang, W. *et al*. Investigation of water-soluble inclusion complex of hypericin with β-cyclodextrin polymer. *Carbohydrate Polymers* **95**, 366–370 (2013).

73. Vesterdal, J. The Agar Cup Method for the Estimation of Penicillin*. *Acta Pharmacologica et Toxicologica* **2**, 9–21 (1946).
74. Di Donato, C. *et al.* Alpha- and Beta-Cyclodextrin Inclusion Complexes with 5-Fluorouracil: Characterization and Cytotoxic Activity Evaluation. *Molecules* 21 06/06/2018; 08/17/2018 (2016).

Acknowledgements
Prof. M.N. Roy would like to acknowledge UGC, New Delhi, Government of India, for being awarded One Time Grant under Basic Scientific Research via the grant-in-Aid no. F.4–10/2010 (BSR). BR is thankful to the "State Fellowship" bearing reference No. 1743/R-2017 dated 18.04.2017 and UGC-SAP DRS-III, New Delhi (no. 540/6/DRS/2007, SAP-1) for providing instrumental facilities according the research. Mr. Goutam Sarkar, the HOD., USIC, University of North Bengal, Darjeeling is also highly acknowledged for executing SEM associated with this paper and his sincere co-operation.

Author Contributions
B.R. designed, performed the experiments and wrote the article, S.S. designed and performed the experiments, K.D. designed and performed the experiments, B.K.B. designed and performed the experiments, S.S. performed cytotoxic activity, A.B. performed cytotoxic activity, MNR supervised the entire work and corresponding author.

Additional Information
Supplementary information accompanies this paper at https://doi.org/10.1038/s41598-018-31373-x.

Competing Interests: The authors declare no competing interests.

Publisher's note: Springer Nature remains neutral with regard to jurisdictional claims in published maps and institutional affiliations.

Journal of Molecular Liquids 282 (2019) 415–427

Contents lists available at ScienceDirect

Journal of Molecular Liquids

journal homepage: www.elsevier.com/locate/molliq

Minimization of the dosage of food preservatives mixing with ionic liquids for controlling risky effect in human body: Physicochemical, antimicrobial and computational study

Biplab Rajbanshi [a], Koyeli Das [a], Khusboo Lepcha [b], Samir Das [a], Debadrita Roy [a], Mitali Kundu [a], Mahendra Nath Roy [a,*]

[a] Department of Chemistry, University of North Bengal, Darjeeling 734013, India
[b] Department of Microbiology, University of North Bengal, Darjeeling 734013, India

ARTICLE INFO

Article history:
Received 11 January 2019
Accepted 6 March 2019
Available online 09 March 2019

Keywords:
Benzyltriethylammoniun chloride
Benzyltrimethylammoniun chloride
Sodium benzoate
Sodium salicylate
Solute-solvent interaction
Anti-microbial activity

ABSTRACT

An analysis on the diverse molecular interactions of implausible food preservatives, Sodium benzoate (SBz), Sodium salicylate (Scyt) in the aqueous solutions of Benzyltriethylammoniun chloride (BTEACl), Benzyltrimethylammoniun chloride (BTMACl) having durable anti-bacterial effect have been explored thoroughly by various physicochemical methodologies such as Density, Refractive index, Viscosity, Electrical conductivity, at five different temperatures ranging from 298.15 K to 318.15 K. Anti-bacterial as well as the anti-fungal effects of the ternary mixtures, (BTEACl + SBz + H_2O), (BTEACl + Scyt + H_2O), (BTMACl + SBz + H_2O) and (BTMACl + Scyt + H_2O) were further analysed for better results and found to act synergistically below the MIC of both the food preservative, thus minimises the hazardous threat, caused by unnecessarily excessive consumption of food preservatives. Association constants governed by diverse intermolecular interactions in the solution phase were studied by UV–vis spectroscopy. Construction of thermodynamic background caused by innumerable interactions taking place in the ternary mixtures was explored by calculating the free energies of various molecular associations. The genesis of diverse interactions was exposed by measurement of the apparent molar volume (ϕ_v), limiting apparent molar volume (ϕ_v^0), molar refraction (R_M), limiting molar refraction (R_M^0) viscosity B coefficients and reveals as strong solute-solvent interaction, over the solute-solute and solvent-solvent interactions. Optimum energies with the optimised geometries of molecular assembly for (BTEACl + SBz), (BTEACl + Scyt), (BTMACl + SBz) and (BTMACl + Scyt) systems were calculated from Ab-initio quantum chemical calculations using Gaussian 09W quantum chemical package which found supportive to the practical outcomes.

1. Introduction

According to our knowledge, it is well known to all, there is so much of food productions all over the world but because of the process of spoilage a large proportion of these is lost. So, it requires a great attention to preserve foods, produced industrially and even at home. There are so many preservatives known, that utterly prevents spoilage of foods, but having some sort of side effects, usedness of these is an inherent threat to the world health. Now, use of these in minimal amount i.e. below the MIC (Minimal Inhibitory Concentration) in food would overcome the threat. The challenge was accepted and reveals that, two well-known food preservatives (FPs), sodium benzoate and sodium salicylate works properly against various fungus as well as gram-positive and gram-negative bacteria below their MIC in the presence of negligible amount of two ammonium based ionic liquids (ILs) benzyltriethylammoniun chloride (BTEACl) and benzyltrimethylammonium chloride (BTMACl).

Sodium benzoate (SBz) (Scheme 1) having inhibitory effect on the microbial growth is strongly recommended as a food preservative and commonly used in foods like soda, fruit juice and a variety of products, such as cosmetics and pharmaceuticals. In acidic medium SBz works better on yeasts, molds, bacterial growth and prevent spoilage [1–5]. In patients with acute hyper-ammonaemia, who were born with urea cycle disorders [6,7] SBz acts as a therapeutic agent and also treats dental carries, blocks D-dopa in the hemi-parkinsonian rat [8]. Beside these bio-medical and pharmaceutical applications SBz have some antagonistic effect, it can damage parts of the DNA affecting the future generations [9]. The acceptable daily intake (ADI) levels of SBz should be 5 mg/kg body weight [10], as strictly recommended by Joint Food and Agriculture Organization of the United Nations/World Health Organization expert committee on food additives, otherwise SBz may be toxic and imperils human health [11]. Research on interaction of antimicrobials shows that, a pair of antimicrobials acting synergistically can

* Corresponding author.
E-mail address: mahendraroy2002@yahoo.co.in (M.N. Roy).

https://doi.org/10.1016/j.molliq.2019.03.034
0167-7322/

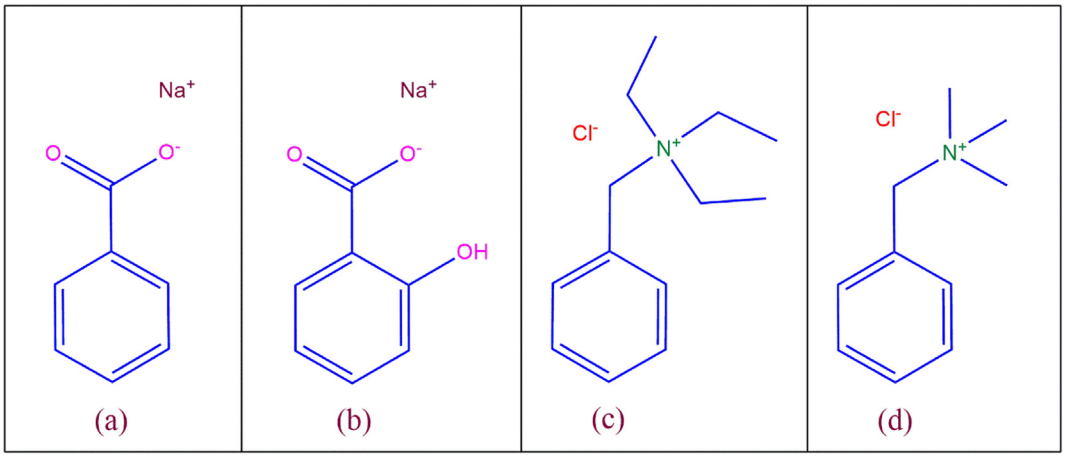

Scheme 1. The molecular structure of (a) Sodium benzoate, (b) Sodium salicylate, (c) Benzyltriethylammonium chloride, (d) Benzyltrimethylammonium chloride.

show satisfactory result and better microbial control could be achieved [12]. In this connection SBz and chitosan found synergistic against spoilage yeast in saline solution [13].

Sodium salicylate (Scyt) (Scheme 1) is a significant antibacterial agent, also enhances the activities of certain antibiotics [14–17]. The bacterial strains, Salmonella, Shigella including *Escherichia coli* that causes diarrhoea used to inhibit by bismuth subsalicylate efficiently [18]. Being an active anti-inflammatory compound Scyt have been used as anti-inflammatory, analgesic and anti-pyretic agent [19] still it has gastric bleeding like serious disadvantage [20]. Scyt acts synergistically with vancomycin and enhances anti-staphylococcal activity significantly. The presence of salicylate in 5 mM concentration, vancomycin prevents biofilm formation and kill bacteria effectively below its MIC [17]. In vitro CPS production can be reduced to 80% or more by Scyt, the major metabolite of aspirin. Scyt also increases synergistic activity of amikacin and imipenem [21].

Quaternary ammonium based ionic liquids also execute some sort of anti-microbial effects for instance positive charge on the Nitrogen atom of these ionic liquids attracts naturally the negatively charged species, such as bacterial proteins and consequently disorganization in the protein chain makes it denature. Ionic liquids, benztltriethylammonim chloride, benztltrimethylammonim chloride (Scheme 1) were used herewith in all four possible combinations to the illustrious food preservative SBz and Scyt. Anti-microbial activities of the set of four combinations were studied warily at concentrations below their MIC and found synergistic to each other.

In this article the synergism activity between the above mentioned food preservatives and ionic liquids against micro-organisms were studied such that, their combination can act properly below their MICs (Minimal Inhibitory Concentration) and as a consequence reduces the unnecessary consumption of hazardous food preservative. In this connection anti-bacterial and anti-fungal activities of both the food preservatives, SBz and Scyt were studied in the presence of trace amount of ionic liquids. Then, volumetric and viscometric analysis as well as refractive index and conductimetric measurement defines the cause of synergism between FPs and ILs.

2. Experimental section

2.1. Materials

All the chemicals, sodium benzoate (purity ≥99.5%), sodium salicylate (purity ≥99.5%), benzyltriethylammoniun chloride (purity 99.0%), benzyltrimethylammonium chloride (purity 97%) were purchased from Sigma Aldrich Germany and used as received taking sufficient precautions.

2.2. Apparatus

All the experimental solutions were prepared by transferring required amount of weighed materials to a volumetric flask and then filled with the solvents up to the mark. The uncertainty in molality of the prepared solutions evaluated as ±0.0001 mol kg^{-3}. Different sets of solutions with various concentration were prepared by proper dilution of the mother solution. The quantity of samples for the preparation of the mother solutions were weighed precociously by Mettler Toledo AG-285 with uncertainty ±0.0003 g.

The molality of the solution which has been calculated from the molar concentration data using the relation [22].

$$m = \frac{1}{[\rho/c - M/1000]} \tag{1}$$

where, m is the molality of the solutions, ρ and c refer to densities and concentration of the solutions respectively, M stands for relative molar mass of the materials used.

The antimicrobial activities of SBz and Scyt were tested in relation to the bacteria *Bacillus subtilis* and *Escherichia coli* by well diffusion assay [23]. Briefly, the bacterial cultures were grown overnight in Nutrient Broth and uniformly spread on the surface of Muller Hington agar plates using sterile cotton swabs. Wells of diameter 8 mm was made using sterile cork borers and SBz, Scyt, BTEACl and BTMACl were used singly and in combinations at concentrations of 3 mg/ml and 6 mg/ml. The plates were incubated overnight at 37 °C and observed for formation of inhibition zones. The "diameter of the inhibition" for positive results was recorded as diameter of zone of inhibition – diameter of the well (8 mm). The diameter of inhibition when no zone was observed was kept at zero.

The solvent as well as the solution densities were measured with vibrating-tube density meter (Anton Paar, DMA 4500M), maintained at 298.15 to 318.15 K. Calibration of the instrument was done with doubly distilled water and dry air. The uncertainty in density was estimated to be ±0.00001 g cm^{-3}.

Digital Refractometer Mettler Toledo was used to measure refractive index. Refractive indices of experimental solutions were measured after rectifying twice the refractometer by distilled water. During measurement calibration of the instrument was done after each few measurements. Temperature of the solutions under measurement was maintained in a Brookfield Digital TC-500 thermostat water bath.

Brookfield DV-III Ultra Programmable Rheometer with fitted spindle size-42was employed to measure viscosities of the solutions. The viscosities were obtained using following programmed equation.

$$\eta = (100/RPM) \times TK \times torque \times SMC \tag{2}$$

where SMC (0.327), RPM, TK (0.09373) stands for spindle multiplier constant, speed, viscometer torque constant respectively. Calibration of the instrument before starting experiment was done with provided standard viscosity samples, water and aqueous $CaCl_2$ solutions. Temperature of the solution was maintained with Brookfield Digital TC-500 thermostat bath.

The conductivity of the experimental solutions was measured in aSystronics-308 conductivity bridge using a dip-type immersion conductivity cell, CD-10, having a cell constant of approximately 0.1 ± 0.001 cm^{-1} of accuracy ±0.01%. Calibration of the conductivity cell was done according the method proposed by Lind et al. [24]. The cell constant was measured using freshly prepared 0.01 M aqueous KCl solution and it was maintained within the range 0.09–1.00 cm^{-1} during experiment. Temperature during experiment was monitored and controlled to the experimental temperature using Brookfield Digital TC-500 thermostat bath. HPLC-grade water with a specific conductance of 6.0 μS m^{-1} was used for conductivity measurement. The conductance data were reported at the accuracy of ±0.3%.

UV–visible spectra were recorded utilizing JASCO V-530 UV–Vis spectrophotometer, with a wavelength accuracy of ±0.5 nm. Cell temperature during the experiment was controlled from 298.15 K to 318.15 K with a digital thermostat.

Theoretical i.e. Ab-initio calculations were executed through Gaussian 09Wquantum chemical package [25].

3. Result and discussion

3.1. Antimicrobial effects of SBz and Scyt in combination with BTEACl and BTMACl reveals synergistic

The results clearly indicated the enhancement of antimicrobial effects of SBz and Scyt when used in combination with ionic liquids BTEACl and BTMACl.

In case of gram positive *B. subtilis* both BTEACl and BTMACl enhanced antimicrobial activity of SBz and Scyt with the effect being comparatively more profound in SBz in combination with BTEACl. The idea of lowering the concentrations to 3 mg was to check the enhancement when SBz and BTEACl individually showed minimal or no zone of inhibition. As expected 3 mg of SBz showed no zone of inhibition and 3 mg BTEACl showed minimal diameter of 2 mm which was enhanced to 8 mm when used in combination indicating enhanced antimicrobial activity. In case of gram negative *E. coli* no susceptibility was observed in case of SBz alone or in combination with ILs. However, *E. coli* showed enhanced susceptibility to Scyt when used in combination with BTEACl and BTMACl (Figs. 1, 2, 3).

The differences in the structure of their cell walls can be accounted for the differences in susceptibility of *Bacillus subtilis* and *E. coli*, with *E. coli* having an outer lipid layer which acts as a molecular filter for hydrophilic compounds [26]. This lipid layer might have reduced the ability of the hydrophilic components to penetrate into the cells and hence exert their potential inhibitory action. The zero antimicrobial effects of SBz and Scyt at concentrations of 3 mg and 6 mg may be because of their concentration being lower than the reported microbial inhibitory concentrations (MIC) of around 10 mg/mL [27]. BTEACl has also showed inhibitory action when used alone which might be due to the presence of quaternary ammonium with ethyl group whereas BTMACl has shown no inhibitory effect when used singly.

The outcome of this study is that SBz and Scyt can exert antimicrobial effects when used with ionic liquids such as BTEACl and BTMACl even at minimal concentrations which normally do not exert antimicrobial effects when used alone. However, the chances of ILs exerting cytotoxic effects on human cell lines will have to be ruled out before its proper application in industries.

3.2. Density and volumetric measurements

Here, we present information concerning the chemistry of food preservative–ionic liquid interactions in aqueous solutions that have been acquired from the apparent molar volume (ϕ_v), limiting apparent molar volume (ϕ_v^0) and (S_v^*) of food preservatives in aqueous solutions of ionic liquids meanwhile all these three parameters evidently be governed by the solvent environment surrounding the solute species and known to cover information belong to the structural penalties of solute–solvent interactions [28]. Apparent molar volume of a substance in solution can be defined as the sum of the geometric volume of the two solute molecules while undergo solvation through solute-solvent interaction with the co-solvent. Densities of the co-solvents of various mass fractions, made by two ionic liquids BTEACl and BTMACl separately with water, were measured at temperature range 298.15 to 318.15 K are listed in (Table S1). The values of (ϕ_v) for the (BTEACl + SBz + H_2O), (BTEACl + Scyt + H_2O) systems (Tables S8, S9, S10) and the same for (BTMACl + SBz + H_2O), (BTMACl + Scyt + H_2O) systems (Tables S11, S12, S13) were calculated by means of density (ρ) data (Tables S2–S4) and (Tables S5–S7) through the following equation [29–32].

$$\phi_v = \frac{M}{\rho} - \frac{1000(\rho - \rho_0)}{m\rho\rho_0} \tag{3}$$

where M is the molar mass of the solute; m is the molality of the solution; ρ and $\rho_0$represents the densities of the solution and solvent respectively. Apparent molar volume at infinite dilution, i.e. limiting molar apparent volume (ϕ_v^0) and experimental slopes (S_v^*) were determined using least squares fitting of linear plots of (ϕ_v) against the square root of molar concentrations ($m^{1/2}$) using the Masson equation [25,33].

$$\phi_v = \phi_v^0 + S_v^* \cdot \sqrt{m} \tag{4}$$

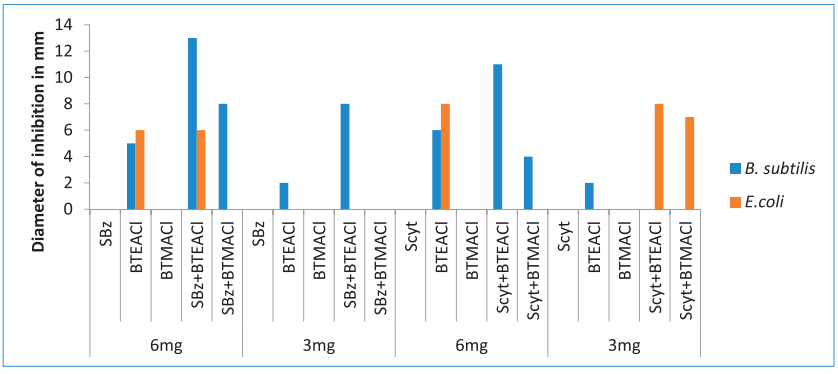

Fig. 1. Graphical presentation of Well diffusion assay (Diameter of inhibition in mm) of Scyt and SBz, singly and in combination with IL1 (BTEACl) and IL2 (BTMACl) applied to *B. subtilis* and *E. coli*.

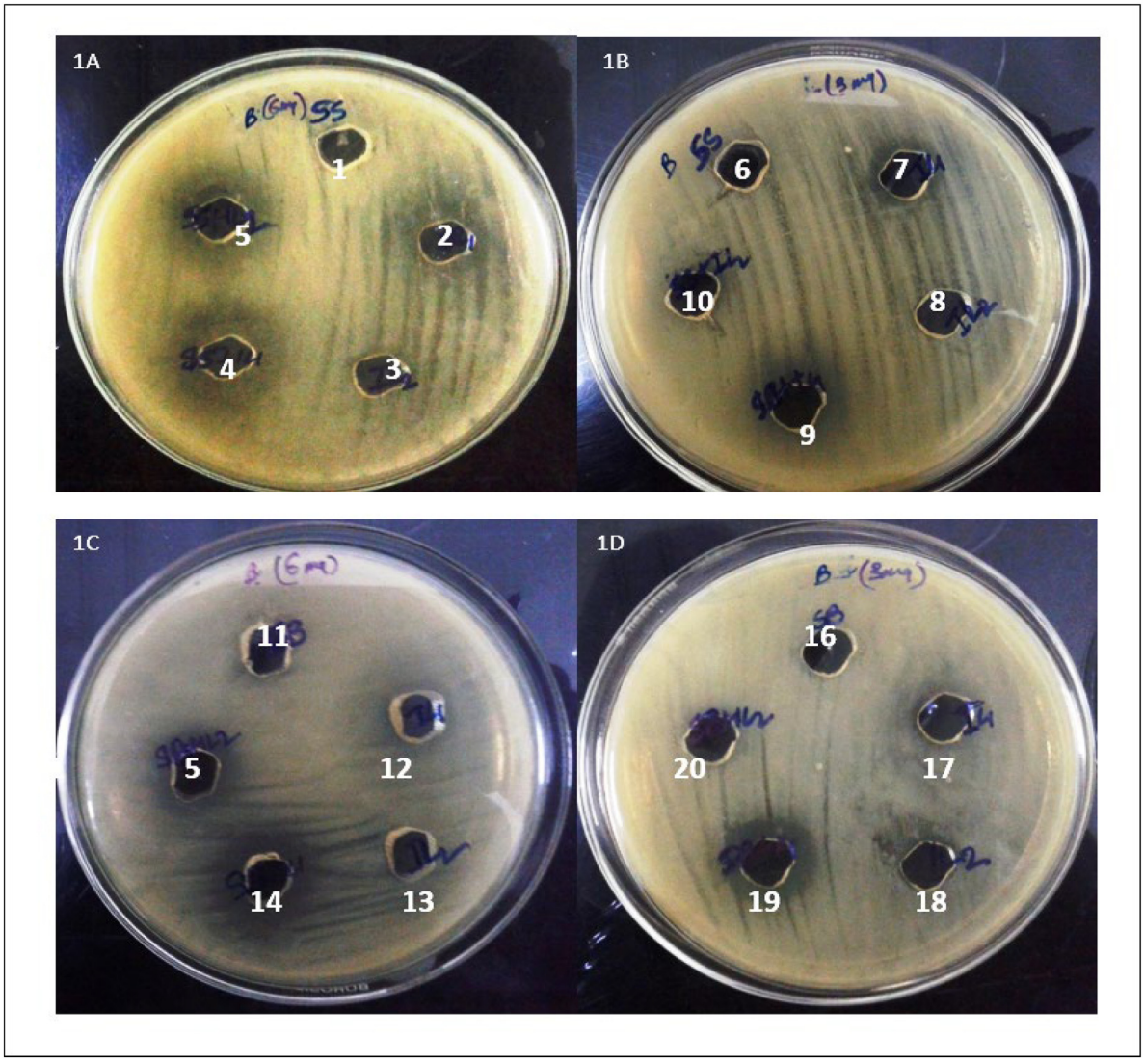

Fig. 2. Well diffusion assay of Scyt and SBz, singly and in combination with IL1 (BTEACl) and IL2 (BTMACl). Plate 1A–B shows susceptibility of *B. subtilis* towards Scyt in combination with IL1 (BTEACl) and IL2 (BTMACl) where, Well 1 contains 6 mg of SS (Scyt), Well 2 contains 6 mg IL1 (BTEACl), Well 3 contains 6 mg IL2 (BTMACl), Well 4 contains 6 mg SS (Scyt) and 6 mg IL1 (BTEACl), Well 5 contains 6 mg SS (Scyt) and 6 mg IL2 (BTMACl), Well 6 contains 3 mg of SS (Scyt), Well 7 contains 3 mg IL1 (BTEACl), Well 8 contains 3 mg IL2 (BTMACl), Well 9 contains 3 mg SS (Scyt) and 3 mg IL1 (BTEACl), Well 10 contains 3 mg SS (Scyt) and 3 mg IL2 (BTMACl). Plate 1C–D shows susceptibility of *B. subtilis* towards SBz in combination with IL1 (BTEACl) and IL2 (BTMACl)where, Well 11 contains 6 mg of SB (SBz), Well 12 contains 6 mg IL1 (BTEACl), Well 13 contains 6 mg IL2 (BTMACl), Well 14 contains 6 mg SB (SBz) and 6 mg IL1 (BTEACl), Well 15 contains 6 mg SB (SBz) and 6 mg IL2 (BTMACl), Well 16 contains 3 mg of SB (SBz), Well 17 contains 3 mg IL1 (BTEACl), Well 18 contains 3 mg IL2 (BTMACl), Well 19 contains 3 mg SB (SBz) and 3 mg IL1 (BTEACl), Well 20 contains 3 mg SB (SBz) and 3 mg IL2 (BTMACl).

The experimental plots, generated from Masson equation and corresponding values of (ϕ_v^0) and (S_v^*) of each plot are shown in (Fig. S1, S2) and (Tables 1, 2). The values of (ϕ_v^0) are found positive for all the systems and is greatest for (BTMACl + Scyt) system, suggesting the presence of stronger solute-solvent interactions in this case than that of the other systems and found to follow the order, (BTMACl + Scyt) > (BTMACl + SBz) > (BTEACl + Scyt) > (BTEACl + Scyt) as represented in (Scheme 2). The dipole–dipole interaction taking place in the solutions explains the truth behind the above mentioned order of solute-solvent interactions since greater the dipole-dipole interaction smaller will be the values of (ϕ_v) as well as (ϕ_v^0) [34]. The dipole moment of SBz, Scyt, BTEACl and BTMACl were calculated theoretically with the help of Gaussian 09W quantum chemical package, are listed in the (Table 7).

Increasing trend in the (ϕ_v^0) values with rise in temperature and mass fraction of BTEACl and BTMACl, suggests the rising trend of solute-solvent interaction as well. This is probably due to the release of a number of the solvent molecules from loose solvation layers during the solute-solvent interactions. The phenomenon drawn above also reflected in the molar conductivity data as discussed in this article. Values of the experimental slope, (S_v^*) assign the extent of ion-ion interaction in the solution, and the negative values indicate the presence of less ion-ion interaction in the medium. Quantitative comparison shows, greater the magnitude of (ϕ_v^0) than (S_v^*) recommends the ion-solvent interactions dominants over ion-ion interactions [35].

Temperature dependency of the limiting apparent molar volume(ϕ_v^0) were studied between the temperature range 298.15 to 318.15 K at the interval of 5 K of temperature and the results obtained were found to follow the following polynomial equation [36]

$$\phi_v^0 = a_o + a_1 T + a_2 T^2 \tag{5}$$

where, a_0, a_1 and a_2 are the empirical coefficients depending on the nature of solute, mass fraction (W) of co-solvent are listed in (Table 3). T represents temperature in Kelvin scale. The values of these coefficients of the above equation. First derivative of Eq. (5) gives the values of

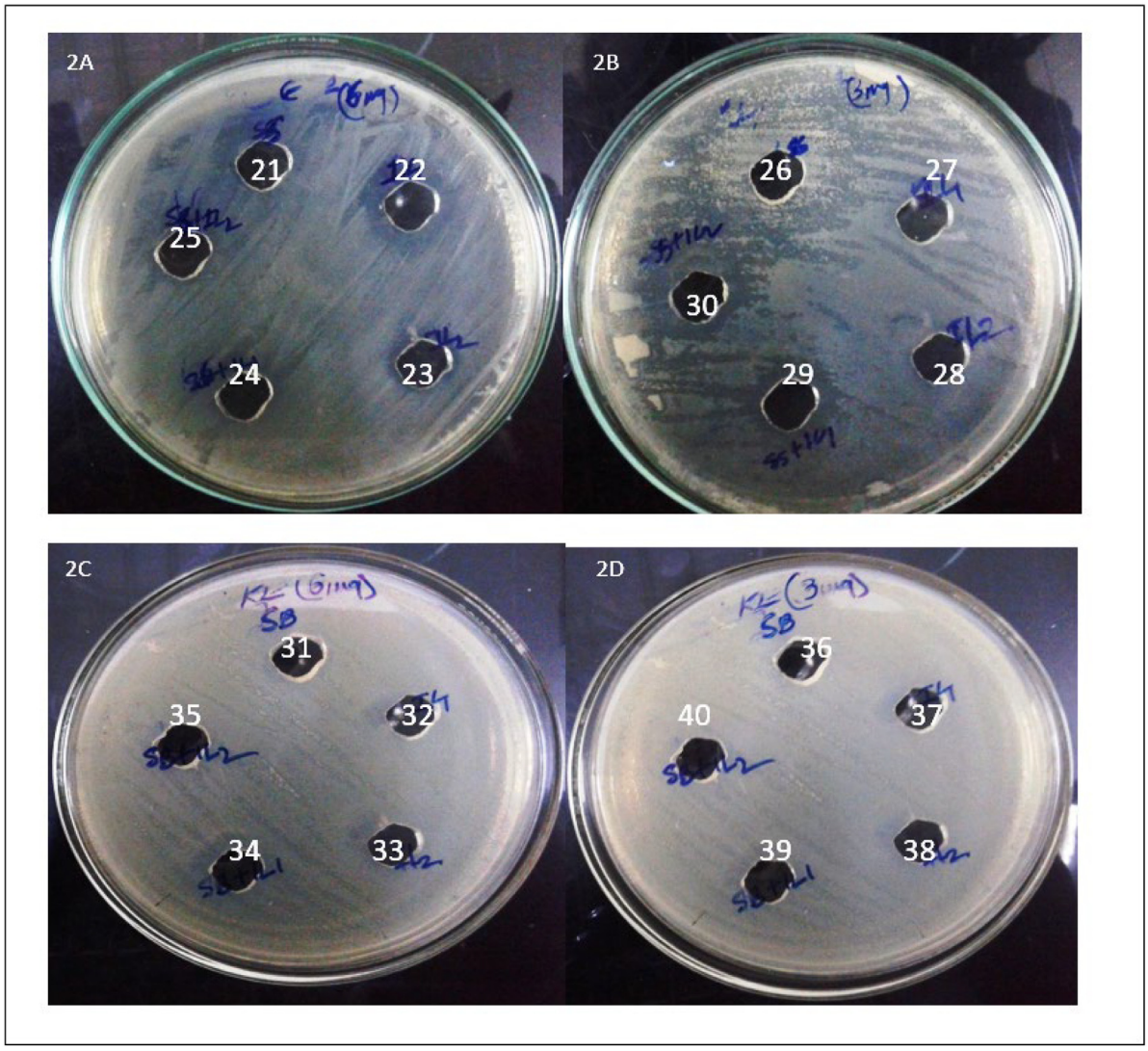

Fig. 3. Well diffusion assay of Scyt and SBz, singly and in combination with IL1 (BTEACl) and IL2 (BTMACl). Plate 2A–B shows susceptibility of *E. coli* towards Scyt in combination with IL1 (BTEACl) and IL2 (BTMACl)where, Well 21 contains 6 mg of SS (Scyt), Well 22 contains 6 mg IL1 (BTEACl), Well 23 contains 6 mg IL2 (BTMACl), Well 24 contains 6 mg SS (Scyt) and 6 mg IL1 (BTEACl), Well 25 contains 6 mg SS (Scyt) and 6 mg IL2 (BTMACl), Well 26 contains 3 mg of SS (Scyt), Well 27 contains 3 mg IL1 (BTEACl), Well 28 contains 3 mg IL2 (BTMACl), Well 29 contains 3 mg SS (Scyt) and 3 mg IL1 (BTEACl), Well 30 contains 3 mg SS (Scyt) and 3 mg IL2 (BTMACl). Plate 2C–D shows susceptibility of *E. coli* towards SBz in combination with IL1 (BTEACl) and IL2 (BTMACl) where, Well 31 contains 6 mg of SB (SBz), Well 32 contains 6 mg IL1 (BTEACl), Well 33 contains 6 mg IL2 (BTMACl), Well 34 contains 6 mg SB (SBz) and 6 mg IL1 (BTEACl), Well 35 contains 6 mg SB (SBz) and 6 mg IL2 (BTMACl), Well 36 contains 3 mg of SB (SBz), Well 37 contains 3 mg IL1 (BTEACl), Well 38 contains 3 mg IL2 (BTMACl), Well 39 contains 3 mg SB (SBz) and 3 mg IL1 (BTEACl), Well 40 contains 3 mg SB (SBz) and 3 mg IL2 (BTMACl).

limiting apparent molar expansibilities (ϕ_E^0) which have been calculated for various temperature and listed in (Table 4).

$$\phi_E^0 = \left(\delta\phi_v^0/\delta T\right)_P = a_1 + 2a_2T \tag{6}$$

Limiting apparent molar expansibilities (ϕ_E^0) for all the systems are found positive signifying the absence of caging or packing effect in the solutions of all the four different systems.

The solute – solvent interaction studied so far is now at a state that, it may be structure breaker or synergistic structure maker interaction. In this connection Hepler developed a way to examine the nature of the solute – solvent interaction taking place in the solution phase [37]. According to Hepler, values of $(\delta\phi_E^0/\delta T)_P$ in the expression given below, determines whether, it is structure breaker or structure maker interaction [38].

$$\left(\delta\phi_E^0/\delta T\right)_P = \left(\delta^2\phi_v^0/\delta T^2\right)_P = 2a_2 \tag{7}$$

Generally, positive or small negative values of $(\delta\phi_E^0/\delta T)_P$ strongly suggests structure making rather than structure breaking interaction. Here, positive and small negative values of $(\delta\phi_E^0/\delta T)_P$ listed in (Table 4) confirms the mode of solute – solvent interaction is structure making.

3.3. Refractive index

Optical data of refractive index of the two studied heterogeneous systems has provided interesting information allied to molecular interactions, structure of solutions in these assay. The refractive index of mixing can be interconnected by the application of a composition-dependent polynomial equation and molar refraction, R_M in solution thus can be estimated from Lorentz-Lorenz relation [39,40].

$$R_M = \frac{(n_D^2-1)}{(n_D^2+2)}\left(\frac{M}{\rho}\right) \tag{8}$$

where, R_M, n_D, M and ρ represents molar refraction, refractive index, molar mass and density of solution respectively.

Table 1
Apparent molar volume (Φ_V^0), Molar Refraction (R_M^0) and viscosity A and viscosity B co-efficient of (BTEACl + SBz + H_2O), (BTEACl + SCyt + H_2O) systems in solution of BTEACl of mass fractions $W_1 = 0.001$, $W_2 = 0.003$, $W_3 = 0.005$, at 298.15 K, 303.15 K, 308.15 K, 313.15 K and 318.15 K.

Temperature T(K[b])	$\Phi_v^0 \times 10^6$ /m^3mol^{-1}	$S_v^* \times 10^6$ /$m^3mol^{-3/2}$ $kg^{1/2}$	R_M^0 /m^3mol^{-1}	A /$dm^{3/2}$ $mol^{-1/2}$	B /dm^3 mol^{-1}
$W_1 = 0.001$[a]	(BTEACl + SBz + H_2O) System				
298.15	99.02	−56.68	29.42	0.034	0.508
303.15	103.60	−62.40	29.46	0.022	0.523
308.15	108.80	−73.10	29.49	0.014	0.544
313.15	112.32	−77.21	29.52	0.0024	0.551
318.15	116.95	−89.10	29.56	0.0019	0.570
$W_1 = 0.003$[a]	(BTEACl + SBz + H_2O) System				
298.15	111.50	−79.40	29.45	0.027	0.515
303.15	116.20	−91.88	29.47	0.017	0.531
308.15	122.10	−100.88	29.49	0.010	0.551
313.15	126.51	−108.52	29.53	0.009	0.565
318.15	128.00	−107.77	29.55	0.004	0.587
$W_1 = 0.005$[a]	(BTEACl + SBz + H_2O) System				
298.15	124.20	−105.81	29.48	0.020	0.520
303.15	128.70	−115.14	29.51	0.011	0.537
308.15	133.40	−120.07	29.54	0.006	0.559
313.15	137.22	−126.81	29.56	0.0005	0.581
318.15	142.75	−133.20	29.60	0.0014	0.595
$W_1 = 0.001$[a]	(BTEACl + SCyt+H_2O) System				
298.15	114.30	−62.17	32.72	0.042	0.513
303.15	118.10	−68.17	32.76	0.030	0.533
308.15	123.50	−78.97	32.81	0.021	0.546
313.15	127.01	−82.35	32.86	0.016	0.570
318.15	131.87	−92.17	32.90	0.006	0.588
$W_1 = 0.003$[a]	(BTEACl + SCyt+H_2O) System				
298.15	121.90	−81.64	32.76	0.037	0.520
303.15	125.00	−86.36	32.80	0.027	0.538
308.15	131.90	−98.03	32.83	0.015	0.552
313.15	136.80	−105.63	32.87	0.028	0.583
318.15	139.19	−107.08	32.91	0.014	0.599
$W_1 = 0.005$[a]	(BTEACl + SCyt+H_2O) System				
298.15	129.60	−97.46	32.79	0.029	0.526
303.15	135.50	−110.58	32.82	0.018	0.545
308.15	139.40	−109.83	32.84	0.009	0.558
313.15	144.18	−119.02	32.86	0.017	0.595
318.15	147.20	−130.68	32.89	0.005	0.595

[a] Standard uncertainties in mass fraction u(W) = ±0.0001 mol Kg^{-1}.
[b] Standard uncertainties in temperature u(T) = ±0.01 K.

Table 2
Apparent molar volume (Φ_V^0), Molar Refraction (R_M^0) and viscosity A and viscosity B co-efficient of (BTMACl + SBz + H_2O), (BTMACl + SCyt + H_2O) systems in solution of BTMACl of mass fractions $W_1 = 0.001$, $W_2 = 0.003$, $W_3 = 0.005$, at 298.15 K, 303.15 K, 308.15 K, 313.15 K and 318.15 K.

Temperature T(K[b])	$\Phi_v^0 \times 10^6$ /m^3mol^{-1}	$S_v^* \times 10^6$ /$m^3mol^{-3/2}$ $kg^{1/2}$	R_M^0 /m^3mol^{-1}	A /$dm^{3/2}$ $mol^{-1/2}$	B /dm^3 mol^{-1}
$W_1 = 0.001$[a]	(BTMACl + SBz + H_2O) System				
298.15	105.45	−99.91	29.47	0.035	0.513
303.15	109.89	−110.76	29.51	0.032	0.526
308.15	114.06	−118.33	29.54	0.017	0.549
313.15	116.16	−120.51	29.59	0.006	0.550
318.15	121.60	−130.61	29.63	0.003	0.560
$W_1 = 0.003$[a]	(BTMACl + SBz + H_2O) System				
298.15	119.81	−146.67	29.51	0.041	0.519
303.15	123.25	−157.20	29.56	0.036	0.531
308.15	126.03	−157.09	29.60	0.010	0.551
313.15	130.21	−160.23	29.67	0.008	0.556
318.15	134.43	−169.08	29.70	0.001	0.568
$W_1 = 0.005$[a]	(BTMACl + SBz + H_2O) System				
298.15	130.37	−166.42	29.55	0.037	0.523
303.15	134.28	−168.25	29.57	0.030	0.535
308.15	138.21	−176.01	29.62	0.026	0.555
313.15	144.46	−185.85	29.70	0.019	0.561
318.15	145.29	−182.24	29.75	0.013	0.574
$W_1 = 0.001$[a]	(BTMACl + SCyt + H_2O) System				
298.15	118.97	−82.80	32.75	0.045	0.518
303.15	123.36	−96.41	32.79	0.042	0.539
308.15	128.20	−108.95	32.85	0.037	0.550
313.15	134.03	−122.95	32.90	0.029	0.563
318.15	135.95	−130.35	32.93	0.014	0.570
$W_1 = 0.003$[a]	(BTMACl + SCyt + H_2O) System				
298.15	124.06	−95.93	32.77	0.041	0.521
303.15	128.90	−106.88	32.82	0.040	0.533
308.15	135.11	−121.50	32.87	0.035	0.554
313.15	140.30	−136.26	32.93	0.025	0.567
318.15	144.74	−142.63	32.97	0.022	0.578
$W_1 = 0.005$[a]	(BTMACl + SCyt + H_2O) System				
298.15	133.83	−121.38	32.84	0.038	0.525
303.15	138.44	−131.90	32.88	0.032	0.536
308.15	143.53	−141.79	32.93	0.029	0.557
313.15	146.48	−150.48	32.93	0.026	0.571
318.15	150.08	−154.30	33.02	0.020	0.581

[a] Standard uncertainties in mass fraction u(W) = ±0.0001 mol Kg^{-1}.
[b] Standard uncertainties in temperature u(T) = ±0.01 K.

Generally, refractive index of a system is the ability to refract light and hence it can simultaneously measure the compactness of that system. The refractive indices (n_D) of (BTEACl + SBz + H_2O), (BTEACl + Scyt + H_2O) systems are reported in (Tables S2–S4) and for(BTMACl + SBz + H_2O), (BTMACl + Scyt + H_2O) systems in (Tables S5–S7). The molar refraction (R_M) of the studied solutions were calculated and listed in the (Tables S8–S10) for (BTEACl + SBz + H_2O), (BTEACl + Scyt + H_2O) systems and (Tables S11–S13) for (BTMACl + SBz + H_2O), (BTMACl + Scyt + H_2O) systems. Analysis of these data enables us to draw the following sequence of compactness of the various (food preservative – ionic liquid) systems in solution phase.

(BTMACl + Scyt) > (BTMACl + SBz) > (BTEACl + Scyt) > (BTEACl + Scyt)

The limiting molar refraction, (R_M^0) listed in Table S can be calculated using the following equation-

$$R_M = R_M^0 + R_S\sqrt{m} \tag{9}$$

where, 'm' is the molality of solution and R_M^0 is the limiting molar refraction that signifies solute – solvent interaction. So, this measurement operates as an expensive tool for studying the molecular interaction in solution. Gradual increase in the values of R_M and R_M^0 (Tables 1, 2 and Figs. 4, S3) with rise in mass fraction of co-solvent also signifies that, solute – solvent interaction predominant over ion-ion interactions as obtained from density measurement.

3.4. Viscosity measurement

In aqueous electrolytic solutions the extent of ionic hydration [41] and structural interactions [42–44] within the ionic hydration co-spheres [45] can be explored easily by studying viscosity coefficient with varying concentration and temperature of the aqueous solution. Experimental values of viscosities for all the food preservative – ionic liquid systems, taken at various concentration and temperature are listed in (Tables S2–S4) and (Tables S5–S7). Viscosity data so obtained were analysed with the help of Jones-Dole equation [46].

$$\eta_r = \frac{\eta}{\eta_0} = 1 + A\sqrt{c} + Bc \tag{10}$$

where, η and η_0 are viscosities of solution and solvent respectively, c is the concentration of solution in molality.

Rearrangement of the above Eq. (8) gives following-

$$\frac{\eta_r - 1}{\sqrt{c}} = A + B\sqrt{c} \tag{11}$$

here, viscosity A coefficient is a constant, also known as Falken hagen coefficient [47], stands for long-range coulombic forces, so represents the solute-solute/ion-ion interaction in solution, while B coefficient is an adjustable parameter, which is the measure of the effective hydrodynamic volume, reflects the solute-solvent interaction. Magnitude of

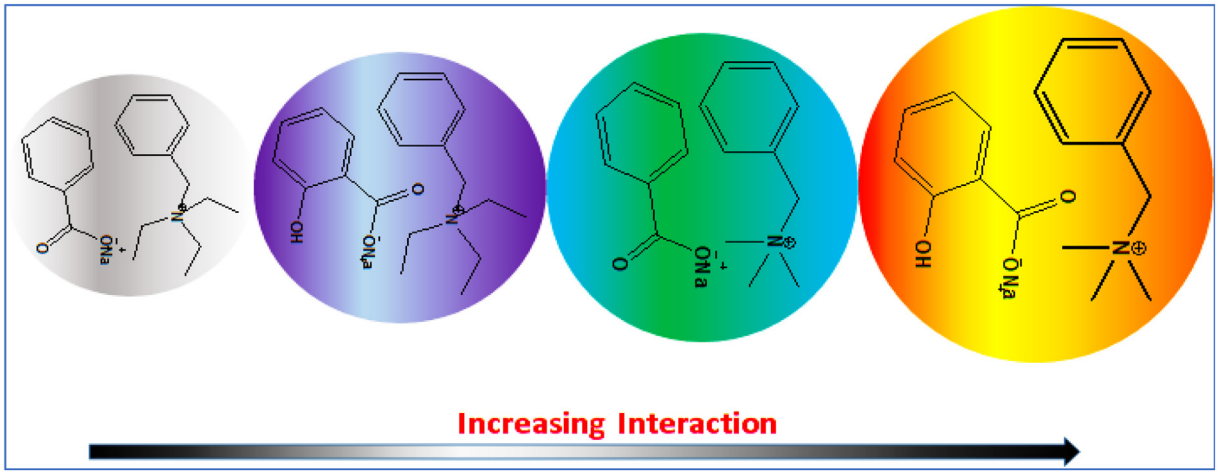

Scheme 2. Schematic representation of molecular interactions taking place between the FPs and ILs interaction in solution.

viscosity B coefficient depends on the shape, size and partial molar entropies of the ions. According to the Jones-Dole equation from the plots of $(\eta_r - 1)/\sqrt{c}$ vs. $\sqrt{c}$ (Figs. S4, S5) viscosity A and B coefficients were obtained by linear least-square analysis, are reported in (Tables 1, 2). Obtained viscosity A and B coefficients are actually the intercept and experimental slopes of the plots (Figs. S4, S5) respectively. An observation and deep investigation on the change in viscosity B coefficient of the various food preservative-ionic liquid systems at a given temperature and mass fraction of co-solvent, enable us to conclude the following sequences of solute-solvent interaction [43,48,49]-(BTMACl + Scyt) > (BTMACl + SBz) > (BTEACl + Scyt) > (BTEACl + Scyt) (Scheme 2). Having near about the same shape and size of both the ionic liquids, size and structural properties of BTEACl and BTMACl can't differentiate the change in viscosity B coefficient, rather it seems to be controlled indirectly by the ion-ion interaction i.e. (SBz-SBz) and (Scyt-Scyt) interaction taking place in SBz and Scyt solution. Lower the ion-ion interaction can enhance

Table 3
Values of empirical coefficients (a_0, a_1, and a_2) of Eq. (5) for aqueous (BTEACl + SBz), (BTEACl + SCyt), (BTMACl + SBz), (BTMACl + SCyt) systems in different mass fraction of aqueous BTEACl/BTMACl solution at 298.15 to 318.15 K.

Mass fraction (W[a])	$a_0 \times 10^6$ /m^3 mol^{-1}	$a_1 \times 10^6$ /m^3 mol^{-1} K^{-1}	$a_2 \times 10^6$ /m^3 mol^{-1} K^{-2}	$a_0 \times 10^6$ /m^3 mol^{-1}	$a_1 \times 10^6$ /m^3 mol^{-1} K^{-1}	$a_2 \times 10^6$ /m^3 mol^{-1} K^{-2}
BTEACl + SBz				BTEACl + SCyt		
0.001	−595.04	3.6738	−0.0045	−86.16	0.476	0.0007
0.003	−2290.90	14.7950	−0.0226	−1082.30	6.949	−0.0098
0.005	172.07	−1.1654	0.0034	−1454.50	9.471	−0.0139
BTMACl + SBz				BTMACl + SCyt		
0.001	−143.26	0.8947	−0.0002	−1218.00	7.848	−0.0113
0.003	706.28	−4.4881	0.0085	−684.10	4.260	−0.0052
0.005	−1149.40	7.5621	−0.0110	−1235.40	8.136	−0.0119

[a] Standard uncertainties in mass fraction u(W) = ±0.0001 mol Kg^{-1}.

Table 4
Values of limiting apparent molar expansibilities (Φ_E^0) of aqueous (BTEACl + SBz), (BTEACl + SCyt), (BTMACl + SBz), (BTMACl + SCyt) systems in different mass fraction of aqueous BTEACl/BTMACl solution at 298.15 to 318.15 K.

Mass fraction (W[a])	$\Phi_E^0 \times 10^6$/m^3 mol^{-1} K^{-1}					$(\frac{\partial \Phi_E^0}{\partial T})_P \times 10^6$ /m^3 mol^{-1} K^{-2}
	298.15	303.15	308.15	313.15	318.15	
(BTEACl + SBz) System						
0.001	0.9905	0.9455	0.9005	0.8555	0.8105	−0.0090
0.003	1.3186	1.0926	0.8666	0.6406	0.4146	−0.0452
0.005	0.8620	0.8960	0.9300	0.9640	0.9980	0.0068
(BTEACl + SCyt) System						
0.001	0.8934	0.9004	0.9074	0.9144	0.9214	0.0014
0.003	1.1053	1.0073	0.9093	0.8113	0.7133	−0.0196
0.005	1.1820	1.0430	0.9040	0.7650	0.6260	−0.0278
(BTMACl + SBz) System						
0.001	0.7754	0.7734	0.7714	0.7694	0.7674	−0.0004
0.003	0.5805	0.6655	0.7505	0.8355	0.9205	0.0170
0.005	1.0028	0.8928	0.7828	0.6728	0.5628	−0.0220
(BTMACl + SCyt) System						
0.001	1.1098	0.9968	0.8838	0.7708	0.6578	−0.0226
0.003	1.1592	1.1072	1.0552	1.0032	0.9512	−0.0104
0.005	1.0400	0.9210	0.8020	0.6830	0.5640	−0.0238

[a] Standard uncertainties in mass fraction u(W) = ±0.0001 mol Kg^{-1}.

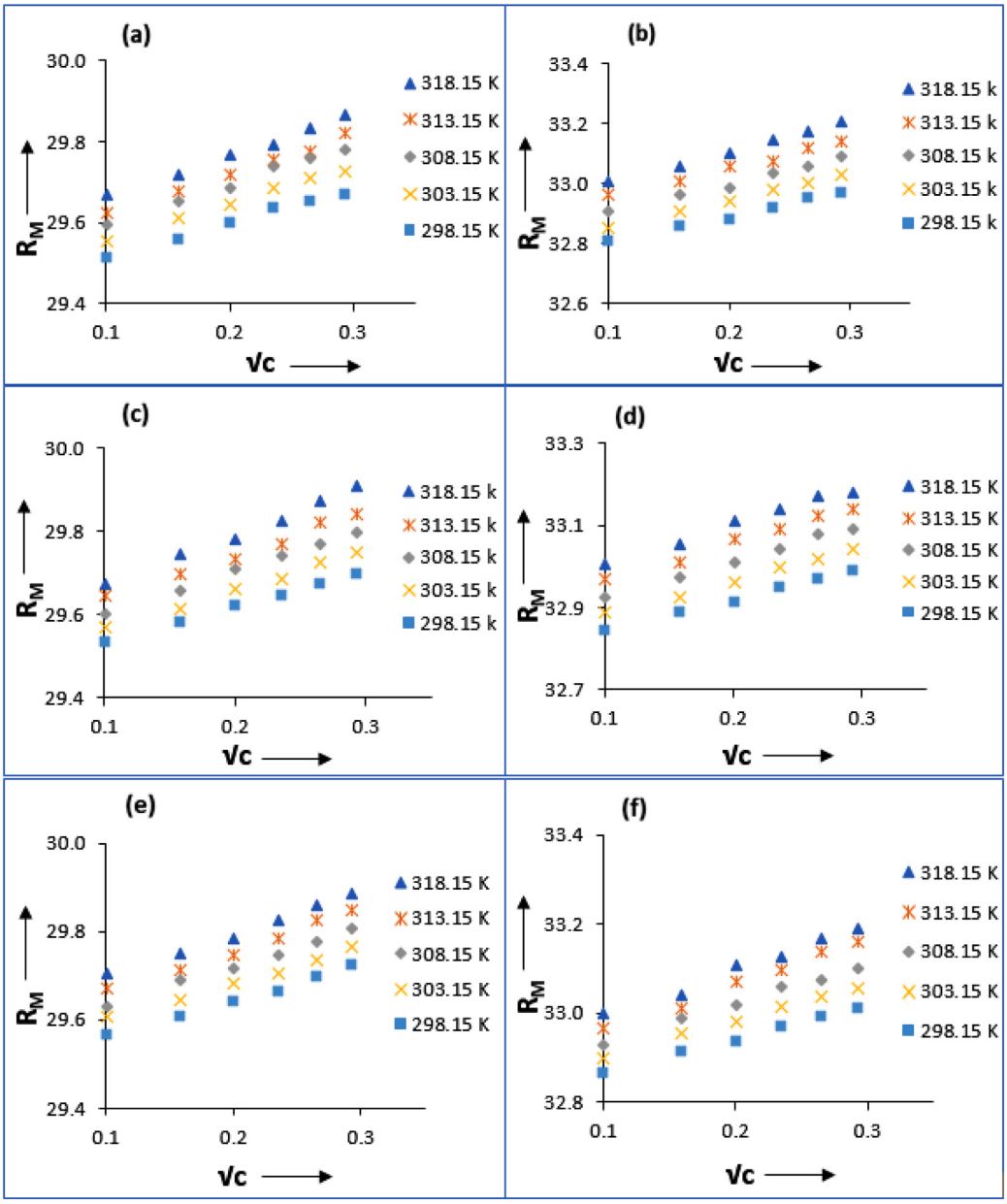

Fig. 4. (a, b, c, d, e, f) Plot of (R_M) Vs √c for (BTEACl + SBz + H_2O), (BTEACl + SCyt + H_2O) systems in aqueous BTEACl solutions of mass fractions (a, b) $W_1 = 0.001$, (c, d) $W_2 = 0.003$, (e, f) $W_3 = 0.005$respectively at 298.15 K, 303.15 K, 308.15 K, 313.15 K and 318.15 K.

dissolution of a solute in solvent through solvation of ions and thereby developing solute-solvent interaction. Now, an inspection on the (Tables 1, 2) shows lower viscosity A coefficient for (Scyt-ionic liquid) than that of (SBz-ionic liquid) systems. This can be accounted by the fact that, benzoate ions originating from SBz in solution can undergo dimerization, whereas dimerization of salicylate ions gets disturbed by the intramolecular H-bonding in Scyt. The innumerable interactions governed in solution which are also responsible for developing solute-solvent interaction can be explained on the basis of the interaction of $R_4N^{\oplus}$ from ionic liquid with the COO^- and OH group originating from food preservative as follows- (i) Lower effective charge accumulation on nitrogen atom of $R_4N^{\oplus}$ in BTEACl than that of BTMACl, caused by greater +I (positive inductive) effect of ($-CH_2$-CH_3) rather than ($-CH_3$) group operating in case of BTEACl. (ii) COO^- and OH group of Scyt interacts with $R_4N^{\oplus}$ in Scyt-ionic liquid systems, while the COO^- interacts alone with $R_4N^{\oplus}$ in case of SBz-ionic liquid systems. On the other hand, at a given temperature, if we deal with a particular food preservative-ionic liquid system viscosity B coefficient found to increase with increasing mass fraction of co-solvent made of ionic liquids in water. The above observation has a ready explanation that, replacement of water molecules by more co-solvent molecules (BTEACl or BTMACl) from the solvation sphere of food preservatives (SBz or Scyt) that, brings solute and co-solvent closer thereby increasing viscosity B coefficients and accounts for the higher solute-solvent interaction. The overall viscometric studies show that, viscosity B coefficients are positive and greater than viscosity A coefficient, suggesting solute–solvent interaction predominant over the solute-solute interaction.

Extensive study of the viscosity B coefficient such that, its first derivative over temperature is an upgradation of viscosity B coefficient in predicting the nature of solute – solvent interaction as structure maker or structure breaker. The value of dB/dT (Table 5) is a measure of activation energy required for the viscous flow in solution. This is the reason, why the measure of dB/dT is indicative towards the structure making or structure breaking ability than sign or magnitude of the B-coefficient [50–53]. The small positive or negative value of dB/dT signifies structure-making (kosmotropic) whereas the larger

Table 5
Values of dB/dT for aqueous (BTEACl + SBz), (BTEACl + SCyt), (BTMACl + SBz), (BTMACl + SCyt) systems in different mass fraction of aqueous BTEACl/BTMACl solution at 298.15 to 318.15 K.

Mass fraction (W)	$(\frac{dB}{dT})$/dm^3 mol^{-1}/K^{-1}			
	BTEACl + SBz	BTEACl + Scyt	BTMACl + SBz	BTMACl + Scyt
0.001	0.0030	0.0037	0.0024	0.0026
0.003	0.0036	0.0041	0.0025	0.0030
0.005	0.0039	0.0038	0.0026	0.0029

positive value identifies it as structure-breaking (chaotropic). The variation of dB/dT with the mass fraction of co-solvents has shown in (Fig. 5).

3.5. Conductimetric study

The conductance study of the interaction (solute – solvent) between Scyt and SBz with the aqueous solution of ILs, BTMACl and BTEACl has been performed at five different temperatures. Advantage of this study is that this measurement provides information about the interaction and transport phenomena of the (Scyt + ILs + H_2O) and (SBz + ILs + H_2O) ternary systems [54].

The molar conductivities [55] (Λ) of aqueous BTEACl and BTMACl has been monitored with increasing the concentration of Scyt and SBz respectively at five different temperatures and have been listed in (Tables S14, S17). The Figs. S6 and S7, shows the resulting plots of (BTMACl + SBz + H_2O), (BTMACl + Scyt + H_2O), (BTEACl + SBz + H_2O) and (BTEACl + Scyt + H_2O) respectively. For every system it has been observed that Λ values increase with increase in temperature and gradual addition of either Scyt or SBz to ILs solution causes a continuous decrease in molar conductance. The mobility of the ionic species in solution playing the leading role, in spite of growing number of ionic species with added aqueous SBz or Scyt solution in step, the molar conductivity decreases [56]. It may be due to the development of solute-solvent interaction governed by the dipole-dipole as well as the pπ – pπ and hydrophobic – hydrophobic interaction in solution mixtures between the solute and solvent molecules. The formation of molecular assembly thus forces the ionic species to lose their independent movement making the ionic species less mobile to show conductivity in solution. The intra-molecular H-bonding of Scyt as discussed in viscosity context also inhibits dimerization between Scyt molecules and makes it available for exerting solute – solvent interaction with ILs more than that of SBz in solution. Conductimetric study thus supports the volumetric, refractometric and viscometric study and echoes the same observation as well.

3.6. UV–vis spectroscopic analysis: The association constants

The stability of the molecular association developed in solution mixtures by the manifestation of solute-solvent interaction were explored by measuring the association constants (K_a). The UV–vis spectroscopic data for the various mixtures of solutions were recorded and employed to determine the association constant (K_a). To determine association constant (K_a), the changes in absorbances (ΔA) of SBz and Scyt at $\lambda_{max} = 220$ nm and $\lambda_{max} = 292$ nm were measured with increasing concentration of BTEACl/BTMACl at 298.15 K (Tables S18–S21). According to the Benesi-Hildebrand method [57], the double reciprocal plots obtained from (Eq. (10)) were found linear that, usually says about the solute: solvent ratio in solution [57,58].

$$\frac{1}{\Delta A} = \frac{1}{\Delta\varepsilon[FPs]K_a}\frac{1}{[ILs]} + \frac{1}{\Delta\varepsilon[FPs]} \tag{12}$$

where, ΔA refers to the difference in absorbances of SBz or Scyt without ILs to the absorbances of the same with the ILs. [FPs] represents the concentration of the SBz and Scyt. For the calculation of the association constants (K_a), listed in the (Table 6), we divide slope by the intercept obtainable from the Benesi-Hildebrand double reciprocal plots [59,60] (Figs. 6, 7).

The well-known association constant – free energy relationship enables us to calculate the free energy change for the molecular association taking place between the respective molecules by the following equation-

$$\Delta G = -RT\ \ln K_a \tag{13}$$

where, ΔG is the change in free energy, K_a stands for association constant, R and T refers to the universal gas constant and temperature in Kelvin respectively. The change in free energies for various (FPs –ILs) systems are listed in (Table 6) and depicts the sequence of interaction as obtained from the previous studies in article.

3.7. Gaussian 09W quantum chemical calculation: Theoretical basis of the interaction

This field is of immense theoretical interest. Here is no use of sequence alignments and no straight use of known structures. Basic idea is to erect empirical function that replicates real physical forces and potentials of chemical contacts. In this manuscript, numerical calculations have been performed using UB3LYP functional. Diffused basis functions have repeatedly been found to be effective in describing weak interaction amid atoms. Therefore, we use 6-31G(d) basis set for an accurate

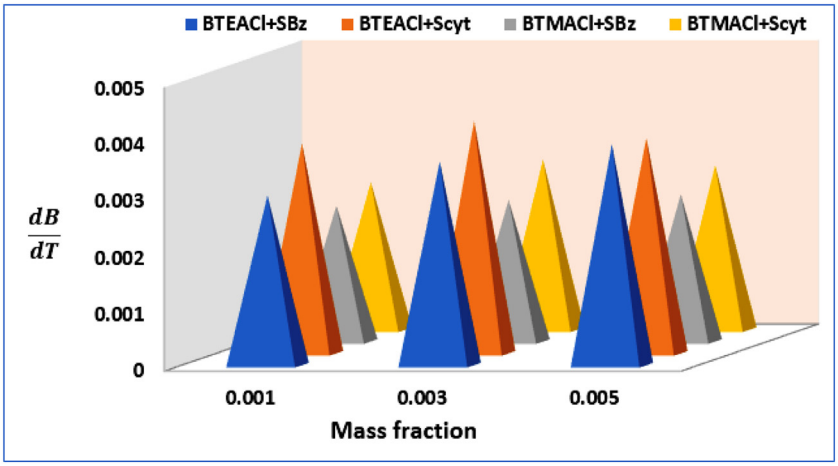

Fig. 5. Variation of $\frac{dB}{dT}$ with the mass fraction of BTEACl and BTMACl separately at their four different combinations, BTEACl + SBz, BTEACl + Scyt, BTMACl + SBz, BTMACl + Scyt.

Table 6
Association constant and Gibb's free energy of (BTEACl + SBz), (BTEACl + SCyt), (BTMACl + SBz) and (BTMACl + SCyt) systems at 298.15 K.

System	(BTEACl + SBz)	(BTEACl + SCyt)	(BTMACl + SBz)	(BTMACl + SCyt)
K_a/M^{-1} ($\times 10^{-3}$)	2.70	3.31	3.05	3.68
ΔG/KJ mol^{-1}	−19.6	−20.1	−19.9	−20.4

description of weak interactions which may prevail in the transition structures.

These calculations are implemented through Gaussian 09W quantum chemical package. The quantum chemical calculations estimate that the O···N···O···, C═O···H—O, H···O—H, weak H-bond interactions in SBz/Scyt clusters in the solvent sphere of aqueous ILs [61] (Scheme 2). The formation of the weak hydrogen bond is an interaction, cohesive interaction [61,62]. Under definite conditions an atom of hydrogen is attracted by rather strong forces to two atoms instead of only one, so that it may be considered to be acting as a bond between them [27]. The aforementioned statements were well thought-out in our present work. We have depicted the existence of SBz···ILs and SCyt···ILs complexes as clusters through quantum chemical calculations and we hereby compared and calculated values with the experimental values in order to verify sequence of interaction as obtained theoretically.

Several approximate properties of varied systems of aqueous SBz - ILs and SCyt - ILs clusters are summarized in (Table 7). The availability of the optimisation energy (E) of pure as well as the molecular assembly makes it possible to calculate the extent of stabilisation (E) while, formation of molecular assembly assorted by solute – solvent interaction between FPs and ILs in solution. Stabilisation energy of molecular assembly i.e. the value of *E*, the optimization energy, which approaches to a minimal value with growing possibility of solute-solvent interactions. From the (Table 7) it is clear that stabilisation through solute – solvent interaction found prominent in case of (BTMACl+Scyt+H_2O) system over the other systems discussed herewith. Specifically, the optimum geometry (Fig. 8) would involve central FPs surrounded by aqueous ILs molecules via weaker non-covalent interactions which can be explained on the basis of solution thermodynamics [63] in addition to solute-solvent interactions.

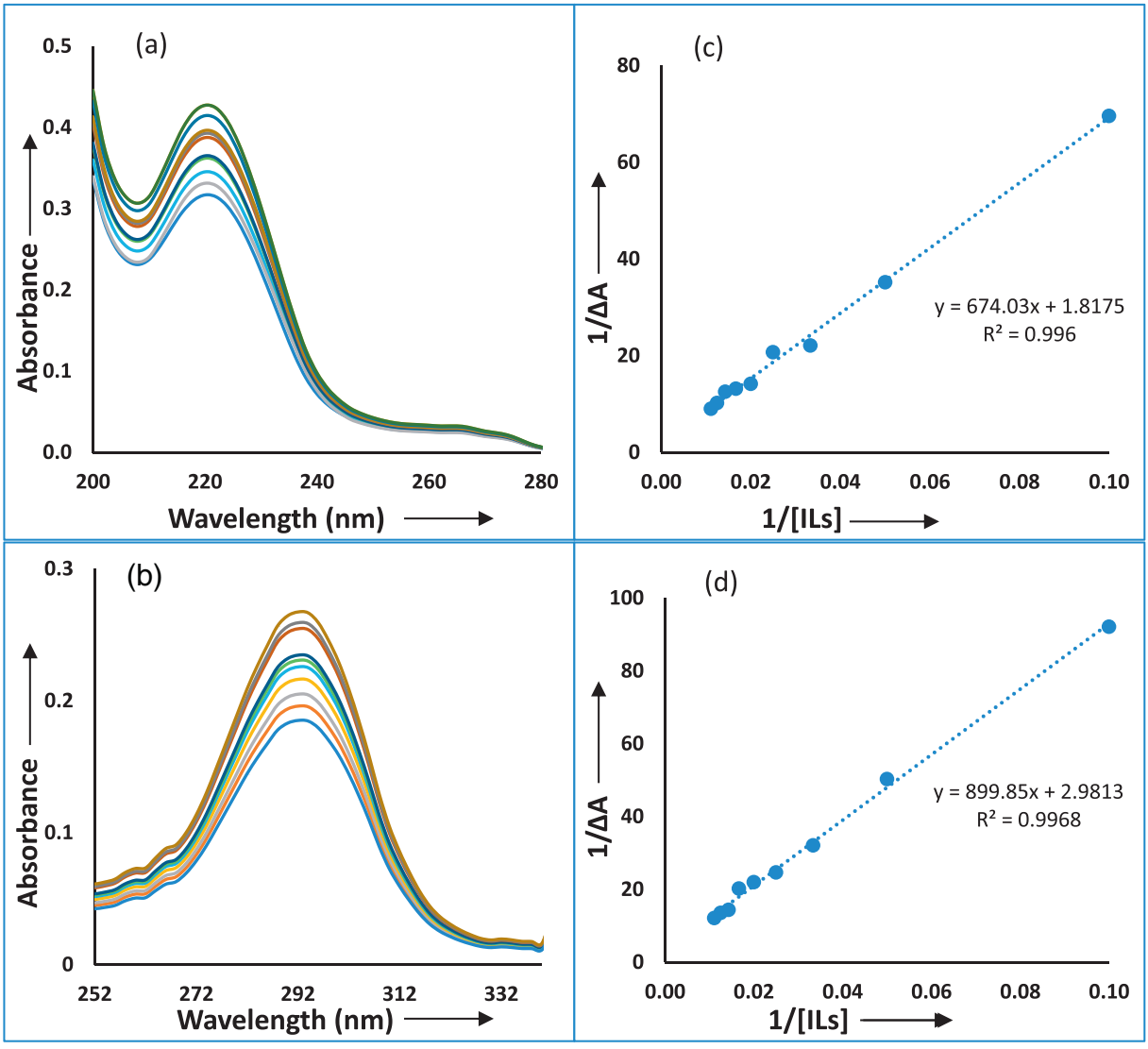

Fig. 6. (a, b, c, d) Spectra for the generation of Benesi-Hildebrand double reciprocal plot of (a) BTEACl + SBz, (b) BTEACl + Scyt systems and corresponding Benesi-Hildebrand double reciprocal plot of (c) BTEACl + SBz, (d) BTEACl + Scyt systems.

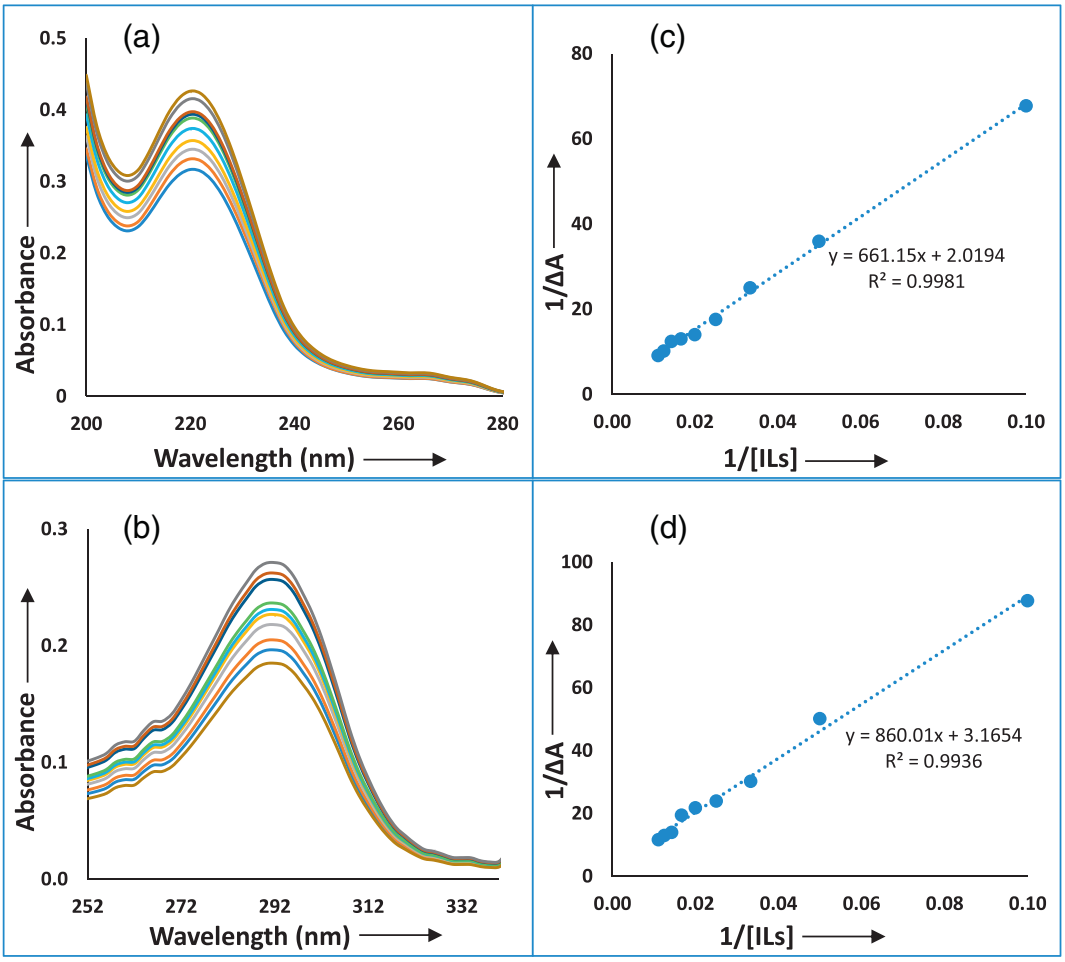

Fig. 7. (a, b, c, d) Spectra for the generation of Benesi-Hildebrand double reciprocal plot of (a) BTMACl + SBz, (b) BTMACl + Scyt systems and corresponding Benesi-Hildebrand double reciprocal plot of (c) BTMACl + SBz, (d) BTMACl + Scyt systems.

4. Conclusion

The motive to reduce unnecessarily-excessive use of food preservative in the preservation of food is reached, since antimicrobial activity of SBz and Scyt studied herewith, in all possible combination with the BTEACl and BTMACl reveal synergistic to kill micro-organisms and found to act properly below their reported MICs. The physico-chemical methodologies, density, viscosity, refractive index and conductance study describes the mode of interaction between the FPs and ILs in solution. Calculation of apparent molar volume, limiting apparent molar volume, molar refraction, limiting molar refraction and viscosity B coefficient makes possible to identify the interaction as predominant solute – solvent interaction. The values of $(\delta\phi_E^0/\delta T)_P$ and (dB/dT) have been calculated to provide the information that, the solute – solvent interaction is structure making. Association constants, optimisation energy and free energy changes for the molecular assembly grown in solution assorted by structure making solute – solvent interaction dictate their stability in solution and consequently, the order of synergism between them. Thus, solution chemistry for all the possible combinations explores the chemistry behind the synergism. This makes one easy to choose a mixture of compounds such that their combination would arise synergistic. Nevertheless, the synergistic combination of food preservatives reduces the level of hazardous food preservative which is used to stop spoilage of foods produced worldwide and makes the world health, safe. So, the study of microbial activity along with solution chemistry would be a great interest in the field of food chemistry for their preservation.

Table 7
Optimisation energies of pure BTEACl, BTMACl, SBz, SCyt and (BTEACl + SBz), (BTEACl + SCyt), (BTMACl + SBz), (BTMACl + SCyt) systems using UB3LYP methodology and 6-31G (d) basis set.

System	Calculation Method	Basis Set	Optimisation energy (a.u.)	Dipole moment (Debye)
SBz	UB3LYP	6-31G(d)	−582.58203318	5.6642
SCyt	UB3LYP	6-31G(d)	−657.78951762	4.4047
BTEACl	UB3LYP	6-31G(d)	−1023.56406394	11.6512
BTMACl	UB3LYP	6-31G(d)	−905.62574200	13.5905
(BTEACl + SBz)	UB3LYP	6-31G(d)	−865.63204549	12.5596
(BTEACl + SCyt)	UB3LYP	6-31G(d)	−940.83809561	11.2236
(BTMACl + SBz)	UB3LYP	6-31G(d)	−983.56112523	12.6819
(BTMACl + SCyt)	UB3LYP	6-31G(d)	−1058.76749759	11.1263

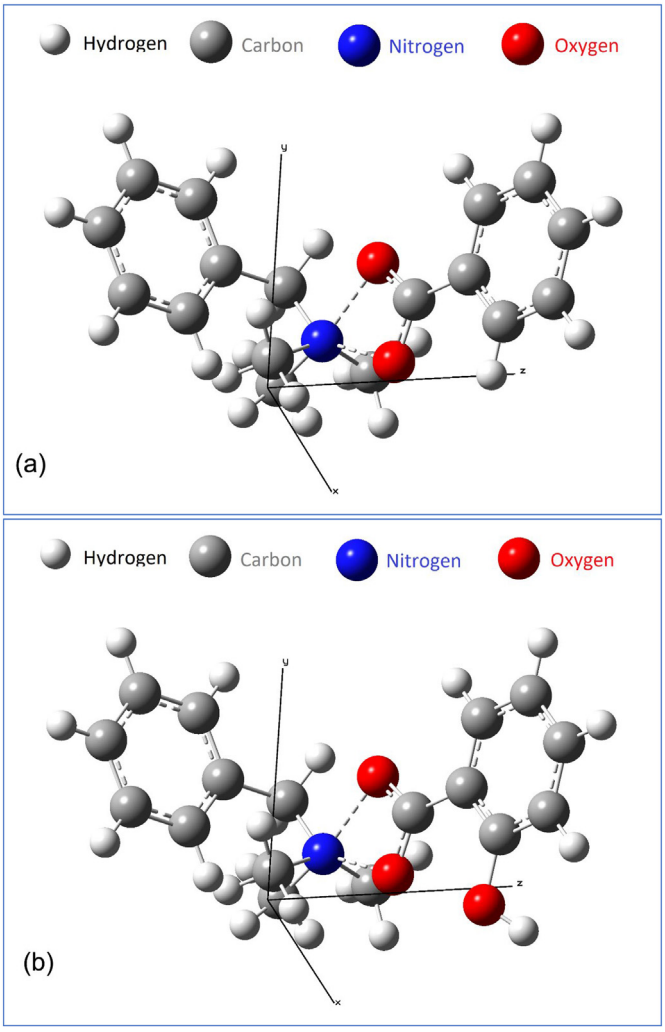

Fig. 8. (a, b): Optimised geometry of (a) BTMACl + SBz and (b) BTMACl + Scyt systems.

Conflicts of interest

There is no conflicts of interest.

Acknowledgements

Prof. M. N. Roy would like to acknowledge UGC, New Delhi, Government of India, for being awarded One Time Grant under Basic Scientific Research via the grant-in-Aid no. F.4-10/2010 (BSR). BR is thankful to the "State Fellowship" bearing reference No. 1743/R-2017 dated 18.04.2017 and UGC-SAP DRS-III, New Delhi (no. 540/6/DRS/2007, SAP-1) for providing instrumental facilities according the research.

Appendix A. Supplementary data

Supplementary data to this article can be found online at https://doi.org/10.1016/j.molliq.2019.03.034.

References

[1] J. Voigt, J. M. Jones: Food Safety. 453 Seiten, zahlr. Abb. und Tab. Eagan Press, St. Paul, Minnesota, 1992. Preis: 50,– $ (USA 42,– $), Food Nahrung, 36 (1992) 425–425.
[2] 4: Final Report on the Safety Assessment of Sorbic Acid and Potassium Sorbate, Journal of the American College of Toxicology, 7 (1988) 837–880.
[3] M.L. Puttemans, C. Branders, L. Dryon, D.L. Massart, Extraction of organic acids by ion-pair formation with tri-n-octylamine. Part 6. Determination of sorbic acid, benzoic acid, and saccharin in yogurt, J Assoc Off Anal Chem, 68 (1985) 80–82.
[4] P.J.H. M, G.M. T, Rapid high-performance liquid chromatography method for the analysis of sodium benzoate and potassium sorbate in foods, Journal of chromatography. A: including electrophoresis and other separation methods, 883 (2000) 299–304.
[5] K. Kubota, T. Ishizaki, Dose-dependent pharmacokinetics of benzoic acid following oral administration of sodium benzoate to humans, Eur. J. Clin. Pharmacol. 41 (1991) 363–368.
[6] V. Praphanphoj, S.A. Boyadjiev, L.J. Waber, S.W. Brusilow, M.T. Geraghty, Three cases of intravenous sodium benzoate and sodium phenylacetate toxicity occurring in the treatment of acute hyperammonaemia, J. Inherit. Metab. Dis. 23 (2000) 129–136.
[7] P. Wittke, F. Walther, Cyclic deformation behavior of friction drilled internal threads in AlSi10Mg and AZ31 profiles, Procedia Struct. Integr. 2 (2016) 3264–3271.
[8] J. Moses, A. Siddiqui, P.B. Silverman, Sodium benzoate differentially blocks circling induced by D- and L-dopa in the hemi-parkinsonian rat, Neurosci. Lett. 218 (1996) 145–148.
[9] N. Zengin, D. Yuzbasioglu, F. Unal, S. Yilmaz, H. Aksoy, The evaluation of the genotoxicity of two food preservatives: sodium benzoate and potassium benzoate, Food Chem. Toxicol. 49 (2011) 763–769.
[10] B.S. Lennerz, S.B. Vafai, N.F. Delaney, C.B. Clish, A.A. Deik, K.A. Pierce, D.S. Ludwig, V.K. Mootha, Effects of sodium benzoate, a widely used food preservative, on glucose homeostasis and metabolic profiles in humans, Mol. Genet. Metab. 114 (2015) 73–79.
[11] D. Liu, Y. Zhu, Z. Li, M. Xiao, C. Jiang, M. Chen, Y. Chen, Microfibrillar polysaccharide-derived biochars as sodium benzoate adsorbents, ACS Omega 2 (2017) 2959–2966.
[12] A. López-Malo, J. Barreto-Valdivieso, E. Palou, F.S. Martín, Aspergillus flavus growth response to cinnamon extract and sodium benzoate mixtures, Food Control 18 (2007) 1358–1362.
[13] S.K. Sagoo, R. Board, S. Roller, Chitosan potentiates the antimicrobial action of sodium benzoate on spoilage yeasts, Lett. Appl. Microbiol. 34 (2002) 168–172.
[14] B.F. Farber, A.G. Wolff, The use of nonsteroidal antiinflammatory drugs to prevent adherence of Staphylococcus epidermidis to medical polymers, J. Infect. Dis. 166 (1992) 861–865.
[15] E. Muller, J. Al-Attar, A.G. Wolff, B.F. Farber, Mechanism of salicylate-mediated inhibition of biofilm in Staphylococcus epidermidis, J. Infect. Dis. 177 (1998) 501–503.
[16] P. Domenico, D.C. Straus, D.E. Woods, B.A. Cunha, Salicylate potentiates amikacin therapy in rodent models of Klebsiella Pneumoniae infection, J. Infect. Dis. 168 (1993) 766–769.
[17] R.E. Polonio, L.A. Mermel, G.E. Paquette, J.F. Sperry, Eradication of biofilm-forming *Staphylococcus epidermidis* (RP62A) by a Combination of Sodium Salicylate and Vancomycin, Antimicrob. Agents Chemother., 45 (2001) 3262.
[18] M.D. Manhart, In vitro antimicrobial activity of bismuth subsalicylate and other bismuth salts, Rev. Infect. Dis. 12 (1990) S11–S15.
[19] S.J. Vane, Aspirin and other anti-inflammatory drugs, Thorax 55 (2000) S3–S9.
[20] E.H. Awtry, J. Loscalzo, Aspirin, Circulation 101 (2000) 1206–1218.
[21] P. Domenico, T. Hopkins, B.A. Cunha, The effect of sodium salicylate on antibiotic susceptibility and synergy in Klebsiella pneumoniae, J. Antimicrob. Chemother. 26 (1990) 343–351.
[22] S.E. Friberg, Interactions of Surfactants With Polymers and Proteins. E.D.Goddard and K.P. Ananthapadmanabhan (eds.), CRC Press, Boca Raton, FL, pp. 1-427, $169.95, J. Dispers. Sci. Technol. 15 (1994) (1993) 399.
[23] M. Balouiri, M. Sadiki, S.K. Ibnsouda, Methods for in vitro evaluating antimicrobial activity: a review, J. Pharm. Anal. 6 (2016) 71–79.
[24] J.E. Lind, J.J. Zwolenik, R.M. Fuoss, Calibration of conductance cells at 25° with aqueous solutions of potassium chloride1, J. Am. Chem. Soc. 81 (1959) 1557–1559.
[25] D.O. Masson, XXVIII, Solute molecular volumes in relation to solvation and ionization, The London, Edinburgh, Dublin Philos. Mag. J. Sci. 8 (1929) 218–235.
[26] R. Benz, K. Bauer, Permeation of hydrophilic molecules through the outer membrane of gram-negative bacteria. Review on bacterial porins, Eur. J. Biochem. 176 (1988) 1–19.
[27] S. Sarkhel, G.R. Desiraju, N-H…O, O-H…O, and C-H…O hydrogen bonds in protein-ligand complexes: strong and weak interactions in molecular recognition, Proteins 54 (2004) 247–259.
[28] M.N. Roy, R. Chanda, R.K. Das, D. Ekka, Densities and viscosities of citric acid in aqueous cetrimonium bromide solutions with reference to the manifestation of solvation, J. Chem. Eng. Data 56 (2011) 3285–3290.
[29] E. Ayranci, Apparent molar volume and viscosity of compounds with asymmetric carbon atoms, J. Chem. Eng. Data 42 (1997) 934–937.
[30] Z. Yan, J. Wang, J. Lu, Apparent molar volumes and viscosities of some α-amino acids in aqueous sodium butyrate solutions at 298.15 K, J. Chem. Eng. Data 46 (2001) 217–222.
[31] Y. Li, X. Wang, Y. Wang, Comparative studies on interactions of bovine serum albumin with cationic Gemini and single-chain surfactants, J. Phys. Chem. B 110 (2006) 8499–8505.
[32] M.T. Zafarani-Moattar, H. Shekaari, P. Jafari, Thermodynamic study of aqueous two-phase systems containing biocompatible cholinium aminoate ionic-liquids and polyethylene glycol di-methyl ether 250 and their performances for bovine serum albumin separation, J. Chem. Thermodyn. 130 (2019) 17–32.
[33] K. Kumar, S. Chauhan, Surface tension and UV–visible investigations of aggregation and adsorption behavior of NaC and NaDC in water–amino acid mixtures, Fluid Phase Equilib. 394 (2015) 165–174.
[34] G. Ravichandran, G. Lakshiminarayanan, D. Ragouramane, Apparent molar volume and ultrasonic studies on some bile salts in water–aprotic solvent mixtures, Fluid Phase Equilib. 356 (2013) 256–263.
[35] D. Ekka, M.N. Roy, Molecular interactions of alpha-amino acids insight into aqueous beta-cyclodextrin systems, Amino Acids 45 (2013) 755–777.

[36] M.N. Roy, V.K. Dakua, B. Sinha, Partial molar volumes, viscosity b-coefficients, and adiabatic compressibilities of sodium molybdate in aqueous 1,3-dioxolane mixtures from 303.15 to 323.15 K, International Journal of Thermophysics, 28 (2007) 1275–1284.
[37] Y. Zhang, P.S. Cremer, Interactions between macromolecules and ions: the Hofmeister series, Curr. Opin. Chem. Biol. 10 (2006) 658–663.
[38] A. Yasmin, S. Barman, B.K. Barman, M.N. Roy, Investigation of diverse interactions of amino acids (Asp and Glu) in aqueous dopamine hydrochloride with the manifestation of the catecholamine molecule recognition tool in solution phase, J. Mol. Liq. 271 (2018) 715–729.
[39] A.Z. Tasic, B.D. Djordjevic, D.K. Grozdanic, N. Radojkovic, Use of mixing rules in predicting refractive indexes and specific refractivities for some binary liquid mixtures, J. Chem. Eng. Data 37 (1992) 310–313.
[40] The Chemistry of Macrocyclic Ligand Complexes L. F. Lindoy Cambridge: Cambridge University Press 1989, pp viii +269 £45.00. SUS 69.50 ISBN 0 521 25261 X, J. Coord. Chem., 21 (1990) 87–87.
[41] H. Eisenberg, Chemical physics of ionic solutions. B. E. Conway and R. G. Barradas, Eds., Wiley, New York, 622 pp. $25.00, J. Polym. Sci. A-2: Polym. Phys. 6 (1968) (1966) 1943.
[42] P.K. Banipal, T.S. Banipal, J.C. Ahluwalia, B.S. Lark, Partial molar heat capacities and volumes of transfer of some saccharides from water to aqueous urea solutions atT = 298.15 K, J. Chem. Thermodyn. 32 (2000) 1409–1432.
[43] H.D.B. Jenkins, Y. Marcus, Viscosity B-coefficients of ions in solution, Chem. Rev. 95 (1995) 2695–2724.
[44] H.T. Briscoe, W.T. Rinehart, Studies of relative viscosity of non-aqueous solutions, J. Phys. Chem. 46 (1942) 387–394.
[45] G.W. Brady, J.T. Krause, Structure in ionic solutions. I, J. Chem. Phys. 27 (1957) 304–308.
[46] G. Jones, M. Dole, The viscosity of aqueous solutions of strong electrolytes with special reference to barium chloride, J. Am. Chem. Soc. 51 (1929) 2950–2964.
[47] A. Ali, S. Hyder, Y. Akther, Viscometric Studies of a –Amino Acid in Aqueous NaCl and MgCl2 at 303 K, 2005.
[48] Y. Marcus, ViscosityB-coefficients, structural entropies and heat capacities, and the effects of ions on the structure of water, J. Solut. Chem. 23 (1994) 831–848.
[49] H.L. Friedman, C.V. Krishnan, Thermodynamics of ionic hydration, in: F. Franks (Ed.), Aqueous Solutions of Simple Electrolytes, Springer US, Boston, MA 1973, pp. 1–118.
[50] W. Devine, B.M. Lowe, Viscosity B-Coefficients at 15 and 25 °C for Glycine, ?-Alanine, 4-Amino-N-Butyric Acid, and 6-Amino-N-Hexanoic Acid in Aqueous Solution, 1971.
[51] T.S. Sarma, J.C. Ahluwalia, Experimental studies on the structures of aqueous solutions of hydrophobic solutes, Chem. Soc. Rev. 2 (1973) 203–232.
[52] I. Pitkänen, J. Suuronen, J. Nurmi, Partial molar volume, ionization, viscosity and structure of Glycine betaine in Aqueous solutions, J. Solut. Chem. 39 (2010) 1609–1626.
[53] M.M. Bhattacharyya, M. Sengupta, Ion–solvent interaction of amino acids. The role of the "Zwitterionic" and the "ionic" forms in the modification of water structure over the temperature range 25–45 °C, Bull. Chem. Soc. Jpn. 61 (1988) 4107–4112.
[54] D. Ekka, M.N. Roy, Conductance, a contrivance to explore ion association and solvation behavior of an ionic liquid (tetrabutylphosphonium tetrafluoroborate) in acetonitrile, tetrahydrofuran, 1,3-dioxolane, and their binaries, J. Phys. Chem. B 116 (2012) 11687–11694.
[55] D. Ekka, T. Ray, K. Roy, M.N. Roy, Exploration of solvation consequence of ionic liquid [Bu4PCH3SO3] in various solvent systems by conductance and FTIR study, J. Chem. Eng. Data 61 (2016) 2187–2196.
[56] X.M. Shen, F. Zhang, G. Dryhurst, Oxidation of dopamine in the presence of cysteine: characterization of new toxic products, Chem. Res. Toxicol. 10 (1997) 147–155.
[57] H.A. Benesi, J.H. Hildebrand, A spectrophotometric investigation of the interaction of iodine with aromatic hydrocarbons, J. Am. Chem. Soc. 71 (1949) 2703–2707.
[58] B. Rajbanshi, S. Saha, K. Das, B.K. Barman, S. Sengupta, A. Bhattacharjee, M.N. Roy, Study to probe subsistence of host-guest inclusion complexes of α and β-cyclodextrins with biologically potent drugs for safety regulatory dischargement, Sci. Rep. 8 (2018) 13031.
[59] M.N. Roy, S. Saha, S. Barman, D. Ekka, Host–guest inclusion complexes of RNA nucleosides inside aqueous cyclodextrins explored by physicochemical and spectroscopic methods, RSC Adv. 6 (2016) 8881–8891.
[60] J.V. Caso, L. Russo, M. Palmieri, G. Malgieri, S. Galdiero, A. Falanga, C. Isernia, R. Iacovino, Investigating the inclusion properties of aromatic amino acids complexing beta-cyclodextrins in model peptides, Amino Acids 47 (2015) 2215–2227.
[61] K. Das, M.C. Roy, B. Rajbanshi, M.N. Roy, Assorted interactions of amino acids prevailing in aqueous vitamin C solutions probed by physicochemical and ab-initio contrivances, Chem. Phys. Lett. 687 (2017) 209–221.
[62] S.K. Panigrahi, G.R. Desiraju, Strong and weak hydrogen bonds in the protein-ligand interface, Proteins 67 (2007) 128–141.
[63] F. Samadi, J. Eckelt, B.A. Wolf, H. Schüle, H. Frey, Branched versus linear oligo (dimethylsiloxane): differences in their thermodynamic interaction with solvents, J. Polym. Sci. B Polym. Phys. 48 (2010) 1309–1318.

Journal of Molecular Liquids 298 (2020) 111952

Contents lists available at ScienceDirect

Journal of Molecular Liquids

journal homepage: www.elsevier.com/locate/molliq

Study to explore host guest inclusion complexes of vitamin B_1 with CD molecules for enhancing stability and innovative application in biological system

Biplab Rajbanshi [a], Ashutosh Dutta [a], Beauty Mahato [a], Debadrita Roy [a], Dilip Kumar Maiti [b], Subires Bhattacharyya [a], Mahendra Nath Roy [a,*,1]

[a] Department of Chemistry, University of North Bengal, Darjeeling, 734013, India
[b] Department of Chemistry, Calcutta University, Kolkata, 700054, India

ARTICLE INFO

Article history:
Received 19 June 2019
Received in revised form 1 September 2019
Accepted 16 October 2019
Available online 28 October 2019

Keywords:
Thiamine hydrochloride
Oligosaccharide
Inclusion complexes
Human serum albumin
Releasing behavior

ABSTRACT

In this article the host-guest inclusion of thiamine hydrochloride(guest) within the hydrophobic cavity of α and β-cyclodextrin molecules (hosts) have been studied scientifically in the solid and solution phases respectively. Various modern spectroscopic techniques had been used to establish the outcome of this work. The UV–Vis study supported the 1:1 stoichiometry of the inclusion complexes and also used to evaluate the association constants along with thermodynamic parameters with high accuracy for the determination of the feasibility of this inclusion process. From the mass spectrometric study, 1:1 stoichiometry of the inclusion complexes had been confirmed in their solid state. Differential scanning calorimetric and infrared studies also supported this fact.^{1}H NMR and 2D ROESY spectroscopic analysis had given the mechanism of inclusion process, and the SEM study exposed their surface structures. Finally, the sustained oozing of the guest molecule from the hydrophobic cavity of the respective cyclodextrin molecules separately had been studied in the presence of human serum albumin in their aqueous buffer solutions with the help of fluorescence spectroscopic technique. This study has a truly intense effect to the stabilization of the respective guest molecule from the external hazardous, such as photolytic degradation, oxidation-reduction, thermal cleavage etc., and also predicts the releasing behavior of thiamine hydrochloride in the presence of human serum albumin without any chemical modification.

1. Introduction

Oligosaccharides, specially cyclodextrins (CDs) regarding host-guest inclusion complexation have very significant importance in food industries [1–3] pharmaceuticals [4,5] and consumer goods [6] due to their unique conical-shaped [7]cyclic structures. Cyclodextrins and their derivatives are commercially available and differ because of the presence of different glucopyranose residues. Cyclodextrins have their distinctive biphasic layers possessing hydrophilic outer and hydrophobic inner surfaces. The inner region allows incorporating hydrophobic surface of different guest or segment(s) of guest molecules into the cavity of a suitable and stable geometrical sized CDs through various kinds of non-covalent interactions [8,9]. Herein, α and β-cyclodextrins bearing 6 and 7 glucopyranose units, respectively, have taken as host molecules. Due to high inclusion efficiency, fitting cavity dimensions, low price, and negligible toxicity [10,11]. The CDs have found widespread application in pharmaceuticals [12], food industries [13], cosmetics [14], tissue engineering [15], bio-medical devices [12,16].Inclusion complexation within the non-polar cavity of CDs (Fig. 1)is employed for protecting the hydrophobic part of different bioactive molecules [17], enzymes [18,19], drugs [20], volatile organic compounds, flavors [21], essential oils [22,23], taxols [24], flavonoids [25], vitamins [26], and etc. to extend their light, air and thermal stability, enhancement of water solubility, bioavailability and shielding side effects.

The B vitamins and their derivatives are a class of water-soluble vitamins and naturally found in food substances. These have significant role in cell metabolism [27]. They have major importance for food processing and biological activities such as transferring the alkyl group, fitting carbon dioxide, decarboxylation and transamination of amino acids, lipids and sugars [28–31]. Fruit juices are one of the main sources of vitamins and the quality of fruit juices in industry is maintained by different techniques including pasteurization, which led to the degradation of vitamins along with other valuable food nutrients. Day to day Consumer's realization about food nutritional value is throwing a challenge to the companies for healthier foods without any change in their

* Corresponding author.
E-mail addresses: dkmchem@caluniv.ac.in (D.K. Maiti), mahendraroy2002@yahoo.co.in (M.N. Roy).
[1] Prof. Mahendra Nath Roy, Department of Chemistry, University of North Bengal.

https://doi.org/10.1016/j.molliq.2019.111952
0167-7322/

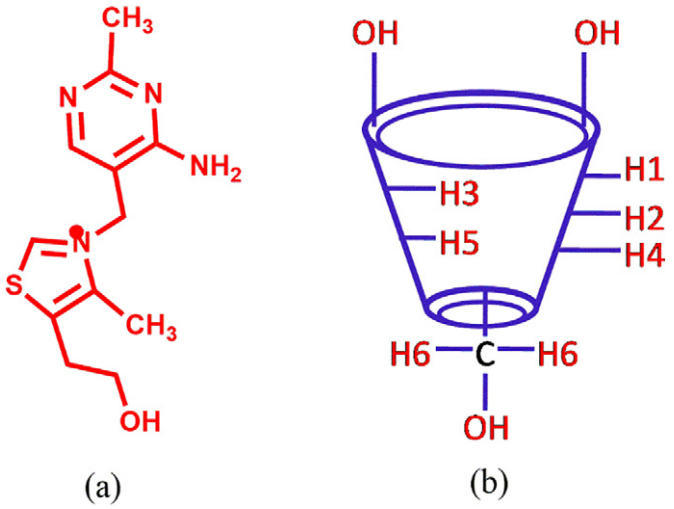

Fig. 1. Molecular structures of (a) thiamine hydrochloride, (b) cyclodextrin.

chemical properties [32,33]. Among all the B vitamins and their derivatives, one of the most common is thiamine (vitamin B_1) chloro hydrochloride (THC, Fig. 1), which is usually used as a component of single vitamin B complex and multivitamin preparations, food supplement, antioxidant, prooxidant, pharmaceutical industries and biological fluids. THC is used to treat in appetence and dermatophytosis. Moreover, it is also helpful to metabolize in human body. [32,34–37], Due to the lack of thiamine hydrochloride, neurotransmission in human body can be affected. Deficiency of THC leads to the occurrence of various malfunctions inside the human body such as beriberi, Wernicke-Korsakoff syndrome, confabulation and an irreversible dementia; even extreme deficiency may lead to heart failure and death [38–40]. Thus thiamine hydrochloride is extensively used in human body; moreover, it can be utilized as feed in agriculture and synthetic intermediates in industry [41]. But THC is very sensitive to light and high temperature processing and also has tend to get oxidize easily in the presence of oxygen which limits their applications to a great extent in different fields. Chemical degradation is very common with vitamin B_1 and the main route of the degradation is its reduction which is caused in the presence of food preservatives such as sodium meta-bisulfite, with very low concentrations (~1 mmol/L). Moreover, it can degrade by some of cell surface enzymes and plant thiamine antagonists [31,33,42].

Based on molecular recognition, inclusion of THC into CDs offers potential advantages in delivery without changing its chemical characteristics. In order to overcome all of these above mentioned foremost problems, we have attempted inclusion of THC within the hydrophobic cavity of α- and β-CD to improve stability and natural characteristics involving preservation for a long existence of time. Several studies have been done to find out the stability of THC within the cavity of CDs against the aforementioned adverse effect.

Human serum albumin (HSA) is one of the most abundant and popular protein in blood-plasma having 585 amino acid sequences. HSA consists of long chain polypeptides. It has tertiary structure consisting of three domains named I, II and III respectively. HSA has only one tryptophan residue (Trp-214) which is located in the subdomain IIA. HSA plays a very important role for the maintenance of life systems [43–46]. According to the two scientists Helms et al. and EI-Kemary et al., serum proteins can take up many conformations from the range of close compact to relaxed form. In recent years there is an ongoing interest and a large field to investigate of plasma proteins with smaller molecules such as drugs, vitamins, hormones and other different kinds of bioactive molecules. The metabolism, distribution, free concentration can change significantly due to binding of HSA [44,47–51]. In the other side, high intake of THC causes several effects such as developing cataracts, kidney disease and dysmenorrheal [52–54]. So, regular dischargement of THC at the targeted site for long term effectively is very important. In this work to get an idea about the regular releasing behavior of THC from the CDs cavity separately in the human body, HSA has taken which will help to formulate THC in pharmaceuticals and food industries.

In this novel work, the inclusion of THC has been aimed within the cavity of α and β-CD separately in both solution and solid states to explore their formation of inclusion complex (IC) for enhancing the stability of THC. Regular release without any chemical alteration of THC in the presence of HSA from the cavity of α and β-CD separately have been monitored with the help of fluorescence spectroscopy. Formation of inclusion complexes have been well characterized by various reliable techniques like 2D ROESY and ^{1}H NMR, IR, UV–Visible spectroscopy, Fluorescence spectroscopy, DSC, ESI-MS, SEM study has been done to get an idea about the surface nature of the corresponding two inclusion complexes. Association parameters, thermodynamic parameters, and stoichiometry have been evaluated to get a clear and quantitative idea about the formation of these ICs.

Hence, this present work mainly approaches towards the stability and regular release of THC inside the body and helps to execute the proposed utilization in the field of food chemistry and pharmaceutical science.

2. Experimental section

2.1. Materials

Thiamine hydrochloride having purity ≥98.0% was purchased from TOKYO CHEMICAL INDUSTRY CO., LTD while human serum albumin, α- and β-cyclodextrins of high purity grade ≥ 97.0% and ≥ 98.0% respectively were purchased from Sigma-Aldrich, Germany. All of these samples were kept in the refrigerator as received and used during the following experiments without further any alteration.

2.2. Apparatus

UV–Visible spectra were recorded with the help of Agilent 8453 UV–Visible Spectrophotometer with an uncertainty of wavelength accuracy of ±0.5 nm and an automated digital thermostat was used to control the temperature of the cell during performing the experiments.

^{1}H NMR and 2D ROESY spectra were recorded in D_2O solvent at 400 MHz in Bruker Avance instrument at 298.15 K. All the signals are shown in terms of δ values (in ppm) by using residual protonated solvent signal (HDO: δ 4.79 ppm) as internal standard and all the data are represented in the form of chemical shift (δ) values.

The DSC thermograms of the samples were recorded with the help of PerkinElmer DSC-6 differential scanning calorimeter at the heating rates of 10 °C min^{-1}. The thermogram was taken by heating 1 mg of samples in aluminum crimped pans under nitrogen gas flow within the temperature range 30–300 °C.

ESI-MS analyses were performed by Q-TOF high resolution are shown with positive mode electro-spray ionization taking the methanol solution of the solid ICs.

According to KBr disk method, FTIR spectra were recorded on a Perkin Elmer spectrometer within 4000-400 cm^{-1} scanning range at room temperature. All KBr disks were made in 1:100 ratios of sample to KBr and during the experimental studies humidity was at 45%.

SEM images had been recorded with the help of JEOL JSM IT 100 Scanning Electron Microscope (SEM) to determine surface morphology. Samples were prepared on a small piece of double adhesive carbon-coated tape attached to brass stubs and then a coating of ultra-thin

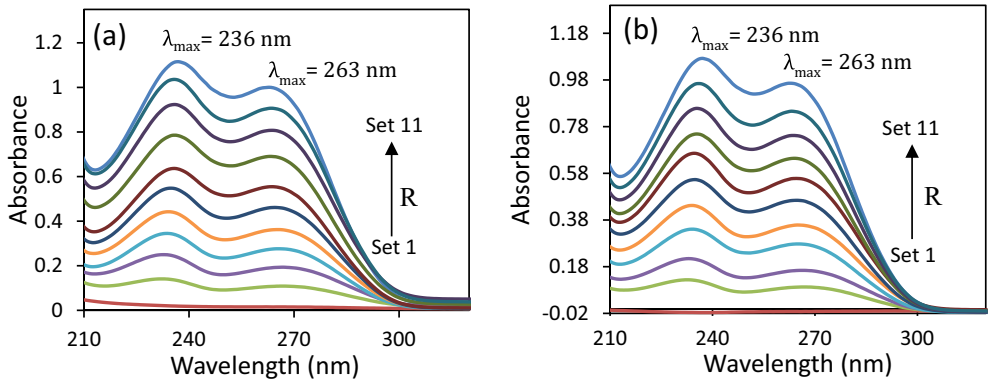

Fig. 2. (a,b): Spectra for the generation of Job plot of (a) THC+α-CD and (b) THC+β-CD systems at 236 and 263 nm.

layer of gold ions was put in a gold-ionization chamber. SEM images were recorded at various resolutions.

Fluorescence spectra were recorded with the help of Bench top spectrofluorimeter from photon technologies International (Quantamaster-40, USA) at room temperature. Data were recorded by taking solutions into Hellma quartz cuvette having optical path length 1.0 cm while excitation and emission slit widths fixed at 5.0 nm and 5.0 nm, respectively.

2.3. Procedure

Solubility of all the required compounds was specifically checked in triply distilled and de-ionized water. Mettler Toledo AG-285 having uncertainty±0.0003 g was used to prepare all the solutions of THC, HSA, α-and β-CD by mass at room temperature. All the stock solutions were prepared by mass dilution and freshly prepared solutions were used during each experiment in phosphate buffer aqueous solution of pH 7.4. Sufficient precautions had been taken during measuring weights, preparing solutions and performing all the respective experiments. Two solid ICs, THC+ α-CD and THC + β-CD had been prepared in 1:1 M ratio of THC and CD. 1.0 mM of α-and β-CD were each separately mixed with water and stirred for 4 h. After that the aqueous solution of 1.0 mM of THC was added dropwise to the respective solutions of CD and left for stirring near about 36 h at 50–55 °C to prepare the corresponding two ICs. Just after filtration of the hot solutions, it is allowed to cool

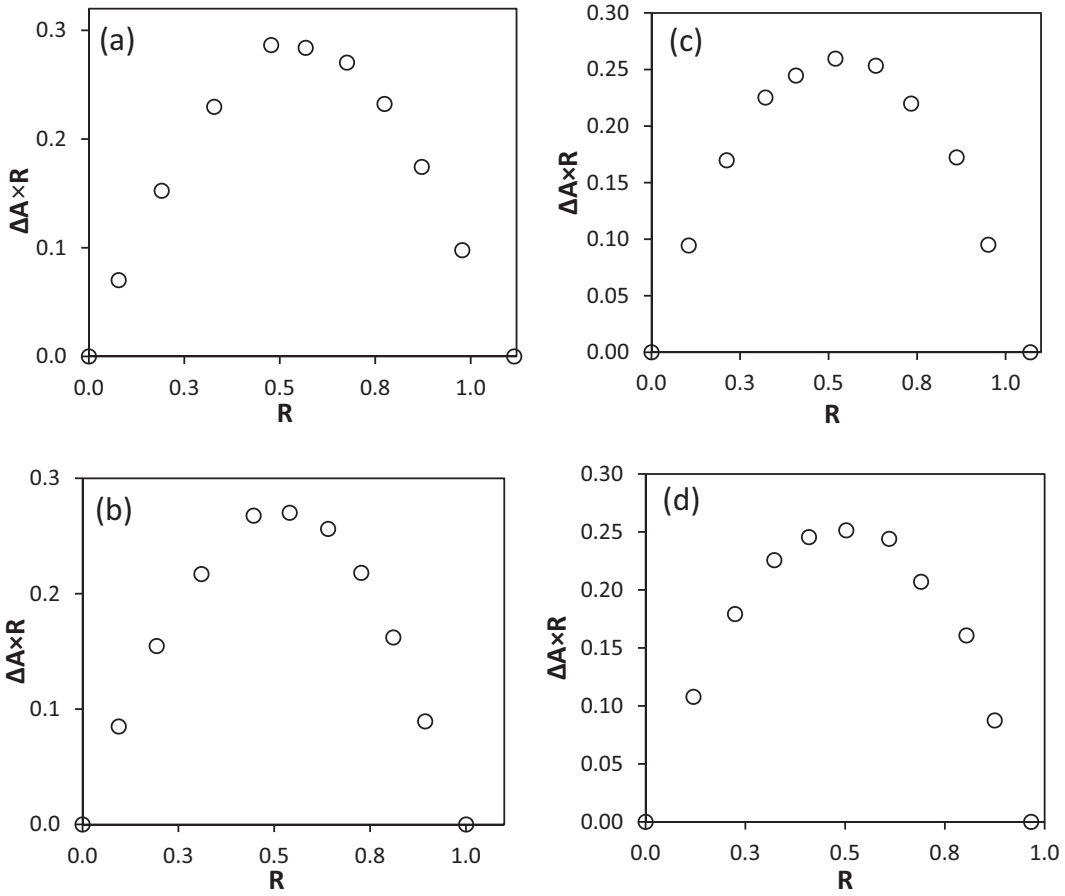

Fig. 3. (a,b,c,d):Job plots of the THC+α-CD system at (a) λ_{max} = 236 nm, (b) λ_{max} = 263 nm and THC+β-CD system at (c) λ_{max} = 236 nm, (d) λ_{max} = 263 nm.

Table 1
Association Constants derived from Benesi-Hildebrand method (K_a) and also from the Nonlinear Program (K_a^τ) using UV–Visible spectroscopic data at 236–263 nm in the temperature range 298.15–308 K.

Host	λ_{max} (nm)	Temperature (K[a])	$K_a(\times 10^3)$	$K_a^\tau(\times 10^3)$
α-CD	236	298.15	1.28	1.30
		303.15	1.12	1.10
		308.15	0.86	0.87
	263	298.15	1.12	1.22
		303.15	0.85	0.81
		308.15	0.62	0.64
β-CD	236	298.15	1.90	2.10
		303.15	1.62	1.52
		308.15	1.33	1.23
	263	298.15	1.67	1.47
		303.15	1.50	1.20
		308.15	1.13	0.93

[a] Standard uncertainty in temperature, u, are u(T) = ± 0.01 K.

down to 5 °C and kept for 12 h without any disturbing. The obtained suspension was then filtered and washed with ethanol and dried in air to get white polycrystalline powder.

3. Result and discussion

3.1. Job plot: stoichiometry of the host-guest inclusion complex

The well-established Job's method, usually known as continuous variation method is used to find out the stoichiometry of host-guest inclusion complex [55]. For this UV–Visible study, a set of solutions of THC had been taken along with host α and β-CD separately varying mole fractions within the range of 0–1 (Table S1-S4) in aqueous solution and experiment was done at 298.15 K. The THC has absorbance with respect to two λ_{max}'s regarding Π–Π* transitions, λ_{max} = 236 nm for pyrimidine ring and = 263 nm for thiazole ring. Hence, the absorbance of THC had been taken at λ_{max} = 236 nm and 263 nm respectively (Fig. 2) for the set of prepared solutions. ΔA × R vs. R were plotted (Fig. 3) of THC+α-CD and THC + β-CD for the graph of Job's plot separately where, ΔA is the difference in absorbance of THC without and with CDs and "R" refers to the mole fraction of THC, i.e. [THC]/([THC] + [CD]). The Y-axis in the Job's plot represents physical property (ΔA × R), that functions as a proxy for the concentration of inclusion complex. From the value of R at the maxima of the plots, the stoichiometry of inclusion complex can be obtained for example if the value of R is 0.33, 0.5 or 0.66 then the stoichiometry of host-guest inclusion complex is 1:2, 1:1 or 2:1 respectively [56]. In this experimental study the value of R had been obtained ~0.5 from the four plots at λ_{max} = 236 and 263 nm for α and β-CD correspondingly which clearly indicates the host-guest inclusion stoichiometry 1:1 for both the cases [57] (Fig. 3) that means both the pyrimidine and thiazole ring form 1:1 inclusion complexes with the respective CDs separately. So, it can be concluded that there is a high probability of formation of a dynamic equilibrium among the pyrimidine and thiazole part of THC with the respective CDs separately in the aqueous solution phase.

3.2. Ultraviolet spectroscopy for the determination of association constants of the ICs

The non-covalent binding capability of the guest molecule within the cavity of host supra-molecules and the binding strength of the respective inclusion complexes had been explored by the evaluated association constants (K_a) of the ICs in the solution state with the help of UV–Visible spectroscopy [20]. The molar extinction co-efficient (ε) of the chromophore of THC was changed on the basis of the solvent polarity as it was changing its environment from polar aqueous medium to apolar cavity of CDs via non-covalent interactions to form host-guest inclusion complexes [58]. For the determination of Ka, the change in absorbance (ΔA) of THC at λ_{max} = 236 and 263 nm for pyrimidine ring and thiazole ring respectively was measured with gradual increasing the concentrations of α-and β-CD separately by varying temperature within the range of 298.15–308.15 K (Table S5-S8). The double reciprocal plots (Figure S1-S2) were drawn with the help of Benesi–Hildebrand method [59–61] for 1:1 host - guest complexation and the corresponding equation is given as follows

$$\frac{1}{\Delta A} = \frac{1}{\Delta\varepsilon}[THC]K_a\frac{1}{[CD]} + \frac{1}{\Delta\varepsilon}[THC] \quad (1)$$

where ΔA is the change in absorbance of THC (at λ_{max} = 236 and 263 nm) and Δε is the change in molar extinction co-efficient of THC from polar environment to apolar environment. The resulting plots are straight line and the Ka for the ICs are evaluated from the intercept to slope of the straight line of the double reciprocal plot (Table 1).

Table 2
Thermodynamic parameters ($\Delta H^0, \Delta S^0, \Delta G^0$) and ($\Delta H^{0\tau}, \Delta S^{0\tau}, \Delta G^{0\tau}$) calculated, using the association constants (K_a, K_a^τ) obtained from Benesi-Hildebrand method, Nonlinear Program for λ_{max} = 236 nm and 263 nm.

Inclusion Complexes (ICs)	λ_{max} (nm)	Application of (K_a) to Van't Hoff equation		Application of (K_a^τ) to Van't Hoff equation	
THC + α-CD	236	ΔH^0 (KJ mol^{-1})	−30.07	$\Delta H^{0\tau}$ (KJ mol^{-1})	−30.32
		ΔS^0 (J mol^{-1} K^{-1})	−41.20	$\Delta S^{0\tau}$ (J mol^{-1} K^{-1})	−41.98
		ΔG^0 (KJ mol^{-1})	−17.79	$\Delta G^{0\tau}$ (KJ mol^{-1})	−17.80
	263	ΔH^0 (KJ mol^{-1})	−44.77	$\Delta H^{0\tau}$ (KJ mol^{-1})	−48.97
		ΔS^0 (J mol^{-1} K^{-1})	−91.69	$\Delta S^{0\tau}$ (J mol^{-1} K^{-1})	−105.35
		ΔG^0 (KJ mol^{-1})	−17.43	$\Delta G^{0\tau}$ (KJ mol^{-1})	−17.56
THC + β-CD	236	ΔH^0 (KJ mol^{-1})	−27.11	$\Delta H^{0\tau}$ (KJ mol^{-1})	−40.81
		ΔS^0 (J mol^{-1} K^{-1})	−28.11	$\Delta S^{0\tau}$ (J mol^{-1} K^{-1})	−73.42
		ΔG^0 (KJ mol^{-1})	−18.73	$\Delta G^{0\tau}$ (KJ mol^{-1})	−18.92
	263	ΔH^0 (KJ mol^{-1})	−29.59	$\Delta H^{0\tau}$ (KJ mol^{-1})	−29.59
		ΔS^0 (J mol^{-1} K^{-1})	−37.28	$\Delta S^{0\tau}$ (J mol^{-1} K^{-1})	−37.28
		ΔG^0 (KJ mol^{-1})	−18.47	$\Delta G^{0\tau}$ (KJ mol^{-1})	−18.47

Mean errors in variables are as follows: $\Delta H^0 = \pm 0.01$ kJ mol^{-1}; $\Delta S^0 = \pm 0.01$ J mol^{-1}K^{-1}; $\Delta G^{0\tau} = \pm 0.01$ kJ mol^{-1}; $\Delta H^{0\tau} = \pm 0.01$ kJ mol^{-1}; $\Delta S^{0\tau} = \pm 0.01$ J mol^{-1}K^{-1}.

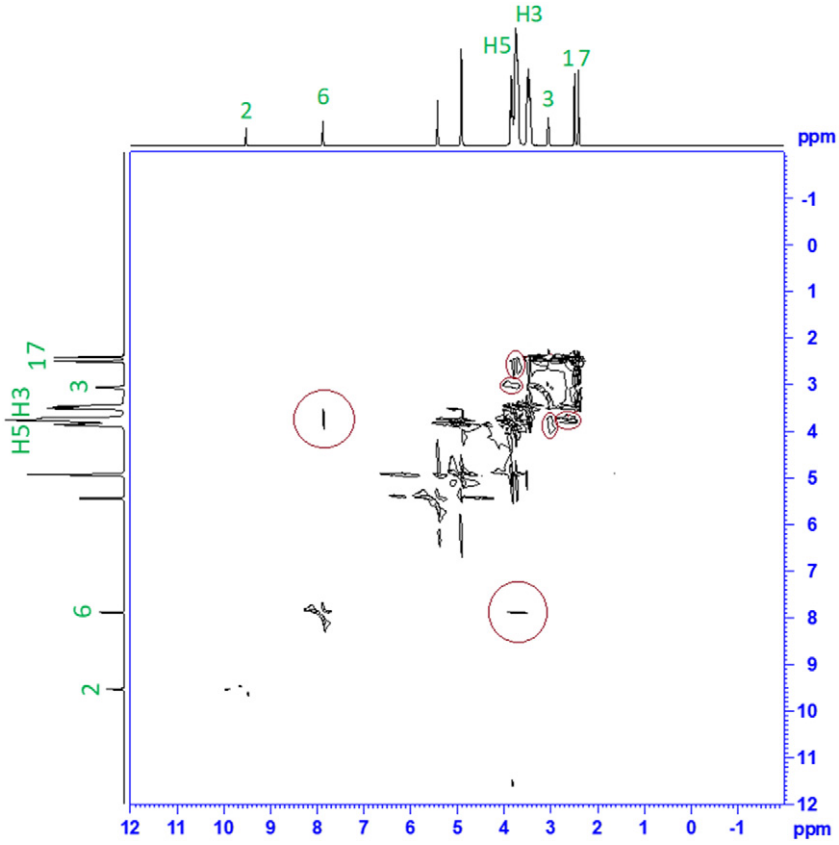

Fig. 4. 2D ROESY NMR spectra of IC-1 (THC+α-CD).

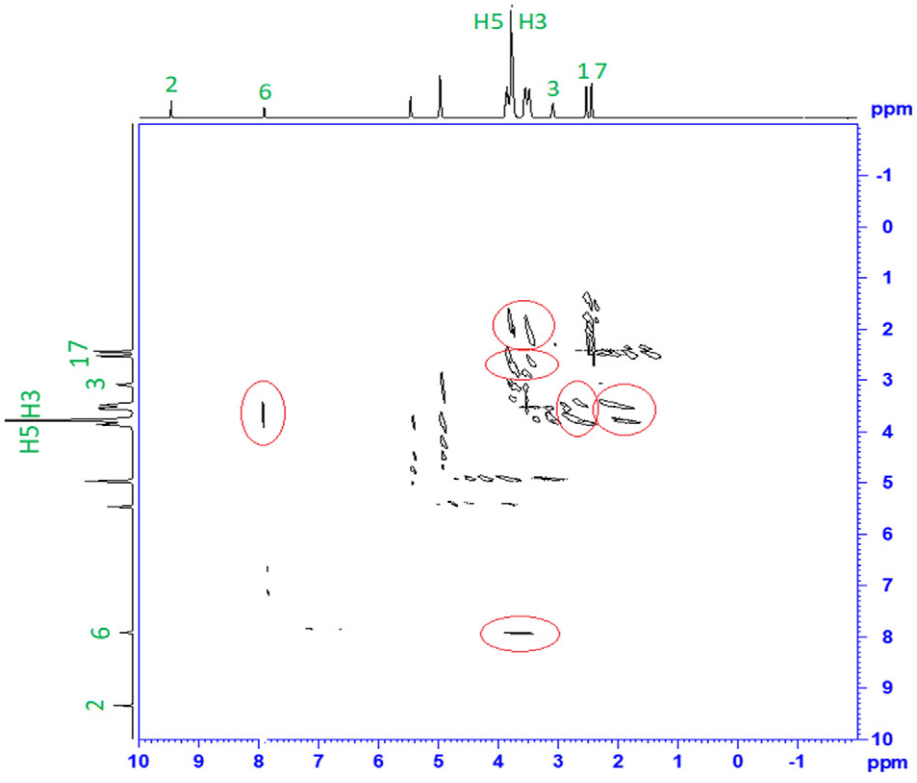

Fig. 5. 2D ROESY NMR spectra of IC-2 (THC+β-CD).

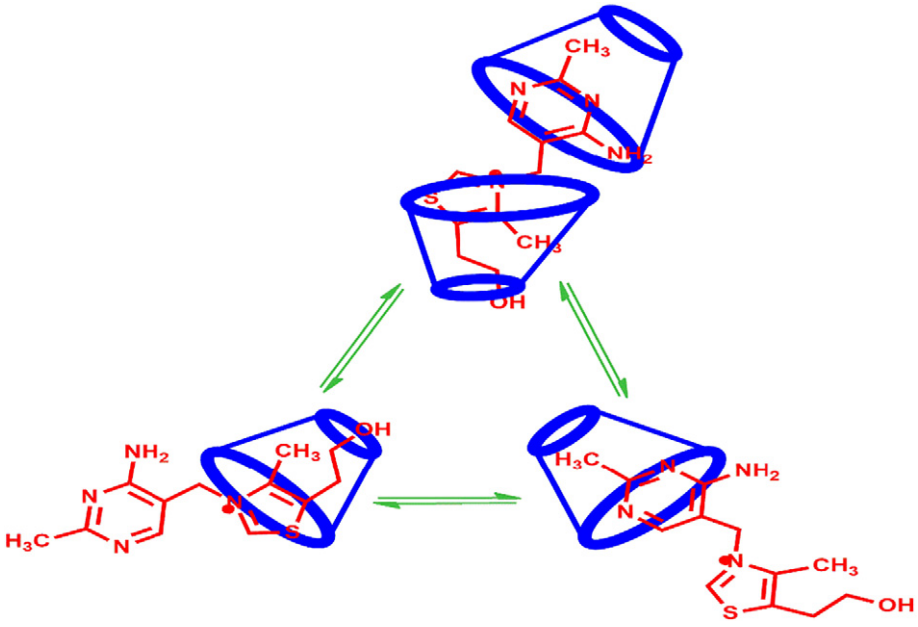

Fig. 6. Plausible mechanism of inclusion complexation through wider rim of cyclodextrin.

K_a's for the respective IC's were also determined with the help of non-linear programmed by the UV–visible study owing to the encapsulation of THC within the hydrophobic cavity of α-CD and β-CD separately. As a result of formation of 1:1 IC in the solution phase, there should be an equilibrium established between host and guest molecules [58,62,63].

$$[THC]_f + [CD]_f \rightleftharpoons_a^K \tau[C,D] \tag{2}$$

The association constant (K_a^τ) for the above equation can be expressed as follows

$$K_a^\tau = \frac{[IC]}{[THC]_f}[CD]_f \tag{3}$$

where [IC], $[THC]_f$ and $[CD]_f$ refer the equilibrium concentrations of IC, free THC and free CD respectively for the above mentioned reaction equation. According to the binding isotherm, the (K_a^τ) for the for the formation of ICs can be written in terms of their absorbance as follows

$$\frac{[CD]_f = [CD]_x - [THC]_x(A_o bs - A_0)}{(A - A_o bs)} \tag{4}$$

Here, A_0 is the initial absorbance for THC molecule, A_{obs} is the absorbance of the THC in the time of ongoing addition of CDs and A denotes the final concentration of THC molecules. $[THC]_x$ and $[CD]_x$ are the concentrations of cyclodextrin and THC molecules respectively. The obtained (K_a^τ) values the respective ICs at both λ_{max} values are listed in the (Table 1) with the help of non-linear programmed.

The association constants of the IC's define the binding ability of the guest into the host as well as their stability as IC. The greater values of the association constants for IC's describes the greatness of their stability. From Table 1, it is clear pyrimidine part of the THC binds more strongly than that of the thiazole part of THC. The IC's formed with β-CD were found more stable than that of the IC's formed with α-CD. With increasing temperature, the thermal stability of IC's decreases as the encapsulation of the guest into host cavity leads to the decrease in enthalpy (Table 2).

3.3. UV–visible spectroscopy, non-linear program based mathematical calculation to determine the thermodynamic parameters

Thermodynamic parameters were calculated basing on the association constants (K_a, K_a^τ) obtained from a variety of isotherms by the above mentioned linear and non-linear methods with the help of van't Hoff equation [20,64,65] (Figure S3-S4, Table S9-S10 and Figure S5-S6, Table S11-S12).

$$\ln K_a = -\frac{\Delta H^0}{RT} + \frac{\Delta S^0}{R} \tag{5}$$

$$\Delta G^0 = \Delta H^0 - T\Delta S^0 \tag{6}$$

where Δ Ho, Δ So, R and T carry their usual meanings. The calculating value of Δ Ho and ΔSo for the formation of ICs were suggesting that the entire inclusion complex formation process in the solution phase are exothermic and entropy restricted means the process is unfavorable in terms entropy (Table 2). From these results it can be concluded that the entire inclusion complex formation process in solution phase is thermodynamically spontaneous but entropically unfavorable as molecular recognition takes place and is highly diminished by the greater value of change in enthalpy ($\Delta H^0, \Delta H^\theta 0$) hence makes the overall process thermodynamically favorable. Thus the Gibbs free energy ΔG^0 becomes negative directing spontaneity in the formation of the ICs.

3.4. ^{1}H NMR and 2D ROESY NMR spectra analysis of solid inclusion complexes

In order to explain the mechanism of the inclusion complexation of THC with the respective cyclodextrin molecules, ^{1}H NMR and 2D-ROESY spectra were recorded. The ^{1}H NMR spectra and the chemical shift (δ) values of THC, α-CD, β-CD and their inclusion complexes are shown in Figure S7-S11 and in Table S13 respectively. As a result of mutual shielding through space among the interacting protons of THC with that of the cyclodextrin molecules, there is a change in their NMR spectra in their corresponding inclusion complexes. Here, change of the chemical shift values of protons of cyclodextrin supramolecules occurs through diamagnetic shielding mainly by the aromatic segments of THC molecule. From the structure of CD (Fig. 1), it can be seen that H3 protons and H5 protons are situated at the wider and narrower rim

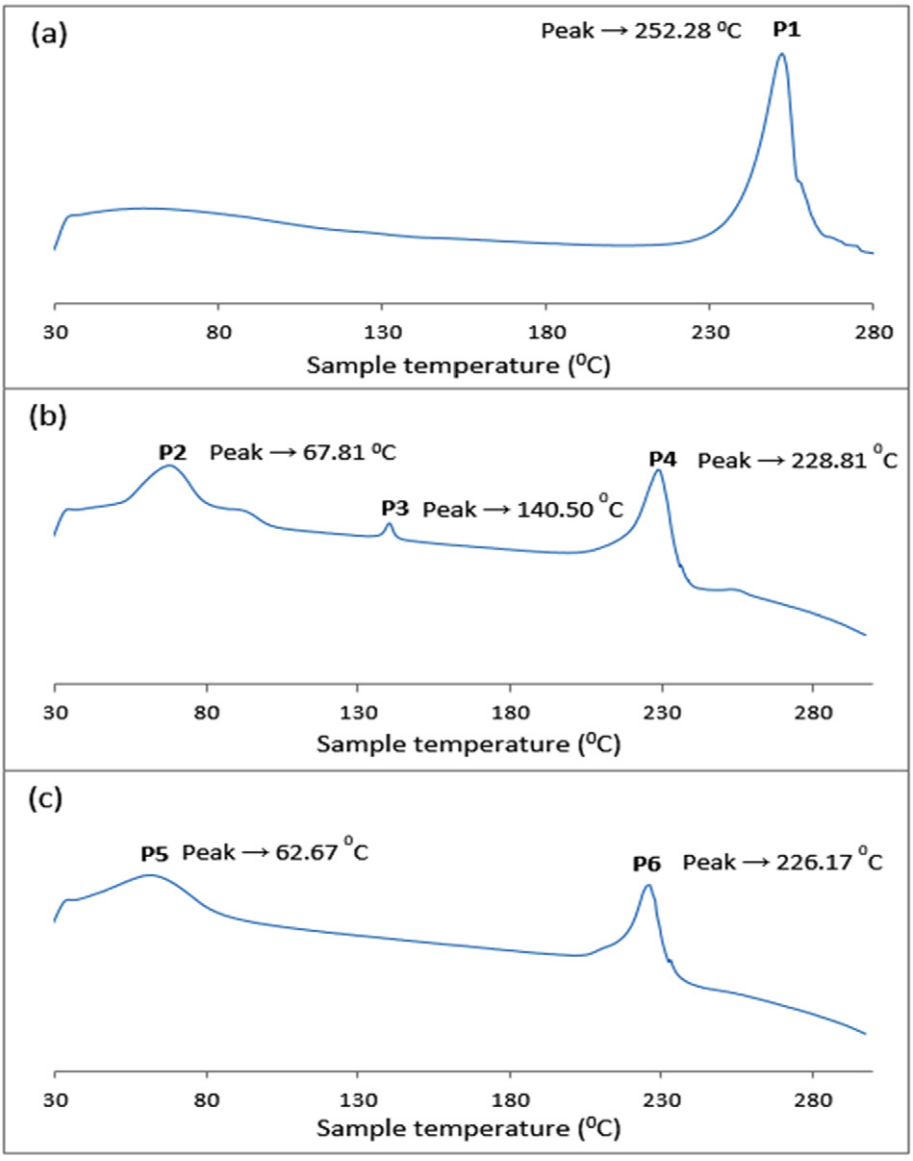

Fig. 7. (a,b,c):DSC thermos-gram of (a) THC, (b) THC+α-CD, (c) THC+β-CD.

sides respectively while the rest of protons are at the exterior area of the CD conical shaped molecule. From Figure S7-S11 of NMR spectra it is clearly seen that there is an upfield shift of H3 and H5 protons of α and β-CD correspondingly which confirms the formation of inclusion complexes with the THC molecule.

To get the clear idea about the mode of interactions of the protons of THC molecule with that of the CD molecules in their inclusion complexes 2D ROESY NMR had been performed and the spectra are shown in Figs. 4 and 5. There are some diagonal and off-diagonal peaks are observed in the spectra in ROESY NMR for the THC-CD complexes if protons are situated within 0.4 nm in space. Off-diagonal peaks are due to the inter cross correlation of the protons of THC with the interior protons i.e. H3 and H5 of CD molecules. In Figs. 4 and 5, there are three off-diagonal peaks are observed due to the inter molecular dipolar cross correlation between H-6 proton of THC with the H3 and H5 of α and β-CD while H-1 and H-7of THC with H3 and H5 of α and β-CD molecule respectively suggesting that the pyrimidine part of THC strongly interacts with the interior protons of CD molecules and resides inside the CD cavity but there is a weak interaction between the thiazole moiety of THC with the CDs probably that positive charge on the N atom of thiazole moiety resists it to stay within CD hydrophobic cavity. As there is no such significant peaks with the H6 protons of CD with that of the THC molecule, it can be concluded that the inclusion occurs through wider rim side (Fig. 6) for both α and β -CD otherwise some changes will be observed as H6 protons reside near narrower side of the rim.

3.5. Differential scanning calorimetric (DSC) study

The thermal characterization of the inclusion complexes had been done with the help of DSC technique [66]. Each pure compound has its own characteristic boiling, melting or sublimation point which frequently disappears or shifts to the different temperature due to the formation of inclusion complexes [67–69]. The DSC thermograms of THC and its ICs are shown in Fig. 7. The DSC thermogram of THC showed a sharp endothermic peak at 252.28 °C corresponds to its melting point. In the ICs a characteristic peak with large shifting in comparison with the THC to the different temperatures were observed. Initially endothermic peaks at 67.81 °C and 140.50 °C for IC-1 could be attributed to the loss of water due the evaporation. Similarly, endothermic peak at 62.67 °C for IC-2 is due to the loss of water molecules owe to the evaporation. Both the peak at 228.81°Cfor IC-1 and at 226.17 °C for IC-2 indicate the loss of crystalline nature of THC molecule and also suggesting

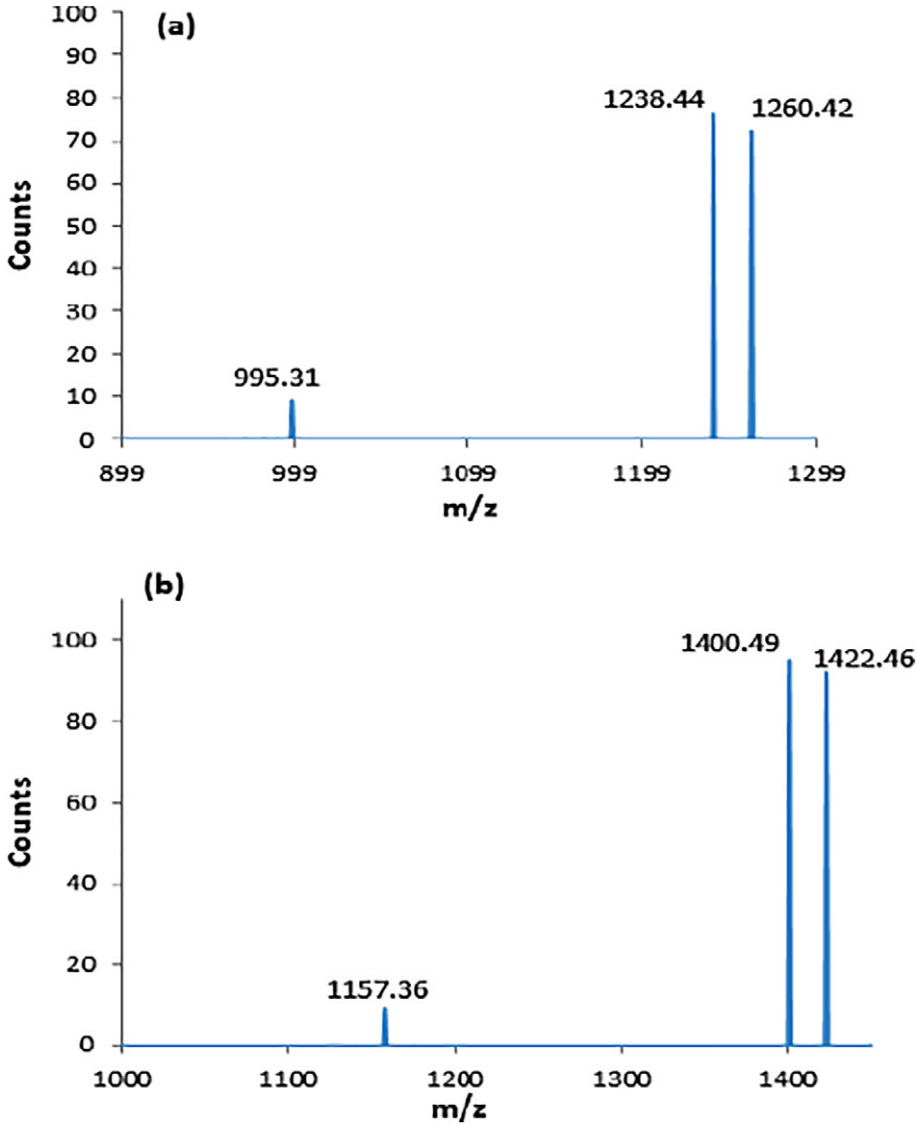

Fig. 8. (a,b): ESI- Mass spectra of (a) IC-1 (THC+α-CD), (b) IC-2 (THC+β-CD).

that there is a strong interaction of THC molecule with β-CD compare to α-CD.

3.6. ESI-mass spectrometric analysis of inclusion complexes

The ICs of THC with α-CD and β-CD separately were further investigated in their solid state with the help of ESI-mass spectrometry by dissolving in methanol. The observed spectra are shown in Fig. 8. The peaks at *m/z* 1238.44 and 1260.42correspond to the $[THC+ \alpha\text{-CD} + H]^+$ and $[THC+\alpha\text{-CD} + Na]^+$ respectively and the peaks at *m/z* 1400.49 and 1422.47 correspond to $[THC+\beta\text{-CD} + H]^+$ and $[THC+\beta\text{-CD} + Na]^+$ respectively. From all of this values, it can be concluded that the ICs of THC with α-CD and β-CD separately have been formed in the solid state and the obtained stoichiometric ratio is 1:1 for the host to guest molecule [70].

3.7. FT-IR spectra of solid inclusion complexes

The formation of inclusion complexes are also well explained with the help of infrared spectroscopic technique [71–73]. KBr disk method had been used to get the IR spectra of the pure THC, α-CD, β-CD and their respective IC's which are shown in Fig. 9. The noteworthy signals which are shifted sufficiently have been listed in Table S14.

For IC-1 means (α-CD + THC) system, the following spectral changes are obtained due the host-guest interactions. (i) The broad signal at 3436.04 $cm^{-1}$of THC generally found due to the merging of the two signals respective to $–NH_2$ and –OH groups together and this peak is found to shift at 3420.09 cm^{-1}in IC-1 while 3410.09 cm^{-1} is observed for –OH groups in α-CD. (ii) The signal of 2361.26 cm^{-1} for ($C^{sp3}H_2$) bending of THC is shifted to 2365.21 cm^{-1} in the complex. (iii) The peak at 1636.35 cm^{-1} for N–H (NH_2) bending of THC is obtained at 1632.02 cm^{-1} while complexed with α-CD. (iv) The peaks from 519.08 cm^{-1} to 1380.15 cm^{-1} of THC are almost completely masked in its complex with α-CD.

For IC-2 means (β-CD + THC) system, the following changes in their spectra are observed owe to the various non-covalent interactions of THC with β–CD. (i) The signal at 3424.05 cm^{-1} for –OH stretching of β-CD is changed to 3401.23 cm^{-1} in IC-2. (ii) The peak at 2361.26 $cm^{-1}$for ($C^{sp3}H_2$) bending of THC is shifted to 2363.29 in its complex with β–CD. (iii) The peak at 1636.35 $cm^{-1}$for N–H (NH_2) bending of THC is now changed to 1632.27 cm^{-1}. (iv) The signals in the range of 519.08 $cm^{-1}$to 1380.15 cm^{-1} are also just as IC-1 masked significantly in IC-2.

Thus, from the above discussions along with Fig. 9 and Table S14, it was seen that, there is no significant appearance of new signals which clearly indicate the absence of formation new chemical bonds between

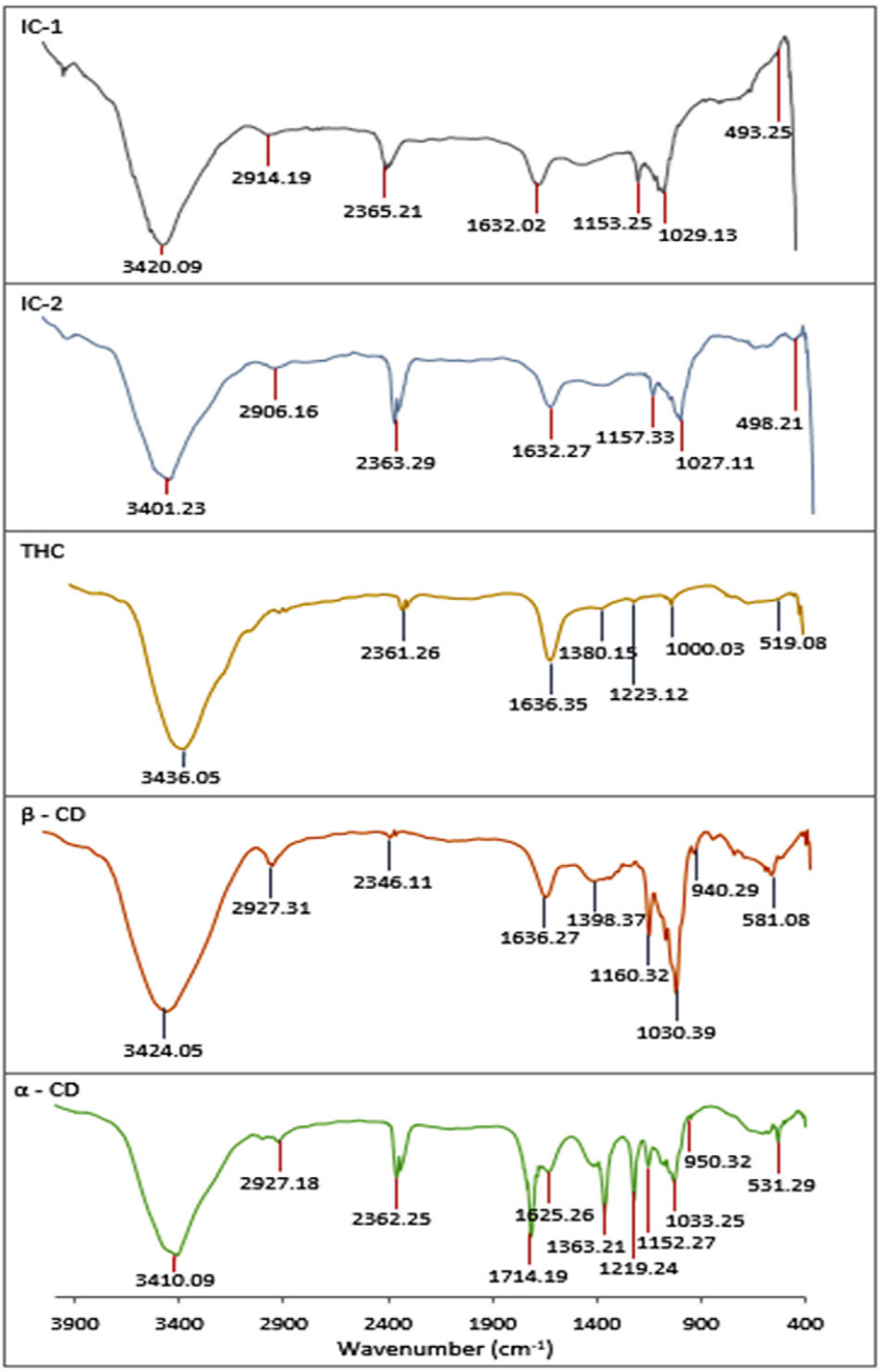

Fig. 9. (a,b,c):FTIR spectra of IC-1 (THC+α-CD), IC-2(THC+β-CD), THC, β-CD and α-CD.

THC and CDs. So, it can be clearly said that the slight shifting of some significant IR signals that may signify hydrophobic-hydrophobic as well as non-covalent interaction of thiazole and pyrimidine ring of THC with CDs causing random weakening and strengthening of the interacting bonds while formation of IC's.

3.8. Scanning electron microscopic study to exhibit the surface structures

Scanning electron microscopy is a well-established technique to analyze the surface morphology and the particle size of the solid substances [9,59,74]. The surface morphology of the pure guest THC, pure hostsα and β-CD separately, their respective ICs and their corresponding physical mixtures have been shown in Figs. 10 and 11. From the SEM images, it is clear that the surface morphology of the ICs is totally different from their raw materials which indicates the formation of new morphology probably indicating the formation of host-guest inclusion complexes as evident from the above mentioned different experimental studies.

3.9. Steady-state fluorescence: association constants from modified Benesi-Hildebrand equation and association constants

The association constants of THC molecule with and without the presence of CD molecule had been derived from the modified Benesi-

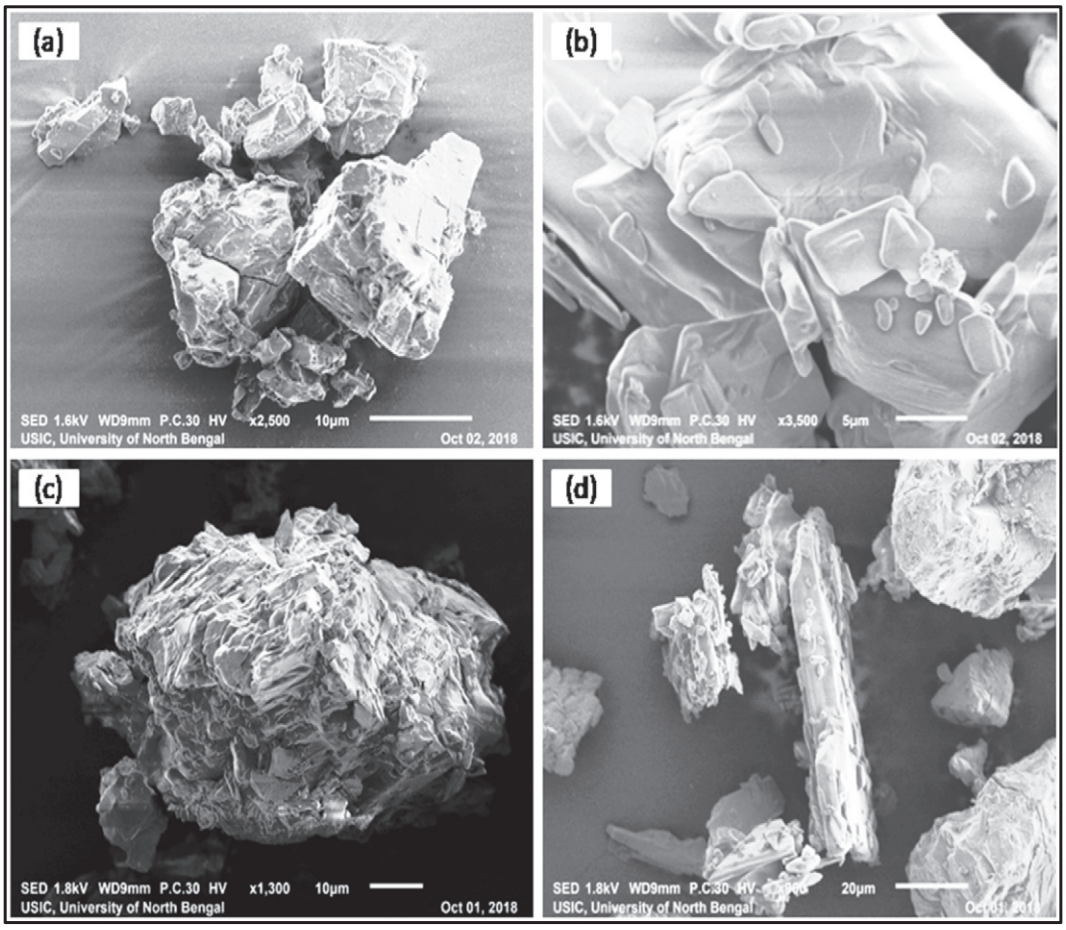

Fig. 10. (a,b,c,d):SEM images of (a) α-CD, (b) THC, (c) (THC+α-CD) IC and (d) (THC+α-CD) physical mixture.

Hildebrand equation by using spectrofluorimetric method [75–77].

$$\frac{1}{I-I_0}=\frac{1}{[I^{/}-I_0}]K_a^{\varphi}\frac{1}{[TH}C]+\frac{1}{I^{/}-I_0} \tag{7}$$

where, I and I_0 represents the fluorescence intensities of HSA in the presence and absence of the THC respectively, $I^{/}$ are the intensities of the HSA while all the guest molecules for a particular system are complexed with THC. [THC] represents the concentration of the Thiamine hydrochloride.

From the above discussions it is clear that there is a formation of 1:1 inclusion complex of THC with CDs. All the fluorescence spectra are taken by exciting the HSA at λ_{max} 280 nm by keeping constant the volume and concentration of HSA and CDs in the respective aqueous solution mixtures while the concentration of THC was varied. The whole experiment was done at phosphate buffer aqueous solutions by maintaining pH 7.4 at 298.15 K. From the plots (Figure S12) drawn by using the above mentioned equation, association constants are evaluated which are shown in Table S15-S17, suggesting the stability of the newly formed complexes in the solution phase at room temperature. The Gibbs free energy value (Table 3) suggesting the spontaneity of the whole complexation processes.

3.10. Binding interaction of the THC molecule in the presence of human serum albumin with and without CDs: the process of dischargement of guest from the cavity of CDs

Fluorescence spectroscopy is a very useful and highly sensitive technique to inspect the change in the microenvironment around the fluorophore depending on the binding with quencher [78,79].

Thus from this study lots of different kind of useful information can be obtained with respect to the binding mechanism [47,48,80]. The release of THC from the inclusion complexes was determined with the help of fluorescence emission spectroscopy by observing the binding interaction of HSA with THC in the presence and absence of CDs in aqueous medium. The intrinsic fluorescence of HSA is due to Trp 214 (hydrophobic moiety) alone having λ_{max} of 280 nm.

For all the set of solutions, excitation had been done at 280 nm to investigate the shift of λ_{max} and the intensity of the HSA molecule with and without the presence of CD molecules, the corresponding spectra was shown in Fig. 12. From these figures, hypochromic shift i.e. a regular decrease in the intensity of the spectra with increasing the concentrations of THC separately in the aqueous buffered solutions of HSA along with respective CDs, was clearly observed probably as a result of strong non-covalent interactions of fluorophore moiety of HSA molecule with the THC molecule. The binding constants of THC:HSA in the presence of CD molecule are $3.03 \times 10^3$and 2.49×10^3 M^{-1} for α and β-CD respectively, where 4.21×10^3 M^{-1} for THC: HSA without CDs suggesting there is a less association of THC with HSA molecule in the presence of CDs as inclusion of THC with CDs decreases the strength of their binding by blocking the non-covalent interactions existing between them. So, HSA strongly competes with CDs to bind THC and in this way it helps in effective delivery of vitamins. Accordingly, it enhances the availability of free THC in blood plasma resulting effective therapeutic effect at the target site. This study also proves the formation of inclusion complexes of THC with both α and β-CD respectively in solution phase.

Hence from this experimental study we can conclude that there is a regularity in the oozing of the guest molecule from the cavity of CDs into the aqueous solution in the presence of HSA molecule.

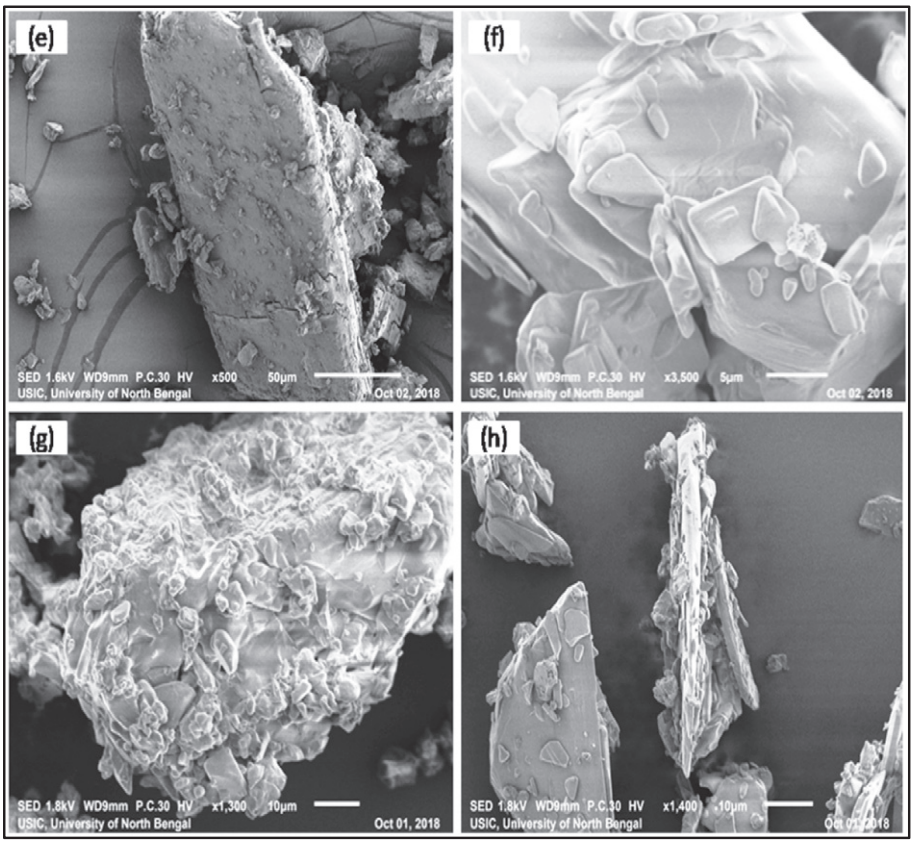

Fig. 11. (e,f,g,h):SEM images of (e) α-CD, (f) THC, (g) (THC+α-CD) IC and (h) (THC+α-CD) physical mixture.

4. Conclusion

1:1 host-guest inclusion complexes of THC within the cavity of α and β-CD are well established by the various techniques in solution phase as well as in the solid state. The entire inclusion process is thermodynamically feasible process as obtained from the calculated thermodynamic parameters and evaluated association constants reveal the stability of the formation of ICs. Molecular recognition due to the dimensional suitability is the major stabilizing factor. The positive entropy factor is also responsible for the formation of ICs via non-covalent interactions such as hydrogen bonding and other hydrophobic interactions as more number of water molecules compare to that of THC molecule are released from the cavity of the CDs for making the free suitable space for the incoming THC molecule. Formation of inclusion complexes enhances the photochemical stability of THC, protect it from thermal degradation and retain its property without any kind of chemical transformation. Moreover, the regulatory dischargement of THC molecule at pH 7.4 from the hydrophobic cavity to the polar aqueous media has been clearly explained in the presence of HSA molecule. So, there is a strong probability to show similar kind of binding behavior of THC with HSA in the human body and successfully will be delivered to the targeted area as per required amount of it. Hence the study for the formation of inclusion complex and the regulatory dischargement of THC from the hydrophobic cavity of CDs into the aqueous solution approach a novel way for the versatile uses and formulation in food, medicinal and pharmaceutical industries without any chemical modification. In conclusion, this article demands far reaching effects by dint of innovative applications in pharmaceutical science.

Disclosure of interest

The authors declare no conflicts of interest.

Acknowledgement

Prof. M. N. Roy would like to acknowledge sponsor-id="https://doi.org/10.13039/501100001501" xlink:role="http://www.elsevier.com/xml/linking-roles/grant-sponsor" xlink:type="simple">UGC, New Delhi, Government of India, for being awarded One Time Grant under Basic Scientific Research via the grant-in-Aid no. F.4-10/2010 (BSR). BR is thankful to the "State Fellowship" bearing reference No. 1743/R-2017 dated April 18, 2017. Mr. Goutam Sarkar, The H.O.D., USIC, University of North Bengal, Darjeeling is also highly acknowledged for executing SEM associated with this paper.

Appendix A. Supplementary data

Supplementary data to this article can be found online at https://doi.org/10.1016/j.molliq.2019.111952.

Table 3
Association constants (K_a^{ϕ}) and standard free energy changes for (HSA + THC), (HSA + THC+α-CD) and (HSA + THC+β-CD) systems at 298.15 K.

System	HSA + THC	HSA + THC+α-CD	HSA + THC+β-CD
$K_a^{\phi} \times 10^3 (M^{-1})$	4.21	3.03	2.49
$\Delta G^{\phi}0$ (KJ mol^{-1})	−20.24	−19.44	−18.97

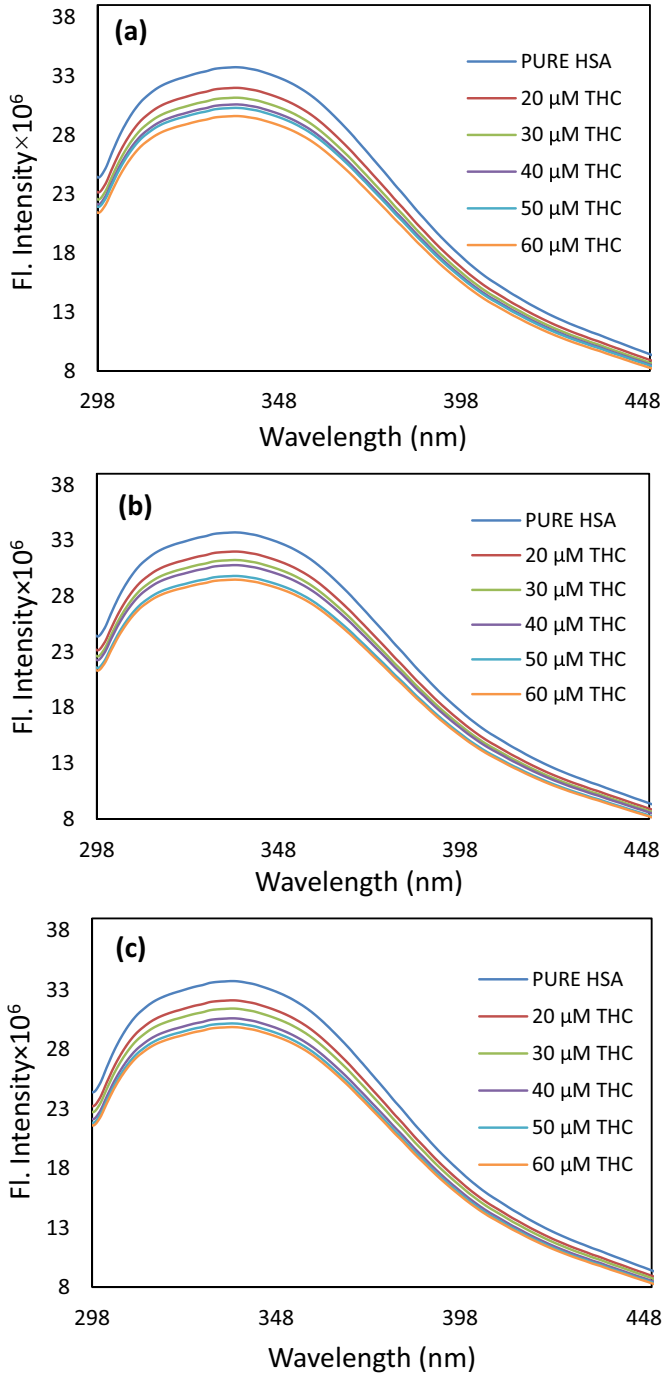

Fig. 12. (a, b, c): Fluorescence spectra of HSA molecule in presence of (a) THC, (b) THC along with β-CD (c) THC along with α-CD at the various concentrations.

References

[1] M.I. Rodríguez-López, M.T. Mercader-Ros, S. López-Miranda, J.A. Pellicer, A. Pérez-Garrido, H. Pérez-Sánchez, E. Núñez-Delicado, J.A. Gabaldón, Thorough characterization and stability of HP-β-cyclodextrin thymol inclusion complexes prepared by microwave technology: a required approach to a successful application in food industry, J. Sci. Food Agric. 99 (2019) 1322–1333.

[2] M. Kfoury, C. Geagea, S. Ruellan, H. Greige-Gerges, S. Fourmentin, Effect of cyclodextrin and cosolvent on the solubility and antioxidant activity of caffeic acid, Food Chem. 278 (2019) 163–169.

[3] I. Mourtzinos, P. Prodromidis, S. Grigorakis, D.P. Makris, C.G. Biliaderis, T. Moschakis, Natural food colorants derived from onion wastes: application in a yoghurt product, Electrophoresis 39 (2018) 1975–1983.

[4] N.K. Bakirhan, T.T. Tok, S.A. Ozkan, The redox mechanism investigation of non-small cell lung cancer drug: erlotinib via theoretical and experimental techniques and its host–guest detection by β-Cyclodextrin nanoparticles modified glassy carbon electrode, Sens. Actuators B Chem. 278 (2019) 172–180.

[5] E. Saidman, A.K. Chattah, L. Aragón, M. Sancho, G. Camí, C. Garnero, M. Longhi, Inclusion complexes of β-cyclodextrin and polymorphs of mebendazole: physicochemical characterization, Eur. J. Pharm. Sci. 127 (2019) 330–338.

[6] N. Singh, O. Sahu, 4 - sustainable cyclodextrin in textile applications, in: I. Shahid ul, B.S. Butola (Eds.), The Impact and Prospects of Green Chemistry for Textile Technology, Woodhead Publishing 2019, pp. 83–105.

[7] S. Cao, J. Chen, G. Lai, C. Xi, X. Li, L. Zhang, G. Wang, Z. Chen, A high efficient adsorbent for plant growth regulators based on ionic liquid and β-cyclodextrin functionalized magnetic graphene oxide, Talanta 194 (2019) 14–25.

[8] B. Strokopytov, D. Penninga, H.J. Rozeboom, K.H. Kalk, L. Dijkhuizen, B.W. Dijkstra, X-ray structure of cyclodextrin glycosyltransferase complexed with acarbose. Implications for the catalytic mechanism of glycosidases, Biochemistry 34 (1995) 2234–2240.

[9] L. Cai, D. Jeremic, H. Lim, Y. Kim, β-Cyclodextrins as sustained-release carriers for natural wood preservatives, Ind. Crops Prod. 130 (2019) 42–48.

[10] L. Bardi, A. Mattei, S. Steffan, M. Marzona, Hydrocarbon degradation by a soil microbial population with β-cyclodextrin as surfactant to enhance bioavailability, Enzym. Microb. Technol. 27 (2000) 709–713.

[11] M.E. Bellringer, T.G. Smith, R. Read, C. Gopinath, P. Olivier, β-Cyclodextrin: 52-Week toxicity studies in the rat and dog, Food Chem. Toxicol. 33 (1995) 367–376.

[12] E. Jalalvandi, A. Shavandi, Shear thinning/self-healing hydrogel based on natural polymers with secondary photocrosslinking for biomedical applications, J. Mech. Behav. Biomed. Mater. 90 (2019) 191–201.

[13] K. Myszka, K. Leja, M. Majcher, A current opinion on the antimicrobial importance of popular pepper essential oil and its application in food industry, J. Essent. Oil Res. 31 (2019) 1–18.

[14] M. Sayed, G.K. Gubbala, H. Pal, Contrasting interactions of DNA-intercalating dye acridine orange with hydroxypropyl derivatives of β-cyclodextrin and γ-cyclodextrin hosts, New J. Chem. 43 (2019) 724–736.

[15] K. Saekhor, W. Udomsinprasert, S. Honsawek, W. Tachaboonyakiat, Preparation of an injectable modified chitosan-based hydrogel approaching for bone tissue engineering, Int. J. Biol. Macromol. 123 (2019) 167–173.

[16] F. van de Manakker, T. Vermonden, C.F. van Nostrum, W.E. Hennink, Cyclodextrin-Based polymeric materials: synthesis, properties, and pharmaceutical/biomedical applications, Biomacromolecules 10 (2009) 3157–3175.

[17] F.J.R. Mejías, M.T. Gutiérrez, A.G. Durán, J.M.G. Molinillo, M.M. Valdivia, F.A. Macías, Provitamin supramolecular polymer micelle with pH responsiveness to control release, bioavailability enhancement and potentiation of cytotoxic efficacy, Colloids Surfaces B Biointerfaces 173 (2019) 85–93.

[18] Y. Li, C. Li, Z. Gu, L. Cheng, Y. Hong, Z. Li, Digestion properties of corn starch modified by α-D-glucan branching enzyme and cyclodextrin glycosyltransferase, Food Hydrocolloids 89 (2019) 534–541.

[19] P. Wang, Z. Ke, J. Yi, X. Liu, L. Hao, Q. Kang, J. Lu, Effects of β-cyclodextrin on the enzymatic hydrolysis of hemp seed oil by lipase Candida sp.99–125, Ind. Crops Prod. 129 (2019) 688–693.

[20] B. Rajbanshi, S. Saha, K. Das, B.K. Barman, S. Sengupta, A. Bhattacharjee, M.N. Roy, Study to probe subsistence of host-guest inclusion complexes of α and β-cyclodextrins with biologically potent drugs for safety regulatory dischargement, Sci. Rep. 8 (2018) 13031.

[21] Y. Yin, K.R. Cadwallader, Spray-chilling encapsulation of 2-acetyl-1-pyrroline zinc chloride using hydrophobic materials: storage stability and flavor application in food, Food Chem. 278 (2019) 738–743.

[22] G. Zhang, C. Yuan, Y. Sun, Effect of selective encapsulation of hydroxypropyl-β-cyclodextrin on components and antibacterial properties of star anise essential oil, Molecules (2018) 23.

[23] J.I.A. Beserra-Filho, A.M. de Macêdo, A.H.F.F. Leão, J.M.M. Bispo, J.R. Santos, A.J. de Oliveira-Melo, P.D.P. Menezes, M.C. Duarte, A.A. de Souza Araújo, R.H. Silva, L.J. Quintans-Júnior, A.M. Ribeiro, Eplingiella fruticosa leaf essential oil complexed with β-cyclodextrin produces a superior neuroprotective and behavioral profile in a mice model of Parkinson's disease, Food Chem. Toxicol. 124 (2019) 17–29.

[24] P. Chowdhury, P.K.B. Nagesh, E. Hatami, S. Wagh, N. Dan, M.K. Tripathi, S. Khan, B.B. Hafeez, B. Meibohm, S.C. Chauhan, M. Jaggi, M.M. Yallapu, Tannic acid-inspired paclitaxel nanoparticles for enhanced anticancer effects in breast cancer cells, J. Colloid Interface Sci. 535 (2019) 133–148.

[25] T. Feng, F. Liu, L. Sun, H. Huo, X. Ren, M. Wang, Associated-extraction efficiency of six cyclodextrins on various flavonoids in puerariae lobatae radix, Molecules (2018) 24.

[26] S. Ho, Y.Y. Thoo, D.J. Young, L.F. Siow, Stability and recovery of cyclodextrin encapsulated catechin in various food matrices, Food Chem. 275 (2019) 594–599.

[27] R.-Y. Gan, C.-L. Chan, Q.-Q. Yang, H.-B. Li, D. Zhang, Y.-Y. Ge, A. Gunaratne, J. Ge, H. Corke, 9 - bioactive compounds and beneficial functions of sprouted grains, in: H. Feng, B. Nemzer, J.W. DeVries (Eds.), Sprouted Grains, AACC International Press 2019, pp. 191–246.

[28] J. Pinela, P. Morales, S. Cabo Verde, A.L. Antonio, A.M. Carvalho, M.B.P.P. Oliveira, M. Cámara, I.C.F.R. Ferreira, Stability of total folates/vitamin B9 in irradiated watercress and buckler sorrel during refrigerated storage, Food Chem. 274 (2019) 686–690.

[29] Y. Yu, C. Li, C. Chen, H. Huang, C. Liang, Y. Lou, X.-B. Chen, Z. Shi, S. Feng, Saccharomyces-derived carbon dots for biosensing pH and vitamin B 12, Talanta 195 (2019) 117–126.

[30] C.H.d.M. Oliveira, A. Assaid Simão, S. Marcussi, Inhibitory effects of ascorbic acid, vitamin E, and vitamin B-complex on the biological activities induced by Bothrops venom, Pharm. Biol. 54 (2016) 845–852.

[31] S. Li, H. Yin, I.W. Wyman, Q. Zhang, D.H. Macartney, R. Wang, Encapsulation of vitamin B1 and its phosphate derivatives by cucurbit[7]uril: tunability of the binding

site and affinity by the presence of phosphate groups, J. Org. Chem. 81 (2016) 1300–1303.
[32] X. Li, D. Han, Y. Wang, S. Du, Y. Liu, J. Zhang, B. Yu, B. Hou, J. Gong, Measurement of solubility of thiamine hydrochloride hemihydrate in three binary solvents and mixing properties of solutions, J. Chem. Eng. Data 61 (2016) 3665–3678.
[33] M.S. Islam, A. Patras, B. Pokharel, M.J. Vergne, M. Sasges, A. Begum, K. Rakariyatham, C. Pan, H. Xiao, Effect of UV irradiation on the nutritional quality and cytotoxicity of apple juice, J. Agric. Food Chem. 64 (2016) 7812–7822.
[34] T.M. Brasky, E. White, C.-L. Chen, Long-term, supplemental, one-carbon metabolism–related vitamin B use in relation to lung cancer risk in the vitamins and lifestyle (VITAL) cohort, J. Clin. Oncol. 35 (2017) 3440–3448.
[35] A.S. Abo Dena, A.A. Ammar, H-point standard addition for simultaneous reagent-free spectrophotometric determination of B1 and B6 vitamins, Spectrochim. Acta A Mol. Biomol. Spectrosc. 206 (2019) 491–497.
[36] D.L. Slawson, N. Fitzgerald, K.T. Morgan, Position of the academy of nutrition and dietetics: the role of nutrition in health promotion and chronic disease prevention, J. Acad. Nutr. Diet. 113 (2013) 972–979.
[37] A. Aloysius, R. Ramanathan, A. Christy, S. Baskaran, N. Antony, Experimental and theoretical studies on the corrosion inhibition of vitamins – thiamine hydrochloride or biotin in corrosion of mild steel in aqueous chloride environment, Egyptian Journal of Petroleum 27 (2018) 371–381.
[38] M.A. Crook, Chapter 6 - methods for assessment of thiamine (vitamin B1), in: D. Harrington (Ed.), Laboratory Assessment of Vitamin Status, Academic Press 2019, pp. 149–164.
[39] A. Nath, T. Tran, T.R. Shope, T.R. Koch, Prevalence of clinical thiamine deficiency in individuals with medically complicated obesity, Nutr. Res. 37 (2017) 29–36.
[40] E. Abdou, A.S. Hazell, Thiamine deficiency: an update of pathophysiologic mechanisms and future therapeutic considerations, Neurochem. Res. 40 (2015) 353–361.
[41] Y. Yang, D. Han, S. Du, S. Wu, J. Gong, Crystal morphology optimization of thiamine hydrochloride in solvent system: experimental and molecular dynamics simulation studies, J. Cryst. Growth 481 (2018) 48–55.
[42] A.L. Voelker, J. Miller, C.A. Running, L.S. Taylor, L.J. Mauer, Chemical stability and reaction kinetics of two thiamine salts (thiamine mononitrate and thiamine chloride hydrochloride) in solution, Food Res. Int. 112 (2018) 443–456.
[43] N. Struch, F. Topić, K. Rissanen, A. Lützen, Electron-deficient trifluoromethyl-substituted sub-components affect the properties of M4L4 tetrahedral cages, Dalton Trans. 46 (2017) 10809–10813.
[44] T. Zhu, J. Du, W. Cao, J. Fan, X. Peng, Microenvironment-sensitive fluorescent dyes for recognition of serum albumin in urine and imaging in living cells, Ind. Eng. Chem. Res. 55 (2016) 527–533.
[45] M.B. Bolattin, S.T. Nandibewoor, S.D. Joshi, S.R. Dixit, S.A. Chimatadar, Interaction of hydralazine with human serum albumin and effect of β-cyclodextrin on binding: insights from spectroscopic and molecular docking techniques, Ind. Eng. Chem. Res. 55 (2016) 5454–5464.
[46] V.D. Suryawanshi, P.V. Anbhule, A.H. Gore, S.R. Patil, G.B. Kolekar, Spectroscopic Investigation on the Interaction of Pyrimidine Derivative, 2-Amino-6-hydroxy-4-(3,4-dimethoxyphenyl)-pyrimidine-5-carbonitrile with human serum albumin: mechanistic and conformational study, Ind. Eng. Chem. Res. vol. 51 (2012) 95–102.
[47] M.J. Weiss-Errico, J. Miksovska, K.E. O'Shea, β-Cyclodextrin reverses binding of perfluorooctanoic acid to human serum albumin, Chem. Res. Toxicol. 31 (2018) 277–284.
[48] L. Wang, J. Yan, Y. Li, K. Xu, S. Li, P. Tang, H. Li, The influence of hydroxypropyl-β-cyclodextrin on the solubility, dissolution, cytotoxicity, and binding of riluzole with human serum albumin, J. Pharm. Biomed. Anal. 117 (2016) 453–463.
[49] P. Sarbadhikary, A. Dube, Spectroscopic investigations on the binding of an iodinated chlorin p6-copper complex to human serum albumin, Photochem. Photobiol. Sci. 16 (2017) 1762–1770.
[50] C. Martin, B. Cohen, I. Gaamoussi, M. Ijjaali, A. Douhal, Ultrafast dynamics of C30 in solution and within CDs and HSA protein, J. Phys. Chem. B 118 (2014) 5760–5771.
[51] B. Cohen, C. Martin Álvarez, N. Alarcos Carmona, J.A. Organero, A. Douhal, Proton-Transfer reaction dynamics within the human serum albumin protein, J. Phys. Chem. B 115 (2011) 7637–7647.
[52] V. Moulin, F. Grandoni, J. Castioni, H. Lu, Pancytopenia in an adult patient with thiamine-responsive megaloblastic anaemia, BMJ Case Rep. 2018 (2018)bcr-2018-225035.
[53] K.D. Wrenn, F. Murphy, C.M. Slovis, A toxicity study of parenteral thiamine hydrochloride, Ann. Emerg. Med. 18 (1989) 867–870.
[54] C.-H. Chern, T.-L. Chern, S.-C. Hu, C.-H. Lee, J.-F. Deng, Complete and partial response to flumazenil in patients with suspected benzodiazepine overdose, Am. J. Emerg. Med. 13 (1995) 372–375.
[55] R. Kumar, R. Bawa, P. Gahlyan, M. Dalela, K. Jindal, P.K. Jha, M. Tomar, V. Gupta, Pyrene appended bis-triazolylated 1,4-dihydropyridine as a selective fluorogenic sensor for Cu2+, Dyes Pigments 161 (2019) 162–171.
[56] F. Ulatowski, K. Dąbrowa, T. Bałakier, J. Jurczak, Recognizing the limited applicability of Job plots in studying host–guest interactions in supramolecular chemistry, J. Org. Chem. 81 (2016) 1746–1756.
[57] C.H. dos Santos, N.M. Uchiyama, I.A. Bagatin, Selective azo dye-based colorimetric chemosensor for F−, CH3COO− and PO43−, Spectrochim. Acta A Mol. Biomol. Spectrosc. 210 (2019) 355–361.
[58] P. Thordarson, Determining association constants from titration experiments in supramolecular chemistry, Chem. Soc. Rev. 40 (2011) 1305–1323.
[59] L. Yuan, S. Li, D. Huo, W. Zhou, X. Wang, D. Bai, J. Hu, Studies on the preparation and photostability of avobenzone and (2-hydroxy)propyl-β-cyclodextrin inclusion complex, J. Photochem. Photobiol. A Chem. 369 (2019) 174–180.
[60] M. Bartolotta, M.T. Buthelezi, Molecular polarity effect on the association constant of cyclodextrin-pyrimidine nucleobases in water, J. Photochem. Photobiol. A Chem. 371 (2019) 382–386.
[61] M. Moncada-Basualto, B. Matsuhiro, A. Mansilla, M. Lapier, J.D. Maya, C. Olea-Azar, Supramolecular hydrogels of β-cyclodextrin linked to calcium homopoly-l-guluronate for release of coumarins with trypanocidal activity, Carbohydr. Polym. 204 (2019) 170–181.
[62] H.N. KiranKumar, H.G. RohitKumar, G.M. Advirao, Synthesis, DNA binding and cytotoxic activity of pyrimido[4′,5′:4,5]thieno(2,3-b)quinoline with 9-hydroxy-4-(3-diethylaminopropylamino) and 8-methoxy-4-(3-diethylaminopropylamino) substitutions, J. Photochem. Photobiol. B Biol. 178 (2018) 1–9.
[63] K.A. Connors, D.D. Pendergast, Microscopic binding constants in cyclodextrin systems: complexation of .alpha.-cyclodextrin with sym-1,4-disubstituted benzenes, J. Am. Chem. Soc. 106 (1984) 7607–7614.
[64] S. Saha, A. Roy, M.N. Roy, Mechanistic investigation of inclusion complexes of a sulfa drug with α- and β-cyclodextrins, Ind. Eng. Chem. Res. 56 (2017) 11672–11683.
[65] S. Saha, A. Roy, K. Roy, M.N. Roy, Study to explore the mechanism to form inclusion complexes of β-cyclodextrin with vitamin molecules, Sci. Rep. 6 (2016) 35764.
[66] Q. Geng, J. Xie, X. Wang, M. Cai, H. Ma, H. Ni, Preparation and characterization of butachlor/(2-hydroxypropyl)-β-cyclodextrin inclusion complex: improve soil mobility and herbicidal activity and decrease fish toxicity, J. Agric. Food Chem. 66 (2018) 12198–12205.
[67] M.I. Sancho, M.G. Russo, M.S. Moreno, E. Gasull, S.E. Blanco, G.E. Narda, Physicochemical characterization of 2-hydroxybenzophenone with β-cyclodextrin in solution and solid state, J. Phys. Chem. B 119 (2015) 5918–5925.
[68] A.P. Sherje, V. Kulkarni, M. Murahari, U.Y. Nayak, P. Bhat, V. Suvarna, B. Dravyakar, Inclusion complexation of etodolac with hydroxypropyl-beta-cyclodextrin and auxiliary agents: formulation characterization and molecular modeling studies, Mol. Pharm. 14 (2017) 1231–1242.
[69] A. do Nascimento Cavalcante, C.M. Feitosa, F.P. da Silva Santos, A.P.R. de Sousa, R. dos Santos Sousa, A.A. de Souza, B.F. Pinto, C.M. Araújo, K. Rashed, Elaboration and characterization of the inclusion complex between β-cyclodextrin and the anticholinesterase 2-oleyl-1,3-dipalmitoyl-glycerol extracted from the seeds of Platonia insignis MART, J. Mol. Struct. 1177 (2019) 286–301.
[70] B.K. Barman, S. Barman, M.N. Roy, Inclusion complexation between tetrabutylphosphonium methanesulfonate as guest and α- and β-cyclodextrin as hosts investigated by physicochemical methodology, J. Mol. Liq. 264 (2018) 80–87.
[71] Z. Aytac, Z.I. Yildiz, F. Kayaci-Senirmak, N.O. San Keskin, S.I. Kusku, E. Durgun, T. Tekinay, T. Uyar, Fast-dissolving, prolonged release, and antibacterial cyclodextrin/limonene-inclusion complex nanofibrous webs via polymer-free electrospinning, J. Agric. Food Chem. 64 (2016) 7325–7334.
[72] H. Guo, J. Yang, J. Zhou, L. Zeng, L. Zhao, B. Xu, Photoresponsive self-assembly of a β-cyclodextrin derivative with an azobenzene terminal group in water, Dyes Pigments 149 (2018) 626–632.
[73] A. Celebioglu, T. Uyar, Antioxidant vitamin E/cyclodextrin inclusion complex electrospun nanofibers: enhanced water solubility, prolonged shelf life, and photostability of vitamin E, J. Agric. Food Chem. 65 (2017) 5404–5412.
[74] L. Gong, T. Li, F. Chen, X. Duan, Y. Yuan, D. Zhang, Y. Jiang, An inclusion complex of eugenol into β-cyclodextrin: preparation, and physicochemical and antifungal characterization, Food Chem. 196 (2016) 324–330.
[75] H. Ikeda, M. Nakamura, N. Ise, N. Oguma, A. Nakamura, T. Ikeda, F. Toda, A. Ueno, Fluorescent cyclodextrins for molecule Sensing: fluorescent properties, NMR characterization, and inclusion phenomena of N-Dansylleucine-Modified cyclodextrins, J. Am. Chem. Soc. 118 (1996) 10980–10988.
[76] A. Banerjee, P.K. Sengupta, Encapsulation of 3-hydroxyflavone and fisetin in β-cyclodextrins: excited state proton transfer fluorescence and molecular mechanics studies, Chem. Phys. Lett. 424 (2006) 379–386.
[77] S. Chaudhuri, S. Chakraborty, P.K. Sengupta, Encapsulation of serotonin in β-cyclodextrin nano-cavities: fluorescence spectroscopic and molecular modeling studies, J. Mol. Struct. 975 (2010) 160–165.
[78] U.S. Sharma, S.V. Balasubramanian, R.M. Straubinger, Pharmaceutical and physical properties of paclitaxel (taxol †) complexes with cyclodextrins ‡, J. Pharm. Sci. 84 (1995) 1223–1230.
[79] R.N. Dsouza, U. Pischel, W.M. Nau, Fluorescent dyes and their supramolecular host/guest complexes with macrocycles in aqueous solution, Chem. Rev. 111 (2011) 7941–7980.
[80] R.S. Naik, S.K. Pawar, R.D. Tandel, S.J., Insights in to the mechanism of interaction of a thrombin inhibitor, dabigatran etexilate with human serum albumin and influence of β-cyclodextrin on binding: spectroscopic and computational approach, J. Mol. Liq. 251 (2018) 119–127.